Compatible discrete operator schemes on polyhedral meshes for elliptic and Stokes equations

Jérôme Bonelle

UNIVERSITÉ PARIS-EST

Thèse

présentée pour obtenir le grade de

Docteur de l'université Paris-Est

École doctorale MSTIC, mention Mathématiques Appliquées

par Jérôme Bonelle

Opérateurs Discrets Compatibles pour la discrétisation sur maillages polyédriques des équations elliptiques et de Stokes

Compatible Discrete Operator schemes on polyhedral meshes for elliptic and Stokes equations

---

Soutenue publiquement le 21 novembre 2014 devant le jury composé de

Rapporteurs	Pr. Snorre H. Christiansen	Université d'Oslo (Norvège)
	Pr. Jérôme Droniou	Université de Monash (Australie)
Examinateurs	Pr. Claire Chainais-Hillairet	Université de Lille
	Pr. Daniele A. Di Pietro	Université de Montpellier
	Pr. Robert Eymard	Université Paris-Est
	Pr. Marc I. Gerritsma	Université Technologique de Delft (Pays-Bas)
	Dr. David Monfort	EDF R&D
Directeur de thèse	Pr. Alexandre Ern	Université Paris-Est

À Aurélie et Adam

"Le véritable voyage de découverte
ne consiste pas à chercher de nouveaux paysages
mais à avoir de nouveaux yeux"
— Marcel Proust

Remerciements

Mes premiers remerciements sont destinés à EDF, mon employeur, et en particulier à Frédéric Archambeau, mon chef de groupe en début de thèse, qui a soutenu mon projet et a permis à cette thèse de voir le jour. Je lui exprime toute ma gratitude.

Mes seconds remerciements sont destinés à Alexandre Ern, mon directeur de thèse, pour sa grande disponibilité, la qualité de son encadrement, et la pédagogie dont il a fait preuve au cours de ces trois années. J'ai beaucoup appris à ses côtés.

Je remercie vivement Snorre Christiansen et Jérôme Droniou de m'avoir fait l'honneur de rapporter ma thèse.

Je remercie également Claire Chainais-Hillairet, Daniele Di Pietro, Robert Eymard, Marc Gerritsma et David Monfort d'avoir accepté de faire partie de mon jury. Je remercie à double titre Daniele, Robert et Marc pour les échanges que nous avons pu avoir au cours de mes travaux et qui je l'espère se poursuivront.

Je souhaite également remercier mes collègues d'EDF R&D à Chatou, et en particulier ceux du groupe I83 de leur soutien et pour nos échanges quotidiens ainsi que ma collègue de bureau, Sophie Bournaud, de sa bienveillance. Je remercie spécifiquement Ophélie Angélini, Bruno Audebert, Martin Ferrand, David Monfort et Jean-Marc Hérard d'avoir suivi et participé aux réunions d'avancement de ma thèse. Je remercie à double titre Bruno et Jean-Marc de leur aide dans le montage de ma thèse. J'exprime aussi ma gratitude à Romain Camy pour sa relecture attentive du manuscrit qui a permis d'éliminer plusieurs "coquilles" passées au travers des relectures. Je tiens à remercier également les responsables (présents et passés) de mon département, Frédéric Baron, Ange Caruso et Isabelle Flour, d'avoir accepté et soutenu cette thèse ainsi que Stéphane Andrieux et Olivier Marchand pour leur avis favorable au lancement de ma thèse.

Je tiens à remercier le CERMICS, son équipe administrative et ses permanents de leur accueil. J'adresse un remerciement particulier à Laurent Monasse qui a partagé son bureau lors de mes passages au CERMICS.

J'adresse également une pensée amicale aux thésards d'EDF et du CERMICS que j'ai côtoyés durant ces trois années : à ceux qui ont fini (Christelle, David, Fabien et Rémi), à ceux qui finissent (Adéla et Antoine), et à ceux qui sont dans le vif du sujet (Cédric, Jean-François, Pierre, Xavier et Yannick).

Je remercie enfin mes proches et particulièrement Aurélie, à qui je témoigne toute mon affection pour son soutien continu au cours de ces années. En guise de conclusion, je tourne mes pensées vers mon petit Adam qui a égaillé ces derniers mois de thèse et qui ouvre un nouveau chapitre de ma vie.

Table des matières

Chapitre 1

Introduction

1.1 Contexte et objectifs

Ce travail de thèse a reçu le soutien d'EDF R&D et plus particulièrement celui du département Mécanique des Fluides, Énergie et Environnement. En effet, les équipes d'EDF R&D développent des codes de simulations numériques pour la mécanique des fluides depuis plus de 30 ans. Pour EDF, les enjeux relatifs à la simulation numérique sont importants. Ces enjeux recouvrent entre autres l'étude du renforcement de la sûreté et de l'allongement de la durée de fonctionnement des moyens de production et de leur optimisation. Parmi les nombreuses applications visées, les études relatives à la thermohydraulique des réacteurs nucléaires constituent une part importante des applications. L'objectif des simulations consiste à étudier les phénomènes physiques en jeu afin d'améliorer le fonctionnement des centrales et prolonger leur durée de vie tout en répondant aux exigences de sûreté. L'étude des écoulements atmosphériques (dispersion de polluants, étude du potentiel éolien) ou la simulation des phénomènes de combustion dans les chaudières du parc de centrales thermiques (compréhension et optimisation des brûleurs à faible rejet d'oxydes d'azote par exemple) sont d'autres applications cibles où la simulation numérique est employée.

Depuis 1998, *Code_Saturne*[1] est le code de référence développé et utilisé à EDF R&D pour l'étude des écoulements monophasiques (cf. Archambeau *et al.* (2004) et Fournier *et al.* (2011) par exemple pour plus de détails). Dans *Code_Saturne*, les équations de Navier–Stokes sont discrétisées à l'aide d'une approche Volumes Finis où les degrés de liberté sont co-localisés au centre des cellules. Il s'agit d'un solveur généraliste adapté aux exigences industrielles (parallélisme et calcul haute performance, traitement des géométries complexes) qui intègre de nombreux modèles physiques dédiés à la turbulence, aux écoulements atmosphériques, à la combustion, aux incendies, aux phénomènes de dépôt et ré-entrainement de particules, aux transferts thermiques, aux turbomachines... Au cours des dernières années, des travaux ont été engagés pour améliorer les méthodes numériques de *Code_Saturne*. Deux axes principaux d'évolutions ont été identifiés.

(a) L'amélioration de la robustesse du code sur des géométries 3D complexes composées d'éléments polyédriques de qualité médiocre constitue le premier axe. En effet, la simulation fine des écoulements dans des géométries industrielles 3D s'appuie sur des maillages hybrides (composés de plusieurs types d'éléments) et/ou polyédriques afin d'offrir plus de souplesse à l'utilisateur lors du maillage de la géométrie.

(b) L'amélioration de la représentativité physique des simulations correspond au second axe. Par représentativité physique, on entend l'absence de modes parasites (potentiellement induits par une mauvaise représentation du noyau des opérateurs différentiels et/ou un traitement inadéquat des conditions aux limites), le respect des bornes physiques (monotonie, principe du maximum), la conservation locale des grandeurs d'intérêt (masse, quantité

1. `http://code-saturne.org`

de mouvement, énergie cinétique...) et une meilleure précision sur maillages grossiers.

A côté de ces deux axes, un impératif d'efficacité en termes de temps de calcul et de consommation mémoire, inhérent au contexte industriel, est également fixé. Ces différents critères ont ainsi guidé les travaux de recherche menés au cours de cette thèse. Suite à une revue bibliographique préalable à la thèse, les schémas dits *mimétiques* ou les *discrétisations compatibles* ont été identifiés comme un axe de recherche pour améliorer les méthodes numériques de *Code_Saturne*. Cette thèse s'inscrit donc dans ce contexte et a pour objectif le développement et l'analyse de schémas de discrétisation compatible pour la mécanique des fluides.

1.2 Contributions de la thèse

Les travaux menés au cours de cette thèse ont permis le développement d'une nouvelle approche de discrétisation sur maillages polyédriques dénommée "Opérateurs Compatibles Discrets" ou "Compatible Discrete Operator" (CDO) en anglais. Deux applications ont été spécifiquement étudiées.

(1) Concernant les problèmes elliptiques (diffusion hétérogène et/ou anisotrope), l'approche CDO propose, à l'aide de l'opérateur de Hodge discret, un cadre unifié à la fois pour l'analyse et l'implémentation de nombreux schémas existants. Deux familles de schémas CDO sont étudiées : les schémas dits *vertex-based* et les schémas dits *cell-based*, en fonction du positionnement des degrés de liberté associés au potentiel. L'analyse a en outre permis de démontrer la convergence du gradient et du flux à l'ordre 1 en norme d'énergie ainsi qu'une convergence à l'ordre 2 en norme L^2 du potentiel (non démontré jusqu'à présent sur des maillages polyédriques relativement généraux à notre connaissance). Par ailleurs, les résultats numériques obtenus à l'aide des schémas CDO sont comparables aux schémas d'ordre bas les plus performants actuellement publiés en termes d'efficacité, de robustesse et de précision. Une étude comparative des schémas CDO proposés est également détaillée.

(2) Concernant les équations de Stokes, l'approche CDO repose sur une formulation à deux ou trois champs utilisant l'opérateur rotationnel. De nouveaux schémas sur maillages polyédriques ont été proposés et analysés pour deux familles de schémas CDO (*vertex-based* et *cell-based*). Ces schémas conservent localement au niveau discret la masse et la quantité de mouvement. La stabilité des schémas CDO a été établie ainsi qu'une convergence à l'ordre 1 du gradient de pression, de la vitesse et de la vorticité. De plus, un traitement robuste des termes source ayant une forte composante solénoïdale ou irrotationnelle a été proposé. Ce traitement particulier, reposant dans un cas sur la définition du terme source sur le maillage dual, a été établi lors de l'analyse d'erreur *a priori*. Des tests numériques ont confirmé la robustesse et l'efficacité de ce traitement. Il est important de signaler que la connaissance de la décomposition de Hodge–Helmholtz du terme source n'est pas requise, ce qui rend ce traitement facilement applicable dans la pratique.

En complément de l'analyse des schémas CDO pour les équations elliptiques et de Stokes, un prototype de solveur basé sur l'approche CDO et s'appuyant sur la structure de *Code_Saturne* a également été développé durant cette thèse afin d'évaluer l'efficacité des schémas CDO et vérifier les résultats théoriques obtenus. En accord avec le cadre industriel dans lequel cette thèse s'inscrit, les travaux de recherche ont été effectués dans une démarche purement 3D que ce soit pour l'analyse, l'implémentation ou les tests numériques.

Publications. Les travaux effectués durant cette thèse ont fait l'objet de deux publications dans des revues internationales avec comité de lecture :

(A) Bonelle, J. & Ern, A. (2014) *Analysis of Compatible Discrete Operator Schemes for Elliptic Problems on Polyhedral Meshes*, ESAIM : Mathematical Modelling and Numerical Analysis, vol. 48, pp. 553–581.

(B) Bonelle, J. & Ern, A. (2014) *Analysis of Compatible Discrete Operator Schemes for the Stokes Equations on Polyhedral Meshes*, (Accepté dans IMA Journal of Numerical Analysis)

Rapports EDF. En complément de ces deux articles, deux rapports internes à EDF ont été publiés. Ils détaillent la prise en compte des conditions aux limites et complètent les résultats numériques présentés dans cette thèse. Leur diffusion est possible sur demande sous réserve de l'accord hiérarchique d'EDF R&D.

(Ra) Bonelle, J. (2012) *Une introduction aux méthodes "Compatible Discrete Operators". Cas d'un problème elliptique.* Rapport EDF R&D H-I83-2012-00741-FR.

(Rb) Bonelle, J. (2013) *Compatible Discrete Operator schemes for the Stokes Problem.* Rapport EDF R&D H-I83-2013-03326-EN.

1.3 Organisation du document

Le présent document est structuré en trois parties dédiées respectivement à la description de l'approche CDO, aux concepts permettant son analyse et à sa mise en œuvre.

Première partie. Cette partie est consacrée à la présentation des schémas CDO. Dans le Chapitre 2, les caractéristiques et les principes à la base des schémas CDO sont exposés. Un état de l'art rappelant les jalons historiques des schémas de discrétisation compatible (ou mimétique) est ensuite présenté. Le positionnement de l'approche CDO par rapport à une sélection de schémas de discrétisation compatible disponibles dans la littérature est ensuite présenté.

Dans le Chapitre 3, les opérateurs discrets et les concepts clés de l'approche CDO sont successivement introduits : la définition des degrés de liberté à partir de l'opérateur de de Rham, les opérateurs différentiels discrets (gradient, rotationnel et divergence), le concept de dualité inhérent à la démarche proposée (maillage dual, degrés de liberté et opérateurs différentiels discrets sur ce maillage), puis l'opérateur de Hodge discret, pierre angulaire de l'approche CDO. Enfin, un diagramme synthétisant les relations entre les différents opérateurs discrets introduits conclut ce chapitre.

Dans le Chapitre 4, les différents schémas CDO proposés pour les équations elliptiques et de Stokes sont détaillés. Deux schémas CDO pour les équations elliptiques sont présentés. Le premier est dénommé *vertex-based* car les degrés de liberté associés au potentiel sont positionnés aux sommets du maillage primal. Le second est denommé *cell-based* car les degrés de liberté associés au potentiel sont cette fois positionnés au centre des cellules du maillage primal (plus précisément aux sommets du maillage dual). Deux schémas CDO sont également proposés pour les équations de Stokes formulées à l'aide de l'opérateur rotationnel. Par analogie au cas elliptique, un schéma *vertex-based pressure* où les degrés de liberté associés à la pression sont positionnés aux sommets du maillage primal, et un schéma *cell-based pressure*, où ces degrés de liberté sont positionnés au centre des cellules, sont explicités.

Deuxième partie. Cette partie est consacrée à la présentation des concepts théoriques permettant l'analyse des schémas CDO. Dans le Chapitre 5, les notions utiles au traitement des maillages polyédriques sont introduites (hypothèses sur la régularité du maillage et définition de la subdivision barycentrique permettant la construction d'un maillage dual barycentrique).

Deux niveaux d'analyse sont ensuite proposés. Dans le Chapitre 6, une analyse algébrique (*i.e.* purement discrète) est développée. Les normes discrètes sur le maillage primal et le maillage dual ainsi que les normes discrètes induites par l'opérateur de Hodges sont définies. Une définition formelle des trois propriétés clés (symétrie, stabilité et consistance) que doit satisfaire un opérateur de Hodge discret est également explicitée. Enfin, des résultats d'approximation

utilisés lors de l'analyse d'erreur des schémas CDO sont établis ainsi que des résultats d'analyse fonctionnelle discrète (injections de Sobolev discrètes), utiles pour démontrer la stabilité des schémas CDO.

Dans le Chapitre 7, un autre point de vue, basé sur les opérateurs de reconstruction, est adopté pour mener l'analyse des schémas CDO. Les opérateurs de reconstruction à partir des degrés de liberté associés aux potentiels, circulations et flux sont successivement détaillés. En outre, ces opérateurs de reconstruction permettent de construire génériquement un opérateur de Hodge discret. Ainsi, ils sont définis de manière à conserver les propriétés de l'opérateur de Hodge discret identifiées dans le chapitre précédent. Des exemples simples d'opérateurs de reconstruction sont ensuite présentés. Plusieurs types d'opérateurs de reconstruction sur maillages polyédriques sont ensuite proposés et classés en fonction des propriétés qu'ils vérifient. Enfin, deux nouvelles inégalités de Poincaré discrètes (Poincaré–Wirtinger et Poincaré pour le rotationnel) s'appuyant sur les opérateurs de reconstruction sont établies.

Troisième partie. Cette partie est dédiée à la discrétisation des équations elliptiques et des équations de Stokes à l'aide des schémas CDO.

Dans le Chapitre 8, s'appuyant sur l'article (A), deux schémas CDO (*vertex-based* et *cell-based)* sont analysés sur un problème de diffusion hétérogène et anisotrope en régime stationnaire. La stabilité, la convergence et des estimations d'erreur *a priori* en norme d'énergie pour le gradient et le flux et en norme L^2 pour le potentiel sont successivement exposées pour les deux familles de schémas. Une hybridation des schémas *cell-based* est ensuite étudiée. Enfin, une série de résultats numériques mettant en évidence la pertinence de la démarche proposée ainsi que les différences entre les trois formulations analysées est présentée.

Dans le Chapitre 9, s'appuyant sur l'article (B), deux familles de schémas CDO (*vertex-based pressure* et *cell-based pressure*) pour les équations de Stokes en formulation rotationnelle et en régime stationnaire sont analysées. La stabilité et la convergence sont établies pour ces deux familles de schémas CDO ainsi que des estimations d'erreur *a priori* pour le gradient de pression, la vitesse et la vorticité. Deux stratégies de discrétisation du terme source sont également exposées ayant pour l'une, une bonne aptitude à représenter les termes source avec une forte composante irrotationnelle et pour l'autre, une bonne aptitude à représenter les termes source avec une forte composante solénoïdale. Enfin, une série de résultats numériques illustrant l'adéquation avec les résultats théoriques conclut ce dernier chapitre.

Part I

Compatible Discrete Operator framework

Chapter 2

Compatible spatial discretizations

Contents

In this chapter, we first recall the main historical contributions and the conceptual roots underpinning this thesis (Section 2.1.1). Then, we introduce the *Compatible Discrete Operator* (CDO) approach and in particular its two leading principles:

(i) The discretization aims at being physically-relevant.

(ii) The discrete setting is based on a fine-grained set of operators on which the analysis is performed.

The first principle along with its consequences is detailed in Section 2.1.2, while the second principle is presented in Section 2.1.3. In Section 2.2, we give an overview of several approaches related to CDO schemes that can be found in the literature. We conclude this chapter with Table 2.2 which summarizes in terms of some selected features the place of the CDO approach among the main related approaches from the literature.

2.1 Compatible Discrete Operator schemes

CDO schemes belong to the broad class of compatible [1] or *mimetic* or *structure-preserving* discretizations. Such discretizations aim at preserving structural properties of the continuous model at the discrete level. All these schemes constitute a class of numerical methods for the discretization of Partial Differential Equations (PDEs) which finds its roots in the seminal works of Kron (1945, 1953), Branin (1966), Tonti (1975a), and Bossavit (1988) oriented toward the electromagnetism community and in those of Whitney (1957), Tikhonov & Samarskii (1962), and Dodziuk (1976) oriented toward the mathematical community. Two papers have also

1. "Compatible Spatial Discretization" is the name of the workshop (and of the book of proceedings) organized in 2004 at the Institute for Mathematics and its Applications of the University of Minnesota. This workshop is one of the first ones dedicated to this field of research. It gathered several of the earlier and main contributors.

set a milestone in the history of compatible spatial discretizations: the "Marker and Cell" (MAC) scheme for solving the Navier–Stokes equations (Harlow & Welch, 1965) and the Yee scheme (Yee, 1966) for solving the Maxwell equations, both on Cartesian grids.

2.1.1 Concepts of differential geometry and algebraic topology

The CDO approach follows the seminal ideas of Tonti (1975b), Frankel (1997), and Bossavit (1998). These previous works rely on concepts of differential geometry and algebraic topology to describe and analyze the geometric structure of the underlying physics. The description of compatible spatial discretizations by means of these concepts is now a widespread viewpoint; see, for instance, Mattiussi (1997); Bossavit (1998); Bochev & Hyman (2005); Arnold *et al.* (2006); Desbrun *et al.* (2006); Gerritsma (2012); Teixeira (2013).

We give an informal and brief overview of these concepts in the present section. We refer the reader interested in a more detailed and precise introduction to these concepts to the book of Abraham *et al.* (1988) for a comprehensive introduction to differential geometry and to the book of Hatcher (2002) for algebraic topology. Even though these concepts are important for the development of CDO schemes, and in general, for the understanding of compatible spatial discretizations, we will be using the language of vector calculus in this thesis so as to facilitate the understanding of the CDO approach by a broad audience (only the term “Hodge operator” is kept).

Differential geometry. In a d-dimensional manifold Ω, there are $(d+1)$ bundles of linear spaces spanned by k-differential forms for $0 \leq k \leq d$. These spaces are generically denoted by $\Lambda^k(\Omega)$. Recasting the continuous problem with differential forms helps one identify the nature of the operators and fields to consider. Roughly speaking, in a three-dimensional space, scalar fields are identified either to a 0-form (a potential) or to a 3-form (a density) and vector fields are identified either to a 1-form (a circulation) or to a 2-form (a flux). A potential, circulation, flux, or density is the proxy field of the corresponding k-differential form.

Operators are divided into two categories: metric and topological operators. An example of metric operator is the Hodge-star operator (cf. Section 3.4). An example of topological operator is the exterior derivative. Via proxy fields, the exterior derivative $\mathrm{d}^k : \Lambda^k(\Omega) \to \Lambda^{k+1}(\Omega)$ corresponds to $\underline{\mathrm{grad}}$ for $k=0$, to $\underline{\mathrm{curl}}$ for $k=1$, and to div for $k=2$. The exterior calculus is also a powerful tool to state fundamental identities of vector calculus in a synthetic way. Namely, $\mathrm{d}^{k+1}\,\mathrm{d}^k = 0$ with $k=0$ and $k=1$ is an equivalent formulation of

$$\underline{\mathrm{curl}}\,\underline{\mathrm{grad}} = \underline{0}, \qquad \text{and} \qquad \mathrm{div}\,\underline{\mathrm{curl}} = 0. \tag{2.1}$$

The association between a set of spaces and a set of operators gives rise to the notion of *complex*. The most popular one is the cochain complex called “de Rham complex” related to the sequence induced by the exterior derivatives on the spaces of differential forms:

$$\mathbb{R} \hookrightarrow \Lambda^0(\Omega) \xrightarrow{\mathrm{d}^0} \Lambda^1(\Omega) \xrightarrow{\mathrm{d}^1} \Lambda^2(\Omega) \xrightarrow{\mathrm{d}^2} \Lambda^3(\Omega) \longrightarrow 0, \tag{2.2}$$

where the first arrow denotes the canonical injection (with $\mathbb{R}$ identified with constant 0-forms). The sequence (2.2) is called a *complex* since the image of an operator from the sequence is included in the kernel of the next operator in the sequence.

Algebraic topology. In the context of spatial discretizations, concepts of algebraic topology are relevant since a mesh (*i.e.* a collection of vertices, edges, faces, and cells with matching faces s.t. they form a partition of the domain $\Omega \subset \mathbb{R}^3$) can be considered as a *cell complex*. A cell complex is a collection of k-cells for $k \in [0,3]$. In our context, a vertex corresponds to a 0-cell, an edge to a 1-cell, a face to 2-cell, and a cell to a 3-cell. Let $c_{(k)}$ denote a k-cell. A k-chain, denoted by $\mathbf{c}_{(k)}$, is a linear combination of k-cells. The set of all the k-chains is a

linear space denoted by C_k. In addition, an orientation is fixed for each k-cell once and for all (by convention a 0-cell is positively oriented). The boundary operator $\partial_k : C_{k+1} \to C_k$ defines a linear combination with weights in $\{+1, -1\}$ of the $(k-1)$-cells constituting the boundary of each k-cell in the k-chain. Namely, the boundary of a cell is described as the combination of its faces, a face as the combination of its edges, an edge as the combination of its vertices where the weights in the combination are either 1 if the orientation of the boundary of the k-cell matches the orientation of the $(k-1)$-cell, or -1 otherwise. Since the boundary of a boundary is empty (*i.e.* $\partial_k \, \partial_{k-1} = 0$), the boundary operators acting on chains yield the following sequence:

$$C_0 \xleftarrow{\partial_0} C_1 \xleftarrow{\partial_1} C_2 \xleftarrow{\partial_2} C_3. \tag{2.3}$$

A k-cochain denoted by $\mathbf{c}^{(k)}$ is a dual object to a k-chain. A k-cochain maps each k-cell to a real value. For instance, a 0-cochain sets a value at each 0-cell (vertex) and a 1-cochain a value at each 1-cell (edge). Acting on a k-chain $\mathbf{c}_{(k)}$, a k-cochain $\mathbf{c}^{(k)}$ produces a real number which is the linear combination of its associated values on each k-cell composing the k-chain. Introducing the duality pairing $\langle \cdot, \cdot \rangle$ between cochains and chains, the latter action is denoted by $\left\langle \mathbf{c}^{(k)}, \mathbf{c}_{(k)} \right\rangle \in \mathbb{R}$. The linear space collecting the k-cochains is denoted by C^k. The coboundary operator $\delta^k : C^k \to C^{k+1}$ is defined as the adjoint operator to the boundary operator ∂_k with respect to the duality pairing:

$$\forall \mathbf{c}^{(k)} \in C^k, \forall \mathbf{c}_{(k+1)} \in C_{k+1}, \qquad \left\langle \delta^k \mathbf{c}^{(k)}, \mathbf{c}_{(k+1)} \right\rangle := \left\langle \mathbf{c}^{(k)}, \partial_k \mathbf{c}_{(k+1)} \right\rangle. \tag{2.4}$$

Since $\partial_k \partial_{k+1} = 0$, $\delta^k \delta^{k+1} = 0$, which produces the following cochain complex:

$$C^0 \xrightarrow{\delta^0} C^1 \xrightarrow{\delta^1} C^2 \xrightarrow{\delta^2} C^3. \tag{2.5}$$

Loosely speaking, a k-cochain can be seen as a discrete field: $k = 0$ for a potential, $k = 1$ for a circulation, $k = 2$ for a flux, and $k = 3$ for a density. The coboundary operator δ^k, $0 \leq k \leq 2$, can be viewed as the discrete counterpart of d^k and thus as a discrete differential operator. In this context, the identity (2.4) can be seen as the discrete counterpart of the generalized Stokes theorem and (2.5) as the discrete counterpart of the de Rham complex (2.2).

Vector calculus	**Differential geometry**	**Algebraic topology**
geometrical objects *point, line, surface, volume*	manifolds	chains
fields *potential, circulation, flux, density*	differential forms	cochains
differential operators grad, curl, div	exterior derivatives	coboundary operators

Table 2.1 – Analogies between terminologies used in vector calculus, differential geometry, and algebraic topology.

2.1.2 A physically-driven strategy of discretization

Since CDO schemes aim at preserving the structural properties of the PDEs at the discrete level, the starting point is an understanding of the physical nature of the fields and equations to discretize.

Firstly, CDO schemes define the degrees of freedom (DoFs) according to the physical nature of fields to discretize: a potential at a vertex, a circulation along an edge, a flux across a face,

and a density inside a cell. The discretization aims at preserving at the discrete level the local conservation property satisfied by these fields, so that the discrete balance equations are locally exact.

Secondly, in CDO schemes, one operates a clear separation between conservation (or balance) laws on the one hand, and constitutive (or closure) relations on the other. The first kind of relation involves topological (or differential) operators and its discretization by CDO schemes does not introduce any consistency error. In particular, the definition of DoFs combined with the fundamental theorem of calculus (for $\underline{\mathrm{grad}}$), the Stokes theorem (for $\underline{\mathrm{curl}}$), and the Gauss theorem (for div) makes it possible to build discrete differential operators which are topological in the sense that these operators are not affected when one stretches or deforms the mesh. In addition, discrete differential operators preserve the key features of their continuous counterpart like relations (2.1). Moreover, a proper representation of the nullspace of the discrete differential operators can help avoiding the emergence of spurious modes.

The second kind of relation involves metric operators and its discretization by CDO schemes leads to approximations. In this way, CDO schemes introduce approximations at the same level as the physical modeling, so that the only source of consistency error stems from the discretization of closure relations (assuming there is no quadrature error related to source terms or boundary conditions).

One crucial idea to design the metric operators in CDO schemes relies on an explicit use of a dual mesh (cf. Section 3.3). DoFs on dual mesh entities are defined similarly to DoFs on primal mesh entities. Furthermore, discrete differential operators are introduced on the dual mesh as well, following the same rationale as for the primal mesh. Discrete differential operators on the primal and dual mesh are related by adjunction properties which are the discrete counterpart of adjunction properties at the continuous level (for instance, between $-\underline{\mathrm{grad}}$ and div).

The discrete closure relations linking DoFs on the primal mesh to DoFs on the dual mesh are formulated using discrete Hodge operators (the discrete counterpart of the Hodge operator appearing when the PDE is formulated in terms of differential forms). In this way, the closure relations relate the same fields at the continuous and discrete levels (for instance, the gradient of a potential and the diffusive flux for an elliptic equation or the velocity circulation and the mass flux for the Stokes equations). The discrete Hodge operator is a metric operator since its definition relies on geometric quantities related to the primal and dual mesh entities and on the evaluation of a material property.

Another benefit of considering a dual mesh explicitly is that it allows one to devise and analyze two families of schemes inside the same framework since two sets of DoFs are available. The first family where potential DoFs are attached to primal vertices leads to *vertex-based* schemes, while the second family where potential DoFs are attached to dual vertices (in one-to-one correspondence with primal cells) leads to *cell-based* schemes. The term *cell-based* stresses the salient role of the primal mesh since this mesh is the only one that needs to be seen by the end-user.

2.1.3 A fine-grained set of operators

In the CDO approach, the discrete setting hinges on a fine-grained set of operators consisting of the discrete differential operators (three on the primal mesh and three on the dual mesh) and of the discrete Hodge operators (four operators, one for each type of mesh entity). This discrete setting is purely algebraic (DoFs are vectors of reals and not polynomial functions). The fundamental properties of the operators of the discrete setting are stated algebraically. In addition to the discrete operators, we consider de Rham (or reduction) operators to define the DoFs and reconstruction (or lifting) operators to define functions from DoFs. All these operators constitute the building blocks of the CDO framework detailed in the following chapters.

The discrete differential operators are uniquely defined, while the discrete Hodge operators are not. The design properties of the discrete Hodge operators can be derived following two strategies, either using an algebraic viewpoint or using reconstruction operators. Within the

algebraic viewpoint, a minimal set of requirements on the design of the discrete Hodge operator is identified so as to perform a purely discrete convergence analysis. When using reconstruction operators, the properties of these operators are identified so as to recover the results derived with an algebraic perspective, but also to derive further theoretical results.

The fine-grained set of operators also allows one to define new operators by combining these operators. For instance, the approximation (also called interpolation or projection) map is the composition of a reconstruction and a reduction map (this operator is mainly used in the Finite Element (FE) literature). Another example is the reconstructed gradient (mainly used in Finite Volume (FV) methods) which is obtained by applying the reconstruction operator to the discrete gradient. In both cases, each choice of the reconstruction operator leads to a specific scheme. Identifying which reconstruction is behind a scheme is therefore a way to draw links between existing schemes (cf. Sections 8.1.3 and 8.2.3). Combining the set of fine-grained operators with the two levels of analysis makes the CDO framework an effective way to analyze compatible spatial discretizations.

2.2 State of the art

During the last decade, compatible spatial discretizations of PDEs have become increasingly popular, making hard to circumscribe the landscape of such schemes. Researches dedicated to this field have led to the development and analysis of new schemes. In addition, new perspectives on existing schemes have been underlined, driven by new design principles and the development of more generic frameworks for the analysis. As a result, many links between compatible discretization schemes have been identified. We now present a brief state of the art (we do not aim at completeness). We divide these contributions according to two axes: lower- or higher-order schemes for the first axis and the type of meshes (specific or polyhedral) supported by the schemes for the second axis.

2.2.1 Lower-order schemes on specific meshes

The electromagnetism community has played a pioneering role in the development of compatible spatial discretizations. This community has developed a geometrical vision of the Maxwell equations based on insightful concepts of differential geometry and algebraic topology.

Relying on concepts of differential geometry, Bossavit (1988) has linked the classical lower-order FE schemes (Lagrange, Nédélec, Raviart–Thomas elements) to the Whitney forms and to the Hodge operator. The *Generalized Finite Difference* method introduced by Bossavit (2001) collects these ideas and gives rise to a reinterpretation of classical FE schemes within a geometrical viewpoint. This work has shed new light on the design principles of discretization schemes. The same geometrical interpretation of the traditional FE method has been pursued in the work of Trevisan & Kettunen (2006) and that of He & Teixeira (2006).

We also mention the work of Mattiussi (1997) who has drawn connections between the main families of spatial discretization schemes: Finite Differences (FD), FV, and FE using concepts of algebraic topology. Clemens & Weiland (2001) with the *Finite Integration Technique* (FIT) and Tonti (2001) with the *Cell Method* on simplicial meshes have followed a similar rationale to devise different schemes.

Independently, three equivalent discretizations on Delaunay–Voronoï meshes have been proposed in different communities: the Covolume method by Hu & Nicolaides (1992) (see also Nicolaides & Trapp (2006) for a reformulation in terms of differential forms), the Two-Point Flux Approximation (TPFA) scheme using a FV approach (Eymard *et al.*, 2000) initially used in petroleum engineering, and the Discrete Exterior Calculus (DEC) approach by Desbrun *et al.* (2005) in computer graphics.

2.2.2 Lower-order schemes on general meshes

Historically, compatible spatial discretizations have been introduced on Cartesian meshes and then on simplicial meshes. An important breakthrough has been the extension of these techniques to general (polyhedral) meshes. The flexibility of polyhedral meshes to pave complex geometries makes such meshes of salient interest in an industrial context.

MFD. The Mimetic Finite Difference (MFD) approach is an evolution of the Support Operator Method (see, for instance, Shashkov & Steinberg, 1995; Hyman & Shashkov, 1997) and is nowadays one of the most popular compatible spatial discretizations dealing with general meshes. A brief history of the approach explaining the different evolutions is detailed in the recent book of Beirão da Veiga *et al.* (2014); see also the recent overview by Lipnikov *et al.* (2014).

For the elliptic case, there exist two families of MFD techniques either based on a mixed formulation (DoFs located at cells and faces) or on a primal formulation (DoFs located at vertices). The first (resp. second) technique has been analyzed by Brezzi *et al.* (2005) (resp. Brezzi *et al.* (2009)) and is equivalent to the lowest-order Raviart–Thomas–Nédélec (resp. P1) FE method on simplicial meshes. The point of view is algebraic, and the definition of a suitable discrete inner product is the key point (see, for instance, Brezzi *et al.*, 2014). This discrete inner product has to verify two design properties: a consistency and a stability condition. In MFD schemes, there are two types of operators: *primary* and *derived* operators. The first type is typically a discrete differential operator. The second type is derived from a primary operator (hence the name) and is defined as the adjoint operator of the primary operator with respect to a discrete inner product. A primary operator is identical to a discrete differential operator on the primal mesh in the CDO approach, while a derived operator is a combination of CDO operators. Moreover, in MFD schemes, reconstruction or lifting operators are only needed in the convergence analysis, but not in the implementation. Neither a dual mesh nor a discrete Hodge operator is explicitly employed. All is implicitly regrouped in the definition of the inner product.

Links between the Covolume approach and the MFD schemes on simplicial meshes have been established by Trapp (2008) and also by Bochev & Hyman (2005) with an additional link to the Whitney forms. In this thesis, we study the correspondences between the nodal MFD (Brezzi *et al.*, 2009) and CDO vertex-based schemes for elliptic problems (cf. Section 8.1.3) and also between mixed MFD (Brezzi *et al.*, 2005) and CDO cell-based schemes for elliptic problems (cf. Section 8.2.3).

FV. FV schemes (see the recent review of Droniou (2014)) intrinsically hinge on some ingredients of compatible discretizations since the divergence operator and DoFs related to a flux are defined in order to verify the Gauss theorem. Moreover, the FV method has been historically the first approach to handle polyhedral meshes.

In mechanical engineering, Perot & Subramanian (2007) proposed the *Discrete Calculus* method in order to generalize *staggered* FV discretizations from Cartesian grids to polyhedral meshes (see also Chénier *et al.* (2014) which shares the same goal). The Discrete Calculus approach relies on the same principles as those introduced in the electromagnetism community, but it deals with a larger class of meshes thanks to a different strategy of reconstruction (Perot *et al.*, 2006). It is worth mentioning that this approach distinguishes two families of schemes according to the positioning of the potential DoFs as in the CDO approach.

Discrete Duality Finite Volume (DDFV) schemes (see Hermeline (2000) for one of the seminal papers and Andreianov *et al.* (2012, 2013) for a recent review), the Hybrid Finite Volume (HFV) scheme (see Eymard *et al.* (2010)) and the Mixed Finite Volume (MFV) scheme (see Droniou & Eymard (2006, 2009)) are examples of new FV schemes which are related to compatible spatial discretizations on polyhedral meshes. The DDFV approach adopts a geometrical viewpoint (a dual and a diamond mesh are considered), and the design of discrete

divergence and discrete gradient operators which are adjoint is at the core of the approach. MFV and HFV schemes do not explicitly consider a dual mesh. However, its implicit use appears in the definition of the reconstruction of the gradient.

A Generalization of the Crouzeix–Raviart element to polyhedral meshes has been proposed by Di Pietro & Lemaire (2015) with an application to linear elasticity and Stokes flow. This approach borrows ideas from cell-centered Galerkin methods (see Di Pietro (2012)) and HFV schemes.

Droniou *et al.* (2010) have established equivalences between MFD in mixed formulation, HFV, and MFV. This class of equivalent schemes is called *Hybrid Mixed Mimetic* (HMM) schemes. Furthermore, Droniou *et al.* (2013) have introduced a more general framework called *Gradient Schemes*. The Gradient Scheme framework embraces a broad class of schemes: some Multi-Point Flux Approximation (MPFA) schemes and DDFV schemes, the HMM schemes, the Mixed FE schemes, the Crouzeix–Raviart FE scheme, and the lower-order conforming FE schemes. All these schemes can be analyzed inside the same theoretical framework. In this thesis, we prove that CDO vertex-based schemes fit the Approximate Gradient Schemes framework described by Eymard *et al.* (2012) for elliptic problems (cf. Section 8.1.3) and that a particular formulation of (hybridized) CDO cell-based schemes corresponds to the SUSHI scheme introduced by Eymard *et al.* (2010) (cf. Section 8.3.2).

DGA. The *Discrete Geometric Approach* (DGA) has been developed by Codecasa & Trevisan (2007) for applications in electromagnetism. This is one of the rare approaches which explicitly defines reconstruction functions on polyhedral meshes from edge- and face-based DoFs. Piecewise constant reconstructions are proposed by Codecasa *et al.* (2010), and the key properties they must satisfy are identified. A geometrical viewpoint is adopted. Namely, a dual mesh, based on a barycentric subdivision (cf. Section 3.3.1) is considered. The convergence analysis of DGA schemes for the Maxwell equations can be found in the work of Codecasa & Trevisan (2010b) for bounded and Lipschitz continuous solutions. DGA schemes fully fit the CDO framework.

2.2.3 Higher-order schemes on specific meshes

The extension of compatible spatial discretizations to higher-order schemes has been first achieved using conforming reconstructions, either with traditional FE basis functions for unstructured tetrahedral or hexahedral meshes, or with spectral elements and splines for structured meshes using the tensor product as a building principle. The reconstruction is said to be conforming when it maps to a (finite dimensional) subspace of the graph space of the corresponding differential operator. For instance, the conformity of a potential (resp. circulation, flux) reconstruction means that the reconstructed potential (resp. circulation, flux) is in $H^1(\Omega)$ (resp. $H(\underline{\mathrm{curl}};\Omega)$, $H(\mathrm{div};\Omega)$). Since reconstructions are generally designed cellwise, the conformity requires matching conditions at mesh faces (continuity for the potential, continuity of the tangential component for the circulation, continuity of the normal component for the flux).

Whitney FE & FEEC. The traditional Lagrange, Nédélec, and Raviart–Thomas elements are particular cases of the more generic Whitney forms as observed by Bossavit (1988) and later formalized by Hiptmair (1999). Following this strategy, Hiptmair (2001b) and Bossavit (2002) have proposed higher-order variants of the above FE schemes relying on Whitney forms. A higher-order extension of the Nédélec element (also called Whitney 1-form or edge element) has also been studied by Rapetti (2007) within the geometrical viewpoint proper to the electromagnetism community.

Arnold *et al.* (2006) have broadened the perspective with the development of the Finite Element Exterior Calculus (FEEC) framework. In their seminal paper, Arnold *et al.* (2010) analyzed FEEC schemes using new concepts relying on de Rham cohomology and Hodge theory;

Hilbert complexes and *bounded cochain projections* are two key ideas in FEEC. The choice of basis functions (or reconstruction functions in our terminology) is the element of differentiation among schemes. Higher-order schemes naturally fit the FEEC framework and can be studied similarly to the lower-order schemes. FEEC schemes encompass Whitney elements, and Brezzi–Douglas–Marini elements, but also lead to the emergence of new elements. This approach does not employ a geometrical viewpoint: neither a dual mesh nor a discrete Hodge operator is explicitly employed. Along with MFD schemes, the FEEC approach stands out as one of the most popular compatible spatial discretizations nowadays.

MSE. Several compatible spatial discretization schemes apply the tensor product as a building principle (Hiemstra *et al.*, 2013). These approaches build multidimensional discretizations from a one-dimensional block by means of tensor products. Therefore, the resulting schemes naturally fit Cartesian/Chebyshev grids, while more geometrically complex elements such as deformed quadrilaterals or hexahedra can be handled using transformations (*pullback* in terms of differential geometry) between the computational domain and a reference domain. Mimetic Spectral Element (MSE) schemes (see Kreeft *et al.* (2011)) combine a geometrical vision (dual mesh, discrete Hodge operator) with a reconstruction based on spectral elements which has been devised by Gerritsma (2011). Recently, Rufat *et al.* (2014) have proposed a similar approach to extend the DEC method to more general meshes.

Reconstruction operators relying on B-splines (or their generalization called NURBS) can replace the spectral elements, leading to compatible isogeometric schemes sharing similar properties; see Buffa *et al.* (2011) and Back & Sonnendrücker (2013).

2.2.4 Higher-order schemes on general meshes

Recently, higher-order schemes on polyhedral meshes have emerged.

MFD & VEM. Beirão da Veiga *et al.* (2013) have proposed an extension of the MFD paradigm leading to the Virtual Element Method (VEM). One important ingredient of the VEM is a reformulation of the MFD approach in a FE spirit, in the sense that a variational formulation is used, but the basis functions are not explicitly defined (hence the terminology *virtual*). Notice that these basis functions can typically belong to suitable polynomial spaces (for the purpose of consistency) but also to non-polynomial spaces (for the purpose of stabilization). This new formalism allows one to design higher-order schemes, and also enforce higher-order continuity conditions between mesh cells.

Another extension of the MFD approach to higher-order schemes has been recently proposed by Lipnikov & Manzini (2014) for diffusion problems on polyhedral meshes relying on cell- and face-based DoFs, while previous works on higher-order schemes on polygonal meshes include that of (Beirão da Veiga *et al.*, 2011).

FES. The notion of Finite Element System (FES) has been developed by Christiansen (2008; 2011). It is an abstract setting generalizing the concept of FE. A *compatible* FES is a set of finite dimensional spaces which constitutes a subcomplex of the de Rham complex (2.2). Considering a polyhedral cell decomposed into subsimplices, a practical example of such compatible FES is the set of piecewise polynomial spaces spanned by the Whitney forms on this decomposition with a specific treatment at the interface of the polyhedral cell to ensure conformity. We detail this example in Section 7.3.2. As a result, considering Whitney forms of higher degree yields higher-order schemes (Christiansen & Rapetti, 2014). Reconstruction operators (on polyhedral meshes) in FES are implicitly defined from the resolutions of local problems. As in VEM schemes, non-polynomial spaces can be considered in the FES approach.

MHO & HHO. In a different context, arbitrary-order schemes on polyhedral meshes for elliptic problems have been recently designed. In this approach, face-based DoFs play a salient role. Mixed High Order (MHO) schemes, based on a mixed formulation, have been introduced by Di Pietro & Ern (2013), and Hybrid High Order (HHO) schemes, based on a primal formulation, have been proposed by Di Pietro *et al.* (2014); Di Pietro & Ern (2015). HHO and MHO schemes use a discrete reconstruction of the flux or gradient in each mesh cell. In MHO schemes, the flux is decomposed into two orthogonal parts, one related to consistency and the other one to stability.

Contrary to VEM, the local reconstruction is explicitly defined and the global reconstruction is non-conforming. In the lowest-order case, links with DGA, MFV, HFV, and the lowest-order Raviart–Thomas, and hence also with the CDO schemes, have been established.

2.2.5 Synthesis

To better localize the CDO approach in the landscape of compatible spatial discretizations, we summarize in Table 2.2 CDO schemes and several related approaches using the following basic features:

— lower-order (LO) or higher-order (HO) schemes;
— conforming (C) or non-conforming (NC) setting;
— the kind of meshes handled by the approach: polyhedral meshes (Poly.) or specific meshes (hexahedral, tetrahedral or meshes built using a "tensor product" strategy);
— the kind of meshes which are explicitly considered to design the scheme: primal (P) or dual (D) or diamond (⋄) meshes;
— the key operator: discrete Hodge operator (Hodge), gradient or flux reconstruction (Reco.), discrete inner product (DIP), or bounded cochain projection (BCP).

	CDO	DDFV	HFV MFV	HHO	MFD VEM	MSE	FEEC	FES
Setting	NC	NC	NC	NC	C	C	C	C
LO/HO	LO	LO	LO	HO	LO/HO	HO	HO	HO
Element	Poly.	Poly.	Poly.	Poly.	Poly.	Tensor Product	Tetra Hexa	Poly. (Subdiv)
Meshes	P+D	P+D+⋄	P	P	P	P+D	P	P (D)
Key Op.	Hodge	Reco.	Reco.	Reco.	DIP	BCP	BCP	Reco.

Table 2.2 – Comparison of the CDO schemes with respect to some recent compatible discretizations.

Chapter 3

Discrete setting

Contents

In this chapter, we present the discrete setting underpinning CDO schemes. We describe the different operators involved in CDO schemes along with their main properties. We start with the primal discrete setting: the DoFs in Section 3.1 and the discrete differential operators in Section 3.2. After introducing the concept of dual mesh, we define in Section 3.3 in a similar way DoFs and discrete differential operators on the dual mesh. The discrete Hodge operators bridging the primal and dual discrete settings are then introduced in Section 3.4. We conclude this chapter with Figure 3.14 which summarizes the discrete setting.

3.1 Degrees of freedom

3.1.1 Primal mesh

The domain Ω over which the PDE is posed is assumed to be an open, bounded, polyhedral set $\Omega \subset \mathbb{R}^3$. Its boundary $\partial\Omega$ has (almost everywhere) a unit outward normal denoted by $\underline{\nu}_{\partial\Omega}$. The discretization of Ω relies on the definition of a *primal* mesh M. This primal mesh is the one produced by the mesh generator and is the only mesh that needs to be seen by the end-user. It carries the information on the domain geometry, the definition of the boundary conditions (BCs), and the material properties.

Definition 3.1 (Primal mesh)**.** *The primal mesh* $\mathrm{M} := \{\mathrm{V}, \mathrm{E}, \mathrm{F}, \mathrm{C}\}$ *collects a set of vertices denoted by* V*, of edges* E*, of faces* F *and of cells* C*. A generic element of* V *(resp.* E*,* F*,* C*) is a vertex denoted by* v *(resp. an edge* e*, a face* f*, a cell* c*); see Figure 3.1.*

We write #X to denote the cardinality of the set X. For instance, #C is the number of primal cells. In what follows, we often denote by X any primal set in V, E, F or C and by x any related primal mesh entity such as v, e, f or c.

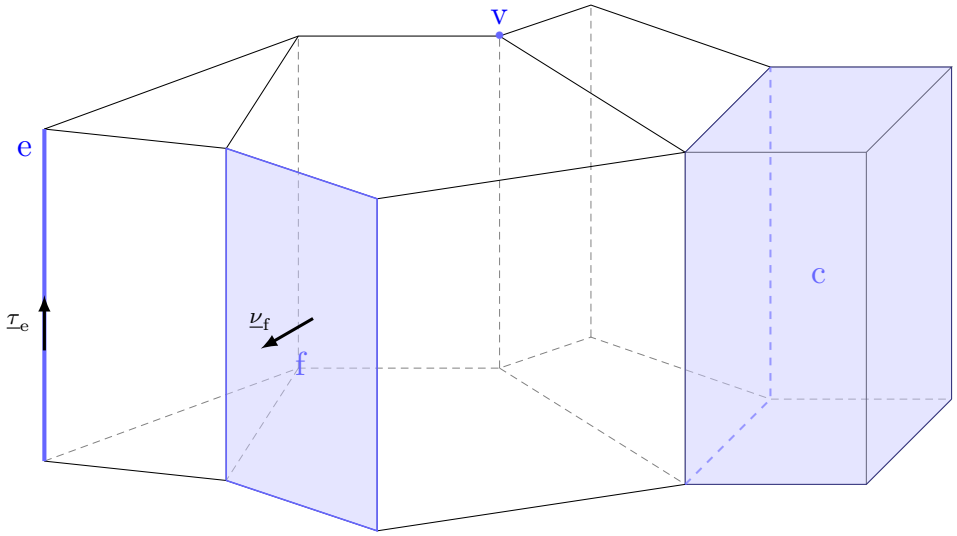

Figure 3.1 – Example of a primal mesh M. A vertex $\mathrm{v} \in \mathrm{V}$, an edge $\mathrm{e} \in \mathrm{E}$ along with its unit tangent vector $\underline{\tau}_{\mathrm{e}}$, a face $\mathrm{f} \in \mathrm{F}$ along with its unit normal vector $\underline{\nu}_{\mathrm{f}}$, and a cell $\mathrm{c} \in \mathrm{C}$ are highlighted in blue.

Definition 3.2 (Subset of mesh entities)**.** *Let* x *be an element of* M *and let* $\mathrm{A} \in \{\mathrm{V}, \mathrm{E}, \mathrm{F}, \mathrm{C}\}$*. If* x *has a dimension larger than that of the elements of* A*, we define the subset* A_{x} *as follows:*

$$\mathrm{A}_{\mathrm{x}} := \{a \in \mathrm{A} \,|\, a \subset \partial \mathrm{x}\};$$

and, otherwise, as follows:

$$\mathrm{A}_{\mathrm{x}} := \{a \in \mathrm{A} \,|\, \mathrm{x} \subset \partial a\}.$$

For instance, $\mathrm{E}_{\mathrm{c}} := \{\mathrm{e} \in \mathrm{E} \,|\, \mathrm{e} \subset \partial \mathrm{c}\}$ *collects the edges of a cell* c*, and* $\mathrm{C}_{\mathrm{e}} := \{\mathrm{c} \in \mathrm{C} \,|\, \mathrm{e} \subset \partial \mathrm{c}\}$ *collects the cells of an edge* e*, and so on.*

Definition 3.3 (Border and interior subsets)**.** *We split mesh entities into an interior subset (superscript* I*) and a border subset (superscript* B*) such that*

$$\begin{aligned}
&\mathrm{V} = \mathrm{V}^{\mathrm{I}} \cup \mathrm{V}^{\mathrm{B}}, \quad \textit{where } \mathrm{V}^{\mathrm{B}} := \{\mathrm{v} \in \mathrm{V} \,|\, \mathrm{v} \subset \partial\Omega\} \quad \textit{and} \quad \mathrm{V}^{\mathrm{I}} := \mathrm{V} \setminus \mathrm{V}^{\mathrm{B}};\\
&\mathrm{E} = \mathrm{E}^{\mathrm{I}} \cup \mathrm{E}^{\mathrm{B}}, \quad \textit{where } \mathrm{E}^{\mathrm{B}} := \{\mathrm{e} \in \mathrm{E} \,|\, \mathrm{e} \subset \partial\Omega\} \quad \textit{and} \quad \mathrm{E}^{\mathrm{I}} := \mathrm{E} \setminus \mathrm{E}^{\mathrm{B}};\\
&\mathrm{F} = \mathrm{F}^{\mathrm{I}} \cup \mathrm{F}^{\mathrm{B}}, \quad \textit{where } \mathrm{F}^{\mathrm{B}} := \{\mathrm{f} \in \mathrm{F} \,|\, \mathrm{f} \subset \partial\Omega\} \quad \textit{and} \quad \mathrm{F}^{\mathrm{I}} := \mathrm{F} \setminus \mathrm{F}^{\mathrm{B}}.
\end{aligned}$$

Furthermore, $|\mathrm{x}|$ represents the measure of the entity $\mathrm{x} \in \{\mathrm{v}, \mathrm{e}, \mathrm{f}, \mathrm{c}\}$. For a vertex, $|\mathrm{v}| = 1$ by convention; $|\mathrm{e}|$ is the length of the edge e, $|\mathrm{f}|$ is the area of the face f, and $|\mathrm{c}|$ is the volume of the cell c.

Links between mesh entities and fields. The starting point in the definition of DoFs is to identify which geometric entity is best suited to reflect the physical nature of a field. The intimate links between geometry and physics have been pointed out earlier in electromagnetism (Tonti, 1975a; Bossavit, 1998, 2000). This connection has also been studied for other physical models by Frankel (1997).

For a three-dimensional domain, four geometric supports have to be considered: point, line, surface, and volume. When one considers a mesh, the discrete counterpart is respectively a vertex, an edge, a face, and a cell.

In addition to the notion of geometric support, we also need a notion of *orientation*. This concept is essentially relevant for edges and faces but applies also to vertices and cells. To each edge $\mathrm{e} \in \mathrm{E}$, we arbitrarily assign a unit tangent vector $\underline{\tau}_\mathrm{e}$. To each face $\mathrm{f} \in \mathrm{F}$, we arbitrarily assign a unit normal vector $\underline{\nu}_\mathrm{f}$ (see Figure 3.1). For the sake of simplicity, we assume that a direct orientation of the ambient space is chosen once and for all. By convention, to each boundary face $\mathrm{f} \in \mathrm{F}^\mathrm{B}$, we assign the orientation given by the outward unit normal to $\partial\Omega$ so that $\underline{\nu}_\mathrm{f} = \underline{\nu}_{\partial\Omega}$ for all $\mathrm{f} \in \mathrm{F}^\mathrm{B}$. These orientations are fixed once and for all.

Remark 3.4 (Inner and outer orientations)**.** *Although they are not made explicit in what follows, the notions of* inner *and* outer *orientation are relevant in compatible spatial discretizations and, in particular, in CDO schemes. An inner-oriented entity is independent of the orientation of the ambient space (for instance, an edge oriented by its unit tangent vector), while an outer-oriented entity depends on that orientation (for instance, a face oriented by its unit normal vector seen as the tangent vector of a line crossing the face). Potentials and circulations are in general attached to inner-oriented quantities, while fluxes and densities are in general attached to outer-oriented quantities; see Bossavit (1998) or Kreeft* et al. *(2011) where the concepts of inner and outer orientations are detailed.*

3.1.2 Spaces of degrees of freedom

The physical fields we consider are either scalar fields like potentials and densities or vector fields like circulations and fluxes. The way one measures a field indicates the appropriate geometric object associated with respect to the field. Since a potential is naturally evaluated at a point, a circulation along a line, a flux across a surface, and a density inside a volume, the DoFs related to a potential are attached to vertices, those of a circulation to edges, those of a flux to faces, and those of a density to cells.

The (finite-dimensional) space of DoFs related to discrete potentials is denoted by $\mathcal{V}$ and collects the values of scalar fields at vertices, that related to discrete circulations is denoted $\mathcal{E}$ and collects the integrals of the tangential component of vector fields along edges (using $\underline{\tau}_\mathrm{e}$), that related to discrete fluxes is denoted $\mathcal{F}$ and collects the integrals of the normal component of vector fields across faces (using $\underline{\nu}_\mathrm{f}$), and that related to discrete densities is denoted $\mathcal{C}$ and collects the integrals of scalar fields over cells. These definitions are in agreement with the underlying physical nature of these fields. The notation used for the spaces aims at stressing the link between these spaces and their related geometric entities (see Figure 3.2).

By construction, $\mathcal{X} \equiv \mathbb{R}^{\#\mathrm{X}}$, so that the elements of $\mathcal{X}$ are algebraically considered as column arrays. Let $\mathbf{a} \in \mathcal{X}$. We denote by $\mathbf{a}_\mathrm{x} \in \mathbb{R}$ the value (*i.e.*, the component of the array) related to the entity $\mathrm{x} \in \mathrm{X}$. For instance, for $\boldsymbol{\phi} \in \mathcal{F}$, $\boldsymbol{\phi}_\mathrm{f}$ is the value of the flux attached to the face f.

Figure 3.2 – Spaces of DoFs.

3.1.3 De Rham maps

De Rham maps (also called reduction maps) act so as to define the DoFs. There are four de Rham maps related to the primal mesh, one for each kind of entity: vertices, edges, faces, and cells. Let $\mathcal{X}$ be any of the spaces in $\{\mathcal{V},\mathcal{E},\mathcal{F},\mathcal{C}\}$. De Rham maps $\mathsf{R}_\mathcal{X} : S_\mathcal{X}(\Omega) \to \mathcal{X}$ are defined as follows:

$$\forall p \in S_\mathcal{V}(\Omega), \qquad \mathsf{R}_\mathcal{V}(p)|_\mathrm{v} := p(\mathrm{v}), \qquad \forall \mathrm{v} \in \mathrm{V}, \tag{3.1a}$$

$$\forall \underline{u} \in S_\mathcal{E}(\Omega), \qquad \mathsf{R}_\mathcal{E}(\underline{u})|_\mathrm{e} := \int_\mathrm{e} \underline{u} \cdot \underline{\tau}_\mathrm{e}, \qquad \forall \mathrm{e} \in \mathrm{E}, \tag{3.1b}$$

$$\forall \underline{\phi} \in S_\mathcal{F}(\Omega), \qquad \mathsf{R}_\mathcal{F}(\underline{\phi})|_\mathrm{f} := \int_\mathrm{f} \underline{\phi} \cdot \underline{\nu}_\mathrm{f}, \qquad \forall \mathrm{f} \in \mathrm{F}, \tag{3.1c}$$

$$\forall s \in S_\mathcal{C}(\Omega), \qquad \mathsf{R}_\mathcal{C}(s)|_\mathrm{c} := \int_\mathrm{c} s, \qquad \forall \mathrm{c} \in \mathrm{C}, \tag{3.1d}$$

where the functional space $S_\mathcal{X}(\Omega)$ is (a particular choice of) the domain of the de Rham map $\mathsf{R}_\mathcal{X}$. The space related to potentials is denoted by $S_\mathcal{V}(\Omega)$, that related to circulations $S_\mathcal{E}(\Omega)$, that related to fluxes $S_\mathcal{F}(\Omega)$, and that related to densities $S_\mathcal{C}(\Omega)$. These spaces have to be spanned by sufficiently smooth functions so that the de Rham maps are well defined. The regularity of the space $S_\mathcal{V}(\Omega)$ has to ensure the existence of a single value of the scalar field at each vertex $\mathrm{v} \in \mathrm{V}$, $S_\mathcal{E}(\Omega)$ the existence of a single value of the tangential component of the vector field along each edge $\mathrm{e} \in \mathrm{E}$, $S_\mathcal{F}(\Omega)$ the existence of a single value of the normal component of the vector field across each face $\mathrm{f} \in \mathrm{F}$, and $S_\mathcal{C}(\Omega)$ the integrability in each cell $\mathrm{c} \in \mathrm{C}$. Several definitions of $S_\mathcal{X}(\Omega)$ are possible. Here is the one we choose.

Definition 3.5 (Domains of the de Rham maps)**.** *Let $d = 3$ be the space dimension and consider real numbers s_0, s_1, s_2 such that $s_k > \frac{d-k}{p}$ for $0 \le k \le 2$ with a real number $p \in [1,+\infty]$. Then, the spaces $S_\mathcal{X}(\Omega)$, $\mathcal{X} \in \{\mathcal{V},\mathcal{E},\mathcal{F},\mathcal{C}\}$ can be defined as follows:*

$$S_\mathcal{V}(\Omega) := W^{s_0,p}(\Omega), \tag{3.2a}$$

$$S_\mathcal{E}(\Omega) := [W^{s_1,p}(\Omega)]^d, \tag{3.2b}$$

$$S_\mathcal{F}(\Omega) := [W^{s_2,p}(\Omega)]^d, \tag{3.2c}$$

$$S_\mathcal{C}(\Omega) := L^1(\Omega), \tag{3.2d}$$

where $W^{s,p}(\Omega)$ denotes the usual Sobolev space. In what follows, we choose $p = 2$ so that, $s_0 > \frac{3}{2}$, $s_1 > 1$, and $s_2 > \frac{1}{2}$; the (Hilbert) Sobolev spaces are then denoted by $H^{s_k}(\Omega)$.

Remark 3.6 (Alternative definitions)**.** *When fields are the solution of a PDE, it can be interesting to give an alternative definition to the spaces $S_\mathcal{X}(\Omega)$ (while keeping the same notation $\mathsf{R}_\mathcal{X}$ for simplicity). Namely, we can infer from the PDE information on the integrability of some differential operator applied to the solution. In this case, one can require less regularity on the field itself and compensate by an additional requirement on the integrability of the differential operator. Let $d = 3$ be the space dimension and q, r, s be real numbers in $[1,+\infty]$. Then, we can set (see Ern & Guermond (2004))*

$$S_\mathcal{E}(\Omega) := \{\underline{u} \in [H^s(\Omega)]^d; \underline{\mathrm{curl}}(\underline{u}) \in [L^q(\Omega)]^d\}, \tag{3.3a}$$

with $s > \frac{1}{2}$ and $q > 2$, and

$$S_\mathcal{F}(\Omega) := \{\underline{\phi} \in [L^s(\Omega)]^d; \mathrm{div}(\underline{\phi}) \in L^q(\Omega)\}, \tag{3.3b}$$

with $s > 2$, $q > r$ such that $\frac{1}{r} = \frac{1}{s} + \frac{1}{d}$.

In addition, when one considers the de Rham complex, the spaces have to ensure the link with differential operators as depicted in Figure 3.3. Therefore, we introduce suitable subspaces of the spaces $S_\mathcal{X}(\Omega)$ in this situation.

Definition 3.7 (Subspaces in de Rham complex)**.**

$$S^{\mathrm{g}}_{\mathcal{V}}(\Omega) := \{p \in S_{\mathcal{V}}(\Omega) \,|\, \underline{\mathrm{grad}}(p) \in S_{\mathcal{E}}(\Omega)\}, \tag{3.4a}$$

$$S^{\mathrm{c}}_{\mathcal{E}}(\Omega) := \{\underline{u} \in S_{\mathcal{E}}(\Omega) \,|\, \underline{\mathrm{curl}}(\underline{u}) \in S_{\mathcal{F}}(\Omega)\}, \tag{3.4b}$$

$$S^{\mathrm{d}}_{\mathcal{F}}(\Omega) := \{\underline{\phi} \in S_{\mathcal{F}}(\Omega) \,|\, \mathrm{div}(\underline{\phi}) \in S_{\mathcal{C}}(\Omega)\}. \tag{3.4c}$$

The definitions (3.1) and the link between continuous and discrete spaces are summarized in Figure 3.3.

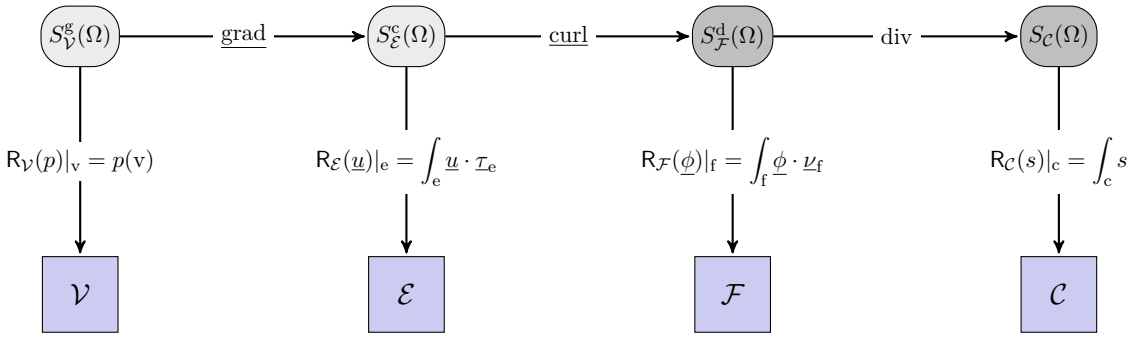

Figure 3.3 – Diagram related to the definition of degrees of freedom on the primal mesh.

3.2 Discrete differential operators

Knowing the definitions of DoFs, the definitions of the discrete differential operators result from the generalized Stokes theorem (in differential geometry, this theorem regroups the fundamental theorem of calculus, the Stokes–Kelvin theorem, and the Gauss theorem). With an obvious correspondence, GRAD, CURL, and DIV designate the discrete counterparts of the differential operators.

3.2.1 Discrete gradient

The starting point is the fundamental theorem of calculus:

$$\int_L \underline{\mathrm{grad}}(p) \cdot \underline{\tau}_L = p(b) - p(a), \tag{3.5}$$

where L is a line (possibly curved) oriented from a to b by the choice of the unit tangent vector $\underline{\tau}_L$.

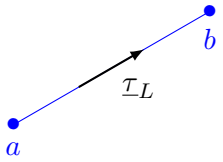

Notice that the value of this integral does not depend on the shape of the path between a and b. DoFs attached to vertices and edges naturally appear in (3.5). We set

$$\mathsf{GRAD} : \mathcal{V} \to \mathcal{E}, \quad \mathsf{GRAD}(\mathbf{p})|_{\mathrm{e}} := \sum_{\mathrm{v} \in \mathrm{V}_{\mathrm{e}}} \iota_{\mathrm{v,e}} \mathbf{p}_{\mathrm{v}}, \quad \forall \mathrm{e} \in \mathrm{E}, \tag{3.6}$$

where $\mathrm{V}_{\mathrm{e}} = \{\mathrm{v} \in \mathrm{V} \,|\, \mathrm{v} \subset \partial \mathrm{e}\}$ and $\iota_{\mathrm{v,e}}$ is the incidence number of the vertex v with respect to the orientation of the edge e. $\iota_{\mathrm{v,e}} = \pm 1$ for vertices in V_{e}. $\iota_{\mathrm{v,e}} = +1$ if $\underline{\tau}_{\mathrm{e}}$ points towards the vertex v and $\iota_{\mathrm{v,e}} = -1$ otherwise. Only the connectivity edge $\to$ vertices contributes to the definition of the discrete gradient. The algebraic realization of GRAD is a rectangular matrix $\mathbb{G}$ of size $\#\mathrm{E} \times \#\mathrm{V}$ with entries in $\{0, \pm 1\}$. This kind of matrix is called an *incidence* matrix.

Example 3.8 (Example of definition of $\mathbb{G}$)**.** *We consider a face of a cube with vertices* $\{\mathrm{v}_1, \ldots, \mathrm{v}_6\}$ *and edges* $\{\mathrm{e}_1, \ldots, \mathrm{e}_8\}$.

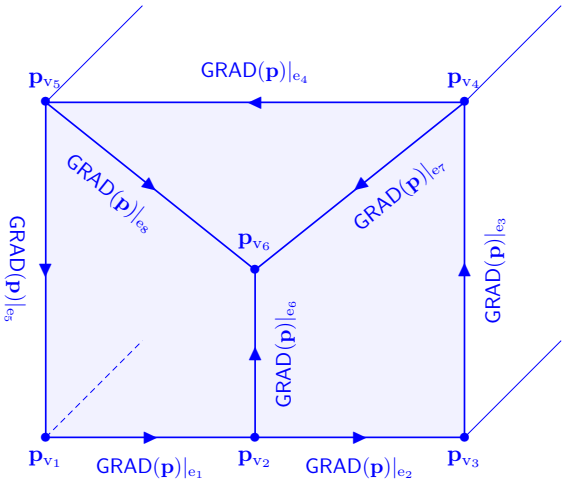

$$\mathbb{G} = \begin{bmatrix} -1 & +1 & 0 & 0 & 0 & 0 & \cdots \\ 0 & -1 & +1 & 0 & 0 & 0 & \\ 0 & 0 & -1 & +1 & 0 & 0 & \\ 0 & 0 & 0 & -1 & +1 & 0 & \\ +1 & 0 & 0 & 0 & -1 & 0 & \\ 0 & -1 & 0 & 0 & 0 & +1 & \\ 0 & 0 & 0 & -1 & 0 & +1 & \\ 0 & 0 & 0 & 0 & -1 & +1 & \\ \cdots & & & & & & \end{bmatrix}$$

3.2.2 Discrete curl

The definition of the discrete curl operator relies on the Stokes–Kelvin theorem:

$$\int_S \underline{\mathrm{curl}}(\underline{u}) \cdot \underline{\nu}_S = \int_{\partial S} \underline{u} \cdot \underline{\tau}_{\partial S}, \tag{3.7}$$

where S is a surface (possibly non-planar) oriented by the choice of a unit normal vector $\underline{\nu}_S$. Given an orientation of the ambient space, $\underline{\nu}_S$ induces an inner-orientation of the surface. The boundary of the surface S is denoted by ∂S and is oriented by a unit tangent vector $\underline{\tau}_{\partial S}$ in accordance with the inner orientation of S.

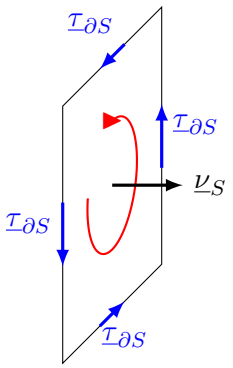

DoFs attached to edges and faces naturally appear in the definition of the discrete curl operator. We set

$$\mathsf{CURL} : \mathcal{E} \to \mathcal{F}, \quad \mathsf{CURL}(\mathbf{u})|_{\mathrm{f}} := \sum_{\mathrm{e} \in \mathrm{E_f}} \iota_{\mathrm{e,f}} \mathbf{u}_{\mathrm{e}}, \quad \forall \mathrm{f} \in \mathrm{F}, \tag{3.8}$$

where $\mathrm{E_f} := \{\mathrm{e} \in \mathrm{E} \,|\, \mathrm{e} \subset \partial \mathrm{f}\}$ and $\iota_{\mathrm{e,f}}$ is the incidence number of the edge e with respect to the orientation of the face f. For an edge $\mathrm{e} \in \mathrm{E_f}$, $\iota_{\mathrm{e,f}} = +1$ if $\underline{\tau}_{\mathrm{e}}$ shares the same orientation as that induced by $\underline{\nu}_{\mathrm{f}}$, $\iota_{\mathrm{e,f}} = -1$ otherwise. Only the connectivity face $\to$ edges contributes to the definition of the discrete curl operator. The algebraic realization of CURL is a rectangular matrix $\mathbb{C}$ of size $\#\mathrm{F} \times \#\mathrm{E}$ with entries in $\{0, \pm 1\}$.

Example 3.9 (Example of definition of $\mathbb{C}$)**.** *We consider a face of a cube with edges* $\{\mathrm{e}_1, \ldots, \mathrm{e}_8\}$ *and faces* $\{\mathrm{f}_1, \mathrm{f}_2, \mathrm{f}_3\}$.

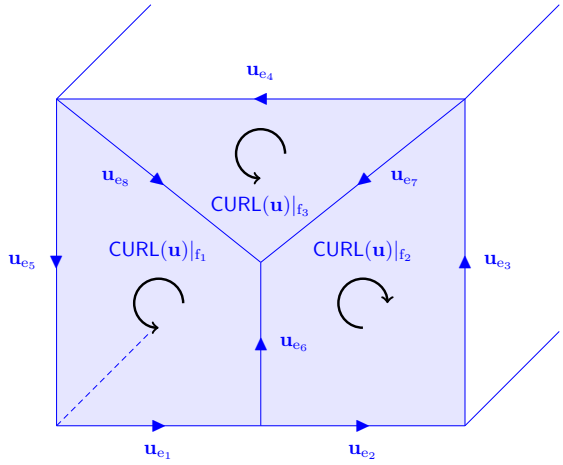

$$\mathbb{C} = \begin{bmatrix} +1 & 0 & 0 & 0 & +1 & +1 & 0 & -1 & \cdots \\ 0 & -1 & -1 & 0 & 0 & +1 & -1 & 0 & \\ 0 & 0 & 0 & +1 & 0 & 0 & -1 & +1 & \\ \cdots & & & & & & & & \end{bmatrix}$$

3.2.3 Discrete divergence

The definition of the discrete divergence operator relies on the Gauss theorem:

$$\int_V \mathrm{div}(\underline{\phi}) = \int_{\partial V} \underline{\phi} \cdot \underline{\nu}_{\partial V}, \tag{3.9}$$

where V is a volume. The boundary of V is a surface, denoted by ∂V, whose orientation is fixed by a unit normal vector $\underline{\nu}_{\partial V}$ pointing outward V.

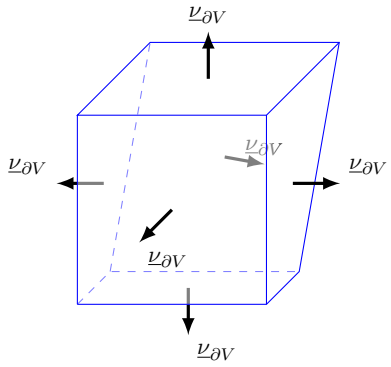

DoFs attached to faces and cells naturally appear in the definition of the discrete divergence operator. We set

$$\mathsf{DIV} : \mathcal{F} \to \mathcal{C}, \quad \mathsf{DIV}(\boldsymbol{\phi})|_{\mathrm{c}} := \sum_{\mathrm{f} \in \mathrm{F_c}} \iota_{\mathrm{f,c}} \boldsymbol{\phi}_{\mathrm{f}}, \quad \forall \mathrm{c} \in \mathrm{C}, \tag{3.10}$$

where $\mathrm{F_c} := \{\mathrm{f} \in \mathrm{F} \,|\, \mathrm{f} \subset \partial \mathrm{c}\}$ and $\iota_{\mathrm{f,c}}$ is the incidence number of the face f with respect to the outward orientation of the boundary of the cell c. For a face $\mathrm{f} \in \mathrm{F_c}$, $\iota_{\mathrm{f,c}} = +1$ if $\underline{\nu}_{\mathrm{f}}$ points outward the cell c, $\iota_{\mathrm{f,c}} = -1$ otherwise. Only the connectivity cell $\to$ faces contributes to the definition of the discrete divergence operator. The algebraic realization of DIV is a rectangular matrix $\mathbb{D}$ of size $\#\mathrm{C} \times \#\mathrm{F}$ with entries in $\{0, \pm 1\}$.

Example 3.10 (Example of definition of $\mathbb{D}$)**.** *We consider a 2D case with* $\mathrm{F} := \{\mathrm{f}_1, \ldots, \mathrm{f}_8\}$ *and* $\mathrm{C} := \{\mathrm{c}_1, \mathrm{c}_2, \mathrm{c}_3\}$.

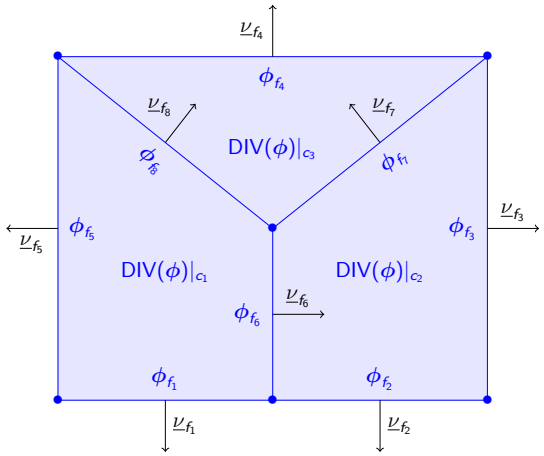

$$\mathbb{D} = \begin{bmatrix} +1 & 0 & 0 & 0 & +1 & +1 & 0 & +1 \\ 0 & +1 & +1 & 0 & 0 & -1 & +1 & 0 \\ 0 & 0 & 0 & +1 & 0 & 0 & -1 & -1 \end{bmatrix}$$

3.2.4 Properties

Since no length, area, volume or material property appears in the definition of GRAD, CURL, and DIV, these operators are metric-free. This reflects the *topological* nature of these operators. One can stretch, rotate, and deform the mesh, the definition remains unchanged. Only the connectivity plays a role in the definition.

Proposition 3.11 (Cochain complex)**.**

$$\mathsf{CURL} \cdot \mathsf{GRAD} = 0_{\mathcal{F}}, \quad \mathsf{DIV} \cdot \mathsf{CURL} = 0_{\mathcal{C}}.$$

Proof. See (Munkres, 1984, § 42). This is a consequence of the fact that the boundary of a boundary is empty. □

Consequently, $\operatorname{Im}\mathsf{GRAD} \subset \operatorname{Ker}\mathsf{CURL}$ and $\operatorname{Im}\mathsf{CURL} \subset \operatorname{Ker}\mathsf{DIV}$, where Im is the range of an operator and Ker its kernel or nullspace. Figure 3.4 summarizes Proposition 3.11.

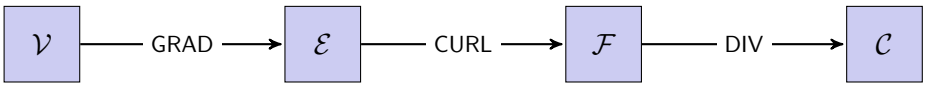

Figure 3.4 – Cochain complex induced by the discrete differential operator on the primal mesh.

Proposition 3.12 (Exactness)**.** *Assume that the domain Ω is simply connected and its boundary $\partial\Omega$ is connected. Then, the following identities hold:*

$$\operatorname{Im}\mathsf{GRAD} = \operatorname{Ker}\mathsf{CURL}, \qquad \operatorname{Im}\mathsf{CURL} = \operatorname{Ker}\mathsf{DIV}.$$

Proof. See (Beirão da Veiga *et al.*, 2014, Lemma 2.4). □

Proposition 3.13 (Commuting property)**.**

$$\mathsf{R}_{\mathcal{E}}(\underline{\mathrm{grad}}) = \mathsf{GRAD}(\mathsf{R}_{\mathcal{V}}), \quad \mathsf{R}_{\mathcal{F}}(\underline{\mathrm{curl}}) = \mathsf{CURL}(\mathsf{R}_{\mathcal{E}}), \quad \mathsf{R}_{\mathcal{C}}(\mathrm{div}) = \mathsf{DIV}(\mathsf{R}_{\mathcal{F}}).$$

Proof. The choice of the definitions (3.1) of DoFs combined with the definitions (3.6), (3.8), and (3.10) of the discrete differential operators based on the generalized Stokes theorem yields the result. □

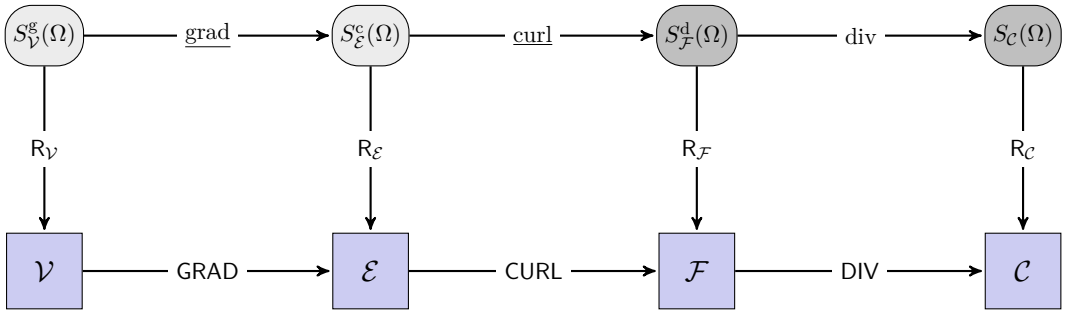

Figure 3.5 – Three commuting diagrams bridging the continuous de Rham complex (top line) and the discrete de Rham complex (bottom line) on the primal mesh. The link between the continuous and discrete setting is operated by de Rham maps.

Figure 3.5 summarizes Proposition 3.13. The discrete differential operators on the primal mesh produce a cochain complex which is the discrete counterpart of the de Rham complex.

3.3 Duality concepts

Duality plays a key role in the CDO framework. We make explicit in this section how this concept is introduced by means of a dual mesh.

3.3.1 Dual mesh

Principles. In addition to the primal mesh M, we define a dual mesh $\widetilde{\mathrm{M}} := \{\widetilde{\mathrm{V}}, \widetilde{\mathrm{E}}, \widetilde{\mathrm{F}}, \widetilde{\mathrm{C}}\}$, where $\widetilde{\mathrm{V}}$ collects dual vertices generically denoted by $\tilde{\mathrm{v}}$, $\widetilde{\mathrm{E}}$ dual edges $\tilde{\mathrm{e}}$, $\widetilde{\mathrm{F}}$ dual faces $\tilde{\mathrm{f}}$, and $\widetilde{\mathrm{C}}$ dual cells $\tilde{\mathrm{c}}$. In general, dual edges are not straight and dual faces are not planar (see Figure 3.6). The primal and dual meshes do not play a symmetric role. The dual mesh does not need to be seen by the end-user, and only the software developer and the mathematician manipulate both meshes. The definition of the primal mesh is an input of the problem, while several definitions of the dual mesh are possible. The Delaunay–Voronoï and the barycentric dual mesh are the most common constructions. We point out the recent contribution of Mullen *et al.* (2011) where *Hodge-optimized* triangulations are proposed leading to the definition of new dual meshes.

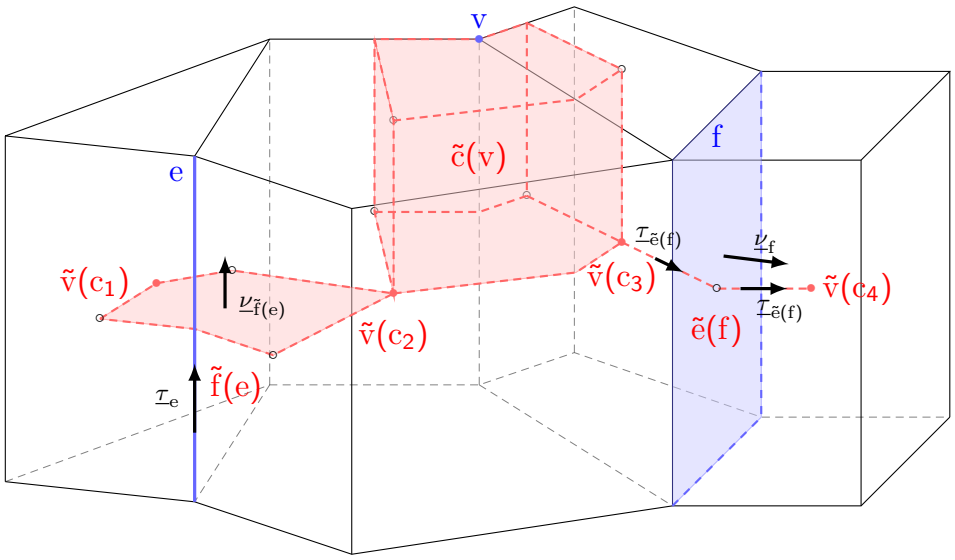

Figure 3.6 – Examples of primal and dual mesh entities.

Design requirements. In the CDO framework, we specify two requirements on the design of the dual mesh.

(1) There exists a *one-to-one pairing* between primal and dual mesh entities. Precisely, each primal vertex $\mathrm{v} \in \mathrm{V}$ is in correspondence with a unique dual cell $\tilde{\mathrm{c}}$. To emphasize this pairing, we often denote by $\tilde{\mathrm{c}}(\mathrm{v})$ the dual cell in association with the primal vertex v. Similarly, to each primal edge $\mathrm{e} \in \mathrm{E}$ corresponds a unique dual face $\tilde{\mathrm{f}}(\mathrm{e})$, to each primal face $\mathrm{f} \in \mathrm{F}$ a unique dual edge $\tilde{\mathrm{e}}(\mathrm{f})$, and to each primal cell $\mathrm{c} \in \mathrm{C}$ a unique dual vertex $\tilde{\mathrm{v}}(\mathrm{c})$; see Figure 3.6.

(2) We apply a *transfer of orientation* between the primal and the dual mesh. The orientation of the unit vector $\underline{\tau}_{\tilde{\mathrm{e}}(\mathrm{f})}$ is determined by $\underline{\nu}_{\mathrm{f}}$ for all $\mathrm{f} \in \mathrm{F}$ and that of $\underline{\nu}_{\tilde{\mathrm{f}}(\mathrm{e})}$ by $\underline{\tau}_{\mathrm{e}}$ for all $\mathrm{e} \in \mathrm{E}$; see Figure 3.6.

A first consequence of the one-to-one pairing is that $\#\widetilde{\mathrm{V}} = \#\mathrm{C}$, $\#\widetilde{\mathrm{E}} = \#\mathrm{F}$, $\#\widetilde{\mathrm{F}} = \#\mathrm{E}$, and $\#\widetilde{\mathrm{C}} = \#\mathrm{V}$. A second consequence is that the dual mesh is not a cellular complex contrary to the primal mesh. Namely, dual cells $\tilde{\mathrm{c}}(\mathrm{v})$ related to a vertex $\mathrm{v} \in \mathrm{V}^{\mathrm{B}}$ (cf. Definition 3.3), dual

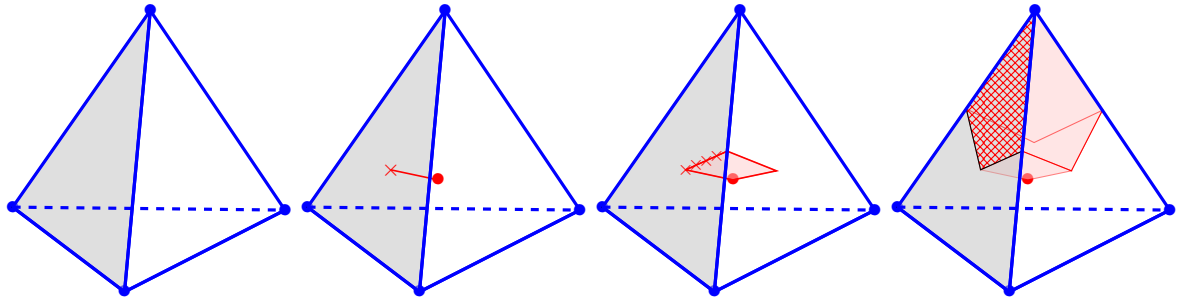

Figure 3.7 – Dual entities related to primal entities lying on the boundary are not closed. Left: Consider a tetrahedral cell with one face touching the boundary $\partial\Omega$ (shaded face); Middle left: The dual edge (associated to the shaded face) does not contain the point (cross) lying on the boundary but contains the point located inside the tetrahedron (bullet); Middle right: The dual face (associated to an edge of the shaded face) does not contain the edge (crossed line) lying on the boundary; Right: The dual cell (associated to a vertex of the shaded face) does not contain the face (crosshatch) lying on the boundary.

faces $\tilde{\mathrm{f}}(\mathrm{e})$ related to an edge $\mathrm{e} \in \mathrm{E}^{\mathrm{B}}$, and dual edges $\tilde{\mathrm{e}}(\mathrm{f})$ related to a face $\mathrm{f} \in \mathrm{F}^{\mathrm{B}}$, are not closed; see Figure 3.7.

A consequence of the transfer of orientation is that the following relations hold:

$$\begin{aligned} \iota_{\mathrm{v,e}} &= -\iota_{\tilde{\mathrm{f}}(\mathrm{e}),\tilde{\mathrm{c}}(\mathrm{v})}, && \forall \mathrm{e} \in \mathrm{E},\ \forall \mathrm{v} \in \mathrm{V}_{\mathrm{e}}; \\ \iota_{\mathrm{e,f}} &= +\iota_{\tilde{\mathrm{e}}(\mathrm{f}),\tilde{\mathrm{f}}(\mathrm{e})}, && \forall \mathrm{f} \in \mathrm{F},\ \forall \mathrm{e} \in \mathrm{E}_{\mathrm{f}}; \\ \iota_{\mathrm{f,c}} &= -\iota_{\tilde{\mathrm{v}}(\mathrm{c}),\tilde{\mathrm{e}}(\mathrm{f})}, && \forall \mathrm{c} \in \mathrm{C},\ \forall \mathrm{f} \in \mathrm{F}_{\mathrm{c}}. \end{aligned} \tag{3.11}$$

As mentioned above, there are several ways to build a dual mesh. The two most common constructions are the Delaunay–Voronoï dual mesh (also called orthogonal dual mesh) and the barycentric dual mesh. The Delaunay–Voronoï dual mesh is used in DEC, TPFA, and Covolume schemes for instance; see Figure 3.8 for an example of this construction. Its advantage is the simplicity of implementation and its efficiency since the stencil is minimal when one considers this dual mesh. However, its main drawback is its limitation to meshes that satisfy the orthogonality conditions $\underline{\tau}_{\mathrm{e}} \cdot \underline{\nu}_{\tilde{\mathrm{f}}(\mathrm{e})} = 1$ for all $\mathrm{e} \in \mathrm{E}$ and $\underline{\nu}_{\mathrm{f}} \cdot \underline{\tau}_{\tilde{\mathrm{e}}(\mathrm{f})} = 1$ for all $\mathrm{f} \in \mathrm{F}$. These conditions are in particular satisfied by Cartesian meshes.

The barycentric dual mesh requires more care in the implementation, but its crucial advantage is that it exists for a broad class of meshes ranging from simplicial to polyhedral meshes with hanging nodes; see Figure 3.9. Owing to its applicability to a broad class of meshes and since we want to consider polyhedral meshes, we focus on the barycentric dual mesh in this thesis. The barycentric dual mesh relies on a barycentric subdivision of the primal mesh. This subdivision along with its main properties are detailed in Section 5.2.

3.3.2 Degrees of freedom

Following the same rationale as for the primal mesh, we introduce spaces of DoFs on the dual mesh. There are four spaces denoted by $\widetilde{\mathcal{V}}$, $\widetilde{\mathcal{E}}$, $\widetilde{\mathcal{F}}$, and $\widetilde{\mathcal{C}}$ defined from de Rham maps related to the corresponding entities of the dual mesh. Let $\widetilde{\mathcal{Y}}$ be any of the spaces in $\{\widetilde{\mathcal{V}}, \widetilde{\mathcal{E}}, \widetilde{\mathcal{F}}, \widetilde{\mathcal{C}}\}$. Then,

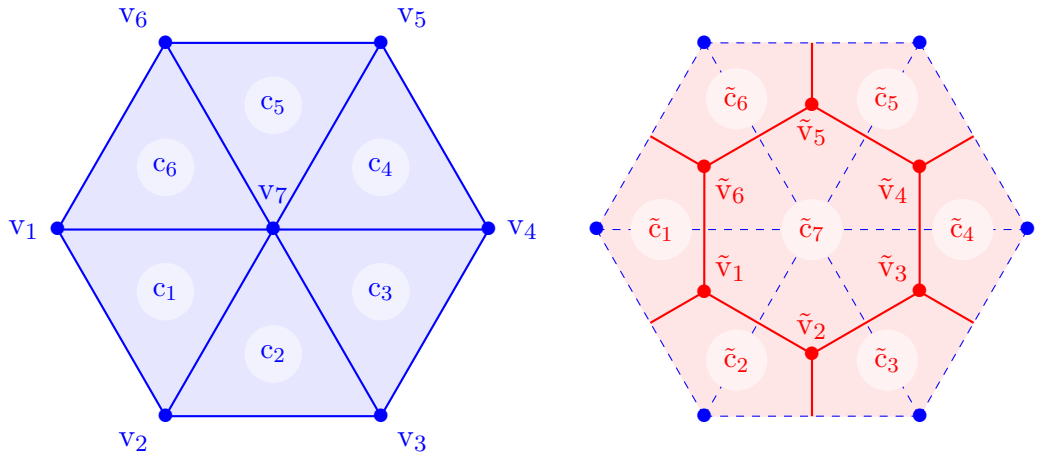

Figure 3.8 – Example of a Delaunay–Voronoï dual mesh (right) and its Delaunay primal mesh (left).

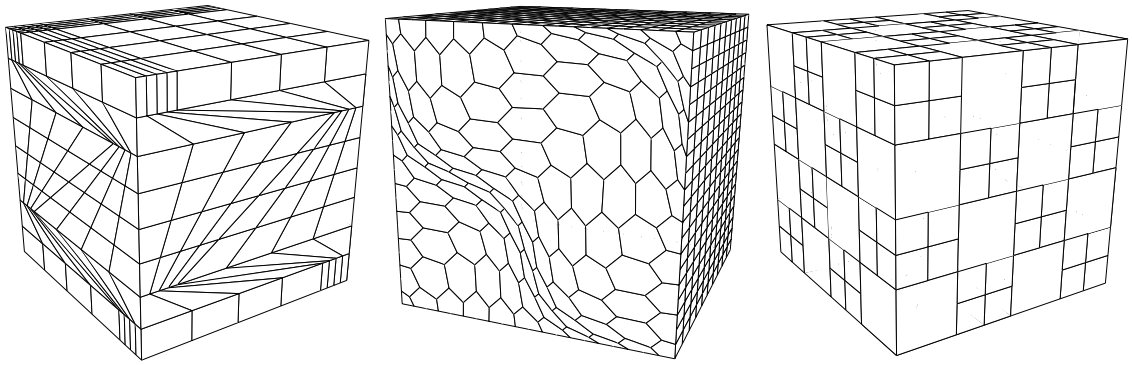

Figure 3.9 – Examples of meshes where a barycentric dual mesh can be considered. Left: Hexahedral mesh with a strong non-orthogonality; Middle: Polyhedral mesh based on the extrusion of a polygonal facet. Right: Polyhedral mesh with hanging nodes.

the (dual) de Rham map $\mathsf{R}_{\widetilde{\mathcal{Y}}} : S_{\widetilde{\mathcal{Y}}}(\Omega) \to \widetilde{\mathcal{Y}}$ acts as follows:

$$\forall p \in S_{\widetilde{\mathcal{V}}}(\Omega), \qquad \mathsf{R}_{\widetilde{\mathcal{V}}}(p)|_{\tilde{\mathrm{v}}(\mathrm{c})} := p(\tilde{\mathrm{v}}(\mathrm{c})), \qquad \forall \mathrm{c} \in \mathrm{C}, \tag{3.12a}$$

$$\forall \underline{u} \in S_{\widetilde{\mathcal{E}}}(\Omega), \qquad \mathsf{R}_{\widetilde{\mathcal{E}}}(\underline{u})|_{\tilde{\mathrm{e}}(\mathrm{f})} := \int_{\tilde{\mathrm{e}}(\mathrm{f})} \underline{u} \cdot \underline{\tau}_{\tilde{\mathrm{e}}(\mathrm{f})}, \qquad \forall \mathrm{f} \in \mathrm{F}, \tag{3.12b}$$

$$\forall \underline{u} \in S_{\widetilde{\mathcal{F}}}(\Omega), \qquad \mathsf{R}_{\widetilde{\mathcal{F}}}(\underline{\phi})|_{\tilde{\mathrm{f}}(\mathrm{e})} := \int_{\tilde{\mathrm{f}}(\mathrm{e})} \underline{\phi} \cdot \underline{\nu}_{\tilde{\mathrm{f}}(\mathrm{e})}, \qquad \forall \mathrm{e} \in \mathrm{E}, \tag{3.12c}$$

$$\forall \underline{u} \in S_{\widetilde{\mathcal{C}}}(\Omega), \qquad \mathsf{R}_{\widetilde{\mathcal{C}}}(s)|_{\tilde{\mathrm{c}}(\mathrm{v})} := \int_{\tilde{\mathrm{c}}(\mathrm{v})} s, \qquad \forall \mathrm{v} \in \mathrm{V}. \tag{3.12d}$$

The functional spaces $S_{\widetilde{\mathcal{Y}}}(\Omega)$ are (a particular choice of) the domains of the de Rham maps $\mathsf{R}_{\widetilde{\mathcal{Y}}}(\Omega)$ and can be defined similarly to Definition 3.5, so that

$$S_{\widetilde{\mathcal{V}}}(\Omega) := S_{\mathcal{V}}(\Omega), \quad S_{\widetilde{\mathcal{E}}}(\Omega) := S_{\mathcal{E}}(\Omega), \quad S_{\widetilde{\mathcal{F}}}(\Omega) := S_{\mathcal{F}}(\Omega), \quad S_{\widetilde{\mathcal{C}}}(\Omega) := S_{\mathcal{C}}(\Omega). \tag{3.13}$$

Two families of CDO schemes. Since we consider primal and dual meshes, we have access to two sets of vertices, edges, faces, and cells. Thus, there are two possibilities to locate DoFs

related to a potential: either on primal vertices or on dual vertices. The same reasoning holds also with edges for a circulation, with faces for a flux, and with cells for a density. In general, once the choice for the potential has been made, all the remaining DoFs are localized in accordance with this first choice as a consequence of the balance equations and the closure relations linking the various fields. This distinction for positioning the DoFs related to the potential leads to two families of CDO schemes: *vertex-based* schemes where the potential DoFs are located at primal vertices and *cell-based* schemes where the potential DoFs are located at dual vertices (in one-to-one correspondence with primal cells). The terminology "cell-based" has been preferred in order to emphasize the salient role of the primal mesh since this mesh is the only one that needs to be seen by the end-user. This distinction of positioning the DoFs has already been underlined in the work of Bossavit (2000) and Perot & Subramanian (2007).

Remark 3.14 (Orientations)**.** *When one considers the concepts of inner and outer orientations (cf. Remark 3.4), choosing a vertex-based scheme corresponds to the choice of an inner-oriented primal mesh (and an outer-oriented dual mesh), while choosing a cell-based scheme corresponds to the choice of an inner-oriented dual mesh (and an outer-oriented primal mesh).*

3.3.3 Discrete differential operators

Definitions. The definition of the discrete differential operators on the dual mesh relies on the same principles as for the primal mesh. As a result, the following definitions hold:

$$\widetilde{\mathsf{GRAD}} : \widetilde{\mathcal{V}} \to \widetilde{\mathcal{E}}, \qquad \forall \tilde{\mathrm{e}} \in \widetilde{\mathrm{E}},\ \forall \mathbf{p} \in \widetilde{\mathcal{V}}, \qquad \widetilde{\mathsf{GRAD}}(\mathbf{p})|_{\tilde{\mathrm{e}}} := \sum_{\tilde{\mathrm{v}} \in \widetilde{\mathrm{V}}_{\tilde{\mathrm{e}}}} \iota_{\tilde{\mathrm{v}},\tilde{\mathrm{e}}} \mathbf{p}_{\tilde{\mathrm{v}}}, \tag{3.14a}$$

where $\widetilde{\mathrm{V}}_{\tilde{\mathrm{e}}} := \{\tilde{\mathrm{v}} \in \widetilde{\mathrm{V}} \,|\, \tilde{\mathrm{v}} \subset \partial\tilde{\mathrm{e}}\}$ and $\iota_{\tilde{\mathrm{v}},\tilde{\mathrm{e}}} = +1$ if $\underline{\tau}_{\tilde{\mathrm{e}}}$ points towards $\tilde{\mathrm{v}}$, $\iota_{\tilde{\mathrm{v}},\tilde{\mathrm{e}}} = -1$ otherwise;

$$\widetilde{\mathsf{CURL}} : \widetilde{\mathcal{E}} \to \widetilde{\mathcal{F}}, \qquad \forall \tilde{\mathrm{f}} \in \widetilde{\mathrm{F}},\ \forall \mathbf{u} \in \widetilde{\mathcal{E}}, \qquad \widetilde{\mathsf{CURL}}(\mathbf{u})|_{\tilde{\mathrm{f}}} := \sum_{\tilde{\mathrm{e}} \in \widetilde{\mathrm{E}}_{\tilde{\mathrm{f}}}} \iota_{\tilde{\mathrm{e}},\tilde{\mathrm{f}}} \mathbf{u}_{\tilde{\mathrm{e}}}, \tag{3.14b}$$

where $\widetilde{\mathrm{E}}_{\tilde{\mathrm{f}}} := \{\tilde{\mathrm{e}} \in \widetilde{\mathrm{E}} \,|\, \tilde{\mathrm{e}} \subset \partial\tilde{\mathrm{f}}\}$ and $\iota_{\tilde{\mathrm{e}},\tilde{\mathrm{f}}} = +1$ if $\underline{\tau}_{\tilde{\mathrm{e}}}$ shares the same orientation as the one induced by $\underline{\nu}_{\tilde{\mathrm{f}}}$ on $\partial\tilde{\mathrm{f}}$, $\iota_{\tilde{\mathrm{e}},\tilde{\mathrm{f}}} = -1$ otherwise;

$$\widetilde{\mathsf{DIV}} : \widetilde{\mathcal{F}} \to \widetilde{\mathcal{C}}, \qquad \forall \tilde{\mathrm{c}} \in \widetilde{\mathrm{C}},\ \forall \boldsymbol{\phi} \in \widetilde{\mathcal{F}}, \qquad \widetilde{\mathsf{DIV}}(\boldsymbol{\phi})|_{\tilde{\mathrm{c}}} := \sum_{\tilde{\mathrm{f}} \in \widetilde{\mathrm{F}}_{\tilde{\mathrm{c}}}} \iota_{\tilde{\mathrm{f}},\tilde{\mathrm{c}}} \boldsymbol{\phi}_{\tilde{\mathrm{f}}}, \tag{3.14c}$$

where $\widetilde{\mathrm{F}}_{\tilde{\mathrm{c}}} := \{\tilde{\mathrm{f}} \in \widetilde{\mathrm{F}} \,|\, \tilde{\mathrm{f}} \subset \partial\tilde{\mathrm{c}}\}$ and $\iota_{\tilde{\mathrm{f}},\tilde{\mathrm{c}}} = +1$ if $\underline{\nu}_{\tilde{\mathrm{f}}}$ points outwards $\tilde{\mathrm{c}}$, $\iota_{\tilde{\mathrm{f}},\tilde{\mathrm{c}}} = -1$ otherwise.

Recall that dual mesh entities touching the boundary $\partial\Omega$ are not closed. This is a consequence of the one-to-one pairing between primal and dual entities. As a result $\widetilde{\mathrm{V}}_{\tilde{\mathrm{e}}}$ contains only one vertex when the dual edge $\tilde{\mathrm{e}}$ is associated to a primal face $\mathrm{f} \in \mathrm{F}^{\mathrm{B}}$, edges $\tilde{\mathrm{e}} \in \widetilde{\mathrm{E}}_{\tilde{\mathrm{f}}}$ do not form a closed path around the dual face $\tilde{\mathrm{f}}$ when $\tilde{\mathrm{f}}$ is associated to a primal edge $\mathrm{e} \in \mathrm{E}^{\mathrm{B}}$, and faces $\tilde{\mathrm{f}} \in \widetilde{\mathrm{F}}_{\tilde{\mathrm{c}}}$ do not close the dual cell $\tilde{\mathrm{c}}$ when the dual cell is associated to a primal vertex $\mathrm{v} \in \mathrm{V}^{\mathrm{B}}$ (see Figure 3.7).

Algebraically, $\widetilde{\mathsf{GRAD}}$ is defined by a rectangular matrix denoted by $\widetilde{\mathbb{G}}$ of size $\#\mathrm{F} \times \#\mathrm{C} = \#\widetilde{\mathrm{E}} \times \#\widetilde{\mathrm{V}}$ (owing to the one-to-one pairing), $\widetilde{\mathsf{CURL}}$ by $\widetilde{\mathbb{C}}$ of size $\#\mathrm{E} \times \#\mathrm{F} = \#\widetilde{\mathrm{F}} \times \#\widetilde{\mathrm{E}}$, and $\widetilde{\mathsf{DIV}}$ by $\widetilde{\mathbb{D}}$ of size $\#\mathrm{V} \times \#\mathrm{E} = \#\widetilde{\mathrm{C}} \times \#\widetilde{\mathrm{F}}$. $\widetilde{\mathbb{G}}$ is associated to the connectivity $\mathrm{f} \to \mathrm{c}$, $\widetilde{\mathbb{C}}$ to the connectivity $\mathrm{e} \to \mathrm{f}$, and $\widetilde{\mathbb{D}}$ to the connectivity $\mathrm{v} \to \mathrm{e}$.

Properties. The discrete differential operators on the dual mesh are *topological* or *metric-free* operators since they are algebraically defined by incidence matrices.

Owing to the one-to-one pairing between primal and dual entities, $\widetilde{\mathcal{V}}$ (resp. $\widetilde{\mathcal{E}}$, $\widetilde{\mathcal{F}}$, $\widetilde{\mathcal{C}}$) is isomorphic to $\mathcal{C}$ (resp. $\mathcal{F}$, $\mathcal{E}$, $\mathcal{V}$). Thus, there are four duality pairings, denoted by $\nu\tilde{c}$, $\varepsilon\tilde{f}$, $f\tilde{\varepsilon}$, and $c\tilde{\nu}$. For each duality pairing, we define a duality product.

Definition 3.15 (Duality products)**.**

$$\forall \mathbf{p} \in \mathcal{V},\ \forall \mathbf{s} \in \widetilde{\mathcal{C}}, \qquad [\![\mathbf{p}, \mathbf{s}]\!]_{\mathcal{V}\widetilde{\mathcal{C}}} := \sum_{\mathrm{v}\in\mathrm{V}} \mathbf{p}_{\mathrm{v}} \mathbf{s}_{\tilde{\mathrm{c}}(\mathrm{v})}, \tag{3.15a}$$

$$\forall \mathbf{u} \in \mathcal{E},\ \forall \boldsymbol{\phi} \in \widetilde{\mathcal{F}}, \qquad [\![\mathbf{u}, \boldsymbol{\phi}]\!]_{\mathcal{E}\widetilde{\mathcal{F}}} := \sum_{\mathrm{e}\in\mathrm{E}} \mathbf{u}_{\mathrm{e}} \boldsymbol{\phi}_{\tilde{\mathrm{f}}(\mathrm{e})}, \tag{3.15b}$$

$$\forall \boldsymbol{\phi} \in \mathcal{F}, \forall \mathbf{u} \in \widetilde{\mathcal{E}}, \qquad [\![\boldsymbol{\phi}, \mathbf{u}]\!]_{\mathcal{F}\widetilde{\mathcal{E}}} := \sum_{\mathrm{f}\in\mathrm{F}} \boldsymbol{\phi}_{\mathrm{f}} \mathbf{u}_{\tilde{\mathrm{e}}(\mathrm{f})}, \tag{3.15c}$$

$$\forall \mathbf{s} \in \mathcal{C},\ \forall \mathbf{p} \in \widetilde{\mathcal{V}}, \qquad [\![\mathbf{s}, \mathbf{p}]\!]_{\mathcal{C}\widetilde{\mathcal{V}}} := \sum_{\mathrm{c}\in\mathrm{C}} \mathbf{s}_{\mathrm{c}} \mathbf{p}_{\tilde{\mathrm{v}}(\mathrm{c})}. \tag{3.15d}$$

Proposition 3.16 (Adjunction property)**.** *The following identities hold:*

$$[\![\mathsf{GRAD}(\mathbf{p}), \boldsymbol{\phi}]\!]_{\mathcal{E}\widetilde{\mathcal{F}}} = -[\![\mathbf{p}, \widetilde{\mathsf{DIV}}(\boldsymbol{\phi})]\!]_{\mathcal{V}\widetilde{\mathcal{C}}}, \qquad \forall \mathbf{p} \in \mathcal{V},\ \forall \boldsymbol{\phi} \in \widetilde{\mathcal{F}}, \tag{3.16a}$$

$$[\![\mathsf{CURL}(\mathbf{u}), \mathbf{v}]\!]_{\mathcal{F}\widetilde{\mathcal{E}}} = [\![\mathbf{u}, \widetilde{\mathsf{CURL}}(\mathbf{v})]\!]_{\mathcal{E}\widetilde{\mathcal{F}}}, \qquad \forall \mathbf{u} \in \mathcal{E},\ \forall \mathbf{v} \in \widetilde{\mathcal{E}}, \tag{3.16b}$$

$$[\![\mathsf{DIV}(\boldsymbol{\phi}), \mathbf{p}]\!]_{\mathcal{C}\widetilde{\mathcal{V}}} = -[\![\boldsymbol{\phi}, \widetilde{\mathsf{GRAD}}(\mathbf{p})]\!]_{\mathcal{F}\widetilde{\mathcal{E}}}, \qquad \forall \boldsymbol{\phi} \in \mathcal{F},\ \forall \mathbf{p} \in \widetilde{\mathcal{V}}. \tag{3.16c}$$

Algebraically, this means that $\widetilde{\mathbb{G}} = -\mathbb{D}^{\mathrm{T}}$, $\widetilde{\mathbb{C}} = \mathbb{C}^{\mathrm{T}}$, *and* $\widetilde{\mathbb{D}} = -\mathbb{G}^{\mathrm{T}}$.

Proof. The adjunction property results from the definitions of the discrete differential operators and the transfer of orientation (3.11). □

Proposition 3.17 (Cochain complex)**.**

$$\widetilde{\mathsf{CURL}} \cdot \widetilde{\mathsf{GRAD}} = 0_{\widetilde{\mathcal{F}}}, \qquad \widetilde{\mathsf{DIV}} \cdot \widetilde{\mathsf{CURL}} = 0_{\widetilde{\mathcal{C}}}. \tag{3.17}$$

Proof. This is a straightforward consequence of Propositions 3.11 and 3.16. □

Consequently, $\operatorname{Im} \widetilde{\mathsf{GRAD}} \subset \operatorname{Ker} \widetilde{\mathsf{CURL}}$ and $\operatorname{Im} \widetilde{\mathsf{CURL}} \subset \operatorname{Ker} \widetilde{\mathsf{DIV}}$. Figure 3.10 summarizes Proposition 3.17.

Figure 3.10 – Cochain complex induced by the discrete differential operator on the dual mesh.

We close this section with a commuting property of the discrete differential operators with the de Rham maps on the dual mesh. This property holds for the interior dual entities since they are closed contrary to those touching the boundary $\partial\Omega$.

Proposition 3.18 (Commuting property with de Rham map)**.** *The following identities hold:*

$$\forall \mathrm{f} \in \mathrm{F}^{\mathrm{I}}, \qquad \mathsf{R}_{\widetilde{\mathcal{E}}}(\underline{\mathrm{grad}})|_{\tilde{\mathrm{e}}(\mathrm{f})} = \widetilde{\mathsf{GRAD}}(\mathsf{R}_{\widetilde{\mathcal{V}}})|_{\tilde{\mathrm{e}}(\mathrm{f})}, \tag{3.18a}$$

$$\forall \mathrm{e} \in \mathrm{E}^{\mathrm{I}}, \qquad \mathsf{R}_{\widetilde{\mathcal{F}}}(\underline{\mathrm{curl}})|_{\tilde{\mathrm{f}}(\mathrm{e})} = \widetilde{\mathsf{CURL}}(\mathsf{R}_{\widetilde{\mathcal{E}}})|_{\tilde{\mathrm{f}}(\mathrm{e})}, \tag{3.18b}$$

$$\forall \mathrm{v} \in \mathrm{V}^{\mathrm{I}}, \qquad \mathsf{R}_{\widetilde{\mathcal{C}}}(\mathrm{div})|_{\tilde{\mathrm{c}}(\mathrm{v})} = \widetilde{\mathsf{DIV}}(\mathsf{R}_{\widetilde{\mathcal{F}}})|_{\tilde{\mathrm{c}}(\mathrm{v})}. \tag{3.18c}$$

Proof. Using the generalized Stokes theorem on the interior dual entities and the definition of the degrees of freedom (3.12) yields the result. □

3.4 Discrete Hodge operators

3.4.1 Principles

The name "Hodge operator" stems from a concept of differential geometry called Hodge-star operator (see Frankel, 1997, Chapter 14, for instance). The Hodge operator embeds a metric (usually induced by a phenomenological parameter) and connects spaces in duality.

A discrete Hodge operator shares the same features. The discrete Hodge operator links spaces of DoFs in duality $x\tilde{y} \in \{\nu\tilde{c}, \varepsilon\tilde{f}, f\tilde{\varepsilon}, c\tilde{\nu}\}$ and is a metric operator since its definition relies on lengths, areas or volumes related to primal or dual entities and on the evaluation of a material property. Let α denote a material property. Then, we use the generic notation $\mathsf{H}_\alpha^{x\tilde{y}}$ for the discrete Hodge operator. In this thesis, α is either a conductivity κ (possibly tensor-valued) when one considers elliptic equations (cf. Section 4.1 and Chapter 8) or a mass density ρ or a viscosity μ when one considers the Stokes equations (cf. Section 4.2 and Chapter 9). The discrete Hodge operator is used to discretize constitutive or closure relations (the Fourier or Darcy law when one considers elliptic equations or the link between velocity and mass flux when one considers the Stokes equations). Observe that a constitutive law results from experiments and is part of a physical model where approximations occur depending on the problem at hand. In the CDO framework, approximations take place at the same level since the discrete Hodge operator is the sole operator leading to a consistency error.

The discrete Hodge operator is the cornerstone of the CDO approach. The definition of this operator is not unique contrary to that of discrete differential operators. Each definition leads to a different scheme, so that the discrete Hodge operator is the element of differentiation between two CDO schemes. Several definitions have been proposed in the literature. Most of the contributions stem from the electromagnetism community. Bossavit (2000) has introduced the concept of *Galerkin Hodge* (see also Tarhasaari *et al.* (1999)) by considering a discrete Hodge operator as a mass matrix weighted by a material property. Auchmann & Kurz (2006) have devised a discrete Hodge operator based on geometrical identities proper to simplicial meshes. We also mention the contribution of Codecasa *et al.* (2010) where a discrete Hodge operator is defined for polyhedral meshes (cf. Section 7.3 for more details).

Remark 3.19 (Unified vision)**.** *An interesting consequence of these multiple definitions is that we end up with a unified vision both of the analysis and of the implementation of CDO schemes. Assuming that the discrete Hodge operator verifies a set of identified properties (cf. next section), then all the analysis holds for the schemes derived from this discrete Hodge operator. This idea has been earlier pointed out by Tarhasaari* et al. *(1999). From the implementation point of view, plugging a discrete Hodge operator gives rise to a specific scheme without altering the remaining part of the code involving, in particular, the discrete differential operators.*

In addition to $\mathsf{H}_\alpha^{x\tilde{y}} : \mathcal{X} \to \widetilde{\mathcal{Y}}$, there exists another category of discrete Hodge operators acting on dual spaces of DoFs and mapping to primal ones $\mathsf{H}_{\alpha^{-1}}^{\tilde{y}x} : \widetilde{\mathcal{Y}} \to \mathcal{X}$ where $\tilde{y}x \in \{\tilde{c}\nu, \tilde{f}\varepsilon, \tilde{\varepsilon}f, \tilde{\nu}c\}$ (see Figure 3.11). Since in general $\mathsf{H}_\alpha^{x\tilde{y}} \neq (\mathsf{H}_{\alpha^{-1}}^{\tilde{y}x})^{-1}$, using $\mathsf{H}_\alpha^{x\tilde{y}}$ or $(\mathsf{H}_{\alpha^{-1}}^{\tilde{y}x})^{-1}$ leads to different schemes. The majority of the work in the literature is dedicated to the discrete Hodge operators $\mathsf{H}_\alpha^{x\tilde{y}}$ acting on the primal DoFs spaces. To our knowledge, only He (2006), Christiansen (2008), and Gillette & Bajaj (2011) have studied the case of discrete Hodge operators $\mathsf{H}_{\alpha^{-1}}^{\tilde{y}x}$ defined from the dual DoFs spaces in non-trivial cases (*i.e.* $\mathsf{H}_{\alpha^{-1}}^{\tilde{y}x} \neq (\mathsf{H}_\alpha^{x\tilde{y}})^{-1}$). He (2006) has considered this kind of discrete Hodge operators to speed up the iterative solver since $\mathsf{H}_1^{\tilde{y}x}$ can be viewed as a sparse approximate inverse of $\mathsf{H}_1^{x\tilde{y}}$. Christiansen (2008) has proposed a generic building principle based on the resolution of local minimization problems discretized on an underlying simplicial submesh of each cell (cf. Section 7.3.2). Gillette & Bajaj (2011) have specifically focused on the operator $\mathsf{H}_1^{\tilde{\nu}c}$ (with $\alpha = 1$) using the concept of *generalized barycentric coordinates* for handling polyhedral cells.

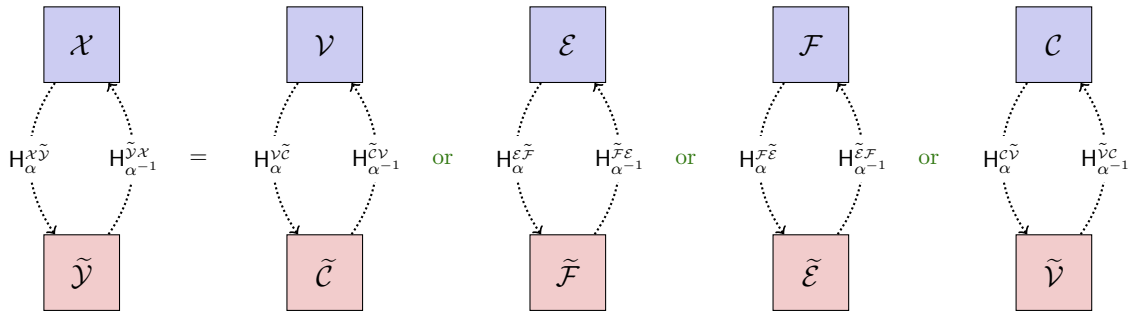

Figure 3.11 – Generic discrete Hodge operators from the primal DoFs spaces and generic discrete Hodge operators from the dual DoFs spaces.

3.4.2 Design

In the CDO framework, the crucial point is the design of the discrete Hodge operator. In the specific case of orthogonal meshes and isotropic material property, a diagonal discrete Hodge operator can be considered (cf. Section 3.4.3). In more general situations (non-orthogonal meshes or anisotropic material property), it is possible to design discrete Hodge operators from the primal mesh to the dual mesh such that the matrix representing this operator is sparse and *symmetric positive definite* (SPD). Since the discrete Hodge operator maps from a vector space to its dual, this implies that the discrete Hodge operator is self-adjoint and (strictly) monotone. In this thesis, we abuse this terminology and say that the discrete Hodge is SPD. A general way to build a (global) discrete Hodge operator is to assemble local discrete Hodge operators defined at the cell level. Design properties are thus stated *locally*. Examples using reconstruction operators are given in Chapter 7. On general meshes, building a global discrete Hodge operator from the dual mesh to the primal mesh with an explicit expression of its entries is still, to our knowledge, a current subject of investigation.

Local design properties. For each primal cell $\mathrm{c} \in \mathrm{C}$, the design of the discrete Hodge operator $\mathsf{H}_\alpha^{\mathcal{X}_\mathrm{c}\tilde{\mathcal{Y}}_\mathrm{c}}$ hinges on three local properties (cf. Section 6.2 for a more formal statement):

(**H0**) A *symmetry* property.

(**H1**) A *local stability* property which states that the eigenvalues of $\mathsf{H}_\alpha^{\mathcal{X}_\mathrm{c}\tilde{\mathcal{Y}}_\mathrm{c}}$ are uniformly bounded from above and from below away from zero.

(**H2**) A *local* $\mathbb{P}_0$*-consistency* which states that the local discrete Hodge operators can exactly represent constant fields.

Assembly. The assembly of the global discrete Hodge operator $\mathsf{H}_\alpha^{\mathcal{X}\tilde{\mathcal{Y}}}$ is performed on primal cells. In what follows, we made the reasonable assumption that the material property is constant (or, more generally, smooth) in each primal cell. The assembly principle is the following. We first introduce local subsets for each $\mathrm{c} \in \mathrm{C}$, as follows:

$$\mathrm{X}_\mathrm{c} := \{\mathrm{x} \in \mathrm{X} \,|\, \mathrm{x} \subseteq \partial\mathrm{c}\}, \qquad \widetilde{\mathrm{Y}}_\mathrm{c} := \{\tilde{\mathrm{y}}_\mathrm{c}(\mathrm{x}) := \tilde{\mathrm{y}}(\mathrm{x}) \cap \mathrm{c},\ \mathrm{x} \in \mathrm{X}_\mathrm{c}\}. \tag{3.19}$$

We define from the local subset X_c (resp. $\widetilde{\mathrm{Y}}_\mathrm{c}$) the local DoFs spaces $\mathcal{X}_\mathrm{c}$ (resp. $\tilde{\mathcal{Y}}_\mathrm{c}$); see Figure 3.12 and Section 6.2 for more details. Then, we introduce a local discrete Hodge operator $\mathsf{H}_\alpha^{\mathcal{X}_\mathrm{c}\tilde{\mathcal{Y}}_\mathrm{c}} : \mathcal{X}_\mathrm{c} \to \tilde{\mathcal{Y}}_\mathrm{c}$ attached to the primal cell c. This local discrete Hodge operator is SPD by construction (owing to (**H0**) and (**H1**)). The *global* discrete Hodge operator $\mathsf{H}_\alpha^{\mathcal{X}\tilde{\mathcal{Y}}}$ is then obtained by a cellwise assembly process of the local discrete Hodge operators as follows:

$$\mathsf{H}_\alpha^{\mathcal{X}\tilde{\mathcal{Y}}} = \sum_{\mathrm{c}\in\mathrm{C}} \mathsf{T}_{\mathrm{X},\mathrm{c}}^* \cdot \mathsf{H}_\alpha^{\mathcal{X}_\mathrm{c}\tilde{\mathcal{Y}}_\mathrm{c}} \cdot \mathsf{T}_{\mathrm{X},\mathrm{c}}, \tag{3.20}$$

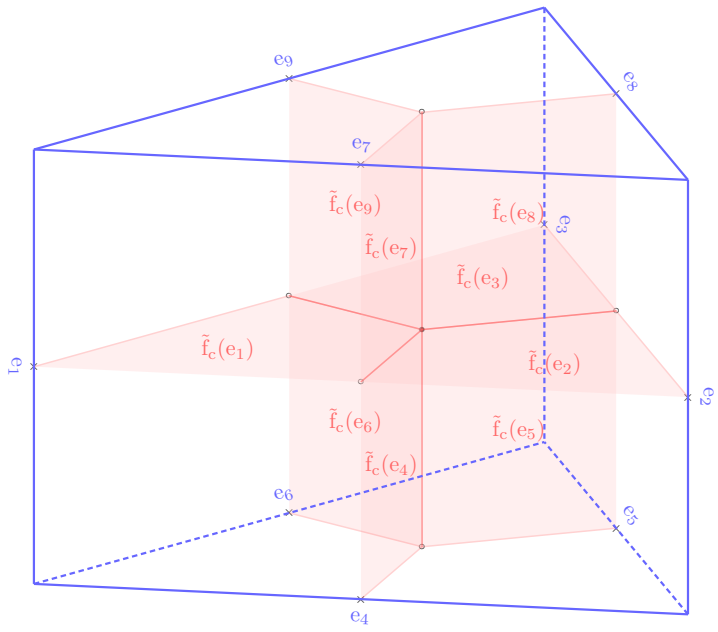

Figure 3.12 – Consider a prismatic cell c. The set of local edges $\mathrm{E_c} = \{\mathrm{e}_1, \dots, \mathrm{e}_9\}$ is depicted in blue and the set of local dual faces $\widetilde{\mathrm{F}}_\mathrm{c} = \{\tilde{\mathrm{f}}_\mathrm{c}(\mathrm{e}_1), \dots, \tilde{\mathrm{f}}_\mathrm{c}(\mathrm{e}_9)\}$ is depicted in red.

where the transfer operator $\mathsf{T}_{\mathrm{X,c}} : \mathbb{R}^{\#\mathrm{X}} \to \mathbb{R}^{\#\mathrm{X_c}}$ is the (full-rank) map from global to local DoFs, and $\mathsf{T}^*_{\mathrm{X,c}} : \mathbb{R}^{\#\mathrm{X_c}} \to \mathbb{R}^{\#\mathrm{X}}$ is the map acting from local to global DoFs. $\mathsf{T}^*_{\mathrm{X,c}}$ is a right inverse of $\mathsf{T}_{\mathrm{X,c}}$ and the algebraic realization of $\mathsf{T}^*_{\mathrm{X,c}}$ and $\mathsf{T}_{\mathrm{X,c}}$ are matrices that are transpose of each other (*i.e.* $\mathsf{T}_{\mathrm{X,c}}\mathsf{T}^*_{\mathrm{X,c}} = \mathsf{Id}_{\mathbb{R}^{\#\mathrm{X_c}}}$ and $[\![\mathbf{a}, \mathsf{T}_{\mathrm{X,c}}(\mathbf{b})]\!]_{\mathcal{X}_\mathrm{c}\widetilde{\mathcal{Y}}_\mathrm{c}} = [\![\mathsf{T}^*_{\mathrm{X,c}}(\mathbf{a}), \mathbf{b}]\!]_{\mathcal{X}\widetilde{\mathcal{Y}}}$ for all $\mathbf{a} \in \mathcal{X}_\mathrm{c}$ and all $\mathbf{b} \in \widetilde{\mathcal{Y}}$).

As a consequence of (3.20), $\mathsf{H}_\alpha^{\mathcal{X}\widetilde{\mathcal{Y}}}$ is algebraically represented by a (large) sparse SPD matrix of size $\#\mathrm{X} = \#\widetilde{\mathrm{Y}}$, while $\mathsf{H}_\alpha^{\mathcal{X}_\mathrm{c}\widetilde{\mathcal{Y}}_\mathrm{c}}$ is algebraically represented by a (small) dense SPD matrix of size $\#\mathrm{X_c} = \#\widetilde{\mathrm{Y}}_\mathrm{c}$.

Design strategies To fulfill the properties (**H0**), (**H1**), and (**H2**), two main strategies are considered in the CDO framework:

(1) The local discrete Hodge operators are designed by setting directly the entries of the matrix associated with the algebraic representation of the operator. These entries are specified in order to verify the three design properties. This strategy, based on an *algebraic* representation of the discrete Hodge operator, is analyzed in Chapter 6. MFD and DEC schemes share this viewpoint; see also Hiptmair (2001a).

(2) The local discrete Hodge operators $\mathsf{H}_\alpha^{\mathcal{X}_\mathrm{c}\widetilde{\mathcal{Y}}_\mathrm{c}}$ are defined from a reconstruction operator $\mathsf{L}_{\mathcal{X}_\mathrm{c}}$ as follows:

$$[\![\mathbf{a}, \mathsf{H}_\alpha^{\mathcal{X}_\mathrm{c}\widetilde{\mathcal{Y}}_\mathrm{c}}(\mathbf{b})]\!]_{\mathcal{X}_\mathrm{c}\widetilde{\mathcal{Y}}_\mathrm{c}} := \int_\mathrm{c} \mathsf{L}_{\mathcal{X}_\mathrm{c}}(\mathbf{a}) \cdot \alpha \mathsf{L}_{\mathcal{X}_\mathrm{c}}(\mathbf{b}), \qquad \forall (\mathbf{a}, \mathbf{b}) \in \mathcal{X}_\mathrm{c} \times \mathcal{X}_\mathrm{c}.$$

In this situation, the design properties of the local discrete Hodge operator are induced by the design properties of the reconstruction operators. This strategy is analyzed in Chapter 7. FEEC, DGA, and MSE schemes adopt this viewpoint; see also the concept of "Galerkin Hodge" introduced by Bossavit (2000).

Remark 3.20 (Comparison with FE and FV)**.** *The algebraic strategy is close to a FV spirit, while the strategy using reconstruction operators is close to a FE spirit.*

3.4.3 Simple examples

In this section, we illustrate the construction of discrete Hodge operators in the case of elliptic equations. In this situation, $\mathsf{H}_{\kappa}^{\mathcal{E}\tilde{\mathcal{F}}}$ and $\mathsf{H}_{\kappa^{-1}}^{\mathcal{F}\tilde{\mathcal{E}}}$, where κ is the conductivity, are the two involved discrete Hodge operators. We give simple examples of diagonal discrete Hodge operators since we consider the case of Delaunay–Voronoï meshes and an isotropic (*i.e.*, scalar-valued, but not necessarily constant) conductivity. Similar definitions hold for Cartesian meshes too.

Construction of $\mathsf{H}_{\kappa}^{\mathcal{E}\tilde{\mathcal{F}}}$. We first recall the local subsets

$$\mathrm{E_c} := \{\mathrm{e} \in \mathrm{E} \,|\, \mathrm{e} \subset \partial \mathrm{c}\} \qquad \text{and} \qquad \widetilde{\mathrm{F}}_\mathrm{c} := \{\tilde{\mathrm{f}}_\mathrm{c}(\mathrm{e}) := \tilde{\mathrm{f}}(\mathrm{e}) \cap \mathrm{c} \,|\, \mathrm{e} \in \mathrm{E_c}\}.$$

The entries of the local discrete Hodge operator in each cell $\mathrm{c} \in \mathrm{C}$ are simply equal to

$$\mathsf{H}_{\kappa}^{\mathcal{E}_\mathrm{c}\tilde{\mathcal{F}}_\mathrm{c}}|_{\tilde{\mathrm{f}}_\mathrm{c}(\mathrm{e}),\mathrm{e}} = \frac{\kappa_\mathrm{c}\,|\tilde{\mathrm{f}}_\mathrm{c}(\mathrm{e})|}{|\mathrm{e}|} \qquad \forall \mathrm{e} \in \mathrm{E_c}, \tag{3.21a}$$

and those of the global discrete Hodge operator to

$$\mathsf{H}_{\kappa}^{\mathcal{E}\tilde{\mathcal{F}}}|_{\tilde{\mathrm{f}}(\mathrm{e}),\mathrm{e}} = \frac{1}{|\mathrm{e}|}\sum_{\mathrm{c}\in\mathrm{C_e}} \kappa_\mathrm{c}\,|\tilde{\mathrm{f}}_\mathrm{c}(\mathrm{e})|, \quad \forall \mathrm{e} \in \mathrm{E}. \tag{3.21b}$$

An arithmetic average of the conductivity naturally appears in the definition of the entries of the global operator.

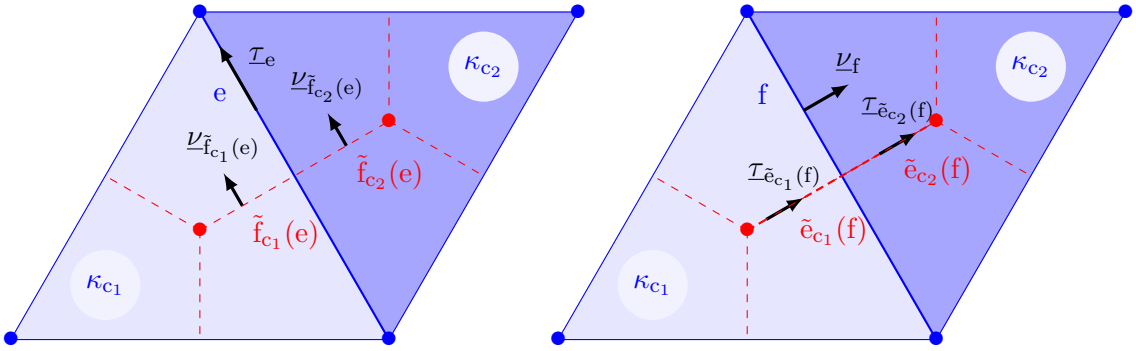

Figure 3.13 – Quantities involved in the definition of diagonal discrete Hodge operators. Left: $\mathsf{H}_{\kappa}^{\mathcal{E}\tilde{\mathcal{F}}}$; Right: $\mathsf{H}_{\kappa^{-1}}^{\mathcal{F}\tilde{\mathcal{E}}}$.

Construction of $\mathsf{H}_{\kappa^{-1}}^{\mathcal{F}\tilde{\mathcal{E}}}$. We first recall the local subsets

$$\mathrm{F_c} := \{\mathrm{f} \in \mathrm{F} \,|\, \mathrm{f} \subset \partial \mathrm{c}\} \qquad \text{and} \qquad \widetilde{\mathrm{E}}_\mathrm{c} := \{\tilde{\mathrm{e}}_\mathrm{c}(\mathrm{f}) := \tilde{\mathrm{e}}(\mathrm{f}) \cap \mathrm{c} \,|\, \mathrm{f} \in \mathrm{F_c}\}.$$

The entries of the local discrete Hodge operator in each cell $\mathrm{c} \in \mathrm{C}$ are simply equal to

$$\mathsf{H}_{\kappa^{-1}}^{\mathcal{F}_\mathrm{c}\tilde{\mathcal{E}}_\mathrm{c}}|_{\tilde{\mathrm{e}}_\mathrm{c}(\mathrm{f}),\mathrm{f}} = \frac{|\tilde{\mathrm{e}}_\mathrm{c}(\mathrm{f})|}{\kappa_\mathrm{c}\,|\mathrm{f}|}, \qquad \forall \mathrm{f} \in \mathrm{F_c}, \tag{3.22a}$$

and those of the global discrete Hodge operator to

$$\mathsf{H}_{\kappa^{-1}}^{\mathcal{F}\tilde{\mathcal{E}}}|_{\tilde{\mathrm{e}}(\mathrm{f}),\mathrm{f}} = \frac{1}{|\mathrm{f}|}\sum_{\mathrm{c}\in\mathrm{C_f}} \kappa_\mathrm{c}^{-1}\,|\tilde{\mathrm{e}}_\mathrm{c}(\mathrm{f})|, \quad \forall \mathrm{f} \in \mathrm{F}. \tag{3.22b}$$

An harmonic average of the conductivity naturally appears in the definition of the entries of the global operator. Moreover, in the present case, a simple choice of discrete Hodge operators from dual to primal spaces of DoFs is $\mathsf{H}_{\kappa^{-1}}^{\widetilde{\mathcal{F}}\mathcal{E}} := (\mathsf{H}_{\kappa}^{\mathcal{E}\widetilde{\mathcal{F}}})^{-1}$ and $\mathsf{H}_{\kappa}^{\widetilde{\mathcal{E}}\mathcal{F}} := (\mathsf{H}_{\kappa^{-1}}^{\mathcal{F}\widetilde{\mathcal{E}}})^{-1}$ since it is straightforward to invert a diagonal matrix.

Adopting the CDO viewpoint, the equivalence between the DEC schemes, the Covolume approach, and the TPFA schemes is straightforward since they all fit the CDO framework and share the same discrete Hodge operator. These approaches are possible on meshes with an orthogonality condition, such as Cartesian and Delaunay–Voronoï meshes, but this condition is too restrictive for handling complex geometries. Therefore, in an industrial context, we do not use this approach. We refer in particular to Chapter 7 for more details.

3.5 Synthesis: fully discrete setting

In the CDO framework, we end up with two discrete de Rham sequences (see Figure 3.14): one on the primal mesh (in blue, top line) and the other one on the dual mesh (in red, bottom line). These two discrete sequences are linked together by the discrete Hodge operators. The horizontal links are topological (or metric-free) relations while the vertical relations are metric-dependent and also rely on material properties. A solid line means a relation free of consistency errors, while a dotted line means the contrary. Table 3.1 summarizes the main features of discrete differential operators and discrete Hodge operators.

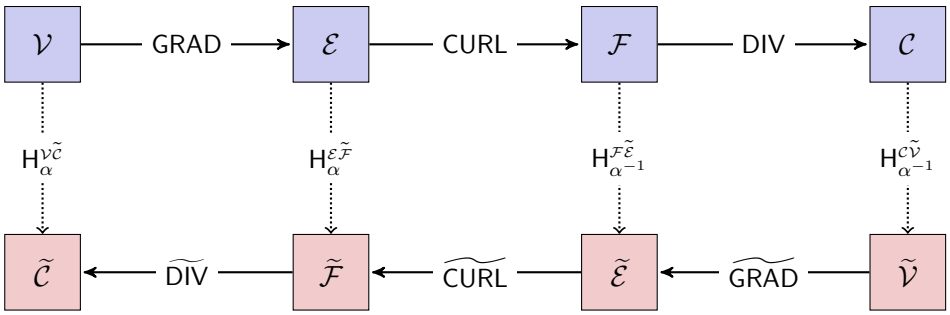

Figure 3.14 – Fully discrete setting.

Discrete Differential Operators	Discrete Hodge Operators
Topological laws	Constitutive relations
Error-free	Approximation
Unique definition	Multiple definitions

Table 3.1 – Main features of discrete differential operators and discrete Hodge operators.

Chapter 4

CDO schemes

Contents

In this chapter, we use the discrete setting introduced in Chapter 3 to devise CDO schemes for elliptic and Stokes equations, postponing the analysis (stability, convergence) to Chapters 8 and 9, resp. For both equations, we propose generic CDO schemes that encompass various schemes (from FE schemes to FV schemes) as soon as one specifies which discrete Hodge operator is used. The present CDO schemes feature several interesting properties. They can be deployed on polyhedral meshes (with an adequate choice of the discrete Hodge operator), and the discrete solution satisfies local conservation properties.

For both elliptic and Stokes equations, two families of schemes are presented depending on the positioning of the DoFs related to the potential. Choosing a positioning on primal vertices leads to *vertex-based* schemes, while choosing a positioning on dual vertices (which are in a one-to-one pairing with primal cells) leads to *cell-based* schemes.

CDO schemes for elliptic equations are detailed in Section 4.1 and those for Stokes equations in Section 4.2.

4.1 Elliptic equations

4.1.1 Vertex-based schemes

Vertex-based schemes rely on writing the elliptic problem in primal formulation as follows:

$$-\operatorname{div}(\underline{\underline{\kappa}}\,\underline{\operatorname{grad}}\, p) = s, \qquad \text{in } \Omega, \tag{4.1}$$

with source term $s \in L^2(\Omega)$. In what follows, p is termed the potential. For simplicity, we focus on homogeneous Dirichlet boundary conditions; non-homogeneous Dirichlet/Neumann boundary conditions for (4.1) can be considered as well. The conductivity $\underline{\underline{\kappa}}$ can be tensor-valued and heterogeneous, and we assume that the tensor is symmetric and its eigenvalues are uniformly bounded from above and from below away from zero. We additionally assume that the conductivity is piecewise constant in each primal cell (it is also possible to assume that the conductivity is piecewise smooth up to additional technicalities).

Following the rationale introduced in Section 2.1, we split equation (4.1) into two topological relations (equations (4.2a) and (4.2c) below) and one constitutive relation (equation (4.2b)); in doing so, we introduce the gradient $\underline{g}$ and the flux $\underline{\phi}$ of the exact solution such that

$$\underline{g} = \underline{\mathrm{grad}}\, p, \tag{4.2a}$$

$$\underline{\phi} = -\underline{\underline{\kappa}}\, \underline{g}, \tag{4.2b}$$

$$\mathrm{div}\, \underline{\phi} = s. \tag{4.2c}$$

In vertex-based schemes, the discrete potential, denoted by $\mathbf{p}$, is attached to primal vertices, the discrete gradient $\mathbf{g}$ to primal edges, the discrete flux $\boldsymbol{\phi}$ to dual faces, and the source term to dual cells. The discrete Hodge operator to consider, which is related to the conductivity $\underline{\underline{\kappa}}$, is

$$\mathsf{H}_{\kappa}^{\mathcal{E}\widetilde{\mathcal{F}}} : \mathcal{E} \to \widetilde{\mathcal{F}}. \tag{4.3}$$

The discrete counterpart of equations (4.2) is

$$\mathbf{g} = \mathsf{GRAD}(\mathbf{p}), \tag{4.4a}$$

$$\boldsymbol{\phi} = -\mathsf{H}_{\kappa}^{\mathcal{E}\widetilde{\mathcal{F}}}(\mathbf{g}), \tag{4.4b}$$

$$\widetilde{\mathsf{DIV}}(\boldsymbol{\phi}) = \mathsf{R}_{\widetilde{\mathcal{C}}}(s). \tag{4.4c}$$

The resulting discrete system is: Find $\mathbf{p} \in \mathcal{V}$ such that

$$-\widetilde{\mathsf{DIV}} \cdot \mathsf{H}_{\kappa}^{\mathcal{E}\widetilde{\mathcal{F}}} \cdot \mathsf{GRAD}(\mathbf{p}) = \mathsf{R}_{\widetilde{\mathcal{C}}}(s). \tag{4.5}$$

For simplicity, we assume there is no quadrature error in the computation of the discrete source term $\mathsf{R}_{\widetilde{\mathcal{C}}}(s)$ on the right-hand side. Since GRAD and $-\widetilde{\mathsf{DIV}}$ are adjoint operators (cf. Proposition 3.16) and the discrete Hodge operator is SPD by construction, the discrete system (4.5) is SPD. The algebraic system is of size #V.

In vertex-based schemes, the balance is expressed on dual cells and is locally exact. Specifically, for all $\mathrm{v} \in \mathrm{V}$,

$$\sum_{\tilde{\mathrm{f}} \in \widetilde{\mathrm{F}}_{\tilde{\mathrm{c}}(\mathrm{v})}} \iota_{\tilde{\mathrm{f}},\tilde{\mathrm{c}}(\mathrm{v})} \boldsymbol{\phi}_{\tilde{\mathrm{f}}} = \mathsf{R}_{\widetilde{\mathcal{C}}}(s)|_{\tilde{\mathrm{c}}(\mathrm{v})}. \tag{4.6}$$

The relations between DoFs and discrete operators can be summarized using a Tonti diagram. The diagram related to equation (4.5) is depicted in Figure 4.1 (compare with the fully discrete setting introduced in Figure 3.14).

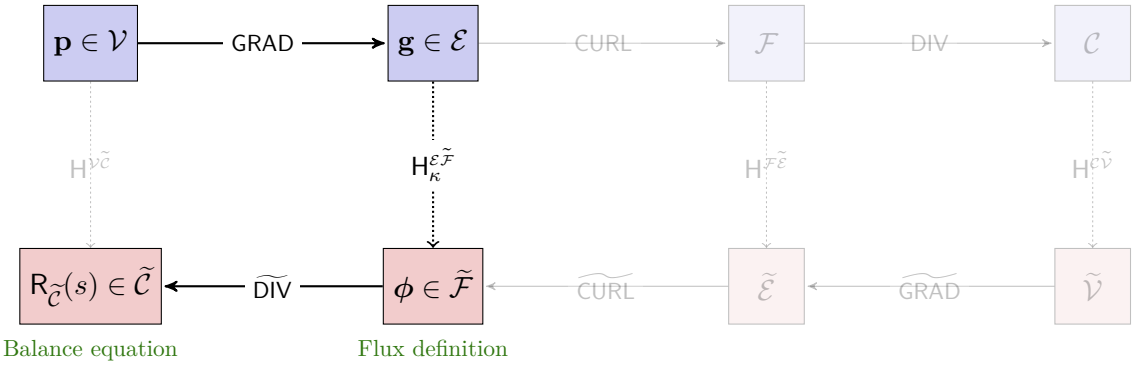

Figure 4.1 – Tonti diagram of vertex-based schemes for elliptic problems.

Remark 4.1 (Dirichlet BC)**.** *In vertex-based schemes, the Dirichlet BC can be strongly enforced by discarding the potential DoFs attached to boundary vertices and the gradient degrees of freedom attached to edges included in the boundary; the corresponding degrees of freedom attached to dual faces and dual cells are also discarded. Their contribution, in the case of a non-homogeneous Dirichlet BC, are thus collected in the right-hand side. This point is detailed in the EDF R&D technical report (Ra) mentioned in Chapter 1.*

Remark 4.2 (Link with FV schemes)**.** *We observe that* (4.5) *is equivalent to a FV scheme on the dual mesh (also called* vertex-centered *FV scheme).*

4.1.2 Cell-based schemes

Cell-based schemes rely on the mixed formulation of the elliptic problem (4.1), defined as follows:

$$\begin{cases} \underline{\underline{\kappa}}^{-1}\underline{\phi} + \underline{\mathrm{grad}}(p) = \underline{0}, & \text{in } \Omega, \\ \mathrm{div}(\underline{\phi}) = s, & \text{in } \Omega. \end{cases} \tag{4.7}$$

In such schemes, the discrete potential is attached to dual vertices ($\mathbf{p} \in \widetilde{\mathcal{V}}$), the discrete gradient to dual edges ($\mathbf{g} \in \widetilde{\mathcal{E}}$), the discrete flux to primal faces ($\boldsymbol{\phi} \in \mathcal{F}$), and the source term to primal cells. The discrete Hodge operator to consider is

$$\mathsf{H}_{\kappa^{-1}}^{\mathcal{F}\widetilde{\mathcal{E}}} : \mathcal{F} \to \widetilde{\mathcal{E}}. \tag{4.8}$$

In cell-based schemes, the resulting discrete system is: Find $(\mathbf{p}, \boldsymbol{\phi}) \in \widetilde{\mathcal{V}} \times \mathcal{F}$ such that

$$\begin{cases} \mathsf{H}_{\kappa^{-1}}^{\mathcal{F}\widetilde{\mathcal{E}}}(\boldsymbol{\phi}) + \widetilde{\mathsf{GRAD}}(\mathbf{p}) = 0_{\widetilde{\mathcal{E}}}, \\ \mathsf{DIV}(\boldsymbol{\phi}) = \mathsf{R}_{\mathcal{C}}(s). \end{cases} \tag{4.9}$$

As for vertex-based schemes, we assume there is no quadrature error related to the computation of the discrete source term $\mathsf{R}_{\mathcal{C}}(s)$ on the right-hand side. Since $-\widetilde{\mathsf{GRAD}}$ and DIV are adjoint operators (cf. Proposition 3.16) and $\mathsf{H}_{\kappa^{-1}}^{\mathcal{F}\widetilde{\mathcal{E}}}$ is SPD by construction, the algebraic system (4.9) is a saddle-point problem of size #C + #F. In cell-based schemes, the balance equation is expressed on primal cells and is locally exact. Specifically, for all c ∈ C,

$$\sum_{\mathrm{f}\in\mathrm{F_c}} \iota_{\mathrm{f,c}}\boldsymbol{\phi}_{\mathrm{f}} = \mathsf{R}_{\mathcal{C}}(s)|_{\mathrm{c}}. \tag{4.10}$$

Remark 4.3 (Dirichlet BC)**.** *Enforcing the Dirichlet BC does not entail discarding DoFs, but the discrete gradient operator explicitly accounts for the boundary condition on dual edges touching the boundary. In the case of a homogeneous Dirichlet BC, the definition of the discrete gradient operator* $\widetilde{\mathsf{GRAD}}$ *remains unchanged.*

Remark 4.4 (Link with FV schemes)**.** *Observe that* (4.9) *is a mixed FV scheme on the primal mesh since there is one unknown per primal cell and one unknown per primal face.*

The Tonti diagram depicted in Figure 4.2 summarizes the relations between DoFs and discrete operators in the cell-based setting (compare with Figure 3.14).

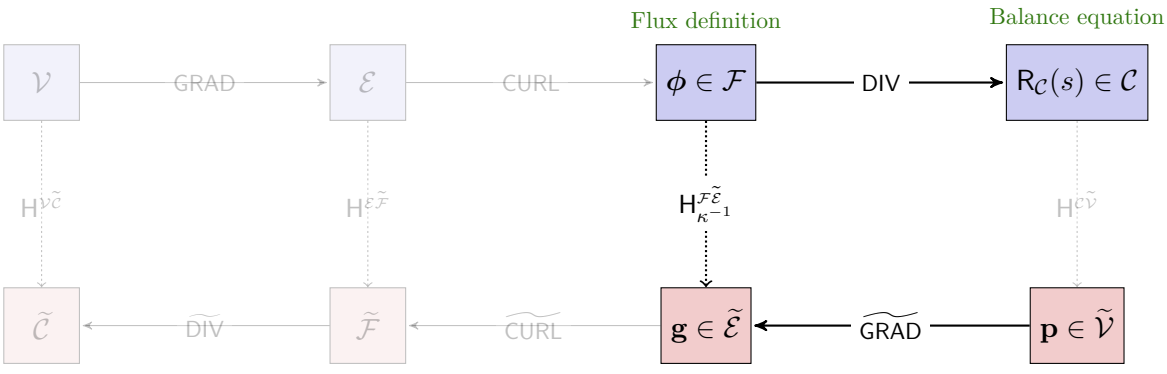

Figure 4.2 – Tonti diagram of cell-based schemes for elliptic problems.

Remark 4.5 (Hybridization)**.** *In general, the resolution of a saddle-point system is not as efficient as the resolution of a SPD system. A classical way to circumvent this point is to hybridize the system* (4.9)*; see Brezzi & Fortin (1991). We develop this technique in the context of cell-based CDO schemes in Section 8.3.*

4.2 Stokes equations

4.2.1 Formulations

The Stokes equations model incompressible flows of viscous fluids where the advective inertial forces are negligible with respect to the viscous forces. In this thesis, we focus on the stationary Stokes equations with constant mass density and constant viscosity. The classical formulation of the Stokes problem uses a vector Laplacian in the momentum balance. This first formulation takes the form

$$\begin{cases} -\underline{\Delta}(\underline{u}) + \underline{\mathrm{grad}}(p) = \underline{f}, & \text{in } \Omega, \\ \mathrm{div}(\underline{u}) = 0, & \text{in } \Omega, \end{cases} \tag{4.11}$$

where p is the pressure, $\underline{u}$ the velocity and $\underline{f}$ the external load. Various schemes were proposed to discretize this formulation on polygonal or polyhedral meshes, including MFV schemes by Droniou & Eymard (2009), MFD schemes by Beirão da Veiga *et al.* (2009, 2010) and Beirão da Veiga & Lipnikov (2010), DDFV schemes by Krell & Manzini (2012), an extension of the Crouzeix–Raviart FE scheme by Di Pietro & Lemaire (2015), and a scheme on triangular meshes based on the FEEC approach by Falk & Neilan (2013). Discretizing the vector Laplacian with CDO schemes is not addressed in this thesis, but is left for future work.

In this thesis, we focus on the Stokes equations formulated with the $\underline{\mathrm{curl}}$ operator. Our starting point is to recast the viscous stresses in the momentum balance using the identity $-\underline{\Delta} = \underline{\mathrm{curl}}\,\underline{\mathrm{curl}} - \underline{\mathrm{grad}}\,\mathrm{div}$, so that all the terms in the Stokes equations can be interpreted using scalar-valued differential forms. We analyze two formulations. The first one, hereafter called *two-field curl formulation*, takes the form

$$\begin{cases} \underline{\mathrm{curl}}(\underline{\mathrm{curl}}(\underline{u})) + \underline{\mathrm{grad}}(p) = \underline{f}, & \text{in } \Omega, \\ \mathrm{div}(\underline{u}) = 0, & \text{in } \Omega. \end{cases} \tag{4.12}$$

Introducing the vorticity $\underline{\omega} := \underline{\mathrm{curl}}\,\underline{u}$, the second formulation, hereafter called *three-field curl formulation* (also called Velocity-Vorticity-Pressure formulation in the literature), takes the form

$$\begin{cases} -\underline{\omega} + \underline{\mathrm{curl}}(\underline{u}) = \underline{0}, & \text{in } \Omega, \\ \underline{\mathrm{curl}}(\underline{\omega}) + \underline{\mathrm{grad}}(p) = \underline{f}, & \text{in } \Omega, \\ \mathrm{div}(\underline{u}) = 0, & \text{in } \Omega. \end{cases} \tag{4.13}$$

Curl formulations of the Stokes equations have been considered, e.g., by Nédélec (1982) and Dubois (1992, 2002) for the three-field curl formulation and by Bramble & Lee (1994) for the two-field curl formulation. Essential and natural boundary conditions (BCs) can be considered for both formulations. The first set of BCs enforces the value of the normal component of the velocity $\underline{u} \cdot \underline{\nu}_{\partial\Omega}$ and that of the tangential components of the vorticity $\underline{\omega} \times \underline{\nu}_{\partial\Omega}$ at the boundary. These BCs are natural for (4.12) and essential for (4.13). As the pressure is then determined up to an additive constant, the additional requirement of p having zero mean-value is typically added. The second set of BCs enforces the value of the tangential components of the velocity $\underline{u} \times \underline{\nu}_{\partial\Omega}$ and the value of the pressure at the boundary. These BCs are essential for (4.12) and natural for (4.13).

In this thesis, we devise and analyze CDO schemes for the Stokes problem in the curl formulations (4.12) and (4.13). Since the pressure plays the role of a potential, its DoFs are located at primal or dual mesh vertices. The former case hinges on (4.12) leading to *vertex-based pressure* schemes, while the latter hinges on (4.13) leading to *cell-based pressure* schemes. Both CDO schemes involve two discrete Hodge operators, one related to the mass density which links the velocity (seen as a circulation) to the mass flux, and the other one related to the viscosity which links the vorticity to the viscous stress.

A benefit from the CDO framework is to deliver two possible discretizations of the external load. To our knowledge, the idea of considering two possible discretizations of the external

load is new. This issue is quite important in practice so as to obtain tight error estimates when the external load has a large curl-free or a large divergence-free part (see Linke (2014) for a related work on classical FE schemes and loads with a large curl-free part). In CDO schemes, both situations can be handled by simply choosing a discretization of the external load on primal or dual mesh entities, without using explicitly any Hodge–Helmholtz decomposition of the external load (cf. Sections 9.1 and 9.2 for the resulting error estimates and Section 9.3 for a numerical illustration).

On specific meshes, previous schemes from the literature can be recovered from the present CDO schemes. On simplicial meshes and using Whitney forms to build the discrete Hodge operator, the present vertex-based (resp., cell-based) pressure schemes yield the recent FE scheme by Abboud *et al.* (2012) (resp., by Nédélec (1982) and Dubois (1992, 2002)). On Delaunay–Voronoï meshes where diagonal discrete Hodge operators can be used, the present CDO schemes are closely related to the recent MAC schemes by Eymard *et al.* (2014) on triangular meshes; see also Perot & Nallapati (2003). Furthermore, the present cell-based pressure schemes share the same algebraic structure (same discrete differential operators, but different discrete Hodge operators) as the recent MSE method on general quadrilateral/hexahedral meshes analyzed by Kreeft & Gerritsma (2013); see also Bernardi & Chorfi (2006). We also mention the DDFV scheme on general 2D meshes by Delcourte & Omnes (2014), which also hinges on the three-field formulation (4.13).

4.2.2 Vertex-based pressure schemes

In vertex-based pressure schemes, the starting formulation is the two-field curl formulation (4.12). Although the mass density ρ and the viscosity μ are constant, we rewrite (4.12) using these material properties so as to identify where a discrete Hodge operator should be used. We obtain

$$\begin{cases} \underline{\mathrm{curl}}(\mu\,\underline{\mathrm{curl}}(\underline{u})) + \rho\,\underline{\mathrm{grad}}(p^*) = \rho\underline{f}^*, & \text{in } \Omega,\\ \mathrm{div}(\rho\underline{u}) = 0, & \text{in } \Omega, \end{cases} \tag{4.14}$$

where we have introduced the pressure potential $p^* := \rho^{-1}p$ and the external load $\underline{f}^* := \rho^{-1}\underline{f}$. In what follows, we also consider the mass flux $\underline{\phi} := \rho\underline{u}$, and the auxiliary field $\underline{\omega}^* := \mu\underline{\omega}$ to which we loosely refer as viscous stress circulation. We focus on natural BCs for (4.14), which are given by

$$\underline{\phi}\cdot\underline{\nu}_{\partial\Omega} = \underline{\phi}_\nu^{\mathrm{bc}}, \quad \underline{\omega}^*\times\underline{\nu}_{\partial\Omega} = \underline{\omega}_\tau^{\mathrm{bc}}, \qquad \text{on } \partial\Omega, \tag{4.15}$$

with data $\underline{\phi}_\nu^{\mathrm{bc}}$ and $\underline{\omega}_\tau^{\mathrm{bc}}$ (for essential BCs, cf. Remark 4.7). Using $\underline{\phi}$ and $\underline{\omega}^*$, (4.14) can be rewritten as

$$\begin{cases} \underline{\mathrm{curl}}(\underline{\omega}^*) + \rho\,\underline{\mathrm{grad}}(p^*) = \rho\underline{f}^*, & \text{in } \Omega,\\ \mathrm{div}(\underline{\phi}) = 0, & \text{in } \Omega. \end{cases} \tag{4.16}$$

At the continuous level, the two unknowns are the pressure potential p^* and the velocity $\underline{u}$. The DoFs of the pressure potential, denoted by $\mathbf{p}^*$, are located at primal vertices. The DoFs of the velocity, denoted by $\mathbf{u}$, are located at primal edges. The velocity field is therefore seen as a circulation. The vorticity DoFs, which are located at primal faces, are directly obtained from the velocity DoFs by setting

$$\boldsymbol{\omega} := \mathsf{CURL}(\mathbf{u}). \tag{4.17}$$

The translational invariance of the discrete pressure potential (the discrete counterpart of the zero mean-value condition on the pressure) is fixed by the condition

$$[\![\mathbf{p}^*, \mathsf{H}_1^{\mathcal{V}\tilde{\mathcal{C}}}(\mathbf{1})]\!]_{\mathcal{V}\tilde{\mathcal{C}}} = 0, \tag{4.18}$$

where $\mathsf{H}_1^{\mathcal{V}\tilde{\mathcal{C}}}$ is a diagonal discrete Hodge operator with diagonal entries set to $|\tilde{\mathrm{c}}(\mathrm{v})|$ and $\mathbf{1}\in\mathcal{V}$ has all its entries equal to 1. The discrete space related to the pressure potential is therefore

$$\mathcal{V}_{\perp\mathbf{1}} := \{\boldsymbol{\theta}\in\mathcal{V};\ [\![\boldsymbol{\theta}, \mathsf{H}_1^{\mathcal{V}\tilde{\mathcal{C}}}(\mathbf{1})]\!]_{\mathcal{V}\tilde{\mathcal{C}}} = 0\}. \tag{4.19}$$

There are two discrete Hodge operators, one related to the mass density ρ and the other to the viscosity μ, such that

$$\mathsf{H}_\rho^{\mathcal{E}\widetilde{\mathcal{F}}} : \mathcal{E} \to \widetilde{\mathcal{F}} \qquad \text{and} \qquad \mathsf{H}_\mu^{\mathcal{F}\widetilde{\mathcal{E}}} : \mathcal{F} \to \widetilde{\mathcal{E}}. \tag{4.20}$$

These operators allow us to define respectively the discrete mass flux $\boldsymbol{\phi}$ located at dual faces and the discrete viscous stress circulation $\boldsymbol{\omega}^*$ located at dual edges as follows:

$$\begin{aligned} \boldsymbol{\phi} &:= \mathsf{H}_\rho^{\mathcal{E}\widetilde{\mathcal{F}}}(\mathbf{u}), && \text{(compare with } \underline{\phi} = \rho\underline{u}\text{)}, \\ \boldsymbol{\omega}^* &:= \mathsf{H}_\mu^{\mathcal{F}\widetilde{\mathcal{E}}}(\boldsymbol{\omega}), && \text{(compare with } \underline{\omega}^* = \mu\underline{\omega}\text{)}. \end{aligned} \tag{4.21}$$

For homogeneous natural BCs, the resulting discrete scheme is: Find $(\mathbf{p}^*, \mathbf{u}) \in \mathcal{V}_{\perp\mathbf{1}} \times \mathcal{E}$ such that

$$\begin{cases} \widetilde{\mathsf{CURL}} \cdot \mathsf{H}_\mu^{\mathcal{F}\widetilde{\mathcal{E}}} \cdot \mathsf{CURL}(\mathbf{u}) + \mathsf{H}_\rho^{\mathcal{E}\widetilde{\mathcal{F}}} \cdot \mathsf{GRAD}(\mathbf{p}^*) = \mathsf{S}^{\mathsf{vb}}(\rho, \underline{f}^*), \\ -\widetilde{\mathsf{DIV}} \cdot \mathsf{H}_\rho^{\mathcal{E}\widetilde{\mathcal{F}}}(\mathbf{u}) = 0_{\widetilde{\mathcal{C}}}. \end{cases} \tag{4.22}$$

The discrete system (4.22) is a saddle-point problem of size #V+#E. Namely, $\widetilde{\mathsf{CURL}} \cdot \mathsf{H}_\mu^{\mathcal{F}\widetilde{\mathcal{E}}} \cdot \mathsf{CURL}$ is SPD since CURL and $\widetilde{\mathsf{CURL}}$ are adjoint (cf. Proposition 3.16) and $\mathsf{H}_\mu^{\mathcal{F}\widetilde{\mathcal{E}}}$ is SPD by construction. In addition, $\mathsf{H}_\rho^{\mathcal{E}\widetilde{\mathcal{F}}} \cdot \mathsf{GRAD}$ and $-\widetilde{\mathsf{DIV}} \cdot \mathsf{H}_\rho^{\mathcal{E}\widetilde{\mathcal{F}}}$ are adjoint, since $\mathsf{H}_\rho^{\mathcal{E}\widetilde{\mathcal{F}}}$ is symmetric by construction and $-\mathsf{GRAD}$ and $\widetilde{\mathsf{DIV}}$ are adjoint (cf. Proposition 3.16). The right-hand side $\mathsf{S}^{\mathsf{vb}}(\rho, \underline{f}^*) \in \widetilde{\mathcal{F}}$ discretizes the external load $\rho\underline{f}^*$. Two discretizations of the external load are studied in Section 9.1 according to the nature of $\underline{f}^*$ (with a large curl-free or divergence-free part).

We observe that in (4.22), mass balance holds in each dual cell and force balance across each dual face. Specifically,

$$\boldsymbol{\tau}_{\tilde{\mathrm{f}}(\mathrm{e})} + \mathbf{g}_{\tilde{\mathrm{f}}(\mathrm{e})} = \mathsf{S}^{\mathsf{vb}}(\rho, \underline{f}^*)|_{\tilde{\mathrm{f}}(\mathrm{e})}, \qquad \forall \mathrm{e} \in \mathrm{E}, \tag{4.23a}$$

$$\sum_{\tilde{\mathrm{f}} \in \widetilde{\mathrm{F}}_{\tilde{\mathrm{c}}(\mathrm{v})}} \iota_{\tilde{\mathrm{f}},\tilde{\mathrm{c}}(\mathrm{v})} \boldsymbol{\phi}_{\tilde{\mathrm{f}}} = 0, \qquad \forall \mathrm{v} \in \mathrm{V}, \tag{4.23b}$$

with the discrete shear stress $\boldsymbol{\tau} := \widetilde{\mathsf{CURL}}(\boldsymbol{\omega}^*) \in \widetilde{\mathcal{F}}$ and the discrete pressure gradient $\mathbf{g} := \mathsf{H}_\rho^{\mathcal{E}\widetilde{\mathcal{F}}} \cdot \mathsf{GRAD}(\mathbf{p}^*) \in \widetilde{\mathcal{F}}$. All the relations in (4.22) between DoFs and discrete operators are summarized in Figure 4.3.

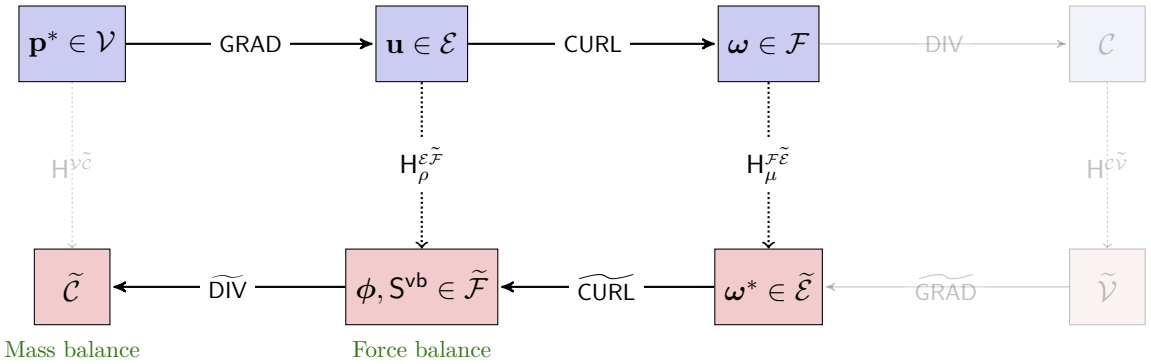

Figure 4.3 – Tonti diagram of vertex-based pressure schemes for the Stokes equations.

Remark 4.6 (Non-homogeneous natural BCs)**.** *Non-homogeneous natural BCs can be easily incorporated by modifying the right-hand side of* (4.22) *accordingly. This point is detailed in the EDF R&D technical report (Rb) mentioned in Chapter 1.*

Remark 4.7 (Essential BCs)**.** *Essential BCs for* (4.14) *are* $\underline{u} \times \underline{\nu}_{\partial\Omega} = \underline{u}_\tau^{\mathrm{bc}}$ *and* $p^* = p^{\mathrm{bc}}$ *on* $\partial\Omega$*. Such BCs can be enforced strongly by removing the corresponding DoFs from the discrete spaces or weakly by a (consistent) penalty method using the full spaces of DoFs. The analysis*

of vertex-based pressure schemes with essential BCs is left for future work; the main point consists of either deriving suitable discrete Poincaré inequalities on smaller spaces of DoFs if strong enforcement is considered or analyzing the consistency and penalty terms if weak enforcement is considered.

4.2.3 Cell-based pressure schemes

Cell-based pressure schemes rely on the three-field curl formulation (4.13). Introducing the mass density ρ and the viscosity μ leads to

$$\begin{cases} -\mu^{-1}\underline{\omega}^* + \underline{\mathrm{curl}}(\rho^{-1}\underline{\phi}) = \underline{0}, & \text{in } \Omega, \\ \rho^{-1}\,\underline{\mathrm{curl}}(\underline{\omega}^*) + \underline{\mathrm{grad}}(p^*) = \underline{f}^*, & \text{in } \Omega, \\ \mathrm{div}(\underline{\phi}) = 0, & \text{in } \Omega, \end{cases} \tag{4.24}$$

recalling that $\underline{\phi} = \rho\underline{u}$, $\underline{\omega} = \underline{\mathrm{curl}}(\underline{u})$, $\underline{\omega}^* = \mu\underline{\omega}$, $p^* = \rho^{-1}p$, and $\underline{f}^* = \rho^{-1}\underline{f}$. We focus on natural BCs for (4.24), which are given by

$$\underline{u} \times \underline{\nu}_{\partial\Omega} = \underline{u}_\tau^{\mathrm{bc}}, \quad p^* = p^{\mathrm{bc}}, \qquad \text{on } \partial\Omega, \tag{4.25}$$

with data $\underline{u}_\tau^{\mathrm{bc}}$ and p^{bc}. A discussion similar to that in Remark 4.7 can be made regarding essential BCs.

At the continuous level, the unknowns are the pressure potential p^*, the mass flux $\underline{\phi}$, and the viscous stress circulation $\underline{\omega}^*$. The DoFs of the pressure potential, denoted by $\mathbf{p}^*$, are located at dual mesh vertices (in one-to-one pairing with primal mesh cells). The DoFs of the mass flux, denoted by $\boldsymbol{\phi}$, are located at primal faces, while the DoFs of the viscous stress circulation, denoted by $\boldsymbol{\omega}^*$, are located at primal edges. There are two discrete Hodge operators, one related to the (reciprocal of) the mass density ρ and the other to the (reciprocal of) the viscosity μ such that

$$\mathsf{H}_{\rho^{-1}}^{\mathcal{F}\widetilde{\mathcal{E}}} : \mathcal{F} \to \widetilde{\mathcal{E}} \qquad \text{and} \qquad \mathsf{H}_{\mu^{-1}}^{\mathcal{E}\widetilde{\mathcal{F}}} : \mathcal{E} \to \widetilde{\mathcal{F}}. \tag{4.26}$$

These operators allow us to define respectively the discrete velocity located at dual edges and the discrete vorticity at dual faces as follows:

$$\begin{aligned} &\mathbf{u} = \mathsf{H}_{\rho^{-1}}^{\mathcal{F}\widetilde{\mathcal{E}}}(\boldsymbol{\phi}), && \text{(compare with } \underline{u} = \rho^{-1}\underline{\phi}\text{)}, \\ &\boldsymbol{\omega} := \mathsf{H}_{\mu^{-1}}^{\mathcal{E}\widetilde{\mathcal{F}}}(\boldsymbol{\omega}^*), && \text{(compare with } \underline{\omega} = \mu^{-1}\underline{\omega}^*\text{)}. \end{aligned} \tag{4.27}$$

Moreover, the following relation holds:

$$\boldsymbol{\omega} = \widetilde{\mathsf{CURL}}(\mathbf{u}). \tag{4.28}$$

The cell-based pressure scheme with homogeneous natural BCs is: Find $(\mathbf{p}^*, \boldsymbol{\phi}, \boldsymbol{\omega}^*) \in \widetilde{\mathcal{V}} \times \mathcal{F} \times \mathcal{E}$ such that

$$\begin{cases} -\mathsf{H}_{\mu^{-1}}^{\mathcal{E}\widetilde{\mathcal{F}}}(\boldsymbol{\omega}^*) + \widetilde{\mathsf{CURL}} \cdot \mathsf{H}_{\rho^{-1}}^{\mathcal{F}\widetilde{\mathcal{E}}}(\boldsymbol{\phi}) = 0_{\widetilde{\mathcal{F}}}, \\ \mathsf{H}_{\rho^{-1}}^{\mathcal{F}\widetilde{\mathcal{E}}} \cdot \mathsf{CURL}(\boldsymbol{\omega}^*) + \widetilde{\mathsf{GRAD}}(\mathbf{p}^*) = \mathsf{S}^{\mathsf{cb}}(\rho, \underline{f}^*), \\ -\mathsf{DIV}(\boldsymbol{\phi}) = 0_{\mathcal{C}}. \end{cases} \tag{4.29}$$

This discrete system is a "double" saddle-point problem of size #C + #F + #E. Namely, $\mathsf{H}_{\rho^{-1}}^{\mathcal{F}\widetilde{\mathcal{E}}} \cdot \mathsf{CURL}$ and $\widetilde{\mathsf{CURL}} \cdot \mathsf{H}_{\rho^{-1}}^{\mathcal{F}\widetilde{\mathcal{E}}}$ are adjoint, $\mathsf{H}_{\mu^{-1}}^{\mathcal{E}\widetilde{\mathcal{F}}}$ is SPD, and $\widetilde{\mathsf{GRAD}}$ and $-\mathsf{DIV}$ are adjoint. These properties are readily verified using the adjunction properties between discrete differential operators (cf. Proposition 3.16) and the fact that $\mathsf{H}_{\rho^{-1}}^{\mathcal{F}\widetilde{\mathcal{E}}}$ and $\mathsf{H}_{\mu^{-1}}^{\mathcal{E}\widetilde{\mathcal{F}}}$ are SPD by construction. The right-hand side $\mathsf{S}^{\mathsf{cb}}(\rho, \underline{f}) \in \widetilde{\mathcal{E}}$ discretizes the external load $\underline{f}$. Two discretizations of the external load are studied in Section 9.2 according to the nature of $\underline{f}^*$ (with a large curl-free or divergence-free part). Furthermore, non-homogeneous natural BCs can be easily incorporated

by modifying the right-hand side of (4.29) accordingly. We observe that in (4.29), mass balance holds in each primal cell and force balance along each dual edge. Specifically,

$$\boldsymbol{\tau}_{\tilde{\mathrm{e}}(\mathrm{f})} + \mathbf{g}_{\tilde{\mathrm{e}}(\mathrm{f})} = \mathsf{S}^{\mathsf{cb}}(\rho, \underline{f}^*)|_{\tilde{\mathrm{e}}(\mathrm{f})}, \qquad \forall \mathrm{f} \in \mathrm{F}, \tag{4.30a}$$

$$\sum_{\mathrm{f}\in\mathrm{F_c}} \iota_{\mathrm{f,c}} \boldsymbol{\phi}_{\mathrm{f}} = 0, \qquad \forall \mathrm{c} \in \mathrm{C}, \tag{4.30b}$$

with the discrete shear stress $\boldsymbol{\tau} := \mathsf{H}^{\mathcal{F}\tilde{\mathcal{E}}}_{\rho^{-1}} \cdot \mathsf{CURL}(\boldsymbol{\omega}^*) \in \widetilde{\mathcal{E}}$ and the discrete pressure gradient $\mathbf{g} := \widetilde{\mathsf{GRAD}}(\mathbf{p}^*) \in \widetilde{\mathcal{E}}$. All the relations in (4.29) between DoFs and discrete operators are summarized in Figure 4.4.

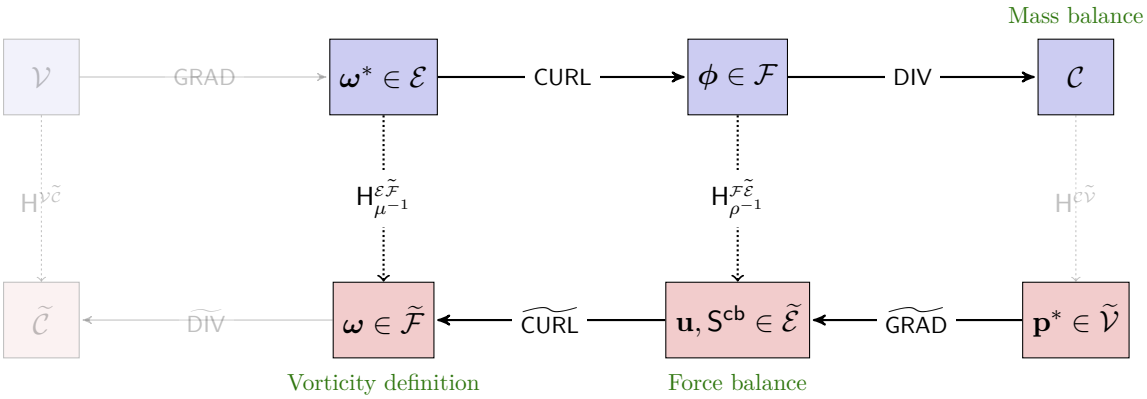

Figure 4.4 – Tonti diagram of cell-based pressure schemes for the Stokes equations.

Part II

Theoretical framework

Chapter 5

Polyhedral meshes

Contents

In this part, we set the mathematical foundations of the CDO framework. This chapter specifically gathers useful concepts to handle polyhedral meshes. In Section 5.1, we introduce the notion of mesh regularity in the twofold context of polyhedral meshes and dual meshes. In Section 5.2, we introduce the *barycentric subdivision* of a polyhedral mesh. The barycentric subdivision plays a salient role in this thesis since we often consider barycentric dual meshes.

5.1 Mesh regularity

In this section, we define a first class of meshes satisfying some mesh regularity requirements. We formulate these requirements by introducing a simplicial submesh. The advantage is that we can then use concepts of FE approximation theory in the analysis. Mesh regularity is an essential ingredient to establish stability and to derive *a priori* error estimates of CDO schemes.

Cellular complex. The primal mesh $\mathrm{M} = \{\mathrm{V}, \mathrm{E}, \mathrm{F}, \mathrm{C}\}$ (cf. Section 3.1.1) has the structure of a *cellular complex*; see, *e.g.*, (Christiansen *et al.*, 2011, § 5.1).

A generic element x of M is a closed subset of Ω which is homeomorphic by a bi-Lipschitz map to the closed unit ball of $\mathbb{R}^k$ for some $0 \le k \le 3$ ($k = 0$ for vertices, $k = 1$ for edges, $k = 2$ for faces, and $k = 3$ for cells). If $k = 0$, then the closed unit ball is set to $\{0\}$. For $k \ge 1$, the boundary of an element x, denoted by ∂x, is the image of the unit sphere of $\mathbb{R}^k$ by the chosen homeomorphism, and its interior is $\mathrm{x} \setminus \partial\mathrm{x}$. The properties of the cellular complex are as follows:

(a) Distinct elements of M have disjoint interiors.

(b) The boundary of any element of M is a union of elements of M.

(c) The union of all elements of M is Ω.

(d) The intersection of two elements of M is a union of elements of M.

Contrary to the primal mesh, the dual mesh $\widetilde{\mathrm{M}} = \{\widetilde{\mathrm{V}}, \widetilde{\mathrm{E}}, \widetilde{\mathrm{F}}, \widetilde{\mathrm{C}}\}$ is not a cellular complex as a consequence of the one-to-one pairing between primal and dual entities. Namely, some part of the boundary of a k-dimensional entity ($1 \le k \le 3$) in $\widetilde{\mathrm{M}}$ is not a union of $(k-1)$-dimensional entities in $\widetilde{\mathrm{M}}$ if this entity touches the boundary $\partial\Omega$ (cf. Section 3.3.1).

Simplicial subcomplex. We first introduce the concept of simplicial subcomplex on which the mesh regularity will be stated.

Definition 5.1 (Simplex)**.** *For all $1 \le k \le 3$, given $(k+1)$ points $\{\underline{x}_0, \ldots, \underline{x}_k\}$, $\mathfrak{s}_{0,\ldots,k}$ denotes the convex hull of these points (yielding, up to degenerate cases, a segment for $k = 1$, a triangle for $k = 2$, and a tetrahedron for $k = 3$).*

Definition 5.2 (Simplicial subcomplex)**.** $\mathfrak{S}(\mathrm{M}, \widetilde{\mathrm{M}})$ *is a simplicial subcomplex common to* M *and* $\widetilde{\mathrm{M}}$ *if it satisfies the following properties:*

(i) $\mathfrak{S}(\mathrm{M}, \widetilde{\mathrm{M}})$ *is a cellular complex consisting of a finite number of tetrahedra $\mathfrak{c} \in \mathfrak{C}$, triangles $\mathfrak{t} \in \mathfrak{T}$, edges $\mathfrak{e} \in \mathfrak{E}$, and vertices $\mathfrak{v} \in \mathfrak{V}$, so that $\mathfrak{S}(\mathrm{M}, \widetilde{\mathrm{M}}) := \{\mathfrak{V}, \mathfrak{E}, \mathfrak{T}, \mathfrak{C}\}$ collects all of these entities;*

(ii) Any primal cell $\mathrm{c} \in \mathrm{C}$ *and any dual cell* $\tilde{\mathrm{c}} \in \widetilde{\mathrm{C}}$ *can be decomposed into a finite number of tetrahedra $\mathfrak{c} \in \mathfrak{C}$, called subtetrahedra. Any primal face* $\mathrm{f} \in \mathrm{F}$ *and any dual face* $\tilde{\mathrm{f}} \in \widetilde{\mathrm{F}}$ *can be decomposed into a finite number of triangles $\mathfrak{t} \in \mathfrak{T}$. Any primal edge* $\mathrm{e} \in \mathrm{E}$ *and any dual edge* $\tilde{\mathrm{e}} \in \widetilde{\mathrm{E}}$ *can be decomposed into a finite number of edges $\mathfrak{e} \in \mathfrak{E}$.*

Remark 5.3 (Barycentric subdivision)**.** *The simplicial subcomplex from Definition 5.2 appears naturally if the dual mesh is built from a barycentric subdivision of each cell, as described in Section 5.2 below.*

Definition 5.4 (Diameter)**.** *For all* $\mathrm{c} \in \mathrm{C}$*, h_c denotes the diameter of the cell* c*.*

$$h_\mathrm{c} := \max_{\underline{x}_1, \underline{x}_2 \in \mathrm{c}} |\underline{x}_1 - \underline{x}_2|, \tag{5.1}$$

where $|\underline{x}_1 - \underline{x}_2|$ denotes the Euclidian distance between $\underline{x}_1$ and $\underline{x}_2$. Moreover, $h := \max_{\mathrm{c}\in\mathrm{C}} h_\mathrm{c}$ denotes the size of the mesh M*.*

Mesh regularity. When working with polyhedral meshes, a rather general way to formulate mesh regularity is the following.

Definition 5.5 (Class **(MR)**)**.** *Consider a sequence of primal meshes $(\mathrm{M}_n)_{n\ge1}$ such that the size of $\mathrm{M}_n \to 0$ as $n \to +\infty$. Denote $\widetilde{\mathrm{M}}_n$ the dual mesh related to M_n. A mesh sequence is of class* **(MR)** *if for all $n \ge 1$, there exists a simplicial subcomplex $\mathfrak{S}(\mathrm{M}_n, \widetilde{\mathrm{M}}_n)$ where the finite number of subtetrahedra, triangles, and edges in Definition 5.2(ii) is uniform in n, and which is shape-regular (in the usual sense of Ciarlet (1978)), i.e. it verifies the following condition: There exists $\varrho > 0$ (independent of n) such that, for all subtetrahedra $\mathfrak{c} \in \mathfrak{C}$, the following inequality holds:*

$$\varrho h_\mathfrak{c} \le r_\mathfrak{c},$$

where $r_\mathfrak{c}$ is the inradius (the diameter of the largest inscribed ball) of the subtetrahedron $\mathfrak{c}$ and $h_\mathfrak{c}$ denotes the diameter of $\mathfrak{c}$ defined similarly to (5.1)*.*

(MR) is a convenient way to exploit classical techniques of FE approximation theory in the convergence analysis of CDO schemes (*e.g.*, inverse inequalities and polynomial approximation properties); see Chapter 1 of Di Pietro & Ern (2012) or Section 1.6 of Beirão da Veiga *et al.* (2014) for a detailed presentation. Note that within **(MR)**, primal faces which are non-planar are necessarily piecewise planar since they are composed of a uniformly finite number of triangles $\mathfrak{t} \in \mathfrak{T}$.

Remark 5.6 (Weaker set of assumptions on mesh regularity)**. (MR)** *can be avoided in the convergence analysis under somewhat stronger regularity assumptions on the exact solution (bounded and Lipschitz gradient); cf. Remark 6.15. For the discrete functional analysis results derived in Chapter 6 (discrete Hölder inequalities and discrete Sobolev embeddings),* **(MR)** *can be also weakened (cf. Section 6.1).*

5.2 Barycentric subdivision

In this section, we define a second class of meshes satisfying the property denoted by **(MB)**. This class of meshes is of interest since a barycentric dual mesh can be built if the mesh is of class **(MB)**.

5.2.1 From barycentric subdivision to barycentric dual mesh

Definition 5.7 (Barycenters)**.** *The barycenter of an edge* $\mathrm{e} \in \mathrm{E}$*, of a face* $\mathrm{f} \in \mathrm{F}$*, and of a cell* $\mathrm{c} \in \mathrm{C}$ *are defined as follows:*

$$\underline{x}_\mathrm{e} := \frac{1}{|\mathrm{e}|}\int_\mathrm{e} \underline{x}, \qquad \underline{x}_\mathrm{f} := \frac{1}{|\mathrm{f}|}\int_\mathrm{f} \underline{x}, \qquad \underline{x}_\mathrm{c} := \frac{1}{|\mathrm{c}|}\int_\mathrm{c} \underline{x}. \tag{5.2}$$

Definition 5.8 (Class **(MB)**)**.** *A mesh* M *belongs to the class* **(MB)** *if*

(MB) *Each face* $\mathrm{f} \in \mathrm{F}$ *is star-shaped with respect to* $\underline{x}_\mathrm{f}$ *and each cell* $\mathrm{c} \in \mathrm{C}$ *is star-shaped with respect to a point* $\underline{x}_{\bar{\mathrm{c}}} \in \mathrm{c}$.

Definition 5.9 (Barycentric subdivision)**.** *Let* M *be of class* **(MB)**. *The barycentric subdivision of each cell* $\mathrm{c} \in \mathrm{C}$ *consists of* $4(\#\mathrm{E_c})$ elementary subsimplices $\mathfrak{s}_{\mathrm{v,e,f,\bar{c}}}$ *defined for all* $\mathrm{f} \in \mathrm{F_c}$, $\mathrm{e} \in \mathrm{E_f}$*, and* $\mathrm{v} \in \mathrm{V_e}$ *as the convex hull of* $\underline{x}_\mathrm{v}$, $\underline{x}_\mathrm{e}$, $\underline{x}_\mathrm{f}$, *and* $\underline{x}_{\bar{\mathrm{c}}}$. *These subsimplices are such that*

$$\mathrm{c} = \bigcup_{\mathrm{f}\in\mathrm{F_c}} \bigcup_{\mathrm{e}\in\mathrm{E_f}} \bigcup_{\mathrm{v}\in\mathrm{V_e}} \mathfrak{s}_{\mathrm{v,e,f,\bar{c}}}, \tag{5.3}$$

see Figure 5.1.

Observe that the set $\mathrm{V_e}$ has cardinality equal to 2 and that $\cup_{\mathrm{f}\in\mathrm{F_c}}\cup_{\mathrm{e}\in\mathrm{E_f}}$ represents the union of $2\#\mathrm{E_c}$ elements. The choice of the point $\underline{x}_{\bar{\mathrm{c}}}$ is the only free parameter in a barycentric subdivision.

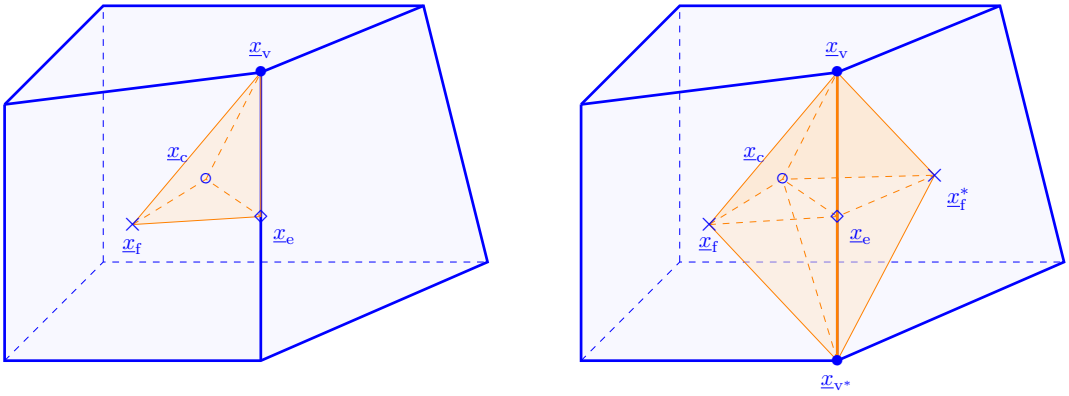

Figure 5.1 – Left: Elementary subsimplex $\mathfrak{s}_{\mathrm{v,e,f,c}}$; Right: The four elementary subsimplices ($\mathfrak{s}_{\mathrm{v,e,f,c}}$, $\mathfrak{s}_{\mathrm{v,e,f^*,c}}$, $\mathfrak{s}_{\mathrm{v^*,e,f,c}}$, $\mathfrak{s}_{\mathrm{v^*,e,f^*,c}}$) associated to an edge $\mathrm{e} \in \mathrm{E_c}$.

Definition 5.10 (Fully barycentric subdivision)**.** *If, for each cell* $\mathrm{c} \in \mathrm{C}$*, the point* $\underline{x}_{\bar{\mathrm{c}}}$ *is the barycenter of* c*, i.e.* $\underline{x}_{\bar{\mathrm{c}}} = \underline{x}_\mathrm{c}$*, then the barycentric subdivision is called* fully barycentric.

Definition 5.11 (Barycentric dual mesh)**.** *A barycentric dual mesh is built from the barycentric subdivision of the primal mesh such that*

$$\begin{aligned}
\tilde{\mathrm{v}}(\mathrm{c}) &:= \mathfrak{s}_{\bar{\mathrm{c}}}, && \forall \mathrm{c} \in \mathrm{C},\\
\tilde{\mathrm{e}}(\mathrm{f}) &:= \bigcup_{\mathrm{c}\in\mathrm{C_f}} \mathfrak{s}_{\mathrm{f,\bar{c}}}, && \forall \mathrm{f} \in \mathrm{F},\\
\tilde{\mathrm{f}}(\mathrm{e}) &:= \bigcup_{\mathrm{f}\in\mathrm{F_e}} \bigcup_{\mathrm{c}\in\mathrm{C_f}} \mathfrak{s}_{\mathrm{e,f,\bar{c}}}, && \forall \mathrm{e} \in \mathrm{E},\\
\tilde{\mathrm{c}}(\mathrm{v}) &:= \bigcup_{\mathrm{e}\in\mathrm{E_v}} \bigcup_{\mathrm{f}\in\mathrm{F_e}} \bigcup_{\mathrm{c}\in\mathrm{C_f}} \mathfrak{s}_{\mathrm{v,e,f,\bar{c}}}, && \forall \mathrm{v} \in \mathrm{V},
\end{aligned} \tag{5.4}$$

where $\mathfrak{s}_{\bar{c}} = \underline{x}_{\bar{c}}$, $\mathfrak{s}_{f,\bar{c}}$ *is the convex hull of* $\underline{x}_f$ *and* $\underline{x}_{\bar{c}}$, *and so on.*

Remark 5.12 (Primal mesh)**.** *The primal mesh entities can also be recovered from the barycentric subdivision as follows:*

$$\begin{aligned}
v &:= \mathfrak{s}_v, && \forall v \in V,\\
e &:= \bigcup_{v\in V_e} \mathfrak{s}_{v,e}, && \forall e \in E,\\
f &:= \bigcup_{e\in E_f}\bigcup_{v\in V_e} \mathfrak{s}_{v,e,f}, && \forall f \in F,\\
c &:= \bigcup_{f\in F_c}\bigcup_{e\in E_f}\bigcup_{v\in V_e} \mathfrak{s}_{v,e,f,\bar{c}}, && \forall c \in C.
\end{aligned}$$

Therefore, the barycentric subdivision is a common simplicial submesh of both primal and dual meshes.

Definition 5.13 (Vectors related to primal edges and primal faces)**.** *For any edge* $e \in E$ *and any face* $f \in F$*, we set*

$$\underline{e} := \int_e \underline{\tau}_e, \qquad \underline{f} := \int_f \underline{\nu}_f, \tag{5.5}$$

where $\underline{\tau}_e$ *is a unit tangent vector assigned to each edge and* $\underline{\nu}_f$ *is a unit normal vector assigned to each face (cf. Section 3.1.1).*

Remark 5.14. *Since* $\underline{\tau}_e$ *is a constant vector along each edge* $e \in E$, $\underline{e} = |e|\underline{\tau}_e$. *If primal faces are planar, then* $\underline{\nu}_f$ *is a constant vector on each face* $f \in F$ *and* $\underline{f} = |f|\underline{\nu}_f$.

Local dual mesh entity. The intersection of a dual mesh entity with a primal cell is frequently used in the CDO framework since the discrete Hodge operators and the reconstruction operators are designed at the level of each primal cell. This intersection is generically defined for $\tilde{y}(x) \in \{\tilde{v}(c), \tilde{e}(f), \tilde{f}(e), \tilde{c}(v)\}$ as follows:

$$\tilde{y}_c(x) := \tilde{y}(x) \cap c, \qquad \forall x \in X_c. \tag{5.6}$$

Definition 5.15 (Intersection of dual mesh entity with a primal cell)**.** *The intersection of dual mesh entities with a cell* $c \in C$ *can be defined from the barycentric subdivision as follows:*

$$\begin{aligned}
\tilde{v}_c(c) &:= \mathfrak{s}_{\bar{c}},\\
\tilde{e}_c(f) &:= \mathfrak{s}_{f,\bar{c}} && \forall f \in F_c,\\
\tilde{f}_c(e) &:= \bigcup_{f\in F_e\cap F_c} \mathfrak{s}_{e,f,\bar{c}}, && \forall e \in E_c,\\
\tilde{c}_c(v) &:= \bigcup_{e\in E_v\cap E_c}\bigcup_{f\in F_e\cap F_c} \mathfrak{s}_{v,e,f,\bar{c}}, && \forall v \in V_c.
\end{aligned} \tag{5.7}$$

For a cell $c \in C$, the local dual vertex associated to that cell is unchanged $\tilde{v}_c(c) = \tilde{v}(c)$, a local dual edge $\tilde{e}_c(f)$ associated to a face $f \in F_c$ is a straight line, a local dual face $\tilde{f}_c(e)$ associated to an edge $e \in E_c$ is the union of two triangles, and a local dual cell $\tilde{c}_c(v)$ associated to a vertex $v \in V_c$ is the union of elementary tetrahedra inside the cell c having v as common vertex.

In the general case where one considers a barycentric dual mesh, a dual edge is a broken segment and a dual face is a union of triangles, so that a dual face is piecewise planar. An illustration of local dual edges (resp. local dual faces) is depicted in Figure 5.2 (resp. Figure 5.3).

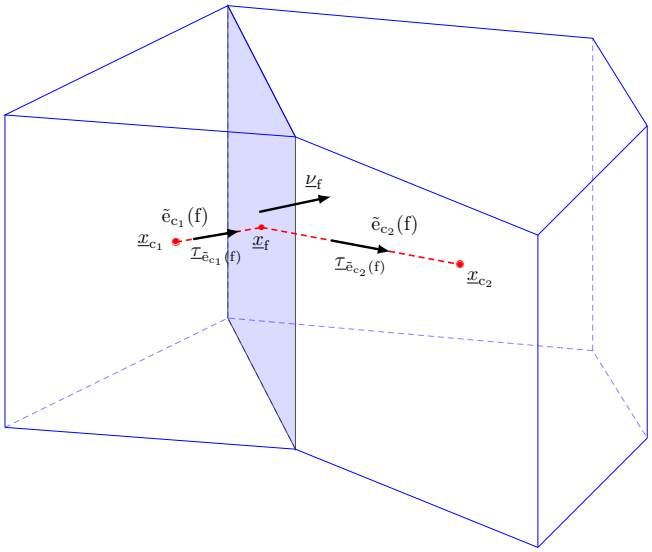

Figure 5.2 – Let c_1 and c_2 be two primal cells. For the face $\mathrm{f} \in \mathrm{F}_{\mathrm{c}_1} \cap \mathrm{F}_{\mathrm{c}_2}$, we represent the dual edge $\tilde{\mathrm{e}}(\mathrm{f})$ (red dashed line) associated to f. $\tilde{\mathrm{e}}(\mathrm{f}) = \tilde{\mathrm{e}}_{\mathrm{c}_1}(\mathrm{f}) \cup \tilde{\mathrm{e}}_{\mathrm{c}_2}(\mathrm{f})$.

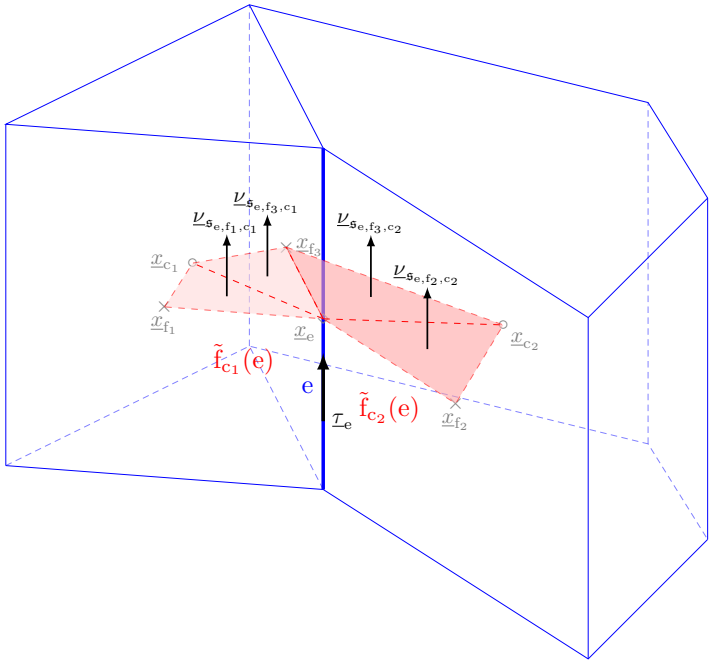

Figure 5.3 – Let c_1 and c_2 be two primal cells. For an $\mathrm{e} \in \mathrm{E}_{\mathrm{c}_1} \cap \mathrm{E}_{\mathrm{c}_2}$, we represent the dual face $\tilde{\mathrm{f}}(\mathrm{e})$ (red) associated to e. $\tilde{\mathrm{f}}(\mathrm{e})$ is composed of $\tilde{\mathrm{f}}_{\mathrm{c}_1}(\mathrm{e})$ (bright red) and $\tilde{\mathrm{f}}_{\mathrm{c}_2}(\mathrm{e})$ (dark red). Each intersection of the dual face $\tilde{\mathrm{f}}(\mathrm{e})$ with a primal cell is composed of two triangles: $\tilde{\mathrm{f}}_{\mathrm{c}_1}(\mathrm{e}) = \mathfrak{s}_{\mathrm{e},\mathrm{f}_1,\mathrm{c}_1} \cup \mathfrak{s}_{\mathrm{e},\mathrm{f}_3,\mathrm{c}_1}$ and $\tilde{\mathrm{f}}_{\mathrm{c}_2}(\mathrm{e}) = \mathfrak{s}_{\mathrm{e},\mathrm{f}_2,\mathrm{c}_2} \cup \mathfrak{s}_{\mathrm{e},\mathrm{f}_3,\mathrm{c}_2}$.

Definition 5.16 (Vectors related to local dual edges and local dual faces)**.** *Let* $c \in C$*. For all* $e \in E_c$ *and all* $f \in F_c$*, we set*

$$\underline{\tilde{e}}_c(f) := \int_{\tilde{e}_c(f)} \underline{\tau}_{\tilde{e}(f)}, \qquad \underline{\tilde{f}}_c(e) := \int_{\tilde{f}_c(e)} \underline{\nu}_{\tilde{f}(e)}, \tag{5.8}$$

where $\underline{\tau}_{\tilde{e}(f)}$ *is the unit tangent vector along* $\tilde{e}_c(f)$ *sharing the same orientation as* $\underline{\nu}_f$ *for all* $f \in F_c$ *and* $\underline{\nu}_{\tilde{f}(e)}$ *is the unit normal vector to* $\tilde{f}_c(e)$ *sharing the same orientation as* $\underline{\tau}_e$ *for all* $e \in E_c$*.*

Remark 5.17. *Since* $\underline{\tau}_{\tilde{e}(f)}$ *is a constant vector along* $\tilde{e}_c(f)$*,* $\underline{\tilde{e}}_c(f) = |\tilde{e}_c(f)|\underline{\tau}_{\tilde{e}_c(f)}$*. Since* $\underline{\nu}_{\tilde{f}(e)}$ *is a piecewise constant vector on* $\tilde{f}_c(e)$*,* $\underline{\tilde{f}}_c(e) = \sum_{f \in F_c \cap F_e} |\mathfrak{s}_{e,f,\bar{c}}| \underline{\nu}_{\mathfrak{s}_{e,f,\bar{c}}}$ *where* $\underline{\nu}_{\mathfrak{s}_{e,f,\bar{c}}}$ *is the unit normal vector to* $\mathfrak{s}_{e,f,\bar{c}}$ *sharing the same orientation as* $\underline{\tau}_e$ *for each face* $f \in F_c \cap F_e$*; see Figure 5.3. Moreover, we readily verify that* $\underline{\tilde{f}}(e) = \sum_{c \in C_e} \underline{\tilde{f}}_c(e)$ *and* $\underline{\tilde{e}}(f) = \sum_{c \in C_f} \underline{\tilde{e}}_c(f)$*.*

5.2.2 Entity-based partitions of a cell

We now introduce three partitions of a cell $c \in C$ hinging on the barycentric subdivision of c: a vertex-based partition relying on subvolumes $\mathfrak{p}_{v,c}$ attached to each vertex $v \in V_c$, an edge-based partition relying on subvolumes $\mathfrak{p}_{e,c}$ attached to each edge $e \in E_c$, and a faced-based partition relying on subvolumes $\mathfrak{p}_{f,c}$ attached to each face $f \in F_c$ (see Figure 5.4). These partitions are used in the definition of discrete functional norms (cf. Section 6.1.1) and in the definition of the reconstruction operators (cf. Section 7.3).

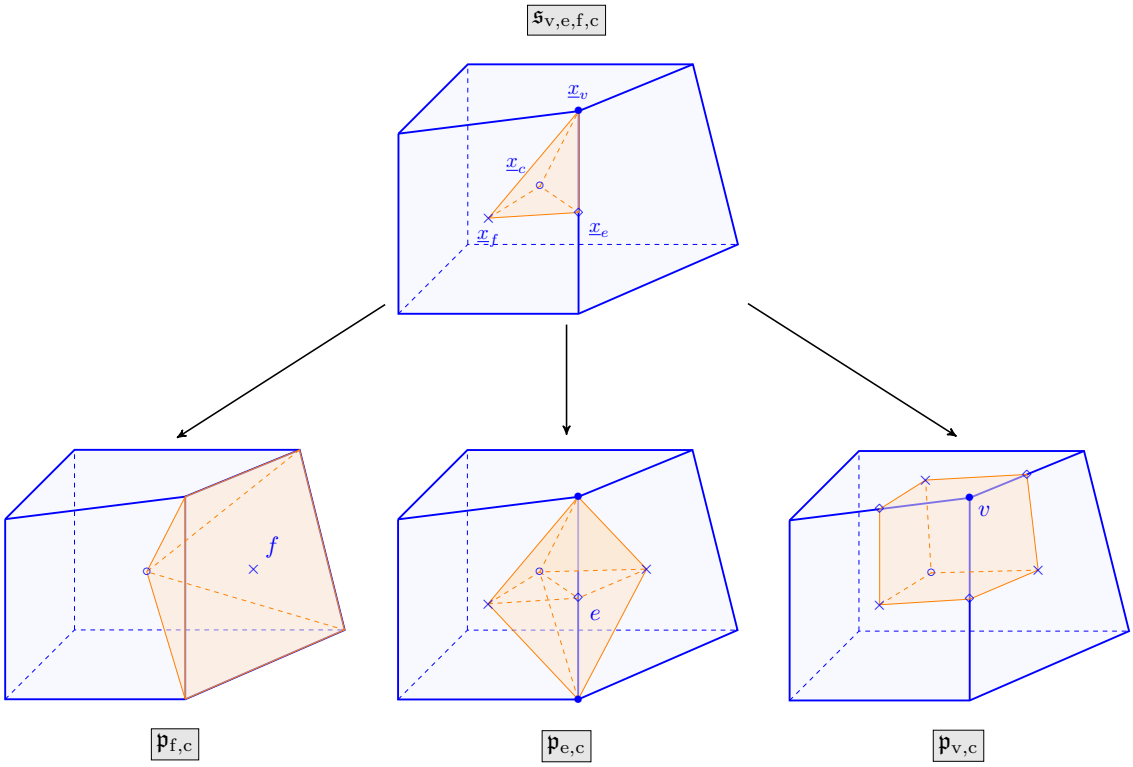

Figure 5.4 – Hexahedral mesh cell c. Above: Elementary subsimplex $\mathfrak{s}_{v,e,f,c}$ of the barycentric subdivision; Below: Example for $\mathfrak{p}_{f,c}$ (left), $\mathfrak{p}_{e,c}$ (center), and $\mathfrak{p}_{v,c}$ (right).

Definition 5.18 (Partitions of a primal cell)**.** *For each cell* $\mathrm{c} \in \mathrm{C}$*, we set:*

$$\mathfrak{p}_{\mathrm{v,c}} := \bigcup_{\mathrm{e}\in\mathrm{E_v}\cap\mathrm{E_c}} \bigcup_{\mathrm{f}\in\mathrm{F_e}\cap\mathrm{F_c}} \mathfrak{s}_{\mathrm{v,e,f,\bar{c}}}, \quad \forall \mathrm{v} \in \mathrm{V_c}; \tag{5.9a}$$

$$\mathfrak{p}_{\mathrm{e,c}} := \bigcup_{\mathrm{f}\in\mathrm{F_e}\cap\mathrm{F_c}} \bigcup_{\mathrm{v}\in\mathrm{V_e}} \mathfrak{s}_{\mathrm{v,e,f,\bar{c}}}, \quad \forall \mathrm{e} \in \mathrm{E_c}; \tag{5.9b}$$

$$\mathfrak{p}_{\mathrm{f,c}} := \bigcup_{\mathrm{e}\in\mathrm{E_f}} \bigcup_{\mathrm{v}\in\mathrm{V_f}} \mathfrak{s}_{\mathrm{v,e,f,\bar{c}}}, \quad \forall \mathrm{f} \in \mathrm{F_c}. \tag{5.9c}$$

The vertex-based partition is denoted by $\mathfrak{P}_{\mathrm{V,c}} := \{\mathfrak{p}_{\mathrm{v,c}}\}_{\mathrm{v}\in\mathrm{V_c}}$*, the edge-based partition* $\mathfrak{P}_{\mathrm{E,c}} := \{\mathfrak{p}_{\mathrm{e,c}}\}_{\mathrm{e}\in\mathrm{E_c}}$*, and the face-based partition* $\mathfrak{P}_{\mathrm{F,c}} := \{\mathfrak{p}_{\mathrm{f,c}}\}_{\mathrm{f}\in\mathrm{F_c}}$*.*

Consider a cell $\mathrm{c} \in \mathrm{C}$. For each edge $\mathrm{e} \in \mathrm{E_c}$ and for each face $\mathrm{f} \in \mathrm{F_c}$, the following identities hold:

$$|\mathfrak{p}_{\mathrm{e,c}}| = \frac{1}{d}\,\underline{\mathrm{e}} \cdot \tilde{\underline{\mathrm{f}}}_{\mathrm{c}}(\mathrm{e}), \qquad |\mathfrak{p}_{\mathrm{f,c}}| = \frac{1}{d}\,\underline{\mathrm{f}} \cdot \tilde{\underline{\mathrm{e}}}_{\mathrm{c}}(\mathrm{f}), \tag{5.10}$$

with d denoting the space dimension (typically $d = 3$). Moreover, observe that $\mathfrak{p}_{\mathrm{v,c}} = \mathrm{c} \cap \tilde{\mathrm{c}}(\mathrm{v})$ for all $\mathrm{v} \in \mathrm{V_c}$. Therefore, we readily infer from (5.9a) that

$$\sum_{\mathrm{f}\in\mathrm{F_v}\cap\mathrm{F_c}} \sum_{\mathrm{e}\in\mathrm{E_v}\cap\mathrm{E_f}} |\mathfrak{s}_{\mathrm{v,e,f,\bar{c}}}| = |\mathrm{c} \cap \tilde{\mathrm{c}}(\mathrm{v})|. \tag{5.11}$$

Proposition 5.19 (Submesh)**.** *Let* $\mathrm{c} \in \mathrm{C}$*. The partition* $\mathfrak{P}_{\mathrm{V,c}}$ *(resp.* $\mathfrak{P}_{\mathrm{E,c}}$*, and* $\mathfrak{P}_{\mathrm{F,c}}$*) forms a partition of unity of* c *in the sense that it constitutes a submesh of the cell* c*. In particular,*

$$\sum_{\mathrm{x}\in\mathrm{X_c}} |\mathfrak{p}_{\mathrm{x,c}}| = |\mathrm{c}|. \tag{5.12}$$

where $\mathrm{X} \in \{\mathrm{V}, \mathrm{E}, \mathrm{F}\}$*.*

Remark 5.20 (Links with different schemes)**.** $\mathfrak{P}_{\mathrm{V,c}}$ *is directly related to the dual mesh since* $\mathfrak{p}_{\mathrm{v,c}} = \tilde{\mathrm{c}}(\mathrm{v}) \cap \mathrm{c}$ *for all* $\mathrm{c} \in \mathrm{C}$ *and all* $\mathrm{v} \in \mathrm{V_c}$*.* $\mathfrak{P}_{\mathrm{F,c}}$ *is directly related to what is called a* diamond *mesh in DDFV (see Andreianov* et al.*, 2012, for instance). An equivalent pyramidal submesh is also considered by Eymard* et al. *(2010) or by Di Pietro & Lemaire (2015) for the stabilization of the reconstruction operator. In the DGA reconstruction introduced by (Codecasa* et al.*, 2010),* $\mathfrak{P}_{\mathrm{E,c}}$ *is considered for the reconstruction from edge DoFs, while* $\mathfrak{P}_{\mathrm{F,c}}$ *is considered for the reconstruction from face DoFs (cf. Section 7.3.1).*

5.2.3 Properties of the barycentric subdivision

This section collects useful properties of the barycentric subdivision.

Proposition 5.21 (Triangle $\mathfrak{t}_{\mathrm{ef}}$)**.** *Let* $\mathrm{c} \in \mathrm{C}$*. For each face* $\mathrm{f} \in \mathrm{F_c}$ *and each edge* $\mathrm{e} \in \mathrm{E_f}$*, we define* $\mathfrak{t}_{\mathrm{ef}} := \bigcup_{\mathrm{v}\in\mathrm{V_e}} \mathfrak{s}_{\mathrm{v,e,f}}$ *(see Figure 5.5 left). Then, for any* $\mathrm{f} \in \mathrm{F_c}$ *and any vertex* $\mathrm{v} \in \mathrm{V_f}$*, the following identity holds:*

$$\frac{1}{2} \sum_{\mathrm{e}\in\mathrm{E_v}\cap\mathrm{E_f}} |\mathfrak{t}_{\mathrm{ef}}| = |\mathrm{f} \cap \tilde{\mathrm{c}}(\mathrm{v})|. \tag{5.13}$$

Proof. By construction, $|\mathrm{f} \cap \tilde{\mathrm{c}}(\mathrm{v})| = \sum_{\mathrm{e}\in\mathrm{E_v}\cap\mathrm{E_f}} |\mathfrak{s}_{\mathrm{v,e,f}}|$ (see Figure 5.5 right). Moreover, for any edge $\mathrm{e} \in \mathrm{E_f}$ with vertices v_0 and $\mathrm{v}_1 \in \mathrm{V_e}$, $|\mathfrak{t}_{\mathrm{ef}}| = \frac{1}{2}|\mathfrak{s}_{\mathrm{v}_0,\mathrm{e,f}}| = \frac{1}{2}|\mathfrak{s}_{\mathrm{v}_1,\mathrm{e,f}}|$ since $\underline{x}_{\mathrm{e}}$ is the barycenter of e. Thus, $|\mathrm{f} \cap \tilde{\mathrm{c}}(\mathrm{v})| = \sum_{\mathrm{e}\in\mathrm{E_v}\cap\mathrm{E_f}} |\mathfrak{s}_{\mathrm{v,e,f}}| = \frac{1}{2} \sum_{\mathrm{e}\in\mathrm{E_v}\cap\mathrm{E_f}} |\mathfrak{t}_{\mathrm{ef}}|$. □

Proposition 5.22 (Link between $\mathfrak{p}_{\mathrm{f,c}}$ and $\tilde{\mathrm{c}}(\mathrm{v}) \cap \mathrm{c}$.)**.** *Consider a barycentric subdivision of a cell* $\mathrm{c} \in \mathrm{C}$*. Then,*

$$\sum_{\mathrm{f}\in\mathrm{F_c}\cap\mathrm{F_v}} \frac{|\mathrm{f} \cap \tilde{\mathrm{c}}(\mathrm{v})|}{|\mathrm{f}|} |\mathfrak{p}_{\mathrm{f,c}}| = |\mathrm{c} \cap \tilde{\mathrm{c}}(\mathrm{v})|. \tag{5.14}$$

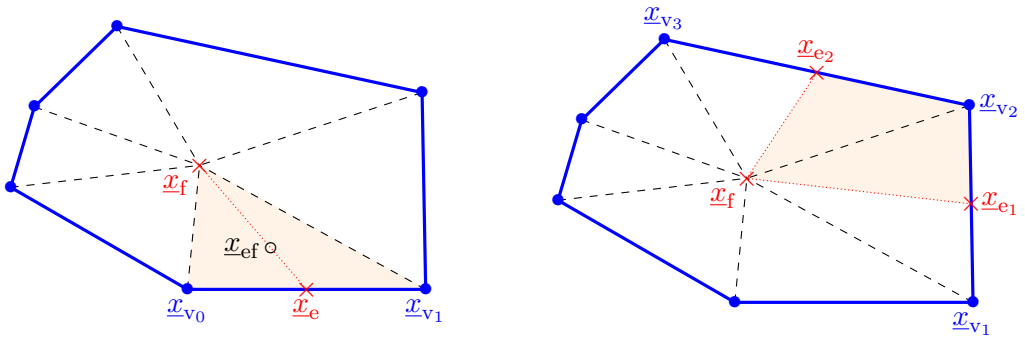

Figure 5.5 – Example of a polygonal face f. Left: For $e \in E_f$ and $v_0, v_1 \in V_e$, the triangle $\mathfrak{t}_{ef}$ is highlighted in orange. Right: For $v_2 \in V_f$, $f \cap \tilde{c}(v_2)$ is highlighted in orange.

Proof. Let $c \in C$. Let $\mathfrak{h}_{\mathfrak{p},f}$ denote the height of the cone $\mathfrak{p}_{f,c}$ for any face $f \in F_c$ (see Figure 5.6 right) so that $|\mathfrak{p}_{f,c}| = \frac{1}{3}\mathfrak{h}_{\mathfrak{p},f}|f|$ and $\frac{1}{6}\mathfrak{h}_{\mathfrak{p},f}|\mathfrak{t}_{ef}| = |\mathfrak{s}_{v,e,f,\tilde{c}}|$. For any $f \in F_c$ and any edge $e \in E_f$, we define $\mathfrak{p}_{ef,c} := \mathfrak{p}_{e,c} \cap \mathfrak{p}_{f,c}$ (see Figure 5.6 left) so that $|\mathfrak{p}_{f,c}| = \sum_{e\in E_f}|\mathfrak{p}_{ef,c}|$. Since $|f| = \sum_{e\in E_f}|\mathfrak{t}_{ef}|$, the following identity holds:

$$|\mathfrak{p}_{f,c}| = \sum_{e\in E_f}|\mathfrak{p}_{ef,c}| = \frac{1}{3}\mathfrak{h}_{\mathfrak{p},f}\sum_{e\in E_f}|\mathfrak{t}_{ef}| = \frac{1}{3}\mathfrak{h}_{\mathfrak{p},f}|f|.$$

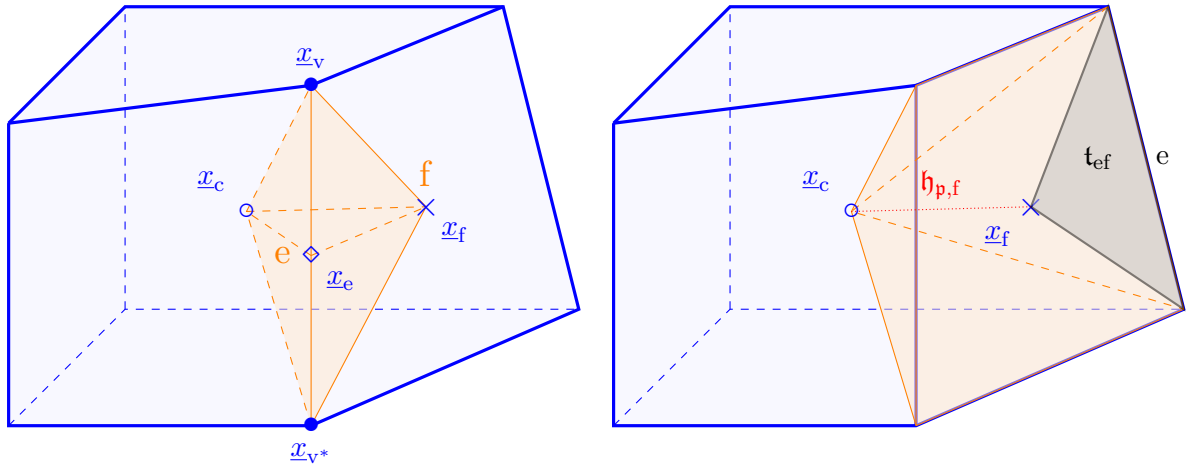

Figure 5.6 – Let c be a hexahedron. Left: For a face $f \in F_c$ and an edge $e \in E_f$, the subvolume $\mathfrak{p}_{ef,c}$ is highlighted. Right: For $f \in F_c$, $\mathfrak{p}_{f,c}$ (in orange), its height $\mathfrak{h}_{\mathfrak{p},f}$ (red dotted line), and the triangle $\mathfrak{t}_{ef}$ (gray) for an edge $e \in E_f$ are highlighted.

Using this identity together with (5.13), we infer that

$$\begin{aligned}\sum_{f\in F_v\cap F_c}\frac{|f\cap\tilde{c}(v)|}{|f|}|\mathfrak{p}_{f,c}| &= \sum_{f\in F_v\cap F_c}\frac{1}{3}\frac{|f\cap\tilde{c}(v)|}{|f|}|f|\mathfrak{h}_{\mathfrak{p},f}\\ &= \sum_{f\in F_v\cap F_c}\sum_{e\in E_f\cap E_v}\frac{1}{6}\mathfrak{h}_{\mathfrak{p},f}|\mathfrak{t}_{ef}| = \sum_{f\in F_v\cap F_c}\sum_{e\in E_f\cap E_v}|\mathfrak{s}_{vefc}| = |c\cap\tilde{c}(v)|.\end{aligned}$$

□

Proposition 5.23 (Properties of $\underline{x}_f$ and $\underline{x}_c$)**.** *Let* M *be of class* **(MB)**. *Consider a barycentric subdivision of a cell* $c \in C$. *Then, the following identity holds for all* $f \in F_c$*:*

$$\sum_{v\in V_f}|f\cap\tilde{c}(v)|(\underline{x}_v - \underline{x}_f) = \underline{0}. \tag{5.15}$$

Moreover, assuming a fully barycentric subdivision, the following identity holds:

$$\sum_{\mathrm{v}\in\mathrm{V_c}} |\mathrm{c}\cap\tilde{\mathrm{c}}(\mathrm{v})|(\underline{x}_\mathrm{v}-\underline{x}_\mathrm{c}) = \underline{0}. \tag{5.16}$$

Proof. We first prove (5.15). Let $\mathfrak{t}_{\mathrm{ef}}$ be the triangle with base $\mathrm{e}\in\mathrm{E_f}$ and apex $\underline{x}_\mathrm{f}$ (see Figure 5.5 left). Consider the simplicial subdivision $\{\mathfrak{t}_{\mathrm{ef}}\}_{\mathrm{e}\in\mathrm{E_f}}$ of the face f induced by the barycentric subdivision. Denote $\underline{x}_{\mathrm{ef}}$ the barycenter of $\mathfrak{t}_{\mathrm{ef}}$. Since $\underline{x}_\mathrm{f}$ is the barycenter of f, we infer that

$$|\mathrm{f}|\underline{x}_\mathrm{f} = \int_\mathrm{f}\underline{x} = \sum_{\mathrm{e}\in\mathrm{E_f}}|\mathfrak{t}_{\mathrm{ef}}|\underline{x}_{\mathrm{ef}} = \frac{1}{3}\sum_{\mathrm{e}\in\mathrm{E_f}}\left[\sum_{\mathrm{v}\in\mathrm{V_e}}|\mathfrak{t}_{\mathrm{ef}}|\underline{x}_\mathrm{v}+|\mathfrak{t}_{\mathrm{ef}}|\underline{x}_\mathrm{f}\right] = \frac{2}{3}\sum_{\mathrm{v}\in\mathrm{V_f}}|\mathrm{f}\cap\tilde{\mathrm{c}}(\mathrm{v})|\underline{x}_\mathrm{v}+\frac{1}{3}|\mathrm{f}|\underline{x}_\mathrm{f},$$

since $\sum_{\mathrm{e}\in\mathrm{E_f}}|\mathfrak{t}_{\mathrm{ef}}| = |\mathrm{f}|$ and $\frac{1}{2}\sum_{\mathrm{e}\in\mathrm{E_v}\cap\mathrm{E_f}}|\mathfrak{t}_{\mathrm{ef}}| = |\mathrm{f}\cap\tilde{\mathrm{c}}(\mathrm{v})|$. We now prove (5.16). Recall that $\mathfrak{p}_{\mathrm{ef,c}} = \mathfrak{p}_{\mathrm{e,c}}\cap\mathfrak{p}_{\mathrm{f,c}}$ for each face $\mathrm{f}\in\mathrm{F_c}$ and each edge $\mathrm{e}\in\mathrm{E_f}$; see also Figure 7.6. Since $\underline{x}_\mathrm{c}$ is the barycenter of c, we infer that

$$\begin{aligned}|\mathrm{c}|\underline{x}_\mathrm{c} &= \int_\mathrm{c}\underline{x} = \sum_{\mathrm{f}\in\mathrm{F_c}}\sum_{\mathrm{e}\in\mathrm{E_f}}\int_{\mathfrak{p}_{\mathrm{ef,c}}}\underline{x} = \sum_{\mathrm{f}\in\mathrm{F_c}}\sum_{\mathrm{e}\in\mathrm{E_f}}\frac{|\mathfrak{p}_{\mathrm{ef,c}}|}{4}\left(\underline{x}_\mathrm{c}+\underline{x}_\mathrm{f}+\sum_{\mathrm{v}\in\mathrm{V_e}}\underline{x}_\mathrm{v}\right)\\ &= \frac{|\mathrm{c}|}{4}\underline{x}_\mathrm{c}+\frac{1}{4}\sum_{\mathrm{f}\in\mathrm{F_c}}|\mathfrak{p}_{\mathrm{f,c}}|\underline{x}_\mathrm{f}+\frac{1}{2}\sum_{\mathrm{f}\in\mathrm{F_c}}\sum_{\mathrm{e}\in\mathrm{E_f}}\sum_{\mathrm{v}\in\mathrm{V_e}}|\mathfrak{s}_{\mathrm{v,e,f,c}}|\underline{x}_\mathrm{v},\end{aligned}$$

since $\sum_{\mathrm{e}\in\mathrm{E_f}}|\mathfrak{p}_{\mathrm{ef,c}}| = |\mathfrak{p}_{\mathrm{f,c}}|$, $\sum_{\mathrm{f}\in\mathrm{f_c}}\sum_{\mathrm{e}\in\mathrm{E_f}}|\mathfrak{p}_{\mathrm{ef,c}}| = |\mathrm{c}|$ and $|\mathfrak{p}_{\mathrm{ef,c}}| = \frac{1}{2}|\mathfrak{s}_{\mathrm{v,e,f,c}}|$ for $\mathrm{v}\in\mathrm{V_e}$. Hence,

$$\begin{aligned}\frac{3}{4}|\mathrm{c}|\underline{x}_\mathrm{c} &= \frac{1}{4}\sum_{\mathrm{v}\in\mathrm{V_c}}\underline{x}_\mathrm{v}\sum_{\mathrm{f}\in\mathrm{F_v}\cap\mathrm{F_c}}\frac{|\mathrm{f}\cap\tilde{\mathrm{c}}(\mathrm{v})|}{|\mathrm{f}|}|\mathfrak{p}_{\mathrm{f,c}}|+\frac{1}{2}\sum_{\mathrm{v}\in\mathrm{V_c}}\underline{x}_\mathrm{v}\sum_{\mathrm{f}\in\mathrm{F_v}\cap\mathrm{F_c}}\sum_{\mathrm{e}\in\mathrm{E_v}\cap\mathrm{E_f}}|\mathfrak{s}_{\mathrm{v,e,f,c}}|\\ &= \frac{3}{4}\sum_{\mathrm{v}\in\mathrm{V_c}}|\mathrm{c}\cap\tilde{\mathrm{c}}(\mathrm{v})|\underline{x}_\mathrm{v},\end{aligned}$$

using (5.15) and (5.14) for the first term and (5.11) for the second term. □

Proposition 5.24. *Let* M *be of class* **(MB)**. *Assume that primal faces are planar. Then, the barycentric subdivision of a cell* $\mathrm{c}\in\mathrm{C}$ *verifies the two following identities:*

$$\sum_{\mathrm{e}\in\mathrm{E_c}}\tilde{\underline{\mathrm{f}}}_\mathrm{c}(\mathrm{e})\otimes\underline{\mathrm{e}} = |\mathrm{c}|\underline{\underline{\mathsf{Id}}}, \tag{5.17a}$$

$$\sum_{\mathrm{f}\in\mathrm{F_c}}\tilde{\underline{\mathrm{e}}}_\mathrm{c}(\mathrm{f})\otimes\underline{\mathrm{f}} = |\mathrm{c}|\underline{\underline{\mathsf{Id}}}, \tag{5.17b}$$

where $\underline{\underline{\mathsf{Id}}}$ *is the* 3×3 *identity tensor. An equivalent formulation of* (5.17) *takes the following form:*

$$\sum_{\mathrm{e}\in\mathrm{E_c}}(\underline{\mathrm{e}}\cdot\underline{a})(\tilde{\underline{\mathrm{f}}}_\mathrm{c}(\mathrm{e})\cdot\underline{b}) = |\mathrm{c}|\underline{a}\cdot\underline{b}, \qquad \forall\underline{a},\,\underline{b}\in\mathbb{R}^3, \tag{5.18a}$$

$$\sum_{\mathrm{f}\in\mathrm{F_c}}(\underline{\mathrm{f}}\cdot\underline{a})(\tilde{\underline{\mathrm{e}}}_\mathrm{c}(\mathrm{f})\cdot\underline{b}) = |\mathrm{c}|\underline{a}\cdot\underline{b}, \qquad \forall\underline{a},\,\underline{b}\in\mathbb{R}^3. \tag{5.18b}$$

Proof. Proofs of (5.17) have been given by Codecasa & Trevisan (2007) and also by Droniou & Eymard (2006) for (5.17b).

(1) Proof of (5.17b). First, observe that (5.17b) is also equivalent to

$$\sum_{\mathrm{f}\in\mathrm{F_c}}(\underline{a}\cdot\underline{\mathrm{f}})\tilde{\underline{\mathrm{e}}}_\mathrm{c}(\mathrm{f}) = |\mathrm{c}|\underline{a}, \qquad \forall\underline{a}\in\mathbb{R}^3.$$

For each cell $c \in C$, we denote by $\underline{\nu}_{f,c}$ the unit normal to the face $f \in F_c$ pointing outward c. Let x^i denote the i-*th* component of the vector $\underline{x}$. Then, using the Gauss theorem and the definition of the face barycenter, the following identities hold:

$$a^i|c| = \int_c \mathrm{div}((x^i - x_c^i)\underline{a}) = \sum_{f\in F_c}\int_f (x^i - x_c^i)\underline{a}\cdot\underline{\nu}_{f,c} = \sum_{f\in F_c} \iota_{f,c}\tilde{e}_c^i(f)(\underline{a}\cdot\iota_{f,c}\underline{f}) = \sum_{f\in F_c}(\underline{a}\cdot\underline{f})\tilde{e}_c^i(f),$$

since $\underline{\nu}_{f,c} = \iota_{f,c}\underline{\nu}_f$, $\underline{\tilde{e}}_c(f) = \iota_{f,c}(\underline{x}_f - \underline{x}_c)$, and $\iota_{f,c}^2 = 1$.

(2) Proof of (5.17a). The proof is presented for the equivalent formulation (5.18a). Let $c \in C$ and denote by $\underline{\nu}_{\partial c}(\underline{x})$ the unit normal vector pointing outward the cell c. For each edge $e \in E_c$ and each vertex $v \in V_e$, we consider the pyramid $\boldsymbol{\pi}_{v,e,c} := \cup_{f\in F_e\cap F_c}\mathfrak{s}_{v,e,f,\bar{c}}$ of base $\tilde{f}_c(e)$ and apex v (see Figure 5.7).

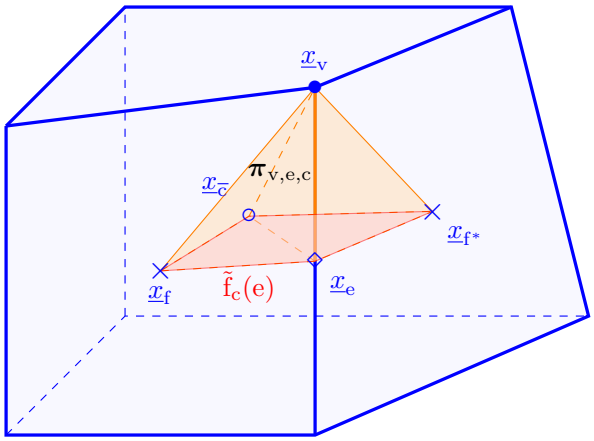

Figure 5.7 – Illustration of the pyramid $\boldsymbol{\pi}_{v,e,c}$ for an edge $e \in E_c$ and a vertex $v \in V_e$.

Its outward unit normal is denoted by $\underline{\nu}_{\partial\boldsymbol{\pi}_{v,e,c}}$. Using the Gauss-Green formula, we infer that

$$\begin{aligned}|c|\underline{a}\cdot\underline{b} &= \sum_{e\in E_c}\sum_{v\in V_e}\int_{\boldsymbol{\pi}_{v,e,c}}\underline{a}\cdot\underline{b} = \sum_{e\in E_c}\sum_{v\in V_e}\int_{\boldsymbol{\pi}_{v,e,c}}\underline{\mathrm{grad}}(\underline{a}\cdot(\underline{x}-\underline{x}_v))\cdot\underline{b}\\ &= \sum_{e\in E_c}\sum_{v\in V_e}\int_{\partial\boldsymbol{\pi}_{v,e,c}}\underline{a}\cdot(\underline{x}-\underline{x}_v)\underline{b}\cdot\underline{\nu}_{\partial\boldsymbol{\pi}_{v,e,c}},\end{aligned}$$

since $\mathrm{div}(\underline{b}) = 0$. Then, decomposing $\partial\boldsymbol{\pi}_{v,e,c}$ into $\tilde{f}_c(e)$, $\cup_{f\in F_e\cap F_c}\mathfrak{s}_{v,e,f}$, and $\cup_{f\in F_e\cap F_c}\mathfrak{s}_{v,f,\bar{c}}$, we introduce T_1, T_2, T_3 such that $|c|\underline{a}\cdot\underline{b} = \sum_{e\in E_c}\sum_{v\in V_e}(T_1+T_2+T_3)$ with

$$\begin{aligned}T_1 &= \int_{\tilde{f}_c(e)}\underline{a}\cdot(\underline{x}-\underline{x}_v)\underline{b}\cdot\underline{\nu}_{\partial\boldsymbol{\pi}_{v,e,c}},\\ T_2 &= \sum_{f\in F_e\cap F_c}\int_{\mathfrak{s}_{v,e,f}}\underline{a}\cdot(\underline{x}-\underline{x}_v)\underline{b}\cdot\underline{\nu}_{\partial c},\\ T_3 &= \sum_{f\in F_e\cap F_c}\int_{\mathfrak{s}_{v,f,\bar{c}}}\underline{a}\cdot(\underline{x}-\underline{x}_v)\underline{b}\cdot\underline{\nu}_{\partial\boldsymbol{\pi}_{v,e,c}}.\end{aligned}$$

Since $\underline{\nu}_{\partial\boldsymbol{\pi}_{v,e,f}}|_{\tilde{f}_c(e)} = \iota_{\tilde{f}(e),\tilde{c}(v)}\underline{\nu}_{\tilde{f}_c(e)}$, $\underline{x}_e - \underline{x}_v = \frac{1}{2}\iota_{\tilde{f}(e),\tilde{c}(v)}\underline{e}$, and $\iota_{\tilde{f}(e),\tilde{c}(v)}^2 = 1$, we infer that

$$\begin{aligned}T_1 &= \int_{\tilde{f}_c(e)}\iota_{\tilde{f}(e),\tilde{c}(v)}\underline{a}\cdot(\underline{x}_e-\underline{x}_v)\underline{b}\cdot\underline{\nu}_{\tilde{f}_c(e)} + \int_{\tilde{f}_c(e)}\underline{a}\cdot(\underline{x}-\underline{x}_e)\underline{b}\cdot\underline{\nu}_{\partial\boldsymbol{\pi}_{v,e,c}}\\ &= \int_{\tilde{f}_c(e)}\frac{1}{2}(\underline{a}\cdot\underline{e})(\underline{b}\cdot\underline{\nu}_{\tilde{f}_c(e)}) + \int_{\tilde{f}_c(e)}\underline{a}\cdot(\underline{x}-\underline{x}_e)\underline{b}\cdot\underline{\nu}_{\partial\boldsymbol{\pi}_{v,e,c}}.\end{aligned}$$

Thus, $\sum_{\mathrm{v}\in\mathrm{V_e}} T_1 = (\underline{a}\cdot\underline{\mathrm{e}})(\underline{b}\cdot\underline{\tilde{\mathrm{f}}}_{\mathrm{c}}(\mathrm{e}))$. For the term T_2, observe that

$$\begin{aligned}\sum_{\mathrm{e}\in\mathrm{E_c}}\sum_{\mathrm{v}\in\mathrm{V_e}} T_2 &= \sum_{\mathrm{f}\in\mathrm{F_c}}\int_{\mathrm{f}}(\underline{a}\cdot\underline{x})\underline{b}\cdot\underline{\nu}_{\partial\mathrm{c}} - \sum_{\mathrm{f}\in\mathrm{F_c}}\sum_{\mathrm{v}\in\mathrm{V_f}}\int_{\mathrm{f}\cap\tilde{\mathrm{c}}(\mathrm{v})}(\underline{a}\cdot\underline{x}_{\mathrm{v}})\underline{b}\cdot\underline{\nu}_{\partial\mathrm{c}}\\ &= \sum_{\mathrm{f}\in\mathrm{F_c}}\sum_{\mathrm{v}\in\mathrm{V_f}}|\mathrm{f}\cap\tilde{\mathrm{c}}(\mathrm{v})|\underline{a}\cdot(\underline{x}_{\mathrm{f}}-\underline{x}_{\mathrm{v}})\underline{b}\cdot\underline{\nu}_{\partial\mathrm{c}} = 0,\end{aligned}$$

owing to (5.15). Moreover, developing T_3 yields

$$\sum_{\mathrm{e}\in\mathrm{E_c}}\sum_{\mathrm{v}\in\mathrm{V_e}} T_3 = \sum_{\mathrm{f}\in\mathrm{F_c}}\sum_{\mathrm{v}\in\mathrm{V_f}}\sum_{\mathrm{e}\in\mathrm{E_v}\cap\mathrm{E_f}}\int_{\mathfrak{s}_{\mathrm{v},\mathrm{f},\mathrm{c}}}\underline{a}\cdot(\underline{x}-\underline{x}_{\mathrm{v}})\underline{b}\cdot\underline{\nu}_{\partial\boldsymbol{\pi}_{\mathrm{v},\mathrm{e},\mathrm{c}}} = 0,$$

since $\sum_{\mathrm{e}\in\mathrm{E_v}\cap\mathrm{E_f}}\underline{\nu}_{\partial\boldsymbol{\pi}_{\mathrm{v},\mathrm{e},\mathrm{c}}}|_{\mathfrak{s}_{\mathrm{v},\mathrm{f},\mathrm{c}}} = \underline{0}$. Adding the results for T_1, T_2, and T_3 yields (5.18a). □

Corollary 5.25. *Let* M *be of class* **(MB)**. *Assume that primal faces are planar. Then, the barycentric subdivision of a cell* $\mathrm{c}\in\mathrm{C}$ *verifies the two following identities:*

$$\sum_{\mathrm{e}\in\mathrm{E_c}}\underline{\mathrm{e}}\otimes\underline{\tilde{\mathrm{f}}}_{\mathrm{c}}(\mathrm{e}) = |\mathrm{c}|\underline{\underline{\mathsf{Id}}}, \tag{5.19a}$$

$$\sum_{\mathrm{f}\in\mathrm{F_c}}\underline{\mathrm{f}}\otimes\underline{\tilde{\mathrm{e}}}_{\mathrm{c}}(\mathrm{f}) = |\mathrm{c}|\underline{\underline{\mathsf{Id}}}, \tag{5.19b}$$

Proof. Take the transposition of (5.17). □

Remark 5.26 (Link with Proposition 5.19)**.** *Since* $\mathrm{tr}(\underline{a}\otimes\underline{b}) = \underline{a}\cdot\underline{b}$ *for all vectors* $\underline{a}$, $\underline{b}\in\mathbb{R}^3$, *we infer from* (5.17) *and* (5.10) *that* $|\mathrm{c}| = \sum_{\mathrm{e}\in\mathrm{E_c}}|\mathfrak{p}_{\mathrm{e},\mathrm{c}}|$ *and* $|\mathrm{c}| = \sum_{\mathrm{f}\in\mathrm{F_c}}|\mathfrak{p}_{\mathrm{f},\mathrm{c}}|$.

Chapter 6

Algebraic analysis

Contents

In this chapter, we set the mathematical basis for the algebraic analysis of CDO schemes. In Section 6.1, we define the discrete norms used in the analysis of CDO schemes along with their basic properties. In Section 6.2, we state formally the three key properties that a discrete Hodge operator has to satisfy: symmetry, stability, and $\mathbb{P}_0$-consistency. We also establish bounds on the consistency error which will be used in Chapters 8 and 9 to derive *a priori* error estimates in the case of elliptic and Stokes equations respectively. Section 6.3 closes this chapter by collecting two results on discrete Sobolev embeddings: the first one related to GRAD and the second one related to $\widetilde{\mathsf{GRAD}}$. As a specific case, the discrete Poincaré inequalities will be useful (in a Hilbertian setting) to establish the stability of CDO schemes.

6.1 Discrete norms

6.1.1 Discrete functional norms

Definition 6.1 (Local discrete norms on the primal mesh)**.** *Let* $\mathcal{X} \in \{\mathcal{V}, \mathcal{E}, \mathcal{F}, \mathcal{C}\}$ *and* $\mathrm{X} \in \{\mathrm{V}, \mathrm{E}, \mathrm{F}, \mathrm{C}\}$*. Let* $\mathrm{c} \in \mathrm{C}$*. Recall that* $\mathrm{X_c}$ *is defined in* (3.19)*. Then, the local mesh-dependent norms are generically defined for* $1 \le p < +\infty$ *as follows:*

$$\forall \mathbf{a} \in \mathcal{X}_\mathrm{c}, \qquad \|\!|\mathbf{a}|\!\|_{p,\mathcal{X}_\mathrm{c}}^p := \sum_{\mathrm{x} \in \mathrm{X_c}} |\mathfrak{p}_{\mathrm{x,c}}| \left(\frac{|\mathbf{a}_\mathrm{x}|}{|\mathrm{x}|} \right)^p, \tag{6.1}$$

where $\mathfrak{p}_{\mathrm{x,c}}$ *for* $\mathrm{x} \in \{\mathrm{v}, \mathrm{e}, \mathrm{f}, \mathrm{c}\}$ *is specified in Definition 5.18. Recall that conventionally* $|\mathrm{v}| = 1$*.*

Remark 6.2 (Simpler definition)**.** *Observe that under the mesh regularity property* **(MR)**, $|\mathfrak{p}_{\mathrm{x,c}}|$ *is uniformly equivalent to* h_c^3*, so that it is possible to consider a simpler definition of the discrete norm as* $\|\!|\mathbf{a}|\!\|_{p,\mathcal{X}_\mathrm{c}}^p := \sum_{\mathrm{x} \in \mathrm{X_c}} h_\mathrm{c}^3 (\frac{|\mathbf{a}_\mathrm{x}|}{|\mathrm{x}|})^p$*. The advantage of Definition 6.1 is that it simplifies the evaluation of constants in the discrete Hölder and Sobolev inequalities presented below.*

We also introduce a global mesh-dependent norms by summing cellwise the local mesh-dependent norms defined by (6.1):

$$\|\!|\mathbf{a}|\!\|_{p,\mathcal{X}}^p := \sum_{\mathrm{c}\in\mathrm{C}} \|\!|\mathsf{T}_{\mathrm{X,c}}(\mathbf{a})|\!\|_{p,\mathcal{X}_\mathrm{c}}^p, \tag{6.2}$$

where the transfer operator $\mathsf{T}_{\mathrm{X,c}}$ is the (full-rank) map from global to local DoFs previously introduced in Section 3.4.2. These norms mimic at the discrete level the $L^p(\Omega)$-norms at the continuous level.

Remark 6.3 (Case $p = +\infty$)**.** *The discrete counterpart of the $L^\infty(\Omega)$ can be defined as*

$$\|\!|\mathbf{a}|\!\|_{\infty,\mathcal{X}} := \max_{\mathrm{x}\in\mathrm{X}} \frac{|\mathbf{a}_\mathrm{x}|}{|\mathrm{x}|}. \tag{6.3}$$

These norms are not needed in what follows.

Discrete Hölder inequalities. As a preliminary result, we derive discrete Hölder inequalities for all discrete norms related to primal mesh entities. No mesh regularity is demanded to derive the following inequalities.

Proposition 6.4 (Discrete Hölder inequalities on the primal mesh)**.** *Let q, r be real numbers such that $1 \le q \le r < +\infty$. Let $\mathcal{X} \in \{\mathcal{V}, \mathcal{E}, \mathcal{F}, \mathcal{C}\}$. Then, the following inequalities hold for all $\mathbf{a} \in \mathcal{X}$:*

$$\|\!|\mathbf{a}|\!\|_{q,\mathcal{X}} \le |\Omega|^{\frac{r-q}{rq}} \|\!|\mathbf{a}|\!\|_{r,\mathcal{X}}. \tag{6.4}$$

Proof. The inequalities rely on the discrete Hölder inequality

$$\sum_{k=1}^n |a_k b_k| \le \left(\sum_{k=1}^n |a_k|^\alpha\right)^{\frac{1}{\alpha}} \left(\sum_{k=1}^n |b_k|^\beta\right)^{\frac{1}{\beta}}, \tag{6.5}$$

with $1 \le \alpha, \beta \le +\infty$, s.t. $\frac{1}{\alpha} + \frac{1}{\beta} = 1$. Take $\alpha = \frac{r}{r-q}$ and $\beta = \frac{r}{q}$. Set $a_k = |\mathfrak{p}_{\mathrm{x,c}}|^{\frac{r-q}{r}}$ and $b_k = |\mathfrak{p}_{\mathrm{x,c}}|^{\frac{q}{r}} (\frac{|\mathbf{a}_\mathrm{x}|}{|\mathrm{x}|})^q$ with $k = \mathrm{x}$. Then (6.4) results from (6.5) since $\sum_{\mathrm{c}\in\mathrm{C}} \sum_{\mathrm{x}\in\mathrm{X}_\mathrm{c}} |\mathfrak{p}_{\mathrm{x,c}}| = |\Omega|$. □

Discrete functional norms on dual entities. The definition of the discrete functional norms on dual entities is somewhat different to those on primal entities. We set

$$\|\!|\mathbf{q}|\!\|_{p,\widetilde{\mathcal{V}}}^p := \sum_{\mathrm{c}\in\mathrm{C}} |\mathrm{c}| |\mathbf{q}_{\tilde{\mathrm{v}}(\mathrm{c})}|^p, \qquad \forall \mathbf{q} \in \widetilde{\mathcal{V}}, \tag{6.6a}$$

$$\|\!|\mathbf{g}|\!\|_{p,\widetilde{\mathcal{E}}}^p := \sum_{\mathrm{f}\in\mathrm{F}} |\mathrm{f}| |\tilde{\mathrm{e}}(\mathrm{f})| \left(\frac{|\mathbf{g}_{\tilde{\mathrm{e}}(\mathrm{f})}|}{|\tilde{\mathrm{e}}(\mathrm{f})|}\right)^p, \qquad \forall \mathbf{g} \in \widetilde{\mathcal{E}}, \tag{6.6b}$$

$$\|\!|\boldsymbol{\phi}|\!\|_{p,\widetilde{\mathcal{F}}}^p := \sum_{\mathrm{e}\in\mathrm{E}} |\mathrm{e}| |\tilde{\mathrm{f}}(\mathrm{e})| \left(\frac{|\boldsymbol{\phi}_{\tilde{\mathrm{f}}(\mathrm{e})}|}{|\tilde{\mathrm{f}}(\mathrm{e})|}\right)^p, \qquad \forall \boldsymbol{\phi} \in \widetilde{\mathcal{F}}, \tag{6.6c}$$

$$\|\!|\mathbf{s}|\!\|_{p,\widetilde{\mathcal{C}}}^p := \sum_{\mathrm{v}\in\mathrm{V}} |\tilde{\mathrm{c}}(\mathrm{v})| \left(\frac{|\mathbf{s}_{\tilde{\mathrm{c}}(\mathrm{v})}|}{|\tilde{\mathrm{c}}(\mathrm{v})|}\right)^p, \qquad \forall \mathbf{s} \in \widetilde{\mathcal{C}}. \tag{6.6d}$$

Other definitions are possible, which are equivalent under mesh regularity. The discrete norms $\|\!|\cdot|\!\|_{p,\widetilde{\mathcal{Y}}}$ also mimic the $L^p(\Omega)$-norm at the continuous level.

Discrete Hölder inequalities. As a preliminary result, we derive discrete Hölder inequalities for all discrete norms related to dual mesh entities. The mesh regularity requirements **(MR)** can be weakened to derive the following inequalities. Specifically, instead of **(MR)**, it suffices to make the two following assumptions: There exists a positive real number $\eta_\perp > 0$ such that, for all $\mathrm{c} \in \mathrm{C}$ and all $\mathrm{e} \in \mathrm{E}_\mathrm{c}$,

$$\eta_\perp |\mathrm{e}||\tilde{\mathrm{f}}_\mathrm{c}(\mathrm{e})| \le \frac{1}{d} \underline{\mathrm{e}} \cdot \tilde{\underline{\mathrm{f}}}_\mathrm{c}(\mathrm{e}) \, (= |\mathfrak{p}_{\mathrm{e},\mathrm{c}}|) \,, \tag{6.7}$$

where $\underline{\mathrm{e}}$ is defined in (5.5) and $\tilde{\underline{\mathrm{f}}}_\mathrm{c}(\mathrm{e})$ in (5.8). Moreover, there exists a positive real number $\eta_{\mathrm{vol}} > 0$ such that, for all $\mathrm{c} \in \mathrm{C}$,

$$\eta_{\mathrm{vol}} \sum_{\mathrm{f} \in \mathrm{F}_\mathrm{c}} |\mathrm{f}||\tilde{\mathrm{e}}(\mathrm{f})| \le |\mathrm{c}|. \tag{6.8}$$

Proposition 6.5 (Discrete Hölder inequalities on the dual mesh)**.** *Let q, r be real numbers such that $1 \le q \le r < +\infty$. The following inequalities hold for all $\mathbf{q} \in \widetilde{\mathcal{V}}$ and all $\mathbf{s} \in \widetilde{\mathcal{C}}$:*

$$\|\mathbf{q}\|_{q,\widetilde{\mathcal{V}}} \le |\Omega|^{\frac{r-q}{rq}} \|\mathbf{q}\|_{r,\widetilde{\mathcal{V}}}, \qquad \|\mathbf{s}\|_{q,\widetilde{\mathcal{C}}} \le |\Omega|^{\frac{r-q}{rq}} \|\mathbf{s}\|_{r,\widetilde{\mathcal{C}}}. \tag{6.9a}$$

Moreover, assuming (6.8)*, the following inequality holds for all $\mathbf{u} \in \widetilde{\mathcal{E}}$:*

$$\|\mathbf{u}\|_{q,\widetilde{\mathcal{E}}} \le (\eta_{\mathrm{vol}}^{-1}|\Omega|)^{\frac{r-q}{rq}} \|\mathbf{u}\|_{r,\widetilde{\mathcal{E}}}, \tag{6.9b}$$

and assuming (6.7)*, the following inequality holds for all $\boldsymbol{\phi} \in \widetilde{\mathcal{F}}$:*

$$\|\boldsymbol{\phi}\|_{q,\widetilde{\mathcal{F}}} \le (\eta_\perp^{-1}|\Omega|)^{\frac{r-q}{rq}} \|\boldsymbol{\phi}\|_{r,\widetilde{\mathcal{F}}}. \tag{6.9c}$$

Proof. We use (6.5) with $\alpha = \frac{r}{r-q}$ and $\beta = \frac{r}{q}$.

(1) *Proof of* (6.9a). Choosing $a_k = |\mathrm{c}|^{\frac{r-q}{r}}$ and $b_k = |\mathrm{c}|^{\frac{q}{r}} |\mathbf{q}_{\tilde{\mathrm{v}}(\mathrm{c})}|^q$ with $k = \mathrm{c}$ in (6.5), and then summing over primal cells leads to the left inequality in (6.9a) for elements of $\widetilde{\mathcal{V}}$. The proof of the right inequality in (6.9a) is similar since $|\Omega| = \sum_{\mathrm{v} \in \mathrm{V}} |\tilde{\mathrm{c}}(\mathrm{v})|$.

(2) *Proof of* (6.9b). Since $|\tilde{\mathrm{e}}(\mathrm{f})| = \sum_{\mathrm{c} \in \mathrm{C}_\mathrm{f}} |\tilde{\mathrm{e}}_\mathrm{c}(\mathrm{f})|$, we can write by inverting the order of the summations

$$\|\mathbf{g}\|_{q,\widetilde{\mathcal{E}}}^q = \sum_{\mathrm{c} \in \mathrm{C}} \sum_{\mathrm{f} \in \mathrm{F}_\mathrm{c}} |\mathrm{f}||\tilde{\mathrm{e}}_\mathrm{c}(\mathrm{f})| \left(\frac{|\mathbf{g}_{\tilde{\mathrm{e}}(\mathrm{f})}|}{|\tilde{\mathrm{e}}(\mathrm{f})|} \right)^q.$$

Then, we derive inequality (6.9b) by noticing that $\sum_{\mathrm{c} \in \mathrm{C}} \sum_{\mathrm{f} \in \mathrm{F}_\mathrm{c}} |\mathrm{f}||\tilde{\mathrm{e}}_\mathrm{c}(\mathrm{f})| \le \eta_{\mathrm{vol}}^{-1}|\Omega|$ owing to (6.8) and $|\tilde{\mathrm{e}}_\mathrm{c}(\mathrm{f})| \le |\tilde{\mathrm{e}}(\mathrm{f})|$ for all $\mathrm{f} \in \mathrm{F}$ and all $\mathrm{c} \in \mathrm{C}_\mathrm{f}$.

(3) *Proof of* (6.9c). To derive (6.9c), we notice that (6.7) implies that $\sum_{\mathrm{e} \in \mathrm{E}_\mathrm{c}} |\mathrm{e}||\tilde{\mathrm{f}}_\mathrm{c}(\mathrm{e})| \le \eta_\perp^{-1}|\mathrm{c}|$, and then proceed similarly to the previous case. □

6.1.2 Discrete norms induced by discrete Hodge operators

Similarly to Definition 3.15, we define *local* duality products for each cell $\mathrm{c} \in \mathrm{C}$, as follows:

$$[\![\mathbf{a}, \mathbf{b}]\!]_{\mathcal{X}_\mathrm{c} \widetilde{\mathcal{Y}}_\mathrm{c}} := \sum_{\mathrm{x} \in \mathrm{X}_\mathrm{c}} \mathbf{a}_\mathrm{x} \mathbf{b}_{\tilde{\mathrm{y}}_\mathrm{c}(\mathrm{x})}, \qquad \forall (\mathbf{a}, \mathbf{b}) \in \mathcal{X}_\mathrm{c} \times \widetilde{\mathcal{Y}}_\mathrm{c}. \tag{6.10}$$

The discrete Hodge operators $\mathsf{H}_\alpha^{\mathcal{X}_\mathrm{c} \widetilde{\mathcal{Y}}_\mathrm{c}}$ being SPD for each cell $\mathrm{c} \in \mathrm{C}$, we can define discrete norms induced by this operator.

Definition 6.6 (Local discrete Hodge norms)**.** *Let $\mathrm{c} \in \mathrm{C}$. Let $\mathbf{a} \in \mathcal{X}_\mathrm{c}$ and $\mathbf{b} \in \widetilde{\mathcal{Y}}_\mathrm{c}$. Then, we set*

$$\|\mathbf{a}\|_{\alpha,\mathcal{X}_\mathrm{c}}^2 := [\![\mathbf{a}, \mathsf{H}_\alpha^{\mathcal{X}_\mathrm{c} \widetilde{\mathcal{Y}}_\mathrm{c}}(\mathbf{a})]\!]_{\mathcal{X}_\mathrm{c} \widetilde{\mathcal{Y}}_\mathrm{c}}, \qquad \|\mathbf{b}\|_{\alpha^{-1},\widetilde{\mathcal{Y}}_\mathrm{c}}^2 := [\![(\mathsf{H}_\alpha^{\mathcal{X}_\mathrm{c} \widetilde{\mathcal{Y}}_\mathrm{c}})^{-1}(\mathbf{b}), \mathbf{b}]\!]_{\mathcal{X}_\mathrm{c} \widetilde{\mathcal{Y}}_\mathrm{c}}. \tag{6.11}$$

From (3.20), $\mathsf{H}_\alpha^{\mathcal{X}\widetilde{\mathcal{Y}}}$ is clearly SPD. Thus, we similarly define discrete norms induced by this operator.

Definition 6.7 (Global discrete Hodge norms)**.** *Let $\mathbf{a} \in \mathcal{X}$ and $\mathbf{b} \in \widetilde{\mathcal{Y}}$. Recalling the Definition 3.15 of the global duality product, we set*

$$\|\mathbf{a}\|_{\alpha,\mathcal{X}}^2 := [\![\mathbf{a}, \mathsf{H}_\alpha^{\mathcal{X}\widetilde{\mathcal{Y}}}(\mathbf{a})]\!]_{\mathcal{X}\widetilde{\mathcal{Y}}}, \qquad \|\mathbf{b}\|_{\alpha^{-1},\widetilde{\mathcal{Y}}}^2 := [\![(\mathsf{H}_\alpha^{\mathcal{X}\widetilde{\mathcal{Y}}})^{-1}(\mathbf{b}), \mathbf{b}]\!]_{\mathcal{X}\widetilde{\mathcal{Y}}}, \tag{6.12}$$

The global norms $\|\cdot\|_{\alpha,\mathcal{X}}$ are readily obtained by summing cellwise the local norms, *i.e.* $\|\mathbf{a}\|_{\alpha,\mathcal{X}}^2 = \sum_{\mathrm{c}\in\mathrm{C}} \|\mathsf{T}_{\mathrm{X},\mathrm{c}}(\mathbf{a})\|_{\alpha,\mathcal{X}_\mathrm{c}}^2$ for all $\mathbf{a} \in \mathcal{X}$.

Proposition 6.8 (Cauchy–Schwarz inequalities)**.** *For each $\mathrm{c} \in \mathrm{C}$, the following local Cauchy–Schwarz inequality holds:*

$$[\![\mathbf{a}, \mathbf{b}]\!]_{\mathcal{X}_\mathrm{c}\widetilde{\mathcal{Y}}_\mathrm{c}} \le \|\mathbf{a}\|_{\alpha,\mathcal{X}_\mathrm{c}} \|\mathbf{b}\|_{\alpha^{-1},\widetilde{\mathcal{Y}}_\mathrm{c}}, \qquad \forall \mathbf{a} \in \mathcal{X}_\mathrm{c},\, \forall \mathbf{b} \in \widetilde{\mathcal{Y}}_\mathrm{c}. \tag{6.13}$$

Moreover, the following global Cauchy–Schwarz inequality holds:

$$[\![\mathbf{a}, \mathbf{b}]\!]_{\mathcal{X}\widetilde{\mathcal{Y}}} \le \|\mathbf{a}\|_{\alpha,\mathcal{X}} \|\mathbf{b}\|_{\alpha^{-1},\widetilde{\mathcal{Y}}}, \qquad \forall \mathbf{a} \in \mathcal{X},\, \forall \mathbf{b} \in \widetilde{\mathcal{Y}}. \tag{6.14}$$

Whenever the context is unambiguous, we write $\|\mathbf{a}\|_\alpha$ (resp. $\|\mathbf{a}\|_{\alpha,\mathrm{c}}$) instead of $\|\mathbf{a}\|_{\alpha,\mathcal{X}}$ (resp. $\|\mathbf{a}\|_{\alpha,\mathcal{X}_\mathrm{c}}$) and $\|\mathbf{b}\|_{\alpha^{-1}}$ (resp. $\|\mathbf{b}\|_{\alpha^{-1},\mathrm{c}}$) instead of $\|\mathbf{b}\|_{\alpha^{-1},\widetilde{\mathcal{Y}}}$ (resp. $\|\mathbf{b}\|_{\alpha^{-1},\widetilde{\mathcal{Y}}_\mathrm{c}}$).

6.2 Results on discrete Hodge operators

6.2.1 Local design properties

We recast in a more formal way the three local design properties of the discrete Hodge operator $\mathsf{H}_\alpha^{\mathcal{X}_\mathrm{c}\widetilde{\mathcal{Y}}_\mathrm{c}}$ previously introduced in Section 3.4.2. In the general case, the material property is tensor-valued (*e.g.* an anisotropic conductivity). Whenever it is relevant, we denote this material property by $\underline{\underline{\alpha}}$. In what follows, we assume that the material property is piecewise constant on the primal mesh (our results can be extended to piecewise Lipschitz material property modulo necessary technicalities), and, in the case of tensor-valued material property, we assume that the tensor is symmetric. We denote, respectively, by $\alpha_{\flat,\mathrm{c}}$ and $\alpha_{\sharp,\mathrm{c}}$ the minimal and maximal eigenvalue of $\underline{\underline{\alpha}}$ on each primal cell. These eigenvalues are uniformly bounded from above and from below:

$$0 < \alpha_{\flat,\mathrm{c}} \le \alpha_{\sharp,\mathrm{c}} < +\infty. \tag{6.15}$$

The corresponding bounds on Ω are denoted by $\alpha_\flat$ and $\alpha_\sharp$ respectively.

Definition 6.9 (Broken domain of de Rham maps)**.** *For all $\mathrm{c} \in \mathrm{C}$, we define $S_{\mathcal{X}}(\mathrm{c})$ (resp. $S_{\widetilde{\mathcal{Y}}}(\mathrm{c})$) similarly to Definition 3.5 (resp. eq. (3.13)) by replacing Ω with c. We denote by $S_{\mathcal{X}}(\mathrm{C})$ the space of functions whose restriction to each cell $\mathrm{c} \in \mathrm{C}$ belongs to $S_{\mathcal{X}}(\mathrm{c})$ and $S_{\widetilde{\mathcal{Y}}}(\mathrm{C})$ the space of functions whose restriction to each cell $\mathrm{c} \in \mathrm{C}$ belongs to $S_{\widetilde{\mathcal{Y}}}(\mathrm{c})$.*

Local de Rham maps. We first introduce local de Rham maps on the primal mesh entities, $\mathsf{R}_{\mathcal{X}_\mathrm{c}} : S_{\mathcal{X}}(\mathrm{c}) \to \mathcal{X}_\mathrm{c}$ for all primal cell $\mathrm{c} \in \mathrm{C}$, acting as follows:

$$\forall p \in S_{\mathcal{V}}(\mathrm{c}), \qquad \mathsf{R}_{\mathcal{V}_\mathrm{c}}(p)|_\mathrm{v} := p(\mathrm{v}), \qquad \forall \mathrm{v} \in \mathrm{V}_\mathrm{c}, \tag{6.16a}$$

$$\forall \underline{u} \in S_{\mathcal{E}}(\mathrm{c}), \qquad \mathsf{R}_{\mathcal{E}_\mathrm{c}}(\underline{u})|_\mathrm{e} := \int_\mathrm{e} \underline{u} \cdot \underline{\tau}_\mathrm{e}, \qquad \forall \mathrm{e} \in \mathrm{E}_\mathrm{c}, \tag{6.16b}$$

$$\forall \underline{\phi} \in S_{\mathcal{F}}(\mathrm{c}), \qquad \mathsf{R}_{\mathcal{F}_\mathrm{c}}(\underline{\phi})|_\mathrm{f} := \int_\mathrm{f} \underline{\phi} \cdot \underline{\nu}_\mathrm{f}, \qquad \forall \mathrm{f} \in \mathrm{F}_\mathrm{c}, \tag{6.16c}$$

$$\forall s \in S_{\mathcal{C}}(\mathrm{c}), \qquad \mathsf{R}_{\mathcal{C}_\mathrm{c}}(s)|_\mathrm{c} := \int_\mathrm{c} s. \tag{6.16d}$$

These definitions are identical to (3.1) but on the local subsets. Local de Rham maps on dual mesh entities, $\mathsf{R}_{\widetilde{\mathcal{Y}}_c} : S_{\widetilde{\mathcal{Y}}}(c) \to \widetilde{\mathcal{Y}}_c$, for all primal cell $c \in C$, act as follows:

$$\forall p \in S_{\widetilde{\mathcal{V}}}(c), \qquad \mathsf{R}_{\widetilde{\mathcal{V}}_c}(p)|_{\tilde{v}(c)} := p(\tilde{v}(c)), \tag{6.17a}$$

$$\forall \underline{u} \in S_{\widetilde{\mathcal{E}}}(c), \qquad \mathsf{R}_{\widetilde{\mathcal{E}}_c}(\underline{u})|_{\tilde{e}_c(f)} := \int_{\tilde{e}_c(f)} \underline{u} \cdot \underline{\tau}_{\tilde{e}_c(f)}, \qquad \forall f \in F_c, \tag{6.17b}$$

$$\forall \underline{u} \in S_{\widetilde{\mathcal{F}}}(c), \qquad \mathsf{R}_{\widetilde{\mathcal{F}}_c}(\underline{\phi})|_{\tilde{f}_c(e)} := \int_{\tilde{f}_c(e)} \underline{\phi} \cdot \underline{\nu}_{\tilde{f}_c(e)}, \qquad \forall e \in E_c, \tag{6.17c}$$

$$\forall \underline{u} \in S_{\widetilde{\mathcal{C}}}(c), \qquad \mathsf{R}_{\widetilde{\mathcal{C}}_c}(s)|_{\tilde{c}_c(v)} := \int_{\tilde{c}_c(v)} s, \qquad \forall v \in V_c. \tag{6.17d}$$

These definitions are similar to (3.12), but one has to restrict the domain of integration from $\tilde{y}$ to $\tilde{y}_c$ ($\tilde{y}_c = \tilde{y} \cap c$, cf. Section 3.3.1).

Local design properties. The symmetry, stability and consistency properties of the local discrete Hodge operators $\mathsf{H}_\alpha^{\mathcal{X}_c\widetilde{\mathcal{Y}}_c}$ assert that

(**H0**) [Symmetry] For all $c \in C$,

$$[\![\mathbf{a}_1, \mathsf{H}_\alpha^{\mathcal{X}_c\widetilde{\mathcal{Y}}_c}(\mathbf{a}_2)]\!]_{\mathcal{X}_c\widetilde{\mathcal{Y}}_c} = [\![\mathbf{a}_2, \mathsf{H}_\alpha^{\mathcal{X}_c\widetilde{\mathcal{Y}}_c}(\mathbf{a}_1)]\!]_{\mathcal{X}_c\widetilde{\mathcal{Y}}_c}, \qquad \forall \mathbf{a}_1, \mathbf{a}_2 \in \mathcal{X}_c. \tag{6.18}$$

(**H1**) [Local stability] There exists $\eta_\alpha > 0$ such that, for all $c \in C$,

$$\eta_\alpha \alpha_{\flat,c} \|\mathbf{a}\|_{2,\mathcal{X}_c}^2 \le \|\mathbf{a}\|_{\alpha,\mathcal{X}_c}^2 \le \eta_\alpha^{-1} \alpha_{\sharp,c} \|\mathbf{a}\|_{2,\mathcal{X}_c}^2, \qquad \forall \mathbf{a} \in \mathcal{X}_c. \tag{6.19}$$

(**H2**) [Local $\mathbb{P}_0$-consistency] The local commuting operator (attached to the commuting diagram depicted in Figure 6.1)

$$\lfloor \alpha, {}_{\mathcal{X}_c}\widetilde{\mathcal{Y}}_c \rceil(\bullet) := \mathsf{H}_\alpha^{\mathcal{X}_c\widetilde{\mathcal{Y}}_c} \cdot \mathsf{R}_{\mathcal{X}_c}(\bullet) - \mathsf{R}_{\widetilde{\mathcal{Y}}_c}(\alpha\, \bullet) \tag{6.20}$$

satisfies $\lfloor \alpha, {}_{\mathcal{X}_c}\widetilde{\mathcal{Y}}_c \rceil(K) = 0$ for any field K which is constant in $c \in C$. One considers a constant scalar-valued field $K \in \mathbb{P}_0(c)$ in the case of $\mathsf{H}_\alpha^{\mathcal{V}_c\widetilde{\mathcal{C}}_c}$ and $\mathsf{H}_\alpha^{\mathcal{C}_c\widetilde{\mathcal{V}}_c}$ and a constant vector-valued field $\underline{K} \in [\mathbb{P}_0(c)]^3$ in the case of $\mathsf{H}_\alpha^{\mathcal{E}_c\widetilde{\mathcal{F}}_c}$ and $\mathsf{H}_\alpha^{\mathcal{F}_c\widetilde{\mathcal{E}}_c}$.

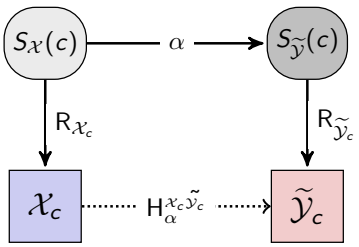

Figure 6.1 – Commuting diagram related to the local consistency property.

Observe that (**H0**) and (**H1**) readily imply that the local discrete Hodge operators are SPD.

Remark 6.10 (Link with MFD)**.** *The local design properties share the same spirit as those introduced for MFD schemes by Brezzi* et al. *(2005, 2009).*

Global properties of discrete Hodge operator. From the cellwise assembly process (3.20), we readily verify that the global discrete Hodge operator is symmetric. Summing cellwise (**H1**) and using (3.20), we infer the global stability property of the discrete Hodge operators

$$\forall \mathbf{a} \in \mathcal{X}, \qquad \eta_\alpha \alpha_\flat \|\mathbf{a}\|_{2,\mathcal{X}}^2 \le \|\mathbf{a}\|_{\alpha,\mathcal{X}}^2 \le \eta_\alpha^{-1} \alpha_\sharp \|\mathbf{a}\|_{2,\mathcal{X}}^2, \tag{6.21}$$

where $\alpha_\flat := \min_{c\in C} \alpha_{\flat,c}$ and $\alpha_\sharp := \max_{c\in C} \alpha_{\sharp,c}$.

The global $\mathbb{P}_0$-consistency property of the discrete Hodge operator is stated using a global commuting operator defined from the local commuting operators as follows:

$$\lfloor \alpha,\, x\tilde{y} \rceil(\bullet) := \sum_{c\in C} \mathsf{T}_{X,c}^* \cdot \lfloor \alpha,\, x_c\tilde{y}_c \rceil(\bullet|_c). \tag{6.22}$$

This global commuting operator acts on functions $u \in S_{\mathcal{X}}(C)$ such that $\alpha u \in S_{\widetilde{\mathcal{Y}}}(C)$. A straightforward consequence of (**H2**) is that for any cellwise constant field K

$$\lfloor \alpha,\, x\tilde{y} \rceil(K) = 0, \tag{6.23}$$

i.e. a cellwise constant solution is exactly captured by the scheme. This property is directly related to the *patch test* condition used in engineering to assess a numerical scheme.

Remark 6.11 (Global de Rham maps)**.** *Observe that a function belonging to $S_{\mathcal{X}}(C)$ is not necessarily in the domain of $\mathsf{R}_{\mathcal{X}}$, while a function belonging to $S_{\widetilde{\mathcal{Y}}}(C)$ is in the domain of $\mathsf{R}_{\widetilde{\mathcal{Y}}}$.*

Link between local and global DoFs. Consider local and global DoFs defined from a field $a \in S_{\mathcal{X}}(\Omega)$ on primal mesh entities. For each cell $c \in C$, the link between the local de Rham map $\mathsf{R}_{\mathcal{X}_c}$ and the global de Rham map $\mathsf{R}_{\mathcal{X}}$ is the following:

$$\mathsf{R}_{\mathcal{X}_c}(a|_c) = \mathsf{T}_{X,c} \cdot \mathsf{R}_{\mathcal{X}}(a). \tag{6.24}$$

Consider now local and global DoFs defined from a field $b \in S_{\widetilde{\mathcal{Y}}}(\Omega)$ on dual mesh entities. For each cell $c \in C$, the link between the local de Rham map $\mathsf{R}_{\widetilde{\mathcal{Y}}_c}$ and the global de Rham map $\mathsf{R}_{\widetilde{\mathcal{Y}}}$ is the following:

$$\mathsf{R}_{\widetilde{\mathcal{Y}}}(b) = \sum_{c\in C} \mathsf{T}_{X,c}^* \cdot \mathsf{R}_{\widetilde{\mathcal{Y}}_c}(b|_c). \tag{6.25}$$

Thus, on primal mesh entities, local DoFs correspond to global DoFs, but on dual mesh entities, this is not the case. One has to collect the local contributions from each primal cell to recover the global DoFs.

Proposition 6.12 (Alternative formulation of the global commuting operator)**.** *Let $a \in S_{\mathcal{X}}(\Omega)$ such that $\alpha\, a \in S_{\widetilde{\mathcal{Y}}}(\Omega)$. Then, the global commuting operator related to the discrete Hodge operator $\mathsf{H}_\alpha^{x\tilde{y}}$ can be formulated as follows:*

$$\lfloor \alpha,\, x\tilde{y} \rceil(a) = \mathsf{H}_\alpha^{x\tilde{y}} \cdot \mathsf{R}_{\mathcal{X}}(a) - \mathsf{R}_{\widetilde{\mathcal{Y}}}(\alpha\, a). \tag{6.26}$$

Proof. Starting from (6.22), using (3.20) and then using (6.24) and (6.25) yields

$$\begin{aligned}
\lfloor \alpha,\, x\tilde{y} \rceil(a) &= \sum_{c\in C} \mathsf{T}_{X,c}^* \cdot \lfloor \alpha,\, x_c\tilde{y}_c \rceil(a|_c) \\
&= \sum_{c\in C} \mathsf{T}_{X,c}^* \cdot \mathsf{H}_\alpha^{x_c\tilde{y}_c} \cdot \mathsf{R}_{\mathcal{X}_c}(a|_c) - \sum_{c\in C} \mathsf{T}_{X,c}^* \cdot \mathsf{R}_{\widetilde{\mathcal{Y}}_c}(\alpha\, a|_c) \\
&= \sum_{c\in C} \mathsf{T}_{X,c}^* \cdot \mathsf{H}_\alpha^{x_c\tilde{y}_c} \cdot \mathsf{T}_{X,c} \cdot \mathsf{R}_{\mathcal{X}}(a) - \sum_{c\in C} \mathsf{T}_{X,c}^* \cdot \mathsf{R}_{\widetilde{\mathcal{Y}}_c}(\alpha\, a|_c) \\
&= \mathsf{H}_\alpha^{x\tilde{y}} \cdot \mathsf{R}_{\mathcal{X}}(a) - \mathsf{R}_{\widetilde{\mathcal{Y}}}(\alpha\, a).
\end{aligned}$$

□

6.2.2 Bounds on consistency error

In this thesis, we often abbreviate $A \lesssim B$ the inequality $A \le cB$ with positive constant c whose value can change at each occurrence and is independent of any mesh size (but can depend on mesh regularity parameters and stability constants). We first state an algebraic result derived by Codecasa & Trevisan (2010a) for operators built from a cellwise assembly process of local operators algebraically defined by SPD matrices.

Lemma 6.13 (Algebraic inequality)**.** *Assume that* $\mathsf{H}_\alpha^{\mathcal{X}_c\widetilde{\mathcal{Y}}_c}$ *satisfies* (**H0**) *and* (**H1**) *for each cell* $c \in C$*. Assume that* $\underline{b} \in S_{\mathcal{X}}(C)$ *and* $\alpha\underline{b} \in S_{\widetilde{\mathcal{Y}}}(C)$*. Then, the following inequality holds:*

$$\|\!|\lfloor \alpha,\, \mathcal{X}\widetilde{\mathcal{Y}}\rceil(b)|\!\|^2_{\alpha^{-1},\widetilde{\mathcal{Y}}} \le \sum_{c\in C} \|\!|\lfloor \alpha,\, \mathcal{X}_c\widetilde{\mathcal{Y}}_c\rceil(b|_c)|\!\|^2_{\alpha^{-1},\widetilde{\mathcal{Y}}_c}. \tag{6.27}$$

Proof. For the sake of completeness, we recall the proof given by Codecasa & Trevisan (2010a). We adopt an algebraic viewpoint. The relation $\mathsf{H}_\alpha^{\mathcal{X}\widetilde{\mathcal{Y}}} = \sum_{c\in C} \mathsf{T}^*_{X,c} \cdot \mathsf{H}_\alpha^{\mathcal{X}_c\widetilde{\mathcal{Y}}_c} \cdot \mathsf{T}_{X,c}$, corresponds to $\mathbb{H}_\alpha^{\mathcal{X}\widetilde{\mathcal{Y}}} = \hat{\mathbb{T}}^T \cdot \hat{\mathbb{H}} \cdot \hat{\mathbb{T}}$ with

$$\hat{\mathbb{H}} = \mathrm{diag}(\{\mathbb{H}_\alpha^{\mathcal{X}_c\widetilde{\mathcal{Y}}_c}\}_{c\in C}) \qquad \text{and} \qquad \hat{\mathbb{T}} = \begin{bmatrix} \mathbb{T}_1 \\ \vdots \\ \mathbb{T}_{\#C} \end{bmatrix},$$

where $\mathbb{T}_j := \mathsf{T}_{X,c_j}$ for all $j \in \{1,\dots,\#C\}$, $\hat{\mathbb{H}}$ is a block diagonal SPD matrix of size $\#\hat{X} := \sum_{c\in C} \#X_c$ since each block is a SPD matrix of size $\#X_c$ for all $c \in C$ (owing to (**H0**) and (**H1**)). $\hat{\mathbb{T}}$ is a full-rank matrix of size $\#\hat{X} \times \#X$. Moreover, the relation $\mathbf{b} = \sum_{c\in C} \mathsf{T}^*_{X,c}(\mathbf{b}_c)$ with $\mathbf{b}_c \in \widetilde{\mathcal{Y}}_c$ for each $c \in C$ corresponds to $\mathbf{b} = \hat{\mathbb{T}}^T(\hat{\mathbf{b}})$, where $\hat{\mathbf{b}}$ is a vector of $\mathbb{R}^{\#\hat{X}}$ defined as follows:

$$\hat{\mathbf{b}} = \begin{bmatrix} \mathbf{b}_1 \\ \vdots \\ \mathbf{b}_{\#C} \end{bmatrix}.$$

In this notation, $\sum_{c\in C} \|\mathbf{b}_c\|^2_{\alpha^{-1},\widetilde{\mathcal{Y}}_c}$ corresponds to $\hat{\mathbf{b}}^T \hat{\mathbb{H}}^{-1} \hat{\mathbf{b}}$.

Let $\hat{\mathbf{x}} \in \mathbb{R}^{\#\hat{X}}$. Then, $\hat{\mathbf{x}}^T\hat{\mathbf{x}} \ge 0$. Setting $\hat{\mathbf{x}} := \hat{\mathbb{H}}^{-\frac{1}{2}} \hat{\mathbf{b}} - \hat{\mathbb{H}}^{\frac{1}{2}} \hat{\mathbb{T}} (\mathbb{H}_\alpha^{\mathcal{X}\widetilde{\mathcal{Y}}})^{-1} \mathbb{T}^T \hat{\mathbf{b}}$ yields

$$\begin{aligned}
\hat{\mathbf{x}}^T\hat{\mathbf{x}} &= \hat{\mathbf{b}}^T\hat{\mathbb{H}}^{-1}\hat{\mathbf{b}} - 2\hat{\mathbf{b}}^T\hat{\mathbb{T}}(\mathbb{H}_\alpha^{\mathcal{X}\widetilde{\mathcal{Y}}})^{-1}\mathbb{T}^T\hat{\mathbf{b}} + \hat{\mathbf{b}}^T\hat{\mathbb{T}}(\mathbb{H}_\alpha^{\mathcal{X}\widetilde{\mathcal{Y}}})^{-1}\mathbb{T}^T\hat{\mathbb{H}}\hat{\mathbb{T}}(\mathbb{H}_\alpha^{\mathcal{X}\widetilde{\mathcal{Y}}})^{-1}\mathbb{T}^T\hat{\mathbf{b}} \\
&= \hat{\mathbf{b}}^T\hat{\mathbb{H}}^{-1}\hat{\mathbf{b}} - \hat{\mathbf{b}}^T\hat{\mathbb{T}}(\mathbb{H}_\alpha^{\mathcal{X}\widetilde{\mathcal{Y}}})^{-1}\mathbb{T}^T\hat{\mathbf{b}} \\
&= \hat{\mathbf{b}}^T\hat{\mathbb{H}}^{-1}\hat{\mathbf{b}} - \mathbf{b}^T(\mathbb{H}_\alpha^{\mathcal{X}\widetilde{\mathcal{Y}}})^{-1}\mathbf{b}
\end{aligned}$$

owing to the symmetry of $\hat{\mathbb{H}}$ and $\mathbb{H}_\alpha^{\mathcal{X}\widetilde{\mathcal{Y}}}$, and the identity $\mathbb{H}_\alpha^{\mathcal{X}\widetilde{\mathcal{Y}}} = \hat{\mathbb{T}}^T \cdot \hat{\mathbb{H}} \cdot \hat{\mathbb{T}}$. Thus, we infer that

$$\|\mathbf{b}\|^2_{\alpha^{-1},\widetilde{\mathcal{Y}}} \le \sum_{c\in C} \|\mathbf{b}_c\|^2_{\alpha^{-1},\widetilde{\mathcal{Y}}_c}.$$

Choosing $\mathbf{b}_c := \lfloor \alpha,\, \mathcal{X}_c\widetilde{\mathcal{Y}}_c\rceil(b|_c)$ for each $c \in C$ so that $\mathbf{b}_{\tilde{y}} = \lfloor \alpha,\, \mathcal{X}_c\widetilde{\mathcal{Y}}_c\rceil(b)|_{\tilde{y}}$ (cf. (6.22)), yields the stated result. □

In CDO schemes, the discrete errors are bounded by the consistency error introduced by the lack of commuting property of the discrete Hodge operators with the de Rham maps; see Bossavit (2000), Hiptmair (2001a), or Codecasa & Trevisan (2010a). We now derive a first-order estimate relying on the three local design properties (**H0**), (**H1**) and (**H2**) of the discrete Hodge operators for smooth enough vector fields. Let $H^1(C)$ denote the broken Sobolev space of piecewise H^1 functions on the primal mesh and $H^1(C)^3$ the corresponding space for vector-valued functions. We first consider the case of the discrete Hodge operator $\mathsf{H}_\alpha^{\mathcal{E}\widetilde{\mathcal{F}}}$.

Lemma 6.14 (Error bound for smooth fields)**.** *Assume* **(MR)**. *Assume that* $\underline{\underline{\alpha}}$ *is piecewise constant on primal cells. Let* $\underline{b} \in [H^1(\mathrm{C})]^3$ *be such that* $\underline{\mathrm{curl}}(\underline{b}) \in L^4(\Omega)^3$. *Let* $\mathsf{H}_\alpha^{\widetilde{\mathcal{E}}\widetilde{\mathcal{F}}}$ *satisfy* (**H0**), (**H1**), *and* (**H2**). *Then, the following inequality holds:*

$$\|\!|\lfloor \alpha,\, \varepsilon^{\widetilde{\mathcal{F}}}\rceil(\underline{b})|\!\|_{\alpha^{-1},\widetilde{\mathcal{F}}} \lesssim h\left(\|\underline{b}\|_{[H^1(\mathrm{C})]^3} + \|\underline{\mathrm{curl}}\,\underline{b}\|_{L^4(\Omega)^3}\right). \tag{6.28}$$

Proof. We first observe that the smoothness assumption on $\underline{b}$ entails that $\underline{b} \in S_{\mathcal{E}}(\mathrm{C})$ and $\underline{\underline{\alpha}}\,\underline{b} \in S_{\widetilde{\mathcal{F}}}(\mathrm{C})$. Namely, for each cell $\mathrm{c} \in \mathrm{C}$, $\underline{b} \in H^s(\mathrm{c})^3$ with $s > \frac{1}{2}$ and $\underline{\mathrm{curl}}(\underline{b}) \in L^q(\mathrm{c})^3$ with $q > 2$ (cf. Remark 3.6), while $\underline{\underline{\alpha}}\,\underline{b} \in H^s(\mathrm{c})^3$ with $s > \frac{1}{2}$ (cf. Definition 3.5) since $\underline{\underline{\alpha}}$ is constant in c. Using the algebraic result of Lemma 6.13 yields $\|\!|\lfloor \alpha,\, \varepsilon^{\widetilde{\mathcal{F}}}\rceil(\underline{b})|\!\|^2_{\alpha^{-1},\widetilde{\mathcal{F}}} \le \sum_{\mathrm{c}\in\mathrm{C}} T_{\mathrm{c}}^2$ where $T_{\mathrm{c}}^2 := \|\!|\lfloor \alpha,\, \varepsilon_{\mathrm{c}}\tilde{\mathcal{F}}_{\mathrm{c}}\rceil(\underline{b})|\!\|^2_{\alpha^{-1},\widetilde{\mathcal{F}}_{\mathrm{c}}}$. Let $\underline{B} \in [\mathbb{P}_0(\mathrm{C})]^3$ be the L^2-orthogonal projection of $\underline{b}$ onto piecewise constant functions on the primal mesh. Owing to the triangle inequality and using (**H2**), we infer, for all $\mathrm{c} \in \mathrm{C}$, that

$$T_{\mathrm{c}}^2 \le 2\left(\|\!|\mathsf{R}_{\mathcal{E}_{\mathrm{c}}}(\underline{b}-\underline{B})|\!\|^2_{\alpha,\mathcal{E}_{\mathrm{c}}} + \|\!|\mathsf{R}_{\widetilde{\mathcal{F}}_{\mathrm{c}}}(\underline{b}-\underline{B})|\!\|^2_{\alpha^{-1},\widetilde{\mathcal{F}}_{\mathrm{c}}}\right).$$

Then, owing to (**H1**) (lower and upper bounds) and **(MR)**, we infer that

$$T_{\mathrm{c}}^2 \lesssim \alpha_{\sharp,\mathrm{c}} h_{\mathrm{c}} \sum_{\mathrm{e}\in\mathrm{E}_{\mathrm{c}}} |T_{\mathrm{e}}|^2 + \alpha_{\flat,\mathrm{c}}^{-1} h_{\mathrm{c}}^{-1} \sum_{\mathrm{e}\in\mathrm{E}_{\mathrm{c}}} |T_{\tilde{\mathrm{f}}_{\mathrm{c}}(\mathrm{e})}|^2,$$

where we have set

$$T_{\tilde{\mathrm{f}}_{\mathrm{c}}(\mathrm{e})} := \int_{\tilde{\mathrm{f}}_{\mathrm{c}}(\mathrm{e})} (\underline{b}-\underline{B})\cdot\underline{\nu}_{\tilde{\mathrm{f}}_{\mathrm{c}}(\mathrm{e})} \quad\text{and}\quad T_{\mathrm{e}} := \int_{\mathrm{e}} (\underline{b}-\underline{B})\cdot\underline{\tau}_{\mathrm{e}}. \tag{6.29}$$

These two terms are estimated using classical FE analysis tools applied on the simplicial submesh of each primal cell considered in **(MR)**. Consider first T_{e}. Pick a (subsimplex) face f of c to which e belongs. Since $\underline{b} \in [H^1(\mathrm{c})]^3$, we infer that $\underline{b} \in [L^4(\mathrm{f})]^3$. We use the result of Amrouche *et al.* (1998) (Lemma 4.7 with $p = 4$). We recall the main steps. Let $\varphi_{\mathrm{e},\partial\mathrm{f}}$ be the characteristic function of e on ∂f. This function is in $W^{\frac{1}{4},\frac{4}{3}}(\partial\mathrm{f})$ and $\|\varphi_{\mathrm{e},\partial\mathrm{f}}\|_{W^{\frac{1}{4},\frac{4}{3}}(\partial\mathrm{f})} \lesssim h_{\mathrm{c}}^{\frac{1}{2}}$ owing to the mesh regularity **(MR)**. The lifting of $\varphi_{\mathrm{e},\partial\mathrm{f}}$ from $W^{\frac{1}{4},\frac{4}{3}}(\partial\mathrm{f})$ to $W^{1,\frac{4}{3}}(\mathrm{f})$ is denoted by $\overline{\varphi}_{\mathrm{e,f}}$. Then, $\overline{\varphi}_{\mathrm{e,f}}$ is extended by zero on ∂c and we denote by $\overline{\overline{\varphi}}_{\mathrm{e,c}}$ the lifting of the last extension from $W^{\frac{1}{4},\frac{4}{3}}(\partial\mathrm{c})$ to $W^{1,\frac{4}{3}}(\mathrm{c})$. As a result, we infer that

$$T_{\mathrm{e}} = \int_{\mathrm{e}} \varphi_{\mathrm{e}}(\underline{b}-\underline{B})\cdot\underline{\tau}_{\mathrm{e}} = \int_{\mathrm{c}} \underline{\mathrm{curl}}(\underline{b}-\underline{B})\cdot\underline{\mathrm{grad}}(\overline{\overline{\varphi}}_{\mathrm{e,c}}) + \int_{\mathrm{f}} ((\underline{b}-\underline{B})\times\underline{\nu}_{\mathrm{f}})\cdot\underline{\mathrm{grad}}\,|_{\mathrm{f}}(\overline{\varphi}_{\mathrm{e,f}})$$

Then, using the Hölder inequality and the stability of the above lifting imply

$$\begin{aligned}|T_{\mathrm{e}}| &\lesssim h_{\mathrm{c}}^{\frac{1}{2}}\left(\|(\underline{b}-\underline{B})|_{\mathrm{c}}\times\underline{\nu}_{\mathrm{f}}\|_{L^4(\mathrm{f})^2} + \|\underline{\mathrm{curl}}\,\underline{b}\|_{L^4(\mathrm{c})^3}\right)\\ &\lesssim h_{\mathrm{c}}^{\frac{1}{2}}\left(\|\underline{b}\|_{H^1(\mathrm{c})^3} + \|\underline{\mathrm{curl}}\,\underline{b}\|_{L^4(\mathrm{c})^3}\right).\end{aligned}$$

The bound on $T_{2,\tilde{\mathrm{f}}_{\mathrm{c}}(\mathrm{e})}$ is simpler since **(MR)** yields

$$|T_{\tilde{\mathrm{f}}_{\mathrm{c}}(\mathrm{e})}| \le |\tilde{\mathrm{f}}_{\mathrm{c}}(\mathrm{e})|^{\frac{1}{2}}\|\underline{b}-\underline{B}\|_{L^2(\tilde{\mathrm{f}}_{\mathrm{c}}(\mathrm{e}))^3} \lesssim |\tilde{\mathrm{f}}_{\mathrm{c}}(\mathrm{e})|^{\frac{1}{2}} h_{\mathrm{c}}^{\frac{1}{2}}\|\underline{b}\|_{H^1(\mathrm{c})^3} \lesssim h_{\mathrm{c}}^{\frac{3}{2}}\|\underline{b}\|_{H^1(\mathrm{c})^3}.$$

Substituting the two contributions into (6.29), we end up with (6.28). □

Remark 6.15 (Stronger regularity assumption)**.** *Simpler arguments can be deployed whenever* $\underline{b}$ *is bounded and Lipschitz (see Codecasa & Trevisan, 2010a). By exploiting this stronger regularity assumption, mesh regularity can be formulated in terms of geometrical requirements without resorting to the simplicial submesh used in* **(MR)**. *Indeed, the terms* T_{e} *and* $T_{\tilde{\mathrm{f}}_{\mathrm{c}}(\mathrm{e})}$ *in the above proof can be readily estimated as* $|T_{\mathrm{e}}| \lesssim |\mathrm{e}|h_{\mathrm{c}}\mathrm{Lip}(\underline{b})$ *and* $|T_{\tilde{\mathrm{f}}_{\mathrm{c}}(\mathrm{e})}| \lesssim |\tilde{\mathrm{f}}_{\mathrm{c}}(\mathrm{e})|h_{\mathrm{c}}\mathrm{Lip}(\underline{b})$, *yielding* $\|\mathsf{R}_{\mathcal{E}}(\underline{b}-\underline{B})\|_\alpha \lesssim \eta_\alpha^{-1/2}\alpha_\sharp^{1/2}h|\Omega|^{\frac{1}{2}}\mathrm{Lip}(\underline{b})$ *(using* $|\mathrm{e}|^2h_{\mathrm{c}} \lesssim |\mathrm{c}|$*) and* $\|\mathsf{R}_{\widetilde{\mathcal{F}}}(\underline{b}-\underline{B})\|_{(\alpha)^{-1}} \lesssim \eta_\alpha^{-1/2}\alpha_\flat^{-1/2}h\mathrm{Lip}(\underline{\phi})$ *(using* $h_{\mathrm{c}}^{-1}|\tilde{\mathrm{f}}_{\mathrm{c}}(\mathrm{e})|^2 \lesssim |\mathrm{c}|$*).*

We now turn to the discrete Hodge operator $\mathsf{H}_\alpha^{\mathcal{F}\tilde{\mathcal{E}}}$.

Lemma 6.16 (Error bound for smooth fields)**.** *Assume* **(MR)**. *Assume that* $\underline{\underline{\alpha}}$ *is piecewise constant on primal cells. Let* $\underline{b} \in [H^1(\mathrm{C})]^3$ *be such that* $\underline{\mathrm{curl}}(\underline{b}) \in L^4(\Omega)^3$. *Let* $\mathsf{H}_\alpha^{\mathcal{F}\tilde{\mathcal{E}}}$ *satisfy* (**H0**), (**H1**), *and* (**H2**). *Then, the following inequality holds:*

$$\left\|\lfloor \alpha,\, {}^{\mathcal{F}\tilde{\mathcal{E}}}\rceil(\underline{b})\right\|_{\alpha^{-1},\tilde{\mathcal{E}}} \lesssim h\left(\|\underline{b}\|_{[H^1(\mathrm{C})]^3} + \|\underline{\mathrm{curl}}\,\underline{b}\|_{L^4(\Omega)^3}\right). \tag{6.30}$$

Proof. The proof follows the same lines as that of Lemma 6.14. □

6.3 Discrete Sobolev embeddings

Discrete functional analysis results presented in this section follow the lines of Eymard *et al.* (2010) for FV schemes (see also Di Pietro & Ern, 2012, for discontinuous Galerkin schemes). To allow for more generality, we consider in this section an arbitrary dimension $d > 1$.

6.3.1 Case of GRAD

For all $\mathbf{p} \in \mathcal{V}$, $\mathtt{L}^0_{\mathcal{V}}(\mathbf{p})$ is defined as the piecewise constant reconstruction of $\mathbf{p}$ on the dual mesh such that, for all $\mathrm{v} \in \mathrm{V}$, $\mathtt{L}^0_{\mathcal{V}}(\mathbf{p})|_{\tilde{\mathrm{c}}(\mathrm{v})} := \mathbf{p}_\mathrm{v}$. For convenience, this reconstruction is extended by zero on $\mathbb{R}^d \setminus \cup_{\mathrm{v}\in\mathrm{V}}\tilde{\mathrm{c}}(\mathrm{v})$. It is clear that $\mathtt{L}^0_{\mathcal{V}}(\mathbf{p}) \in L^1(\mathbb{R}^d)$. For a function $v \in L^1(\mathbb{R}^d)$, its $\|\cdot\|_{\mathrm{BV}}$-norm is defined as

$$\|v\|_{\mathrm{BV}} := \sup_{\underline{\psi}\in C_0^\infty(\mathbb{R}^d,\mathbb{R}^d),\|\underline{\psi}\|_{[L^\infty(\mathbb{R}^d)]^d}\le 1} \int_{\mathbb{R}^d} v\,\mathrm{div}(\underline{\psi}). \tag{6.31}$$

In what follows, we consider the space $\mathcal{V}_0 := \{\mathbf{p} \in \mathcal{V} \,|\, \mathbf{p}_\mathrm{v} = 0, \forall \mathrm{v} \in \mathrm{V}^\mathrm{B}\}$ where V^B is introduced in Definition 3.3. If $\mathbf{p} \in \mathcal{V}_0$, then $\mathsf{GRAD}(\mathbf{p}) \in \mathcal{E}_0 := \{\mathbf{g} \in \mathcal{E} \,|\, \mathbf{g}_\mathrm{e} = 0, \forall \mathrm{e} \in \mathrm{E}^\mathrm{B}\}$. Typically, the spaces $\mathcal{V}_0$ and $\mathcal{E}_0$ play a role when one considers vertex-based CDO schemes for an elliptic equation with strongly enforced homogeneous Dirichlet BCs.

Lemma 6.17 (Bound on $\|\cdot\|_{\mathrm{BV}}$-norm)**.** *Assume* (6.7). *Then, for all* $\mathbf{p} \in \mathcal{V}_0$, *the following inequality holds:*

$$\|\mathtt{L}^0_{\mathcal{V}}(\mathbf{p})\|_{\mathrm{BV}} \le \frac{\sqrt{d}}{\eta_\perp}\|\mathsf{GRAD}(\mathbf{p})\|_{1,\mathcal{E}}. \tag{6.32}$$

Proof. Owing to the adjunction property of Proposition 3.16 and the commuting property of Proposition 3.18 on the $\widetilde{\mathsf{DIV}}$ operator (since $\mathbf{p} \in \mathcal{V}_0$), we infer that

$$\int_{\mathbb{R}^d} \mathtt{L}^0_{\mathcal{V}}(\mathbf{p})\,\mathrm{div}(\underline{\psi}) = [\![\mathbf{p}, \mathsf{R}_{\tilde{\mathcal{C}}}(\mathrm{div}(\underline{\psi}))]\!]_{\mathcal{V}\tilde{\mathcal{C}}} = [\![\mathbf{p}, \widetilde{\mathsf{DIV}}(\mathsf{R}_{\tilde{\mathcal{F}}}(\underline{\psi}))]\!]_{\mathcal{V}\tilde{\mathcal{C}}} = -[\![\mathsf{GRAD}(\mathbf{p}), \mathsf{R}_{\tilde{\mathcal{F}}}(\underline{\psi})]\!]_{\mathcal{E}\tilde{\mathcal{F}}}.$$

Since all the components of $\underline{\psi}$ are bounded by 1, we infer that $|\mathsf{R}_{\tilde{\mathcal{F}}}(\underline{\psi})|_{\tilde{\mathrm{f}}(\mathrm{e})}| \le \sqrt{d}|\tilde{\mathrm{f}}(\mathrm{e})|$ for all $\mathrm{e} \in \mathrm{E}$, so that

$$\left|[\![\mathsf{GRAD}(\mathbf{p}), \mathsf{R}_{\tilde{\mathcal{F}}}(\underline{\psi})]\!]_{\mathcal{E}\tilde{\mathcal{F}}}\right| \le \sqrt{d}\sum_{\mathrm{e}\in\mathrm{E}}|(\mathsf{GRAD}(\mathbf{p}))_\mathrm{e}||\tilde{\mathrm{f}}(e)| = \sqrt{d}\sum_{\mathrm{e}\in\mathrm{E}}\sum_{\mathrm{c}\in\mathrm{C}_\mathrm{e}}|(\mathsf{GRAD}(\mathbf{p}))_\mathrm{e}||\tilde{\mathrm{f}}_\mathrm{c}(\mathrm{e})|.$$

Inverting the order of the summations, observing that $|\mathfrak{p}_{\mathrm{e,c}}| = \frac{1}{d}|\tilde{\mathrm{f}}_\mathrm{c}(\mathrm{e})||\mathrm{e}|\underline{\tau}_\mathrm{e}\cdot\underline{\nu}_{\tilde{\mathrm{f}}_\mathrm{c}(\mathrm{e})}$ and using (6.7) yield (6.32). □

An important consequence of Lemma 6.17 is the following discrete Sobolev embedding.

Theorem 6.18 (Discrete Sobolev embedding)**.** *Let* $d > 1$. *Let* $1 \le p < +\infty$. *Assume* (6.7). *Then, for all real number* q *satisfying*

- $1 \le q \le p^* := \frac{pd}{d-p}$ *if* $1 \le p < d$,
- $1 \le q < +\infty$ *if* $d \le p < +\infty$,

there is $C_{pq}^{(0)}$ *such that, for all* $\mathbf{p} \in \mathcal{V}_0$,

$$\|\!|\mathbf{p}|\!\|_{q,\mathcal{V}} \le C_{pq}^{(0)} \|\!|\mathsf{GRAD}(\mathbf{p})|\!\|_{p,\mathcal{E}}. \tag{6.33}$$

In particular, the choice $p = q = 2$ *leads to the following discrete Poincaré inequality:*

$$\|\!|\mathbf{p}|\!\|_{2,\mathcal{V}} \le C_{\mathrm{P}}^{(0)} \|\!|\mathsf{GRAD}(\mathbf{p})|\!\|_{2,\mathcal{E}}, \tag{6.34}$$

where $C_{\mathrm{P}}^{(0)} := C_{22}^{(0)}$.

Proof. Let a real number $1 \le p < +\infty$. Let $\mathbf{p} \in \mathcal{V}_0$ and set $\mathbf{g} := \mathsf{GRAD}(\mathbf{p}) \in \mathcal{E}_0$. We first observe that whenever $p < d$, it suffices to prove the bound (6.33) for $q = p^* := \frac{pd}{d-p}$, since the bounds for $1 \le q < p^*$ then result from the bound for $q = p^*$ and the Hölder inequality (6.4).

(1) The case $p = 1$. Set $1^* = \frac{d}{d-1}$. A classical result (see, *e.g.*, Eymard *et al.*, 2000) states that, for all $v \in L^1(\mathbb{R}^d)$ with bounded $\|\cdot\|_{\mathrm{BV}}$-norm, $\|v\|_{L^{1^*}(\mathbb{R}^d)} \le (2d)^{-1}\|v\|_{\mathrm{BV}}$. Hence, using Lemma 6.17, we infer that

$$\|\mathtt{L}_{\mathcal{V}}^0(\mathbf{p})\|_{L^{1^*}(\mathbb{R}^d)} \le (2d)^{-1}\|\mathtt{L}_{\mathcal{V}}^0(\mathbf{p})\|_{\mathrm{BV}} \le (2\sqrt{d}\eta_\perp)^{-1}\|\!|\mathbf{g}|\!\|_{1,\mathcal{E}}.$$

Since $\|\!|\mathbf{p}|\!\|_{1^*,\mathcal{V}} = \|\mathtt{L}_{\mathcal{V}}^0(\mathbf{p})\|_{L^{1^*}(\mathbb{R}^d)}$, we infer the desired bound (6.33) for $q = 1^*$.

(2) The case $1 < p < d$. Let $\mu := \frac{p(d-1)}{d-p} > 1$ and observe that $p^* = \mu 1^*$. Let $|\mathbf{p}|^\mu$ denote the element of $\mathcal{V}_0$ whose components are, for all $\mathrm{v} \in \mathrm{V}$, $|\mathbf{p}_\mathrm{v}|^\mu$. Applying the above bound to $|\mathbf{p}|^\mu$ yields

$$\|\!|\mathbf{p}|\!\|_{p^*,\mathcal{V}}^\mu = \|\!||\mathbf{p}|^\mu|\!\|_{1^*,\mathcal{V}} \le (2\sqrt{d}\eta_\perp)^{-1}\|\!|\mathsf{GRAD}(|\mathbf{p}|^\mu)|\!\|_{1,\mathcal{E}}.$$

Let $\mathrm{e} \in \mathrm{E}$ with vertices v_1 and v_2; since $|\mathsf{GRAD}(|\mathbf{p}|^\mu)|_\mathrm{e} \le \mu(|\mathbf{p}_{\mathrm{v}_1}|^{\mu-1} + |\mathbf{p}_{\mathrm{v}_2}|^{\mu-1})|\mathbf{g}_\mathrm{e}|$, we infer that

$$\|\!|\mathsf{GRAD}(|\mathbf{p}|^\mu)|\!\|_{1,\mathcal{E}} \le \mu \sum_{\mathrm{c}\in\mathrm{C}} \sum_{\mathrm{e}\in\mathrm{E}_\mathrm{c}} \sum_{\mathrm{v}\in\mathrm{V}_\mathrm{e}} |\mathfrak{p}_{\mathrm{e,c}}||\mathbf{p}_\mathrm{v}|^{\mu-1} \left(\frac{|\mathbf{g}_\mathrm{e}|}{|\mathrm{e}|}\right).$$

Using the Hölder inequality (6.5) with $\alpha = p$, $\beta = \frac{p}{p-1}$ (so that $\beta(\mu-1) = p^*$), $a_k = \frac{|\mathbf{g}_\mathrm{e}|}{|\mathrm{e}|}|\mathfrak{p}_{\mathrm{e,c}}|^{\frac{1}{p}}$, $b_k = |\mathfrak{p}_{\mathrm{e,c}}|^{\frac{1}{\beta}}|\mathbf{p}_\mathrm{v}|^{\mu-1}$, and $k = \{\mathrm{c},\mathrm{e},\mathrm{v}\}$ leads to

$$\|\!|\mathsf{GRAD}(|\mathbf{p}|^\mu)|\!\|_{1,\mathcal{E}} \le 2^{\frac{1}{p}}\mu\|\!|\mathbf{g}|\!\|_{p,\mathcal{E}} \left(\sum_{\mathrm{c}\in\mathrm{C}} \sum_{\mathrm{e}\in\mathrm{E}_\mathrm{c}} \sum_{\mathrm{v}\in\mathrm{V}_\mathrm{e}} |\mathfrak{p}_{\mathrm{e,c}}||\mathbf{p}_\mathrm{v}|^{p^*}\right)^{\frac{1}{\beta}}.$$

Moreover,

$$\sum_{\mathrm{c}\in\mathrm{C}} \sum_{\mathrm{e}\in\mathrm{E}_\mathrm{c}} \sum_{\mathrm{v}\in\mathrm{V}_\mathrm{e}} |\mathfrak{p}_{\mathrm{e,c}}||\mathbf{p}_\mathrm{v}|^{p^*} = 2\sum_{\mathrm{c}\in\mathrm{C}} \sum_{\mathrm{v}\in\mathrm{V}_\mathrm{c}} |\tilde{\mathrm{c}}(\mathrm{v}) \cap \mathrm{c}||\mathbf{p}_\mathrm{v}|^{p^*},$$

since $\sum_{\mathrm{e}\in\mathrm{E}_\mathrm{c}\cap\mathrm{E}_\mathrm{v}} |\mathfrak{p}_{\mathrm{e,c}}| = 2|\tilde{\mathrm{c}}(\mathrm{v}) \cap \mathrm{c}|$ for all $\mathrm{v} \in \mathrm{V}_\mathrm{c}$. As a result, we obtain

$$\|\!|\mathbf{p}|\!\|_{p^*,\mathcal{V}}^\mu \le \frac{\mu}{\sqrt{d}\eta_\perp} \|\!|\mathbf{p}|\!\|_{p^*,\mathcal{V}}^{\frac{p^*}{\beta}} \|\!|\mathbf{g}|\!\|_{p,\mathcal{E}}.$$

Combining the above bounds with the fact that $\mu = \frac{p^*}{\beta} + 1$ yields the desired bound (6.33) for $q = p^*$ with the constant $\mu(\sqrt{d}\eta_\perp)^{-1}$.

(3) The case $d \le p$. Let $q_1 > d$ and set $p_1 := \frac{dq_1}{d+q_1}$. Observe that $1 < p_1 < d$ and $p_1^* = q_1$, so that $\|\!|\mathbf{p}|\!\|_{q_1,\mathcal{V}} \le C_{p_1q_1}^{(0)}\|\!|\mathbf{g}|\!\|_{p_1,\mathcal{E}}$. Since $p_1 < d \le p$, the right-hand side can be bounded by $\|\!|\mathbf{g}|\!\|_{p,\mathcal{E}}$ owing to Hölder's inequality (6.4), whence the desired bound (6.33) for q_1. □

6.3.2 Case of $\widetilde{\mathsf{GRAD}}$

For all $\mathbf{p} \in \widetilde{\mathcal{V}}$, $\mathtt{L}^0_{\widetilde{\mathcal{V}}}(\mathbf{p})$ is the piecewise constant reconstruction of $\mathbf{p}$ on the primal mesh with $\mathtt{L}^0_{\widetilde{\mathcal{V}}}(\mathbf{p})|_{\mathrm{c}} = \mathbf{p}_{\tilde{\mathrm{v}}(\mathrm{c})}$. For convenience, $\mathtt{L}^0_{\widetilde{\mathcal{V}}}(\mathbf{p})$ is extended by zero outside Ω.

Lemma 6.19 (Bound on $\|\cdot\|_{\mathrm{BV}}$-norm)**.** *For all $\mathbf{p} \in \widetilde{\mathcal{V}}$, the following inequality holds:*

$$\|\mathtt{L}^0_{\widetilde{\mathcal{V}}}(\mathbf{p})\|_{\mathrm{BV}} \le \sqrt{d} \|\widetilde{\mathsf{GRAD}}(\mathbf{p})\|_{1,\widetilde{\mathcal{E}}}.$$

Proof. Owing to the adjunction property between $-\widetilde{\mathsf{GRAD}}$ and DIV (Proposition 3.16) and the commuting property of DIV with the de Rham maps (Proposition 3.13), we first infer, for all $\underline{\psi} \in C^\infty_0(\mathbb{R}^d, \mathbb{R}^d)$ s.t. $\|\underline{\psi}\|_{[L^\infty(\mathbb{R}^d)]^d} = 1$, that

$$\left| \int_{\mathbb{R}^d} \mathtt{L}^0_{\widetilde{\mathcal{V}}}(\mathbf{p}) \operatorname{div}(\underline{\psi}) \right| = \left| [\![\mathbf{g}, \mathsf{R}_{\mathcal{F}}(\underline{\psi})]\!]_{\widetilde{\mathcal{E}}\mathcal{F}} \right| \le \sqrt{d} \sum_{\mathrm{f}\in\mathrm{F}} |\mathrm{f}| |\mathbf{g}_{\tilde{\mathrm{e}}(\mathrm{f})}| = \sqrt{d} \|\mathbf{g}\|_{1,\widetilde{\mathcal{E}}},$$

where we have set $\mathbf{g} := \widetilde{\mathsf{GRAD}}(\mathbf{p})$ and used the fact that for all $\mathrm{f} \in \mathrm{F}$, $|\mathsf{R}_{\mathcal{F}}(\underline{\psi})|_{\mathrm{f}}| \le \sqrt{d}|\mathrm{f}|$, since all the components of $\underline{\psi}$ are bounded by 1. □

Theorem 6.20 (Discrete Sobolev embedding)**.** *Let $d > 1$. Let $1 \le p < +\infty$. Assume* (6.8)*. Then, for all real number q as in Theorem 6.18, there is $C^{(\tilde{0})}_{pq}$ such that, for all $\mathbf{p} \in \widetilde{\mathcal{V}}$,*

$$\|\mathbf{p}\|_{q,\widetilde{\mathcal{V}}} \le C^{(\tilde{0})}_{pq} \|\widetilde{\mathsf{GRAD}}(\mathbf{p})\|_{p,\widetilde{\mathcal{E}}}.$$

In particular, the choice $p = q = 2$ leads to the following discrete Poincaré inequality:

$$\|\mathbf{p}\|_{2,\widetilde{\mathcal{V}}} \le C^{(\tilde{0})}_{\mathrm{P}} \|\widetilde{\mathsf{GRAD}}(\mathbf{p})\|_{2,\widetilde{\mathcal{E}}}, \tag{6.35}$$

where $C^{(\tilde{0})}_{\mathrm{P}} := C^{(\tilde{0})}_{22}$.

Proof. (1) The case $1 \le q \le 1^*$. We infer that $\|\mathbf{p}\|_{q,\widetilde{\mathcal{V}}} \le C^{(\tilde{0})}_{1q} \|\widetilde{\mathsf{GRAD}}(\mathbf{p})\|_{1,\widetilde{\mathcal{E}}}$ using Lemma 6.19, the classical result $\|\mathtt{L}^0_{\widetilde{\mathcal{V}}}(\mathbf{p})\|_{L^{1^*}(\mathbb{R}^d)} \le (2d)^{-1} \|\mathtt{L}^0_{\widetilde{\mathcal{V}}}(\mathbf{p})\|_{\mathrm{BV}}$, the identity $\|\mathtt{L}^0_{\widetilde{\mathcal{V}}}(\mathbf{p})\|_{L^{1^*}(\mathbb{R}^d)} = \|\mathbf{p}\|_{1^*,\widetilde{\mathcal{V}}}$ and Hölder's inequality (6.9a).

(2) The case $1 \le q \le p^*$. We define μ as in Theorem 6.18. Owing to Lemma 6.19, we infer that $\|\mathbf{p}\|^\mu_{p^*,\widetilde{\mathcal{V}}} = \||\mathbf{p}|^\mu\|_{1^*,\widetilde{\mathcal{V}}} \le (2\sqrt{d})^{-1} \|\widetilde{\mathsf{GRAD}}(|\mathbf{p}|^\mu)\|_{1,\widetilde{\mathcal{E}}}$. We set $\mathbf{g} = \widetilde{\mathsf{GRAD}}(\mathbf{p})$. Since $\widetilde{\mathsf{GRAD}}(|\mathbf{p}|^\mu)|_{\tilde{\mathrm{e}}(\mathrm{f})} \le \mu \mathbf{g}_{\tilde{\mathrm{e}}(\mathrm{f})} \sum_{\mathrm{c}\in\mathrm{C_f}} |\mathbf{p}_{\tilde{\mathrm{v}}(\mathrm{c})}|^{\mu-1}$ for each $\mathrm{f} \in \mathrm{F}$, we infer using Hölder's inequality (6.5) with $\alpha = p$, $\beta = \frac{p}{p-1}$, $a_k = (|\mathrm{f}||\tilde{\mathrm{e}}(\mathrm{f})|)^{\frac{1}{p}} \frac{|\mathbf{g}_{\tilde{\mathrm{e}}(\mathrm{f})}|}{|\tilde{\mathrm{e}}(\mathrm{f})|}$, $b_k = (|\mathrm{f}||\tilde{\mathrm{e}}(\mathrm{f})|)^{\frac{1}{\beta}} |\mathbf{p}_{\tilde{\mathrm{v}}(\mathrm{c})}|^{\mu-1}$, and $k = \{\mathrm{f}, \mathrm{c}\}$ that

$$\|\widetilde{\mathsf{GRAD}}(|\mathbf{p}|^\mu)\|_{1,\widetilde{\mathcal{E}}} \le \mu 2^{\frac{1}{p}} \|\mathbf{g}\|_{p,\widetilde{\mathcal{E}}} \left(\sum_{\mathrm{f}\in\mathrm{F}} \sum_{\mathrm{c}\in\mathrm{C_f}} |\mathrm{f}||\tilde{\mathrm{e}}(\mathrm{f})| |\mathbf{p}_{\tilde{\mathrm{v}}(\mathrm{c})}|^{\beta(\mu-1)} \right)^{\frac{1}{\beta}} \le \mu \eta_{\mathrm{vol}}^{\frac{1}{\beta}} 2^{\frac{1}{p}} \|\mathbf{g}\|_{p,\widetilde{\mathcal{E}}} \|\mathbf{p}\|^{\frac{p^*}{\beta}}_{p^*,\widetilde{\mathcal{V}}}.$$

To obtain the last inequality, we have inverted the order of summations and used (6.8). Notice that $\mu - 1 = \frac{p^*}{\beta}$. Using Hölder's inequality (6.9a) yields $\|\mathbf{p}\|_{q,\widetilde{\mathcal{V}}} \le C^{(\tilde{0})}_{pq} \|\widetilde{\mathsf{GRAD}}(\mathbf{p})\|_{p,\widetilde{\mathcal{E}}}$.

(3). The proof of the case $d \le p$ follows the same lines as Theorem 6.18. □

Remark 6.21. *Note that in Theorem 6.20, $\mathbf{p} \in \widetilde{\mathcal{V}}$ as opposed to Theorem 6.18 where $\mathbf{p} \in \mathcal{V}_0$ (and not $\mathcal{V}$). The reason is that for all dual edges touching the boundary $\partial\Omega$, $\widetilde{\mathsf{GRAD}}(\mathbf{p})|_{\tilde{\mathrm{e}}}$ only contains one vertex contribution (namely that from the vertex of $\tilde{\mathrm{e}}$ in Ω).*

Chapter 7

Analysis using reconstruction operators

Contents

In the previous chapter, an algebraic analysis based on finite-dimensional DoFs spaces has been developed. The use of reconstruction operators allows us to adopt a new viewpoint on CDO schemes (in a spirit closer to the FE approach) that extends the algebraic analysis. In this chapter, we assume that the meshes belong to the class **(MB)** and that primal faces are planar. This is a relatively weak assumption which is verified by several meshes (see Figure 3.9 for examples). In Section 7.1, we detail the principles underpinning the reconstruction operators. As for the discrete Hodge operator, the design properties are stated locally. In Section 7.2, we give simple examples of reconstruction operators for the potential, circulation, and flux on specific meshes and a simple potential reconstruction operator on polyhedral meshes. In Section 7.3, we define reconstruction operators on polyhedral meshes. Three families of reconstructions are successively introduced according to their properties: piecewise constant reconstructions, piecewise polynomial and conforming (we will precise the meaning in what follows) reconstructions, and piecewise polynomial and conforming reconstructions which satisfy a "dual consistency" property. These three families of reconstruction operators are introduced either to derive further theoretical results or to implement new discrete Hodge operators. We conclude this chapter by deriving new discrete Poincaré inequalities in Section 7.4.

7.1 Reconstruction operators

7.1.1 Local reconstruction operators

Loosely speaking, a reconstruction (or lifting) operator generates a field from a set of DoFs and it acts as an approximate inverse of the de Rham map. A reconstruction operator acting on the DoFs of the space $\mathcal{X}$ is denoted by $\mathtt{L}_{\mathcal{X}}$. Similarly to the discrete Hodge operator, the reconstruction operator is devised locally on the cells of the primal mesh.

Definition 7.1 (Local reconstruction operator)**.** *Let* $\mathrm{c} \in \mathrm{C}$*. The* local *reconstruction operator* $\mathtt{L}_{\mathcal{X}_\mathrm{c}} : \mathcal{X}_\mathrm{c} \to P_{\mathcal{X}}(\mathrm{c})$ *is defined in terms of a family of* $\#\mathrm{X}_\mathrm{c}$ *linearly independent functions* $\{\ell_{\mathrm{x},\mathrm{c}}\}_{\mathrm{x}\in\mathrm{X}_\mathrm{c}}$ *spanning the finite-dimensional space* $P_{\mathcal{X}}(\mathrm{c})$*, called the* approximation *space, so that the reconstructed field* $\mathtt{L}_{\mathcal{X}_\mathrm{c}}(\mathbf{a})$ *is defined by*

$$\mathtt{L}_{\mathcal{X}_\mathrm{c}}(\mathbf{a})(\underline{x}) := \sum_{\mathrm{x}\in\mathrm{X}_\mathrm{c}} \mathbf{a}_\mathrm{x}\ell_{\mathrm{x},\mathrm{c}}(\underline{x}), \qquad \forall \mathbf{a} \in \mathcal{X}_\mathrm{c},\ \forall \underline{x} \in \mathrm{c}.$$

Whenever needed, we distinguish the case of scalar-valued reconstruction operators $\mathtt{L}_{\mathcal{X}}$ when $\mathcal{X} \in \{\mathcal{V}, \mathcal{C}\}$ and that of vector-valued reconstruction operators $\underline{\mathtt{L}}_{\mathcal{X}}$ when $\mathcal{X} \in \{\mathcal{E}, \mathcal{F}\}$. The space $P_{\mathcal{X}}(\mathrm{c})$ is generally a broken polynomial space spanned by scalar-valued polynomials when $\mathcal{X} \in \{\mathcal{V}, \mathcal{C}\}$ and by vector-valued polynomials when $\mathcal{X} \in \{\mathcal{E}, \mathcal{F}\}$. In what follows, we focus on the case $\mathcal{X} \in \{\mathcal{V}, \mathcal{E}, \mathcal{F}\}$. The case $\mathcal{X} = \mathcal{C}$, which follows the same lines, is straightforward (cf. Remark 7.8). We assume that the functions in $P_{\mathcal{X}}(\mathrm{c})$ are in the domain of the local de Rham map $\mathsf{R}_{\mathcal{X}_\mathrm{c}}$, *i.e.* $P_{\mathcal{X}}(\mathrm{c}) \subset S_{\mathcal{X}}(\mathrm{c})$.

Remark 7.2 (Local conformity)**.** *The concept of conformity with respect to a functional space is a key element of distinction between the reconstruction operators. Let* S *be a functional space. A reconstruction is said to be* S*-conforming if the range of the reconstruction operator is a subspace of* S*. There are three relevant conformities to consider in our context:* H^1*-conformity for potentials (i.e.* $P_{\mathcal{V}}(\mathrm{c}) \subset H^1(\mathrm{c})$ *for each cell* $\mathrm{c} \in \mathrm{C}$*),* $H(\underline{\mathrm{curl}})$*-conformity for circulations (i.e.* $P_{\mathcal{E}}(\mathrm{c}) \subset H(\underline{\mathrm{curl}};\mathrm{c})$ *for each cell* $\mathrm{c} \in \mathrm{C}$*), and* $H(\mathrm{div})$*-conformity for fluxes (i.e.* $P_{\mathcal{F}}(\mathrm{c}) \subset H(\mathrm{div};\mathrm{c})$ *for each cell* $\mathrm{c} \in \mathrm{C}$*). We use the superscript* conf *to indicate the conformity of a reconstruction operator. Notice that, in general, the reconstruction operators we consider are non-conforming.*

Link with discrete Hodge operators. A local reconstruction operator or equivalently a set of local reconstruction functions induces a local discrete Hodge operator. Namely, given a set of functions $\{\ell_{\mathrm{x},\mathrm{c}}\}_{\mathrm{x}\in\mathrm{X}_\mathrm{c}}$, the local discrete Hodge operator $\mathsf{H}_\alpha^{\mathcal{X}_\mathrm{c}\tilde{\mathcal{Y}}_\mathrm{c}}$ is generically defined by

$$\mathsf{H}_\alpha^{\mathcal{X}_\mathrm{c}\tilde{\mathcal{Y}}_\mathrm{c}}|_{\mathrm{x}',\tilde{\mathrm{y}}(\mathrm{x})} := \int_\mathrm{c} \ell_{\mathrm{x},\mathrm{c}}(\underline{x})\,\alpha\ell_{\mathrm{x}',\mathrm{c}}(\underline{x}), \qquad \forall \mathrm{x},\mathrm{x}' \in \mathrm{X}_\mathrm{c}, \tag{7.1}$$

so that, owing to Definition 7.1, we infer that

$$[\![\mathbf{a}_1, \mathsf{H}_\alpha^{\mathcal{X}_\mathrm{c}\tilde{\mathcal{Y}}_\mathrm{c}}(\mathbf{a}_2)]\!]_{\mathcal{X}_\mathrm{c}\tilde{\mathcal{Y}}_\mathrm{c}} := \int_\mathrm{c} \mathtt{L}_{\mathcal{X}_\mathrm{c}}(\mathbf{a}_1)\,\alpha\mathtt{L}_{\mathcal{X}_\mathrm{c}}(\mathbf{a}_2), \qquad \forall \mathbf{a}_1, \mathbf{a}_2 \in \mathcal{X}_\mathrm{c}. \tag{7.2}$$

Here, α is the considered material property which we assume to be piecewise constant on the primal mesh. As previously noticed by Bossavit (2000) (cf. the concept of *Galerkin Hodge* when the Whitney reconstruction functions are used), a discrete Hodge operator defined by (7.1) is a mass matrix weighted by the material property α. The link between the CDO approach and the FE approach appears naturally in (7.1) since FE basis functions can be considered as CDO reconstruction functions.

Besides the generic definition (7.2) which allows us to build local discrete Hodge operators, the reconstruction operator is also useful to derive further theoretical results, for instance,

the discrete Poincaré inequalities (cf. Lemmata 7.45 and 7.47 below) or the second-order convergence rate in L^2-norm for the potential in elliptic problems (cf. Theorems 8.13 and 8.23 below). Moreover, the reconstruction operators are also of practical interest for postprocessing the discrete solution.

7.1.2 Local design properties

The design of the reconstruction operators hinges on local properties whose aim is to recover the three properties stated in Section 6.2.1 for the local discrete Hodge operator: symmetry (**H0**), stability (**H1**), and $\mathbb{P}_0$-consistency (**H2**). Notice that (**H0**) is readily satisfied using (7.2). There are two equivalent ways to state these design properties.

Direct approach on reconstruction functions. This approach is considered by Codecasa & Trevisan (2010a) (except for (**R1**)). For all $\mathrm{c} \in \mathrm{C}$, we require that:

(**R1**) [*Stability*] There exists a real constant $\eta_{\mathcal{X}} > 0$ uniform w.r.t. c such that

$$\eta_{\mathcal{X}} \|\!|\mathbf{a}|\!\|_{2,\mathcal{X}_\mathrm{c}}^2 \le \|\mathsf{L}_{\mathcal{X}_\mathrm{c}}(\mathbf{a})\|_{L^2(\mathrm{c})}^2 \le \eta_{\mathcal{X}}^{-1} \|\!|\mathbf{a}|\!\|_{2,\mathcal{X}_\mathrm{c}}^2, \qquad \forall \mathbf{a} \in \mathcal{X}_\mathrm{c}.$$

(**R2**) [*Partition of unity*] For any constant field K in c, the following identity holds:

$$\mathsf{L}_{\mathcal{X}_\mathrm{c}} \mathsf{R}_{\mathcal{X}_\mathrm{c}}(K) = K.$$

(**R3**) [*Dual consistency*] For any constant field $\widetilde{K}$ in c, the following identity holds:

$$\int_\mathrm{c} \mathsf{L}_{\mathcal{X}_\mathrm{c}}(\mathbf{a}) \cdot \widetilde{K} = [\![\mathbf{a}, \mathsf{R}_{\widetilde{\mathcal{Y}}_\mathrm{c}}(\widetilde{K})]\!]_{\mathcal{X}_\mathrm{c}\widetilde{\mathcal{Y}}_\mathrm{c}}, \qquad \forall \mathbf{a} \in \mathcal{X}_\mathrm{c}.$$

(**R4**) [*Unisolvence*] $\mathsf{L}_{\mathcal{X}_\mathrm{c}}$ is a right inverse of $\mathsf{R}_{\mathcal{X}_\mathrm{c}}$, *i.e.*

$$\mathsf{R}_{\mathcal{X}_\mathrm{c}} \mathsf{L}_{\mathcal{X}_\mathrm{c}} = \mathsf{Id}_{\mathcal{X}_\mathrm{c}}.$$

Proposition 7.3. *Let* $\mathsf{H}_\alpha^{\mathcal{X}_\mathrm{c}\widetilde{\mathcal{Y}}_\mathrm{c}}$ *be defined by* (7.2)*. Assume* (**R1**)–(**R3**)*. Then,* (**H0**)*,* (**H1**)*, and* (**H2**) *hold.*

Proof. (**H0**) is readily verified. The stability property (**H1**) results from (**R1**) and (7.2). Let K be a constant field on c. Recall that α is constant in c. (**H2**) results from

$$\begin{aligned}
\forall \mathbf{a} \in \mathcal{X}_\mathrm{c}, \quad [\![\mathbf{a}, \mathsf{H}_\alpha^{\mathcal{X}_\mathrm{c}\widetilde{\mathcal{Y}}_\mathrm{c}} \cdot \mathsf{R}_{\mathcal{X}_\mathrm{c}}(K)]\!]_{\mathcal{X}_\mathrm{c}\widetilde{\mathcal{Y}}_\mathrm{c}} &= \int_\mathrm{c} \mathsf{L}_{\mathcal{X}_\mathrm{c}}(\mathbf{a}) \cdot \alpha \mathsf{L}_{\mathcal{X}_\mathrm{c}} \mathsf{R}_{\mathcal{X}_\mathrm{c}}(K) && \text{by (7.2)}, \\
&= \int_\mathrm{c} \mathsf{L}_{\mathcal{X}_\mathrm{c}}(\mathbf{a}) \cdot \alpha K && \text{by (\textbf{R2})}, \\
&= [\![\mathbf{a}, \mathsf{R}_{\widetilde{\mathcal{Y}}_\mathrm{c}}(\alpha K)]\!]_{\mathcal{X}_\mathrm{c}\widetilde{\mathcal{Y}}_\mathrm{c}} && \text{by (\textbf{R3})}.
\end{aligned}$$

The conclusion follows since $\mathbf{a}$ is arbitrary in $\mathcal{X}_\mathrm{c}$. □

Therefore, every discrete Hodge operator built from (7.2) with a reconstruction operator verifying the three properties (**R1**)–(**R3**) inherits the theoretical results derived in Chapter 6.

Remark 7.4 (Unisolvence)**.** *Observe that the unisolvence property* (**R4**) *is not needed to satisfy the design properties of the discrete Hodge operator identified in Chapter 6.*

Local design properties on reconstruction functions. We now specify what are the equivalences in terms of reconstruction functions of the properties (**R2**)–(**R4**) for each type of primal DoFs. We only state the results since the proofs are straightforward. In what follows, K is a constant scalar-valued field in the case of $\mathcal{V}_\mathrm{c}$ and a constant vector-valued field in the case of $\mathcal{E}_\mathrm{c}$ and $\mathcal{F}_\mathrm{c}$.

Proposition 7.5 (Requirements for $\ell_{\mathrm{v,c}}$)**.** *Let* $\mathrm{c} \in \mathrm{C}$. *The following properties of the reconstruction functions* $\{\ell_{\mathrm{v,c}}\}_{\mathrm{v}\in\mathrm{V_c}}$ *are equivalent to* (**R2**)–(**R4**) *for* $\mathsf{L}_{\mathcal{V}_\mathrm{c}}$*:*

$$(\mathbf{R2}) \quad \mathsf{L}_{\mathcal{V}_\mathrm{c}}\mathsf{R}_{\mathcal{V}_\mathrm{c}}(K) = K \qquad \Longleftrightarrow \qquad \sum_{\mathrm{v}\in\mathrm{V_c}} \ell_{\mathrm{v,c}}(\underline{x}) = 1, \qquad \forall \underline{x} \in \mathrm{c}, \tag{7.3a}$$

and for all $\mathbf{a} \in \mathcal{V}_\mathrm{c}$*,*

$$(\mathbf{R3}) \quad \int_\mathrm{c} \mathsf{L}_{\mathcal{V}_\mathrm{c}}(\mathbf{a}) = \sum_{\mathrm{v}\in\mathrm{V_c}} \mathbf{a}_\mathrm{v}|\tilde{\mathrm{c}}(\mathrm{v}) \cap \mathrm{c}| \quad \Longleftrightarrow \quad \int_\mathrm{c} \ell_{\mathrm{v,c}} = |\mathrm{c} \cap \tilde{\mathrm{c}}(\mathrm{v})|, \qquad \forall \mathrm{v} \in \mathrm{V_c}, \tag{7.3b}$$

$$(\mathbf{R4}) \quad \mathsf{R}_{\mathcal{V}_\mathrm{c}}\mathsf{L}_{\mathcal{V}_\mathrm{c}}(\mathbf{a}) = \mathbf{a} \qquad \Longleftrightarrow \quad \ell_{\mathrm{v}',\mathrm{c}}(\underline{x}_\mathrm{v}) = \delta_{\mathrm{v},\mathrm{v}'}, \qquad \forall \mathrm{v}, \mathrm{v}' \in \mathrm{V_c}. \tag{7.3c}$$

In addition, whenever the *linear completeness* property

$$\sum_{\mathrm{v}\in\mathrm{V_c}} \underline{x}_\mathrm{v} \ell_{\mathrm{v,c}}(\underline{x}) = \underline{x}, \qquad \forall \underline{x} \in \mathrm{c}, \tag{7.4}$$

holds along with (**R2**), this induces the $\mathbb{P}_1$-consistency property, *i.e.* for any affine field A, $\mathsf{L}_{\mathcal{V}_\mathrm{c}}\mathsf{R}_{\mathcal{V}_\mathrm{c}}(A) = A$. Indeed, in each cell $\mathrm{c} \in \mathrm{C}$, A can be written as $A(\underline{x}) := A(\underline{x}_\mathrm{c}) + \underline{G} \cdot (\underline{x} - \underline{x}_\mathrm{c})$ with $\underline{G}$ constant in c, so that

$$\begin{aligned}\mathsf{L}_{\mathcal{V}_\mathrm{c}}\mathsf{R}_{\mathcal{V}_\mathrm{c}}(A(\underline{x})) &= \sum_{\mathrm{v}\in\mathrm{V_c}} A(\underline{x}_\mathrm{v})\ell_{\mathrm{v,c}}(\underline{x}) = \sum_{\mathrm{v}\in\mathrm{V_c}} \left(A(\underline{x}_\mathrm{c}) - \underline{G} \cdot (\underline{x}_\mathrm{v} - \underline{x}_\mathrm{c})\right) \ell_{\mathrm{v,c}}(\underline{x}) \\ &= A(\underline{x}_\mathrm{c}) + \underline{G} \cdot (\underline{x} - \underline{x}_\mathrm{c}) = A(\underline{x}).\end{aligned}$$

Proposition 7.6 (Requirements for $\underline{\ell}_{\mathrm{e,c}}$)**.** *Let* $\mathrm{c} \in \mathrm{C}$. *The following properties of the reconstruction functions* $\{\underline{\ell}_{\mathrm{e,c}}\}_{\mathrm{e}\in\mathrm{E_c}}$ *are equivalent to* (**R2**)–(**R4**) *for* $\underline{\mathsf{L}}_{\mathcal{E}_\mathrm{c}}$*:*

$$(\mathbf{R2}) \quad \underline{\mathsf{L}}_{\mathcal{E}_\mathrm{c}}\mathsf{R}_{\mathcal{E}_\mathrm{c}}(\underline{K}) = \underline{K} \qquad \Longleftrightarrow \qquad \sum_{\mathrm{e}\in\mathrm{E_c}} \underline{\ell}_{\mathrm{e,c}}(\underline{x}) \otimes \underline{\mathrm{e}} = \underline{\underline{\mathsf{Id}}}, \qquad \forall \underline{x} \in \mathrm{c}, \tag{7.5a}$$

where $\underline{\mathrm{e}} = \int_\mathrm{e} \underline{\tau}_\mathrm{e}$ *(cf. Definition 5.13), and for all* $\mathbf{a} \in \mathcal{E}_\mathrm{c}$*,*

$$(\mathbf{R3}) \quad \int_\mathrm{c} \underline{\mathsf{L}}_{\mathcal{E}_\mathrm{c}}(\mathbf{a}) = \sum_{\mathrm{e}\in\mathrm{E_c}} \mathbf{a}_\mathrm{e}\tilde{\underline{\mathrm{f}}}_\mathrm{c}(\mathrm{e}) \quad \Longleftrightarrow \quad \int_\mathrm{c} \underline{\ell}_{\mathrm{e,c}} = \tilde{\underline{\mathrm{f}}}_\mathrm{c}(\mathrm{e}), \qquad \forall \mathrm{e} \in \mathrm{E_c}, \tag{7.5b}$$

where $\tilde{\underline{\mathrm{f}}}_\mathrm{c}(\mathrm{e}) = \int_{\tilde{\mathrm{f}}_\mathrm{c}(\mathrm{e})} \underline{\nu}_{\tilde{\mathrm{f}}_\mathrm{c}(\mathrm{e})}$ *(cf. Definition 5.16),*

$$(\mathbf{R4}) \quad \mathsf{R}_{\mathcal{E}_\mathrm{c}}\underline{\mathsf{L}}_{\mathcal{E}_\mathrm{c}}(\mathbf{a}) = \mathbf{a} \qquad \Longleftrightarrow \qquad \int_\mathrm{e} \underline{\ell}_{\mathrm{e}',\mathrm{c}} \cdot \underline{\tau}_\mathrm{e} = \delta_{\mathrm{e},\mathrm{e}'}, \qquad \forall \mathrm{e}, \mathrm{e}' \in \mathrm{E_c}. \tag{7.5c}$$

Proposition 7.7 (Requirements for $\underline{\ell}_{\mathrm{f,c}}$)**.** *Let* $\mathrm{c} \in \mathrm{C}$. *The following properties of the reconstruction functions* $\{\underline{\ell}_{\mathrm{f,c}}\}_{\mathrm{f}\in\mathrm{F_c}}$ *are equivalent to* (**R2**)–(**R4**) *for* $\underline{\mathsf{L}}_{\mathcal{F}_\mathrm{c}}$*:*

$$(\mathbf{R2}) \quad \underline{\mathsf{L}}_{\mathcal{F}_\mathrm{c}}\mathsf{R}_{\mathcal{F}_\mathrm{c}}(\underline{K}) = \underline{K} \qquad \Longleftrightarrow \qquad \sum_{\mathrm{f}\in\mathrm{F_c}} \underline{\ell}_{\mathrm{f,c}}(\underline{x}) \otimes \underline{\mathrm{f}} = \underline{\underline{\mathsf{Id}}}, \qquad \forall \underline{x} \in \mathrm{c}, \tag{7.6a}$$

where $\underline{\mathrm{f}} = \int_\mathrm{f} \underline{\nu}_\mathrm{f}$ *(cf. Definition 5.13), and for all* $\mathbf{a} \in \mathcal{F}_\mathrm{c}$*,*

$$(\mathbf{R3}) \quad \int_\mathrm{c} \underline{\mathsf{L}}_{\mathcal{F}_\mathrm{c}}(\mathbf{a}) = \sum_{\mathrm{f}\in\mathrm{F_c}} \mathbf{a}_\mathrm{f}\tilde{\underline{\mathrm{e}}}_\mathrm{c}(\mathrm{f}) \quad \Longleftrightarrow \quad \int_\mathrm{c} \underline{\ell}_{\mathrm{f,c}} = \tilde{\underline{\mathrm{e}}}_\mathrm{c}(\mathrm{f}), \qquad \forall \mathrm{f} \in \mathrm{F_c}, \tag{7.6b}$$

where $\tilde{\underline{e}}_c(f) = \int_{\tilde{e}_c(f)} \underline{\tau}_{\tilde{e}_c(f)}$ *(cf. Definition 5.16),*

$$(\mathbf{R4}) \quad \mathsf{R}_{\mathcal{F}_c} \underline{\mathsf{L}}_{\mathcal{F}_c}(\mathbf{a}) = \mathbf{a} \qquad \Longleftrightarrow \qquad \int_f \underline{\ell}_{f',f} \cdot \underline{\nu}_f = \delta_{f,f'}, \qquad \forall f, f' \in F_c. \tag{7.6c}$$

Remark 7.8 (Density reconstruction)**.** $\mathsf{L}_{\mathcal{C}_c}$ *is derived from a single reconstruction function* ℓ_c *since* $\#C_c = 1$*. For each* $c \in C$*, property* (**R2**)*, corresponding to* $|c|\ell_c(\underline{x}) = 1$ *for all* $\underline{x} \in c$*, gives the definition of* ℓ_c*. We easily verify that this definition is in agreement with* (**R3**) *(since* $\int_c \mathsf{L}_{\mathcal{C}_c}(\mathbf{a}) = \mathbf{a}_c \int_c \ell_c = \mathbf{a}_c$*) and* (**R4**) *(since* $\int_c \ell_c = 1$*).*

Remark 7.9 (Physical dimension)**.** *Observe that the reconstruction functions* $\ell_{v,c}$ *are dimensionless,* $\underline{\ell}_{e,c}$ *scale as the reciprocal of a length,* $\underline{\ell}_{f,c}$ *scale as the reciprocal of a surface, and* ℓ_c *as the reciprocal of a volume.*

Orthogonal decomposition of the reconstruction operator. The second approach operates a decomposition of the reconstruction operator $\mathsf{L}_{\mathcal{X}_c}$ into a *consistent* part $\mathsf{C}_{\mathcal{X}_c}$ and a *stabilization* part $\mathsf{S}_{\mathcal{X}_c}$, so that, for all $c \in C$,

$$\mathsf{L}_{\mathcal{X}_c} := \mathsf{C}_{\mathcal{X}_c} + \mathsf{S}_{\mathcal{X}_c}, \tag{7.7}$$

with the consistent part $\mathsf{C}_{\mathcal{X}_c} : \mathcal{X}_c \to \mathbb{P}_0(c)$ and the stabilization part $\mathsf{S}_{\mathcal{X}_c} : \mathcal{X}_c \to P_{\mathcal{X}}(c)$. This kind of decomposition has already been introduced by Brezzi *et al.* (2005) in the context of MFD schemes and by Eymard *et al.* (2010) for the reconstruction of gradients in the context of HFV schemes. More recently, Di Pietro & Ern (2013) extended this viewpoint to higher-order gradient reconstructions.

For all $c \in C$, we require, in addition to (**R1**) and (**R4**), that:

(**R2**$*$) For any constant field K,

$$\mathsf{C}_{\mathcal{X}_c} \mathsf{R}_{\mathcal{X}_c}(K) = K \qquad \text{and} \qquad \mathsf{S}_{\mathcal{X}_c} \mathsf{R}_{\mathcal{X}_c}(K) = 0, \tag{7.8}$$

(**R3**$*$) For all $\mathbf{a} \in \mathcal{X}_c$,

$$\int_c \mathsf{S}_{\mathcal{X}_c}(\mathbf{a}) = 0. \tag{7.9}$$

In the case of lower-order schemes (based on a barycentric subdivision), the consistent part of the reconstruction is given on each cell $c \in C$ for any constant field $\widetilde{K}$ by

$$\mathsf{C}_{\mathcal{X}_c}(\mathbf{a}) \cdot \widetilde{K} := \frac{1}{|c|} [\![\mathbf{a}, \mathsf{R}_{\widetilde{\mathcal{Y}}_c}(\widetilde{K})]\!]_{\mathcal{X}_c \widetilde{\mathcal{Y}}_c}, \qquad \forall \mathbf{a} \in \mathcal{X}_c. \tag{7.10}$$

In the specific case of $\mathcal{V}$, $\mathcal{E}$, and $\mathcal{F}$, this leads to the following expressions:

$$\mathsf{C}_{\mathcal{V}_c}(\mathbf{p}) := \frac{1}{|c|} \sum_{v \in V_c} \mathbf{p}_v \, |\tilde{c}(v) \cap c|, \qquad \forall \mathbf{p} \in \mathcal{V}_c, \tag{7.11a}$$

$$\underline{\mathsf{C}}_{\mathcal{E}_c}(\mathbf{u}) := \frac{1}{|c|} \sum_{e \in E_c} \mathbf{u}_e \, \tilde{\underline{f}}_c(e), \qquad \forall \mathbf{u} \in \mathcal{E}_c, \tag{7.11b}$$

$$\underline{\mathsf{C}}_{\mathcal{F}_c}(\boldsymbol{\phi}) := \frac{1}{|c|} \sum_{f \in F_c} \boldsymbol{\phi}_f \, \tilde{\underline{e}}_c(f), \qquad \forall \boldsymbol{\phi} \in \mathcal{F}_c. \tag{7.11c}$$

Proposition 7.10. *Let* $c \in C$*. Then, for any constant fields* K*,* $\widetilde{K}$ *in* c*, the following identity holds:*

$$[\![\mathsf{R}_{\mathcal{X}_c}(K), \mathsf{R}_{\widetilde{\mathcal{Y}}_c}(\widetilde{K})]\!]_{\mathcal{X}_c \widetilde{\mathcal{Y}}_c} = |c| K \cdot \widetilde{K}. \tag{7.12}$$

Proof. This property relies on the barycentric subdivision. Namely, (7.12) is readily verified owing to (5.18a) if $\mathcal{X}$ is $\mathcal{E}$, owing to (5.18b) if $\mathcal{X}$ is $\mathcal{F}$, and owing to (5.12) if $\mathcal{X}$ is $\mathcal{V}$. □

A straightforward consequence of Proposition 7.10 is that the definition (7.10) (and, as a result the definitions (7.11)) automatically ensure that for any constant field K, $\mathtt{C}_{\mathcal{X}_c}\mathsf{R}_{\mathcal{X}_c}(K) = K$.

Proposition 7.11 (Link between the two sets of properties)**.** *Set* $\mathtt{L}_{\mathcal{X}_c} = \mathtt{C}_{\mathcal{X}_c} + \mathtt{S}_{\mathcal{X}_c}$ *with* $\mathtt{C}_{\mathcal{X}_c}$ *defined according to* (7.11)*. Then,* (**R2**$*$) *and* (**R3**$*$) *are equivalent to* (**R2**) *and* (**R3**)*, respectively.*

Proof. (**R2**) readily results from (**R2**$*$) and (7.7). Moreover, (**R3**$*$) yields for any constant field $\widetilde{K}$,

$$\int_c \mathtt{L}_{\mathcal{X}_c}(\mathbf{a}) \cdot \widetilde{K} = \int_c \mathtt{C}_{\mathcal{X}_c}(\mathbf{a}) \cdot \widetilde{K} = [\![\mathbf{a}, \mathsf{R}_{\widetilde{\mathcal{Y}}_c}(\widetilde{K})]\!]_{\mathcal{X}_c\widetilde{\mathcal{Y}}_c},$$

so that (**R3**) holds. The converse statement is proven with similar arguments. □

A straightforward consequence of Proposition 7.11 is that every discrete Hodge operator built using reconstruction operators satisfying properties (**R1**), (**R2**$*$), and (**R3**$*$) along with a consistent part of the reconstruction defined as in (7.11) inherits the theoretical results derived in Chapter 6. Owing to property (**R3**$*$) and since $\mathtt{C}_{\mathcal{X}_c}$ maps onto constant fields, the local discrete Hodge operator can be decomposed as

$$\forall \mathbf{a}_1, \mathbf{a}_2 \in \mathcal{X}_c, \quad [\![\mathbf{a}_1, \mathsf{H}_\alpha^{\mathcal{X}_c\widetilde{\mathcal{Y}}_c}(\mathbf{a}_2)]\!]_{\mathcal{X}_c\widetilde{\mathcal{Y}}_c} := \int_c \mathtt{C}_{\mathcal{X}_c}(\mathbf{a}_1)\, \alpha \mathtt{C}_{\mathcal{X}_c}(\mathbf{a}_2) + \int_c \mathtt{S}_{\mathcal{X}_c}(\mathbf{a}_1)\, \alpha \mathtt{S}_{\mathcal{X}_c}(\mathbf{a}_2). \tag{7.13}$$

All the schemes based on this decomposition share the same consistent part. The distinction between two different schemes stems from the stabilization part. From (7.13) and (7.11), we infer that the entries of the local Hodge operator related to the consistent part are the following:

$$\mathsf{H}_\alpha^{\mathcal{V}_c\widetilde{\mathcal{C}}_c}|_{\tilde{c}_c(v),v'} = |c|^{-1}|\tilde{c}(v) \cap c| \cdot \alpha|\tilde{c}(v') \cap c| \qquad \forall v, v' \in V_c, \tag{7.14a}$$

$$\mathsf{H}_\alpha^{\mathcal{E}_c\widetilde{\mathcal{F}}_c}|_{\tilde{f}_c(e),e'} = |c|^{-1}\underline{\tilde{f}}_c(e) \cdot \underline{\underline{\alpha}}\, \underline{\tilde{f}}_c(e') \qquad \forall e, e' \in E_c, \tag{7.14b}$$

$$\mathsf{H}_\alpha^{\mathcal{F}_c\widetilde{\mathcal{E}}_c}|_{\tilde{e}_c(f),f'} = |c|^{-1}\underline{\tilde{e}}_c(f) \cdot \underline{\underline{\alpha}}\, \underline{\tilde{e}}_c(f') \qquad \forall f, f' \in F_c. \tag{7.14c}$$

7.1.3 Global reconstruction operators

Definition 7.12 (Global reconstruction operator)**.** *Let* $P_{\mathcal{X}}(C)$ *be the set of functions whose restriction to each cell* $c \in C$ *belongs to* $P_{\mathcal{X}}(c)$*. Then, the global reconstruction operator* $\mathtt{L}_{\mathcal{X}} : \mathcal{X} \to P_{\mathcal{X}}(C)$ *is defined from the local reconstruction operators by collecting the local contributions on each cell* $c \in C$ *as follows:*

$$\mathtt{L}_{\mathcal{X}}(\mathbf{a})|_c := \mathtt{L}_{\mathcal{X}_c}(\mathsf{T}_{X,c}(\mathbf{a})) \qquad \forall \mathbf{a} \in \mathcal{X}. \tag{7.15}$$

Using (7.2), (3.20) along with (7.15), we readily verify that

$$[\![\mathbf{a}_1, \mathsf{H}_\alpha^{\mathcal{X}\widetilde{\mathcal{Y}}}(\mathbf{a}_2)]\!]_{\mathcal{X}\widetilde{\mathcal{Y}}} = \int_\Omega \mathtt{L}_{\mathcal{X}}(\mathbf{a}_1) \cdot\, \alpha \mathtt{L}_{\mathcal{X}}(\mathbf{a}_2), \qquad \forall \mathbf{a}_1, \mathbf{a}_2 \in \mathcal{X}. \tag{7.16}$$

Remark 7.13 (Global density reconstruction)**.** *The global reconstruction operator* $\mathtt{L}_{\mathcal{C}}$ *is simply defined from* (7.15) *and Remark 7.8 as follows:*

$$\mathtt{L}_{\mathcal{C}}(\mathbf{s}) := \sum_{c \in C} \frac{\mathbf{s}_c}{|c|}, \qquad \forall \mathbf{s} \in \mathcal{C}. \tag{7.17}$$

The discrete Hodge operator built using this global reconstruction operator is diagonal with entries equal to $|c|^{-1}$*.*

Proposition 7.14 (Global stability)**.** *Let* $\mathsf{L}_{\mathcal{X}}$ *be a global reconstruction operator built from local reconstruction operators* $\mathsf{L}_{\mathcal{X}_\mathrm{c}}$ *satisfying* (**R1**) *in each cell* $\mathrm{c} \in \mathrm{C}$*. Then, the following inequalities hold: There exists a real constant* $\eta_{\mathcal{X}} > 0$ *such that*

$$\eta_{\mathcal{X}} |||\mathbf{a}|||_{2,\mathcal{X}}^2 \le \|\mathsf{L}_{\mathcal{X}}(\mathbf{a})\|_{L^2(\Omega)}^2 \le \eta_{\mathcal{X}}^{-1} |||\mathbf{a}|||_{2,\mathcal{X}}^2, \qquad \forall \mathbf{a} \in \mathcal{X}. \tag{7.18}$$

Proof. Summing cellwise (**R1**) and owing to (6.2), we infer the global stability property. □

Proposition 7.15 (Global dual consistency)**.** *Let* $\mathsf{L}_{\mathcal{X}}$ *be a global reconstruction operator built from local reconstruction operators* $\mathsf{L}_{\mathcal{X}_\mathrm{c}}$ *satisfying* (**R3**) *in each cell* $\mathrm{c} \in \mathrm{C}$*. Then, the following identity holds for any piecewise constant field* $\widetilde{K}$ *on the primal mesh:*

$$\int_\Omega \mathsf{L}_{\mathcal{X}}(\mathbf{a}) \cdot \widetilde{K} = [\![\mathbf{a}, \mathsf{R}_{\widetilde{\mathcal{Y}}}(\widetilde{K})]\!]_{\mathcal{X}\widetilde{\mathcal{Y}}}, \qquad \forall \mathbf{a} \in \mathcal{X}. \tag{7.19}$$

Proof. Since a piecewise constant field on the primal mesh belongs to $S_{\widetilde{\mathcal{Y}}}(\mathrm{C})$, we infer from (**R3**) that

$$\begin{aligned}
\int_\Omega \mathsf{L}_{\mathcal{X}}(\mathbf{a}) \cdot \widetilde{K} &= \sum_{\mathrm{c}\in\mathrm{C}} \int_\mathrm{c} \mathsf{L}_{\mathcal{X}}(\mathbf{a})|_\mathrm{c} \cdot \widetilde{K} = \sum_{\mathrm{c}\in\mathrm{C}} \int_\mathrm{c} \mathsf{L}_{\mathcal{X}_\mathrm{c}}(\mathsf{T}_{\mathrm{X},\mathrm{c}}(\mathbf{a})) \cdot \widetilde{K} && \text{by (7.15)},\\
&= \sum_{\mathrm{c}\in\mathrm{C}} [\![\mathsf{T}_{\mathrm{X},\mathrm{c}}(\mathbf{a}), \mathsf{R}_{\widetilde{\mathcal{Y}}_\mathrm{c}}(\widetilde{K}|_\mathrm{c})]\!]_{\mathcal{X}_\mathrm{c}\widetilde{\mathcal{Y}}_\mathrm{c}} && \text{by (\textbf{R3})},\\
&= \sum_{\mathrm{c}\in\mathrm{C}} [\![\mathbf{a}, \mathsf{T}_{\mathrm{X},\mathrm{c}}^* \mathsf{R}_{\widetilde{\mathcal{Y}}_\mathrm{c}}(\widetilde{K}|_\mathrm{c})]\!]_{\mathcal{X}\widetilde{\mathcal{Y}}}\\
&= [\![\mathbf{a}, \mathsf{R}_{\widetilde{\mathcal{Y}}}(\widetilde{K})]\!]_{\mathcal{X}\widetilde{\mathcal{Y}}} && \text{by (6.25)}.
\end{aligned}$$

□

Remark 7.16 (Conformity)**.** *Observe that the cellwise definition* (7.15) *of the global reconstruction operator does not entail any conformity property for* $\mathsf{L}_{\mathcal{X}}$*. When this property is actually satisfied, we use the notation* $\mathsf{L}_{\mathcal{X}}^{\mathrm{conf}}$*; note that the conformity of* $\mathsf{L}_{\mathcal{X}}^{\mathrm{conf}}$ *requires that of* $\mathsf{L}_{\mathcal{X}_\mathrm{c}}^{\mathrm{conf}}$ *in each cell* $\mathrm{c} \in \mathrm{C}$ *(cf. Remark 7.2) as well as suitable matching conditions across interior mesh faces. Whenever the global reconstruction operators are conforming, it is interesting to consider the additional property of commutativity with the differential operators in the form*

$$\underline{\mathrm{grad}}(\mathsf{L}_{\mathcal{V}}^{\mathrm{conf}}) = \underline{\mathsf{L}}_{\mathcal{E}}^{\mathrm{conf}}(\mathsf{GRAD}), \quad \underline{\mathrm{curl}}(\underline{\mathsf{L}}_{\mathcal{E}}^{\mathrm{conf}}) = \underline{\mathsf{L}}_{\mathcal{F}}^{\mathrm{conf}}(\mathsf{CURL}), \quad \mathrm{div}(\underline{\mathsf{L}}_{\mathcal{F}}^{\mathrm{conf}}) = \mathsf{L}_{\mathcal{C}}(\mathsf{DIV}). \tag{7.20}$$

This leads to the commuting diagrams of Figure 7.1 where $P_{\mathcal{V}}(\Omega) := P_{\mathcal{V}}(\mathrm{C}) \cap H^1(\Omega)$*,* $P_{\mathcal{E}}(\Omega) := P_{\mathcal{E}}(\mathrm{C}) \cap H(\underline{\mathrm{curl}};\Omega)$*, and* $P_{\mathcal{F}}(\Omega) := P_{\mathcal{F}}(\mathrm{C}) \cap H(\mathrm{div};\Omega)$*.*

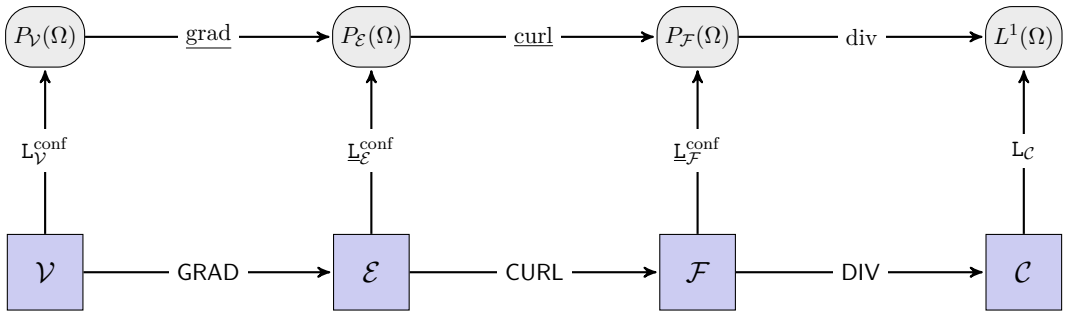

Figure 7.1 – Three commuting diagrams linking the de Rham complex related to the finite-dimensional approximation spaces (top line) and the discrete de Rham complex (bottom line) on the primal mesh. These links are operated by conforming reconstruction operators which commute with differential operators.

Remark 7.17 (Analogies with MFD)**.** *In MFD, the reconstruction operator is mainly used for theoretical purposes. The properties are stated locally as in CDO schemes.* (**R2**) *and* (**R4**) *are required in addition to a commuting property with some differential operator (hence, the reconstruction operators are locally conforming) and a data locality property (Beirão da Veiga* et al.*, 2014).*

7.1.4 Approximation maps

Definition 7.18 (Local approximation map)**.** *Let* $\mathrm{c} \in \mathrm{C}$*. We define the local approximation map* $\mathtt{A}_{\mathcal{X}_\mathrm{c}} : S_{\mathcal{X}}(\mathrm{c}) \to P_{\mathcal{X}}(\mathrm{c})$ *by*

$$\mathtt{A}_{\mathcal{X}_\mathrm{c}} := \mathtt{L}_{\mathcal{X}_\mathrm{c}} \mathsf{R}_{\mathcal{X}_\mathrm{c}}. \tag{7.21}$$

Combining (7.21) with (7.2), we infer the following property of the local discrete Hodge operator:

$$\int_\mathrm{c} \mathtt{A}_{\mathcal{X}_\mathrm{c}}(u) \cdot \alpha \mathtt{A}_{\mathcal{X}_\mathrm{c}}(v) = [\![\mathsf{R}_{\mathcal{X}_\mathrm{c}}(u), \mathsf{H}_\alpha^{\mathcal{X}_\mathrm{c}\tilde{\mathcal{Y}}_\mathrm{c}} \cdot \mathsf{R}_{\mathcal{X}_\mathrm{c}}(v)]\!]_{\mathcal{X}_\mathrm{c}\tilde{\mathcal{Y}}_\mathrm{c}}, \qquad \forall u, v \in S_{\mathcal{X}}(\mathrm{c}). \tag{7.22}$$

Proposition 7.19. *Let* $\mathrm{c} \in \mathrm{C}$*.*

(i) Under assumption (**R2**)*,* $\mathtt{A}_{\mathcal{X}_\mathrm{c}}(K) = K$ *for any constant field* K*.*

(ii) Under assumption (**R4**)*,* $\mathtt{A}_{\mathcal{X}_\mathrm{c}} \cdot \mathtt{A}_{\mathcal{X}_\mathrm{c}} = \mathtt{A}_{\mathcal{X}_\mathrm{c}}$ *(i.e.* $\mathtt{A}_{\mathcal{X}_\mathrm{c}}$ *is a projector).*

Proof. (i) is readily verified using (**R2**) and the definition of $\mathtt{A}_{\mathcal{X}_\mathrm{c}}$. Concerning (ii), $\mathtt{A}_{\mathcal{X}_\mathrm{c}}$ is a projector since $\mathtt{A}_{\mathcal{X}_\mathrm{c}}\mathtt{A}_{\mathcal{X}_\mathrm{c}} = \mathtt{L}_{\mathcal{X}_\mathrm{c}}(\mathsf{R}_{\mathcal{X}_\mathrm{c}}\mathtt{L}_{\mathcal{X}_\mathrm{c}})\mathsf{R}_{\mathcal{X}_\mathrm{c}} = \mathtt{L}_{\mathcal{X}_\mathrm{c}}\mathsf{R}_{\mathcal{X}_\mathrm{c}} = \mathtt{A}_{\mathcal{X}_\mathrm{c}}$ owing to (**R4**). □

Definition 7.20 (Global approximation map)**.** *The global approximation map* $\mathtt{A}_{\mathcal{X}} : S_{\mathcal{X}}(\mathrm{C}) \to P_{\mathcal{X}}(\mathrm{C})$ *is defined from the local approximation maps by collecting their contributions as follows:*

$$\forall \mathrm{c} \in \mathrm{C}, \qquad \mathtt{A}_{\mathcal{X}}(u)|_\mathrm{c} := \mathtt{A}_{\mathcal{X}_\mathrm{c}}(u|_\mathrm{c}), \qquad \forall u \in S_{\mathcal{X}}(\mathrm{C}). \tag{7.23}$$

Based on this definition, we infer by summing cellwise (7.22) that the global discrete Hodge operator verifies

$$\int_\Omega \mathtt{A}_{\mathcal{X}}(u) \cdot \alpha \mathtt{A}_{\mathcal{X}}(v) = [\![\mathsf{R}_{\mathcal{X}}(u), \mathsf{H}_\alpha^{\mathcal{X}\tilde{\mathcal{Y}}} \cdot \mathsf{R}_{\mathcal{X}}(v)]\!]_{\mathcal{X}\tilde{\mathcal{Y}}}, \qquad \forall u, v \in S_{\mathcal{X}}(\Omega), \tag{7.24}$$

owing to Definition 7.20, the fact that $\mathsf{R}_{\mathcal{X}_\mathrm{c}}(u|_\mathrm{c}) = \mathsf{T}_{\mathrm{X},\mathrm{c}}\mathsf{R}_{\mathcal{X}}(u)$, and (3.20).

Proposition 7.21 (Approximation property of $\underline{\mathtt{A}}_{\mathcal{E}}$)**.** *Assume that the mesh sequence is of class* (**MR**)*. Consider local reconstruction operators* $\underline{\mathtt{L}}_{\mathcal{E}_\mathrm{c}}$ *verifying the properties* (**R1**) *and* (**R2**) *in each cell* $\mathrm{c} \in \mathrm{C}$*. Then, for all* $\underline{b} \in [H^1(\mathrm{C})]^3$ *such that* $\underline{\mathrm{curl}}\, \underline{b} \in [L^4(\Omega)]^3$*, the following inequality holds:*

$$\|\underline{b} - \underline{\mathtt{A}}_{\mathcal{E}}(\underline{b})\|_{L^2(\Omega)^3} \lesssim h \left(\|\underline{b}\|_{[H^1(\mathrm{C})]^3} + \|\underline{\mathrm{curl}}\, \underline{b}\|_{[L^4(\Omega)]^3} \right). \tag{7.25}$$

Proof. Let $\underline{B}$ be the L^2-orthogonal projection of $\underline{b}$ onto $[\mathbb{P}_0(\mathrm{C})]^3$. First, observe that $\underline{b} \in S_{\mathcal{E}}(\mathrm{C})$ since $\underline{b} \in [H^1(\mathrm{C})]^3$ and $\underline{\mathrm{curl}}\, \underline{b} \in [L^4(\Omega)]^3$. The bound (7.25) is derived locally. Since

$$\|\underline{b} - \underline{\mathtt{A}}_{\mathcal{E}}(\underline{b})\|_{L^2(\Omega)^3}^2 = \sum_{\mathrm{c}\in\mathrm{C}} \|\underline{b} - \underline{\mathtt{A}}_{\mathcal{E}_\mathrm{c}}(\underline{b}|_\mathrm{c})\|_{L^2(\mathrm{c})^3}^2,$$

using (**R2**) in each cell, $\underline{\mathtt{A}}_{\mathcal{E}_\mathrm{c}}(\underline{B}|_\mathrm{c}) = \underline{B}|_\mathrm{c}$ and the triangle inequality, we infer that

$$\|\underline{b} - \underline{\mathtt{A}}_{\mathcal{E}}(\underline{b})\|_{L^2(\Omega)^3}^2 \le \sum_{\mathrm{c}\in\mathrm{C}} \left(\|\underline{b} - \underline{B}\|_{L^2(\mathrm{c})^3}^2 + \|\underline{\mathtt{L}}_{\mathcal{E}_\mathrm{c}} \mathsf{R}_{\mathcal{E}_\mathrm{c}}((\underline{b} - \underline{B})|_\mathrm{c})\|_{L^2(\mathrm{c})^3}^2 \right).$$

Clearly, $\|\underline{b} - \underline{B}\|_{L^2(\mathrm{c})^3} \lesssim h_\mathrm{c} \|\underline{b}\|_{H^1(\mathrm{c})^3}$ using **(MR)** and standard approximation properties. Moreover, owing to the upper bound in (**R1**) and to **(MR)**, we infer that $\|\underline{\mathtt{L}}_{\mathcal{E}_\mathrm{c}} \mathsf{R}_{\mathcal{E}_\mathrm{c}}((\underline{b} - \underline{B})|_\mathrm{c})\|_{L^2(\mathrm{c})^3}^2 \lesssim h_\mathrm{c} \sum_{\mathrm{e}\in\mathrm{E}_\mathrm{c}} |T_\mathrm{e}|^2$, where $T_\mathrm{e} = \int_\mathrm{e} (\underline{b} - \underline{B}) \cdot \underline{\tau}_\mathrm{e}$ has been bounded in the proof of Lemma 6.14 by $|T_\mathrm{e}| \lesssim h_\mathrm{c}^{\frac{1}{2}} (\|\underline{b}\|_{H^1(\mathrm{c})^3} + \|\underline{\mathrm{curl}}\, \underline{b}\|_{L^4(\mathrm{c})^3})$. Thus, $\|\underline{b} - \underline{\mathtt{A}}_{\mathcal{E}}(\underline{b})\|_{L^2(\Omega)^3}^2 \lesssim \sum_{\mathrm{c}\in\mathrm{C}} h_\mathrm{c}^2 \left(\|\underline{b}\|_{H^1(\mathrm{c})^3}^2 + \|\underline{\mathrm{curl}}\, \underline{b}\|_{L^4(\mathrm{c})^3}^2 \right)$. □

Proposition 7.22 (Approximation property of $\underline{\mathtt{A}}_{\mathcal{F}}$)**.** *Assume that the mesh sequence is of class* **(MR)**. *Consider local reconstruction operators* $\underline{\mathtt{L}}_{\mathcal{F}_\mathrm{c}}$ *verifying the properties* (**R1**) *and* (**R2**) *in each cell* $\mathrm{c} \in \mathrm{C}$. *Then, for all* $\underline{b} \in [H^1(\mathrm{C})]^3$, *the following inequality holds:*

$$\|\underline{b} - \underline{\mathtt{A}}_{\mathcal{F}}(\underline{b})\|_{L^2(\Omega)^3} \lesssim h \|\underline{b}\|_{[H^1(\mathrm{C})]^3}. \tag{7.26}$$

Proof. Since $\underline{b} \in [H^1(\mathrm{C})]^3$, $\underline{b} \in S_{\mathcal{F}}(\mathrm{C})$. The proof follows the same lines as that of Proposition 7.21. The only difference is that we now use $\|\underline{\mathtt{L}}_{\mathcal{F}_\mathrm{c}} \mathsf{R}_{\mathcal{F}_\mathrm{c}}((\underline{b} - \underline{B})|_\mathrm{c})\|^2_{L^2(\mathrm{c})^3} \lesssim h_\mathrm{c}^{-1} \sum_{\mathrm{f} \in \mathrm{F}_\mathrm{c}} |T_\mathrm{f}|^2$, where $T_\mathrm{f} = \int_\mathrm{f} (\underline{b} - \underline{B}) \cdot \underline{\nu}_\mathrm{f}$ satisfies $|T_\mathrm{f}| \lesssim h_\mathrm{c}^{\frac{3}{2}} \|\underline{b}\|_{H^1(\mathrm{c})^3}$. This is shown as in the proof of Lemma 6.14 by replacing $\tilde{\mathrm{f}}$ by f. □

Remark 7.23 (Conformity)**.** *Consider an approximation map* $\mathtt{A}_{\mathcal{X}}^{\mathrm{conf}} := \mathtt{L}_{\mathcal{X}}^{\mathrm{conf}} \mathsf{R}_{\mathcal{X}}$ *built from a conforming reconstruction operator which has the commuting property* (7.20) *with the differential operators. Then, owing to the Proposition 3.13, the following properties hold (see Figure 7.2):*

$$\underline{\mathrm{grad}}\, \mathtt{A}_{\mathcal{V}}^{\mathrm{conf}} = \underline{\mathtt{A}}_{\mathcal{E}}^{\mathrm{conf}}\, \underline{\mathrm{grad}}, \qquad \underline{\mathrm{curl}}\, \underline{\mathtt{A}}_{\mathcal{E}}^{\mathrm{conf}} = \underline{\mathtt{A}}_{\mathcal{F}}^{\mathrm{conf}}\, \underline{\mathrm{curl}}, \qquad \mathrm{div}\, \underline{\mathtt{A}}_{\mathcal{F}}^{\mathrm{conf}} = \mathtt{A}_{\mathcal{C}}\, \mathrm{div}\,. \tag{7.27}$$

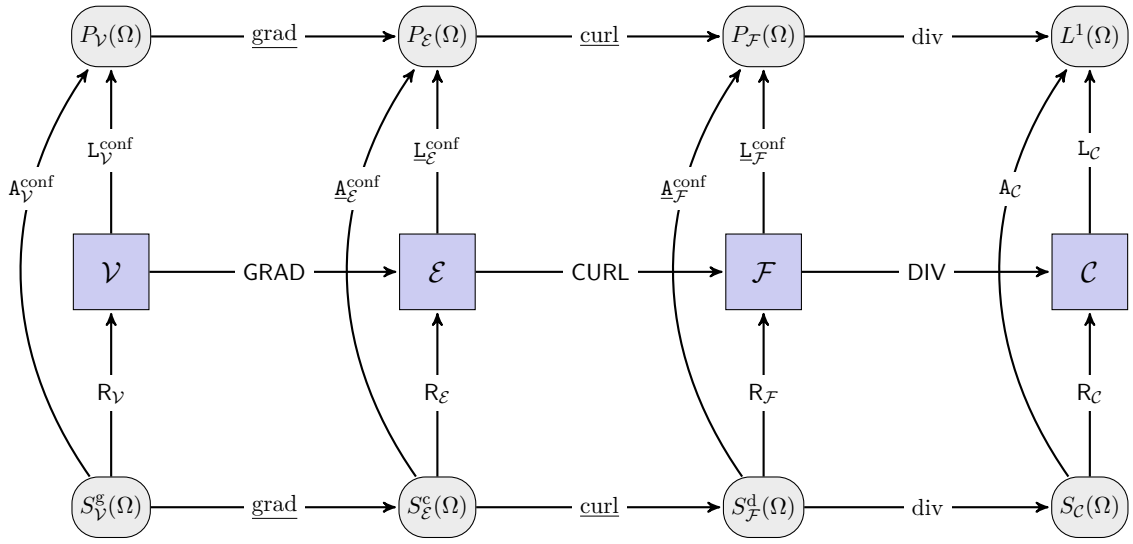

Figure 7.2 – Commuting diagrams linking the de Rham complex related to the finite-dimensional approximation spaces (top line), the discrete de Rham complex (center line), and the continuous de Rham complex (bottom line). These links are operated by conforming approximation operators which commute with differential operators.

Remark 7.24 (Link with FEEC)**.** *The approximation map (also called* interpolation *or* projection *operator) is extensively used in the FE framework. In the FEEC framework (Arnold* et al.*, 2010), the key concept of* bounded cochain projection *translates as a conforming approximation map which commutes with the differential operator and which has the stability property* (**R1**).

7.2 Simple examples

The discrete Hodge operator is the key ingredient in the design of CDO schemes. Since the definition (7.2) of the discrete Hodge operator depends on the choice of the reconstruction operator, choosing a specific reconstruction operator leads to a specific CDO scheme. In Sections 7.2.1 and 7.2.2, we present two simple examples of reconstruction functions on specific meshes and, in Section 7.2.3, we present a simple potential reconstruction operator on polyhedral meshes.

7.2.1 Simplicial meshes

The Whitney reconstruction functions are a well-known example of conforming FE basis functions for simplicial meshes. Whitney functions embrace the lowest-order Lagrange FE for vertex-based DoFs, the lowest-order Nédélec FE for edge-based DoFs, the lowest-order Raviart–Thomas–Nédélec FE face-based DoFs, and the cellwise constant functions for cell-based DoFs (cf. Remark 7.8). Let $\mathrm{c} \in \mathrm{C}$ belong to a simplicial mesh. Then, the Whitney reconstruction operators are given as follows:

$$\underline{\mathtt{L}}^{\mathrm{W}}_{\mathcal{V}_\mathrm{c}}(\mathbf{p}) = \sum_{\mathrm{v}\in\mathrm{V_c}} \mathbf{p}_\mathrm{v}\ell^{\mathrm{LAG}}_{\mathrm{v,c}}(\underline{x}), \qquad \forall \mathbf{p} \in \mathcal{V}_\mathrm{c}, \tag{7.28a}$$

$$\underline{\mathtt{L}}^{\mathrm{W}}_{\mathcal{E}_\mathrm{c}}(\mathbf{u}) = \sum_{\mathrm{e}\in\mathrm{E_c}} \mathbf{u}_\mathrm{e}\underline{\ell}^{\mathrm{NED}}_{\mathrm{e,c}}(\underline{x}), \qquad \forall \mathbf{u} \in \mathcal{E}_\mathrm{c}, \tag{7.28b}$$

$$\underline{\mathtt{L}}^{\mathrm{W}}_{\mathcal{F}_\mathrm{c}}(\boldsymbol{\phi}) = \sum_{\mathrm{f}\in\mathrm{F_c}} \boldsymbol{\phi}_\mathrm{f}\underline{\ell}^{\mathrm{RTN}}_{\mathrm{f,c}}(\underline{x}), \qquad \forall \boldsymbol{\phi} \in \mathcal{F}_\mathrm{c}, \tag{7.28c}$$

where $\ell^{\mathrm{LAG}}_{\mathrm{v,c}}$ is the local lowest-order Lagrange FE shape function attached to the vertex v, $\underline{\ell}^{\mathrm{NED}}_{\mathrm{e,c}}$ the local lowest-order Nédélec edge FE shape function attached to the edge e, and $\underline{\ell}^{\mathrm{RTN}}_{\mathrm{f,c}}$ the local lowest-order Raviart–Thomas–Nédélec FE shape function attached to the face f.

Let c be a tetrahedron. In a tetrahedron, there are as many as faces as vertices (*i.e.* $\#\mathrm{F_c} = \#\mathrm{V_c}$). Thus, to each face $\mathrm{f} \in \mathrm{F_c}$, we can associate a unique vertex $\mathrm{v} \in \mathrm{V_c}$ such that $\mathrm{v} \notin \mathrm{V_f}$. We denote by $\mathrm{f}(\mathrm{v})$ this correspondence (see Figure 7.3). Similarly, we denote by $\mathrm{v}(\mathrm{f})$ the converse correspondence. To each edge $\mathrm{e} \in \mathrm{E_c}$, we can associate a unique opposite edge $\mathrm{e}' \in \mathrm{E_c}$ defined such that $\mathrm{V_e} \cap \mathrm{V_{e'}} = \emptyset$. We denote this association by $\mathrm{e}' := \mathrm{e}(\mathrm{e})$ (see, for instance, edges e_1 and e_6 in Figure 7.3). We can now turn to the definition of the shape functions.

Definition 7.25 (Whitney reconstruction functions)**.** *Let* c *be a tetrahedron. For each vertex* $\mathrm{v} \in \mathrm{V_c}$*, we define* $\ell^{\mathrm{LAG}}_{\mathrm{v,c}}$ *as follows:*

$$\ell^{\mathrm{LAG}}_{\mathrm{v,c}}(\underline{x}) := 1 - \frac{(\underline{x} - \underline{x}_\mathrm{v}) \cdot \underline{\nu}_{\mathrm{f(v),c}}}{(\underline{x}_{\mathrm{f(v)}} - \underline{x}_\mathrm{v}) \cdot \underline{\nu}_{\mathrm{f(v),c}}}, \qquad \forall \underline{x} \in \mathrm{c}, \tag{7.29a}$$

where we recall that $\underline{\nu}_{\mathrm{f(v),c}}$ *is the unit normal to* $\mathrm{f(v)}$ *pointing outward* c*. For each edge* $\mathrm{e} \in \mathrm{E_c}$*, we define* $\underline{\ell}^{\mathrm{NED}}_{\mathrm{e,c}}$ *as follows:*

$$\underline{\ell}^{\mathrm{NED}}_{\mathrm{e,c}}(\underline{x}) := \frac{(\underline{x} - \underline{x}_{\mathrm{e(e)}}) \times \underline{\tau}_{\mathrm{e(e)}}}{\underline{\mathrm{e}} \cdot \Big((\underline{x}_\mathrm{e} - \underline{x}_{\mathrm{e(e)}}) \times \underline{\tau}_{\mathrm{e(e)}}\Big)}, \qquad \forall \underline{x} \in \mathrm{c}, \tag{7.29b}$$

where we recall that $\underline{\mathrm{e}} = \int_\mathrm{e} \underline{\tau}_\mathrm{e}$*. For each face* $\mathrm{f} \in \mathrm{F_c}$*, we define* $\underline{\ell}^{\mathrm{RTN}}_{\mathrm{f,c}}$ *as follows:*

$$\underline{\ell}^{\mathrm{RTN}}_{\mathrm{f,c}}(\underline{x}) := \frac{\underline{x} - \underline{x}_{\mathrm{v(f)}}}{d|\mathrm{c}|}, \qquad \forall \underline{x} \in \mathrm{c}. \tag{7.29c}$$

Remark 7.26 (Definition of $\ell^{\mathrm{LAG}}_{\mathrm{v,c}}$)**.** *In the definition* (7.29a)*, the point* $\underline{x}_{\mathrm{f(v)}}$ *is not the only choice. Any point lying inside* f *is an admissible choice.*

Remark 7.27 (Alternative definition of $\underline{\ell}^{\mathrm{NED}}_{\mathrm{e,c}}$ and $\underline{\ell}^{\mathrm{RTN}}_{\mathrm{f,c}}$)**.** *Let* c *be a tetrahedron. Consider an edge* $\mathrm{e} \in \mathrm{E_c}$ *and its vertices* v_1 *and* v_2*. If* $\underline{\tau}_\mathrm{e}$ *points from* v_1 *to* v_2*, then we can also define* $\underline{\ell}^{\mathrm{NED}}_{\mathrm{e,c}}$ *as follows:*

$$\underline{\ell}^{\mathrm{NED}}_{\mathrm{e,c}} := \ell^{\mathrm{LAG}}_{\mathrm{v}_1,\mathrm{c}}\nabla(\ell^{\mathrm{LAG}}_{\mathrm{v}_2,\mathrm{c}}) - \ell^{\mathrm{LAG}}_{\mathrm{v}_2,\mathrm{c}}\nabla(\ell^{\mathrm{LAG}}_{\mathrm{v}_1,\mathrm{c}}). \tag{7.30a}$$

Consider now a face $\mathrm{f} \in \mathrm{F_c}$ *and its vertices* v_1*,* v_2*, and* v_3 *such that* $\big((\underline{x}_{\mathrm{v}_1} - \underline{x}_{\mathrm{v}_2}) \times (\underline{x}_{\mathrm{v}_2} - \underline{x}_{\mathrm{v}_3})\big) \cdot \underline{\nu}_{\mathrm{f,c}} > 0$ *(i.e. we give an orientation to the face* f*). Then, we can also define* $\underline{\ell}^{\mathrm{RTN}}_{\mathrm{f,c}}$ *as follows:*

$$\underline{\ell}^{\mathrm{RTN}}_{\mathrm{f,c}} := 2\left(\ell^{\mathrm{LAG}}_{\mathrm{v}_1,\mathrm{c}}\nabla(\ell^{\mathrm{LAG}}_{\mathrm{v}_2,\mathrm{c}}) \times \nabla(\ell^{\mathrm{LAG}}_{\mathrm{v}_3,\mathrm{c}}) + \ell^{\mathrm{LAG}}_{\mathrm{v}_2,\mathrm{c}}\nabla(\ell^{\mathrm{LAG}}_{\mathrm{v}_3,\mathrm{c}}) \times \nabla(\ell^{\mathrm{LAG}}_{\mathrm{v}_1,\mathrm{c}}) + \ell^{\mathrm{LAG}}_{\mathrm{v}_3,\mathrm{c}}\nabla(\ell^{\mathrm{LAG}}_{\mathrm{v}_1,\mathrm{c}}) \times \nabla(\ell^{\mathrm{LAG}}_{\mathrm{v}_2,\mathrm{c}})\right). \tag{7.30b}$$

Proposition 7.28 (Properties of Whitney reconstructions)**.** *Let* $\mathrm{c} \in \mathrm{C}$*. Assume the mesh is of class* **(MR)** *and* **(MB)***. Then, the reconstruction operators* $\mathsf{L}^{\mathrm{W}}_{\mathcal{V}_\mathrm{c}}$*,* $\underline{\mathsf{L}}^{\mathrm{W}}_{\mathcal{E}_\mathrm{c}}$*, and* $\underline{\mathsf{L}}^{\mathrm{W}}_{\mathcal{F}_\mathrm{c}}$ *satisfy the four properties* (**R1**)–(**R4**)*. Moreover, the set* $\{\ell^{\mathrm{LAG}}_{\mathrm{v,c}}\}_{\mathrm{v}\in\mathrm{V_c}}$ *satisfies the linear completeness property* (7.4)*. In addition, the global reconstruction operators built according to* (7.15) *are conforming and commute with the differential operators, i.e.*

$$\underline{\mathrm{grad}}\cdot\mathsf{L}^{\mathrm{LAG}}_{\mathcal{V}} = \underline{\mathsf{L}}^{\mathrm{NED}}_{\mathcal{E}}\cdot\mathsf{GRAD}, \qquad \underline{\mathrm{curl}}\cdot\underline{\mathsf{L}}^{\mathrm{NED}}_{\mathcal{E}} = \underline{\mathsf{L}}^{\mathrm{RTN}}_{\mathcal{F}}\cdot\mathsf{CURL}, \qquad \mathrm{div}\cdot\underline{\mathsf{L}}^{\mathrm{RTN}}_{\mathcal{F}} = \mathsf{L}_{\mathcal{C}}\cdot\mathsf{DIV}. \tag{7.31}$$

Proof. (**R1**) is established using **(MR)**. For (**R2**)–(**R4**), we refer to Bossavit (2000), no.5 "The Galerkin Hodge" . The linear completeness of $\ell^{\mathrm{LAG}}_{\mathrm{v,c}}$ is straightforward since $\ell^{\mathrm{LAG}}_{\mathrm{v,c}}$ is a barycentric coordinate. The conformity and the commuting property of the global Whitney reconstructions are classical results (see, *e.g.* Ern & Guermond (2004), Chapter 1). □

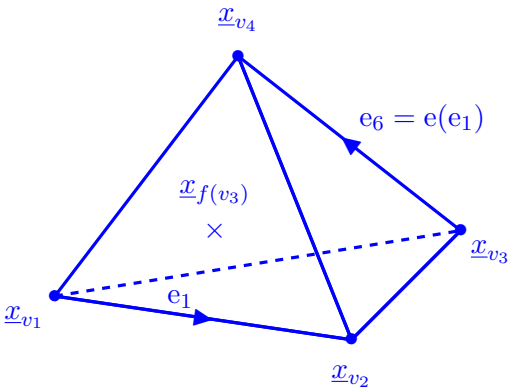

Figure 7.3 – Tetrahedron.

7.2.2 Cartesian meshes

Let $\mathrm{c} \in \mathrm{C}$ belong to a Cartesian mesh. Consider a fully barycentric subdivision of c (cf. Definition 5.10). Two examples of non-conforming reconstructions on Cartesian meshes are the following:

(a) For all $\mathrm{e} \in \mathrm{E_c}$, letting $\mathfrak{p}^{\mathrm{CAR}}_{\mathrm{e,c}} := \cup_{\mathrm{v}\in\mathrm{V_e}}\cup_{\mathrm{e}'\in\mathrm{E_v}\cap\mathrm{E_c}}\cup_{\mathrm{f}\in\mathrm{F_{e'}}\cap\mathrm{F_c}}\mathfrak{s}_{\mathrm{v,e',f,c}}$ (composed of 12 elementary subsimplices; see Figure 7.4 left), we set

$$\underline{\ell}^{\mathrm{CAR}}_{\mathrm{e,c}}(\underline{x}) := \begin{cases} |\mathrm{e}|^{-1}\underline{\tau}_\mathrm{e} & \text{if } \underline{x}\in\mathfrak{p}^{\mathrm{CAR}}_{\mathrm{e,c}},\\ \underline{0} & \text{otherwise.}\end{cases} \tag{7.32}$$

(b) For all $\mathrm{f} \in \mathrm{F_c}$, letting $\mathfrak{p}^{\mathrm{CAR}}_{\mathrm{f,c}} := \cup_{\mathrm{v}\in\mathrm{V_f}}\cup_{\mathrm{e}\in\mathrm{E_v}\cap\mathrm{E_c}}\cup_{\mathrm{f}'\in\mathrm{F_e}\cap\mathrm{F_c}}\mathfrak{s}_{\mathrm{v,e,f'},\mathrm{c}}$ (see Figure 7.4 right), we set

$$\underline{\ell}^{\mathrm{CAR}}_{\mathrm{f,c}}(\underline{x}) := \begin{cases} |\mathrm{f}|^{-1}\underline{\nu}_\mathrm{f} & \text{if } \underline{x}\in\mathfrak{p}^{\mathrm{CAR}}_{\mathrm{f,c}},\\ \underline{0} & \text{otherwise.}\end{cases} \tag{7.33}$$

In both cases, the local design properties (**R1**)–(**R4**) are easily verified. Moreover, the local discrete Hodge operator defined by (7.1) is diagonal for isotropic material property α. Using (7.32) yields the discrete Hodge operator defined in (3.21), while using (7.33) the one defined in (3.22). The case $\ell^{\mathrm{CAR}}_{\mathrm{v,c}}$ for all $\mathrm{v} \in \mathrm{V_c}$ is detailed in a more general context (cf. Section 7.2.3 below).

7.2.3 Simple potential reconstruction on polyhedral meshes

For each cell $\mathrm{c} \in \mathrm{C}$ belonging to a polyhedral mesh, the piecewise constant potential reconstruction operator $\mathsf{L}^0_{\mathcal{V}_\mathrm{c}}$ is defined as follows:

$$\mathsf{L}^0_{\mathcal{V}_\mathrm{c}} : \mathcal{V}_\mathrm{c} \to \mathbb{P}_0(\mathfrak{P}_{\mathrm{V,c}}), \qquad \mathsf{L}^0_{\mathcal{V}_\mathrm{c}}(\mathbf{p})|_{\tilde{\mathrm{c}}(\mathrm{v})\cap\mathrm{c}} := \mathbf{p}_\mathrm{v}, \qquad \forall \mathrm{v}\in\mathrm{V_c},\ \forall \mathbf{p}\in\mathcal{V}_\mathrm{c}. \tag{7.34}$$

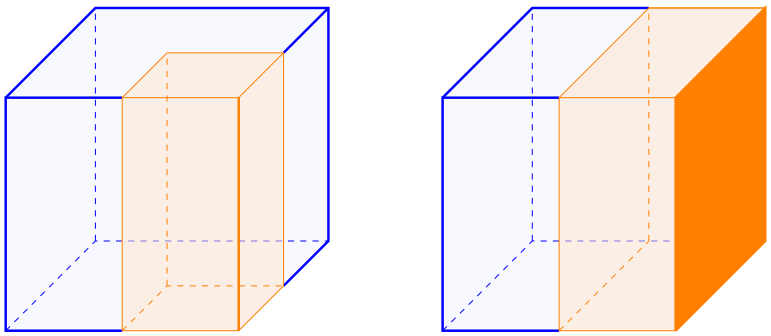

Figure 7.4 – Volume to consider for the definition of the reconstruction functions in MAC schemes on a Cartesian mesh. Left: $\mathfrak{p}_{\mathrm{e,c}}^{\mathrm{CAR}}$; Right: $\mathfrak{p}_{\mathrm{f,c}}^{\mathrm{CAR}}$.

This local potential reconstruction operator verifies (**R1**)–(**R4**) and induces a local discrete Hodge operator $\mathsf{H}_1^{\mathcal{C}_\mathrm{c}\tilde{\mathcal{V}}_\mathrm{c}}$ which is diagonal with entries equal to $|\tilde{\mathrm{c}}(\mathrm{v})\cap\mathrm{c}|$. The global reconstruction operator $\mathsf{L}_{\mathcal{V}}^0$ resulting from definition (7.34) is cellwise constant on the dual mesh and verifies

$$\|\mathsf{L}_{\mathcal{V}}^0(\mathbf{p})\|_{L^2(\Omega)}^2 = \|\mathbf{p}\|_{2,\mathcal{V}}^2. \tag{7.35}$$

Remark 7.29 (Simple reconstruction operators $\underline{\mathsf{L}}_{\mathcal{E}_\mathrm{c}}^0$ and $\underline{\mathsf{L}}_{\mathcal{F}_\mathrm{c}}^0$)**.** *Defining* $\underline{\mathsf{L}}_{\mathcal{E}_\mathrm{c}}^0$ *and* $\underline{\mathsf{L}}_{\mathcal{F}_\mathrm{c}}^0$ *following the same building principle as* $\mathsf{L}_{\mathcal{V}_\mathrm{c}}^0$ *leads to*

$$\begin{aligned}
&\underline{\mathsf{L}}_{\mathcal{E}_\mathrm{c}}^0 : \mathcal{E}_\mathrm{c} \to \mathbb{P}_0(\mathfrak{P}_{\mathrm{E,c}}), && \underline{\mathsf{L}}_{\mathcal{E}_\mathrm{c}}^0(\mathbf{u})|_{\mathfrak{p}_{\mathrm{e,c}}} := \frac{\mathbf{u}_\mathrm{e}}{|\mathrm{e}|}\underline{\tau}_\mathrm{e}, && \forall \mathrm{e}\in\mathrm{E_c},\ \forall \mathbf{u}\in\mathcal{E}_\mathrm{c},\\
&\underline{\mathsf{L}}_{\mathcal{F}_\mathrm{c}}^0 : \mathcal{F}_\mathrm{c} \to \mathbb{P}_0(\mathfrak{P}_{\mathrm{F,c}}), && \underline{\mathsf{L}}_{\mathcal{F}_\mathrm{c}}^0(\boldsymbol{\phi})|_{\mathfrak{p}_{\mathrm{f,c}}} := \frac{\boldsymbol{\phi}_\mathrm{f}}{|\mathrm{f}|}\underline{\nu}_\mathrm{f}, && \forall \mathrm{f}\in\mathrm{F_c},\ \forall \boldsymbol{\phi}\in\mathcal{F}_\mathrm{c}.
\end{aligned} \tag{7.36}$$

These two reconstruction operators lead to diagonal discrete Hodge operators. However, properties (**R2**) *and* (**R3**) *are not verified by these reconstructions on general meshes.*

7.3 Reconstruction operators on polyhedral meshes

The goal of this section is to reconstruct potential (resp. circulation, flux) fields from vertex-based (resp. edge-based, face-based) DoFs defined on polyhedral meshes. The devised reconstruction operators have to fulfill *a minima* properties (**R1**), (**R2**), and (**R3**) (or, equivalently (**R1**), (**R2**$*$), and (**R3**$*$)), so that the discrete Hodge operator satisfies the theoretical results derived in Chapter 6.

In what follows, we detail three classes of reconstruction operators. The first class is introduced in Section 7.3.1. It consists of piecewise constant non-conforming reconstruction operators $\mathsf{L}_{\mathcal{V}}$, $\underline{\mathsf{L}}_{\mathcal{E}}$, and $\underline{\mathsf{L}}_{\mathcal{F}}$. These reconstruction operators embrace as a particular case, the reconstruction operators devised by Codecasa *et al.* (2010), hereafter called DGA reconstruction, and the reconstruction proposed by Eymard *et al.* (2010) for the discrete gradient, hereafter called SUSHI reconstruction. This class of reconstruction operators is of practical interest since they are explicitly defined (which is clearly attractive from an implementation viewpoint).

The second class of operators comprising piecewise polynomial conforming reconstruction operators, is introduced in Section 7.3.2. In contrast to those of Section 7.3.1, these reconstruction operators are conforming and commute with the differential operators. However, the dual consistency property (**R3**) is not proved for these operators. These reconstruction operators are implicitly defined (their evaluation typically requires solving a local linear system) and are mainly used for deriving further theoretical results (cf. Section 7.4). Such reconstruction operators have been addressed in several works: Buffa & Christiansen (2007) in the two-dimensional case for $\mathsf{L}_{\mathcal{X}_\mathrm{c}}^{\mathrm{conf}}$, and extended by Christiansen (2008) in the context of FES to the three-dimensional case; see also Euler (2007) for a similar approach in the context of FIT.

In all cases, the definition relies on a constrained problem on each polygonal or polyhedral cell subdivided into subsimplices, so that a preprocessing stage is needed to evaluate numerically the local reconstruction functions.

The third class of operators comprising piecewise polynomial conforming reconstruction operators satisfying the dual consistency property (**R3**), is described in Section 7.3.3. We only consider $\mathsf{L}_{\mathcal{V}_c}^{\mathrm{conf}}$ and $\underline{\mathsf{L}}_{\mathcal{F}_c}^{\mathrm{conf}}$, and not $\underline{\mathsf{L}}_{\mathcal{E}_c}^{\mathrm{conf}}$ (which is not needed in what follows). These reconstruction operators also commute with differential operators. $\underline{\mathsf{L}}_{\mathcal{F}_c}^{\mathrm{conf}}$ is implicitly defined, while $\underline{\mathsf{L}}_{\mathcal{V}_c}^{\mathrm{conf}}$ is explicitly defined using geometrical relation specific to the fully barycentric subdivision. To our knowledge, the potential reconstruction operator $\mathsf{L}_{\mathcal{V}_c}^{\mathrm{conf}}$ is new, while $\underline{\mathsf{L}}_{\mathcal{F}_c}^{\mathrm{conf}}$ is inspired from Vohralík & Wohlmuth (2013) in the context of Mixed FE methods.

Remark 7.30 (Potential reconstruction)**.** *Potential reconstructions are extensively treated in the FE literature for specific elements (tetrahedron, hexahedron, pyramid...). A typical way to extend these reconstructions to polyhedral meshes is to use the concept of* generalized barycentric coordinates*; see Wachspress (1975), Floater* et al. *(2005), Warren* et al. *(2007), Hormann & Sukumar (2008),Gillette & Bajaj (2011); Gillette* et al. *(2012), and reference therein.*

7.3.1 Piecewise constant non-conforming reconstruction

For each primal cell $c \in C$, a simple way to design piecewise constant non-conforming reconstruction operators $\mathsf{L}_{\mathcal{X}_c}$ based on the orthogonal decomposition (7.7) is the following. Recall that the mesh is assumed to be of class **(MB)** and that the dual barycentric mesh is considered.

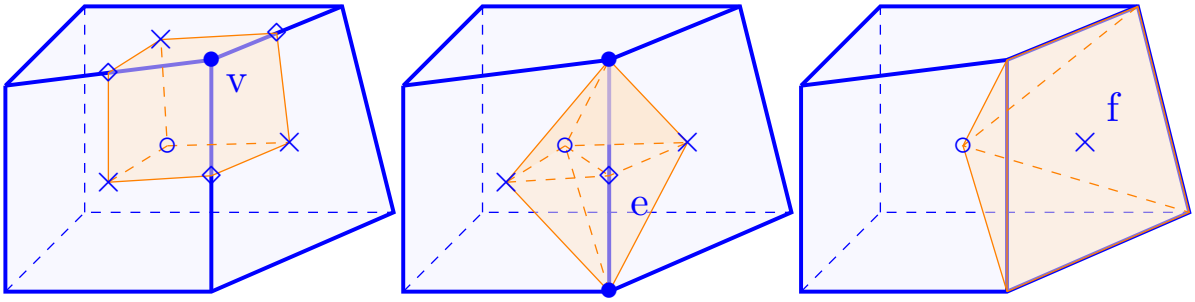

Figure 7.5 – Example of partition of a hexahedral cell c. Left: $\mathfrak{p}_{v,c}$ for a vertex $v \in V_c$; Middle: $\mathfrak{p}_{e,c}$ for an edge $e \in E_c$; Right: $\mathfrak{p}_{f,c}$ for a face $f \in F_c$. Crosses indicate barycenters of faces and diamonds barycenters of edges.

Definition 7.31. *Let $c \in C$ and let $X \in \{V, E, F\}$. Recall the partitions $\mathfrak{P}_{X,c} := \{\mathfrak{p}_{x,c}\}_{x \in X_c}$ introduced in Definition 5.18 (see also Figure 7.5). Then, for all $\mathbf{a} \in \mathcal{X}_c$, set*

$$\mathsf{L}_{\mathcal{X}_c}(\mathbf{a}) := \mathsf{C}_{\mathcal{X}_c}(\mathbf{a}) + \hat{\mathsf{S}}_{\mathcal{X}_c}\left((\mathsf{Id}_{\mathcal{X}_c} - \mathsf{R}_{\mathcal{X}_c}\mathsf{C}_{\mathcal{X}_c})(\mathbf{a})\right),$$

with $\mathsf{C}_{\mathcal{X}_c} : \mathcal{X}_c \to \mathbb{P}_0(c)$ and $\hat{\mathsf{S}}_{\mathcal{X}_c} : \mathcal{X}_c \to \mathbb{P}_0(\mathfrak{P}_{X,c})$ (the space of piecewise constant functions in each $\mathfrak{p}_{x,c}$) acting as follows for any constant field $\widetilde{K}$ in c:

$$\mathsf{C}_{\mathcal{X}_c}(\mathbf{a}) \cdot \widetilde{K} := \frac{1}{|c|}[\![\mathbf{a}, \mathsf{R}_{\widetilde{\mathcal{Y}}_c}(\widetilde{K})]\!]_{\mathcal{X}_c\widetilde{\mathcal{Y}}_c}, \qquad (\hat{\mathsf{S}}_{\mathcal{X}_c}(\mathbf{a}) \cdot \widetilde{K})|_{\mathfrak{p}_{x,c}} := \beta \frac{\mathsf{R}_{\widetilde{\mathcal{Y}}_c}(\widetilde{K})|_{\tilde{y}_c(x)}}{|\mathfrak{p}_{x,c}|} \cdot \mathbf{a}_x, \ \forall x \in X_c. \quad (7.37)$$

where $\beta > 0$ is a free-parameter related to the stabilization. Comparing with (7.7), the stabilization part takes the form

$$\mathsf{S}_{\mathcal{X}_c} = \hat{\mathsf{S}}_{\mathcal{X}_c} \circ (\mathsf{Id} - \mathsf{C}_{\mathcal{X}_c}\mathsf{R}_{\mathcal{X}_c}). \quad (7.38)$$

Proposition 7.32. *Assume that the mesh is of class* **(MR)** *and* **(MB)**. *Assume that primal faces are planar. Let $c \in C$. Then, the reconstruction operator $\mathsf{L}_{\mathcal{X}_c}$ from Definition 7.31 satisfies properties* **(R1)**, **(R2$*$)**, *and* **(R3$*$)**.

Proof. (**R1**) stems from the regularity of the barycentric subdivision. (**R2**$*$) is a straightforward consequence of the definition of the consistent and stabilization parts. In particular, (7.12) implies that $\mathtt{C}_{\mathcal{X}_c}\mathsf{R}_{\mathcal{X}_c}(K) = K$ for any constant field K in c.

Let us now verify (**R3**$*$). For any constant field $\widetilde{K}$ in c, we infer that

$$\begin{aligned}\int_c \mathtt{S}_{\mathcal{X}_c}(\mathbf{a})\cdot\widetilde{K} &= \sum_{x\in X_c}\int_{\mathfrak{p}_{x,c}} \mathtt{S}_{\mathcal{X}_c}(\mathbf{a})|_{\mathfrak{p}_{x,c}}\cdot\widetilde{K} = \beta\left(\sum_{x\in X_c}(\mathbf{a}_x - \mathsf{R}_{\mathcal{X}_c}\mathtt{C}_{\mathcal{X}_c}(\mathbf{a})|_x)\cdot\mathsf{R}_{\widetilde{\mathcal{Y}}_c}(\widetilde{K})|_{\tilde{y}_c(x)}\right)\\ &= \beta\left(\llbracket\mathbf{a},\mathsf{R}_{\widetilde{\mathcal{Y}}_c}(\widetilde{K})\rrbracket_{\mathcal{X}_c\tilde{\mathcal{Y}}_c} - \llbracket\mathsf{R}_{\mathcal{X}_c}\mathtt{C}_{\mathcal{X}_c}(\mathbf{a}),\mathsf{R}_{\widetilde{\mathcal{Y}}_c}(\widetilde{K})\rrbracket_{\mathcal{X}_c\tilde{\mathcal{Y}}_c}\right)\\ &= \beta|c|\left(\mathtt{C}_{\mathcal{X}_c}(\mathbf{a})\cdot\widetilde{K} - \mathtt{C}_{\mathcal{X}_c}(\mathbf{a})\cdot\widetilde{K}\right) = 0,\end{aligned}$$

owing to (7.37) for the first term and (7.12) for the second term (since $\underline{\mathtt{C}}_{\mathcal{X}_c}(\mathbf{a})$ is constant in c). □

Potential reconstruction. For each $c\in C$, the reconstruction operator $\mathtt{L}_{\mathcal{V}_c}$ is constant in each $\mathfrak{p}_{v,c}$ associated to the vertex $v\in V_c$. In this case, (7.37) becomes $\mathtt{C}_{\mathcal{V}_c}:\mathcal{V}_c\to\mathbb{P}_0(c)$ and $\hat{\mathtt{S}}_{\mathcal{V}_c}:\mathcal{V}_c\to\mathbb{P}_0(\mathfrak{P}_{V,c})$ such that for all $\mathbf{p}\in\mathcal{V}_c$,

$$\mathtt{C}_{\mathcal{V}_c}(\mathbf{p}) := \frac{1}{|c|}\sum_{v\in V_c}\mathbf{p}_v\,|c\cap\tilde{c}(v)|,\qquad \hat{\mathtt{S}}_{\mathcal{V}_c}(\mathbf{p})|_{\mathfrak{p}_{v,c}} := \beta\,\mathbf{p}_v,\ \forall v\in V_c. \tag{7.39}$$

It turns out that the stabilization part is $\mathtt{S}_{\mathcal{V}_c}(\mathbf{p})|_{\mathfrak{p}_{v',c}} = \beta|c|^{-1}\sum_{v\in V_c}|c\cap\tilde{c}(v)|\,(\mathbf{p}_{v'}-\mathbf{p}_v)$ yielding

$$\mathtt{L}_{\mathcal{V}_c}(\mathbf{p})|_{\mathfrak{p}_{v',c}} = \frac{1}{|c|}\sum_{v\in V_c}|c\cap\tilde{c}(v)|\,(\beta(\mathbf{p}_{v'}-\mathbf{p}_v)+\mathbf{p}_v). \tag{7.40}$$

The set of local reconstruction functions $\{\ell_{v,c}\}_{v\in V_c}$ associated with (7.40) is piecewise constant on $\mathfrak{P}_{V,c}$ and is such that

$$\ell_{v,c}(\underline{x})|_{\mathfrak{p}_{v',c}} := \beta\delta_{v,v'} + \frac{|c\cap\tilde{c}(v)|}{|c|}(1-\beta). \tag{7.41}$$

We stress that the value of these functions is not necessarily continuous across the faces of the submesh (induced by $\mathfrak{P}_{V,c}$) lying inside c, so that, in general, $\mathtt{L}_{\mathcal{V}_c}$ does not map into $H^1(c)$. In what follows, we do not use this reconstruction since a conforming potential reconstruction on polyhedral meshes can be defined explicitly with more properties (cf. Section 7.3.3).

Circulation reconstruction. For each $c\in C$, the reconstruction operator $\underline{\mathtt{L}}_{\mathcal{E}_c}$ is constant in each $\mathfrak{p}_{e,c}$ associated to the edge $e\in E_c$. In this case, (7.37) becomes $\underline{\mathtt{C}}_{\mathcal{E}_c}:\mathcal{E}_c\to[\mathbb{P}_0(c)]^3$ and $\underline{\hat{\mathtt{S}}}_{\mathcal{E}_c}:\mathcal{E}_c\to[\mathbb{P}_0(\mathfrak{P}_{E,c})]^3$ such that for all $\mathbf{u}\in\mathcal{E}_c$,

$$\underline{\mathtt{C}}_{\mathcal{E}_c}(\mathbf{u}) := \frac{1}{|c|}\sum_{e\in E_c}\mathbf{u}_e\tilde{\underline{f}}_c(e),\qquad \underline{\hat{\mathtt{S}}}_{\mathcal{E}_c}(\mathbf{u})|_{\mathfrak{p}_{e,c}} := \beta\,\frac{\tilde{\underline{f}}_c(e)}{|\mathfrak{p}_{e,c}|}\,\mathbf{u}_e,\ \forall e\in E_c. \tag{7.42}$$

Then, we readily infer that the constant value taken by $\underline{\mathtt{L}}_{\mathcal{E}_c}(\mathbf{u})$ in each $\mathfrak{p}_{e,c}$, for $e\in E_c$, is

$$\underline{\mathtt{L}}_{\mathcal{E}_c}(\mathbf{u})|_{\mathfrak{p}_{e,c}} = \underline{\mathtt{C}}_{\mathcal{E}_c}(\mathbf{u}) + \beta\frac{\tilde{\underline{f}}_c(e)}{|\mathfrak{p}_{e,c}|}\left(\mathbf{u}_e - \underline{e}\cdot\underline{\mathtt{C}}_{\mathcal{E}_c}(\mathbf{u})\right). \tag{7.43}$$

The set of local reconstruction functions $\{\underline{\ell}_{e,c}\}_{e\in E_c}$ associated with (7.42) is piecewise constant on $\mathfrak{P}_{E,c}$ and is such that

$$\underline{\ell}_{e,c}(\underline{x})|_{\mathfrak{p}_{e',c}} := \frac{\beta}{|\mathfrak{p}_{e,c}|}\tilde{\underline{f}}_c(e)\delta_{e',e} + \left(\underline{\underline{\mathsf{Id}}} - \beta\frac{\tilde{\underline{f}}_c(e')\otimes\underline{e}'}{|\mathfrak{p}_{e',c}|}\right)\frac{\tilde{\underline{f}}_c(e)}{|c|}. \tag{7.44}$$

Recall that $|\mathfrak{p}_{e,c}| = \frac{1}{d}\underline{e}\cdot\tilde{\underline{f}}_c(e)$ where d is the space dimension. We stress that the tangential component of these functions is not necessarily continuous on the edges of the submesh (induced by $\mathfrak{P}_{E,c}$) lying inside c, so that, in general, $\underline{\mathtt{L}}_{\mathcal{E}_c}$ does not map into $H(\underline{\mathrm{curl}};c)$.

Flux reconstruction. For each $\mathrm{c} \in \mathrm{C}$, the reconstruction operator $\underline{\mathtt{L}}_{\mathcal{F}_\mathrm{c}}$ is constant in each $\mathfrak{p}_{\mathrm{f},\mathrm{c}}$ associated to the face $\mathrm{f} \in \mathrm{F}_\mathrm{c}$. In this case, (7.37) becomes $\underline{\mathtt{C}}_{\mathcal{F}_\mathrm{c}} : \mathcal{F}_\mathrm{c} \to [\mathbb{P}_0(\mathrm{c})]^3$ and $\hat{\underline{\mathtt{S}}}_{\mathcal{F}_\mathrm{c}} : \mathcal{F}_\mathrm{c} \to [\mathbb{P}_0(\mathfrak{P}_{\mathrm{F},\mathrm{c}})]^3$ such that for all $\boldsymbol{\phi} \in \mathcal{F}_\mathrm{c}$,

$$\underline{\mathtt{C}}_{\mathcal{F}_\mathrm{c}}(\boldsymbol{\phi}) := \frac{1}{|\mathrm{c}|}\sum_{\mathrm{f}\in\mathrm{F}_\mathrm{c}} \boldsymbol{\phi}_\mathrm{f}\tilde{\underline{\mathrm{e}}}_\mathrm{c}(\mathrm{f}), \qquad \hat{\underline{\mathtt{S}}}_{\mathcal{F}_\mathrm{c}}(\boldsymbol{\phi})|_{\mathfrak{p}_{\mathrm{f},\mathrm{c}}} := \beta\frac{\tilde{\underline{\mathrm{e}}}_\mathrm{c}(\mathrm{f})}{|\mathfrak{p}_{\mathrm{f},\mathrm{c}}|}\boldsymbol{\phi}_\mathrm{f},\ \forall \mathrm{f} \in \mathrm{F}_\mathrm{c}. \tag{7.45}$$

Then, we readily infer that the constant value taken by $\underline{\mathtt{L}}_{\mathcal{F}_\mathrm{c}}(\boldsymbol{\phi})$ in each $\mathfrak{p}_{\mathrm{f},\mathrm{c}}$, for $\mathrm{f} \in \mathrm{F}_\mathrm{c}$, is

$$\underline{\mathtt{L}}_{\mathcal{F}_\mathrm{c}}(\boldsymbol{\phi})|_{\mathfrak{p}_{\mathrm{f},\mathrm{c}}} = \underline{\mathtt{C}}_{\mathcal{F}_\mathrm{c}}(\boldsymbol{\phi}) + \beta\frac{\tilde{\underline{\mathrm{e}}}_\mathrm{c}(\mathrm{f})}{|\mathfrak{p}_{\mathrm{f},\mathrm{c}}|}\left(\boldsymbol{\phi}_\mathrm{f} - \underline{\mathrm{f}}\cdot\underline{\mathtt{C}}_{\mathcal{F}_\mathrm{c}}(\boldsymbol{\phi})\right). \tag{7.46}$$

The set of local reconstruction functions $\{\underline{\ell}_{\mathrm{f},\mathrm{c}}\}_{\mathrm{f}\in\mathrm{F}_\mathrm{c}}$ associated with (7.45) is piecewise constant on $\mathfrak{P}_{\mathrm{F},\mathrm{c}}$ and is such that

$$\underline{\ell}_{\mathrm{f},\mathrm{c}}(\underline{x})|_{\mathfrak{p}_{\mathrm{f}',\mathrm{c}}} := \frac{\beta}{|\mathfrak{p}_{\mathrm{f},\mathrm{c}}|}\tilde{\underline{\mathrm{e}}}_\mathrm{c}(\mathrm{f})\delta_{\mathrm{f},\mathrm{f}'} + \left(\underline{\underline{\mathsf{Id}}} - \beta\frac{\tilde{\underline{\mathrm{e}}}_\mathrm{c}(\mathrm{f}')\otimes\underline{\mathrm{f}}'}{|\mathfrak{p}_{\mathrm{f}',\mathrm{c}}|}\right)\frac{\tilde{\underline{\mathrm{e}}}_\mathrm{c}(\mathrm{f})}{|\mathrm{c}|}. \tag{7.47}$$

We stress that the normal component of these functions is not necessarily continuous accross the faces of the submesh (induced by $\mathfrak{P}_{\mathrm{F},\mathrm{c}}$) lying inside c, so that, in general, $\underline{\mathtt{L}}_{\mathcal{F}_\mathrm{c}}$ does not map into $H(\mathrm{div};\mathrm{c})$.

Proposition 7.33 (Unisolvence)**.** *The reconstruction operators detailed in Definition 7.31 satisfy property* (**R4**) *if and only if*

- $\beta = \frac{1}{d}$ *for circulation and flux reconstructions,*
- $\beta = 1$ *for potential reconstructions.*

Proof. In the case of potential reconstructions, the proof is straightforward considering (7.41). In the case of circulation reconstructions, since $|\mathfrak{p}_{\mathrm{e},\mathrm{c}}| = \frac{1}{d}\underline{\mathrm{e}}\cdot\tilde{\underline{\mathrm{f}}}_\mathrm{c}(\mathrm{e})$ for all cells $\mathrm{c} \in \mathrm{C}$ and for all edges $\mathrm{e} \in \mathrm{E}_\mathrm{c}$, (7.44) yields

$$\int_\mathrm{e}\underline{\ell}_{\mathrm{e},\mathrm{c}}\cdot\underline{\tau}_\mathrm{e} = \underline{\mathrm{e}}\cdot\tilde{\underline{\mathrm{f}}}_\mathrm{c}(\mathrm{e})\left(\frac{1}{|\mathrm{c}|} + \frac{\beta}{|\mathfrak{p}_{\mathrm{e},\mathrm{c}}|} - \frac{\beta\underline{\mathrm{e}}\cdot\tilde{\underline{\mathrm{f}}}_\mathrm{c}(\mathrm{e})}{|\mathfrak{p}_{\mathrm{e},\mathrm{c}}||\mathrm{c}|}\right) = 1 + (\beta d - 1)(1 - \frac{d|\mathfrak{p}_{\mathrm{e},\mathrm{c}}|}{|\mathrm{c}|}),$$

and the right-hand side equals 1 if and only if $\beta = \frac{1}{d}$. In the case of flux reconstructions, the proof follows the same lines; see also Codecasa *et al.* (2010), Property 1. □

Remark 7.34 (SUSHI vs. DGA)**.** *Considering circulation and flux reconstructions, the choice $\beta = \frac{1}{d}$ yields the DGA reconstructions while the choice $\beta = \frac{1}{\sqrt{d}}$ corresponds to the choice made in SUSHI schemes.* (**R4**) *holds only for the choice $\beta = \frac{1}{d}$, so that, for all* $\mathrm{c} \in \mathrm{C}$, $\underline{\mathtt{A}}_{\mathcal{E}_\mathrm{c}}$ *and* $\underline{\mathtt{A}}_{\mathcal{F}_\mathrm{c}}$ *are projectors (cf. Proposition 7.19) only when one considers the DGA reconstruction. However, the SUSHI-like reconstructions have the practical advantage to yield a diagonal discrete Hodge operator when the mesh is superadmissible and the material property is isotropic (see Eymard* et al. *(2010), Lemma 2.1).*

Remark 7.35 (Comparison with Perot et al.)**.** *Perot* et al. *(2006) have proposed a reconstruction operator $\underline{\mathtt{L}}_{\mathcal{E}_\mathrm{c}}$ (resp. $\underline{\mathtt{L}}_{\mathcal{F}_\mathrm{c}}$) on polyhedral meshes with only a consistent part defined as in* (7.11b) *(resp.* (7.11c)*). However, these reconstructions seem to suffer from a lack of stability.*

7.3.2 Piecewise polynomial conforming reconstruction

For the sake of completeness, we recall in this section the construction proposed by Christiansen (2008) since we consider these reconstruction operators for deriving the theoretical results of Section 7.4. The construction is cellwise. In each polyhedral cell $\mathrm{c} \in \mathrm{C}$, the local reconstruction functions devised by Christiansen for potentials, $\ell^\mathrm{C}_{\mathrm{v},\mathrm{c}}$, circulations, $\underline{\ell}^\mathrm{C}_{\mathrm{e},\mathrm{c}}$, and

fluxes, $\underline{\ell}^{\mathrm{C}}_{\mathrm{f,c}}$ are built solving mixed FE problems on a simplicial submesh of the cell c. Since we assume that the mesh is of class **(MB)**, we can consider the simplicial submesh arising from the barycentric subdivision of each cell in what follows (observe that the barycentric subdivision is not required in the original construction). Similar to Chapter 5, the simplicial submesh is denoted by $\mathfrak{S} := \{\mathfrak{V}, \mathfrak{E}, \mathfrak{T}, \mathfrak{C}\}$ where $\mathfrak{V}$ collects the vertices $\mathfrak{v}$ (including those of M), $\mathfrak{E}$ the edges $\mathfrak{e}$, $\mathfrak{T}$ the triangles $\mathfrak{t}$, and $\mathfrak{C}$ the subtetrahedra $\mathfrak{c}$. In what follows, we denote by $\mathfrak{E}_{\mathrm{e}} := \{\mathfrak{e} \in \mathfrak{E} \,|\, \mathfrak{e} \subset \mathrm{e}\}$ for each edge $\mathrm{e} \in \mathrm{E}$, $\mathfrak{T}_{\mathrm{f}} := \{\mathfrak{t} \in \mathfrak{T} \,|\, \mathfrak{t} \subset \mathrm{f}\}$ for each face $\mathrm{f} \in \mathrm{F}$, and $\mathfrak{C}_{\mathrm{c}} := \{\mathfrak{c} \in \mathfrak{C} \,|\, \mathfrak{c} \subset \mathrm{c}\}$ for each cell $\mathrm{c} \in \mathrm{C}$.

Remark 7.36 (FIT)**.** *In the context of FIT schemes, Euler (2007) has proposed a similar approach to define potential, circulation, and flux reconstruction functions on polyhedral meshes based on the use of Whitney reconstruction functions on an underlying simplicial submesh.*

Potential reconstruction. Let $\mathrm{c} \in \mathrm{C}$. For each vertex $\mathrm{v} \in \mathrm{V}_{\mathrm{c}}$, we proceed as follows:

1. We assign $\ell^{\mathrm{C}}_{\mathrm{v,c}}(\underline{x}_{\mathrm{v}'}) = \delta_{\mathrm{v,v}'}$ for all $\mathrm{v}' \in \mathrm{V}_{\mathrm{c}}$ (δ is the Kronecker symbol).
2. For each $\mathrm{e} \in \mathrm{E}_{\mathrm{c}}$, we denote by $\mathbb{P}^{\mathrm{conf}}_1(\mathfrak{E}_{\mathrm{e}}) := \{\theta \in C^0(\mathrm{e}) \,|\, \forall \mathfrak{e} \in \mathfrak{E}_{\mathrm{e}},\, \theta|_{\mathfrak{e}} \in \mathbb{P}_1(\mathfrak{e})\}$ and $\mathbb{P}^{\mathrm{conf}}_{1,0}(\mathfrak{E}_{\mathrm{e}})$ the subspace of $\mathbb{P}^{\mathrm{conf}}_1(\mathfrak{E}_{\mathrm{e}})$ spanned by functions with homogeneous Dirichlet BCs on $\partial\mathrm{e}$. Then, $\ell^{\mathrm{C}}_{\mathrm{v,c}}|_{\mathrm{e}}$ is defined by solving the following problem:

$$\int_{\mathrm{e}} \underline{\mathbf{grad}}(\ell^{\mathrm{C}}_{\mathrm{v,c}}) \cdot \underline{\mathbf{grad}}(\theta) = 0, \qquad \forall \theta \in \mathbb{P}^{\mathrm{conf}}_{1,0}(\mathfrak{E}_{\mathrm{e}}). \tag{7.48a}$$

   The Dirichlet boundary conditions of $\ell^{\mathrm{C}}_{\mathrm{v,c}}$ on $\partial\mathrm{e}$ results from the previous step.

3. For each face $\mathrm{f} \in \mathrm{F}_{\mathrm{c}}$, we denote by $\mathbb{P}^{\mathrm{conf}}_1(\mathfrak{T}_{\mathrm{f}}) := \{\theta \in C^0(\mathrm{f}) \,|\, \forall \mathfrak{t} \in \mathfrak{T}_{\mathrm{f}},\, \theta|_{\mathfrak{t}} \in \mathbb{P}_1(\mathfrak{t})\}$ and $\mathbb{P}^{\mathrm{conf}}_{1,0}(\mathfrak{T}_{\mathrm{f}})$ the subspace of $\mathbb{P}^{\mathrm{conf}}_1(\mathfrak{T}_{\mathrm{f}})$ spanned by functions with homogeneous Dirichlet BCs on $\partial\mathrm{f}$. Then, $\ell^{\mathrm{C}}_{\mathrm{v,c}}|_{\mathrm{f}}$ is defined by solving the following problem:

$$\int_{\mathrm{f}} \underline{\mathbf{grad}}(\ell^{\mathrm{C}}_{\mathrm{v,c}}) \cdot \underline{\mathbf{grad}}(\theta) = 0, \qquad \forall \theta \in \mathbb{P}^{\mathrm{conf}}_{1,0}(\mathfrak{T}_{\mathrm{f}}). \tag{7.48b}$$

   The Dirichlet boundary conditions of $\ell^{\mathrm{C}}_{\mathrm{v,c}}$ on $\partial\mathrm{f}$ results from the previous step.

4. In c, we denote by $\mathbb{P}^{\mathrm{conf}}_1(\mathfrak{C}_{\mathrm{c}}) := \{\theta \in C^0(\mathrm{c}) \,|\, \forall \mathfrak{c} \in \mathfrak{C}_{\mathrm{c}},\, \theta|_{\mathfrak{c}} \in \mathbb{P}_1(\mathfrak{c})\}$ and $\mathbb{P}^{\mathrm{conf}}_{1,0}(\mathfrak{C}_{\mathrm{c}})$ the subspace of $\mathbb{P}^{\mathrm{conf}}_1(\mathfrak{C}_{\mathrm{c}})$ spanned by functions with homogeneous Dirichlet BCs on $\partial\mathrm{c}$. Then, $\ell^{\mathrm{C}}_{\mathrm{v,c}}$ is defined by solving the following problem:

$$\int_{\mathrm{c}} \underline{\mathbf{grad}}(\ell^{\mathrm{C}}_{\mathrm{v,c}}) \cdot \underline{\mathbf{grad}}(\theta) = 0, \qquad \forall \theta \in \mathbb{P}^{\mathrm{conf}}_{1,0}(\mathfrak{C}_{\mathrm{c}}). \tag{7.48c}$$

   The Dirichlet boundary conditions of $\ell^{\mathrm{C}}_{\mathrm{v,c}}$ on $\partial\mathrm{c}$ results from the previous step.

Circulation reconstruction. Let $\mathbb{N}_0(\mathfrak{t})$ (resp. $\mathbb{N}_0(\mathfrak{c})$) be the lowest-order Nédélec space on a triangle $\mathfrak{t}$ (resp. tetrahedron $\mathfrak{c}$). Let $\mathrm{c} \in \mathrm{C}$. For each edge $\mathrm{e} \in \mathrm{E}_{\mathrm{c}}$, we proceed as follows:

1. We assign $\int_{\mathrm{e}'} \underline{\ell}^{\mathrm{C}}_{\mathrm{e,c}} \cdot \underline{\tau}_{\mathrm{e}'} = \delta_{\mathrm{e,e}'}$ for all $\mathrm{e}' \in \mathrm{E}_{\mathrm{c}}$.
2. For each face $\mathrm{f} \in \mathrm{F}_{\mathrm{c}}$, we denote by $\mathbb{N}_0(\mathfrak{T}_{\mathrm{f}}) := \{\underline{\psi} \in L^2(\mathrm{f})^2 \,|\, \forall \mathfrak{t} \in \mathfrak{T}_{\mathrm{f}},\, \underline{\psi}|_{\mathfrak{t}} \in \mathbb{N}_0(\mathfrak{t})\}$ and $\mathbb{N}_{0,0}(\mathfrak{T}_{\mathrm{f}})$ the subspace of $\mathbb{N}_0(\mathfrak{T}_{\mathrm{f}})$ spanned by functions with homogeneous tangential component on $\partial\mathrm{f}$. Then, $\underline{\ell}^{\mathrm{C}}_{\mathrm{e,c}}|_{\mathrm{f}}$ is defined by solving the following problem:

$$\begin{cases} \displaystyle\int_{\mathrm{f}} \underline{\mathbf{curl}}(\underline{\ell}^{\mathrm{C}}_{\mathrm{e,c}}) \cdot \underline{\mathbf{curl}}(\underline{\psi}) = 0, & \forall \underline{\psi} \in \mathbb{N}_{0,0}(\mathfrak{T}_{\mathrm{f}}), \\ \displaystyle\int_{\mathrm{f}} \underline{\ell}^{\mathrm{C}}_{\mathrm{e,c}} \cdot \underline{\mathbf{grad}}(\theta) = 0, & \forall \theta \in \mathbb{P}^{\mathrm{conf}}_{1,0}(\mathfrak{T}_{\mathrm{f}}). \end{cases} \tag{7.49a}$$

   The tangential boundary conditions of $\underline{\ell}^{\mathrm{C}}_{\mathrm{e,c}}$ on $\partial\mathrm{f}$ results from the previous step.

3. In c, we denote by $\mathbb{N}_0(\mathfrak{C}_c) := \{\underline{\psi} \in L^2(c)^3 \,|\, \forall \mathfrak{c} \in \mathfrak{C}_c,\, \underline{\psi}|_{\mathfrak{c}} \in \mathbb{N}_0(\mathfrak{c})\}$ and $\mathbb{N}_{0,0}(\mathfrak{C}_c)$ the subspace of $\mathbb{N}_0(\mathfrak{C}_c)$ spanned by functions with homogeneous tangential component on ∂c. Then, $\underline{\ell}^C_{e,c}$ is defined by solving the following problem:

$$\begin{cases} \displaystyle\int_c \underline{\mathrm{curl}}(\underline{\ell}^C_{e,c}) \cdot \underline{\mathrm{curl}}(\underline{\psi}) = 0, & \forall \underline{\psi} \in \mathbb{N}_{0,0}(\mathfrak{C}_c), \\ \displaystyle\int_c \underline{\ell}^C_{e,c} \cdot \underline{\mathrm{grad}}(\theta) = 0, & \forall \theta \in \mathbb{P}^{\mathrm{conf}}_{1,0}(\mathfrak{C}_c). \end{cases} \tag{7.49b}$$

The tangential boundary conditions of $\underline{\ell}^C_{e,c}$ on ∂c results from the previous step.

Flux reconstruction. Let $\mathbb{RTN}_0(\mathfrak{c})$ be the lowest-order Raviart–Thomas–Nédélec space on a tetrahedron $\mathfrak{c}$. Let $c \in C$. For each face $f \in F_c$, we proceed as follows:

1. We assign $\int_{f'} \underline{\ell}^C_{f,c} \cdot \underline{\nu}_{f'} = \delta_{f,f'}$ for all $f' \in F_c$.
2. In c, we denote by $\mathbb{RTN}_0(\mathfrak{C}_c) := \{\underline{\phi} \in L^2(c)^3 \,|\, \forall \mathfrak{c} \in \mathfrak{C}_c,\, \underline{\phi}|_{\mathfrak{c}} \in \mathbb{RTN}_0(\mathfrak{c})\}$ and $\mathbb{RTN}_{0,0}(\mathfrak{C}_c)$ the subspace of $\mathbb{RTN}_0(\mathfrak{C}_c)$ spanned by functions with homogeneous normal component on ∂c. Then, $\underline{\ell}^C_{f,c}$ is defined by solving the following problem:

$$\begin{cases} \displaystyle\int_c \mathrm{div}(\underline{\ell}^C_{f,c}) \cdot \mathrm{div}(\underline{\phi}) = 0, & \forall \underline{\phi} \in \mathbb{RTN}_{0,0}(\mathfrak{C}_c), \\ \displaystyle\int_c \underline{\ell}^C_{f,c} \cdot \underline{\mathrm{curl}}(\underline{\psi}) = 0, & \forall \underline{\psi} \in \mathbb{N}_{0,0}(\mathfrak{C}_c). \end{cases} \tag{7.50}$$

The normal boundary conditions of $\underline{\ell}^C_{f,c}$ on ∂c results from the previous step.

Properties. The global reconstruction operators $\mathtt{L}^C_{\mathcal{V}}$, $\underline{\mathtt{L}}^C_{\mathcal{E}}$, and $\underline{\mathtt{L}}^C_{\mathcal{F}}$ are defined as in (7.15) from the local reconstruction operators.

Proposition 7.37 (Properties of Christiansen's reconstruction operators)**.** *Assume that the mesh is of class* **(MR)** *with planar primal faces. Then, the local reconstruction operators* $\mathtt{L}^C_{\mathcal{V}_c}$, $\underline{\mathtt{L}}^C_{\mathcal{E}_c}$, *and* $\underline{\mathtt{L}}^C_{\mathcal{F}_c}$ *satisfy* (**R1**), (**R2**), *and* (**R4**). *Moreover, the global reconstruction operators* $\mathtt{L}^C_{\mathcal{V}}$, $\underline{\mathtt{L}}^C_{\mathcal{E}}$, *and* $\underline{\mathtt{L}}^C_{\mathcal{F}}$ *are conforming and commute with differential operators.*

Proof. See Christiansen (2008). The assumption on planar primal faces is required to represent exactly constant fields (*i.e.* to achieve (**R2**)). □

Remark 7.38 (Potential reconstructions in MFD)**.** *In MFD schemes, Beirão da Veiga* et al. *(2014) have proposed an alternative definition of a conforming reconstruction operator having properties* (**R2**) *and* (**R4**) *along with the commuting property with differential operators. Brezzi* et al. *(2009) have also devised a conforming potential reconstruction operator having properties* (**R1**), (**R2**), *and* (**R4**). *The commuting property with* $\underline{\mathrm{grad}}$ *is not addressed since only the potential reconstruction is considered in this work.*

7.3.3 Piecewise polynomial conforming reconstruction with dual consistency

In this section, we devise potential and flux reconstruction operators on polyhedral meshes which share the same properties as the reconstruction operators of the previous section (cf. Proposition 7.37), but which are different since the additional property (**R3**) (dual consistency) is satisfied. Devising a circulation reconstruction operator with such properties is left to future work.

Potential reconstruction. The conforming potential reconstruction $\mathrm{L}_{\mathcal{V}}^{\mathrm{conf}}$ is built as a continuous and piecewise affine function on a simplicial submesh of each primal cell. Let $\mathrm{c} \in \mathrm{C}$. For the definition of $\mathrm{L}_{\mathcal{V}_\mathrm{c}}^{\mathrm{conf}}$, we consider a new partition of the cell, denoted by $\mathfrak{P}_{\mathrm{EF,c}}$ of c composed of the set of tetrahedra $\{\mathfrak{p}_{\mathrm{ef,c}}\}_{\mathrm{f}\in\mathrm{F_c},\mathrm{e}\in\mathrm{E_f}}$ defined as follows:

$$\mathfrak{p}_{\mathrm{ef,c}} := \mathfrak{p}_{\mathrm{e,c}} \cap \mathfrak{p}_{\mathrm{f,c}}, \qquad \forall \mathrm{f} \in \mathrm{F_c}, \forall \mathrm{e} \in \mathrm{E_f}. \tag{7.51}$$

For each face $\mathrm{f} \in \mathrm{F_c}$ and each edge $\mathrm{e} \in \mathrm{E_f}$, $\mathfrak{p}_{\mathrm{ef,c}}$ is a simplex composed of two elementary subsimplices $\mathfrak{p}_{\mathrm{ef,c}} = \cup_{\mathrm{v}\in\mathrm{V_e}}\mathfrak{s}_{\mathrm{v,e,f,c}}$ (see Figure 7.6, left).

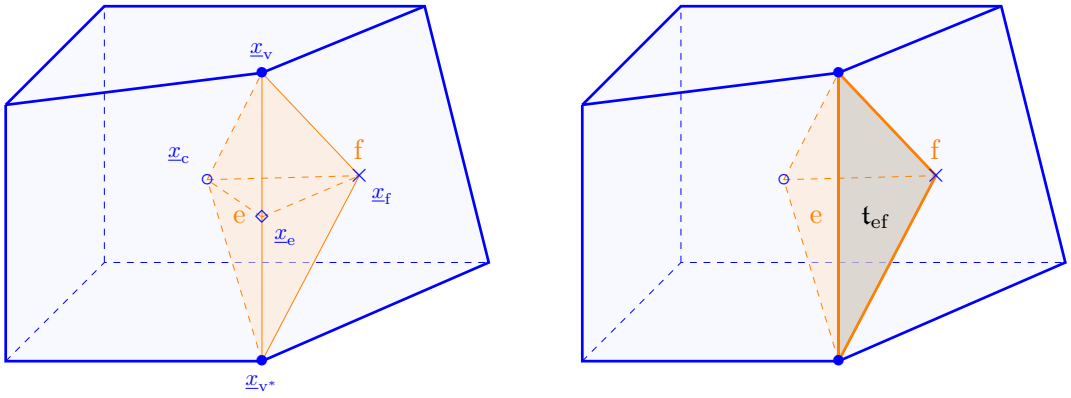

Figure 7.6 – Let c be a hexahedron. For a face $\mathrm{f} \in \mathrm{F_c}$ and an edge $\mathrm{e} \in \mathrm{E_f}$, we highlight the subvolume $\mathfrak{p}_{\mathrm{ef,c}}$ (left) and the triangle $\mathfrak{t}_{\mathrm{ef}}$ (right).

In what follows, we consider

$$\mathbb{P}_1^{\mathrm{conf}}(\mathfrak{P}_{\mathrm{EF,c}}) := \{q \in C^0(\mathrm{c}) \,|\, \forall \mathrm{f} \in \mathrm{F_c}, \forall \mathrm{e} \in \mathrm{E_f}, \, q|_{\mathfrak{p}_{\mathrm{ef,c}}} \in \mathbb{P}_1(\mathfrak{p}_{\mathrm{ef,c}})\}, \tag{7.52}$$

the space spanned by continuous and piecewise affine functions on $\mathfrak{P}_{\mathrm{EF,c}}$. The local conforming reconstruction operator $\mathrm{L}_{\mathcal{V}_\mathrm{c}}^{\mathrm{conf}} : \mathcal{V}_\mathrm{c} \to \mathbb{P}_1^{\mathrm{conf}}(\mathfrak{P}_{\mathrm{EF,c}})$ is built by prescribing its values at the vertices of $\mathfrak{P}_{\mathrm{EF,c}}$ that is, at $\underline{x}_\mathrm{v}$ for all $\mathrm{v} \in \mathrm{V_c}$, at $\underline{x}_\mathrm{f}$ for all $\mathrm{f} \in \mathrm{F_c}$, and at $\underline{x}_\mathrm{c}$. Let $\mathbf{p} \in \mathcal{V}_\mathrm{c}$. We set $\mathrm{L}_{\mathcal{V}_\mathrm{c}}^{\mathrm{conf}}(\mathbf{p})(\underline{x}_\mathrm{v}) := \mathbf{p}_\mathrm{v}$ for all $\mathrm{v} \in \mathrm{V_c}$, and prescribe $\mathrm{L}_{\mathcal{V}_\mathrm{c}}^{\mathrm{conf}}(\mathbf{p})(\underline{x}_\mathrm{f})$ for all $\mathrm{f} \in \mathrm{F_c}$ and $\mathrm{L}_{\mathcal{V}_\mathrm{c}}^{\mathrm{conf}}(\mathbf{p})(\underline{x}_\mathrm{c})$ as follows:

$$\mathrm{L}_{\mathcal{V}_\mathrm{c}}^{\mathrm{conf}}(\mathbf{p})(\underline{x}_\mathrm{f}) := \frac{1}{|\mathrm{f}|}\sum_{\mathrm{v}\in\mathrm{V_f}} |\mathrm{f} \cap \tilde{\mathrm{c}}(\mathrm{v})|\mathbf{p}_\mathrm{v}, \qquad \forall \mathrm{f} \in \mathrm{F_c}, \tag{7.53a}$$

$$\mathrm{L}_{\mathcal{V}_\mathrm{c}}^{\mathrm{conf}}(\mathbf{p})(\underline{x}_\mathrm{c}) := \frac{1}{|\mathrm{c}|}\sum_{\mathrm{v}\in\mathrm{V_c}} |\mathrm{c} \cap \tilde{\mathrm{c}}(\mathrm{v})|\mathbf{p}_\mathrm{v}. \tag{7.53b}$$

Definition 7.39 (Local conforming potential reconstruction on polyhedral meshes)**.** *Assume there exists a fully barycentric subdivision of the mesh. Let* $\mathrm{c} \in \mathrm{C}$. *Then, we set* $\mathrm{L}_{\mathcal{V}_\mathrm{c}}^{\mathrm{conf}}(\mathbf{p}) = \sum_{\mathrm{v}\in\mathrm{V_c}} \mathbf{p}_\mathrm{v}\ell_{\mathrm{v,c}}^{\mathrm{conf}}$ *for all* $\mathbf{p} \in \mathcal{V}_\mathrm{c}$ *with the local reconstruction functions* $\{\ell_{\mathrm{v,c}}^{\mathrm{conf}}\}_{\mathrm{v}\in\mathrm{V_c}}$ *defined in each* $\mathfrak{p}_{\mathrm{ef,c}}$ *for all* $\mathrm{f} \in \mathrm{F_c}$ *and all* $\mathrm{e} \in \mathrm{E_f}$, *as follows:*

$$\ell_{\mathrm{v,c}}^{\mathrm{conf}}(\underline{x})|_{\mathfrak{p}_{\mathrm{ef}}} := \delta_\mathrm{e}(\mathrm{v})\ell_\mathrm{v}^{\mathrm{LAG}}(\underline{x}) + \delta_\mathrm{f}(\mathrm{v})\frac{|\mathrm{f} \cap \tilde{\mathrm{c}}(\mathrm{v})|}{|\mathrm{f}|}\ell_\mathrm{f}^{\mathrm{LAG}}(\underline{x}) + \frac{|\mathrm{c} \cap \tilde{\mathrm{c}}(\mathrm{v})|}{|\mathrm{c}|}\ell_\mathrm{c}^{\mathrm{LAG}}(\underline{x}), \tag{7.54}$$

where ℓ^{LAG} *are the Lagrange shape functions related to the vertices of* $\mathfrak{p}_{\mathrm{ef,c}}$ *located at* $\underline{x}_\mathrm{c}$, $\{\underline{x}_\mathrm{f}\}_{\mathrm{f}\in\mathrm{F_c}}$, *and* $\{\underline{x}_\mathrm{v}\}_{\mathrm{v}\in\mathrm{V_e}}$. $\delta_\mathrm{e}(\mathrm{v}) = 1$ *if* $\mathrm{v} \in \mathrm{V_e}$, 0 *otherwise, and* $\delta_\mathrm{f}(\mathrm{v}) = 1$ *if* $\mathrm{v} \in \mathrm{V_f}$, 0 *otherwise.*

As a consequence, the local potential reconstruction operator is such that for all $\mathrm{f} \in \mathrm{F_c}$ and all $\mathrm{e} \in \mathrm{E_f}$,

$$\mathrm{L}_{\mathcal{V}_\mathrm{c}}^{\mathrm{conf}}(\mathbf{p})|_{\mathfrak{p}_{\mathrm{ef,c}}} = \mathrm{L}_{\mathcal{V}_\mathrm{c}}^{\mathrm{conf}}(\mathbf{p})(\underline{x}_\mathrm{c})\ell_\mathrm{c}^{\mathrm{LAG}}(\underline{x}) + \mathrm{L}_{\mathcal{V}_\mathrm{c}}^{\mathrm{conf}}(\mathbf{p})(\underline{x}_\mathrm{f})\ell_\mathrm{f}^{\mathrm{LAG}}(\underline{x}) + \sum_{\mathrm{v}\in\mathrm{V_e}} \mathbf{p}_\mathrm{v}\ell_\mathrm{v}^{\mathrm{LAG}}(\underline{x}). \tag{7.55}$$

Lemma 7.40 (Properties of $\mathsf{L}_{\mathcal{V}_c}^{\rm conf}$)**.** *Assume that the mesh is of class* **(MR)** *and* **(MB)** *with a fully barycentric subdivision. Assume that primal faces are planar. Then, for each cell* $c \in C$, $\mathsf{L}_{\mathcal{V}_c}$ *satisfies the four properties* (**R1**)–(**R4**)*. Moreover,* $\mathsf{L}_{\mathcal{V}_c}^{\rm conf}$ *satisfies the following additional properties:*

(i) (Local conformity) $\mathsf{L}_{\mathcal{V}_c}^{\rm conf} : \mathcal{V}_c \to H^1(c)$*;*

(ii) ($\mathbb{P}_1$*-consistency) For all* $A \in \mathbb{P}_1(c)$*,* $\mathsf{L}_{\mathcal{V}_c}\mathsf{R}_{\mathcal{V}_c}(A) = A$*.*

Proof. (**R1**) can be proved using the mesh regularity **(MR)**. Let us now consider (**R2**). For any constant field K in c, we infer from (7.55) that, for all $f \in F_c$ and all $e \in E_f$,

$$\begin{aligned}\mathsf{L}_{\mathcal{V}_c}^{\rm conf}\mathsf{R}_{\mathcal{V}_c}(K)|_{\mathfrak{p}_{ef,c}} &= K\left[\left(\sum_{v\in V_c}\frac{|c\cap\tilde{c}(v)|}{|c|}\right)\ell_c^{\rm LAG} + \left(\sum_{v\in V_f}\frac{|f\cap\tilde{c}(v)|}{|f|}\right)\ell_f^{\rm LAG} + \sum_{v\in V_e}\ell_v^{\rm LAG}\right]\\ &= K\left(\ell_c^{\rm LAG} + \ell_f^{\rm LAG} + \sum_{v\in V_e}\ell_v^{\rm LAG}\right) = K,\end{aligned}$$

since the Lagrange shape functions form a partition of unity.

(**R3**) corresponds to $\int_c \ell_{v,c}^{\rm conf} = |c\cap\tilde{c}(v)|$ for any vertex $v \in V_c$. Since $\int_{\mathfrak{p}_{ef}} \ell_{\mathfrak{v}}^{\rm LAG} = \frac{1}{4}|\mathfrak{p}_{ef}|$ for any vertex $\mathfrak{v}$ of $\mathfrak{p}_{ef}$, we infer for any vertex $v \in V_c$ that

$$\begin{aligned}\int_c \ell_{v,c}^{\rm conf} &= \sum_{f\in F_c}\sum_{e\in E_f}\int_{\mathfrak{p}_{ef,c}}\ell_{v,c}^{\rm conf} = \sum_{f\in F_c}\sum_{e\in E_f}\frac{1}{4}|\mathfrak{p}_{ef,c}|\left(\frac{|c\cap\tilde{c}(v)|}{|c|} + \delta_f(v)\frac{|f\cap\tilde{c}(v)|}{|f|} + \delta_e(v)\right)\\ &= T_1 + T_2 + T_3.\end{aligned}$$

We readily verify that $T_1 = \frac{1}{4}|c\cap\tilde{c}(v)|$. By definition of $\delta_f(v)$ and owing to Proposition 5.22, we infer that

$$T_2 = \frac{1}{4}\sum_{f\in F_v\cap F_c}\frac{|f\cap\tilde{c}(v)|}{|f|}\sum_{e\in E_f}|\mathfrak{p}_{ef,c}| = \frac{1}{4}\sum_{f\in F_v\cap F_c}\frac{|f\cap\tilde{c}(v)|}{|f|}|\mathfrak{p}_{f,c}| = \frac{1}{4}|c\cap\tilde{c}(v)|.$$

By definition of $\delta_e(v)$ and since $\underline{x}_e$ is the barycenter of e for each edge $e \in E_c$, we infer that

$$T_3 = \frac{1}{4}\sum_{f\in F_v\cap F_c}\sum_{e\in E_f\cap E_v}|\mathfrak{p}_{ef,c}| = \frac{1}{2}\sum_{f\in F_v\cap F_c}\sum_{e\in E_f\cap E_v}|\mathfrak{s}_{v,e,f,c}| = \frac{1}{2}|c\cap\tilde{c}(v)|.$$

(**R4**) is readily verified using the definition (7.54).

Local conformity (i) holds by construction. Finally, the $\mathbb{P}_1$-consistency (ii) results from the linear completeness property (7.4) since (**R2**) holds. Indeed, for any face $f \in F_c$ and any edge $e \in E_f$, the following property holds in any $\underline{x} \in \mathfrak{p}_{ef,c}$:

$$\begin{aligned}\sum_{v\in V_c}\underline{x}_v\ell_{v,c}^{\rm conf}(\underline{x}) &= \left(\sum_{v\in V_c}\frac{|c\cap\tilde{c}(v)|}{|c|}\underline{x}_v\right)\ell_c^{\rm LAG}(\underline{x}) + \left(\sum_{v\in V_f}\frac{|f\cap\tilde{c}(v)|}{|f|}\underline{x}_v\right)\ell_f^{\rm LAG}(\underline{x}) + \sum_{v\in V_e}\underline{x}_v\ell_v^{\rm LAG}(\underline{x})\\ &= \underline{x}_c\ell_c^{\rm LAG}(\underline{x}) + \underline{x}_f\ell_f^{\rm LAG}(\underline{x}) + \sum_{v\in V_e}\underline{x}_v\ell_v^{\rm LAG}(\underline{x}) = \underline{x},\end{aligned}$$

owing to Proposition 5.23, and the linear completeness of the Lagrange shape functions. □

Lemma 7.41 (Properties of $\mathsf{L}_{\mathcal{V}}^{\rm conf}$)**.** *Under the assumptions of Lemma 7.40, the global conforming potential reconstruction operator* $\mathsf{L}_{\mathcal{V}}^{\rm conf}$ *assembled cellwise from* $\mathsf{L}_{\mathcal{V}_c}^{\rm conf}$ *following the relation* (7.15) *satisfies the following properties:*

(i) (Conformity) $\mathsf{L}_{\mathcal{V}}^{\rm conf} : \mathcal{V} \to H^1(\Omega)$*;*

(ii) (Unisolvence) $\mathsf{R}_{\mathcal{V}}\mathsf{L}_{\mathcal{V}}^{\rm conf} = \mathsf{Id}_{\mathcal{V}}$*;*

(iii) (Stability) There exists a real number $\eta_{\mathcal{V},\mathrm{conf}} > 0$ *such that, for all* $\mathbf{p} \in \mathcal{V}$,

$$\eta_{\mathcal{V},\mathrm{conf}} |||\mathbf{p}|||_{2,\mathcal{V}}^2 \le \|\mathtt{L}_{\mathcal{V}}^{\mathrm{conf}}(\mathbf{p})\|_{L^2(\Omega)}^2 \le \eta_{\mathcal{V},\mathrm{conf}}^{-1} |||\mathbf{p}|||_{2,\mathcal{V}}^2. \tag{7.56}$$

(iv) (Dual consistency) $\mathtt{L}_{\mathcal{V}}^{\mathrm{conf}}$ *and any global potential reconstruction operator* $\mathtt{L}_{\mathcal{V}}$ *built from a local potential reconstruction operator satisfying* (**R3**) *have the same mean value. In particular, for any* $\mathbf{p} \in \mathcal{V}$*, the following identity holds:*

$$\int_\Omega \mathtt{L}_{\mathcal{V}}^{\mathrm{conf}}(\mathbf{p}) = \sum_{\mathrm{v}\in\mathrm{V}} |\tilde{\mathrm{c}}(\mathrm{v})| \mathbf{p}_{\mathrm{v}} = \int_\Omega \mathtt{L}_{\mathcal{V}}(\mathbf{p}). \tag{7.57}$$

Proof. (i) Conformity holds by construction.

(ii) Unisolvence results from the property (**R4**) of $\mathtt{L}_{\mathcal{V}_{\mathrm{c}}}^{\mathrm{conf}}$ in each cell $\mathrm{c} \in \mathrm{C}$ and the continuity of the global reconstruction.

(iii) Stability results from Proposition 7.14.

(iv) Dual consistency results from the property (**R3**) of $\mathtt{L}_{\mathcal{V}_{\mathrm{c}}}^{\mathrm{conf}}$ and $\mathtt{L}_{\mathcal{V}_{\mathrm{c}}}$ in each cell $\mathrm{c} \in \mathrm{C}$.

$$\int_\Omega \mathtt{L}_{\mathcal{V}_{\mathrm{conf}}}(\mathbf{p}) = \sum_{\mathrm{c}\in\mathrm{C}} \sum_{\mathrm{v}\in\mathrm{V}} \mathbf{p}_{\mathrm{v}} \int_{\mathrm{c}} \ell_{\mathrm{v,c}}^{\mathrm{conf}} = \sum_{\mathrm{c}\in\mathrm{C}} \sum_{\mathrm{v}\in\mathrm{V}_{\mathrm{c}}} |\mathrm{c} \cap \tilde{\mathrm{c}}(\mathrm{v})| \mathbf{p}_{\mathrm{v}} = \sum_{\mathrm{v}\in\mathrm{V}} |\tilde{\mathrm{c}}(\mathrm{v})| \mathbf{p}_{\mathrm{v}},$$

and the same relations hold replacing $\mathtt{L}_{\mathcal{V}}^{\mathrm{conf}}$ by $\mathtt{L}_{\mathcal{V}}$. □

Flux reconstruction. We take inspiration from a construction by Vohralík & Wohlmuth (2013). The reconstruction devised shares similarities with the reconstruction operator $\underline{\mathtt{L}}_{\mathcal{F}_{\mathrm{c}}}^{\mathrm{c}}$ (cf. Section 7.3.2) but the present construction is different since an additional property related to the dual consistency (**R3**) is satisfied.

The construction is cellwise. Let $\mathrm{c} \in \mathrm{C}$. For all $\mathrm{f} \in \mathrm{F}_{\mathrm{c}}$ and all $\mathrm{e} \in \mathrm{E}_{\mathrm{f}}$, we consider $\mathfrak{p}_{\mathrm{ef,c}}$ defined in (7.51) and we define the triangle $\mathfrak{t}_{\mathrm{ef}} := \mathfrak{p}_{\mathrm{ef,c}} \cap \mathrm{f}$ (see Figure 7.6 right). Let $\mathbb{RTN}_0(\mathfrak{P}_{\mathrm{EF,c}})$ be the lowest-order Raviart–Thomas–Nédélec FE space on the submesh $\mathfrak{P}_{\mathrm{EF,c}}$ and let $\mathbb{P}_0^*(\mathfrak{P}_{\mathrm{EF,c}})$ be spanned by piecewise constant functions with zero mean-value on c.

Definition 7.42 (Local conforming flux reconstruction)**.** *Assume that the mesh is of class* **(MR)** *and of class* **(MB)** *with a fully barycentric subdivision. Assume that the primal faces are planar. Let* $\mathrm{c} \in \mathrm{C}$*. For all* $\mathrm{f} \in \mathrm{F}_{\mathrm{c}}$ *and all* $\mathrm{e} \in \mathrm{E}_{\mathrm{f}}$*, we build the function* $\underline{\ell}_{\mathrm{ef,c}} \in \mathbb{RTN}_0(\mathfrak{P}_{\mathrm{EF,c}})$ *by solving the following mixed FE problem:*

$$\begin{cases} \displaystyle\int_{\mathrm{c}} \underline{\ell}_{\mathrm{ef,c}} \cdot \underline{\psi}_h - \int_{\mathrm{c}} \pi_{\mathrm{ef,c}} \operatorname{div}(\underline{\psi}_h) = 0, & \forall \underline{\psi}_h \in \mathbb{RTN}_{0,0}(\mathfrak{P}_{\mathrm{EF,c}}), \\ \displaystyle\int_{\mathrm{c}} \operatorname{div}(\underline{\ell}_{\mathrm{ef,c}}) q_h = \int_{\mathrm{c}} d_{\mathrm{f,c}} q_h, & \forall q_h \in \mathbb{P}_0^*(\mathfrak{P}_{\mathrm{EF,c}}), \end{cases} \tag{7.58}$$

with prescribed normal component

$$\int_{\mathfrak{t}_{\mathrm{e'f'}}} \underline{\ell}_{\mathrm{ef,c}} \cdot \underline{\nu}_{\mathrm{f'}} := \delta_{\mathrm{e,e'}} \delta_{\mathrm{f,f'}}, \tag{7.59}$$

(observe that $\underline{\nu}_{\mathrm{f}}$ *is constant in* f *since* f *is planar). Additionally, we prescribed a (constant) divergence*

$$d_{\mathrm{f,c}} := |\mathrm{c}|^{-1} \iota_{\mathrm{f,c}}. \tag{7.60}$$

In (7.58)*,* $\mathbb{RTN}_{0,0}(\mathfrak{P}_{\mathrm{EF,c}})$ *is the subspace of* $\mathbb{RTN}_0(\mathfrak{P}_{\mathrm{EF,c}})$ *spanned by functions with zero normal component on* $\partial\mathrm{c}$*, and* $\pi_{\mathrm{ef,c}} \in \mathbb{P}_0^*(\mathfrak{P}_{\mathrm{EF,c}})$ *is the Lagrange multiplier. Then, for all* $\mathrm{f} \in \mathrm{F}_{\mathrm{c}}$*, we set*

$$\underline{\ell}_{\mathrm{f,c}}^{\mathrm{conf}} := \frac{1}{|\mathrm{f}|} \sum_{\mathrm{e}\in\mathrm{E}_{\mathrm{f}}} |\mathfrak{t}_{\mathrm{ef}}| \underline{\ell}_{\mathrm{ef,c}}, \tag{7.61}$$

and, for all $\boldsymbol{\phi} \in \mathcal{F}_{\mathrm{c}}$*,* $\underline{\mathtt{L}}_{\mathcal{F}_{\mathrm{c}}}^{\mathrm{conf}}(\boldsymbol{\phi}) := \sum_{\mathrm{f}\in\mathrm{F}_{\mathrm{c}}} \boldsymbol{\phi}_{\mathrm{f}} \underline{\ell}_{\mathrm{f,c}}^{\mathrm{conf}}$*.*

Lemma 7.43 (Properties of $\underline{\mathsf{L}}^{\rm conf}_{\mathcal{F}_{\rm c}}$)**.** *Assume that the mesh is of class* **(MR)** *and of class* **(MB)** *with a fully barycentric subdivision. Assume that the primal faces are planar. Then, for each cell* $\mathrm{c} \in \mathrm{C}$, $\underline{\mathsf{L}}^{\rm conf}_{\mathcal{F}_{\rm c}}$ *is a local conforming flux reconstruction, i.e.*

$$\underline{\mathsf{L}}^{\rm conf}_{\mathcal{F}_{\rm c}} : \mathcal{F}_{\rm c} \to H(\mathrm{div};\mathrm{c}),$$

and it satisfies the four properties (**R1**)–(**R4**).

Proof. Conformity holds by construction since $\underline{\ell}_{\mathrm{f,c}} \in \mathbb{RTN}_0(\mathfrak{P}_{\mathrm{EF,c}}) \subset H(\mathrm{div};\mathrm{c})$.

(**R1**). Let $\boldsymbol{\phi} \in \mathcal{F}_{\rm c}$. Then, by linearity, $\underline{\mathsf{L}}^{\rm conf}_{\mathcal{F}_{\rm c}}(\boldsymbol{\phi})$ is in $\mathbb{RTN}_0(\mathfrak{P}_{\mathrm{EF,c}})$ and solves

$$\begin{cases} \displaystyle\int_{\rm c} \underline{\mathsf{L}}^{\rm conf}_{\mathcal{F}_{\rm c}}(\boldsymbol{\phi}) \cdot \underline{\psi}_h - \int_{\rm c} \pi_{\boldsymbol{\phi}}\, \mathrm{div}(\underline{\psi}_h) = 0, & \forall \underline{\psi}_h \in \mathbb{RTN}_{0,0}(\mathfrak{P}_{\mathrm{EF,c}}), \\ \displaystyle\int_{\rm c} \mathrm{div}(\underline{\mathsf{L}}^{\rm conf}_{\mathcal{F}_{\rm c}}(\boldsymbol{\phi}))q_h = \int_{\rm c} d_{\boldsymbol{\phi}} q_h, & \forall q_h \in \mathbb{P}^*_0(\mathfrak{P}_{\mathrm{EF,c}}), \end{cases}$$

with prescribed normal component $\int_{\mathrm{t_{ef}}} \underline{\mathsf{L}}^{\rm conf}_{\mathcal{F}_{\rm c}}(\boldsymbol{\phi}) \cdot \underline{\nu}_{\rm f} := \frac{|\mathrm{t_{ef}}|}{|\mathrm{f}|}\boldsymbol{\phi}_{\rm f}$, and prescribed (constant) divergence $d_{\boldsymbol{\phi}} := |\mathrm{c}|^{-1}\mathsf{DIV}(\boldsymbol{\phi})|_{\rm c}$. Using **(MR)** and classical stability estimates of mixed FE problems yield (**R1**).

(**R3**). This property is equivalent to $\int_{\rm c} \underline{\ell}^{\rm conf}_{\mathrm{f,c}} = \underline{\tilde{\mathrm{e}}}_{\rm c}(\mathrm{f}) = \iota_{\mathrm{f,c}}(\underline{x}_{\rm f} - \underline{x}_{\rm c})$. Let $\underline{B}$ be a constant vector field in c. Since $\mathrm{div}(\underline{\ell}_{\mathrm{ef,c}})$ is constant in c, $\underline{\ell}_{\rm ef} \in \mathbb{RTN}_0(\mathfrak{P}_{\mathrm{EF,c}})$, and $\underline{x}_{\rm c}$ is the barycenter of c (fully barycentric subdivision), integration by parts yields

$$\int_{\rm c} \underline{\ell}_{\mathrm{ef,c}} \cdot \underline{B} = \int_{\rm c} \underline{\ell}_{\mathrm{ef,c}} \cdot \underline{\mathrm{grad}}(\underline{B}\cdot(\underline{x}-\underline{x}_{\rm c})) = \sum_{\mathrm{f}'\in\mathrm{F_c}} \int_{\mathrm{f}'} (\underline{\ell}_{\mathrm{ef,c}} \cdot \underline{\nu}_{\mathrm{f}',\mathrm{c}})(\underline{B}\cdot(\underline{x}-\underline{x}_{\rm c})) = \iota_{\mathrm{f,c}}\underline{B}\cdot(\underline{x}_{\rm ef}-\underline{x}_{\rm c}),$$

where $\underline{x}_{\rm ef}$ denotes the barycenter of $\mathrm{t_{ef}}$. For each face $\mathrm{f} \in \mathrm{F_c}$, summing over $\mathrm{e} \in \mathrm{E_f}$ and using (7.61) yields the desired result since $\sum_{\mathrm{e}\in\mathrm{E_f}} |\mathrm{t_{ef}}|\underline{x}_{\rm ef} = |\mathrm{f}|\underline{x}_{\rm f}$.

(**R2**). We consider a constant vector field $\underline{\Phi}$ in c. First, using (**R3**) and the property of the barycentric subdivision (5.17b), we infer that

$$\frac{1}{|\mathrm{c}|}\int_{\rm c} \underline{\mathsf{L}}^{\rm conf}_{\mathcal{F}_{\rm c}} \mathsf{R}_{\mathcal{F}_{\rm c}}(\underline{\Phi}) = \frac{1}{|\mathrm{c}|}\int_{\rm c} \sum_{\mathrm{f}\in\mathrm{F_c}} (\underline{\Phi}\cdot\underline{\mathrm{f}})\underline{\ell}^{\rm conf}_{\mathrm{f,c}} = \frac{1}{|\mathrm{c}|}\left(\sum_{\mathrm{f}\in\mathrm{F_c}} \underline{\tilde{\mathrm{e}}}_{\rm c}(\mathrm{f})\otimes\underline{\mathrm{f}}\right)\underline{\Phi} = \underline{\Phi},$$

so that $\|\underline{\Phi}\|_{L^2(\mathrm{c})^3} \le \|\underline{\mathsf{L}}^{\rm conf}_{\mathcal{F}_{\rm c}}\mathsf{R}_{\mathcal{F}_{\rm c}}(\underline{\Phi})\|_{L^2(\mathrm{c})^3}$. However, $\underline{\Phi}$ is in $\mathbb{RTN}_0(\mathfrak{P}_{\mathrm{EF,c}})$ and satisfies the prescriptions on the normal component and (constant) divergence. Since $\underline{\mathsf{L}}^{\rm conf}_{\mathcal{F}_{\rm c}}\mathsf{R}_{\mathcal{F}_{\rm c}}(\underline{\Phi})$ minimizes the L^2-norm in this space under these constraints, we infer that $\underline{\mathsf{L}}^{\rm conf}_{\mathcal{F}_{\rm c}}\mathsf{R}_{\mathcal{F}_{\rm c}}(\underline{\Phi}) = \underline{\Phi}$.

(**R4**). Unisolvence is a straightforward consequence of (7.59) and (7.61). □

In what follows, we consider the cellwise constant reconstruction operator $\mathsf{L}_{\mathcal{C}}$ defined such that $\mathsf{L}_{\mathcal{C}}(\mathbf{s})|_{\rm c} := |\mathrm{c}|^{-1}\mathbf{s}_{\rm c}$ for all $\mathrm{c} \in \mathrm{C}$ and all $\mathbf{s} \in \mathcal{C}$ (cf. Remark 7.13).

Lemma 7.44 (Properties of $\underline{\mathsf{L}}^{\rm conf}_{\mathcal{F}}$)**.** *Under the assumptions of Lemma 7.43, the global conforming flux reconstruction operator* $\underline{\mathsf{L}}^{\rm conf}_{\mathcal{F}}$ *assembled cellwise from* $\underline{\mathsf{L}}^{\rm conf}_{\mathcal{F}_{\rm c}}$ *following the relation* (7.15) *satisfies the following properties:*

(i) (Conformity) $\underline{\mathsf{L}}^{\rm conf}_{\mathcal{F}} : \mathcal{F} \to H(\mathrm{div};\Omega)$*;*

(ii) (Unisolvence) $\mathsf{R}_{\mathcal{F}}\underline{\mathsf{L}}^{\rm conf}_{\mathcal{F}} = \mathsf{Id}_{\mathcal{F}}$*;*

(iii) (Compatibility with div*)* $\mathrm{div}(\underline{\mathsf{L}}^{\rm conf}_{\mathcal{F}}(\boldsymbol{\phi})) = \mathsf{L}_{\mathcal{C}}(\mathsf{DIV}(\boldsymbol{\phi}))$ *for all* $\boldsymbol{\phi} \in \mathcal{F}$*;*

(iv) (Stability) There exists a real constant $\eta_{\mathcal{F},\rm conf} > 0$ *such that, for all* $\boldsymbol{\phi} \in \mathcal{F}$*,*

$$\eta_{\mathcal{F},\rm conf}\|\boldsymbol{\phi}\|^2_{2,\mathcal{F}} \le \|\underline{\mathsf{L}}^{\rm conf}_{\mathcal{F}}(\boldsymbol{\phi})\|^2_{L^2(\Omega)} \le \eta^{-1}_{\mathcal{F},\rm conf}\|\boldsymbol{\phi}\|^2_{2,\mathcal{F}}. \tag{7.62}$$

(v) (Dual consistency) $\underline{\mathsf{L}}_{\mathcal{F}}^{\mathrm{conf}}$ *and any global potential reconstruction operator* $\underline{\mathsf{L}}_{\mathcal{F}}$ *built from a local potential reconstruction operator satisfying* (**R3**) *have the same mean value. In particular, for any* $\boldsymbol{\phi} \in \mathcal{F}$*, the following identity holds:*

$$\int_\Omega \underline{\mathsf{L}}_{\mathcal{F}}^{\mathrm{conf}}(\boldsymbol{\phi}) = \sum_{\mathrm{f}\in\mathrm{F}} \boldsymbol{\phi}_{\mathrm{f}} \underline{\tilde{\mathrm{e}}}(\mathrm{f}) = \int_\Omega \mathsf{L}_{\mathcal{F}}(\boldsymbol{\phi}). \tag{7.63}$$

Proof. The conformity (i) of the reconstruction holds by construction. The unisolvence (ii) results from the property (**R4**) of $\underline{\mathsf{L}}_{\mathcal{F}_\mathrm{c}}^{\mathrm{conf}}$ in each cell $\mathrm{c} \in \mathrm{C}$ and the continuity of the normal component of the global reconstruction. The compatibility with div (iii) results from (7.61) and the prescribed value of $\operatorname{div} \underline{\ell}_{\mathrm{ef,c}}$. The stability (iv) results from Proposition 7.14. The dual consistency (v) results from the property (**R3**) of $\underline{\mathsf{L}}_{\mathcal{F}_\mathrm{c}}^{\mathrm{conf}}$ and $\underline{\mathsf{L}}_{\mathcal{F}_\mathrm{c}}$ in each cell $\mathrm{c} \in \mathrm{C}$. Indeed,

$$\int_\Omega \underline{\mathsf{L}}_{\mathcal{F}_\mathrm{c}}^{\mathrm{conf}}(\boldsymbol{\phi}) = \sum_{\mathrm{c}\in\mathrm{C}} \sum_{\mathrm{f}\in\mathrm{F}_\mathrm{c}} \boldsymbol{\phi}_{\mathrm{f}} \underline{\tilde{\mathrm{e}}}_{\mathrm{c}}(\mathrm{f}) = \sum_{\mathrm{f}\in\mathrm{F}} \boldsymbol{\phi}_{\mathrm{f}} \underline{\tilde{\mathrm{e}}}(\mathrm{f}),$$

and the same relations hold if $\underline{\mathsf{L}}_{\mathcal{F}_\mathrm{c}}^{\mathrm{conf}}$ is replaced by $\underline{\mathsf{L}}_{\mathcal{F}_\mathrm{c}}$. □

7.4 Discrete functional analysis

The following two discrete Poincaré inequalities are important tools for the analysis of CDO schemes (especially when applied to the Stokes equations; cf. Chapter 9). Similar discrete Poincaré inequalities have been derived by Arnold *et al.* (2010) in a conforming setting where the discrete functions belong to the functional spaces where the continuous Poincaré inequalities hold, *e.g.*, $H^1(\Omega)$, $H(\underline{\mathrm{curl}};\Omega)$, and so on. The difference is that the present inequalities are stated on the spaces of DoFs (and not on discrete functions) and, more importantly, that the orthogonality is stated using a discrete Hodge operator; even if this operator is devised from local reconstruction functions, the latter need not be conforming. Moreover, these inequalities hold on polyhedral meshes. To our knowledge, the following two discrete Poincaré inequalities are new results.

Suitable conforming reconstructions. The proof of the discrete Poincaré inequalities hinges on the existence of conforming reconstruction operators which are are polynomial-valued and such that

$$\mathsf{L}_{\mathcal{V}}^{\mathrm{conf}} : \mathcal{V} \to H^1(\Omega), \quad \underline{\mathsf{L}}_{\mathcal{E}}^{\mathrm{conf}} : \mathcal{E} \to H(\underline{\mathrm{curl}};\Omega), \quad \underline{\mathsf{L}}_{\mathcal{F}}^{\mathrm{conf}} : \mathcal{F} \to H(\mathrm{div};\Omega), \tag{7.64}$$

with right inverse properties

$$\mathsf{R}_{\mathcal{V}}\mathsf{L}_{\mathcal{V}}^{\mathrm{conf}} = \mathsf{Id}_{\mathcal{V}}, \quad \mathsf{R}_{\mathcal{E}}\mathsf{L}_{\mathcal{E}}^{\mathrm{conf}} = \mathsf{Id}_{\mathcal{E}}, \tag{7.65}$$

commuting properties with the differential operators

$$\underline{\mathrm{grad}}(\mathsf{L}_{\mathcal{V}}^{\mathrm{conf}}) = \underline{\mathsf{L}}_{\mathcal{E}}^{\mathrm{conf}}(\mathsf{GRAD}), \quad \underline{\mathrm{curl}}(\underline{\mathsf{L}}_{\mathcal{E}}^{\mathrm{conf}}) = \underline{\mathsf{L}}_{\mathcal{F}}^{\mathrm{conf}}(\mathsf{CURL}), \tag{7.66}$$

and having the following stability properties:

$$C_{\mathcal{V}}^{\flat}\|\mathbf{p}\|_{2,\mathcal{V}} \le \|\mathsf{L}_{\mathcal{V}}^{\mathrm{conf}}(\mathbf{p})\|_{L^2(\Omega)}, \quad \|\mathsf{L}_{\mathcal{E}}^{\mathrm{conf}}(\mathbf{u})\|_{L^2(\Omega)^3} \le C_{\mathcal{E}}^{\sharp}\|\mathbf{u}\|_{2,\mathcal{E}}, \quad \|\mathsf{L}_{\mathcal{F}}^{\mathrm{conf}}(\boldsymbol{\phi})\|_{L^2(\Omega)^3} \le C_{\mathcal{F}}^{\sharp}\|\boldsymbol{\phi}\|_{2,\mathcal{F}}. \tag{7.67}$$

One possibility is to use the reconstruction operators of Christiansen (2008), detailed in Section 7.3.2, hinging on local constrained minimization problems using Whitney FE on a simplicial submesh of each mesh cell.

7.4.1 Discrete Poincaré–Wirtinger inequality for GRAD

The discrete Hodge operator $\mathsf{H}_1^{\mathcal{V}\tilde{\mathcal{C}}}$ in Lemma 7.45 is diagonal with entries equal to $|\tilde{\mathrm{c}}(\mathrm{v})|$. $\mathbf{1} \in \mathcal{V}$ has all its entries equal to 1.

Lemma 7.45 (Discrete Poincaré–Wirtinger inequality)**.** *Assume that the mesh is of class* **(MR)**. *Then, there exists a constant $C_{\mathrm{P}}^{(0)}$ (independent of the mesh size, but dependent on mesh regularity and stability constants) such that, for all $\mathbf{p} \in \mathcal{V}$ verifying $[\![\mathbf{p}, \mathsf{H}_1^{\mathcal{V}\tilde{\mathcal{C}}}(\mathbf{1})]\!]_{\mathcal{V}\tilde{\mathcal{C}}} = 0$, the following inequality holds:*

$$\|\mathbf{p}\|_{2,\mathcal{V}} \le C_{\mathrm{P}}^{(0)} \|\mathsf{GRAD}(\mathbf{p})\|_{2,\mathcal{E}}. \tag{7.68}$$

Proof. Let $\mathbf{p} \in \mathcal{V}$ be such that $[\![\mathbf{p}, \mathsf{H}_1^{\mathcal{V}\tilde{\mathcal{C}}}(\mathbf{1})]\!]_{\mathcal{V}\tilde{\mathcal{C}}} = 0$. Set $z := \mathsf{L}_{\mathcal{V}}^{\mathrm{conf}}(\mathbf{p}) - \langle \mathsf{L}_{\mathcal{V}}^{\mathrm{conf}}(\mathbf{p}) \rangle_\Omega \in H^1(\Omega)$ where $\langle\cdot\rangle_\Omega$ denotes the mean-value in Ω. Owing to the continuous Poincaré–Wirtinger inequality,

$$\|z\|_{L^2(\Omega)} \le C_{\mathrm{P},\Omega}^{(0)} \|\underline{\mathrm{grad}}\, z\|_{L^2(\Omega)^3}.$$

Moreover, owing to the properties of $\mathsf{L}_{\mathcal{V}}^{\mathrm{conf}}$ and $\underline{\mathsf{L}}_{\mathcal{E}}^{\mathrm{conf}}$, we infer that

$$\|\underline{\mathrm{grad}}\, z\|_{L^2(\Omega)^3} = \|\underline{\mathrm{grad}}(\mathsf{L}_{\mathcal{V}}^{\mathrm{conf}}(\mathbf{p}))\|_{L^2(\Omega)^3} = \|\underline{\mathsf{L}}_{\mathcal{E}}^{\mathrm{conf}}(\mathsf{GRAD}(\mathbf{p}))\|_{L^2(\Omega)^3} \le C_{\mathcal{E}}^{\sharp} \|\mathsf{GRAD}(\mathbf{p})\|_{2,\mathcal{E}},$$

so that $\|z\|_{L^2(\Omega)} \le C_{\mathrm{P},\Omega}^{(0)} C_{\mathcal{E}}^{\sharp} \|\mathsf{GRAD}(\mathbf{p})\|_{2,\mathcal{E}}$. Furthermore, since $\mathbf{p} - \mathsf{R}_{\mathcal{V}}(z) = \langle \mathsf{L}_{\mathcal{V}}^{\mathrm{conf}}(\mathbf{p}) \rangle_\Omega \mathbf{1}$, we infer that

$$\|\mathbf{p}\|_{2,\mathcal{V}}^2 = [\![\mathbf{p}, \mathsf{H}_1^{\mathcal{V}\tilde{\mathcal{C}}}(\mathbf{p})]\!]_{\mathcal{V}\tilde{\mathcal{C}}} = [\![\mathbf{p}, \mathsf{H}_1^{\mathcal{V}\tilde{\mathcal{C}}}(\mathbf{p} - \mathsf{R}_{\mathcal{V}}(z))]\!]_{\mathcal{V}\tilde{\mathcal{C}}} + [\![\mathbf{p}, \mathsf{H}_1^{\mathcal{V}\tilde{\mathcal{C}}} \mathsf{R}_{\mathcal{V}}(z)]\!]_{\mathcal{V}\tilde{\mathcal{C}}} = [\![\mathbf{p}, \mathsf{H}_1^{\mathcal{V}\tilde{\mathcal{C}}} \mathsf{R}_{\mathcal{V}}(z)]\!]_{\mathcal{V}\tilde{\mathcal{C}}},$$

so that $\|\mathbf{p}\|_{2,\mathcal{V}} \le \|\mathsf{R}_{\mathcal{V}}(z)\|_{2,\mathcal{V}}$. Finally, since $\|\mathsf{R}_{\mathcal{V}}(z)\|_{2,\mathcal{V}} \le (C_{\mathcal{V}}^{\flat})^{-1} \|\mathsf{L}_{\mathcal{V}}^{\mathrm{conf}}(\mathsf{R}_{\mathcal{V}}(z))\|_{L^2(\Omega)}$ and $\mathsf{L}_{\mathcal{V}}^{\mathrm{conf}}(\mathsf{R}_{\mathcal{V}}(z)) = z$ (observe in particular that $\mathsf{R}_{\mathcal{V}}(1) = \mathbf{1}$ and $\mathsf{L}_{\mathcal{V}}^{\mathrm{conf}}(\mathbf{1}) = 1$), we infer (7.68) with $C_{\mathrm{P}}^{(0)} = C_{\mathrm{P},\Omega}^{(0)} C_{\mathcal{E}}^{\sharp} (C_{\mathcal{V}}^{\flat})^{-1}$. □

Remark 7.46 (DDFV schemes)**.** *Using a similar approach to that developed in Section 6.3, Bessemoulin-Chatard* et al. *(2014) have derived a discrete Poincaré–Wirtinger inequality in the context of DDFV schemes.*

7.4.2 Discrete Poincaré inequality for CURL

Lemma 7.47 (Discrete Poincaré inequality for the curl)**.** *Assume that Ω is simply connected and $\partial\Omega$ is connected. Assume that the mesh is of class* **(MR)**. *Let $\mathsf{H}_\alpha^{\mathcal{E}\tilde{\mathcal{F}}}$ satisfy a global stability property. Then, there exists a constant $C_{\mathrm{P}}^{(1)}$ (independent of the mesh size, but dependent on mesh regularity and stability constants) such that, for all $\mathbf{u} \in \mathcal{E}$ such that $[\![\mathbf{u}, \mathsf{H}_\alpha^{\mathcal{E}\tilde{\mathcal{F}}}(\mathbf{v})]\!]_{\mathcal{E}\tilde{\mathcal{F}}} = 0$ for all $\mathbf{v} \in \operatorname{Ker} \mathsf{CURL}$, the following inequality holds:*

$$\|\mathbf{u}\|_{2,\mathcal{E}} \le C_{\mathrm{P}}^{(1)} \|\mathsf{CURL}(\mathbf{u})\|_{2,\mathcal{F}}. \tag{7.69}$$

Proof. Let $\mathbf{u} \in \mathcal{E}$ be such that $[\![\mathbf{u}, \mathsf{H}_\alpha^{\mathcal{E}\tilde{\mathcal{F}}}(\mathbf{v})]\!]_{\mathcal{E}\tilde{\mathcal{F}}} = 0$ for all $\mathbf{v} \in \operatorname{Ker} \mathsf{CURL}$. There is $\underline{z} \in H(\underline{\mathrm{curl}}; \Omega)$ such that

$$\begin{cases} \underline{\mathrm{curl}}(\underline{z}) = \underline{\mathrm{curl}}(\underline{\mathsf{L}}_{\mathcal{E}}^{\mathrm{conf}}(\mathbf{u})), & \text{in } \Omega, \\ \mathrm{div}(\underline{z}) = 0, & \text{in } \Omega, \end{cases}$$

and $\underline{z} \cdot \underline{\nu}_{\partial\Omega} = 0$. Since Ω is simply connected and $\partial\Omega$ is connected, for all $\underline{v} \in \operatorname{Ker}(\underline{\mathrm{curl}})$, there is $\vartheta \in H^1(\Omega)$ such that $\underline{v} = \underline{\mathrm{grad}}(\vartheta)$ so that

$$\int_\Omega \underline{z} \cdot \underline{v} = \int_\Omega \mathrm{div}(\underline{z}) \vartheta + \int_{\partial\Omega} (\underline{z} \cdot \underline{\nu}_{\partial\Omega}) \vartheta = 0.$$

Owing to the continuous Poincaré inequality for the curl,

$$\|\underline{z}\|_{L^2(\Omega)^3} \le C_{\mathrm{P},\Omega}^{(1)} \|\underline{\mathrm{curl}}(\underline{z})\|_{L^2(\Omega)^3}.$$

Moreover, owing to (Amrouche *et al.*, 1998, Prop. 3.7), there is $s > \frac{1}{2}$ such that

$$\|\underline{z}\|_{H^s(\Omega)^3} \le C_{H^s} C^{(1)}_{\mathrm{P},\Omega} \|\underline{\mathrm{curl}}(\underline{z})\|_{L^2(\Omega)^3}.$$

This bound implies that $\underline{z}$ is in the domain of the Nédélec FE interpolation operator on the simplicial submesh, so that, using **(MR)**, the proof of Proposition 4.6 in the above reference, and the fact that $\underline{\mathrm{curl}}(\underline{z})$ is polynomial-valued, we infer that

$$\|\mathsf{R}_{\mathcal{E}}(\underline{z})\|_{2,\mathcal{E}} \le C_{\mathrm{N}} C_{H^s} C^{(1)}_{\mathrm{P},\Omega} \|\underline{\mathrm{curl}}(\underline{z})\|_{L^2(\Omega)^3}. \tag{7.70}$$

Furthermore, we observe that

$$[\![\mathbf{u}, \mathsf{H}^{\mathcal{E}\tilde{\mathcal{F}}}_{\alpha}(\mathbf{u})]\!]_{\mathcal{E}\tilde{\mathcal{F}}} = [\![\mathbf{u}, \mathsf{H}^{\mathcal{E}\tilde{\mathcal{F}}}_{\alpha}(\mathbf{u} - \mathsf{R}_{\mathcal{E}}(\underline{z}))]\!]_{\mathcal{E}\tilde{\mathcal{F}}} + [\![\mathbf{u}, \mathsf{H}^{\mathcal{E}\tilde{\mathcal{F}}}_{\alpha}(\mathsf{R}_{\mathcal{E}}(\underline{z}))]\!]_{\mathcal{E}\tilde{\mathcal{F}}} = [\![\mathbf{u}, \mathsf{H}^{\mathcal{E}\tilde{\mathcal{F}}}_{\alpha}(\mathsf{R}_{\mathcal{E}}(\underline{z}))]\!]_{\mathcal{E}\tilde{\mathcal{F}}},$$

since $\mathsf{CURL}(\mathbf{u} - \mathsf{R}_{\mathcal{E}}(\underline{z})) = \mathsf{CURL}(\mathsf{R}_{\mathcal{E}}(\underline{\mathrm{L}}^{\mathrm{conf}}_{\mathcal{E}}(\mathbf{u}) - \underline{z})) = \mathsf{R}_{\mathcal{F}}(\underline{\mathrm{curl}}(\underline{\mathrm{L}}^{\mathrm{conf}}_{\mathcal{E}}(\mathbf{u}) - \underline{z})) = 0$. Hence, $[\![\mathbf{u}]\!]_{\alpha} \le [\![\mathsf{R}_{\mathcal{E}}(\underline{z})]\!]_{\alpha}$, and owing to the global stability of $\mathsf{H}^{\mathcal{E}\tilde{\mathcal{F}}}_{\alpha}$ and (7.70), we infer that

$$\eta_{\alpha} [\![\mathbf{u}]\!]_{2,\mathcal{E}} \le C_{\mathrm{N}} C_{H^s} C^{(1)}_{\mathrm{P},\Omega} \|\underline{\mathrm{curl}}(\underline{\mathrm{L}}^{\mathrm{conf}}_{\mathcal{E}}(\mathbf{u}))\|_{L^2(\Omega)^3}.$$

Observing that $\underline{\mathrm{curl}}(\underline{z}) = \underline{\mathrm{curl}}(\underline{\mathrm{L}}^{\mathrm{conf}}_{\mathcal{E}}(\mathbf{u})) = \underline{\mathrm{L}}^{\mathrm{conf}}_{\mathcal{F}}(\mathsf{CURL}(\mathbf{u}))$ and using the stability of $\underline{\mathrm{L}}^{\mathrm{conf}}_{\mathcal{F}}$, we infer (7.69) with $C^{(1)}_{\mathrm{P}} = \eta_{\alpha}^{-1} C_{\mathrm{N}} C_{H^s} C^{(1)}_{\mathrm{P},\Omega} C^{\sharp}_{\mathcal{F}}$. □

Remark 7.48 (Connectedness)**.** *The assumption related to the connectedness of the domain Ω avoids to enter into the technicalities necessary to handle the case of harmonic forms.*

Part III

Applications

Chapter 8

Elliptic equations

Contents

This chapter is devoted to the analysis of the vertex- and cell-based CDO schemes for elliptic equations presented in Section 4.1. Two levels of analysis are considered for the two families of CDO schemes, depending on the positioning of the DoFs associated to the potential (vertex-based and cell-based). Stability, convergence, and *a priori* error estimates are established. The first level of analysis hinges on the theoretical results derived in Chapter 6 based on an algebraic representation of the discrete Hodge operator (Sections 8.1.1 and 8.2.1 for vertex-based and cell-based schemes respectively). The main result is an energy error estimate with first-order convergence rate for smooth enough solutions. The second level of analysis hinges on the theoretical results derived in Chapter 7 using reconstruction operators for defining the discrete Hodge operator (Sections 8.1.2 and 8.2.2 for vertex-based and cell-based schemes respectively). In this case, an optimal L^2-error estimate is proved for the potential for smooth solutions in addition to energy error estimate. Moreover, links with related compatible discretizations are drawn for both families of CDO schemes. In Section 8.3, the hybridization of CDO cell-based schemes is detailed. This is an important aspect of cell-based schemes to enhance their computational efficiency. To conclude this chapter, the results of three test cases run on polyhedral meshes are presented in Section 8.4, and a comparative study of the computational effectiveness of CDO schemes is carried out.

8.1 Vertex-based schemes

The starting point is the elliptic problem (4.1) in primal formulation

$$-\operatorname{div}(\underline{\underline{\kappa}}\,\underline{\operatorname{grad}}(p)) = s, \qquad \text{in } \Omega, \tag{8.1}$$

which is detailed in Section 4.1.1.

Boundary conditions. We consider the elliptic equation (8.1) with homogeneous Dirichlet BCs. Nonhomogeneous Dirichlet/Neumann BCs can be considered as well (cf. the EDF R&D technical report (Ra) mentioned in Chapter 1). To take into account the homogeneous Dirichlet BCs, we introduce the DoFs spaces

$$\mathcal{V}_0 := \{\mathbf{p} \in \mathcal{V} \,|\, \mathbf{p}_\mathrm{v} = 0,\ \forall \mathrm{v} \in \mathrm{V}^\mathrm{B}\} \qquad \text{and} \qquad \mathcal{E}_0 := \{\mathbf{g} \in \mathcal{E} \,|\, \mathbf{g}_\mathrm{e} = 0,\ \forall \mathrm{e} \in \mathrm{E}^\mathrm{B}\}. \tag{8.2}$$

$\mathcal{V}_0$ has dimension $\#\mathrm{V}^\mathrm{I}$ (the number of interior vertices) and $\mathcal{E}_0$ has dimension $\#\mathrm{E}^\mathrm{I}$ (the number of interior edges). The space of DoFs in duality with $\mathcal{V}_0$ is denoted by $\widetilde{\mathcal{C}}_0$. It collects values for all dual cells associated to a vertex $\mathrm{v} \in \mathrm{V}^\mathrm{I}$. The space of DoFs in duality with $\mathcal{E}_0$ is denoted by $\widetilde{\mathcal{F}}_0$. It collects values for all dual faces associated to an edge $\mathrm{e} \in \mathrm{E}^\mathrm{I}$. Thus, the related discrete gradient becomes $\mathsf{GRAD}_0 : \mathcal{V}_0 \to \mathcal{E}_0$ and the discrete divergence $\widetilde{\mathsf{DIV}}_0 : \widetilde{\mathcal{F}}_0 \to \widetilde{\mathcal{C}}_0$. For simplicity, we keep the previous notation for the DoFs spaces (*i.e.* $\mathcal{V}$, $\mathcal{E}$, $\widetilde{\mathcal{F}}$, and $\widetilde{\mathcal{C}}$) and for the discrete differential operators (*i.e.* GRAD and $\widetilde{\mathsf{DIV}}$) since the properties of these operators remain the same.

8.1.1 Analysis from an algebraic viewpoint

Discrete systems. In this section, we focus on the discrete system (4.5) that we recall for the sake of completeness: Find $\mathbf{p} \in \mathcal{V}$ such that

$$-\widetilde{\mathsf{DIV}} \cdot \mathsf{H}_\kappa^{\mathcal{E}\widetilde{\mathcal{F}}} \cdot \mathsf{GRAD}(\mathbf{p}) = \mathsf{R}_{\widetilde{\mathcal{C}}}(s). \tag{8.3}$$

Owing to the adjunction property (Proposition 3.16), the discrete variational formulation takes the form: Find $\mathbf{p} \in \mathcal{V}$ such that

$$[\![\mathsf{GRAD}(\mathbf{p}), \mathsf{H}_\kappa^{\mathcal{E}\widetilde{\mathcal{F}}} \cdot \mathsf{GRAD}(\mathbf{q})]\!]_{\mathcal{E}\widetilde{\mathcal{F}}} = [\![\mathbf{q}, \mathsf{R}_{\widetilde{\mathcal{C}}}(s)]\!]_{\mathcal{V}\widetilde{\mathcal{C}}}, \qquad \forall \mathbf{q} \in \mathcal{V}. \tag{8.4}$$

We recall that we neglect quadrature errors on the source term s. We assume that the local discrete Hodge operator satisfies the three properties (**H0**), (**H1**), and (**H2**) stated in Section 6.2.1, which we recall in the specific case of $\mathsf{H}_\kappa^{\mathcal{E}_\mathrm{c}\widetilde{\mathcal{F}}_\mathrm{c}}$.

(**H0**) [Symmetry] $\mathsf{H}_\kappa^{\mathcal{E}_\mathrm{c}\widetilde{\mathcal{F}}_\mathrm{c}}$ is symmetric.

(**H1**) [Local stability] There exists $\eta_\kappa > 0$ such that, for all $\mathrm{c} \in \mathrm{C}$,

$$\eta_\kappa \kappa_{\flat,\mathrm{c}} \|\mathbf{g}\|_{2,\mathcal{E}_\mathrm{c}}^2 \le [\![\mathbf{g}, \mathsf{H}_\kappa^{\mathcal{E}_\mathrm{c}\widetilde{\mathcal{F}}_\mathrm{c}}(\mathbf{g})]\!]_{\mathcal{E}_\mathrm{c}\widetilde{\mathcal{F}}_\mathrm{c}} \le \eta_\kappa^{-1} \kappa_{\sharp,\mathrm{c}} \|\mathbf{g}\|_{2,\mathcal{E}_\mathrm{c}}^2, \qquad \forall \mathbf{g} \in \mathcal{E}_\mathrm{c}. \tag{8.5}$$

(**H2**) [Local $\mathbb{P}_0$-consistency] The local commuting operator

$$\lfloor \kappa,\, \varepsilon_\mathrm{c}\widetilde{\mathcal{F}}_\mathrm{c} \rceil(\bullet) := \mathsf{H}_\kappa^{\mathcal{E}_\mathrm{c}\widetilde{\mathcal{F}}_\mathrm{c}} \cdot \mathsf{R}_{\mathcal{E}_\mathrm{c}}(\bullet) - \mathsf{R}_{\widetilde{\mathcal{F}}_\mathrm{c}}(\underline{\underline{\kappa}}\,\bullet) \tag{8.6}$$

satisfies $\lfloor \kappa,\, \varepsilon_\mathrm{c}\widetilde{\mathcal{F}}_\mathrm{c} \rceil(\underline{K}) = 0$ for any vector field $\underline{K}$ which is constant in $\mathrm{c} \in \mathrm{C}$.

Following the rationale detailed in Section 6.1.2, the discrete Hodge operator $\mathsf{H}_\kappa^{\mathcal{E}_\mathrm{c}\widetilde{\mathcal{F}}_\mathrm{c}}$ induces for each cell $\mathrm{c} \in \mathrm{C}$, the following local discrete norms:

$$\|\mathbf{g}\|_{\kappa,\mathrm{c}}^2 := [\![\mathbf{g}, \mathsf{H}_\kappa^{\mathcal{E}_\mathrm{c}\widetilde{\mathcal{F}}_\mathrm{c}}(\mathbf{g})]\!]_{\mathcal{E}_\mathrm{c}\widetilde{\mathcal{F}}_\mathrm{c}} \qquad \text{and} \qquad \|\boldsymbol{\phi}\|_{\kappa^{-1},\mathrm{c}}^2 := [\![(\mathsf{H}_\kappa^{\mathcal{E}_\mathrm{c}\widetilde{\mathcal{F}}_\mathrm{c}})^{-1}(\boldsymbol{\phi}), \boldsymbol{\phi}]\!]_{\mathcal{E}_\mathrm{c}\widetilde{\mathcal{F}}_\mathrm{c}}, \tag{8.7}$$

and the global discrete norms:

$$\|\mathbf{g}\|_\kappa^2 := [\![\mathbf{g}, \mathsf{H}_\kappa^{\mathcal{E}\widetilde{\mathcal{F}}}(\mathbf{g})]\!]_{\mathcal{E}\widetilde{\mathcal{F}}} \qquad \text{and} \qquad \|\boldsymbol{\phi}\|_{\kappa^{-1}}^2 := [\![(\mathsf{H}_\kappa^{\mathcal{E}\widetilde{\mathcal{F}}})^{-1}(\boldsymbol{\phi}), \boldsymbol{\phi}]\!]_{\mathcal{E}\widetilde{\mathcal{F}}}. \tag{8.8}$$

Owing to the Cauchy–Schwarz inequality (6.14), we infer that

$$[\![\mathbf{g}, \boldsymbol{\phi}]\!]_{\mathcal{E}\widetilde{\mathcal{F}}} \le \|\mathbf{g}\|_\kappa \, \|\boldsymbol{\phi}\|_{\kappa^{-1}}. \tag{8.9}$$

Stability. The global stability property (6.21) of the discrete Hodge operator $\mathsf{H}_\kappa^{\mathcal{E}\widetilde{\mathcal{F}}}$, stemming from (**H1**) and (3.20), takes the form:

$$\eta_\kappa \kappa_\flat \|\mathbf{g}\|_{2,\mathcal{E}}^2 \le \|\mathbf{g}\|_\kappa^2 \le \eta_\kappa^{-1} \kappa_\sharp \|\mathbf{g}\|_{2,\mathcal{E}}^2, \qquad \forall \mathbf{g} \in \mathcal{E}, \tag{8.10}$$

where $\kappa_\flat := \min_{\mathrm{c}\in\mathrm{C}} \kappa_{\flat,\mathrm{c}}$ and $\kappa_\sharp := \max_{\mathrm{c}\in\mathrm{C}} \kappa_{\sharp,\mathrm{c}}$. A consequence of the discrete Poincaré inequality (6.34) is the following stability of the vertex-based scheme.

Lemma 8.1 (Discrete stability)**.** *Assume the mesh regularity property* (6.7)*. Let* $\mathbf{p} \in \mathcal{V}$ *solve* (8.3)*. Then, the following inequality holds with* $C = (\eta_\kappa \kappa_\flat)^{-1} C_{\mathrm{P}}^{(0)}$*:*

$$\|\mathsf{GRAD}(\mathbf{p})\|_{2,\mathcal{E}} \le C \|s\|_{L^2(\Omega)}, \tag{8.11}$$

where $C_{\mathrm{P}}^{(0)}$ *stems from the discrete Poincaré inequality* (6.34)*.*

Proof. Since $\mathbf{p} \in \mathcal{V}$ solves (8.3), setting $\boldsymbol{\phi} = -\mathsf{H}_\kappa^{\mathcal{E}\widetilde{\mathcal{F}}} \cdot \mathsf{GRAD}(\mathbf{p})$, the identity $\widetilde{\mathsf{DIV}}(\boldsymbol{\phi}) = \mathsf{R}_{\widetilde{\mathcal{C}}}(s)$ holds. Hence, using the adjunction property of Proposition 3.16 and the lower bound in (8.10), we infer that

$$\begin{aligned}\llbracket \mathbf{p}, \mathsf{R}_{\widetilde{\mathcal{C}}}(s) \rrbracket_{\mathcal{V}\widetilde{\mathcal{C}}} &= \llbracket \mathbf{p}, \widetilde{\mathsf{DIV}}(\boldsymbol{\phi}) \rrbracket_{\mathcal{V}\widetilde{\mathcal{C}}} = \llbracket \mathsf{GRAD}(\mathbf{p}), \mathsf{H}_\kappa^{\mathcal{E}\widetilde{\mathcal{F}}} \mathsf{GRAD}(\mathbf{p}) \rrbracket_{\mathcal{E}\widetilde{\mathcal{F}}} \\ &= \|\mathsf{GRAD}(\mathbf{p})\|_\kappa^2 \ge \eta_\kappa \kappa_\flat \|\mathsf{GRAD}(\mathbf{p})\|_{2,\mathcal{E}}^2.\end{aligned}$$

Moreover, using two times the Cauchy–Schwarz inequality yields

$$\llbracket \mathbf{p}, \mathsf{R}_{\widetilde{\mathcal{C}}}(s) \rrbracket_{\mathcal{V}\widetilde{\mathcal{C}}} \le \|\mathbf{p}\|_{2,\mathcal{V}} \left(\sum_{\mathrm{v}\in\mathrm{V}} |\tilde{\mathrm{c}}(\mathrm{v})|^{-1} \left(\int_{\tilde{\mathrm{c}}(\mathrm{v})} s \right)^2 \right)^{1/2} \le \|\mathbf{p}\|_{2,\mathcal{V}} \|s\|_{L^2(\Omega)}.$$

We conclude using the discrete Poincaré inequality (6.34). □

Consistency error. The diagram in Figure 8.1 shows that the exact problem (8.1) and the discrete scheme (8.3) are linked through the de Rham maps. Owing to Propositions 3.13 and 3.18, the diagrams D_1 and D_3 are commutative (for D_3, recall that we only consider interior dual mesh entities here), but this is (in general) not the case for D_2. This lack of commutation produces a consistency error. This fact has been recognized in the seminal work of (Bossavit, 2000, no 3) and Hiptmair (2001a); see also Codecasa & Trevisan (2010a).

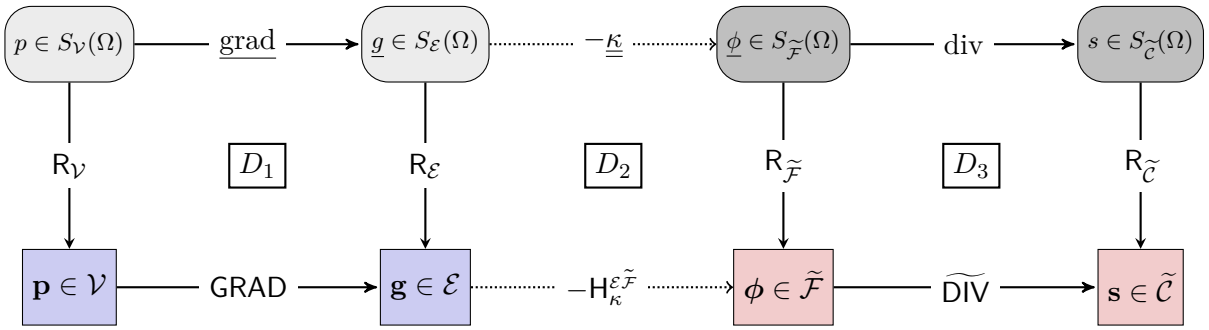

Figure 8.1 – Diagram depicting the links between the exact problem (8.1) and the vertex-based scheme (8.3).

Lemma 8.2 (Basic error bound)**.** *Let* $\mathbf{g}$ *be the discrete gradient and* $\boldsymbol{\phi}$ *the discrete flux resulting from* (8.3)*. Let* $\underline{g}$ *be the exact gradient and* $\underline{\phi}$ *the exact flux. Assume that* $\underline{g}$*,* $\underline{\phi} \in H^s(\Omega)^3$ *with* $s > \frac{1}{2}$*. Then, the following inequality holds:*

$$\max(\|\mathsf{R}_{\mathcal{E}}(\underline{g}) - \mathbf{g}\|_\kappa, \|\mathsf{R}_{\widetilde{\mathcal{F}}}(\underline{\phi}) - \boldsymbol{\phi}\|_{\kappa^{-1}}) \le \|\lfloor \kappa, \varepsilon^{\widetilde{\mathcal{F}}} \rceil(\underline{g})\|_{\kappa^{-1}}, \tag{8.12}$$

where the global commuting operator for diagram D_2 of Figure 4.1 is defined from (6.26) *as follows:*

$$\lfloor \kappa,\, \varepsilon^{\widetilde{\mathcal{F}}} \rceil(\underline{g}) := \mathsf{H}_\kappa^{\varepsilon^{\widetilde{\mathcal{F}}}} \cdot \mathsf{R}_{\mathcal{E}}(\underline{g}) - \mathsf{R}_{\widetilde{\mathcal{F}}}(\kappa\, \underline{g}). \tag{8.13}$$

Proof. For completeness, we sketch the proof. We preliminarily observe that the regularity assumption on $\underline{\phi}$ and $\underline{g}$ entails that $\underline{\phi} \in S_{\widetilde{\mathcal{F}}}(\Omega)$ and $\underline{g} \in S_{\mathcal{E}}(\Omega)$ since $\underline{g}$ is curl-free (cf. Definition 3.5 and Remark 3.6). Therefore, $\mathsf{R}_{\mathcal{E}}(\underline{g})$, $\mathsf{R}_{\widetilde{\mathcal{F}}}(\underline{\phi})$, and the global commuting operator (8.13) are well-defined. Owing to the commuting properties of Propositions 3.13 and 3.18,

$$\begin{aligned}
\mathsf{R}_{\mathcal{E}}(\underline{g}) - \mathbf{g} &= \mathsf{GRAD}(\mathsf{R}_{\mathcal{V}}(p)) - \mathsf{GRAD}(\mathbf{p}) = \mathsf{GRAD}(\mathsf{R}_{\mathcal{V}}(p) - \mathbf{p}),\\
\widetilde{\mathsf{DIV}}(\mathsf{R}_{\widetilde{\mathcal{F}}}(\underline{\phi}) - \boldsymbol{\phi}) &= \mathsf{R}_{\widetilde{\mathcal{C}}}(\operatorname{div} \underline{\phi}) - \mathsf{R}_{\widetilde{\mathcal{C}}}(s) = 0.
\end{aligned}$$

The adjunction of gradient and divergence of Proposition 3.16 then yields

$$[\![\mathsf{R}_{\mathcal{E}}(\underline{g}) - \mathbf{g}, \mathsf{R}_{\widetilde{\mathcal{F}}}(\underline{\phi}) - \boldsymbol{\phi}]\!]_{\varepsilon^{\widetilde{\mathcal{F}}}} = 0. \tag{8.14}$$

Moreover, a direct calculation shows that

$$\mathsf{R}_{\widetilde{\mathcal{F}}}(\underline{\phi}) - \boldsymbol{\phi} = -\mathsf{R}_{\widetilde{\mathcal{F}}}(\underline{\kappa}\, \underline{g}) + \mathsf{H}_\kappa^{\varepsilon^{\widetilde{\mathcal{F}}}}(\mathbf{g}) = \lfloor \kappa,\, \varepsilon^{\widetilde{\mathcal{F}}} \rceil(\underline{g}) - \mathsf{H}_\kappa^{\varepsilon^{\widetilde{\mathcal{F}}}}(\mathsf{R}_{\mathcal{E}}(\underline{g}) - \mathbf{g}). \tag{8.15}$$

Applying the discrete duality product $[\![\mathsf{R}_{\mathcal{E}}(\underline{g}) - \mathbf{g}, \cdot]\!]_{\varepsilon^{\widetilde{\mathcal{F}}}}$ to (8.15), using the definition of the discrete norm $|\!|\!|\cdot|\!|\!|_\kappa$ and (8.14), we obtain

$$|\!|\!|\mathsf{R}_{\mathcal{E}}(\underline{g}) - \mathbf{g}|\!|\!|_\kappa^2 = [\![\mathsf{R}_{\mathcal{E}}(\underline{g}) - \mathbf{g}, \lfloor \kappa,\, \varepsilon^{\widetilde{\mathcal{F}}} \rceil(\underline{g})]\!]_{\varepsilon^{\widetilde{\mathcal{F}}}}.$$

Using the Cauchy–Schwarz inequality (8.9) yields the bound on the discrete energy error. The other bound is obtained similarly. □

Recall that the discrete Hodge operator is built in the CDO framework by a cellwise assembly process (cf. Section 3.4) of local discrete Hodge operators attached to primal cells. Using the local $\mathbb{P}_0$-consistency property of these local discrete Hodge operators transforms the result of Lemma 8.2 into the following error bound.

Lemma 8.3 (Tighter error bound)**.** *Let $[\mathbb{P}_0(\mathrm{C})]^3$ be spanned by piecewise constant functions on the primal mesh. Assume that $\underline{g}$, $\underline{\phi} \in H^s(\Omega)^3$ with $s > \frac{1}{2}$. Then, the following inequality holds:*

$$\max(|\!|\!|\mathsf{R}_{\mathcal{E}}(\underline{g}) - \mathbf{g}|\!|\!|_\kappa, |\!|\!|\mathsf{R}_{\widetilde{\mathcal{F}}}(\underline{\phi}) - \boldsymbol{\phi}|\!|\!|_{\kappa^{-1}}) \le \inf_{\underline{G} \in [\mathbb{P}_0(\mathrm{C})]^3} \left\{ \sum_{\mathrm{c} \in \mathrm{C}} |\!|\!| \lfloor \kappa,\, \varepsilon_{\mathrm{c}} \tilde{\mathcal{F}}_{\mathrm{c}} \rceil((\underline{g} - \underline{G})|_{\mathrm{c}}) |\!|\!|_{\kappa^{-1},\mathrm{c}}^2 \right\}^{\frac{1}{2}}, \tag{8.16}$$

with the local norm $|\!|\!|\boldsymbol{\phi}|\!|\!|_{\kappa^{-1},\mathrm{c}}^2$ defined in (8.7)*.*

Proof. Owing to the algebraic result of Lemma 6.13, the following inequality holds:

$$|\!|\!| \lfloor \kappa,\, \varepsilon^{\widetilde{\mathcal{F}}} \rceil(\underline{g}) |\!|\!|_{\kappa^{-1}}^2 \le \sum_{\mathrm{c} \in \mathrm{C}} |\!|\!| \lfloor \kappa,\, \varepsilon_{\mathrm{c}} \tilde{\mathcal{F}}_{\mathrm{c}} \rceil(\underline{g}|_{\mathrm{c}}) |\!|\!|_{\kappa^{-1},\mathrm{c}}^2.$$

We conclude using the result of Lemma 8.2 together with (**H2**) for the local discrete Hodge operator $\mathsf{H}_\kappa^{\varepsilon_{\mathrm{c}} \tilde{\mathcal{F}}_{\mathrm{c}}}$ in each cell $\mathrm{c} \in \mathrm{C}$. □

Remark 8.4 (Exact solution for piecewise affine functions)**.** *Whenever the exact solution turns out to be piecewise affine on the primal mesh, it is clear from* (8.16) *that the solution of the scheme is the image by the de Rham map of the exact solution. Indeed, since $\underline{g} \in [\mathbb{P}_0(\mathrm{C})]^3$, the infimum in* (8.16) *is zero so that $\mathbf{g} = \mathsf{R}_{\mathcal{E}}(\underline{g})$ and $\boldsymbol{\phi} = \mathsf{R}_{\widetilde{\mathcal{F}}}(\underline{\phi})$; moreover, owing to the Poincaré inequality* (6.34)*, $\mathbf{p} = \mathsf{R}_{\mathcal{V}}(p)$. This property can be used by practitioners to verify the scheme on coarse meshes (see, e.g. Eymard* et al.*, 2012, p. 277).*

Convergence rate for smooth solutions. We now derive from the result of Lemma 8.3 a first-order convergence result for the discrete energy and complementary energy errors in the case of smooth solutions.

Definition 8.5 (Energy norms)**.** *For all $\underline{g} \in L^2(\Omega)^3$, we define the so-called energy norm and for all $\underline{\phi} \in L^2(\Omega)^3$, the complementary energy norm as follows:*

$$\|\underline{g}\|_\kappa^2 := \int_\Omega \underline{g} \cdot \underline{\underline{\kappa}}\, \underline{g} \qquad \text{and} \qquad \|\underline{\phi}\|_{\kappa^{-1}}^2 := \int_\Omega \underline{\phi} \cdot \underline{\underline{\kappa}}^{-1} \underline{\phi}. \tag{8.17}$$

For all $\mathbf{g} \in \mathcal{E}$ and all $\boldsymbol{\phi} \in \widetilde{\mathcal{F}}$, the discrete counterparts of (8.17) are $\|\mathbf{g}\|_\kappa$ and $\|\boldsymbol{\phi}\|_{\kappa^{-1}}$ respectively, defined in (8.8).

Theorem 8.6 (Convergence rate for smooth solutions)**.** *Let h denote the maximal diameter of primal cells. Let $\mathbf{g}$ be the discrete gradient and $\boldsymbol{\phi}$ the discrete flux resulting from* (8.3)*. Let $\underline{g}$ be the exact gradient and $\underline{\phi}$ the exact flux. Assume that $\underline{g}, \underline{\phi} \in [H^1(\mathrm{C})]^3$. Assume that the sequence of meshes is of class* **(MR)***. Then, the following inequality holds:*

$$\|\lfloor \kappa,\, \varepsilon^{\widetilde{\mathcal{F}}} \rceil(\underline{g})\|_{\kappa^{-1}} \lesssim h \left(\kappa_\sharp^{1/2} \|\underline{g}\|_{[H^1(\mathrm{C})]^3} + \kappa_\flat^{-1/2} \|\underline{\phi}\|_{[H^1(\mathrm{C})]^3} \right). \tag{8.18}$$

Moreover, assuming that $\underline{g}$, $\underline{\phi} \in H^s(\Omega)^3$ with $s > \frac{1}{2}$, then,

$$\max(\|\mathsf{R}_{\mathcal{E}}(\underline{g}) - \mathbf{g}\|_\kappa, \|\mathsf{R}_{\widetilde{\mathcal{F}}}(\underline{\phi}) - \boldsymbol{\phi}\|_{\kappa^{-1}}) \lesssim h \left(\kappa_\sharp^{1/2} \|\underline{g}\|_{[H^1(\mathrm{C})]^3} + \kappa_\flat^{-1/2} \|\underline{\phi}\|_{[H^1(\mathrm{C})]^3} \right). \tag{8.19}$$

Proof. First, observe that $\underline{g} \in S_{\mathcal{E}}(\mathrm{C})$ and $\underline{\phi} \in S_{\widetilde{\mathcal{F}}}(\mathrm{C})$ since $\underline{g}, \underline{\phi} \in [H^1(\mathrm{C})]^3$. Thus, applying Lemma 6.14 with $\underline{b} = \underline{g}$ and $\underline{\underline{\alpha}} = \underline{\underline{\kappa}}$ to the bound (8.12) yields the error estimate (8.18). The second inequality readily results from (8.18) and Lemma 8.2. □

Remark 8.7 (Regularity requirements)**.** *In order to ensure that $\mathsf{R}_{\mathcal{E}}(\underline{g})$ and $\mathsf{R}_{\widetilde{\mathcal{F}}}(\underline{\phi})$ are well-defined, we additionally assume in Theorem 8.6 that $\underline{g}$ and $\underline{\phi} \in H^s(\Omega)^3$ with $s > \frac{1}{2}$. In fact, only the assumption $\underline{g} \in H^s(\Omega)^3$ with $s > \frac{1}{2}$ is needed since $\underline{\phi} \in [H^1(\mathrm{C})]^3 \subset S_{\widetilde{\mathcal{F}}}(\Omega)$ (cf. Remark 6.11).*

Remark 8.8 (Estimate on the potential)**.** *Using the discrete Poincaré inequality* (6.35)*, the lower bound in* (8.10)*, and the commuting property of Proposition 3.13, we infer that*

$$\begin{aligned}(C_{\mathrm{P}}^{(0)})^{-1} \|\mathsf{R}_{\mathcal{V}}(p) - \mathbf{p}\|_{2,\mathcal{V}} &\le \|\mathsf{GRAD}(\mathsf{R}_{\mathcal{V}}(p) - \mathbf{p})\|_{2,\mathcal{E}} \\ &\le (\eta_\kappa \kappa_\flat)^{-1/2} \|\mathsf{GRAD}(\mathsf{R}_{\mathcal{V}}(p) - \mathbf{p})\|_\kappa = (\eta_\kappa \kappa_\flat)^{-1/2} \|\mathsf{R}_{\mathcal{E}}(\underline{g}) - \mathbf{g}\|_\kappa.\end{aligned}$$

Hence, the right-hand side of (8.19) *also bounds $(\eta_\kappa \kappa_\flat)^{1/2} (C_{\mathrm{P}}^{(0)})^{-1} \|\mathsf{R}_{\mathcal{V}}(p) - \mathbf{p}\|_{2,\mathcal{V}}$.*

Remark 8.9 (First-order error estimate in energy norm)**.** *A similar error estimate has been derived recently by Codecasa & Trevisan (2010a) under the stronger, piecewise Lipschitz assumption on the exact gradient and flux.*

Remark 8.10 (Verifying the regularity assumption)**.** *The regularity assumption $\underline{g}, \underline{\phi} \in [H^1(\mathrm{C})]^3$ is satisfied if, for instance, the exact potential sits in $H^2(\Omega)$ and, more generally, if the potential is in $S_{\mathcal{V}}(\Omega)$ and is piecewise H^2 on a partition of Ω to which the primal mesh is conforming.*

8.1.2 Analysis using reconstruction operators

In this section, we assume that the primal mesh is of class **(MB)** (*i.e.* one can define a barycentric subdivision) and that primal faces are planar. This section relies on the existence of suitable local gradient reconstruction operators in each cell $\mathrm{c} \in \mathrm{C}$ which are introduced in Chapter 7. We only require that the local gradient reconstruction operator $\underline{\mathsf{L}}_{\mathcal{E}_\mathrm{c}} : \mathcal{E}_\mathrm{c} \to P_{\mathcal{E}}(\mathrm{c})$ satisfies the three properties (**R1**), (**R2**), and (**R3**) so that the algebraic analysis of the previous

section holds (cf. Proposition 7.3). Functions in $P_{\mathcal{E}}(\mathrm{c}) \subset [L^2(\mathrm{c})]^3$ are typically piecewise polynomials on a submesh of c composed of elementary subsimplices or aggregations thereof; we stress that the tangential component of these functions is not necessarily continuous across the edges of this submesh lying inside c, so that, in general $P_{\mathcal{E}}(\mathrm{c}) \not\subset H(\underline{\mathrm{curl}};\mathrm{c})$ (*i.e.* $\underline{\mathtt{L}}_{\mathcal{E}_\mathrm{c}}$ is non-conforming) but functions in $P_{\mathcal{E}}(\mathrm{c})$ are sufficiently smooth to apply the local de Rham map $\mathsf{R}_{\mathcal{E}_\mathrm{c}}$ on them. Examples and properties of operators $\underline{\mathtt{L}}_{\mathcal{E}_\mathrm{c}}$ are detailed in Section 7.3.1.

The starting point for analyzing the vertex-based scheme (8.3) using reconstruction operators is the following identity for each cell $\mathrm{c} \in \mathrm{C}$:

$$[\![\mathbf{g}_1, \mathsf{H}_\kappa^{\mathcal{E}_\mathrm{c}\tilde{\mathcal{F}}_\mathrm{c}}(\mathbf{g}_2)]\!]_{\mathcal{E}_\mathrm{c}\tilde{\mathcal{F}}_\mathrm{c}} = \int_\mathrm{c} \underline{\mathtt{L}}_{\mathcal{E}_\mathrm{c}}(\mathbf{g}_1)\cdot\underline{\underline{\kappa}}\,\underline{\mathtt{L}}_{\mathcal{E}_\mathrm{c}}(\mathbf{g}_2), \qquad \forall \mathbf{g}_1,\mathbf{g}_2 \in \mathcal{E}_\mathrm{c}. \tag{8.20}$$

Therefore, the vertex-based scheme (8.4) can be recast into the functional form: Find $\mathbf{p} \in \mathcal{V}$ such that

$$\int_\Omega \underline{\mathtt{L}}_{\mathcal{E}}(\mathsf{GRAD}(\mathbf{p}))\cdot\underline{\underline{\kappa}}\,\underline{\mathtt{L}}_{\mathcal{E}}(\mathsf{GRAD}(\mathbf{q})) = \int_\Omega s\mathtt{L}^0_{\mathcal{V}}(\mathbf{q}), \qquad \forall \mathbf{q} \in \mathcal{V}, \tag{8.21}$$

where the operator $\mathtt{L}^0_{\mathcal{V}}$ is defined for all $\mathbf{p} \in \mathcal{V}$ as $\mathtt{L}^0_{\mathcal{V}}(\mathbf{p})|_{\tilde{\mathrm{c}}(\mathrm{v})} = \mathbf{p}_\mathrm{v}$ for each primal vertex $\mathrm{v} \in \mathrm{V}$ (cf. Section 7.2.3). A straightforward consequence of (8.17) and (8.20) is that for all $\mathbf{g} \in \mathcal{E}$, the following identity holds:

$$|\!|\!|\mathbf{g}|\!|\!|_\kappa = \|\underline{\mathtt{L}}_{\mathcal{E}}(\mathbf{g})\|_\kappa. \tag{8.22}$$

Lemma 8.11 (Error estimate in energy norms on reconstructed gradient and flux)**.** *Assume that the mesh sequence is of class* **(MR)** *and* **(MB)**. *Assume that primal faces are planar. Assume that* $\underline{\mathtt{L}}_{\mathcal{E}_\mathrm{c}}$ *satisfies* (**R1**), (**R2**), *and* (**R3**) *for each cell* $\mathrm{c} \in \mathrm{C}$. *Let* $\underline{g}$ *be the exact gradient and* $\underline{\phi}$ *the exact flux. Assume* $\underline{g} \in [H^1(\mathrm{C})]^3 \cap S_{\mathcal{E}}(\Omega)$ *and* $\underline{\phi} \in [H^1(\mathrm{C})]^3$. *Let* $\mathbf{g}$ *be the discrete gradient and* $\boldsymbol{\phi}$ *the discrete flux resulting from* (8.3). *Then, letting* $\underline{\mathtt{L}}_{\tilde{\mathcal{F}}}(\boldsymbol{\phi}) := -\underline{\underline{\kappa}}\,\underline{\mathtt{L}}_{\mathcal{E}}(\mathbf{g})$, *the following inequality holds:*

$$\|\underline{g} - \underline{\mathtt{L}}_{\mathcal{E}}(\mathbf{g})\|_\kappa = \|\underline{\phi} - \underline{\mathtt{L}}_{\tilde{\mathcal{F}}}(\boldsymbol{\phi})\|_{\kappa^{-1}} \lesssim h\left(\kappa_\sharp^{\frac12}\|\underline{g}\|_{[H^1(\mathrm{C})]^3} + \kappa_\flat^{-\frac12}\|\underline{\phi}\|_{[H^1(\mathrm{C})]^3}\right). \tag{8.23}$$

Proof. Using the triangle inequality, we infer that

$$\|\underline{g} - \underline{\mathtt{L}}_{\mathcal{E}}(\mathbf{g})\|_\kappa \le \|\underline{g} - \underline{\mathtt{A}}_{\mathcal{E}}(\underline{g})\|_\kappa + \|\underline{\mathtt{A}}_{\mathcal{E}}(\underline{g}) - \underline{\mathtt{L}}_{\mathcal{E}}(\mathbf{g})\|_\kappa = T_1 + T_2.$$

Owing to bounds on $\underline{\underline{\kappa}}$ and Proposition 7.21 (and taking into account the fact that $\underline{g}$ is curl-free), we infer that $T_1 \lesssim h\kappa_\sharp^{\frac12}\|\underline{g}\|_{[H^1(\mathrm{C})]^3}$. Using (8.22) and then Theorem 8.6 yields

$$T_2 \lesssim h\left(\kappa_\sharp^{\frac12}\|\underline{g}\|_{[H^1(\mathrm{C})]^3} + \kappa_\flat^{-\frac12}\|\underline{\phi}\|_{[H^1(\mathrm{C})]^3}\right).$$

The estimate on the flux is straightforward owing to the definition of $\underline{\mathtt{L}}_{\tilde{\mathcal{F}}}$. □

L^2 error estimate. For simplicity, we assume in this paragraph that $\underline{\underline{\kappa}}$ is the identity tensor. Moreover, we assume that the dual mesh is built using a fully barycentric subdivision. The proof of our L^2-error estimate hinges on the existence of a conforming potential reconstruction $\mathtt{L}^{\mathrm{conf}}_{\mathcal{V}}$ with suitable properties. Such a potential reconstruction has been devised in Section 7.3.3. This reconstruction verifies the four properties (**R1**)–(**R4**) along with conformity and $\mathbb{P}_1$-consistency (cf. Lemmata 7.40 and 7.41). We recall that the potential reconstruction $\mathtt{L}^{\mathrm{conf}}_{\mathcal{V}}$ defines a continuous and piecewise affine field relying on a set of local reconstruction functions $\{\ell^{\mathrm{conf}}_{\mathrm{v,c}}\}_{\mathrm{v}\in\mathrm{V_c}}$ in each cell $\mathrm{c} \in \mathrm{C}$ defined as follows:

$$\ell^{\mathrm{conf}}_{\mathrm{v,c}}(\underline{x})|_{\mathfrak{p}_{\mathrm{ef,c}}} := \delta_\mathrm{e}(\mathrm{v})\ell^{\mathrm{LAG}}_\mathrm{v}(\underline{x}) + \delta_\mathrm{f}(\mathrm{v})\frac{|\mathrm{f}\cap\tilde{\mathrm{c}}(\mathrm{v})|}{|\mathrm{f}|}\ell^{\mathrm{LAG}}_\mathrm{f}(\underline{x}) + \frac{|\mathrm{c}\cap\tilde{\mathrm{c}}(\mathrm{v})|}{|\mathrm{c}|}\ell^{\mathrm{LAG}}_\mathrm{c}(\underline{x}), \tag{8.24}$$

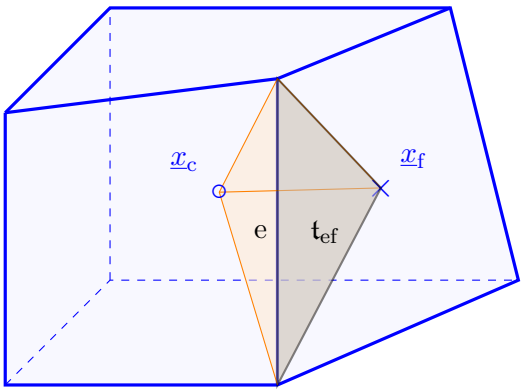

Figure 8.2 – Consider a hexahedral cell c. For a face $f \in F_c$ and an edge $e \in E_f$, we highlight the subvolume $\mathfrak{p}_{ef,c}$ (orange) and the triangle $\mathfrak{t}_{ef}$ (grey).

where ℓ_a^{LAG} is the Lagrange shape function on a tetrahedron related to the vertex located at $\underline{x}_a$, $\delta_e(v) = 1$ if $v \in V_e$, 0 otherwise, $\delta_f(v) = 1$ if $v \in V_f$, 0 otherwise, and $\mathfrak{p}_{ef,c} = \mathfrak{p}_{e,c} \cap \mathfrak{p}_{f,c}$ for each face $f \in F_c$, each edge $e \in E_f$ (see Figure 8.2). We first establish additional properties for $\underline{\mathrm{grad}}\, \mathsf{L}_{\mathcal{V}}^{\mathrm{conf}}$.

Proposition 8.12 (Properties of $\underline{\mathrm{grad}}\, \mathsf{L}_{\mathcal{V}}^{\mathrm{conf}}$)**.** *Assume that the mesh sequence is of class* **(MR)** *and* **(MB)** *with a fully barycentric subdivision. Assume that primal faces are planar. Consider the global conforming potential reconstruction operator* $\mathsf{L}_{\mathcal{V}}^{\mathrm{conf}}$ *built using* (7.15) *from the local reconstruction operators* $\mathsf{L}_{\mathcal{V}_c}^{\mathrm{conf}}$ *in each cell* $c \in C$ *(cf. Definition 7.39). Then, the following properties are satisfied:*

(i) Local stability. For all $c \in C$ *and all* $\mathbf{p} \in \mathcal{V}_c$,

$$\|\underline{\mathrm{grad}}(\mathsf{L}_{\mathcal{V}_c}^{\mathrm{conf}}(\mathbf{p}))\|_{L^2(c)^3} \lesssim \|\mathsf{GRAD}(\mathbf{p})\|_{2,\mathcal{E}_c}. \tag{8.25}$$

(ii) Approximation. Set $\mathtt{A}_{\mathcal{V}}^{\mathrm{conf}} := \mathsf{L}_{\mathcal{V}}^{\mathrm{conf}} \mathsf{R}_{\mathcal{V}}$*. For all* $\zeta \in H^2(\Omega)$,

$$\|\underline{\mathrm{grad}}(\zeta) - \underline{\mathrm{grad}}(\mathtt{A}_{\mathcal{V}}^{\mathrm{conf}}(\zeta))\|_{L^2(\Omega)^3} \lesssim h\|\zeta\|_{H^2(\Omega)}. \tag{8.26}$$

(iii) Mean consistency. For all $c \in C$*, for all* $\mathbf{p} \in \mathcal{V}_c$ *and any* $\underline{\mathsf{L}}_{\mathcal{E}_c}$ *satisfying* **(R3)** *(cf.* (7.5b)*),*

$$\int_c \underline{\mathrm{grad}}\, \mathsf{L}_{\mathcal{V}_c}^{\mathrm{conf}}(\mathbf{p}) = \int_c \underline{\mathsf{L}}_{\mathcal{E}_c}(\mathsf{GRAD}(\mathbf{p})). \tag{8.27}$$

Proof. (i) Local stability. The stability can be proved using the mesh regularity **(MR)**.

(ii) Approximation. The estimate is proved locally on each primal cell. Adding and subtracting the gradient of the L^2-orthogonal projection of ζ on $\mathbb{P}_1(c)$ denoted by Z_c^1 yields

$$\|\underline{\mathrm{grad}}(\zeta) - \underline{\mathrm{grad}}(\mathtt{A}_{\mathcal{V}_c}^{\mathrm{conf}}(\zeta))\|_{L^2(c)^3} \le \|\underline{\mathrm{grad}}(\zeta) - \underline{\mathrm{grad}}(Z_c^1)\|_{L^2(c)^3} + \|\underline{\mathrm{grad}}(\mathsf{L}_{\mathcal{V}_c}^{\mathrm{conf}}(\mathsf{R}_{\mathcal{V}_c}(Z_c^1 - \zeta)))\|_{L^2(c)^3},$$

using the triangle inequality and the $\mathbb{P}_1$-consistency of $\mathsf{L}_{\mathcal{V}_c}^{\mathrm{conf}}$. Then, applying classical results from FE approximation theory for the first term and the local stability (i) and the commuting property (cf. Proposition 3.13) for the second term, we infer that

$$\|\underline{\mathrm{grad}}(\zeta) - \underline{\mathrm{grad}}(\mathtt{A}_{\mathcal{V}_c}^{\mathrm{conf}}(\zeta))\|_{L^2(c)^3} \lesssim h_c\|\underline{\mathrm{grad}}(\zeta)\|_{H^1(c)^3} + \|\mathsf{R}_{\mathcal{E}_c}(\underline{\mathrm{grad}}(\zeta - Z_c^1))\|_{2,\mathcal{E}_c}.$$

The second term is bounded by $h_c\|\underline{\mathrm{grad}}(\zeta)\|_{H^1(c)^3}$ as in the proof of Lemma 6.14. We infer (8.26) by summing cellwise.

(iii) Mean consistency. As a preliminary result, we show that

$$\int_f \ell_{v,c}^{\mathrm{conf}} = |f \cap \tilde{c}(v)|, \qquad \forall f \in F_c,\ \forall v \in V_f.$$

Since $\int_{\mathfrak{t}_{\mathrm{ef}}} \ell_a^{\mathrm{LAG}} = \frac{1}{3}|\mathfrak{t}_{\mathrm{ef}}|$ for any vertex a of $\mathfrak{t}_{\mathrm{ef}}$ (see Figure 8.2), using (8.24), we infer for all $\mathrm{v} \in \mathrm{V_f}$ that

$$\int_{\mathrm{f}} \ell_{\mathrm{v,c}}^{\mathrm{conf}} = \sum_{\mathrm{e}\in\mathrm{E_f}} \delta_{\mathrm{e}}(\mathrm{v}) \int_{\mathfrak{t}_{\mathrm{ef}}} \ell_{\mathrm{v}}^{\mathrm{LAG}} + \frac{|\mathrm{f}\cap\tilde{\mathrm{c}}(\mathrm{v})|}{|\mathrm{f}|}\ell_{\mathrm{f}}^{\mathrm{LAG}} = \sum_{\mathrm{e}\in\mathrm{E_v}\cap\mathrm{E_f}} \frac{1}{3}|\mathfrak{t}_{\mathrm{ef}}| + \frac{|\mathrm{f}\cap\tilde{\mathrm{c}}(\mathrm{v})|}{3} = |\mathrm{f}\cap\tilde{\mathrm{c}}(\mathrm{v})|,$$

since $\sum_{\mathrm{e}\in\mathrm{E_f}}|\mathfrak{t}_{\mathrm{ef}}| = |\mathrm{f}|$ and $\sum_{\mathrm{e}\in\mathrm{E_v}\cap\mathrm{E_f}}|\mathfrak{t}_{\mathrm{ef}}| = 2|\mathrm{f}\cap\tilde{\mathrm{c}}(\mathrm{v})|$ (cf. Proposition 5.21).

Moreover, for each $\mathrm{v} \in \mathrm{V_c}$, the set of faces of the polyhedron $\mathrm{c}\cap\tilde{\mathrm{c}}(\mathrm{v})$ consists of the dual faces $\tilde{\mathrm{f}}_{\mathrm{c}}(\mathrm{e})$ for all $\mathrm{e} \in \mathrm{E_v}\cap\mathrm{E_c}$ and of subfaces $\mathrm{f}\cap\tilde{\mathrm{c}}(\mathrm{v})$ for all $\mathrm{f} \in \mathrm{F_c}\cap\mathrm{F_v}$. Since $\underline{\nu}_{\mathrm{f,c}}$ (the unit normal to f pointing outward c) is constant (primal faces are planar), we infer from the divergence theorem that

$$\sum_{\mathrm{f}\in\mathrm{F_v}\cap\mathrm{F_c}} |\mathrm{f}\cap\tilde{\mathrm{c}}(\mathrm{v})|\underline{\nu}_{\mathrm{f,c}} = \sum_{\mathrm{e}\in\mathrm{E_v}\cap\mathrm{E_c}} \iota_{\mathrm{v,e}}\underline{\tilde{\mathrm{f}}}_{\mathrm{c}}(\mathrm{e}). \tag{8.28}$$

The two last identities imply that

$$\int_{\mathrm{c}} \underline{\mathrm{grad}}(\ell_{\mathrm{v,c}}^{\mathrm{conf}}) = \int_{\mathrm{c}} \underline{\mathrm{div}}(\ell_{\mathrm{v,c}}^{\mathrm{conf}}\underline{\underline{\mathsf{Id}}}) = \sum_{\mathrm{f}\in\mathrm{F_v}\cap\mathrm{F_c}} |\mathrm{f}\cap\tilde{\mathrm{c}}(\mathrm{v})|\underline{\nu}_{\mathrm{f,c}} = \sum_{\mathrm{e}\in\mathrm{E_v}\cap\mathrm{E_c}} \iota_{\mathrm{v,e}}\underline{\tilde{\mathrm{f}}}_{\mathrm{c}}(\mathrm{e}).$$

Then, since $\underline{\mathtt{L}}_{\mathcal{E}_{\mathrm{c}}}$ satisfies (**R3**),

$$\begin{aligned}\int_{\mathrm{c}} \underline{\mathrm{grad}}(\mathtt{L}_{\mathcal{V}_{\mathrm{c}}}^{\mathrm{conf}}(\mathbf{p})) &= \sum_{\mathrm{v}\in\mathrm{V_c}} \mathbf{p}_{\mathrm{v}} \int_{\mathrm{c}} \underline{\mathrm{grad}}(\ell_{\mathrm{v,c}}^{\mathrm{conf}}) = \sum_{\mathrm{v}\in\mathrm{V_c}} \mathbf{p}_{\mathrm{v}} \left(\sum_{\mathrm{e}\in\mathrm{E_v}\cap\mathrm{E_c}} \iota_{\mathrm{v,e}}\underline{\tilde{\mathrm{f}}}_{\mathrm{c}}(\mathrm{e})\right)\\ &= \sum_{\mathrm{e}\in\mathrm{E_c}} \left(\sum_{\mathrm{v}\in\mathrm{V_e}} \iota_{\mathrm{v,e}}\mathbf{p}_{\mathrm{v}}\right)\underline{\tilde{\mathrm{f}}}_{\mathrm{c}}(\mathrm{e}) = \sum_{\mathrm{e}\in\mathrm{E_c}} (\mathsf{GRAD}(\mathbf{p}))_{\mathrm{e}}\underline{\tilde{\mathrm{f}}}_{\mathrm{c}}(\mathrm{e}) = \int_{\mathrm{c}} \underline{\mathtt{L}}_{\mathcal{E}_{\mathrm{c}}}(\mathsf{GRAD}(\mathbf{p})).\end{aligned}$$

□

We can now turn to the main result of this section. We underline that the next result applies to all vertex-based schemes based on formulation (8.21) with a reconstruction operator $\underline{\mathtt{L}}_{\mathcal{E}}$ satisfying (**R1**), (**R2**), and (**R3**). $\mathtt{L}_{\mathcal{V}}^{\mathrm{conf}}$ is only used as a postprocessing of the discrete solution.

Theorem 8.13. *Assume that the mesh sequence is of class* **(MR)** *and* **(MB)** *with a fully barycentric subdivision. Assume that primal faces are planar. Assume that the model problem* (8.1) *with* $\underline{\underline{\kappa}} = \underline{\underline{\mathsf{Id}}}$ *has elliptic regularity. Assume* $s \in H^1(\Omega)$*. Let* p *be the exact potential and let* $\mathbf{p}$ *be the discrete potential resulting from* (8.3)*. Assume that* $p \in H^2(\Omega)$ *Then,*

$$\|p - \mathtt{L}_{\mathcal{V}}^{\mathrm{conf}}(\mathbf{p})\|_{L^2(\Omega)} \lesssim h^2\left(\|p\|_{H^2(\Omega} + \|s\|_{H^1(\Omega)}\right). \tag{8.29}$$

Proof. Let $\underline{g}$ be the exact gradient and $\mathbf{g} := \mathsf{GRAD}(\mathbf{p})$ the discrete gradient. Let $\zeta \in H^2(\Omega)\cap H_0^1(\Omega)$ solve the model problem (8.1) with source $p - \mathtt{L}_{\mathcal{V}}^{\mathrm{conf}}(\mathbf{p})$. Let $\underline{g}^{\zeta}$ be the gradient of ζ. Integrating by parts yields $\|p-\mathtt{L}_{\mathcal{V}}^{\mathrm{conf}}(\mathbf{p})\|_{L^2(\Omega)}^2 = \int_{\Omega}(\underline{g} - \underline{\mathrm{grad}}(\mathtt{L}_{\mathcal{V}}^{\mathrm{conf}}(\mathbf{p})))\cdot\underline{g}^{\zeta}$ so that (recalling the approximation operator $\underline{\mathtt{A}}_{\mathcal{E}} = \underline{\mathtt{L}}_{\mathcal{E}}\mathsf{R}_{\mathcal{E}}$)

$$\begin{aligned}\|p - \mathtt{L}_{\mathcal{V}}^{\mathrm{conf}}(\mathbf{p})\|_{L^2(\Omega)}^2 = &\int_{\Omega}(\underline{g} - \underline{\mathtt{L}}_{\mathcal{E}}(\mathbf{g}))\cdot(\underline{g}^{\zeta} - \underline{\mathtt{A}}_{\mathcal{E}}(\underline{g}^{\zeta})) + \int_{\Omega}(\underline{g} - \underline{\mathtt{L}}_{\mathcal{E}}(\mathbf{g}))\cdot\underline{\mathtt{A}}_{\mathcal{E}}(\underline{g}^{\zeta})\\ &+ \int_{\Omega}(\underline{\mathtt{L}}_{\mathcal{E}}(\mathbf{g}) - \underline{\mathrm{grad}}(\mathtt{L}_{\mathcal{V}}^{\mathrm{conf}}(\mathbf{p})))\cdot\underline{g}^{\zeta} := T_1 + T_2 + T_3.\end{aligned}$$

The Cauchy–Schwarz inequality together with the bounds (7.25) and (8.23) yields

$$|T_1| \lesssim h^2\|\underline{g}\|_{H^1(\Omega)^3}\|\underline{g}^{\zeta}\|_{H^1(\Omega)^3}.$$

Moreover, setting $\boldsymbol{\zeta} = \mathsf{R}_{\mathcal{V}}(\zeta)$ and $\mathbf{g}^{\boldsymbol{\zeta}} = \mathsf{GRAD}(\boldsymbol{\zeta}) = \mathsf{R}_{\mathcal{E}}(\underline{g}^{\boldsymbol{\zeta}})$ so that $\underline{\mathtt{A}}_{\mathcal{E}}(\underline{g}^{\boldsymbol{\zeta}}) = \underline{\mathtt{L}}_{\mathcal{E}}(\mathbf{g}^{\boldsymbol{\zeta}})$, we obtain

$$T_2 = \int_\Omega \underline{g} \cdot (\underline{\mathtt{L}}_{\mathcal{E}}(\mathbf{g}^{\boldsymbol{\zeta}}) - \underline{\mathrm{grad}}(\mathtt{L}_{\mathcal{V}}^{\mathrm{conf}}(\boldsymbol{\zeta}))) + \int_\Omega \underline{g} \cdot \underline{\mathrm{grad}}(\mathtt{L}_{\mathcal{V}}^{\mathrm{conf}}(\boldsymbol{\zeta})) - \int_\Omega \underline{\mathtt{L}}_{\mathcal{E}}(\mathbf{g}) \cdot \underline{\mathtt{L}}_{\mathcal{E}}(\mathbf{g}^{\boldsymbol{\zeta}}).$$

Using the variational form for the exact and discrete potentials and setting $\mathtt{A}_{\mathcal{V}}^0 := \mathtt{L}_{\mathcal{V}}^0 \mathsf{R}_{\mathcal{V}}$ while recalling that $\mathtt{A}_{\mathcal{V}}^{\mathrm{conf}} = \mathtt{L}_{\mathcal{V}}^{\mathrm{conf}} \mathsf{R}_{\mathcal{V}}$, we infer that

$$T_2 = \int_\Omega \underline{g} \cdot (\underline{\mathtt{L}}_{\mathcal{E}}(\mathbf{g}^{\boldsymbol{\zeta}}) - \underline{\mathrm{grad}}(\mathtt{L}_{\mathcal{V}}^{\mathrm{conf}}(\boldsymbol{\zeta}))) + \int_\Omega s\,(\mathtt{A}_{\mathcal{V}}^{\mathrm{conf}}(\zeta) - \mathtt{A}_{\mathcal{V}}^0(\zeta)) := T_{2,1} + T_{2,2}.$$

To bound $T_{2,1}$, we use the mean consistency of $\underline{\mathrm{grad}}(\mathtt{L}_{\mathcal{V}}^{\mathrm{conf}})$, stated in (8.27), to subtract from $\underline{g}$ its mean-value on each primal cell yielding

$$|T_{2,1}| \lesssim h \|\underline{g}\|_{H^1(\Omega)^3} \|\underline{\mathtt{L}}_{\mathcal{E}}(\mathbf{g}^{\boldsymbol{\zeta}}) - \underline{\mathrm{grad}}(\mathtt{L}_{\mathcal{V}}^{\mathrm{conf}}(\boldsymbol{\zeta}))\|_{L^2(\Omega)^3},$$

and the last factor is bounded as

$$\begin{aligned}\|\underline{\mathtt{L}}_{\mathcal{E}}(\mathbf{g}^{\boldsymbol{\zeta}}) - \underline{\mathrm{grad}}(\mathtt{L}_{\mathcal{V}}^{\mathrm{conf}}(\boldsymbol{\zeta}))\|_{L^2(\Omega)^3} &\le \|\underline{g}^{\boldsymbol{\zeta}} - \underline{\mathtt{A}}_{\mathcal{E}}(\underline{g}^{\boldsymbol{\zeta}})\|_{L^2(\Omega)^3} + \|\underline{g}^{\boldsymbol{\zeta}} - \underline{\mathrm{grad}}(\mathtt{L}_{\mathcal{V}}^{\mathrm{conf}}(\boldsymbol{\zeta}))\|_{L^2(\Omega)^3} \\ &= \|\underline{g}^{\boldsymbol{\zeta}} - \underline{\mathtt{A}}_{\mathcal{E}}(\underline{g}^{\boldsymbol{\zeta}})\|_{L^2(\Omega)^3} + \|\underline{\mathrm{grad}}(\zeta) - \underline{\mathrm{grad}}(\mathtt{A}_{\mathcal{V}}^{\mathrm{conf}}(\zeta))\|_{L^2(\Omega)^3} \\ &\lesssim h \|\underline{g}^{\boldsymbol{\zeta}}\|_{H^1(\Omega)^3},\end{aligned}$$

owing to the approximation properties of $\underline{\mathtt{A}}_{\mathcal{E}}$ (Proposition 7.21) and $\mathtt{A}_{\mathcal{V}}^{\mathrm{conf}}$ (Proposition 8.12).

The term $T_{2,2}$ is bounded similarly: owing to the dual consistency property for both $\mathtt{L}_{\mathcal{V}}^{\mathrm{conf}}$ and $\mathtt{L}_{\mathcal{V}}^0$ (cf. Lemma 7.41), the mean-value of s can be subtracted from s on each primal cell, so that using the regularity of s yields

$$|T_{2,2}| \lesssim h \|s\|_{H^1(\Omega)} \|\mathtt{A}_{\mathcal{V}}^{\mathrm{conf}}(\zeta) - \mathtt{A}_{\mathcal{V}}^0(\zeta)\|_{L^2(\Omega)}.$$

We add and subtract ζ in the last term on the right-hand side, use the triangle inequality together with the fact that $\mathtt{A}_{\mathcal{V}}^{\mathrm{conf}}(\zeta)$ and $\mathtt{A}_{\mathcal{V}}^0(\zeta)$ both approximate ζ to first-order in the L^2-norm to infer

$$|T_{2,2}| \lesssim h^2 \|s\|_{H^1(\Omega)} \|\zeta\|_{H^2(\Omega)}.$$

Turning to T_3, using again the mean consistency of $\underline{\mathrm{grad}}\,\mathtt{L}_{\mathcal{V}}^{\mathrm{conf}}$ to subtract cellwise the mean value of $\underline{g}^{\boldsymbol{\zeta}}$ yields

$$|T_3| \lesssim h \|\underline{g}^{\boldsymbol{\zeta}}\|_{H^1(\Omega)^3} \|\underline{\mathtt{L}}_{\mathcal{E}}(\mathbf{g}) - \underline{\mathrm{grad}}(\mathtt{L}_{\mathcal{V}}^{\mathrm{conf}}(\mathbf{p}))\|_{L^2(\Omega)^3},$$

and by the triangle inequality

$$\begin{aligned}\|\underline{\mathtt{L}}_{\mathcal{E}}(\mathbf{g}) - \underline{\mathrm{grad}}(\mathtt{L}_{\mathcal{V}}^{\mathrm{conf}}(\mathbf{p}))\|_{L^2(\Omega)^3} \le{}& \|\underline{\mathtt{L}}_{\mathcal{E}}(\mathbf{g}) - \underline{g}\|_{L^2(\Omega)^3} + \|\underline{\mathrm{grad}}(p) - \underline{\mathrm{grad}}(\mathtt{A}_{\mathcal{V}}^{\mathrm{conf}}(p))\|_{L^2(\Omega)^3} \\ &+ \|\underline{\mathrm{grad}}(\mathtt{L}_{\mathcal{V}}^{\mathrm{conf}}(\mathsf{R}_{\mathcal{V}}(p) - \mathbf{p}))\|_{L^2(\Omega)^3}.\end{aligned}$$

The first term on the right-hand side is bounded using (8.23), the second using the approximation property (8.26) of $\underline{\mathrm{grad}}\,\mathtt{A}_{\mathcal{V}}^{\mathrm{conf}}$, and the third using the stability (8.25) of $\underline{\mathrm{grad}}\,\mathtt{L}_{\mathcal{V}}^{\mathrm{conf}}$, the commuting property of Proposition 3.13, the lower bound of (8.10), and Theorem 8.6. Finally, collecting the above bounds and using elliptic regularity so that $\|\zeta\|_{H^2(\Omega)} + \|\underline{g}^{\boldsymbol{\zeta}}\|_{H^1(\Omega)^3} \lesssim \|p - \mathtt{L}_{\mathcal{V}}^{\mathrm{conf}}(\mathbf{p})\|_{L^2(\Omega)}$ yields the desired L^2-error estimate. □

Remark 8.14 (Conforming gradient reconstruction)**.** *It is possible to define a conforming gradient reconstruction of discrete gradients by setting* $\underline{\mathtt{L}}_{\mathcal{E}}^{\mathrm{conf}}(\mathsf{GRAD}(\mathbf{p})) = \underline{\mathrm{grad}}(\mathtt{L}_{\mathcal{V}}^{\mathrm{conf}}(\mathbf{p}))$ *for all* $\mathbf{p} \in \mathcal{V}$ *(we only define this operator on the subspace* $\mathsf{GRAD}(\mathcal{V})$ *and not on the whole space* $\mathcal{E}$*). It is readily seen that* $\underline{\mathtt{L}}_{\mathcal{E}}^{\mathrm{conf}} : \mathsf{GRAD}(\mathcal{V}) \to H(\underline{\mathrm{curl}};\Omega)$ *with zero tangential component on the boundary (conformity),* $\mathsf{R}_{\mathcal{E}} \underline{\mathtt{L}}_{\mathcal{E}}^{\mathrm{conf}} = \mathsf{Id}_{\mathcal{E}}$ *on* $\mathsf{GRAD}(\mathcal{V})$ *(unisolvence),* $\|\underline{\mathtt{L}}_{\mathcal{E}}^{\mathrm{conf}}(\mathbf{g})\|_{L^2(\Omega)^3} \lesssim \|\mathbf{g}\|_{2,\mathcal{E}}$ *for all* $\mathbf{g} = \mathsf{GRAD}(\mathbf{p})$ *(stability),* $\mathtt{A}_{\mathcal{E}}^{\mathrm{conf}} := \underline{\mathtt{L}}_{\mathcal{E}}^{\mathrm{conf}} \mathsf{R}_{\mathcal{E}}$ *leaves invariant the gradients of piecewise affine functions on primal cells (restricted* $\mathbb{P}_0$*-consistency), and* $\underline{\mathtt{L}}_{\mathcal{E}}^{\mathrm{conf}}(\mathbf{g})$ *has the same mean-value on primal cells as* $\underline{\mathtt{L}}_{\mathcal{E}}(\mathbf{g})$ *for all* $\mathbf{g} = \mathsf{GRAD}(\mathbf{p})$ *(mean consistency).*

8.1.3 Link with existing schemes

Link with classical schemes on specific meshes. Using the reconstruction functions $\{\underline{\ell}_{\mathrm{e}}^{\mathrm{NED}}\}_{\mathrm{e}\in\mathrm{E}}$ on simplicial meshes defined in Section 7.2.1, the vertex-based scheme (8.3) then coincides with the classical first-order Lagrange FE approximation (up to a quadrature on the source term).

Using the reconstruction functions $\{\underline{\ell}_{\mathrm{e}}^{\mathrm{CART}}\}_{\mathrm{e}\in\mathrm{E}}$ on Cartesian meshes defined in (7.32), the vertex-based scheme (8.3) then coincides with a vertex-centered TPFA scheme.

Link with nodal MFD schemes. We show that the vertex-based scheme (8.3) belongs to the family of nodal MFD schemes analyzed by Brezzi *et al.* (2009). The starting point is the discrete variational formulation (8.4) of vertex-based schemes.

Similarly to (3.6), we define the local discrete gradient operator $\mathsf{GRAD}_{\mathrm{c}}:\mathcal{V}_{\mathrm{c}}\to\mathcal{E}_{\mathrm{c}}$ for all $\mathrm{c}\in\mathrm{C}$. Letting $\mathsf{T}_{\mathrm{V,c}}:\mathcal{V}\to\mathcal{V}_{\mathrm{c}}$ be the (full-rank) map from global to local DoFs attached to vertices and recalling the map $\mathsf{T}_{\mathrm{E,c}}$ from global to local DoFs attached to edges, it is easily seen that the commuting property $\mathsf{GRAD}_{\mathrm{c}}\cdot\mathsf{T}_{\mathrm{V,c}}=\mathsf{T}_{\mathrm{E,c}}\cdot\mathsf{GRAD}$ holds on $\mathcal{V}$ and for all $\mathrm{c}\in\mathrm{C}$. Then, for all $\mathbf{p},\mathbf{q}\in\mathcal{V}_{\mathrm{c}}$, we define the following bilinear form:

$$[\![\mathbf{p},\mathbf{q}]\!]_{\mathrm{c}}^{\mathrm{MFD}}:=[\![\mathsf{GRAD}_{\mathrm{c}}(\mathbf{p}),\mathsf{H}_{\kappa}^{\mathcal{E}_{\mathrm{c}}\tilde{\mathcal{F}}_{\mathrm{c}}}\cdot\mathsf{GRAD}_{\mathrm{c}}(\mathbf{q})]\!]_{\mathcal{E}_{\mathrm{c}}\tilde{\mathcal{F}}_{\mathrm{c}}},\tag{8.30}$$

which readily inherits the symmetry property of $\mathsf{H}_{\kappa}^{\mathcal{E}_{\mathrm{c}}\tilde{\mathcal{F}}_{\mathrm{c}}}$. Owing to the cellwise assembly (3.20) of the discrete Hodge operator $\mathsf{H}_{\kappa}^{\mathcal{E}\tilde{\mathcal{F}}}$ and the above commuting property, the left-hand side of (8.4) can be rewritten as

$$\begin{aligned}[\![\mathsf{GRAD}(\mathbf{p}),\mathsf{H}_{\kappa}^{\mathcal{E}\tilde{\mathcal{F}}}\cdot\mathsf{GRAD}(\mathbf{q})]\!]_{\mathcal{E}\tilde{\mathcal{F}}}&=\sum_{\mathrm{c}\in\mathrm{C}}[\![\mathsf{T}_{\mathrm{E,c}}\cdot\mathsf{GRAD}(\mathbf{p}),\mathsf{H}_{\kappa}^{\mathcal{E}_{\mathrm{c}}\tilde{\mathcal{F}}_{\mathrm{c}}}\cdot\mathsf{T}_{\mathrm{E,c}}\cdot\mathsf{GRAD}(\mathbf{q})]\!]_{\mathcal{E}_{\mathrm{c}}\tilde{\mathcal{F}}_{\mathrm{c}}}\\&=\sum_{\mathrm{c}\in\mathrm{C}}[\![\mathsf{T}_{\mathrm{V,c}}(\mathbf{p}),\mathsf{T}_{\mathrm{V,c}}(\mathbf{q})]\!]_{\mathrm{c}}^{\mathrm{MFD}},\end{aligned}$$

so that the vertex-based scheme (8.4) fits the general form of nodal MFD schemes. We now verify that the bilinear form (8.30) satisfies the two abstract properties identified in Brezzi *et al.* (2009) for the convergence of nodal MFD schemes.

Proposition 8.15. *Let* $\mathsf{H}_{\kappa}^{\mathcal{E}_{\mathrm{c}}\tilde{\mathcal{F}}_{\mathrm{c}}}$ *satisfy, for all* $\mathrm{c}\in\mathrm{C}$*, the design properties* (**H0**)*,* (**H1**)*, and* (**H2**)*. Then, the two properties (Brezzi* et al.*, 2009, Eqs. (5.14)-(5.15)) hold for the bilinear form* $[\![\cdot,\cdot]\!]_{\mathrm{c}}^{\mathrm{MFD}}$*.*

Proof. Property (Brezzi *et al.*, 2009, Eq. (5.15)) is a direct consequence of (**H1**). To verify (Brezzi *et al.*, 2009, Eq. (5.14)), we consider a cell $\mathrm{c}\in\mathrm{C}$ and $r\in\mathbb{P}_1(\mathrm{c})$ so that $\underline{\underline{\kappa}}\,\underline{\mathrm{grad}}\,r$ is constant in c. Then, for all $\mathbf{q}\in\mathcal{V}_{\mathrm{c}}$, letting $\mathsf{R}_{\mathcal{V}_{\mathrm{c}}}(r)$ collect the DoFs of r at local vertices, we obtain

$$\begin{aligned}[\![\mathbf{q},\mathsf{R}_{\mathcal{V}_{\mathrm{c}}}(r)]\!]_{\mathrm{c}}^{\mathrm{MFD}}&=[\![\mathsf{GRAD}_{\mathrm{c}}(\mathbf{q}),\mathsf{H}_{\kappa}^{\mathcal{E}_{\mathrm{c}}\tilde{\mathcal{F}}_{\mathrm{c}}}\cdot\mathsf{GRAD}_{\mathrm{c}}(\mathsf{R}_{\mathcal{V}_{\mathrm{c}}}(r))]\!]_{\mathcal{E}_{\mathrm{c}}\tilde{\mathcal{F}}_{\mathrm{c}}}\\&=[\![\mathsf{GRAD}_{\mathrm{c}}(\mathbf{q}),\mathsf{H}_{\kappa}^{\mathcal{E}_{\mathrm{c}}\tilde{\mathcal{F}}_{\mathrm{c}}}\cdot\mathsf{R}_{\mathcal{E}_{\mathrm{c}}}(\underline{\mathrm{grad}}\,r)]\!]_{\mathcal{E}_{\mathrm{c}}\tilde{\mathcal{F}}_{\mathrm{c}}}&&\text{by Proposition 3.13}\\&=[\![\mathsf{GRAD}_{\mathrm{c}}(\mathbf{q}),\mathsf{R}_{\tilde{\mathcal{F}}_{\mathrm{c}}}(\underline{\underline{\kappa}}\,\underline{\mathrm{grad}}\,r)]\!]_{\mathcal{E}_{\mathrm{c}}\tilde{\mathcal{F}}_{\mathrm{c}}}&&\text{by (\textbf{H2})}\\&=\sum_{\mathrm{e}\in\mathrm{E}_{\mathrm{c}}}\sum_{\mathrm{v}\in\mathrm{V}_{\mathrm{e}}}\iota_{\mathrm{v,e}}\mathbf{q}_{\mathrm{v}}(\underline{\underline{\kappa}}\,\underline{\mathrm{grad}}\,r)\cdot\tilde{\underline{\mathrm{f}}}_{\mathrm{c}}(\mathrm{e})&&\text{by definition of }\mathsf{R}_{\tilde{\mathcal{F}}_{\mathrm{c}}}\\&=\sum_{\mathrm{v}\in\mathrm{V}_{\mathrm{c}}}\mathbf{q}_{\mathrm{v}}(\underline{\underline{\kappa}}\,\underline{\mathrm{grad}}\,r)\cdot\left(\sum_{\mathrm{e}\in\mathrm{E}_{\mathrm{v}}\cap\mathrm{E}_{\mathrm{c}}}\iota_{\mathrm{v,e}}\tilde{\underline{\mathrm{f}}}_{\mathrm{c}}(\mathrm{e})\right).\end{aligned}$$

Using (8.28), we infer that

$$[\![\mathbf{q},\mathsf{R}_{\mathcal{V}_{\mathrm{c}}}(r)]\!]_{\mathrm{c}}^{\mathrm{MFD}}=\sum_{\mathrm{v}\in\mathrm{V}_{\mathrm{c}}}\sum_{\mathrm{f}\in\mathrm{F}_{\mathrm{v}}\cap\mathrm{F}_{\mathrm{c}}}\mathbf{q}_{\mathrm{v}}(\underline{\underline{\kappa}}\,\underline{\mathrm{grad}}\,r)\cdot\int_{\mathrm{f}\cap\tilde{\mathrm{c}}(\mathrm{v})}\underline{\nu}_{\mathrm{f,c}}=\sum_{\mathrm{f}\in\mathrm{F}_{\mathrm{c}}}\sum_{\mathrm{v}\in\mathrm{V}_{\mathrm{f}}}\mathbf{q}_{\mathrm{v}}(\underline{\underline{\kappa}}\,\underline{\mathrm{grad}}\,r)\cdot\int_{\mathrm{f}\cap\tilde{\mathrm{c}}(\mathrm{v})}\underline{\nu}_{\mathrm{f,c}},$$

which is a specific form of (Brezzi *et al.*, 2009, Eq. (5.14)) for a suitable integration formula on the faces of c. If primal faces are planar, then the weight $\omega_{\mathrm{f}}^{\mathrm{v}}$ of (5.14) corresponds to $|\mathrm{f} \cap \tilde{\mathrm{c}}(\mathrm{v})|$. □

Link with Approximate Gradient Schemes. Approximate Gradient Schemes have been introduced by Eymard *et al.* (2012). We first observe that (8.21) matches the general form of (Eymard *et al.*, 2012, Eq. (1.2)) with the potential reconstruction $\mathtt{L}_{\mathcal{V}}^0(\mathbf{p}) \in L^2(\Omega)$ and the gradient reconstruction $\underline{\mathtt{L}}_{\mathcal{E}}(\mathsf{GRAD}(\mathbf{p})) \in [L^2(\Omega)]^3$. The convergence analysis of Approximate Gradient Schemes hinges on three properties (we adopt the terminology of Eymard *et al.* (2012)).

(i) The *coercivity*, stating that, there is a real constant C such that, uniformly in h,

$$\max_{\mathbf{q}\in\mathcal{V}\setminus\{0\}} \frac{\|\mathtt{L}_{\mathcal{V}}^0(\mathbf{q})\|_{L^2(\Omega)}}{\|\underline{\mathtt{L}}_{\mathcal{E}}(\mathsf{GRAD}(\mathbf{q}))\|_{L^2(\Omega)^3}} \le C. \tag{8.31}$$

(ii) The *strong consistency*, stating that, for all $\varphi \in H_0^1(\Omega)$,

$$S_{\mathrm{M}}(\varphi) := \min_{\mathbf{q}\in\mathcal{V}} \left\{ \|\mathtt{L}_{\mathcal{V}}^0(\mathbf{q}) - \varphi\|_{L^2(\Omega)} + \|\underline{\mathtt{L}}_{\mathcal{E}}(\mathsf{GRAD}(\mathbf{q})) - \underline{\mathrm{grad}}\,\varphi\|_{L^2(\Omega)^3} \right\} \xrightarrow{h\to 0} 0. \tag{8.32}$$

(iii) The *dual consistency* (or conformity), stating that, for all $\underline{\psi} \in H(\mathrm{div};\Omega)$,

$$W_{\mathrm{M}}(\underline{\psi}) := \max_{\mathbf{q}\in\mathcal{V}\setminus\{0\}} \frac{1}{\|\underline{\mathtt{L}}_{\mathcal{E}}(\mathsf{GRAD}(\mathbf{q}))\|_{L^2(\Omega)^3}} \left| \int_\Omega \left\{ \underline{\mathtt{L}}_{\mathcal{E}}(\mathsf{GRAD}(\mathbf{q})) \cdot \underline{\psi} + \mathtt{L}_{\mathcal{V}}^0(\mathbf{q})\,\mathrm{div}(\underline{\psi}) \right\} \right| \xrightarrow{h\to 0} 0. \tag{8.33}$$

Proposition 8.16 (Link with Approximate Gradient Schemes)**.** *Let* $\mathsf{H}_\kappa^{\varepsilon\tilde{\mathcal{F}}}$ *be defined by* (8.20) *with local reconstruction operators satisfying* (**R1**)*,* (**R2**)*, and* (**R3**)*. Then,* (8.31)*,* (8.32)*, and* (8.33) *hold with first-order convergence rates:*

$$S_{\mathrm{M}}(\varphi) \lesssim h\|\varphi\|_{H^2(\Omega)} \qquad \textit{and} \qquad W_{\mathrm{M}}(\underline{\psi}) \lesssim (\kappa_\sharp/\kappa_\flat) h \|\underline{\psi}\|_{H^1(\Omega)^3}.$$

Proof. To prove (8.31), we use the discrete Poincaré inequality (6.34) and the lower bound in (**R1**) yielding, for all $\mathbf{q} \in \mathcal{V}$,

$$\|\mathtt{L}_{\mathcal{V}}^0(\mathbf{q})\|_{L^2(\Omega)} = \|\mathbf{q}\|_{2,\mathcal{V}} \le C_{\mathrm{P}}^{(0)} \|\mathsf{GRAD}(\mathbf{q})\|_{2,\mathcal{E}} \le C_{\mathrm{P}}^{(0)} \eta_{\mathcal{E}}^{-\frac{1}{2}} \|\underline{\mathtt{L}}_{\mathcal{E}}(\mathsf{GRAD}(\mathbf{q}))\|_{L^2(\Omega)^3}.$$

To prove (8.32), it suffices by density (Eymard *et al.*, 2012, Lemma 2.5) to consider $\varphi \in C_0^\infty(\Omega)$. We take $\mathbf{q} = \mathsf{R}_{\mathcal{V}}(\varphi)$ so that, owing to the commuting property of Proposition 3.13,

$$\underline{\mathtt{L}}_{\mathcal{E}}(\mathsf{GRAD}(\mathbf{q})) = \underline{\mathtt{L}}_{\mathcal{E}}(\mathsf{GRAD}(\mathsf{R}_{\mathcal{V}}(\varphi))) = \underline{\mathtt{L}}_{\mathcal{E}}\mathsf{R}_{\mathcal{E}}(\underline{\mathrm{grad}}\,\varphi) = \underline{\mathtt{A}}_{\mathcal{E}}(\underline{\mathrm{grad}}\,\varphi),$$

whence we infer $\|\underline{\mathtt{L}}_{\mathcal{E}}(\mathsf{GRAD}(\mathbf{q})) - \underline{\mathrm{grad}}\,\varphi\|_{L^2(\Omega)^3} \lesssim h\|\varphi\|_{H^2(\Omega)}$ owing to Proposition 7.21. Moreover, the definition of $\mathtt{L}_{\mathcal{V}}^0$ yields $\|\mathtt{L}_{\mathcal{V}}^0\mathsf{R}_{\mathcal{V}}(\varphi) - \varphi\|_{L^2(\Omega)} \lesssim h\|\varphi\|_{H^1(\Omega)}$, so that the same bound holds on $S_{\mathrm{M}}(\varphi)$.

To prove (8.33), it suffices by density (Eymard *et al.*, 2012, Lemma 2.5) to consider $\underline{\psi} \in [C^1(\overline{\Omega})]^3$. We set $\underline{g} := -\underline{\underline{\kappa}}^{-1}\underline{\psi}$. Then, for all $\mathbf{q} \in \mathcal{V}$, we first observe that, owing to the definition of $\mathtt{L}_{\mathcal{V}}^0$ and the commuting and adjunction properties of Propositions 3.13 and 3.16 respectively, the following identities hold:

$$\int_\Omega \mathtt{L}_{\mathcal{V}}^0(\mathbf{q})\,\mathrm{div}(\underline{\psi}) = [\![\mathbf{q}, \mathsf{R}_{\tilde{\mathcal{C}}}(\mathrm{div}(\underline{\psi}))]\!]_{\mathcal{V}\tilde{\mathcal{C}}} = [\![\mathbf{q}, \widetilde{\mathsf{DIV}}(\mathsf{R}_{\tilde{\mathcal{F}}}(\underline{\psi}))]\!]_{\mathcal{V}\tilde{\mathcal{C}}} = -[\![\mathsf{GRAD}(\mathbf{q}), \mathsf{R}_{\tilde{\mathcal{F}}}(\underline{\psi})]\!]_{\mathcal{E}\tilde{\mathcal{F}}}.$$

Hence,

$$\int_\Omega \left\{\underline{\mathsf{L}}_{\mathcal{E}}(\mathsf{GRAD}(\mathbf{q}))\cdot\underline{\psi}+\mathsf{L}^0_{\mathcal{V}}(\mathbf{q})\,\mathrm{div}(\underline{\psi})\right\} = \int_\Omega \underline{\mathsf{L}}_{\mathcal{E}}(\mathsf{GRAD}(\mathbf{q}))\cdot\underline{\psi} - [\![\mathsf{GRAD}(\mathbf{q}),\mathsf{R}_{\widetilde{\mathcal{F}}}(\underline{\psi})]\!]_{\mathcal{E}\widetilde{\mathcal{F}}}$$
$$= \int_\Omega \underline{\mathsf{L}}_{\mathcal{E}}(\mathsf{GRAD}(\mathbf{q}))\cdot\underline{\underline{\kappa}}(\underline{\mathsf{A}}_{\mathcal{E}}(\underline{g})-\underline{g}) - [\![\mathsf{GRAD}(\mathbf{q}),\lfloor\kappa,\,\varepsilon^{\widetilde{\mathcal{F}}}\rceil(\underline{g})]\!]_{\mathcal{E}\widetilde{\mathcal{F}}} := T_1+T_2,$$

since

$$\int_\Omega \underline{\mathsf{L}}_{\mathcal{E}}(\mathsf{GRAD}(\mathbf{q}))\cdot\underline{\underline{\kappa}}\,\underline{\mathsf{A}}_{\mathcal{E}}(\underline{g}) = \int_\Omega \underline{\mathsf{L}}_{\mathcal{E}}(\mathsf{GRAD}(\mathbf{q}))\cdot\underline{\underline{\kappa}}\,\underline{\mathsf{L}}_{\mathcal{E}}(\mathsf{R}_{\mathcal{E}}(\underline{g})) = [\![\mathsf{GRAD}(\mathbf{q}),\mathsf{H}^{\mathcal{E}\widetilde{\mathcal{F}}}_{\kappa}\mathsf{R}_{\mathcal{E}}(\underline{g})]\!]_{\mathcal{E}\widetilde{\mathcal{F}}}.$$

Then,

$$\frac{|T_1|}{\|\underline{\mathsf{L}}_{\mathcal{E}}(\mathsf{GRAD}(\mathbf{q}))\|_{L^2(\Omega)^3}} \le \kappa_\sharp\|\underline{g}-\underline{\mathsf{A}}_{\mathcal{E}}(\underline{g})\|_{L^2(\Omega)^3} \lesssim \kappa_\sharp h\|\underline{g}\|_{[H^1(\mathrm{C})]^3} \le (\kappa_\sharp/\kappa_\flat)h\|\underline{\psi}\|_{H^1(\Omega)^3}$$

owing to Proposition 7.21. Moreover, (8.22) implies $\|\mathbf{g}\|_\kappa = \|\underline{\mathsf{L}}_{\mathcal{E}}(\mathbf{g})\|_\kappa \le \kappa_\sharp^{1/2}\|\underline{\mathsf{L}}_{\mathcal{E}}(\mathbf{g})\|_{L^2(\Omega)^3}$ for all $\mathbf{g}\in\mathcal{E}$, so that we obtain

$$|T_2| \le \kappa_\sharp^{1/2}\|\underline{\mathsf{L}}_{\mathcal{E}}(\mathsf{GRAD}(\mathbf{q}))\|_{L^2(\Omega)^3}\|\lfloor\kappa,\,\varepsilon^{\widetilde{\mathcal{F}}}\rceil(\underline{g})\|_{\kappa^{-1}},$$

and the last factor has been estimated in Lemma 6.14, yielding the desired bound on $W_{\mathrm{M}}(\underline{\psi})$. □

8.2 Cell-based schemes

In this section, we analyze cell-based schemes for elliptic equations from an algebraic viewpoint and then using reconstruction operators. Our theoretical results are similar to those derived for vertex-based schemes. Some proofs are omitted since they hinge on an adaptation of the previous ones. For the sake of completeness, we recall the discrete system (4.9) for cell-based schemes: Find $(\boldsymbol{\phi},\mathbf{p})\in\mathcal{F}\times\widetilde{\mathcal{V}}$ such that

$$\begin{cases}\mathsf{H}^{\mathcal{F}\widetilde{\mathcal{E}}}_{\kappa^{-1}}(\boldsymbol{\phi}) + \widetilde{\mathsf{GRAD}}(\mathbf{p}) = 0,\\ \mathsf{DIV}(\boldsymbol{\phi}) = \mathsf{R}_{\mathcal{C}}(s).\end{cases}\tag{8.34}$$

We also recall that we neglect quadrature errors on the source term s for simplicity and take $\mathsf{R}_{\mathcal{C}}(s)$ on the right-hand side of (8.34). We consider homogeneous Dirichlet BCs. Nonhomogeneous Dirichlet/Neumann BCs can be considered as well (cf. the EDF R&D technical report (Ra) mentioned in Chapter 1). The discrete variational formulation of the system (8.34) is the following: Find $(\boldsymbol{\phi},\mathbf{p})\in\mathcal{F}\times\widetilde{\mathcal{V}}$ such that

$$\begin{cases}[\![\boldsymbol{\sigma},\mathsf{H}^{\mathcal{F}\widetilde{\mathcal{E}}}_{\kappa^{-1}}(\boldsymbol{\phi})]\!]_{\mathcal{F}\widetilde{\mathcal{E}}} - [\![\mathsf{DIV}(\boldsymbol{\sigma}),\mathbf{p}]\!]_{\mathcal{C}\widetilde{\mathcal{V}}} = 0, & \forall\boldsymbol{\sigma}\in\mathcal{F},\\ [\![\mathsf{DIV}(\boldsymbol{\phi}),\mathbf{q}]\!]_{\mathcal{C}\widetilde{\mathcal{V}}} = [\![\mathsf{R}_{\mathcal{C}}(s),\mathbf{q}]\!]_{\mathcal{C}\widetilde{\mathcal{V}}}, & \forall\mathbf{q}\in\widetilde{\mathcal{V}},\end{cases}\tag{8.35}$$

where we have used the adjunction property between DIV and $-\widetilde{\mathsf{GRAD}}$ (cf. Proposition 3.16) in the first equation.

8.2.1 Analysis from an algebraic viewpoint

The discrete Hodge operator $\mathsf{H}^{\mathcal{F}\widetilde{\mathcal{E}}}_{\kappa^{-1}}$ is designed from a cellwise assembly process of local discrete Hodge operators $\mathsf{H}^{\mathcal{F}_{\mathrm{c}}\widetilde{\mathcal{E}}_{\mathrm{c}}}_{\kappa^{-1}}$ for each cell $\mathrm{c}\in\mathrm{C}$ as detailed in Section 3.4.2. The three

properties (**H0**), (**H1**), and (**H2**) stated in Section 6.2.1 are recalled in the specific case of $\mathsf{H}_{\kappa^{-1}}^{\mathcal{F}_c\tilde{\mathcal{E}}_c}$.

(**H0**) [Symmetry] $\mathsf{H}_{\kappa^{-1}}^{\mathcal{F}_c\tilde{\mathcal{E}}_c}$ is symmetric.

(**H1**) [Local stability] There exists $\eta_{\kappa^{-1}} > 0$ such that, for all $c \in \mathrm{C}$,

$$\eta_{\kappa^{-1}}\kappa_{\sharp,c}^{-1}\|\boldsymbol{\phi}\|_{2,\mathcal{F}_c}^2 \le [\![\boldsymbol{\phi}, \mathsf{H}_{\kappa^{-1}}^{\mathcal{F}_c\tilde{\mathcal{E}}_c}(\boldsymbol{\phi})]\!]_{\mathcal{F}_c\tilde{\mathcal{E}}_c} \le \eta_{\kappa^{-1}}^{-1}\kappa_{\flat,c}^{-1}\|\boldsymbol{\phi}\|_{2,\mathcal{F}_c}^2, \qquad \forall \boldsymbol{\phi} \in \mathcal{F}_c. \tag{8.36}$$

(**H2**) [Local $\mathbb{P}_0$-consistency] The local commuting operator

$$\lfloor \kappa^{-1}, {}_{\mathcal{F}_c}\tilde{\mathcal{E}}_c \rceil(\bullet) := \mathsf{H}_{\kappa^{-1}}^{\mathcal{F}_c\tilde{\mathcal{E}}_c} \cdot \mathsf{R}_{\mathcal{F}_c}(\bullet) - \mathsf{R}_{\tilde{\mathcal{E}}_c}(\underline{\underline{\kappa}}^{-1}\,\bullet) \tag{8.37}$$

satisfies $\lfloor \kappa^{-1}, {}_{\mathcal{F}_c}\tilde{\mathcal{E}}_c \rceil(\underline{K}) = 0$ for any vector field $\underline{K}$ which is constant in $c \in \mathrm{C}$.

Following the rationale detailed in Section 6.1.2, the discrete Hodge operator $\mathsf{H}_{\kappa}^{\mathcal{F}\tilde{\mathcal{E}}}$ induces the following discrete norms:

$$\|\boldsymbol{\phi}\|_{\kappa^{-1}}^2 := [\![\boldsymbol{\phi}, \mathsf{H}_{\kappa^{-1}}^{\mathcal{F}\tilde{\mathcal{E}}}(\boldsymbol{\phi})]\!]_{\mathcal{F}\tilde{\mathcal{E}}} \qquad \text{and} \qquad \|\mathbf{g}\|_{\kappa}^2 := [\![(\mathsf{H}_{\kappa^{-1}}^{\mathcal{F}\tilde{\mathcal{E}}})^{-1}(\boldsymbol{\phi}), \boldsymbol{\phi}]\!]_{\mathcal{F}\tilde{\mathcal{E}}}, \tag{8.38}$$

and for each cell $c \in \mathrm{C}$,

$$\|\boldsymbol{\phi}\|_{\kappa^{-1},c}^2 := [\![\boldsymbol{\phi}, \mathsf{H}_{\kappa^{-1}}^{\mathcal{F}_c\tilde{\mathcal{E}}_c}(\boldsymbol{\phi})]\!]_{\mathcal{F}_c\tilde{\mathcal{E}}_c} \qquad \text{and} \qquad \|\mathbf{g}\|_{\kappa,c}^2 := [\![(\mathsf{H}_{\kappa^{-1}}^{\mathcal{F}_c\tilde{\mathcal{E}}_c})^{-1}(\mathbf{g}), \mathbf{g}]\!]_{\mathcal{F}_c\tilde{\mathcal{E}}_c}. \tag{8.39}$$

Owing to the Cauchy–Schwarz inequality (6.14), we infer that

$$[\![\boldsymbol{\phi}, \mathbf{g}]\!]_{\mathcal{F}\tilde{\mathcal{E}}} \le \|\mathbf{g}\|_{\kappa}\,\|\boldsymbol{\phi}\|_{\kappa^{-1}}. \tag{8.40}$$

Discrete stability. The global stability property (6.21) of the discrete Hodge operator $\mathsf{H}_{\kappa^{-1}}^{\mathcal{F}\tilde{\mathcal{E}}}$, stemming from (**H1**) and (3.20), takes the form:

$$\eta_{\kappa^{-1}}\kappa_{\sharp}^{-1}\|\boldsymbol{\phi}\|_{2,\mathcal{F}}^2 \le \|\boldsymbol{\phi}\|_{\kappa^{-1}}^2 \le (\eta_{\kappa^{-1}}\kappa_{\flat})^{-1}\|\boldsymbol{\phi}\|_{2,\mathcal{F}}^2, \qquad \forall \boldsymbol{\phi} \in \mathcal{F}. \tag{8.41}$$

A consequence of (8.41) and the discrete Poincaré inequality (6.35) is the stability of the cell-based scheme.

Proposition 8.17 (Discrete stability)**.** *Assume the mesh regularity property* (6.8)*. Let* $(\mathbf{p}, \boldsymbol{\phi}) \in \widetilde{\mathcal{V}} \times \mathcal{F}$ *solve* (8.34)*. Then, the two following inequalities hold:*

$$\|\boldsymbol{\phi}\|_{\kappa^{-1}} \lesssim (\eta_{\kappa^{-1}}\kappa_{\flat})^{-\frac{1}{2}} C_{\mathrm{P}}^{(\tilde{0})} \|s\|_{L^2(\Omega)}, \qquad \|\mathbf{p}\|_{2,\widetilde{\mathcal{V}}} \lesssim (\eta_{\kappa^{-1}}\kappa_{\flat})^{-1} (C_{\mathrm{P}}^{(\tilde{0})})^2 \|s\|_{L^2(\Omega)}, \tag{8.42}$$

where $C_{\mathrm{P}}^{(\tilde{0})}$ *stems from the discrete Poincaré inequality* (6.35)*.*

Proof. Let $\mathbf{q} \in \widetilde{\mathcal{V}}$ and define $\boldsymbol{\psi} \in \mathcal{F}$ such that $\mathsf{H}_{\kappa^{-1}}^{\mathcal{F}\tilde{\mathcal{E}}}(\boldsymbol{\psi}) = -\widetilde{\mathsf{GRAD}}(\mathbf{q})$. As a preliminary result, we prove that

$$\|\widetilde{\mathsf{GRAD}}(\mathbf{q})\|_{2,\tilde{\mathcal{E}}} \lesssim (\eta_{\kappa^{-1}}\kappa_{\flat})^{-1}\|\boldsymbol{\psi}\|_{\kappa^{-1}}. \tag{8.43}$$

First, for each cell $c \in \mathrm{C}$ and each face $f \in \mathrm{F}_c$, we consider $\boldsymbol{\delta}_{c,f} \in \mathcal{F}_c$ such that $\boldsymbol{\delta}_{c,f}|_{f'} = \delta_{f,f'}$ for all $f' \in \mathrm{F}_c$ (δ is the Kronecker symbol). For each face $f \in \mathrm{F}$, the following identities hold:

$$\widetilde{\mathsf{GRAD}}(\mathbf{q})|_{\tilde{e}(f)} = -\sum_{c\in\mathrm{C}_f}\sum_{f'\in\mathrm{F}_c} \mathsf{H}_{\kappa^{-1}}^{\mathcal{F}_c\tilde{\mathcal{E}}_c}(\boldsymbol{\psi})|_{\tilde{e}(f),f'}\mathsf{T}_{\mathrm{F},c}(\boldsymbol{\psi})|_{f'} = -\sum_{c\in\mathrm{C}_f} [\![\boldsymbol{\delta}_{c,f}, \mathsf{H}_{\kappa^{-1}}^{\mathcal{F}_c\tilde{\mathcal{E}}_c}(\mathsf{T}_{\mathrm{F},c}(\boldsymbol{\psi}))]\!]_{\mathcal{F}_c\tilde{\mathcal{E}}_c}.$$

Using twice the Cauchy–Schwarz inequality yields

$$\widetilde{\mathsf{GRAD}}(\mathbf{q})|_{\tilde{e}(f)}^2 \le \#\mathrm{C}_f \sum_{c\in\mathrm{C}_f} [\![\boldsymbol{\delta}_{c,f}, \mathsf{H}_{\kappa^{-1}}^{\mathcal{F}_c\tilde{\mathcal{E}}_c}(\mathsf{T}_{\mathrm{F},c}(\boldsymbol{\psi}))]\!]_{\mathcal{F}_c\tilde{\mathcal{E}}_c}^2 \le 2\sum_{c\in\mathrm{C}_f} \|\boldsymbol{\delta}_{c,f}\|_{\kappa^{-1},c}^2 \|\mathsf{T}_{\mathrm{F},c}(\boldsymbol{\psi})\|_{\kappa^{-1},c}^2,$$

since $\#\mathrm{C_f} \le 2$. From (**H1**) and the definition (6.1), we infer that

$$\|\boldsymbol{\delta}_{\mathrm{c,f}}\|_{\kappa^{-1},\mathrm{c}}^2 \le (3|\mathrm{f}|\eta_{\kappa^{-1}}\kappa_\flat)^{-1}\tilde{\underline{\mathrm{e}}}_{\mathrm{c}}(\mathrm{f})\cdot\underline{\nu}_{\mathrm{f}}.$$

Moreover, the definition (6.6b) of $\|\cdot\|_{2,\widetilde{\mathcal{E}}}$ yields

$$\begin{aligned}\|\widetilde{\mathsf{GRAD}}(\mathbf{q})\|_{2,\widetilde{\mathcal{E}}}^2 &= \sum_{\mathrm{f}\in\mathrm{F}}\frac{|\mathrm{f}|}{|\tilde{\mathrm{e}}(\mathrm{f})|}\widetilde{\mathsf{GRAD}}(\mathbf{q})|_{\tilde{\mathrm{e}}(\mathrm{f})}^2 \le \sum_{\mathrm{f}\in\mathrm{F}}\sum_{\mathrm{c}\in\mathrm{C_f}}\frac{2}{3\eta_{\kappa^{-1}}\kappa_\flat|\tilde{\mathrm{e}}(\mathrm{f})|}\tilde{\underline{\mathrm{e}}}_{\mathrm{c}}(\mathrm{f})\cdot\underline{\nu}_{\mathrm{f}}\|\mathsf{T}_{\mathrm{F,c}}(\boldsymbol{\psi})\|_{\kappa^{-1},\mathrm{c}}^2\\ &\le (\eta_{\kappa^{-1}}\kappa_\flat)^{-1}\sum_{\mathrm{f}\in\mathrm{F}}\sum_{\mathrm{c}\in\mathrm{C_f}}\|\mathsf{T}_{\mathrm{F,c}}(\boldsymbol{\psi})\|_{\kappa^{-1},\mathrm{c}}^2 = (\eta_{\kappa^{-1}}\kappa_\flat)^{-1}\sum_{\mathrm{c}\in\mathrm{C}}\sum_{\mathrm{f}\in\mathrm{F_c}}\|\mathsf{T}_{\mathrm{F,c}}(\boldsymbol{\psi})\|_{\kappa^{-1},\mathrm{c}}^2\\ &\le \max_{\mathrm{c}\in\mathrm{C}}(\#\mathrm{F_c})(\eta_{\kappa^{-1}}\kappa_\flat)^{-1}\|\boldsymbol{\psi}\|_{\kappa^{-1}}^2,\end{aligned}$$

since $\frac{2}{3}\tilde{\underline{\mathrm{e}}}_{\mathrm{c}}(\mathrm{f})\cdot\underline{\nu}_{\mathrm{f}}/|\tilde{\mathrm{e}}(\mathrm{f})| \le 1$ for all $\mathrm{f}\in\mathrm{F}$ and all $\mathrm{c}\in\mathrm{C_f}$. Thus, (8.43) holds.

We now prove (8.42). We denote by $\mathsf{L}^0_{\widetilde{\mathcal{V}}}$ the cellwise constant potential reconstruction such that $\mathsf{L}^0_{\widetilde{\mathcal{V}}}(\mathbf{p})|_{\mathrm{c}} := \mathbf{p}_{\tilde{\mathrm{v}}(\mathrm{c})}$ for all $\mathbf{p}\in\widetilde{\mathcal{V}}$. Since $\boldsymbol{\phi}$ solves (8.35), we infer that

$$\|\boldsymbol{\phi}\|_{\kappa^{-1}}^2 = [\![\mathsf{DIV}(\boldsymbol{\phi}),\mathbf{p}]\!]_{\mathcal{C}\widetilde{\mathcal{V}}} = [\![\mathsf{R_c}(s),\mathbf{p}]\!]_{\mathcal{C}\widetilde{\mathcal{V}}} = \sum_{\mathrm{c}\in\mathrm{C}}\mathbf{p}_{\tilde{\mathrm{v}}(\mathrm{c})}\int_{\mathrm{c}}s = \int_\Omega \mathsf{L}^0_{\widetilde{\mathcal{V}}}(\mathbf{p})s \le \|\mathsf{L}^0_{\widetilde{\mathcal{V}}}(\mathbf{p})\|_{L^2(\Omega)}\|s\|_{L^2(\Omega)},$$

using Proposition 3.16) and the Cauchy–Schwarz inequality. Since $\|\mathsf{L}^0_{\widetilde{\mathcal{V}}}(\mathbf{p})\| = \|\mathbf{p}\|_{2,\widetilde{\mathcal{V}}}$, we infer using the Poincaré inequality (6.35) that

$$\|\boldsymbol{\phi}\|_{\kappa^{-1}}^2 \le \|\mathbf{p}\|_{2,\widetilde{\mathcal{V}}}\|s\|_{L^2(\Omega)} \le C_{\mathrm{P}}^{(0)}\|\widetilde{\mathsf{GRAD}}(\mathbf{p})\|_{2,\widetilde{\mathcal{E}}}\|s\|_{L^2(\Omega)}.$$

Using (8.43) yields the first inequality in (8.42), while applying again (8.43) then the Poincaré inequality (6.35) yields the second inequality. □

Consistency error. The Tonti diagrams for the exact problem and the discrete scheme (8.34) are linked through the de Rham maps as shown in Figure 8.3. As in vertex-based schemes, the diagrams D_4 and D_6 are commutative, but this is (in general) not the case for D_5.

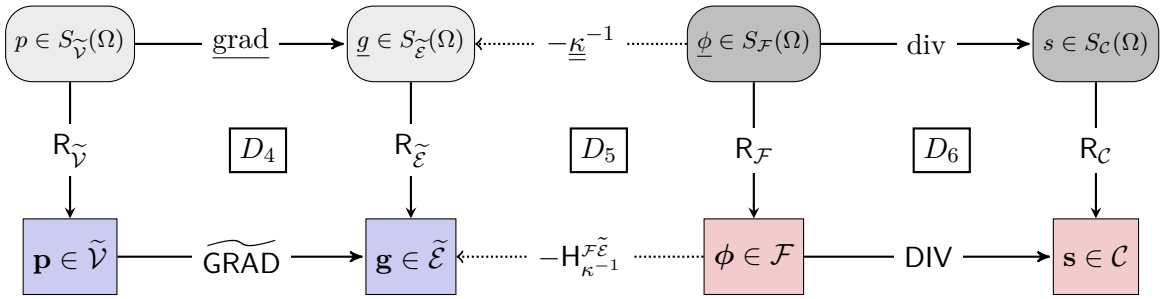

Figure 8.3 – Tonti diagrams for the exact problem and the cell-based scheme (8.34).

The counterpart of Lemma 8.2 for cell-based schemes is the following lemma.

Lemma 8.18 (Basic error bound)**.** *Let* $\mathbf{g}$ *be the discrete gradient and* $\boldsymbol{\phi}$ *be the discrete flux resulting from* (8.34)*. Let* $\underline{g}$ *be the exact gradient and* $\underline{\phi}$ *be the exact flux. Assume that* $\underline{g}$*,* $\underline{\phi}\in H^s(\Omega)^3$ *with* $s>\frac{1}{2}$*. Then, the following inequality holds:*

$$\max(\|\mathsf{R}_{\widetilde{\mathcal{E}}}(\underline{g})-\mathbf{g}\|_\kappa, \|\mathsf{R}_{\mathcal{F}}(\underline{\phi})-\boldsymbol{\phi}\|_{\kappa^{-1}}) \le \|\lfloor\kappa^{-1},\,{}^{\mathcal{F}}\tilde{\mathcal{E}}\rceil(\underline{\phi})\|_\kappa, \tag{8.44}$$

where the global commuting operator related to diagram D_5 *of Figure 8.3 is defined from* (6.26) *as follows:*

$$\lfloor\kappa^{-1},\,{}^{\mathcal{F}}\tilde{\mathcal{E}}\rceil(\underline{\phi}) := \mathsf{H}^{\mathcal{F}\widetilde{\mathcal{E}}}_{\kappa^{-1}}\cdot\mathsf{R}_{\mathcal{F}}(\underline{\phi}) - \mathsf{R}_{\widetilde{\mathcal{E}}}(\underline{\underline{\kappa}}^{-1}\underline{\phi}). \tag{8.45}$$

The counterpart of Lemma 8.3 is the following lemma.

Lemma 8.19 (Tighter error bound)**.** *Assume that* $\underline{g}$, $\underline{\phi} \in H^s(\Omega)^3$ *with* $s > \frac{1}{2}$*. Then, the following inequality holds:*

$$\max(\|\mathsf{R}_{\widetilde{\mathcal{E}}}(\underline{g}) - \mathbf{g}\|_\kappa, \|\mathsf{R}_{\mathcal{F}}(\underline{\phi}) - \boldsymbol{\phi}\|_{\kappa^{-1}}) \le \inf_{\underline{\Phi}\in[\mathbb{P}_0(\mathrm{C})]^3} \left\{ \sum_{\mathrm{c}\in\mathrm{C}} \|\lfloor \kappa^{-1},\, {}_{\mathcal{F}_\mathrm{c}}\tilde{\varepsilon}_\mathrm{c}\rceil((\underline{\phi} - \underline{\Phi})|_\mathrm{c})\|^2_{\kappa,\mathrm{c}} \right\}^{\frac{1}{2}}. \quad (8.46)$$

As for vertex-based schemes, a consequence of (8.46) is that, if the exact solution is piecewise affine on the primal mesh, then the solution of the cell-based scheme is the image by the de Rham map of the exact solution.

Convergence in discrete energy norms.

Theorem 8.20 (Convergence rate for smooth solutions)**.** *Let* h *denote the maximal diameter of primal cells. Let* $\underline{g}$ *be the exact gradient and* $\underline{\phi}$ *the exact flux. Let* $\mathbf{g}$ *be the discrete gradient and* $\boldsymbol{\phi}$ *the discrete flux resulting from* (8.34)*. Assume that* $\underline{g}, \underline{\phi} \in [H^1(\mathrm{C})]^3$*. Assume that the mesh sequence is of class* **(MR)***. Then, the following inequality holds:*

$$\|\lfloor \kappa^{-1},\, {}_{\mathcal{F}}\tilde{\varepsilon}\rceil(\underline{\phi})\|_\kappa \lesssim h \left(\kappa_\sharp^{\frac{1}{2}} \|\underline{g}\|_{[H^1(\mathrm{C})]^3} + \kappa_\flat^{-\frac{1}{2}} \|\underline{\phi}\|_{[H^1(\mathrm{C})]^3} \right). \quad (8.47)$$

Moreover, assuming that $\underline{g}$, $\underline{\phi} \in H^s(\Omega)^3$ *with* $s > \frac{1}{2}$*, then*

$$\max(\|\mathsf{R}_{\widetilde{\mathcal{E}}}(\underline{g}) - \mathbf{g}\|_\kappa, \|\mathsf{R}_{\mathcal{F}}(\underline{\phi}) - \boldsymbol{\phi}\|_{\kappa^{-1}}) \lesssim h \left(\kappa_\sharp^{\frac{1}{2}} \|\underline{g}\|_{[H^1(\mathrm{C})]^3} + \kappa_\flat^{-\frac{1}{2}} \|\underline{\phi}\|_{[H^1(\mathrm{C})]^3} \right). \quad (8.48)$$

Proof. First, observe that $\underline{g} \in S_{\widetilde{\mathcal{E}}}(\mathrm{C})$ and $\underline{\phi} \in S_{\mathcal{F}}(\mathrm{C})$ since $\underline{g}, \underline{\phi} \in [H^1(\mathrm{C})]^3$. Then, the proof follows the same lines as the proof of Theorem 8.6 (applying this time, Lemma 6.16 and Lemma 8.18). □

Remark 8.21 (Regularity requirements)**.** *In order to ensure that* $\mathsf{R}_{\widetilde{\mathcal{E}}}(\underline{g})$ *and* $\mathsf{R}_{\mathcal{F}}(\underline{\phi})$ *are well-defined, we additionally assume in Theorem 8.20 that* $\underline{g}$ *and* $\underline{\phi} \in H^s(\Omega)^3$ *with* $s > \frac{1}{2}$*. In fact, only the assumption* $\underline{\phi} \in H^s(\Omega)^3$ *with* $s > \frac{1}{2}$ *is needed since* $\underline{g}$ *is curl-free and* $\underline{g} \in [H^1(\mathrm{C})]^3$*,* $\underline{g} \in S_{\widetilde{\mathcal{E}}}(\Omega)$ *(cf. Remark 6.11).*

8.2.2 Analysis using reconstruction operators

In this section, we assume that the primal mesh is of class **(MB)** (*i.e.* one can define a barycentric subdivision) and that primal faces are planar. This section relies on the existence of suitable local flux reconstruction operators in each cell $\mathrm{c} \in \mathrm{C}$ which are introduced in Chapter 7. We only require that the local reconstruction operator $\underline{\mathsf{L}}_{\mathcal{F}_\mathrm{c}} : \mathcal{F}_\mathrm{c} \to P_{\mathcal{F}}(\mathrm{c})$ satisfies the three properties (**R1**), (**R2**), and (**R3**) so that the algebraic analysis of the previous section holds (cf. Proposition 7.3). Examples of local flux reconstruction operators $\underline{\mathsf{L}}_{\mathcal{F}_\mathrm{c}}$ are detailed in Section 7.3.1. Functions in $P_{\mathcal{F}}(\mathrm{c}) \subset [L^2(\mathrm{c})]^3$ are typically piecewise polynomials on a submesh of c composed of elementary subsimplices or aggregations thereof; we stress that the normal component of these functions is not necessarily continuous across the faces of this submesh lying inside c, so that, in general $P_{\mathcal{F}}(\mathrm{c}) \not\subset H(\mathrm{div};\mathrm{c})$ (*i.e.* $\underline{\mathsf{L}}_{\mathcal{F}_\mathrm{c}}$ is non-conforming), but functions in $P_{\mathcal{F}}(\mathrm{c})$ are sufficiently smooth to apply the local de Rham map $\mathsf{R}_{\mathcal{F}_\mathrm{c}}$ on them.

The starting point for analyzing the cell-based scheme (8.34) using reconstruction operators is the following identity for each cell $\mathrm{c} \in \mathrm{C}$:

$$[\![\boldsymbol{\phi}_1, \mathsf{H}_{\kappa^{-1}}^{\mathcal{F}_\mathrm{c}\tilde{\mathcal{E}}_\mathrm{c}}(\boldsymbol{\phi}_2)]\!]_{\mathcal{F}_\mathrm{c}\tilde{\mathcal{E}}_\mathrm{c}} = \int_\mathrm{c} \underline{\mathsf{L}}_{\mathcal{F}_\mathrm{c}}(\boldsymbol{\phi}_1) \cdot \underline{\underline{\kappa}}^{-1} \underline{\mathsf{L}}_{\mathcal{F}_\mathrm{c}}(\boldsymbol{\phi}_2), \qquad \forall \boldsymbol{\phi}_1, \boldsymbol{\phi}_2 \in \mathcal{F}_\mathrm{c}. \quad (8.49)$$

Lemma 8.22 (Error estimate in energy norms on reconstructed gradient and flux)**.** *Assume that the mesh sequence is of class* **(MR)** *and* **(MB)**. *Assume that primal faces are planar. Assume that* $\underline{\mathtt{L}}_{\mathcal{F}_\mathrm{c}}$ *satisfies* (**R1**), (**R2**), *and* (**R3**) *for each cell* $\mathrm{c} \in \mathrm{C}$. *Let* $\underline{g}$ *be the exact gradient and* $\underline{\phi}$ *the exact flux. Assume* $\underline{g} \in [H^1(\mathrm{C})]^3$, $\underline{\phi} \in [H^1(\mathrm{C})]^3 \cap S_{\mathcal{F}}(\Omega)$. *Let* $\mathbf{g}$ *be the discrete gradient and* $\boldsymbol{\phi}$ *the discrete flux resulting from* (8.34). *Then, letting* $\underline{\mathtt{L}}_{\widetilde{\mathcal{E}}}(\mathbf{g}) := -\underline{\underline{\kappa}}^{-1}\underline{\mathtt{L}}_{\mathcal{F}}(\boldsymbol{\phi})$,

$$\|\underline{g} - \underline{\mathtt{L}}_{\widetilde{\mathcal{E}}}(\mathbf{g})\|_\kappa = \|\underline{\phi} - \underline{\mathtt{L}}_{\mathcal{F}}(\boldsymbol{\phi})\|_{\kappa^{-1}} \lesssim h(\kappa_\sharp^{1/2}\|\underline{g}\|_{[H^1(\mathrm{C})]^3} + \kappa_\flat^{-1/2}\|\underline{\phi}\|_{[H^1(\mathrm{C})]^3}). \tag{8.50}$$

Proof. The proof follows the same lines as the proof of Lemma 8.11 (use Proposition 7.22 and Theorem 8.20). □

L^2-error estimate. For simplicity, we assume in this paragraph that $\underline{\underline{\kappa}}$ is the identity tensor. Moreover, we assume a fully barycentric subdivision. The proof of our L^2-error estimate proceeds somewhat differently than that for the vertex-based scheme; herein, we consider the conforming flux reconstruction $\underline{\mathtt{L}}_{\mathcal{F}}^{\mathrm{conf}}$ defined in Section 7.3.3 and whose properties are stated in Lemmata 7.43 and 7.44. Recall that $\mathtt{L}_{\mathcal{C}} : \mathcal{C} \to L^2(\Omega)$ reconstructs cellwise constant functions on the primal mesh with $\mathtt{L}_{\mathcal{C}}(\mathbf{s})|_\mathrm{c} = |\mathrm{c}|^{-1}\mathbf{s}_\mathrm{c}$ for all $\mathrm{c} \in \mathrm{C}$ and for all $\mathbf{s} \in \mathcal{C}$; and $\mathtt{L}_{\widetilde{\mathcal{V}}}^0$ reconstructs cellwise constant functions on the primal mesh with $\mathtt{L}_{\widetilde{\mathcal{V}}}^0(\mathbf{p})|_\mathrm{c} = \mathbf{p}_{\tilde{\mathrm{v}}(\mathrm{c})}$ for all $\mathrm{c} \in \mathrm{C}$ and all $\mathbf{p} \in \widetilde{\mathcal{V}}$. Reconstruction operators $\mathtt{L}_{\mathcal{C}}$ and $\mathtt{L}_{\widetilde{\mathcal{V}}}^0$ clearly satisfy the four properties (**R1**)–(**R4**).

We now turn to the main result of this section; note that the L^2-error estimate is established with respect to the mean-value of the exact potential on primal cells, as is classical in mixed FE and cell-centered FV schemes. We also underline that the next result applies to all cell-based schemes built with a discrete Hodge operator $\mathsf{H}_{\kappa^{-1}}^{\mathcal{F}\widetilde{\mathcal{E}}}$ defined from a reconstruction operator $\underline{\mathtt{L}}_{\mathcal{F}}$ satisfying (**R1**), (**R2**), and (**R3**).

Theorem 8.23. *Assume that the mesh sequence is of class* **(MR)** *and* **(MB)** *with a fully barycentric subdivision. Assume that primal faces are planar. Assume that the model problem* (8.1) *with* $\underline{\underline{\kappa}} = \underline{\underline{\mathsf{Id}}}$ *has elliptic regularity. Assume* $s \in H^1(\Omega)$. *Let* p *be the exact potential and let* $\mathbf{p}$ *be the discrete potential resulting from* (8.34). *Assume that* $p \in H^2(\Omega)$. *Then,*

$$\|\mathtt{L}_{\mathcal{C}}\mathsf{R}_{\mathcal{C}}(p) - \mathtt{L}_{\widetilde{\mathcal{V}}}^0(\mathbf{p})\|_{L^2(\Omega)} \lesssim h^2\left(\|p\|_{H^2(\Omega)} + \|s\|_{H^1(\Omega)}\right). \tag{8.51}$$

Proof. Let $\underline{\phi}$ be the exact flux and $\boldsymbol{\phi}$ the discrete flux. Let $\zeta \in H^2(\Omega) \cap H_0^1(\Omega)$ solve the model problem (8.1) with source $\mathtt{L}_{\mathcal{C}}\mathsf{R}_{\mathcal{C}}(p) - \mathtt{L}_{\widetilde{\mathcal{V}}}^0(\mathbf{p})$. Let $\underline{\phi}^\zeta$ be the flux of ζ. We observe that

$$\|\mathtt{L}_{\mathcal{C}}\mathsf{R}_{\mathcal{C}}(p) - \mathtt{L}_{\widetilde{\mathcal{V}}}^0(\mathbf{p})\|_{L^2(\Omega)}^2 = \int_\Omega \left(\mathtt{L}_{\mathcal{C}}\mathsf{R}_{\mathcal{C}}(p) - \mathtt{L}_{\widetilde{\mathcal{V}}}^0(\mathbf{p})\right) \cdot \mathrm{div}(\underline{\phi}^\zeta).$$

Using the adjunction of $-\widetilde{\mathsf{GRAD}}$ and DIV (Proposition 3.16), the fact that $\widetilde{\mathsf{GRAD}}(\mathbf{p}) = -\mathsf{H}_{\kappa^{-1}}^{\mathcal{F}\widetilde{\mathcal{E}}}(\boldsymbol{\phi})$, and the definition (7.16) of the discrete Hodge operator, we infer that

$$\int_\Omega \mathtt{L}_{\widetilde{\mathcal{V}}}^0(\mathbf{p})\,\mathrm{div}(\underline{\phi}^\zeta) = [\![\mathbf{p}, \mathsf{R}_{\mathcal{C}}(\mathrm{div}\,\underline{\phi}^\zeta)]\!]_{\widetilde{\mathcal{V}}\mathcal{C}} = [\![\mathbf{p}, \mathsf{DIV}(\mathsf{R}_{\mathcal{F}}(\underline{\phi}^\zeta))]\!]_{\widetilde{\mathcal{V}}\mathcal{C}} = \int_\Omega \mathtt{L}_{\mathcal{F}}(\boldsymbol{\phi}) \cdot \underline{\mathtt{A}}_{\mathcal{F}}(\underline{\phi}^\zeta).$$

Observing that $\mathtt{L}_{\mathcal{C}}\mathsf{R}_{\mathcal{C}}(p)|_\mathrm{c} = |\mathrm{c}|^{-1}\int_\mathrm{c} p$ yields $\int_\Omega \mathtt{L}_{\mathcal{C}}\mathsf{R}_{\mathcal{C}}(p)\,\mathrm{div}(\underline{\phi}^\zeta) = \int_\Omega p\mathtt{L}_{\mathcal{C}}\mathsf{R}_{\mathcal{C}}(\mathrm{div}(\underline{\phi}^\zeta))$. Then, owing to the commuting property with de Rham maps (cf. Proposition 3.13) and the commuting property of $\underline{\mathtt{L}}_{\mathcal{F}}^{\mathrm{conf}}$ (cf. Lemma 7.44(iii)), we infer that

$$\int_\Omega p\mathtt{L}_{\mathcal{C}}\mathsf{R}_{\mathcal{C}}(\mathrm{div}(\underline{\phi}^\zeta)) = \int_\Omega p\mathtt{L}_{\mathcal{C}}(\mathsf{DIV}(\mathsf{R}_{\mathcal{F}}(\underline{\phi}^\zeta))) = \int_\Omega p\,\mathrm{div}(\mathtt{L}_{\mathcal{F}}^{\mathrm{conf}}(\mathsf{R}_{\mathcal{F}}(\underline{\phi}^\zeta))) = \int_\Omega p\,\mathrm{div}(\underline{\mathtt{A}}_{\mathcal{F}}^{\mathrm{conf}}(\underline{\phi}^\zeta)),$$

so that $\int_\Omega p\mathtt{L}_{\mathcal{C}}(\mathsf{R}_{\mathcal{C}}(\mathrm{div}\,\underline{\phi}^\zeta)) = \int_\Omega \underline{\phi} \cdot \underline{\mathtt{A}}_{\mathcal{F}}^{\mathrm{conf}}(\underline{\phi}^\zeta)$ using integration by parts. As a result,

$$\|\mathtt{L}_{\mathcal{C}}\mathsf{R}_{\mathcal{C}}(p) - \mathtt{L}_{\widetilde{\mathcal{V}}}^0(\mathbf{p})\|_{L^2(\Omega)}^2 = \int_\Omega \underline{\phi} \cdot \underline{\mathtt{A}}_{\mathcal{F}}^{\mathrm{conf}}(\underline{\phi}^\zeta) - \int_\Omega \mathtt{L}_{\mathcal{F}}(\boldsymbol{\phi}) \cdot \underline{\mathtt{A}}_{\mathcal{F}}(\underline{\phi}^\zeta),$$

Splitting the last identity into four terms yields

$$\begin{aligned}\|\mathsf{L}_{\mathcal{C}}\mathsf{R}_{\mathcal{C}}(p)-\mathsf{L}^0_{\widetilde{\mathcal{V}}}(\mathbf{p})\|^2_{L^2(\Omega)} &= \int_\Omega \underline{\phi}\cdot(\underline{\mathtt{A}}^{\mathrm{conf}}_{\mathcal{F}}-\underline{\mathtt{A}}_{\mathcal{F}})(\underline{\phi}^\zeta)-\int_\Omega(\underline{\phi}-\underline{\mathtt{L}}_{\mathcal{F}}(\boldsymbol{\phi}))\cdot(\underline{\phi}^\zeta-\underline{\mathtt{A}}_{\mathcal{F}}(\underline{\phi}^\zeta))\\ &\quad+\int_\Omega(\underline{\mathtt{L}}^{\mathrm{conf}}_{\mathcal{F}}-\underline{\mathtt{L}}_{\mathcal{F}})(\boldsymbol{\phi})\cdot\underline{\phi}^\zeta+\int_\Omega(\underline{\phi}-\underline{\mathtt{L}}^{\mathrm{conf}}_{\mathcal{F}}(\boldsymbol{\phi}))\cdot\underline{\phi}^\zeta\\ &= T_1+T_2+T_3+T_4.\end{aligned}$$

T_1 and T_3 are bounded as in the proof of Theorem 8.13. T_2 is bounded using (8.50) and (7.26). Turning to T_4, using integration by parts, Lemma 7.44(iii) and the cell-based scheme (8.34), yields

$$\begin{aligned}T_4 &= \int_\Omega \operatorname{div}(\underline{\phi}-\underline{\mathtt{L}}^{\mathrm{conf}}_{\mathcal{F}}(\boldsymbol{\phi}))\zeta=\int_\Omega(\operatorname{div}\underline{\phi}-\mathsf{L}_{\mathcal{C}}(\mathsf{DIV}(\boldsymbol{\phi})))\zeta=\int_\Omega(s-\mathsf{L}_{\mathcal{C}}\mathsf{R}_{\mathcal{C}}(s))\zeta\\ &=\int_\Omega(s-\mathsf{L}_{\mathcal{C}}\mathsf{R}_{\mathcal{C}}(s))(\zeta-\mathsf{L}^0_{\widetilde{\mathcal{V}}}\mathsf{R}_{\widetilde{\mathcal{V}}}(\zeta)),\end{aligned}$$

which is easily bounded since $s\in H^1(\Omega)$. We conclude the proof similarly to the proof of Theorem 8.13. □

8.2.3 Link with existing schemes

Link with classical schemes on specific meshes. Using the reconstruction functions $\{\underline{\ell}^{\mathrm{RTN}}_{\mathrm{f}}\}_{\mathrm{f}\in\mathrm{F}}$ on simplicial meshes defined in Section 7.2.1, the cell-based scheme (8.34) then coincides with the classical lowest-order mixed FE approximation on the primal mesh (up to a quadrature on the source term).

Link with MFD schemes. We show in this section that the (mixed) cell-based CDO schemes fit the family of MFD schemes analyzed by Brezzi *et al.* (2005). We first translate the quantities used in MFD schemes in our notation. In MFD, the space associated to the flux is denoted by X^d and that associated to the potential Q^d. The relation between the DoFs related to the flux is

$$\forall\boldsymbol{\phi}\in\mathcal{F},\qquad \boldsymbol{\phi}^{\mathtt{MFD}}_{\mathrm{c,f}}:=\frac{\iota_{\mathrm{f,c}}\boldsymbol{\phi}_{\mathrm{f}}}{|\mathrm{f}|},\qquad\forall\mathrm{c}\in\mathrm{C},\,\forall\mathrm{f}\in\mathrm{F}_{\mathrm{c}}. \tag{8.52a}$$

In MFD schemes, the DoFs related to the potential are defined as follows:

$$\forall\hat{\mathbf{p}}\in\mathcal{C},\qquad \mathbf{p}^{\mathtt{MFD}}:=\mathsf{H}_1^{\mathcal{C}\widetilde{\mathcal{V}}}(\hat{\mathbf{p}}), \tag{8.52b}$$

where $\mathsf{H}_1^{\mathcal{C}\widetilde{\mathcal{V}}}$ is a diagonal discrete Hodge operator of size #C with entries equal to $|\mathrm{c}|^{-1}$. The discrete divergence operators used in MFD schemes and CDO schemes are linked as follows:

$$\mathsf{DIV}^{\mathtt{MFD}}(\boldsymbol{\phi}^{\mathtt{MFD}})|_{\mathrm{c}}:=\frac{1}{|\mathrm{c}|}\mathsf{DIV}(\boldsymbol{\phi}),\qquad\forall\mathrm{c}\in\mathrm{C},\,\forall\boldsymbol{\phi}\in\mathcal{F}. \tag{8.52c}$$

Moreover, the two MFD scalar products $[\cdot,\cdot]_{X^d}$ for the DoFs related to the flux and $[\cdot,\cdot]_{Q^d}$ for the DoFs related to the potential correspond in our notation to

$$\begin{aligned}[\mathbf{p}^{\mathtt{MFD}},\mathbf{q}^{\mathtt{MFD}}]_{Q^d}&:=[\![\hat{\mathbf{p}},\mathsf{H}_1^{\mathcal{C}\widetilde{\mathcal{V}}}(\hat{\mathbf{q}})]\!]_{\mathcal{C}\widetilde{\mathcal{V}}},&&\forall\hat{\mathbf{p}},\hat{\mathbf{q}}\in\mathcal{C}.\\ [\boldsymbol{\phi}^{\mathtt{MFD}},\boldsymbol{\sigma}^{\mathtt{MFD}}]_{X^d}&:=[\![\boldsymbol{\phi},\mathsf{H}^{\mathcal{F}\widetilde{\mathcal{E}}}_{\kappa^{-1}}(\boldsymbol{\sigma})]\!]_{\mathcal{F}\widetilde{\mathcal{E}}},&&\forall\boldsymbol{\phi},\boldsymbol{\sigma}\in\mathcal{F}.\end{aligned} \tag{8.52d}$$

The MFD system defined in (Brezzi *et al.*, 2005, eq. (4.1) and (4.2)) corresponds to: Find $(\boldsymbol{\phi}^{\mathtt{MFD}},\mathbf{p}^{\mathtt{MFD}})\in X^d\times Q^d$ such that

$$\begin{cases}[\boldsymbol{\phi}^{\mathtt{MFD}},\boldsymbol{\sigma}^{\mathtt{MFD}}]_{X^d}-[\mathbf{p}^{\mathtt{MFD}},\mathsf{DIV}^{\mathtt{MFD}}(\boldsymbol{\sigma}^{\mathtt{MFD}})]_{Q^d}=0, & \forall\boldsymbol{\sigma}^{\mathtt{MFD}}\in X^d,\\ [\mathsf{DIV}^{\mathtt{MFD}}(\boldsymbol{\phi}^{\mathtt{MFD}}),\mathbf{q}^{\mathtt{MFD}}]_{Q^d}=[\mathbf{s}^{\mathtt{MFD}},\mathbf{q}^{\mathtt{MFD}}]_{Q^d}, & \forall\mathbf{q}^{\mathtt{MFD}}\in Q^d,\end{cases} \tag{8.53}$$

where $\mathbf{s}^{\mathtt{MFD}}\in Q^d$ is the discretization of the source term.

Proposition 8.24 (Link with MFD schemes)**.** *Assume that the mesh is of class* **(MR)** *and* **(MB)** *with a fully barycentric subdivision. Assume that the discrete Hodge operators* $\mathsf{H}_{\kappa^{-1}}^{\mathcal{F}_c\tilde{\mathcal{E}}_c}$ *satisfy the three properties* (**H0**)*,* (**H1**)*, and* (**H2**) *for all* $c \in C$*. Let* $\mathsf{H}_1^{\mathcal{C}\tilde{\mathcal{V}}}$ *be the diagonal discrete Hodge operator with entries equal to* $|c|^{-1}$ *for all* $c \in C$*. Then, the MFD system* (8.53) *is equivalent to the CDO system* (8.35)*. Moreover, the stability property* (S_1) *and the consistency property* (S_2) *of MFD schemes (Brezzi* et al.*, 2005, eq. (3.10) and (5.1)) are verified.*

Proof. Using (8.52), (8.53) can be recast as follows: Find $(\boldsymbol{\phi}, \hat{\mathbf{p}}) \in \mathcal{F} \times \mathcal{C}$ such that

$$\begin{cases} [\![\boldsymbol{\sigma}, \mathsf{H}_{\kappa^{-1}}^{\mathcal{F}\tilde{\mathcal{E}}}(\boldsymbol{\phi})]\!]_{\mathcal{F}\tilde{\mathcal{E}}} - [\![\mathsf{DIV}(\boldsymbol{\sigma}), \mathsf{H}_1^{\mathcal{C}\tilde{\mathcal{V}}}(\hat{\mathbf{p}})]\!]_{\mathcal{C}\tilde{\mathcal{V}}} = 0, & \forall \boldsymbol{\sigma} \in \mathcal{F}, \\ [\![\mathsf{DIV}(\boldsymbol{\phi}), \mathsf{H}_1^{\mathcal{C}\tilde{\mathcal{V}}}(\hat{\mathbf{q}})]\!]_{\mathcal{C}\tilde{\mathcal{V}}} = [\![\mathsf{R}_{\mathcal{C}}(s), \mathsf{H}_1^{\mathcal{C}\tilde{\mathcal{V}}}(\hat{\mathbf{q}})]\!]_{\mathcal{C}\tilde{\mathcal{V}}}, & \forall \hat{\mathbf{q}} \in \mathcal{C}, \end{cases} \tag{8.54}$$

with the source term s defined as in the CDO cell-based system (8.35). Then, starting from (8.54), the equivalence between the MFD and CDO system is straightforward since $\mathsf{H}_1^{\mathcal{C}\tilde{\mathcal{V}}}$ is an isomorphism between $\mathcal{C}$ and $\widetilde{\mathcal{V}}$.

(S_1) is a consequence of the mesh regularity and (**H1**). In each cell $c \in C$, recalling that we consider a piecewise constant material property on the primal mesh, (S_2) corresponds in our notation to

$$[\![\boldsymbol{\phi}, \mathsf{H}_{\kappa^{-1}}^{\mathcal{F}_c\tilde{\mathcal{E}}_c} \cdot \mathsf{R}_{\mathcal{F}_c}(\underline{\underline{\kappa}}\, \underline{\mathrm{grad}}(q^1))]\!]_{\mathcal{F}_c\tilde{\mathcal{E}}_c} = \sum_{f \in F_c} \boldsymbol{\phi}^{\mathtt{MFD}} q^1 - \int_c q^1 \mathsf{DIV}^{\mathtt{MFD}}(\boldsymbol{\phi}^{\mathtt{MFD}}), \tag{8.55}$$

for all $q^1 \in \mathbb{P}_1(c)$. The identity (8.55) holds since

$$\begin{aligned} [\![\boldsymbol{\phi}, \mathsf{H}_{\kappa^{-1}}^{\mathcal{F}_c\tilde{\mathcal{E}}_c} \cdot \mathsf{R}_{\mathcal{F}_c}(\underline{\underline{\kappa}}\, \underline{\mathrm{grad}}(q^1))]\!]_{\mathcal{F}_c\tilde{\mathcal{E}}_c} &= [\![\boldsymbol{\phi}, \mathsf{R}_{\tilde{\mathcal{E}}_c}(\underline{\mathrm{grad}}(q^1))]\!]_{\mathcal{F}_c\tilde{\mathcal{E}}_c} && \text{by (H2)}, \\ &= \sum_{f \in F_c} \boldsymbol{\phi}_f \int_{\tilde{e}_c(f)} \underline{\mathrm{grad}}(q^1) \cdot \underline{\tau}_{\tilde{e}_c(f)} && \text{by definition}, \\ &= \sum_{f \in F_c} \boldsymbol{\phi}_f \iota_{f,c} \left(q^1(\underline{x}_f) - q^1(\underline{x}_c) \right) && \text{by (5.8)}, \\ &= \sum_{f \in F_c} \int_f \frac{\iota_{f,c}\boldsymbol{\phi}_f}{|f|} q^1 - \int_c q^1 \frac{1}{|c|} \sum_{f \in F_c} \iota_{f,c}\boldsymbol{\phi}_f \\ &= \sum_{f \in F_c} \int_f \boldsymbol{\phi}^{\mathtt{MFD}} q^1 - \int_c \mathsf{DIV}^{\mathtt{MFD}}(\boldsymbol{\phi}^{\mathtt{MFD}}), \end{aligned}$$

where we have used that q^1 is linear, $\underline{x}_f$ is the barycenter of f, and $\underline{x}_c$ is the barycenter of c (this is where the fully barycentric subdivision is needed). The last identity results from (8.52b), (8.52a), and (8.52c). □

Since (S_1) and (S_2) are satisfied, we recover the analysis derived in Brezzi *et al.* (2005). As a consequence, cell-based schemes fit the HMM framework derived by Droniou *et al.* (2010).

8.3 Hybridization of cell-based schemes

The hybridization of mixed systems is a classical technique (see, for instance, Arnold & Brezzi (1985) and Brezzi & Fortin (1991)) to circumvent the saddle-point formulation arising from the mixed formulation and recover a SPD system which can be solved more efficiently.

8.3.1 Mixed hybrid cell-based schemes

Hybridization consists of an exact algebraic reformulation of the cell-based scheme (8.34) by using two new discrete linear spaces, one related to the discrete fluxes denoted by $\hat{\mathcal{F}}$, and another one related to the discrete potential denoted by $\widetilde{\mathcal{L}}$ whose elements act as Lagrange

multipliers to ensure flux continuity between two adjacent cells. The linear space $\hat{\mathcal{F}}$ collects the fluxes across faces of the primal mesh as $\mathcal{F}$ but, contrary to $\mathcal{F}$, two fluxes are defined for each interior face $\mathrm{f} \in \mathrm{F}^{\mathrm{I}}$ (one for each cell $\mathrm{c} \in \mathrm{C}_{\mathrm{f}}$). Thus, the dimension of the linear space $\hat{\mathcal{F}}$ is $2\#\mathrm{F}^{\mathrm{I}} + \#\mathrm{F}^{\mathrm{B}}$. The linear space $\widetilde{\mathcal{L}}$ can be viewed as collecting the values of the potential at the barycenter of each face $\mathrm{f} \in \mathrm{F}$. Since we consider homogeneous Dirichlet BCs, the value at each boundary face $\mathrm{f} \in \mathrm{F}^{\mathrm{B}}$ of an element of $\widetilde{\mathcal{L}}$ is set to 0. Thus, $\widetilde{\mathcal{L}}$ is a subspace of $\mathbb{R}^{\#\mathrm{F}}$ isomorphic to $\mathbb{R}^{\#\mathrm{F}^{\mathrm{I}}}$.

In what follows, it is useful to localize DoFs to a given cell $\mathrm{c} \in \mathrm{C}$. For all $\hat{\boldsymbol{\phi}} \in \hat{\mathcal{F}}$, $\hat{\boldsymbol{\phi}}_{\mathrm{c}} \in \mathcal{F}_{\mathrm{c}}$ collects all the components of $\hat{\boldsymbol{\phi}}$ attached to the faces $\mathrm{f} \in \mathrm{F}_{\mathrm{c}}$, and we denote by $\hat{\boldsymbol{\phi}}_{\mathrm{c,f}}$ the component of $\hat{\boldsymbol{\phi}}$ attached to the cell $\mathrm{c} \in \mathrm{C}$ and to the face $\mathrm{f} \in \mathrm{F}_{\mathrm{c}}$, *i.e.* $\hat{\boldsymbol{\phi}}_{\mathrm{c}} := \{\hat{\boldsymbol{\phi}}_{\mathrm{c,f}}\}_{\mathrm{f}\in\mathrm{F}_{\mathrm{c}}}$. Similarly, $\boldsymbol{\lambda}_{\mathrm{c}} \in \widetilde{\mathcal{L}}_{\mathrm{c}}$ collects all the components of $\boldsymbol{\lambda} \in \widetilde{\mathcal{L}}$ attached to the faces $\mathrm{f} \in \mathrm{F}_{\mathrm{c}}$, *i.e.* $\boldsymbol{\lambda}_{\mathrm{c}} := \{\boldsymbol{\lambda}_{\mathrm{f}}\}_{\mathrm{f}\in\mathrm{F}_{\mathrm{c}}}$. We also use the notation $\mathcal{C}_{\mathrm{c}}$ and $\widetilde{\mathcal{V}}_{\mathrm{c}}$ for the one-dimensional spaces of DoFs attached to c and $\tilde{\mathrm{v}}(\mathrm{c})$. Observe that

$$\hat{\mathcal{F}} = \bigtimes_{\mathrm{c}\in\mathrm{C}} \hat{\mathcal{F}}_{\mathrm{c}} \qquad \text{and} \qquad \widetilde{\mathcal{V}} = \bigtimes_{\mathrm{c}\in\mathrm{C}} \widetilde{\mathcal{V}}_{\mathrm{c}}. \tag{8.56}$$

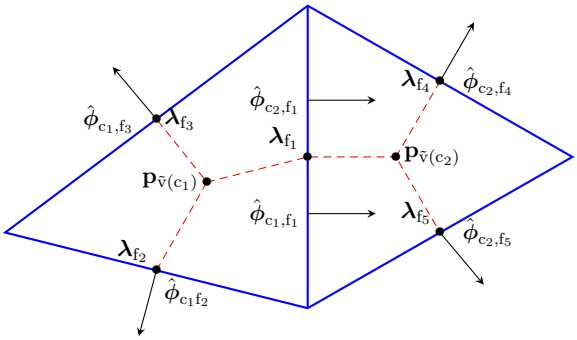

Figure 8.4 – Positionning of DoFs within the hybrid formulation.

Discrete system. The discrete system related to the hybrid formulation of (8.34) is defined as follows: Find $(\hat{\boldsymbol{\phi}}, \mathbf{p}, \boldsymbol{\lambda}) \in \hat{\mathcal{F}} \times \widetilde{\mathcal{V}} \times \mathcal{L}$ such that

$$\begin{cases} \mathsf{H}_{\kappa^{-1}}^{\mathcal{F}_{\mathrm{c}}\widetilde{\mathcal{E}}_{\mathrm{c}}}(\hat{\boldsymbol{\phi}}_{\mathrm{c}}) + \widetilde{\mathsf{G}}_{\mathrm{c}}^{\mathrm{Hy}}(\mathbf{p}_{\mathrm{c}}, \boldsymbol{\lambda}_{\mathrm{c}}) = 0_{\widetilde{\mathcal{E}}_{\mathrm{c}}} \\ \mathsf{DIV}_{\mathrm{c}}(\hat{\boldsymbol{\phi}}_{\mathrm{c}}) = \mathsf{R}_{\mathcal{C}}(s)|_{\mathrm{c}} \end{cases} \qquad \text{for all } \mathrm{c} \in \mathrm{C}, \tag{8.57a}$$

and

$$\sum_{\mathrm{c}\in\mathrm{C}_{\mathrm{f}}} \iota_{\mathrm{f,c}} \hat{\boldsymbol{\phi}}_{\mathrm{c,f}} = 0, \qquad \forall \mathrm{f} \in \mathrm{F}^{\mathrm{I}}. \tag{8.57b}$$

In (8.57a), $\mathsf{DIV}_{\mathrm{c}} : \mathcal{F}_{\mathrm{c}} \to \mathcal{C}_{\mathrm{c}}$ is simply defined as the restriction to a cell $\mathrm{c} \in \mathrm{C}$ of DIV and $\widetilde{\mathsf{G}}_{\mathrm{c}}^{\mathrm{Hy}} : \widetilde{\mathcal{V}}_{\mathrm{c}} \times \widetilde{\mathcal{L}}_{\mathrm{c}} \to \widetilde{\mathcal{E}}_{\mathrm{c}}$ is defined as follows:

$$\widetilde{\mathsf{G}}_{\mathrm{c}}^{\mathrm{Hy}}(\mathbf{p}, \boldsymbol{\lambda})|_{\tilde{\mathrm{e}}_{\mathrm{c}}(\mathrm{f})} = \iota_{\mathrm{f,c}}(\boldsymbol{\lambda}_{\mathrm{f}} - \mathbf{p}_{\tilde{\mathrm{v}}(\mathrm{c})}), \qquad \forall \mathrm{f} \in \mathrm{F}_{\mathrm{c}}. \tag{8.58}$$

The discrete system (8.57) consists of a collection of local discrete problems (8.57a) in each cell $\mathrm{c} \in \mathrm{C}$ and of equations enforcing the flux continuity across each interior face $\mathrm{f} \in \mathrm{F}^{\mathrm{I}}$.

Definition 8.25 (Local face-based product)**.** *For each cell* $\mathrm{c} \in \mathrm{C}$*, we introduce a local product defined as follows:*

$$\langle\!\langle \mathbf{a}\,,\, \mathbf{b} \rangle\!\rangle_{\mathcal{F}_{\mathrm{c}}\widetilde{\mathcal{L}}_{\mathrm{c}}} := \sum_{\mathrm{f}\in\mathrm{F}_{\mathrm{c}}} \iota_{\mathrm{f,c}} \mathbf{a}_{\mathrm{f}} \mathbf{b}_{\mathrm{f}}, \qquad \forall (\mathbf{a}, \mathbf{b}) \in \mathcal{F}_{\mathrm{c}} \times \widetilde{\mathcal{L}}_{\mathrm{c}}. \tag{8.59}$$

Proposition 8.26 (Adjunction). *Let* $\mathrm{c} \in \mathrm{C}$. *For all* $\hat{\boldsymbol{\phi}} \in \hat{\mathcal{F}}_\mathrm{c}$, *all* $\mathbf{p} \in \widetilde{\mathcal{V}}_\mathrm{c}$ *and all* $\boldsymbol{\lambda} \in \widetilde{\mathcal{L}}_\mathrm{c}$, *the following identity holds:*

$$[\![\hat{\boldsymbol{\phi}}, \widetilde{\mathsf{G}}_\mathrm{c}^{\mathrm{Hy}}(\mathbf{p}, \boldsymbol{\lambda})]\!]_{\mathcal{F}_\mathrm{c}\widetilde{\mathcal{E}}_\mathrm{c}} = -[\![\mathsf{DIV}_\mathrm{c}(\hat{\boldsymbol{\phi}}), \mathbf{p}]\!]_{\mathcal{C}_\mathrm{c}\widetilde{\mathcal{V}}_\mathrm{c}} + \langle\!\langle \hat{\boldsymbol{\phi}}\,,\, \boldsymbol{\lambda} \rangle\!\rangle_{\mathcal{F}_\mathrm{c}\widetilde{\mathcal{L}}_\mathrm{c}}, \tag{8.60}$$

where $[\![\cdot,\cdot]\!]_{\mathcal{C}_\mathrm{c}\widetilde{\mathcal{V}}_\mathrm{c}}$ *simply denotes the product of two real numbers.*

Proof. The result follows from the fact that $[\![\hat{\boldsymbol{\phi}}, \widetilde{\mathsf{G}}_\mathrm{c}^{\mathrm{Hy}}(\mathbf{p}, \boldsymbol{\lambda})]\!]_{\mathcal{F}_\mathrm{c}\widetilde{\mathcal{E}}_\mathrm{c}} = \sum_{\mathrm{f}\in\mathrm{F}_\mathrm{c}} \hat{\boldsymbol{\phi}}_{\mathrm{c,f}} \iota_{\mathrm{f,c}}(\boldsymbol{\lambda}_\mathrm{f} - \mathbf{p}_{\tilde{\mathrm{v}}(\mathrm{c})})$ and $\mathsf{DIV}_\mathrm{c}(\hat{\boldsymbol{\phi}}) = \sum_{\mathrm{f}\in\mathrm{F}_\mathrm{c}} \iota_{\mathrm{f,c}} \hat{\boldsymbol{\phi}}_{\mathrm{c,f}}$. □

Proposition 8.27 (Variational hybrid scheme). *The variational formulation of* (8.57) *is: Find* $(\hat{\boldsymbol{\phi}}, \mathbf{p}, \boldsymbol{\lambda}) \in \hat{\mathcal{F}} \times \widetilde{\mathcal{V}} \times \widetilde{\mathcal{L}}$ *such that*

$$\sum_{\mathrm{c}\in\mathrm{C}} [\![\hat{\boldsymbol{\sigma}}_\mathrm{c}, \mathsf{H}_{\kappa^{-1}}^{\mathcal{F}_\mathrm{c}\widetilde{\mathcal{E}}_\mathrm{c}}(\hat{\boldsymbol{\phi}}_\mathrm{c})]\!]_{\mathcal{F}_\mathrm{c}\widetilde{\mathcal{E}}_\mathrm{c}} - \sum_{\mathrm{c}\in\mathrm{C}} [\![\mathsf{DIV}_\mathrm{c}(\hat{\boldsymbol{\sigma}}_\mathrm{c}), \mathbf{p}_\mathrm{c}]\!]_{\mathcal{C}_\mathrm{c}\widetilde{\mathcal{V}}_\mathrm{c}} + \sum_{\mathrm{c}\in\mathrm{C}} \langle\!\langle \hat{\boldsymbol{\sigma}}_\mathrm{f}\,,\, \boldsymbol{\lambda}_\mathrm{c} \rangle\!\rangle_{\mathcal{F}_\mathrm{c}\widetilde{\mathcal{L}}_\mathrm{c}} = 0, \quad \forall \hat{\boldsymbol{\sigma}} \in \hat{\mathcal{F}}, \tag{8.61a}$$

$$\sum_{\mathrm{c}\in\mathrm{C}} [\![\mathsf{DIV}_\mathrm{c}(\hat{\boldsymbol{\phi}}_\mathrm{c}), \mathbf{q}_\mathrm{c}]\!]_{\mathcal{C}_\mathrm{c}\widetilde{\mathcal{V}}_\mathrm{c}} = [\![\mathsf{R}_\mathcal{C}(s), \mathbf{q}]\!]_{\mathcal{C}_\mathrm{c}\widetilde{\mathcal{V}}_\mathrm{c}}, \qquad \forall \mathbf{q} \in \widetilde{\mathcal{V}}, \tag{8.61b}$$

$$\sum_{\mathrm{c}\in\mathrm{C}} \langle\!\langle \hat{\boldsymbol{\phi}}_\mathrm{c}\,,\, \boldsymbol{\mu}_\mathrm{c} \rangle\!\rangle_{\mathcal{F}_\mathrm{c}\widetilde{\mathcal{L}}_\mathrm{c}} = 0, \qquad \forall \boldsymbol{\mu} \in \widetilde{\mathcal{L}}. \tag{8.61c}$$

Proof. For each cell $\mathrm{c} \in \mathrm{C}$, the variational form of (8.57a) is the following system:

$$\begin{cases} [\![\hat{\boldsymbol{\sigma}}_\mathrm{c}, \mathsf{H}_{\kappa^{-1}}^{\mathcal{F}_\mathrm{c}\widetilde{\mathcal{E}}_\mathrm{c}}(\hat{\boldsymbol{\phi}}_\mathrm{c})]\!]_{\mathcal{F}_\mathrm{c}\widetilde{\mathcal{E}}_\mathrm{c}} + [\![\hat{\boldsymbol{\sigma}}_\mathrm{c}, \widetilde{\mathsf{G}}_\mathrm{c}^{\mathrm{Hy}}(\mathbf{p}_\mathrm{c}, \boldsymbol{\lambda}_\mathrm{c})]\!]_{\mathcal{F}_\mathrm{c}\widetilde{\mathcal{E}}_\mathrm{c}} = 0, & \forall \hat{\boldsymbol{\sigma}}_\mathrm{c} \in \hat{\mathcal{F}}_\mathrm{c}, \\ [\![\mathsf{DIV}_\mathrm{c}(\hat{\boldsymbol{\phi}}_\mathrm{c}), \mathbf{q}_\mathrm{c}]\!]_{\mathcal{C}_\mathrm{c}\widetilde{\mathcal{V}}_\mathrm{c}} = [\![\mathsf{R}_\mathcal{C}(s)|_\mathrm{c}, \mathbf{q}_\mathrm{c}]\!]_{\mathcal{C}\widetilde{\mathcal{V}}}, & \forall \mathbf{q}_\mathrm{c} \in \widetilde{\mathcal{V}}_\mathrm{c}. \end{cases}$$

This is equivalent to (8.61a) and (8.61b) owing to (8.56) and using (8.60) in the first equation. Furthermore, (8.61c) implies (8.57b) by taking for each face $\mathrm{f} \in \mathrm{F}^\mathrm{I}$, $\boldsymbol{\mu}_\mathrm{f} = 1$ and $\boldsymbol{\mu}_{\mathrm{f}'} = 0$ if $\mathrm{f} \neq \mathrm{f}'$. Conversely, (8.57b) implies (8.61c). Indeed, for each $\boldsymbol{\mu} \in \widetilde{\mathcal{L}}$, multiply (8.57b) with $\boldsymbol{\mu}_\mathrm{f}$ and sum over interior faces to infer $\sum_{\mathrm{c}\in\mathrm{C}} \sum_{\mathrm{f}\in\mathrm{F}_\mathrm{c}^\mathrm{I}} \iota_{\mathrm{f,c}} \hat{\boldsymbol{\phi}}_{\mathrm{c,f}} \boldsymbol{\mu}_\mathrm{f} = 0$ which is equal to $\sum_{\mathrm{c}\in\mathrm{C}} \langle\!\langle \hat{\boldsymbol{\phi}}_\mathrm{c}\,,\, \boldsymbol{\mu}_\mathrm{c} \rangle\!\rangle_{\mathcal{F}_\mathrm{c}\widetilde{\mathcal{L}}_\mathrm{c}} = 0$ since $\boldsymbol{\mu}_\mathrm{f} = 0$ if $\mathrm{f} \in \mathrm{F}^\mathrm{B}$. □

Lemma 8.28 (Link hybrid → cell-based). *Let* $(\hat{\boldsymbol{\phi}}, \mathbf{p}, \boldsymbol{\lambda}) \in \hat{\mathcal{F}} \times \widetilde{\mathcal{V}} \times \widetilde{\mathcal{L}}$ *solve* (8.61). *Then, for all* $\mathrm{f} \in \mathrm{F}^\mathrm{I}$, *the value* $\hat{\boldsymbol{\phi}}_{\mathrm{c,f}}$ *is independent of* $\mathrm{c} \in \mathrm{C}_\mathrm{f}$. *Moreover, denoting* $\boldsymbol{\phi}_\mathrm{f}$ *this common value and defining* $\boldsymbol{\phi}_\mathrm{f} := \hat{\boldsymbol{\phi}}_{\mathrm{c,f}}$ *for all face* $\mathrm{f} \in \mathrm{F}^\mathrm{B}$ *where* c *is the unique cell in* C_f, $(\boldsymbol{\phi}, \mathbf{p}) \in \mathcal{F} \times \widetilde{\mathcal{V}}$ *solves* (8.34).

Proof. The flux continuity imposed in (8.61c) on $\hat{\boldsymbol{\phi}}$ defines a unique value $\boldsymbol{\phi}_\mathrm{f}$ for each face $\mathrm{f} \in \mathrm{F}^\mathrm{I}$. Testing (8.61a) with $\hat{\boldsymbol{\sigma}} \in \hat{\mathcal{F}}$ such that $\forall \mathrm{f} \in \mathrm{F}^\mathrm{I}$, $\sum_{\mathrm{c}\in\mathrm{C}_\mathrm{f}} \iota_{\mathrm{f,c}} \hat{\boldsymbol{\sigma}}_{\mathrm{f,c}} = 0$ (and, thus considering $\boldsymbol{\sigma} \in \mathcal{F}$ built from $\hat{\boldsymbol{\sigma}}$ as $\boldsymbol{\phi}$ is built from $\hat{\boldsymbol{\phi}}$) yields

$$\sum_{\mathrm{c}\in\mathrm{C}} [\![\mathsf{T}_{\mathrm{F,c}}(\boldsymbol{\sigma}), \mathsf{H}_{\kappa^{-1}}^{\mathcal{F}_\mathrm{c}\widetilde{\mathcal{E}}_\mathrm{c}}(\mathsf{T}_{\mathrm{F,c}}(\boldsymbol{\phi}))]\!]_{\mathcal{F}_\mathrm{c}\widetilde{\mathcal{E}}_\mathrm{c}} - \sum_{\mathrm{c}\in\mathrm{C}} [\![\mathsf{DIV}_\mathrm{c}(\mathsf{T}_{\mathrm{F,c}}(\boldsymbol{\sigma})), \mathbf{p}_\mathrm{c}]\!]_{\mathcal{C}_\mathrm{c}\widetilde{\mathcal{V}}_\mathrm{c}} = 0, \qquad \forall \boldsymbol{\sigma} \in \mathcal{F},$$

where we recall that $\mathsf{T}_{\mathrm{F,c}}$ denotes the full-rank map from global to local DoFs from $\mathcal{F}$ to $\mathcal{F}_\mathrm{c}$. Using (3.20), the fact that $\mathsf{DIV} := \sum_{\mathrm{c}\in\mathrm{C}} \mathsf{T}_{\mathrm{C,c}}^* \cdot \mathsf{DIV}_\mathrm{c} \cdot \mathsf{T}_{\mathrm{F,c}}$, and the adjunction between $-\widetilde{\mathsf{GRAD}}$ and DIV (cf. Proposition 3.16), we infer that

$$[\![\boldsymbol{\sigma}, \mathsf{H}_{\kappa^{-1}}^{\mathcal{F}\widetilde{\mathcal{E}}}(\boldsymbol{\phi})]\!]_{\mathcal{F}\widetilde{\mathcal{E}}} + [\![\boldsymbol{\sigma}, \widetilde{\mathsf{GRAD}}(\mathbf{p})]\!]_{\mathcal{F}\widetilde{\mathcal{E}}} = 0.$$

Moreover, we readily verify that (8.61b) yields $[\![\mathsf{DIV}(\boldsymbol{\phi}), \mathbf{q}]\!]_{\mathcal{C}\widetilde{\mathcal{V}}} = [\![\mathsf{R}_\mathcal{C}(s), \mathbf{q}]\!]_{\mathcal{C}\widetilde{\mathcal{V}}}$, for all $\mathbf{q} \in \widetilde{\mathcal{V}}$. Hence, $(\boldsymbol{\phi}, \mathbf{p})$ solves (8.34). □

Lemma 8.29 (Link cell-based → hybrid). *Let* $(\boldsymbol{\phi}, \mathbf{p}) \in \mathcal{F} \times \widetilde{\mathcal{V}}$ *solve* (8.34). *Then, there exists* $\boldsymbol{\lambda} \in \widetilde{\mathcal{L}}$ *such that, setting* $\hat{\boldsymbol{\phi}}_{\mathrm{c,f}} := \boldsymbol{\phi}_\mathrm{f}$ *for all* $\mathrm{c} \in \mathrm{C}$ *and all* $\mathrm{f} \in \mathrm{F}_\mathrm{c}$, $(\hat{\boldsymbol{\phi}}, \mathbf{p}, \boldsymbol{\lambda}) \in \hat{\mathcal{F}} \times \widetilde{\mathcal{V}} \times \widetilde{\mathcal{L}}$ *solves* (8.61).

Proof. By definition of $\hat{\boldsymbol{\phi}}$, the flux continuity is readily verified for each interior face $\mathrm{f} \in \mathrm{F}^{\mathrm{I}}$. Thus, (8.61c) holds. Since $(\boldsymbol{\phi}, \mathbf{p})$ solves (8.34), we infer that for each cell $\mathrm{c} \in \mathrm{C}$, $\mathsf{DIV}(\boldsymbol{\phi})|_{\mathrm{c}} = \mathsf{R}_{\mathcal{C}}(s)|_{\mathrm{c}}$. By definition, $\mathsf{DIV}(\boldsymbol{\phi})|_{\mathrm{c}} = \sum_{\mathrm{f}\in\mathrm{F}_{\mathrm{c}}} \iota_{\mathrm{f,c}}\boldsymbol{\phi}_{\mathrm{f}} = \sum_{\mathrm{f}\in\mathrm{F}_{\mathrm{c}}} \iota_{\mathrm{f,c}}\hat{\boldsymbol{\phi}}_{\mathrm{c,f}} = \mathsf{DIV}_{\mathrm{c}}(\hat{\boldsymbol{\phi}}_{\mathrm{c}})$. Thus, (8.61b) holds. Finally, we show that there is $\boldsymbol{\lambda} \in \widetilde{\mathcal{L}}$ such that, for each cell $\mathrm{c} \in \mathrm{C}$,

$$\mathsf{H}_{\kappa^{-1}}^{\mathcal{F}_{\mathrm{c}}\widetilde{\mathcal{E}}_{\mathrm{c}}}(\boldsymbol{\phi}_{\mathrm{c}}) + \widetilde{\mathsf{G}}_{\mathrm{c}}^{\mathrm{Hy}}(\mathbf{p}_{\mathrm{c}}, \boldsymbol{\lambda}_{\mathrm{c}}) = 0_{\widetilde{\mathcal{E}}_{\mathrm{c}}}. \tag{8.62}$$

(8.62) readily defines a collection of (possibly) multi-valued quantities $\boldsymbol{\lambda}_{\mathrm{c,f}}$ for all $\mathrm{c} \in \mathrm{C}$ and all $\mathrm{f} \in \mathrm{F}_{\mathrm{c}}$. Let us show that $\boldsymbol{\lambda}$ is single-valued on each interior face $\mathrm{f} \in \mathrm{F}^{\mathrm{I}}$. Summing (8.62) over cells and then considering a face $\mathrm{f} \in \mathrm{F}^{\mathrm{I}}$, we infer that

$$\mathsf{H}_{\kappa^{-1}}^{\mathcal{F}\widetilde{\mathcal{E}}}(\boldsymbol{\phi})|_{\tilde{\mathrm{e}}(\mathrm{f})} + \sum_{\mathrm{c}\in\mathrm{C}_{\mathrm{f}}} \widetilde{\mathsf{G}}_{\mathrm{c}}^{\mathrm{Hy}}(\mathbf{p}_{\mathrm{c}}, \boldsymbol{\lambda}_{\mathrm{c}}) = 0,$$

owing to (3.20). Since $\mathsf{H}_{\kappa^{-1}}^{\mathcal{F}\widetilde{\mathcal{E}}}(\boldsymbol{\phi}) = -\widetilde{\mathsf{GRAD}}(\mathbf{p})$, $\iota_{\tilde{\mathrm{v}}(\mathrm{c}),\tilde{\mathrm{e}}(\mathrm{f})} = -\iota_{\mathrm{f,c}}$ (cf. (3.11)) and owing to the definition (8.58) of $\widetilde{\mathsf{G}}_{\mathrm{c}}^{\mathrm{Hy}}$, we infer that $\sum_{\mathrm{c}\in\mathrm{C}_{\mathrm{f}}} \iota_{\mathrm{f,c}}\boldsymbol{\lambda}_{\mathrm{f,c}} = 0$ so that $\boldsymbol{\lambda}$ is single-valued for all $\mathrm{f} \in \mathrm{F}^{\mathrm{I}}$. For each border face $\mathrm{f} \in \mathrm{F}^{\mathrm{B}}$, we infer that $\boldsymbol{\lambda}_{\mathrm{f}} = 0$ with the same arguments. Thus, there exists $\boldsymbol{\lambda} \in \widetilde{\mathcal{L}}$ such that (8.62) holds in each cell. Since (8.61a) readily results from (8.62), we conclude that $(\hat{\boldsymbol{\phi}}, \mathbf{p}, \boldsymbol{\lambda}) \in \hat{\mathcal{F}} \times \widetilde{\mathcal{V}} \times \widetilde{\mathcal{L}}$ solves (8.61). □

Remark 8.30 (Well-posedness of (8.61))**.** *The linear system* (8.61) *is well-posed (and, hence, $\boldsymbol{\lambda} \in \widetilde{\mathcal{L}}$ from Lemma 8.29 is unique). We return to this fact in Remark 8.33 below.*

8.3.2 Primal hybrid cell-based schemes

We now consider the following discrete system: Find $(\mathbf{p}, \boldsymbol{\lambda}) \in \widetilde{\mathcal{V}} \times \widetilde{\mathcal{L}}$ such that

$$\sum_{\mathrm{c}\in\mathrm{C}} [\![(\mathsf{H}_{\kappa^{-1}}^{\mathcal{F}_{\mathrm{c}}\widetilde{\mathcal{E}}_{\mathrm{c}}})^{-1} \cdot \widetilde{\mathsf{G}}_{\mathrm{c}}^{\mathrm{Hy}}(\mathbf{p}_{\mathrm{c}}, \boldsymbol{\lambda}_{\mathrm{c}}), \widetilde{\mathsf{G}}_{\mathrm{c}}^{\mathrm{Hy}}(\mathbf{q}_{\mathrm{c}}, \boldsymbol{\mu}_{\mathrm{c}})]\!]_{\mathcal{F}_{\mathrm{c}}\widetilde{\mathcal{E}}_{\mathrm{c}}} = [\![\mathsf{R}_{\mathcal{C}}(s), \mathbf{q}]\!]_{\mathcal{C}\widetilde{\mathcal{V}}}, \qquad \forall (\mathbf{q}, \boldsymbol{\mu}) \in \widetilde{\mathcal{V}} \times \widetilde{\mathcal{L}}. \tag{8.63}$$

This discrete system is known in the literature as a primal hybrid formulation (Raviart & Thomas, 1977). We first show that this system is equivalent to the hybrid system (8.61).

Lemma 8.31 (Equivalence between (8.61) and (8.63))**.** *The two following assertions hold:*

(i) Let $(\hat{\boldsymbol{\phi}}, \mathbf{p}, \boldsymbol{\lambda}) \in \hat{\mathcal{F}} \times \widetilde{\mathcal{V}} \times \widetilde{\mathcal{L}}$ solve (8.61)*. Then, $(\mathbf{p}, \boldsymbol{\lambda}) \in \widetilde{\mathcal{V}} \times \widetilde{\mathcal{L}}$ solves* (8.63)*.*

(ii) Let $(\mathbf{p}, \boldsymbol{\lambda}) \in \widetilde{\mathcal{V}} \times \widetilde{\mathcal{L}}$ solve (8.63)*. Then, setting $\hat{\boldsymbol{\phi}}_{\mathrm{c}} := -(\mathsf{H}_{\kappa^{-1}}^{\mathcal{F}_{\mathrm{c}}\widetilde{\mathcal{E}}_{\mathrm{c}}})^{-1} \cdot \widetilde{\mathsf{G}}_{\mathrm{c}}^{\mathrm{Hy}}(\mathbf{p}_{\mathrm{c}}, \boldsymbol{\lambda}_{\mathrm{c}})$ for each cell $\mathrm{c} \in \mathrm{C}$, $(\hat{\boldsymbol{\phi}}, \mathbf{p}, \boldsymbol{\lambda}) \in \hat{\mathcal{F}} \times \widetilde{\mathcal{V}} \times \widetilde{\mathcal{L}}$ solves* (8.61)*.*

Proof. (i). Let $(\hat{\boldsymbol{\phi}}, \mathbf{p}, \boldsymbol{\lambda}) \in \hat{\mathcal{F}} \times \widetilde{\mathcal{V}} \times \widetilde{\mathcal{L}}$ solve (8.61). Then, owing to (8.61b), $\sum_{\mathrm{c}\in\mathrm{C}} [\![\mathsf{DIV}_{\mathrm{c}}(\hat{\boldsymbol{\phi}}), \mathbf{q}_{\mathrm{c}}]\!]_{\mathcal{C}_{\mathrm{c}}\widetilde{\mathcal{V}}_{\mathrm{c}}} = [\![\mathsf{R}_{\mathcal{C}}(s), \mathbf{q}]\!]_{\mathcal{C}\widetilde{\mathcal{V}}}$ for all $\mathbf{q} \in \widetilde{\mathcal{V}}$. Moreover, applying cellwise (8.60) and using the fact that $\hat{\boldsymbol{\phi}}$ verifies (8.61c), we infer that $\sum_{\mathrm{c}\in\mathrm{C}} -[\![\hat{\boldsymbol{\phi}}_{\mathrm{c}}, \widetilde{\mathsf{G}}_{\mathrm{c}}^{\mathrm{Hy}}(\mathbf{q}_{\mathrm{c}}, \boldsymbol{\mu}_{\mathrm{c}})]\!]_{\mathcal{F}_{\mathrm{c}}\widetilde{\mathcal{E}}_{\mathrm{c}}} = [\![\mathsf{R}_{\mathcal{C}}(s), \mathbf{q}]\!]_{\mathcal{C}\widetilde{\mathcal{V}}}$. Finally, since $\hat{\boldsymbol{\phi}}_{\mathrm{c}} = -(\mathsf{H}_{\kappa^{-1}}^{\mathcal{F}_{\mathrm{c}}\widetilde{\mathcal{E}}_{\mathrm{c}}})^{-1} \cdot \widetilde{\mathsf{G}}_{\mathrm{c}}^{\mathrm{Hy}}(\mathbf{p}_{\mathrm{c}}, \boldsymbol{\lambda}_{\mathrm{c}})$ owing to (8.62), we infer that $(\mathbf{p}, \boldsymbol{\lambda}) \in \widetilde{\mathcal{V}} \times \widetilde{\mathcal{L}}$ solves (8.63).

(ii). Let $(\mathbf{p}, \boldsymbol{\lambda}) \in \widetilde{\mathcal{V}} \times \widetilde{\mathcal{L}}$ solve (8.63). Set $\hat{\boldsymbol{\phi}}_{\mathrm{c}} := -(\mathsf{H}^{\mathcal{F}_{\mathrm{c}}\widetilde{\mathcal{E}}_{\mathrm{c}}})_{\kappa}^{-1} \cdot \widetilde{\mathsf{G}}_{\mathrm{c}}^{\mathrm{Hy}}(\mathbf{p}_{\mathrm{c}}, \boldsymbol{\lambda}_{\mathrm{c}})$ on each cell $\mathrm{c} \in \mathrm{C}$. Then, (8.63) can be recast as follows:

$$-\sum_{\mathrm{c}\in\mathrm{C}} [\![\hat{\boldsymbol{\phi}}_{\mathrm{c}}, \widetilde{\mathsf{G}}_{\mathrm{c}}^{\mathrm{Hy}}(\mathbf{q}_{\mathrm{c}}, \boldsymbol{\mu}_{\mathrm{c}})]\!]_{\mathcal{F}_{\mathrm{c}}\widetilde{\mathcal{E}}_{\mathrm{c}}} = [\![\mathsf{R}_{\mathcal{C}}(s), \mathbf{q}]\!]_{\mathcal{C}\widetilde{\mathcal{V}}}, \qquad \forall \mathbf{q} \in \widetilde{\mathcal{V}},\ \forall \boldsymbol{\mu} \in \widetilde{\mathcal{L}}.$$

Owing to (8.60), we infer that

$$\sum_{\mathrm{c}\in\mathrm{C}} [\![\mathsf{DIV}_{\mathrm{c}}(\hat{\boldsymbol{\phi}}_{\mathrm{c}}), \mathbf{q}_{\mathrm{c}}]\!]_{\mathcal{C}_{\mathrm{c}}\widetilde{\mathcal{V}}_{\mathrm{c}}} - \sum_{\mathrm{c}\in\mathrm{C}} \langle\!\langle \hat{\boldsymbol{\phi}}_{\mathrm{c}}\,,\, \boldsymbol{\mu}_{\mathrm{c}} \rangle\!\rangle_{\mathcal{F}_{\mathrm{c}}\widetilde{\mathcal{L}}_{\mathrm{c}}} = [\![\mathsf{R}_{\mathcal{C}}(s), \mathbf{q}]\!]_{\mathcal{C}\widetilde{\mathcal{V}}},$$

which corresponds to (8.61b) combined with (8.61c). Since we can choose independently $\boldsymbol{\mu}$ and $\mathbf{q}$, the global constraint on the flux continuity and the balance equation hold simultaneously. Finally, for all $\hat{\boldsymbol{\sigma}} \in \hat{\mathcal{F}}$, summing cellwise $(\mathsf{H}_{\kappa^{-1}}^{\mathcal{F}_{\mathrm{c}}\widetilde{\mathcal{E}}_{\mathrm{c}}})^{-1}\hat{\boldsymbol{\phi}}_{\mathrm{c}} + \widetilde{\mathsf{G}}_{\mathrm{c}}^{\mathrm{Hy}}(\mathbf{p}_{\mathrm{c}}, \boldsymbol{\lambda}_{\mathrm{c}}) = 0_{\widetilde{\mathcal{E}}_{\mathrm{c}}}$ tested with $\hat{\boldsymbol{\sigma}}_{\mathrm{c}} \in \mathcal{F}_{\mathrm{c}}$, and using (8.60) yields (8.61a). We conclude that $(\hat{\boldsymbol{\phi}}, \mathbf{p}, \boldsymbol{\lambda}) \in \hat{\mathcal{F}} \times \widetilde{\mathcal{V}} \times \widetilde{\mathcal{L}}$ solves (8.61). □

Proposition 8.32 (Well-posedness)**.** (8.63) *is well-posed.*

Proof. Existence results from Lemma 8.29 (recall that (8.34) is well-posed) and Lemma 8.31(i). This also implies uniqueness since (8.63) is a square linear system with arbitrary right-hand side. Uniqueness can also be proven directly by considering a zero right-hand side. Indeed, the stability of the discrete Hodge operator implies that, for all cell $\mathrm{c} \in \mathrm{C}$, $\widetilde{\mathsf{G}}_{\mathrm{c}}^{\mathrm{Hy}}(\mathbf{p}_{\mathrm{c}}, \boldsymbol{\lambda}_{\mathrm{c}}) = 0_{\widetilde{\mathcal{E}}_{\mathrm{c}}}$. Then, $\boldsymbol{\lambda}_{\mathrm{f}} = \mathbf{p}_{\mathrm{c}}$ for all $\mathrm{f} \in \mathrm{F}_{\mathrm{c}}$. This implies that $\mathbf{p}$ takes the same value at all dual vertices and, since $\boldsymbol{\lambda}_{\mathrm{f}} = 0$ for all $\mathrm{f} \in \mathrm{F}^{\mathrm{B}}$, we infer that $\boldsymbol{\lambda} = 0_{\widetilde{\mathcal{L}}}$ and $\mathbf{p} = 0_{\widetilde{\mathcal{V}}}$. □

Remark 8.33 (Well-posedness of (8.61))**.** (8.61) *is well-posed. Indeed, since this is a square linear system, it suffices to show uniqueness. Lemma 8.31(i) implies that* $(\mathbf{p}, \boldsymbol{\lambda})$ *is unique (since* (8.63) *is well-posed) and Lemma 8.28 implies that* $\hat{\boldsymbol{\phi}}$ *is unique (since* (8.34) *is well-posed).*

Dual to primal discrete Hodge operator. To recover the solution of the cell-based scheme (8.34) from (8.63), we have to consider the local inverse operator $(\mathsf{H}_{\kappa^{-1}}^{\mathcal{F}_{\mathrm{c}}\widetilde{\mathcal{E}}_{\mathrm{c}}})^{-1}$ in each cell $\mathrm{c} \in \mathrm{C}$, *i.e.* to compute the inverse of a small matrix of size $\#\mathrm{F}_{\mathrm{c}}$. We now want to explore a second approach where we directly build a local discrete Hodge operator $\mathsf{H}_{\kappa}^{\widetilde{\mathcal{E}}_{\mathrm{c}}\mathcal{F}_{\mathrm{c}}}$ in each cell $\mathrm{c} \in \mathrm{C}$ so as to avoid the local inversions. This approach leads to the following discrete system: Find $(\mathbf{p}, \boldsymbol{\lambda}) \in \widetilde{\mathcal{V}} \times \widetilde{\mathcal{L}}$ such that

$$\sum_{\mathrm{c}\in\mathrm{C}} [\![\mathsf{H}_{\kappa}^{\widetilde{\mathcal{E}}_{\mathrm{c}}\mathcal{F}_{\mathrm{c}}} \cdot \widetilde{\mathsf{G}}_{\mathrm{c}}^{\mathrm{Hy}}(\mathbf{p}_{\mathrm{c}}, \boldsymbol{\lambda}_{\mathrm{c}}), \widetilde{\mathsf{G}}_{\mathrm{c}}^{\mathrm{Hy}}(\mathbf{q}_{\mathrm{c}}, \boldsymbol{\mu}_{\mathrm{c}})]\!]_{\mathcal{F}_{\mathrm{c}}\widetilde{\mathcal{E}}_{\mathrm{c}}} = [\![\mathsf{R}_{\mathcal{C}}(s), \mathbf{q}]\!]_{\mathcal{C}\widetilde{\mathcal{V}}}, \qquad \forall (\mathbf{q}, \boldsymbol{\mu}) \in \widetilde{\mathcal{V}} \times \widetilde{\mathcal{L}}. \tag{8.64}$$

Lemma 8.34 (Equivalence between (8.61) and (8.64))**.** *The two following assertions hold:*

(i) Let $(\hat{\boldsymbol{\phi}}, \mathbf{p}, \boldsymbol{\lambda}) \in \hat{\mathcal{F}} \times \widetilde{\mathcal{V}} \times \widetilde{\mathcal{L}}$ *solve* (8.61)*. Set* $\mathsf{H}_{\kappa}^{\widetilde{\mathcal{E}}_{\mathrm{c}}\mathcal{F}_{\mathrm{c}}} := (\mathsf{H}_{\kappa^{-1}}^{\mathcal{F}_{\mathrm{c}}\widetilde{\mathcal{E}}_{\mathrm{c}}})^{-1}$*. Then,* $(\mathbf{p}, \boldsymbol{\lambda}) \in \widetilde{\mathcal{V}} \times \widetilde{\mathcal{L}}$ *solves* (8.64)*.*

(ii) Let $(\mathbf{p}, \boldsymbol{\lambda}) \in \widetilde{\mathcal{V}} \times \widetilde{\mathcal{L}}$ *solve* (8.64)*. Set* $\mathsf{H}_{\kappa^{-1}}^{\mathcal{F}_{\mathrm{c}}\widetilde{\mathcal{E}}_{\mathrm{c}}} := (\mathsf{H}_{\kappa}^{\widetilde{\mathcal{E}}_{\mathrm{c}}\mathcal{F}_{\mathrm{c}}})^{-1}$ *and* $\hat{\boldsymbol{\phi}}_{\mathrm{c}} := -\mathsf{H}_{\kappa}^{\widetilde{\mathcal{E}}_{\mathrm{c}}\mathcal{F}_{\mathrm{c}}} \cdot \widetilde{\mathsf{G}}_{\mathrm{c}}^{\mathrm{Hy}}(\mathbf{p}_{\mathrm{c}}, \boldsymbol{\lambda}_{\mathrm{c}})$ *for each* $\mathrm{c} \in \mathrm{C}$*. Then,* $(\hat{\boldsymbol{\phi}}, \mathbf{p}, \boldsymbol{\lambda}) \in \hat{\mathcal{F}} \times \widetilde{\mathcal{V}} \times \widetilde{\mathcal{L}}$ *solves* (8.61)*.*

Proof. This is a direct consequence of Lemma 8.31. □

Design of $\mathsf{H}_{\kappa}^{\widetilde{\mathcal{E}}_{\mathrm{c}}\mathcal{F}_{\mathrm{c}}}$. The question we now address is to identify the design properties of $\mathsf{H}_{\kappa}^{\widetilde{\mathcal{E}}_{\mathrm{c}}\mathcal{F}_{\mathrm{c}}}$ so that $\mathsf{H}_{\kappa^{-1}}^{\mathcal{F}_{\mathrm{c}}\widetilde{\mathcal{E}}_{\mathrm{c}}} := (\mathsf{H}_{\kappa}^{\widetilde{\mathcal{E}}_{\mathrm{c}}\mathcal{F}_{\mathrm{c}}})^{-1}$ satisfies the three design properties (**H0**), (**H1**), and (**H2**) identified in Section 6.2.1. Indeed, asserting these properties implies that the convergence analysis of the original cell-based system (8.34) also holds for the primal hybrid system (8.64).

Proposition 8.35 (Design properties of $\mathsf{H}_{\kappa}^{\widetilde{\mathcal{E}}_{\mathrm{c}}\mathcal{F}_{\mathrm{c}}}$)**.** *Let* $\mathrm{c} \in \mathrm{C}$*. Then,* $\mathsf{H}_{\kappa^{-1}}^{\mathcal{F}_{\mathrm{c}}\widetilde{\mathcal{E}}_{\mathrm{c}}} := (\mathsf{H}_{\kappa}^{\widetilde{\mathcal{E}}_{\mathrm{c}}\mathcal{F}_{\mathrm{c}}})^{-1}$ *satisfies* (**H0**)*,* (**H1**)*, and* (**H2**)*, meaning that* $\mathsf{H}_{\kappa^{-1}}^{\mathcal{F}_{\mathrm{c}}\widetilde{\mathcal{E}}_{\mathrm{c}}}$ *is symmetric, uniformly positive definite, and* $\mathbb{P}_0$*-consistent, if and only if* $\mathsf{H}_{\kappa}^{\widetilde{\mathcal{E}}_{\mathrm{c}}\mathcal{F}_{\mathrm{c}}}$ *is symmetric, uniformly positive definite, and satisfies the following* $\mathbb{P}_0$*-consistency property:*

$$\mathsf{H}_{\kappa}^{\widetilde{\mathcal{E}}_{\mathrm{c}}\mathcal{F}_{\mathrm{c}}} \cdot \mathsf{R}_{\widetilde{\mathcal{E}}_{\mathrm{c}}}(\underline{G}) - \mathsf{R}_{\mathcal{F}_{\mathrm{c}}}(\underline{\underline{\kappa}}\,\underline{G}) = \underline{0}, \tag{8.65}$$

for all constant vector field $\underline{G}$ *in* c*.*

Proof. The equivalence for the symmetry and the uniformly positive definiteness is straightforward. The equivalence for the $\mathbb{P}_0$-consistency is shown by taking $\underline{\Phi} = -\underline{\underline{\kappa}}\,\underline{G}$ and multiplying (8.65) by $\mathsf{H}_{\kappa^{-1}}^{\mathcal{F}_{\mathrm{c}}\widetilde{\mathcal{E}}_{\mathrm{c}}}$. The converse proof is similar. □

Following the rationale detailed in Section 7.3.1 (in particular the reconstruction of circulations), we define the local discrete Hodge operator $\mathsf{H}_{\kappa}^{\widetilde{\mathcal{E}}_{\mathrm{c}}\mathcal{F}_{\mathrm{c}}}$ in each cell $\mathrm{c} \in \mathrm{C}$ as follows:

$$[\![\mathsf{H}_{\kappa}^{\widetilde{\mathcal{E}}_{\mathrm{c}}\mathcal{F}_{\mathrm{c}}}(\mathbf{b}_1), \mathbf{b}_2]\!]_{\mathcal{F}_{\mathrm{c}}\widetilde{\mathcal{E}}_{\mathrm{c}}} := \int_{\mathrm{c}} \underline{\mathrm{L}}_{\widetilde{\mathcal{E}}_{\mathrm{c}}}(\mathbf{b}_1) \cdot \underline{\underline{\kappa}}\,\underline{\mathrm{L}}_{\widetilde{\mathcal{E}}_{\mathrm{c}}}(\mathbf{b}_2), \qquad \forall \mathbf{b}_1, \mathbf{b}_2 \in \widetilde{\mathcal{E}}_{\mathrm{c}}, \tag{8.66}$$

and our aim is now to define the local reconstruction operator $\underline{\mathsf{L}}_{\widetilde{\mathcal{E}}_\mathrm{c}}$ so that $\mathsf{H}_\kappa^{\widetilde{\mathcal{E}}_\mathrm{c}\mathcal{F}_\mathrm{c}}$ defined from (8.66) satisfies the properties identified in Proposition 8.35.

Definition 8.36 (Piecewise constant reconstruction)**.** *Let* $\mathrm{c}\in\mathrm{C}$*. Recall the partition* $\mathfrak{P}_{\mathrm{F},\mathrm{c}}:=\{\mathfrak{p}_{\mathrm{f},\mathrm{c}}\}_{\mathrm{f}\in\mathrm{F}_\mathrm{c}}$ *from Definition 5.18. Then, the local reconstruction operator* $\underline{\mathsf{L}}_{\widetilde{\mathcal{E}}_\mathrm{c}}$ *(constant on each* $\mathfrak{p}_{\mathrm{f},\mathrm{c}}$*) is defined for all* $\mathbf{b}_\mathrm{c}\in\widetilde{\mathcal{E}}_\mathrm{c}$ *as follows:*

$$\underline{\mathsf{L}}_{\widetilde{\mathcal{E}}_\mathrm{c}}(\mathbf{b}_\mathrm{c}):=\underline{\mathsf{C}}_{\widetilde{\mathcal{E}}_\mathrm{c}}(\mathbf{b}_\mathrm{c})+\hat{\underline{\mathsf{S}}}_{\widetilde{\mathcal{E}}_\mathrm{c}}\left((\mathsf{Id}_{\widetilde{\mathcal{E}}_\mathrm{c}}-\mathsf{R}_{\widetilde{\mathcal{E}}_\mathrm{c}}\underline{\mathsf{C}}_{\widetilde{\mathcal{E}}_\mathrm{c}})(\mathbf{b}_\mathrm{c})\right),\tag{8.67a}$$

where $\underline{\mathsf{C}}_{\widetilde{\mathcal{E}}_\mathrm{c}}:\widetilde{\mathcal{E}}_\mathrm{c}\to[\mathbb{P}_0(\mathrm{c})]^3$ *and* $\hat{\underline{\mathsf{S}}}_{\widetilde{\mathcal{E}}_\mathrm{c}}:\widetilde{\mathcal{E}}_\mathrm{c}\to[\mathbb{P}_0(\mathfrak{P}_{\mathrm{F},\mathrm{c}})]^3$ *act as follows:*

$$\underline{\mathsf{C}}_{\widetilde{\mathcal{E}}_\mathrm{c}}(\mathbf{b}_\mathrm{c}):=\frac{1}{|\mathrm{c}|}\sum_{\mathrm{f}\in\mathrm{F}_\mathrm{c}}\mathbf{b}_{\tilde{\mathrm{e}}_\mathrm{c}(\mathrm{f})}\underline{\mathrm{f}},\qquad\text{and}\qquad\hat{\underline{\mathsf{S}}}_{\widetilde{\mathcal{E}}_\mathrm{c}}(\mathbf{b}_\mathrm{c})|_{\mathfrak{p}_{\mathrm{f},\mathrm{c}}}:=\beta\,\frac{\underline{\mathrm{f}}}{|\mathfrak{p}_{\mathrm{f},\mathrm{c}}|}\,\mathbf{b}_{\tilde{\mathrm{e}}_\mathrm{c}(\mathrm{f})},\qquad\forall\mathrm{f}\in\mathrm{F}_\mathrm{c},\tag{8.67b}$$

and $\beta>0$ *is a free-parameter related to the stabilization.*

Then, we readily infer that the constant value taken by $\underline{\mathsf{L}}_{\widetilde{\mathcal{E}}_\mathrm{c}}(\mathbf{b}_\mathrm{c})$ in each $\mathfrak{p}_{\mathrm{f},\mathrm{c}}$, for $\mathrm{f}\in\mathrm{F}_\mathrm{c}$, is

$$\underline{\mathsf{L}}_{\widetilde{\mathcal{E}}_\mathrm{c}}(\mathbf{b}_\mathrm{c})|_{\mathfrak{p}_{\mathrm{f},\mathrm{c}}}=\underline{\mathsf{C}}_{\widetilde{\mathcal{E}}_\mathrm{c}}(\mathbf{b}_\mathrm{c})+\beta\frac{\underline{\mathrm{f}}}{|\mathfrak{p}_{\mathrm{f},\mathrm{c}}|}\left(\mathbf{b}_{\tilde{\mathrm{e}}_\mathrm{c}(\mathrm{f})}-\tilde{\mathrm{e}}_\mathrm{c}(\mathrm{f})\cdot\underline{\mathsf{C}}_{\widetilde{\mathcal{E}}_\mathrm{c}}(\mathbf{b}_\mathrm{c})\right).\tag{8.68}$$

Proposition 8.37 (Properties of $\underline{\mathsf{L}}_{\widetilde{\mathcal{E}}_\mathrm{c}}$)**.** *Assume that the mesh is of class* **(MR)** *and* **(MB)**. *Assume that primal faces are planar. Let* $\mathrm{c}\in\mathrm{C}$*. Then,* $\underline{\mathsf{L}}_{\widetilde{\mathcal{E}}_\mathrm{c}}$ *from Definition 8.36 satisfies for any value of* $\beta>0$ *the following properties:*

($\widetilde{\mathbf{R}}\mathbf{1}$) *[Stability] There exists* $\eta_{\widetilde{\mathcal{E}}}>0$ *uniform w.r.t.* c *such that*

$$\eta_{\widetilde{\mathcal{E}}}\|\mathbf{b}\|_{2,\widetilde{\mathcal{E}}_\mathrm{c}}^2\le\|\underline{\mathsf{L}}_{\widetilde{\mathcal{E}}_\mathrm{c}}(\mathbf{b})\|_{L^2(\mathrm{c})}^2\le\eta_{\widetilde{\mathcal{E}}}^{-1}\|\mathbf{b}\|_{2,\widetilde{\mathcal{E}}_\mathrm{c}}^2,\qquad\forall\mathbf{b}\in\widetilde{\mathcal{E}}_\mathrm{c}.$$

($\widetilde{\mathbf{R}}\mathbf{2}$) *[Partition of unity] For any constant vector field* $\underline{K}$ *in* c*, the following identity holds:*

$$\underline{\mathsf{L}}_{\widetilde{\mathcal{E}}_\mathrm{c}}\mathsf{R}_{\widetilde{\mathcal{E}}_\mathrm{c}}(\underline{K})=\underline{K}.$$

($\widetilde{\mathbf{R}}\mathbf{3}$) *[Dual consistency] For all* $\mathrm{c}\in\mathrm{C}$*, the following identity holds:*

$$\int_\mathrm{c}\underline{\mathsf{L}}_{\widetilde{\mathcal{E}}_\mathrm{c}}(\mathbf{a})=\sum_{\mathrm{f}\in\mathrm{F}_\mathrm{c}}\mathbf{b}_{\tilde{\mathrm{e}}_\mathrm{c}(\mathrm{f})}\underline{\mathrm{f}},\qquad\forall\mathbf{b}\in\widetilde{\mathcal{E}}_\mathrm{c}.$$

Moreover, the following property holds if and only if $\beta=\frac{1}{d}$*:*

($\widetilde{\mathbf{R}}\mathbf{4}$) *[Unisolvence] For all* $\mathbf{a}\in\mathcal{X}_\mathrm{c}$*,*

$$\mathsf{R}_{\widetilde{\mathcal{E}}_\mathrm{c}}\underline{\mathsf{L}}_{\widetilde{\mathcal{E}}_\mathrm{c}}=\mathsf{Id}_{\widetilde{\mathcal{E}}_\mathrm{c}}.$$

Proof. The proof follows the same lines as that of Proposition 7.32. □

Using the local reconstruction operator from Definition 8.36, the discrete system (8.64) is readily recast as follows: Find $(\mathbf{p},\boldsymbol{\lambda})\in\widetilde{\mathcal{V}}\times\widetilde{\mathcal{L}}$ such that

$$\sum_{\mathrm{c}\in\mathrm{C}}\int_\mathrm{c}\underline{\mathsf{L}}_{\widetilde{\mathcal{E}}_\mathrm{c}}(\widetilde{\mathsf{G}}_\mathrm{c}^{\mathrm{Hy}}(\mathbf{p}_\mathrm{c},\boldsymbol{\lambda}_\mathrm{c}))\cdot\underline{\kappa}\,\underline{\mathsf{L}}_{\widetilde{\mathcal{E}}_\mathrm{c}}(\widetilde{\mathsf{G}}_\mathrm{c}^{\mathrm{Hy}}(\mathbf{q}_\mathrm{c},\boldsymbol{\mu}_\mathrm{c}))=[\![\mathsf{R}_\mathcal{C}(s),\mathbf{q}]\!]_{\mathcal{C}\widetilde{\mathcal{V}}},\qquad\forall(\mathbf{q},\boldsymbol{\mu})\in\widetilde{\mathcal{V}}\times\widetilde{\mathcal{L}}.\tag{8.69}$$

Proposition 8.38 (Link with SUSHI schemes)**.** *The hybrid SUSHI scheme introduced by Eymard* et al. *(2010) is equivalent to the primal hybrid CDO scheme* (8.69) *using a reconstruction operator* $\underline{\mathsf{L}}_{\widetilde{\mathcal{E}}_\mathrm{c}}$ *defined in* (8.67) *with the choice* $\beta=\frac{1}{\sqrt{d}}$.

Proof. The space of DoFs $\mathcal{X}_\mathcal{D}$ in the hybrid SUSHI scheme corresponds to $\widetilde{\mathcal{V}} \times \widetilde{\mathcal{L}}$ since $\mathcal{X}_\mathcal{D}$ collects values at the cell centers and at the interfaces of the control volumes, *i.e.* the faces $\mathrm{f} \in \mathrm{F}$ in our notation. In what follows, we refer to equations (22), (24) and (25) of the paper by Eymard *et al.* (2010). Eymard *et al.* (2010) consider a discrete gradient of $u \in \mathcal{X}_\mathcal{D}$, denoted by $\nabla_\mathcal{D}(u)$, which is decomposed into a consistent part, denoted by $\nabla_K(u)$ (K is c in our notation), and a stabilized part, denoted by $R_{K,\sigma}(u)\mathbf{n}_{K,\sigma}$ (σ is f and $\mathbf{n}_{\mathbf{K},\sigma}$ is $\iota_{\mathrm{f,c}}\underline{\nu}_\mathrm{f}$ in our notation). The consistent part corresponds to $\underline{\mathsf{C}}_{\widetilde{\mathcal{E}}_\mathrm{c}}(\widetilde{\mathsf{G}}_\mathrm{c}^{\mathrm{Hy}}(\mathbf{p},\boldsymbol{\lambda}))$. The stabilized part is constant on each cone $D_{K,\sigma}$ of base σ and apex $\underline{x}_K$ (since $\underline{x}_K$ is $\underline{x}_\mathrm{c}$, this cone corresponds to $\mathfrak{p}_{\mathrm{f,c}}$ in our notation). Choosing $\beta = \frac{1}{\sqrt{d}}$ in the definition of $\underline{\mathsf{S}}_{\widetilde{\mathcal{E}}_\mathrm{c}}(\widetilde{\mathsf{G}}_\mathrm{c}^{\mathrm{Hy}}(\mathbf{p},\boldsymbol{\lambda}))$ leads to the same stabilized part. The discrete system obtained with the hybrid SUSHI scheme is: Find $u \in \mathcal{X}_\mathcal{D}$ such that

$$\sum_{K\in\mathcal{M}} \int_K \nabla_\mathcal{D}(u)\cdot\underline{\underline{\kappa}}\nabla_\mathcal{D}(v) = \sum_{K\in\mathcal{M}} v_K \int_K s, \qquad \forall v \in \mathcal{X}_\mathcal{D}, \tag{8.70}$$

where $\mathcal{M}$ is C in our notation. Since $[\![\mathsf{R}_\mathcal{C}(s),\mathbf{q}]\!]_{\mathcal{C}\widetilde{\mathcal{V}}} = \sum_{\mathrm{c}\in\mathrm{C}} \mathbf{q}_{\widetilde{\mathrm{v}}(\mathrm{c})} \int_\mathrm{c} s$ by definition, we readily verify the equivalence between the primal hybrid CDO scheme (8.69) and the hybrid SUSHI scheme (8.70). □

8.3.3 Static condensation

We adopt an algebraic viewpoint to present the technique of static condensation following the lines of Brezzi & Fortin (1991). We first recast the system (8.57) as follows:

$$\begin{bmatrix} \mathsf{A} & \mathsf{B}^\mathrm{T} & \mathsf{C}^\mathrm{T} \\ \mathsf{B} & 0 & 0 \\ \mathsf{C} & 0 & 0 \end{bmatrix} \begin{bmatrix} \hat{\boldsymbol{\phi}} \\ \mathbf{p} \\ \boldsymbol{\lambda} \end{bmatrix} = \begin{bmatrix} 0_{\hat{\mathcal{F}}} \\ -\mathsf{R}_\mathcal{C}(s) \\ 0_{\widetilde{\mathcal{L}}} \end{bmatrix}, \tag{8.71}$$

where we identify operators with their algebraic realization as follows:

$$\mathsf{A} : \hat{\mathcal{F}} \to \hat{\mathcal{F}}, \qquad \mathsf{A} := \sum_{\mathrm{c}\in\mathrm{C}} \mathsf{T}^*_{\hat{\mathrm{F}},\mathrm{c}} \cdot \mathsf{H}_{\kappa^{-1}}^{\mathcal{F}_\mathrm{c}\widetilde{\mathcal{E}}_\mathrm{c}} \cdot \mathsf{T}_{\hat{\mathrm{F}},\mathrm{c}}, \tag{8.72a}$$

$$\mathsf{B} : \hat{\mathcal{F}} \to \mathcal{C}, \qquad \mathsf{B} := -\sum_{\mathrm{c}\in\mathrm{C}} \mathsf{T}^*_{\mathrm{C},\mathrm{c}} \cdot \mathsf{DIV}_\mathrm{c} \cdot \mathsf{T}_{\hat{\mathrm{F}},\mathrm{c}}, \tag{8.72b}$$

$$\mathsf{C} : \hat{\mathcal{F}} \to \widetilde{\mathcal{L}}, \qquad \mathsf{C} := \sum_{\mathrm{c}\in\mathrm{C}} \mathsf{T}^*_{\mathrm{F},\mathrm{c}} \cdot \mathsf{I}_{\mathrm{F},\mathrm{c}} \cdot \mathsf{T}_{\hat{\mathrm{F}},\mathrm{c}}. \tag{8.72c}$$

Here, $\mathsf{T}_{\hat{\mathrm{F}},\mathrm{c}}$, $\mathsf{T}_{\mathrm{F},\mathrm{c}}$, and $\mathsf{T}_{\mathrm{C},\mathrm{c}}$ denote as usual the full-rank map from global to local DoFs, and, in each cell $\mathrm{c} \in \mathrm{C}$, $\mathsf{I}_{\mathrm{F},\mathrm{c}} : \mathbb{R}^{\#\mathrm{F}_\mathrm{c}} \to \mathbb{R}^{\#\mathrm{F}_\mathrm{c}}$ is such that $\mathsf{I}_{\mathrm{F},\mathrm{c}}(\mathbf{a})|_\mathrm{f} = \iota_{\mathrm{f,c}}\mathbf{a}_\mathrm{f}$ for all $\mathrm{f} \in \mathrm{F}_\mathrm{c}$ and all $\mathbf{a} \in \mathbb{R}^{\#\mathrm{F}_\mathrm{c}}$.

The operator C ensures the continuity of the discrete flux. Namely, $\mathsf{C}(\hat{\boldsymbol{\phi}})|_\mathrm{f} = \sum_{\mathrm{c}\in\mathrm{C}_\mathrm{f}} \iota_{\mathrm{f,c}}\hat{\boldsymbol{\phi}}_{\mathrm{c,f}}$ for all $\mathrm{f} \in \mathrm{F}$. B^T (resp. C^T) is the transpose of the matrix B (resp. C). A has a block diagonal structure, where each diagonal block is a local discrete Hodge operator $\mathsf{H}_{\kappa^{-1}}^{\mathcal{F}_\mathrm{c}\widetilde{\mathcal{E}}_\mathrm{c}}$:

$$\mathsf{A} = \operatorname{diag}\left(\mathsf{H}_{\kappa^{-1}}^{\mathcal{F}_\mathrm{c}\widetilde{\mathcal{E}}_\mathrm{c}}\right)_{\mathrm{c}\in\mathrm{C}}. \tag{8.73}$$

From (8.71), we infer that $\hat{\boldsymbol{\phi}} = -\mathsf{A}^{-1}(\mathsf{B}^\mathrm{T}(\mathbf{p}) + \mathsf{C}^\mathrm{T}(\boldsymbol{\lambda}))$. Eliminating the discrete flux yields

$$\begin{bmatrix} \mathsf{B}\mathsf{A}^{-1}\mathsf{B}^\mathrm{T} & \mathsf{B}\mathsf{A}^{-1}\mathsf{C}^\mathrm{T} \\ \mathsf{C}\mathsf{A}^{-1}\mathsf{B}^\mathrm{T} & \mathsf{C}\mathsf{A}^{-1}\mathsf{C}^\mathrm{T} \end{bmatrix} \begin{bmatrix} \mathbf{p} \\ \boldsymbol{\lambda} \end{bmatrix} = \begin{bmatrix} \mathsf{R}_\mathcal{C}(s) \\ 0_{\widetilde{\mathcal{L}}} \end{bmatrix}. \tag{8.74}$$

which is the algebraic representation of (8.64). The first row states the conservation law and the second raw states the continuity of the flux across each interior face. The key point is

to observe that $\mathsf{B}\mathsf{A}^{-1}\mathsf{B}^{\mathrm{T}}$ is a diagonal matrix of rank #C with entry for a cell c equal to $d_{\mathrm{c}} := \sum_{\mathrm{f}\in\mathrm{F_c}}\sum_{\mathrm{f}'\in\mathrm{F_c}} \iota_{\mathrm{f,c}}\iota_{\mathrm{f}',\mathrm{c}}(\mathsf{H}_{\kappa^{-1}}^{\mathcal{F}_{\mathrm{c}}\widetilde{\mathcal{E}}_{\mathrm{c}}})^{-1}|_{\mathrm{f}',\tilde{\mathrm{e}}(\mathrm{f})}$, since for all $\mathbf{a}\in\mathbb{R}^{\#\mathrm{X_c}}$ ($\mathrm{X}\in\{\mathrm{F},\hat{\mathrm{F}},\mathrm{C}\}$),

$$\mathsf{T}_{\mathrm{X,c}}^{*}\cdot\mathsf{T}_{\mathrm{X,c}}(\mathbf{a}) := \begin{cases}\mathbf{a}_{\mathrm{x}}, & \text{if } \mathrm{x}\in\mathrm{X_c},\\ 0, & \text{otherwise,}\end{cases} \tag{8.75}$$

and, thus $\mathsf{T}_{\mathrm{X,c}}^{*}\cdot\mathsf{T}_{\mathrm{X,c'}} = 0_{\mathrm{X}}$ if $\mathrm{c}\neq\mathrm{c}'$. As a consequence, one can easily eliminate the potential DoFs by setting

$$\mathbf{p} = (\mathsf{B}\mathsf{A}^{-1}\mathsf{B}^{\mathrm{T}})^{-1}\left(\mathsf{R}_{\mathcal{C}}(s) - \mathsf{B}\mathsf{A}^{-1}\mathsf{C}^{\mathrm{T}}(\boldsymbol{\lambda})\right). \tag{8.76}$$

Using (8.76) in (8.74) yields a discrete system on the sole discrete Lagrange multiplier: Find $\boldsymbol{\lambda}\in\widetilde{\mathcal{L}}$ such that

$$\left[\mathsf{C}\mathsf{A}^{-1}\mathsf{B}^{\mathrm{T}}\cdot\left(\mathsf{B}\mathsf{A}^{-1}\mathsf{B}^{\mathrm{T}}\right)^{-1}\cdot\mathsf{B}\mathsf{A}^{-1}\mathsf{C}^{\mathrm{T}} - \mathsf{C}\mathsf{A}^{-1}\mathsf{C}^{\mathrm{T}}\right](\boldsymbol{\lambda}) = \mathsf{C}\mathsf{A}^{-1}\mathsf{B}^{\mathrm{T}}\cdot\left(\mathsf{B}\mathsf{A}^{-1}\mathsf{B}^{\mathrm{T}}\right)^{-1}\mathsf{R}_{\mathcal{C}}(s). \tag{8.77}$$

The discrete system (8.77) is SPD and of size $\#\mathrm{F}^{\mathrm{I}}$ since A^{-1} is SPD by construction.

8.4 Numerical results

In this section, we assess and compare the reliability and efficiency of vertex-based, mixed cell-based, and hybrid cell-based CDO schemes for three-dimensional diffusion problems. We investigate numerically vertex-based schemes (8.3), mixed cell-based schemes (8.34), and hybrid cell-based scheme (8.77). For each family of schemes, we examine two different discrete Hodge operators based on piecewise constant reconstruction operators (cf. Section 7.3.1). We consider discrete Hodge operators built using either the DGA reconstruction (corresponding to the choice $\beta = d^{-1}$), or the SUSHI-like reconstruction (corresponding to the choice $\beta = d^{-\frac{1}{2}}$). We recall that β is the multiplicative coefficient of the stabilization part of the reconstruction operator in (7.37). In what follows, we denote by `Vb-DGA` and `Vb-SUSHI` the two vertex-based schemes that have been tested, and similarly, by `Cb-DGA` and `Cb-SUSHI` the two mixed cell-based schemes, and by `HCb-DGA` and `HCb-SUSHI`, the two hybrid cell-based schemes.

We underline that hybrid cell-based schemes and mixed cell-based schemes are different schemes since mixed cell-based schemes rely on a local discrete Hodge operator $\mathsf{H}_{\kappa^{-1}}^{\mathcal{F}_{\mathrm{c}}\widetilde{\mathcal{E}}_{\mathrm{c}}}$ (κ is the conductivity) for each cell $\mathrm{c}\in\mathrm{C}$ built using the reconstruction operator $\underline{\mathsf{L}}_{\mathcal{F}_{\mathrm{c}}}$ and hybrid cell-based schemes rely on a local discrete Hodge operator $\mathsf{H}_{\kappa}^{\widetilde{\mathcal{E}}_{\mathrm{c}}\mathcal{F}_{\mathrm{c}}}$ built using the reconstruction operator $\underline{\mathsf{L}}_{\widetilde{\mathcal{E}}_{\mathrm{c}}}$. With our choice of $\underline{\mathsf{L}}_{\mathcal{F}_{\mathrm{c}}}$ and $\underline{\mathsf{L}}_{\widetilde{\mathcal{E}}_{\mathrm{c}}}$, $\mathsf{H}_{\kappa}^{\widetilde{\mathcal{E}}_{\mathrm{c}}\mathcal{F}_{\mathrm{c}}}$ is not equal to $(\mathsf{H}_{\kappa^{-1}}^{\mathcal{F}_{\mathrm{c}}\widetilde{\mathcal{E}}_{\mathrm{c}}})^{-1}$.

Three test cases are considered. The first test case is an isotropic and heterogeneous diffusion problem having a continuous and piecewise affine solution (cf. Section 8.4.2). The two other test cases are taken from the FVCA benchmark (Eymard *et al.*, 2011). They respectively correspond to an anisotropic diffusion problem (cf. Section 8.4.3) and an anistropic and heterogeneous diffusion problem (cf. Section 8.4.4) having a solution expressed as a combination of sine functions.

Computations are run on the unit cube $[0,1]^3$. The three-dimensional mesh sequences consist of successive uniform refinements of an initial mesh. These mesh sequences are taken from the FVCA benchmark (see Figure 8.5). We considered different mesh sequences according to the test case. There are six mesh sequences respectively defined from Cartesian meshes and denoted by `Hex`, from prismatic meshes `PrT`, from prismatic meshes with polygonal basis `PrG`, from Cartesian meshes with locally refined subdomain `HLR`, from checkerboard meshes `CB`, and from hexahedral meshes with a strong non-orthogonality `Ker` (in reference to Kershaw meshes). The `PrG`, `HLR` and `CB` mesh sequences are examples of polyhedral meshes. The `HLR` and `CB` mesh sequences constitute a classical example of so-called non-matching meshes (see Figure 8.5). All these mesh sequences are detailed in Appendix A along with mesh regularity criteria identified in the analysis.

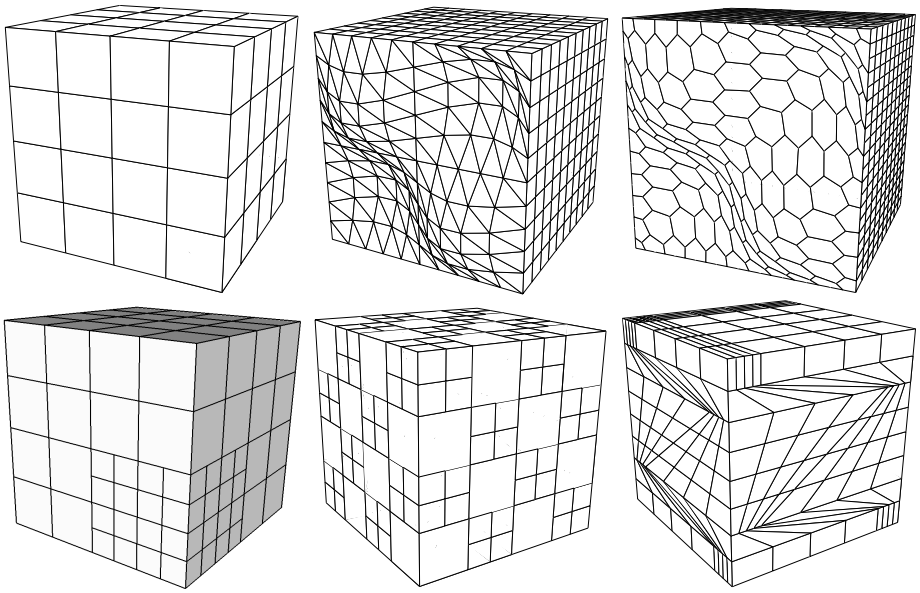

Figure 8.5 – Coarsest mesh of each mesh sequence considered for numerical tests. From top left to bottom right: `Hex`, `PrT`, `PrG`, `HLR`, `CB`, and `Ker` mesh sequences.

8.4.1 Postprocessed quantities

Quantities related to convergence. We compute discrete and continuous error norms to evaluate the convergence rates of CDO schemes. Two generic discrete error norms are considered: one based on the discrete functional norms and the other one induced by a discrete Hodge operator.

Definition 8.39 (Discrete error norms)**.** *Let $a \in S_{\mathcal{X}}(\Omega)$ be an exact solution of a diffusion problem and let $\mathbf{a} \in \mathcal{X}$ be the related discrete solution. Then, we set*

$$\mathbf{Er}_{\mathcal{X}}(\mathbf{a}) := \frac{\|\mathsf{R}_{\mathcal{X}}(a) - \mathbf{a}\|_{2,\mathcal{X}}}{\|\mathsf{R}_{\mathcal{X}}(a)\|_{2,\mathcal{X}}}, \qquad \mathbf{Er}_{\alpha,\mathcal{X}}(\mathbf{a}) := \frac{\|\mathsf{R}_{\mathcal{X}}(a) - \mathbf{a}\|_{\alpha,\mathcal{X}}}{\|\mathsf{R}_{\mathcal{X}}(a)\|_{\alpha,\mathcal{X}}}. \tag{8.78}$$

We recall that the discrete norms $\|\cdot\|_{2,\mathcal{X}}$ and $\|\cdot\|_{\alpha,\mathcal{X}}$ are defined in Section 6.1.

In what follows, we compute $\mathbf{Er}_{\mathcal{V}}(\mathbf{p})$ and $\mathbf{Er}_{\kappa,\mathcal{E}}(\mathbf{g})$ to evaluate the discrete error on the potential and its gradient in vertex-based schemes, $\mathbf{Er}_{\widetilde{\mathcal{V}}}(\mathbf{p})$ and $\mathbf{Er}_{\kappa^{-1},\mathcal{F}}(\boldsymbol{\phi})$ to evaluate the discrete error on the potential and its flux in mixed cell-based schemes, and $\mathbf{Er}_{\widetilde{\mathcal{V}}}(\mathbf{p})$ and $\mathbf{Er}^*_{\kappa,\widetilde{\mathcal{E}}}(\mathbf{g})$ to evaluate the discrete error on the potential and its gradient in hybrid cell-based schemes. The last discrete error is adapted from (8.78) as follows:

$$\mathbf{Er}^*_{\kappa,\widetilde{\mathcal{E}}}(\mathbf{g})^2 := \frac{\sum_{\mathrm{c}\in\mathrm{C}} \|\mathsf{R}_{\widetilde{\mathcal{E}}_\mathrm{c}}(\underline{g}) - \mathbf{g}_\mathrm{c}\|^2_{\kappa,\widetilde{\mathcal{E}}_\mathrm{c}}}{\sum_{\mathrm{c}\in\mathrm{C}} \|\mathsf{R}_{\widetilde{\mathcal{E}}_\mathrm{c}}(\underline{g})\|^2_{\kappa,\widetilde{\mathcal{E}}_\mathrm{c}}}, \tag{8.79}$$

where $\|\mathbf{b}_\mathrm{c}\|^2_{\kappa,\widetilde{\mathcal{E}}_\mathrm{c}} := [\![\mathsf{H}^{\widetilde{\mathcal{E}}_\mathrm{c}\mathcal{F}_\mathrm{c}}_\kappa(\mathbf{b}_\mathrm{c}), \mathbf{b}_\mathrm{c}]\!]_{\mathcal{F}_\mathrm{c}\widetilde{\mathcal{E}}_\mathrm{c}}$ for all $\mathrm{c} \in \mathrm{C}$ and all $\mathbf{b}_\mathrm{c} \in \widetilde{\mathcal{E}}_\mathrm{c}$. Two continuous error norms are also evaluated.

Definition 8.40 (Continuous error norms)**.** *Let $a \in S_{\mathcal{X}}(\Omega)$ be an exact solution of a diffusion problem and $\mathbf{a} \in \mathcal{X}$ be the related discrete solution. Then, we set*

$$Er_{L^2}(\mathbf{a}) := \frac{\|a - \mathtt{L}_{\mathcal{X}}(\mathbf{a})\|_{L^2(\Omega)}}{\|a\|_{L^2(\Omega)}}, \qquad Er_{\alpha}(\mathbf{a}) := \frac{\|a - \mathtt{L}_{\mathcal{X}}(\mathbf{a})\|_{\alpha}}{\|a\|_{\alpha}}, \tag{8.80}$$

where we recall that $\|a\|^2_\alpha = \int_\Omega a \cdot \alpha\, a$.

In what follows, we compute $Er_{L^2}(\mathbf{p})$ and $Er_\kappa(\mathbf{g})$ to evaluate the error on the potential and its gradient in vertex-based schemes, $Er^*_{L^2}(\mathbf{p})$ and $Er_{\kappa^{-1}}(\boldsymbol{\phi})$ to evaluate the error on the potential and its flux in mixed cell-based schemes, and $Er^*_{L^2}(\mathbf{p})$ and $Er^*_\kappa(\mathbf{g})$ to evaluate the error on the potential and its gradient in hybrid cell-based schemes.

In vertex-based schemes, $Er_{L^2}(\mathbf{p})$ is computed using the conforming potential reconstruction $\mathtt{L}^{\mathrm{conf}}_{\mathcal{V}}$ in order to verify the second-order convergence rate stated in Theorem 8.13. In mixed cell-based and hybrid cell-based schemes, $Er^*_{L^2}(\mathbf{p})$ is defined somewhat differently. We adapt the definition so that it corresponds to the quantity used in Theorem 8.23, *i.e.*

$$Er^*_{L^2}(\mathbf{p}) := \frac{\|\mathtt{L}_{\mathcal{C}}\mathtt{R}_{\mathcal{C}}(p) - \mathtt{L}^0_{\widetilde{\mathcal{V}}}(\mathbf{p})\|}{\|p\|_{L^2(\Omega)}}. \tag{8.81}$$

In hybrid cell-based schemes, the definition is different since only the set of local reconstruction operators $\{\underline{\mathtt{L}}_{\widetilde{\mathcal{E}}_\mathrm{c}}\}_{\mathrm{c}\in\mathrm{C}}$ is defined. Thus, we adapt (8.80) as follows:

$$Er^*_\kappa(\mathbf{g})^2 := \frac{\sum_{\mathrm{c}\in\mathrm{C}}\|\underline{g} - \underline{\mathtt{L}}_{\widetilde{\mathcal{E}}_\mathrm{c}}(\mathbf{g}_\mathrm{c})\|^2_{\kappa,\mathrm{c}}}{\sum_{\mathrm{c}\in\mathrm{C}}\|\underline{g}\|^2_{\kappa,\mathrm{c}}}. \tag{8.82}$$

The rate of convergence is computed for any quantity Q using the same rationale. We set

$$\mathrm{R} := -3\frac{\log\left(\frac{Q_i}{Q_{i-1}}\right)}{\log\left(\frac{\#\mathrm{X}_i}{\#\mathrm{X}_{i-1}}\right)}, \tag{8.83}$$

where Q_i and Q_{i-1} are the quantities computed on the i^{th} and $(i-1)^{\mathrm{th}}$ meshes of the sequence, and $\#\mathrm{X}_i$ and $\#\mathrm{X}_{i-1}$ are the numbers of DoFs related to theses quantities and associated to the i^{th} and $(i-1)^{\mathrm{th}}$ meshes of the sequence.

Quantities related to minimum/maximum principle. We investigate numerically if CDO schemes ensure a discrete minimum/maximum principle for the potential.

Definition 8.41 (Min./Max. bounds)**.** *Let p be an exact solution of a diffusion problem and $\mathbf{p}\in\mathcal{X}$ be the related discrete solution ($\mathcal{X}$ being any of the DoFs space $\mathcal{V}$, $\widetilde{\mathcal{V}}$ or $\widetilde{\mathcal{L}}$ according to the CDO scheme). Then, we define the two following quantities:*

$$\mathbf{p}_{\min} := \min_{\mathrm{x}\in\mathrm{X}}\mathbf{p}_\mathrm{x}, \qquad \mathbf{p}_{\max} := \max_{\mathrm{x}\in\mathrm{X}}\mathbf{p}_\mathrm{x}. \tag{8.84}$$

If $\mathbf{p}_{\min}\geq\min_{\underline{x}\in\overline{\Omega}}p(\underline{x})$, then we consider that the discrete minimum principle is numerically satisfied. If $\mathbf{p}_{\max}\leq\max_{\underline{x}\in\overline{\Omega}}p(\underline{x})$, then we consider that the discrete maximum principle is numerically satisfied.

Quantities related to linear algebra. Linear systems arising in CDO schemes are solved using iterative solvers. The tolerance of the iterative solver is denoted by ϵ. We denote by $\mathrm{n}_{\mathrm{Ite}}$ the number of iterations performed by the iterative solver to reduce the Euclidean norm of the residual below the required accuracy. In addition, we denote by $\mathrm{n}_{\mathrm{Sys}}$ and NNZ the size and the number of non-zeros in the system matrix. We define the stencil of a scheme as the maximal number of non-zeros in a row of the system matrix. In order to compare the efficiency to solve the linear systems produced by vertex-based, mixed cell-based, and hybrid cell-based schemes, we define the following quantity:

$$\boldsymbol{\chi} := \mathrm{NNZ}\times\mathrm{n}_{\mathrm{Ite}}. \tag{8.85}$$

$\boldsymbol{\chi}$ corresponds to an approximation of the computational cost to solve the linear system since the most costly operation in an iterative solver is the matrix-vector product. The quantity $\boldsymbol{\chi}$ is also useful to evaluate the influence of the element shapes on the conditioning of the system matrix.

Since the linear system (8.3) for vertex-based schemes or (8.77) for hybrid cell-based schemes is SPD by construction, a Conjugate Gradient (CG) method preconditioned with a Symmetric Successive OverRelaxation (SSOR) technique is employed. For mixed cell-based schemes, the saddle-point problem is solved using an augmented Lagrangian-Uzawa (ALU) algorithm (Fortin & Glowinski, 1983). Recasting the system (8.34) into the more generic form

$$\begin{bmatrix} \mathsf{A} & \mathsf{B}^{\mathrm{T}} \\ \mathsf{B} & 0 \end{bmatrix} \begin{bmatrix} \boldsymbol{\phi} \\ \mathbf{p} \end{bmatrix} = \begin{bmatrix} 0_{\mathcal{E}} \\ \mathbf{s} \end{bmatrix}, \tag{8.86}$$

each iteration of ALU solves the following system:

$$\left(\underbrace{\mathsf{A} + r\mathsf{B}^{\mathrm{T}}\mathsf{B}}_{\mathsf{A}_r} \right) (\boldsymbol{\phi}^{(k+1)}) = r\mathsf{B}^{\mathrm{T}}(\mathbf{s}) - \mathsf{B}^{\mathrm{T}}(\mathbf{p}^{(k)}), \tag{8.87}$$

until the norm of the global residual is below the required tolerance. The real number $r > 0$ is the parameter related to the ALU algorithm. Numerical experiments suggest that a convenient choice of r is the reciprocal of $\max_{\mathrm{c}\in\mathrm{C}}|\mathrm{c}|$. The second step of the ALU algorithm consists of updating the discrete potential as follows:

$$\mathbf{p}^{(k+1)} = \mathbf{p}^{(k)} + \mathsf{B}(\boldsymbol{\phi}^{(k+1)}) - \mathbf{s}. \tag{8.88}$$

To compare mixed cell-based schemes with vertex-based and hybrid cell-based schemes, the quantity $\boldsymbol{\chi}$ is computed using $\mathrm{n_{Ite}}$ equal to the accumulated number of iterations of CG algorithm and NNZ corresponds to that of the matrix A_r. For meshes with more elements, more sophisticated techniques like algebraic multigrid could be employed to increase the efficiency of the resolution of the linear system.

8.4.2 Continuous and piecewise affine solution

We consider the following test case adapted from Perot & Subramanian (2007); see Figure 8.6. A jump of the value of the conductivity coefficient is located at the plane $\{x = 0.5\}$. We only consider the `Hex`, `PrT`, `HLR` and `CB` mesh sequences for this test case since the plane $\{x = 0.5\}$ is not an interface of the primal mesh for the other mesh sequences. There is no source term and non-homogeneous Dirichlet BCs are imposed in such a way that the solution is

$$p(\underline{x}) = \begin{cases} x + y + 1 & x \leq 0.5, \\ \dfrac{\kappa_1}{\kappa_2} x + y + \left(1 - \dfrac{\kappa_1 - \kappa_2}{2\kappa_2}\right) & x > 0.5, \end{cases} \tag{8.89}$$

where $\kappa_1 = 0.1$ and $\kappa_2 = 10^3$. Vertex-based (8.3), mixed cell-based (8.34), and hybrid cell-based (8.77) schemes capture exactly the solution in the sense that the error norms on potential and its gradient (or flux) are reduced down to machine precision ($\approx 10^{-16}$) for all meshes of the tested sequences.

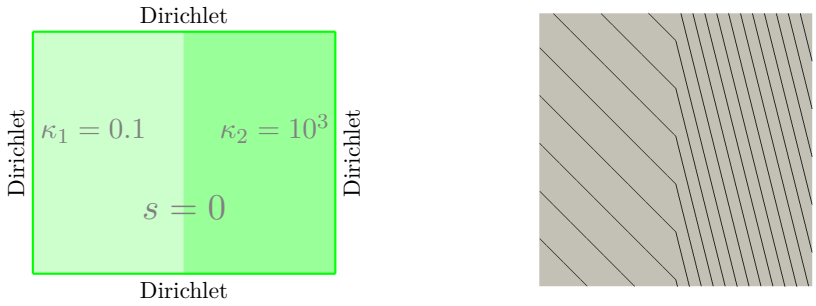

Figure 8.6 – Left: Description of the problem; Right: Isovalues of the computed potential.

8.4.3 Anisotropic diffusion problem

We now consider the first test case of the FVCA benchmark. The exact potential and the conductivity tensor in (8.1) are defined as follows:

$$p(x,y,z) := 1 + \sin(\pi x)\sin\left(\pi\left(y+\frac{1}{2}\right)\right)\sin\left(\pi\left(z+\frac{1}{3}\right)\right), \qquad \underline{\underline{\kappa}} := \begin{bmatrix} 1 & 0.5 & 0 \\ 0.5 & 1 & 0.5 \\ 0 & 0.5 & 1 \end{bmatrix}. \quad (8.90)$$

The source term and the Dirichlet boundary condition are set so that (8.90) solves (8.1). The integral of the source term is computed using the barycentric subdivision of each primal cell. We simply collect the value at the barycenter of each subtetrahedra weighted by its volume. This quadrature is of order 1.

Convergence rates. We summarize the results related to the convergence rates of the potential and its gradient (or flux) by indicating for each CDO scheme the computed convergence rate between the two finest meshes of each mesh sequence. Table 8.1 collects results for vertex-based schemes, Table 8.2 for mixed cell-based schemes, and Table 8.3 for hybrid cell-based schemes.

Numerical results gathered in Table 8.1 are in agreement with the theoretical results derived in Section 8.1. Namely, expected (or greater) convergence rates are observed for all the mesh sequences and all the errors except for $Er_{L^2}(\mathbf{p})$ in the case of the `Ker` mesh sequence. The reason is that this mesh sequence does not satisfy **(MR)** since $\eta_\perp$ (cf. (6.7)) is not uniformly bounded during the successive refinements (cf. Appendix A for more details). Moreover, a super-convergent behavior is observed for the two discrete errors except for $\mathbf{Er}_{\kappa,\mathcal{E}}(\mathbf{g})$ in the case of the `CB` mesh sequence. `Vb-DGA` and `Vb-SUSHI` deliver close results for all the mesh sequences except for the `Ker` mesh sequence, for which a better convergence rate is observed with `Vb-DGA`.

	$\mathbf{Er}_{\mathcal{V}}(\mathbf{p})$		$Er_{L^2}(\mathbf{p})$		$\mathbf{Er}_{\kappa,\mathcal{E}}(\mathbf{g})$		$Er_{\kappa}(\mathbf{g})$	
Vb-	DGA	SUSHI	DGA	SUSHI	DGA	SUSHI	DGA	SUSHI
Hex	2.1	2.1	2.1	2.1	2.1	2.0	1.0	1.0
PrT	2.0	2.0	2.0	2.0	2.0	2.0	1.0	1.0
PrG	2.0	1.9	2.0	2.0	1.8	1.8	1.0	1.0
CB	2.0	2.0	2.0	2.0	1.0	1.0	1.0	1.0
Ker	1.6	1.1	1.6	1.2	1.8	1.4	0.9	0.8

Table 8.1 – Computed convergence rates of the errors on the potential and its gradient between the two finest meshes of each sequence for vertex-based schemes using either the DGA reconstruction or the SUSHI-like reconstruction.

Remark 8.42 (Alternative potential reconstruction)**.** *Let* $\mathtt{L}^1_{\mathcal{V}}(\mathbf{p})$ *be piecewise affine on the submesh* $\mathfrak{P}_{\mathrm{E,c}}$ *(cf. Chapter 5) such that, for all* $\mathrm{c} \in \mathrm{C}$ *and all* $\mathrm{e} \in \mathrm{E}$*,*

$$\mathtt{L}^1_{\mathcal{V}}(\mathbf{p})(\underline{x})|_{\mathfrak{p}_{\mathrm{e,c}}} := \frac{1}{2}\sum_{\mathrm{v}\in\mathrm{V_e}} \mathbf{p} + \underline{\mathtt{L}}_{\mathcal{E}}(\mathsf{GRAD}(\mathbf{p}))|_{\mathfrak{p}_{\mathrm{e,c}}} \cdot (\underline{x} - \underline{x}_{\mathrm{e}}), \qquad \forall \mathbf{p} \in \mathcal{V}, \tag{8.91}$$

where $\underline{\mathtt{L}}_{\mathcal{E}}$ *is a piecewise constant circulation reconstruction operator in each primal cell defined in Section 7.3.1. Then, our numerical experiments indicate that the discrete error* $Er_{L^2}(\mathbf{p})$ *computed using this potential reconstruction operator also converges to second-order in the* L^2*-norm.*

Numerical results gathered in Table 8.2 are in agreement with the theoretical results derived in Section 8.2. Comments are similar to those of Table 8.1. Mixed cell-based schemes appear to be more sensitive to the non-orthogonality criteria than vertex-based schemes. Namely, lower convergence rates are observed in the case of the `Ker` mesh sequence for all the errors.

	$\mathbf{Er}_{\widetilde{\mathcal{V}}}(\mathbf{p})$		$Er^*_{L^2}(\mathbf{p})$		$\mathbf{Er}_{\kappa^{-1},\mathcal{F}}(\boldsymbol{\phi})$		$Er_{\kappa^{-1}}(\boldsymbol{\phi})$	
Cb-	DGA	SUSHI	DGA	SUSHI	DGA	SUSHI	DGA	SUSHI
Hex	2.0	2.0	2.0	2.0	2.0	1.9	1.0	1.0
PrT	1.8	1.9	1.9	1.9	1.1	1.1	1.0	1.0
PrG	1.9	1.9	2.0	2.0	1.6	1.7	1.0	1.0
CB	2.0	2.0	2.0	2.0	1.0	1.0	1.0	1.0
Ker	1.1	0.7	1.1	0.7	1.4	1.1	0.6	0.5

Table 8.2 – Computed convergence rates of the errors on the potential and its flux between the two finest meshes of each sequence for mixed cell-based schemes using either the DGA reconstruction or the SUSHI-like reconstruction.

Numerical results gathered in Table 8.3 are in agreement with the theoretical results derived in Section 8.3. Comments are similar to those of Table 8.1. There are three differences with respect to vertex-based schemes. Firstly, better convergence rates are observed for the `Ker` sequence using hybrid cell-based schemes. Hybrid cell-based schemes seem to be less sensitive to the regularity criterion $\eta_\perp$. Secondly, no super-convergent behavior is observed for the discrete error $\mathbf{Er}_{\kappa,\widetilde{\mathcal{E}}}(\mathbf{g})$. Thirdly, `HCb-SUSHI` and `HCb-DGA` deliver close results, but `HCb-SUSHI` appears to deliver better convergence rates in the case of the `Ker` mesh sequence (in opposition to what has been observed in vertex-based schemes).

	$\mathbf{Er}_{\widetilde{\mathcal{V}}}(\mathbf{p})$		$Er^*_{L^2}(\mathbf{p})$		$\mathbf{Er}^*_{\kappa,\widetilde{\mathcal{E}}}(\mathbf{g})$		$Er^*_{\kappa}(\mathbf{g})$	
HCb-	DGA	SUSHI	DGA	SUSHI	DGA	SUSHI	DGA	SUSHI
Hex	2.0	2.0	2.0	2.0	0.9	1.0	1.0	1.0
PrT	1.9	1.9	2.0	1.9	1.0	1.0	1.0	1.0
PrG	2.0	2.0	2.0	2.0	0.9	0.9	1.0	1.0
CB	2.0	2.0	2.0	2.0	1.0	1.0	1.0	1.0
Ker	1.8	1.9	1.8	1.9	0.8	1.1	1.1	1.2

Table 8.3 – Computed convergence rates of the errors on the potential and its gradient between the two finest meshes of each sequence for hybrid cell-based schemes using either the DGA reconstruction or the SUSHI reconstruction.

Discrete min./max. principle. In Table 8.4, we collect results on the discrete min./max. principle for this test case. The exact minimal and maximal bounds on the potential are 0 and 2 (cf. (8.90)). For each couple (mesh sequence, scheme), Y in the "min" (resp. "max") column indicates that all the meshes of the sequence satisfy the discrete minimum (resp. maximum) principle (cf. Definition 8.41), N indicates that at least one mesh of the sequence does not satisfy the property.

Only vertex-based schemes satisfy the discrete min./max. principle for all the meshes of the tested sequences. In mixed cell-based schemes, `Cb-DGA` satisfies the discrete min./max. principle for all meshes except the `Ker` mesh sequence, while `Cb-SUSHI` almost never satisfies the discrete min./max. principle. The almost converse situation is found for hybrid cell-based schemes. `HCb-DGA` never satisfies the discrete min./max. principle, while `HCb-SUSHI` satisfies the min./max. principle for the `Hex`, `PrT`, and `PrG` mesh sequences.

	Vb-DGA		Vb-SUSHI		Cb-DGA		Cb-SUSHI		HCb-DGA		HCb-SUSHI	
	min	max	min	max	min	max	min	max	min	max	min	max
Hex	Y	Y	Y	Y	Y	Y	N	N	N	N	Y	Y
PrT	Y	Y	Y	Y	Y	Y	N	N	N	N	Y	Y
PrG	Y	Y	Y	Y	Y	Y	Y	N	N	N	Y	Y
CB	Y	Y	Y	Y	Y	Y	N	N	N	N	N	N
Ker	Y	Y	Y	Y	N	N	N	N	N	N	N	N

Table 8.4 – Synthesis of results related to the discrete min./max. principle.

Remark 8.43 (Non-planar faces)**.** *Additional tests show that if the primal faces are non-planar, then the discrete min./max. principle is not satisfied by vertex-based schemes.*

Remark 8.44 (Face unknowns in hybrid cell-based schemes)**.** *If we only consider the face unknowns to check the min./max. principle, we observe that `HCb-DGA` satisfies the property for the `Hex`, `PrT`, and `PrG` mesh sequences.*

Linear algebra. Table 8.5 collects the stencil observed for each scheme according to the mesh sequence. Hybrid and mixed cell-based schemes yield the same stencil, independently of the choice of the reconstruction operator. This is not the case of vertex-based schemes. `Vb-SUSHI` yields a smaller stencil than `Vb-DGA` for Cartesian meshes (cf. Remark 7.34). Moreover, vertex-based schemes yield a stencil two or three times larger than hybrid and mixed cell-based schemes.

	Vb-DGA	Vb-SUSHI	Cb-DGA	Cb-SUSHI	HCb-DGA	HCb-SUSHI
Hex	25	19	11	11	11	11
PrT	21	21	9	9	9	9
PrG	39	39	15	15	15	15
CB	93	93	29	29	29	29
Ker	27	27	11	11	11	11

Table 8.5 – Stencil of the system matrix of the finest mesh of each sequence and for each CDO scheme.

	Vb-DGA	Vb-SUSHI	Cb-DGA	Cb-SUSHI	HCb-DGA	HCb-SUSHI
Hex	1.0	1.1	39.5	31.6	2.3	2.6
PrT	1.0	1.2	125.0	116.7	6.3	6.3
PrG	1.0	1.6	20.0	20.0	0.9	1.0
CB	1.0	1.6	56.7	57.5	1.8	1.9
Ker	1.0	1.3	52.5	45.0	3.0	2.7

Table 8.6 – Values of the relative computational cost $\boldsymbol{\chi}_{\mathrm{R}}$ for each mesh sequence and the different CDO schemes.

In Table 8.6, we compute the relative computational cost $\boldsymbol{\chi}_{\mathrm{R}}$ of a mesh sequence M for a given scheme S as follows:

$$\boldsymbol{\chi}_{\mathrm{R}}(\mathtt{S},\mathtt{M}) := \frac{\boldsymbol{\chi}(\mathtt{S},\mathtt{M})}{\boldsymbol{\chi}(\mathtt{Vb\text{-}DGA},\mathtt{M})}, \tag{8.92}$$

where $\boldsymbol{\chi}(\mathtt{S},\mathtt{M})$ is the computational cost associated to the finest mesh of the sequence M for the scheme S. We observe that mixed cell-based schemes are much more computationally intensive than hybrid cell-based and vertex-based schemes due to the saddle-point formulation. Therefore, in what follows, we only detail the comparison between vertex-based and hybrid cell-based schemes. Additional results related to mixed cell-based schemes are presented in Appendix B.1. Even if vertex-based schemes yield the largest stencil, they are in most cases less computationally intensive than hybrid cell-based schemes. Furthermore, Vb-DGA (resp. HCb-DGA) appears to be slightly less computationally-intensive than Vb-SUSHI (resp. HCb-SUSHI).

Sequence	Hex	PrT	PrG	CB	Ker
Thumbnail	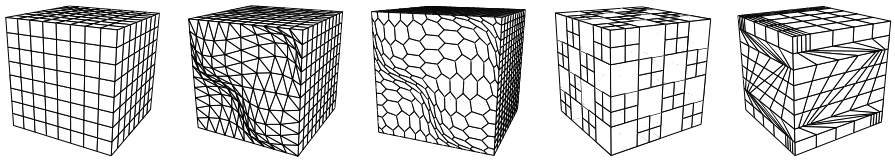				
Labels A					
Labels B					

Table 8.7 – Labels associated to each mesh sequence.

Analysis of vertex-based and hybrid cell-based schemes. In what follows, we assign a label to each mesh sequence as depicted in Table 8.7. To analyze the different schemes, we study the accuracy of the potential and its gradient approximation. We also analyze the cost-effectiveness of each scheme, that is the ratio error to cost.

For Vb-DGA and Vb-SUSHI schemes, we plot in Figure 8.8 the error on potential in discrete and continuous norms, the error on its gradient in discrete and continuous energy norms. In both cases, Vb-DGA is more accurate than Vb-SUSHI. The hierarchy in terms of accuracy between the different mesh sequences is the following: Ker $<$ CB $<$ PrG $<$ PrT $<$ Hex. In addition, the computational-effectiveness for the potential and its gradient are depicted in Figure 8.8 (bottom row). For the two quantities, Vb-DGA turns out to be more cost-effective than Vb-SUSHI.

Remark 8.45 (Stiffness matrix)**.** *We observe that on simplicial meshes, the stiffness matrix built using the DGA circulation reconstruction operator is identical to that obtained with the Whitney circulation reconstruction operator.*

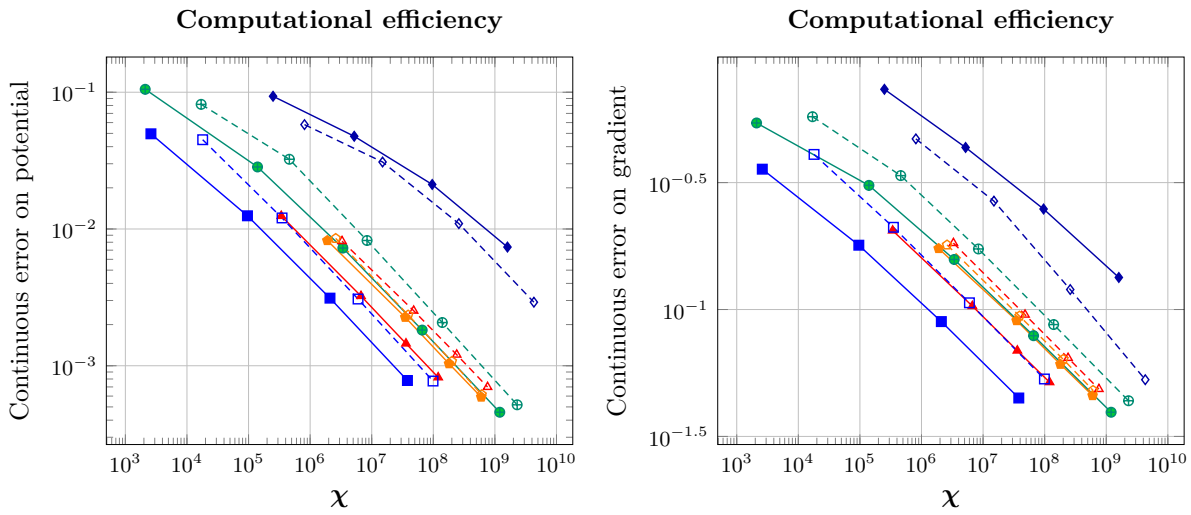

Figure 8.7 – Comparison of the cost-effectiveness between `Vb-DGA` (labels A) and `HCb-SUSHI` (labels B) schemes for the continuous error on the potential (left) and the error on the gradient in continuous energy norm (right).

In Figure 8.9, we plot the error on potential and its gradient in discrete and continuous norms for `HCb-DGA` and `HCb-SUSHI` schemes. Contrary to vertex-based schemes, the SUSHI reconstruction leads to a more accurate scheme for the potential and its gradient than that using the DGA reconstruction. The hierarchy in terms of accuracy between the different mesh sequences remains the same: `Ker` $<$ `CB` $<$ `PrG` $<$ `PrT` $<$ `Hex`. The computational-effectiveness of the two schemes for the potential and its gradient can be assessed from Figure 8.9 (bottom row). In both cases, `HCb-SUSHI` turns out to be more cost-effective than `HCb-DGA`.

Comparison of vertex-based and hybrid cell-based schemes. To compare vertex-based and hybrid cell-based schemes, we consider `Vb-DGA` and `HCb-SUSHI` which are the best (tested) cost-effective schemes of each family (cf. Figure 8.8 and Figure 8.9). In Figure 8.7, we plot the accuracy on the potential approximation (in terms of $Er_{L^2}(\mathbf{p})$ for `Vb-DGA` and $Er^*_{L^2}(\mathbf{p})$ for `HCb-SUSHI`) and the accuracy of the gradient approximation (in terms of $Er_\kappa(\mathbf{g})$) against the computational cost. For the `Hex`, `PrT`, `PrG`, and `CB` mesh sequences, `Vb-DGA` turns out to be more cost-effective than `HCb-SUSHI` for this test case. This is the opposite situation for the `Ker` mesh sequence.

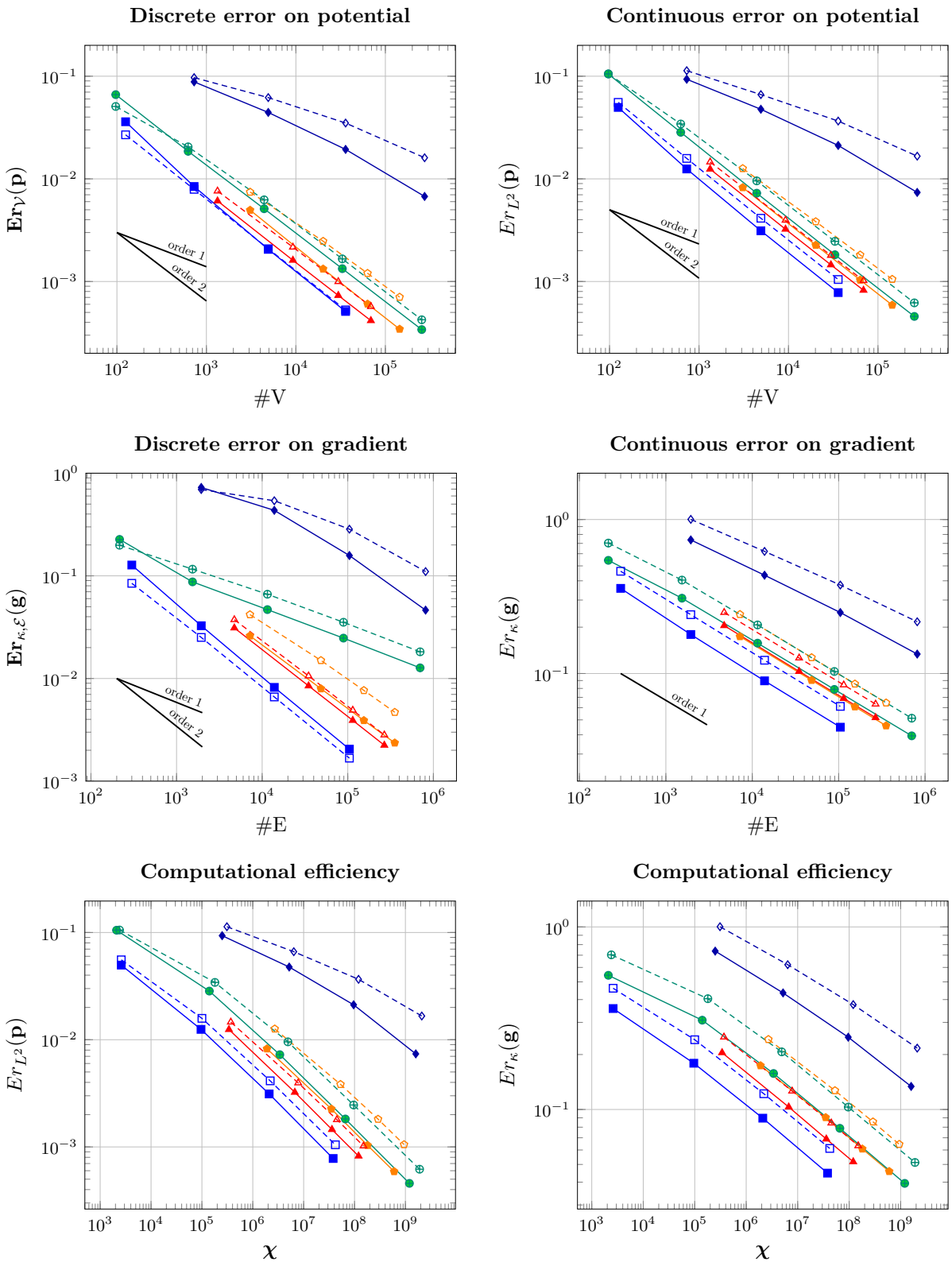

Figure 8.8 – Comparison between `Vb-DGA` (labels A) and `Vb-SUSHI` (labels B) schemes of the error on potential (top row), of the error on its gradient (middle row), and of the cost-effectiveness (bottom row).

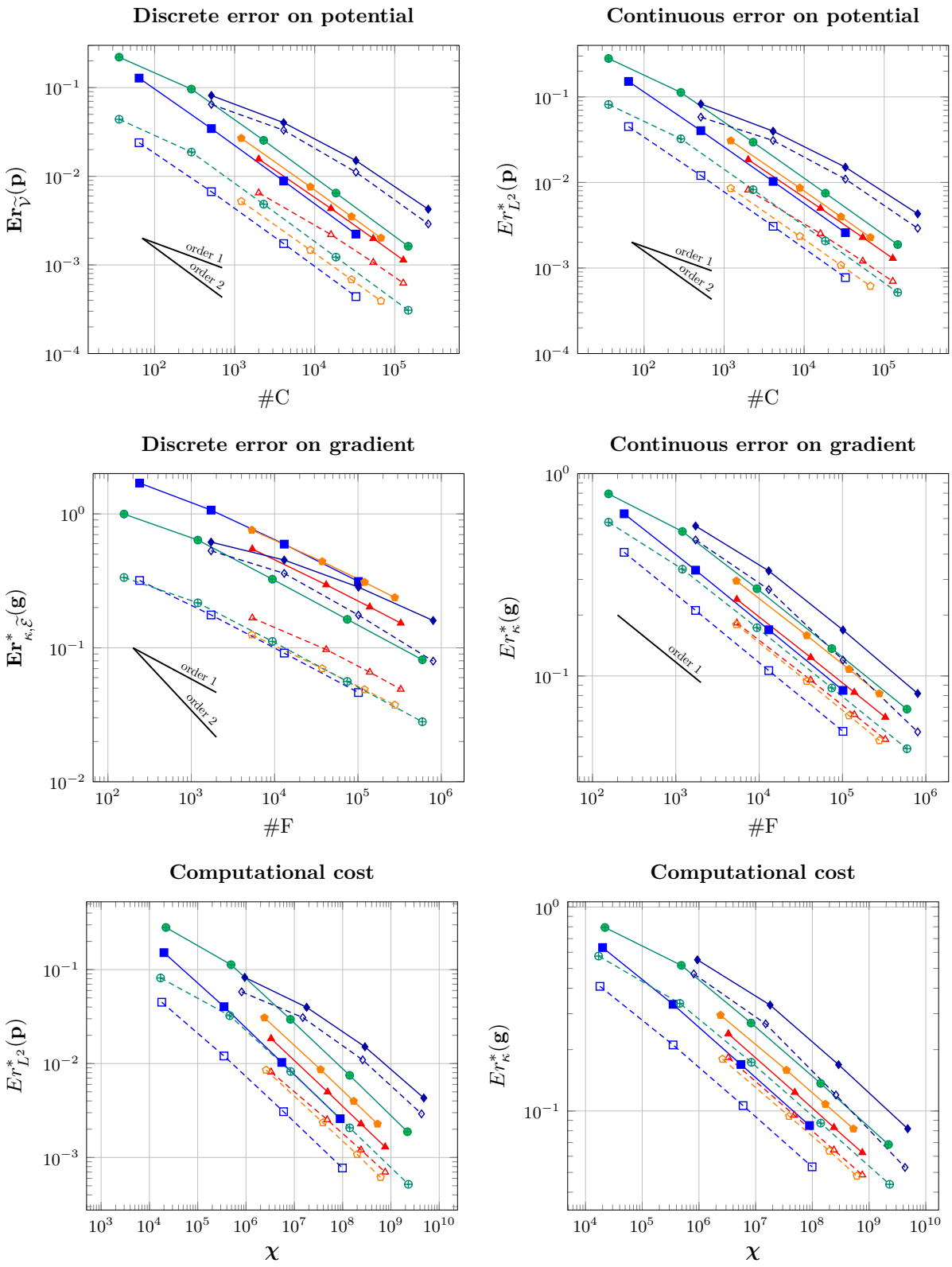

Figure 8.9 – Comparison between `HCb-DGA` (labels A) and `HCb-SUSHI` (labels B) schemes of the error on potential (top row), of the error on its gradient (middle row), and of the cost-effectiveness (bottom row).

8.4.4 Anisotropic and heterogeneous diffusion problem

We now consider the fifth test case of the FVCA benchmark (see Figure 8.10). The unit cube is subdivided into four partitions

$$\begin{aligned} \Omega_1 &:= \{(x,y,z)\,|\,y \le 0.5, z \le 0.5\}, & \Omega_2 &:= \{(x,y,z)\,|\,y > 0.5, z \le 0.5\}, \\ \Omega_3 &:= \{(x,y,z)\,|\,y > 0.5, z > 0.5\}, & \Omega_4 &:= \{(x,y,z)\,|\,y \le 0.5, z > 0.5\}. \end{aligned} \tag{8.93}$$

The exact potential is specified in each partition as follows

$$p(x,y,z)|_{\Omega_i} := \gamma_i \sin(2\pi x)\sin(2\pi y)\sin(2\pi z), \tag{8.94}$$

where $\gamma_1 = 0.1$, $\gamma_2 = 10$, $\gamma_3 = 100$, and $\gamma_4 = 0.01$ and the conductivity tensor as follows:

$$\begin{aligned} \underline{\underline{\kappa}}|_{\Omega_1} &:= \begin{bmatrix} 1 & 0 & 0 \\ 0 & 10 & 0 \\ 0 & 0 & 0.01 \end{bmatrix} & \underline{\underline{\kappa}}|_{\Omega_2} &:= \begin{bmatrix} 1 & 0 & 0 \\ 0 & 0.1 & 0 \\ 0 & 0 & 100 \end{bmatrix} \\ \underline{\underline{\kappa}}|_{\Omega_3} &:= \begin{bmatrix} 1 & 0 & 0 \\ 0 & 0.01 & 0 \\ 0 & 0 & 10 \end{bmatrix} & \underline{\underline{\kappa}}|_{\Omega_4} &:= \begin{bmatrix} 1 & 0 & 0 \\ 0 & 100 & 0 \\ 0 & 0 & 0.01 \end{bmatrix}. \end{aligned} \tag{8.95}$$

The source term and the Dirichlet boundary conditions are set so that (8.94) solves (8.1). The integral of the source term is computed using the barycentric subdivision of each primal cell. We simply collect the value at the barycenter of each subtetrahedra weighted by its volume. This quadrature is of order 1.

We only consider the `Hex` and `HLR` mesh sequences for this test case since these sequences naturally match the inner interfaces induced by the partitioning of Ω into four subdomains.

Convergence rates. Table 8.8 (resp. 8.9 and 8.10) collects the computed convergence rates between the two finest meshes of each mesh sequence for vertex-based schemes (resp. mixed cell-based schemes and hybrid cell-based schemes). These convergence rates are in agreement with the theoretical results derived in this chapter. Moreover, a superconvergent behavior is observed for the error in discrete energy norm in the case of vertex-based and mixed cell-based schemes.

Discrete min./max. principle. The exact minimal and maximal bounds are -100 and 100. If at least one mesh of the sequence does not preserve these bounds, we write `N` otherwise `Y`. Table 8.11 collects the results on the discrete min./max. principle. The results are quite different from the previous test case. All tested mixed and hybrid cell-based schemes respect the min./max. principle while only the `Vb-SUSHI` scheme respects the principle.

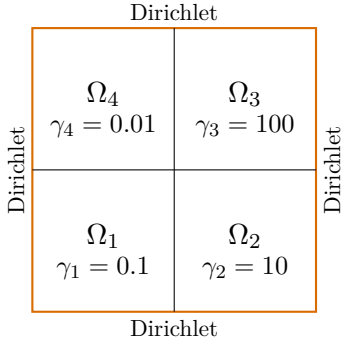

Figure 8.10 – Description of the problem.

	$\mathbf{Er}_{\mathcal{V}}(\mathbf{p})$		$Er_{L^2}(\mathbf{p})$		$\mathbf{Er}_{\kappa,\mathcal{E}}(\mathbf{g})$		$Er_{\kappa}(\mathbf{g})$	
Vb-	DGA	SUSHI	DGA	SUSHI	DGA	SUSHI	DGA	SUSHI
Hex	2.1	1.7	2.1	2.0	2.1	1.9	1.0	1.0
HLR	2.1	1.7	2.1	2.0	2.1	1.9	1.0	1.0

Table 8.8 – Computed convergence rates of the errors on the potential and its gradient between the two finest meshes of each sequence for vertex-based schemes using either the DGA reconstruction or the SUSHI-like reconstruction.

	$\mathbf{Er}_{\widetilde{\mathcal{V}}}(\mathbf{p})$		$Er^*_{L^2}(\mathbf{p})$		$\mathbf{Er}_{\kappa^{-1},\mathcal{F}}(\boldsymbol{\phi})$		$Er_{\kappa^{-1}}(\boldsymbol{\phi})$	
Cb-	DGA	SUSHI	DGA	SUSHI	DGA	SUSHI	DGA	SUSHI
Hex	2.0	2.0	2.0	2.0	2.0	2.0	1.0	1.0
HLR	2.0	2.0	2.0	2.0	2.0	2.0	1.0	1.0

Table 8.9 – Computed convergence rates of the errors on the potential and its flux between the two finest meshes of each sequence for mixed cell-based schemes using either the DGA reconstruction or the SUSHI-like reconstruction.

	$\mathbf{Er}_{\widetilde{\mathcal{V}}}(\mathbf{p})$		$Er^*_{L^2}(\mathbf{p})$		$\mathbf{Er}^*_{\kappa,\widetilde{\mathcal{E}}}(\mathbf{g})$		$Er^*_{\kappa}(\mathbf{g})$	
HCb-	DGA	SUSHI	DGA	SUSHI	DGA	SUSHI	DGA	SUSHI
Hex	2.0	2.0	2.0	2.0	1.0	1.0	1.0	1.0
HLR	2.0	2.0	2.0	2.0	1.0	1.0	1.0	1.0

Table 8.10 – Computed convergence rates of the errors on the potential and its gradient between the two finest meshes of each sequence for hybrid cell-based schemes using either the DGA reconstruction or the SUSHI reconstruction.

	Vb-DGA		Vb-SUSHI		Cb-DGA		Cb-SUSHI		HCb-DGA		HCb-SUSHI	
	min	max	min	max	min	max	min	max	min	max	min	max
Hex	N	N	Y	Y	Y	Y	Y	Y	Y	Y	Y	Y
HLR	N	N	Y	Y	Y	Y	Y	Y	Y	Y	Y	Y

Table 8.11 – Synthesis of results related to the discrete min./max. principle.

Computational cost. Table 8.12 collects values of the relative computational cost associated to each scheme for the two mesh sequences. $\boldsymbol{\chi}_{\mathrm{R}}$ is defined in (8.92) using the `Vb-DGA` scheme as reference. Contrary to the previous test case, the less computationally-intensive scheme is the `Vb-SUSHI` scheme. The reason is that the stencil of the system matrix is reduced with the SUSHI-like reconstruction in the case of vertex-based schemes since the conductivity tensor is diagonal and the `Hex` meshes super-admissible meshes (`HLR` meshes benefit also from a reduction of stencil since they are built as an assembly of super-admissible meshes). Namely, the stencil for the `Hex` mesh sequence is equal to 27 in the case of `Vb-DGA` and to 7 in the case of `Vb-SUSHI`.

	Vb-DGA	Vb-SUSHI	Cb-DGA	Cb-SUSHI	HCb-DGA	HCb-SUSHI
Hex	1.0	0.3	9.6	8.3	1.3	1.3
HLR	1.0	0.5	52.6	39.5	1.6	1.7

Table 8.12 – Relative computational cost $\boldsymbol{\chi}_{\mathrm{R}}$ for each mesh sequence and for the different schemes

Comparison of vertex-based and hybrid cell-based schemes. In what follows, we only consider the vertex-based and hybrid cell-based schemes since the mixed cell-based is much more computationally-intensive. We assign a generic label to each mesh sequence as depicted in Table 8.13.

Sequence	Hex	HLR
Thumbnail	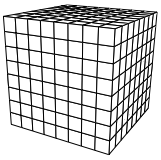	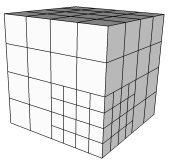
Labels A		
Labels B		

Table 8.13 – Labels associated to each mesh sequence.

In Figure 8.11, we compare the behavior of `Vb-DGA` and `Vb-SUSHI` schemes in terms of accuracy and cost-effectiveness. We successively plot the error on potential in the discrete and continuous norms, the error on the gradient in the discrete and continuous energy norms and the error on potential (resp. gradient) versus the computational cost. We observe that `Vb-SUSHI` is more accurate than `Vb-DGA` in discrete norms and the converse situation in continuous norms. In terms of computational efficiency, `Vb-SUSHI` scheme appears to be better than `Vb-DGA` for this test case.

In Figure 8.12, we compare compare the behavior of `HCb-DGA` and `HCb-SUSHI` schemes in terms of accuracy and cost-effectiveness. We plot the similar quantities as in Figure 8.11. We observe that `HCb-SUSHI` is more accurate than `HCb-DGA` for all quantities. In terms of computational efficiency, `HCb-SUSHI` scheme appears to be better than `HCb-DGA` for this test case.

In Figure 8.13, we compare the computational efficiency of `Vb-SUSHI` and `HCb-SUSHI`. We conclude that `HCb-SUSHI` turns out to be more cost-effective than `Vb-SUSHI` in terms of potential approximation while this is the converse situation in terms of gradient approximation.

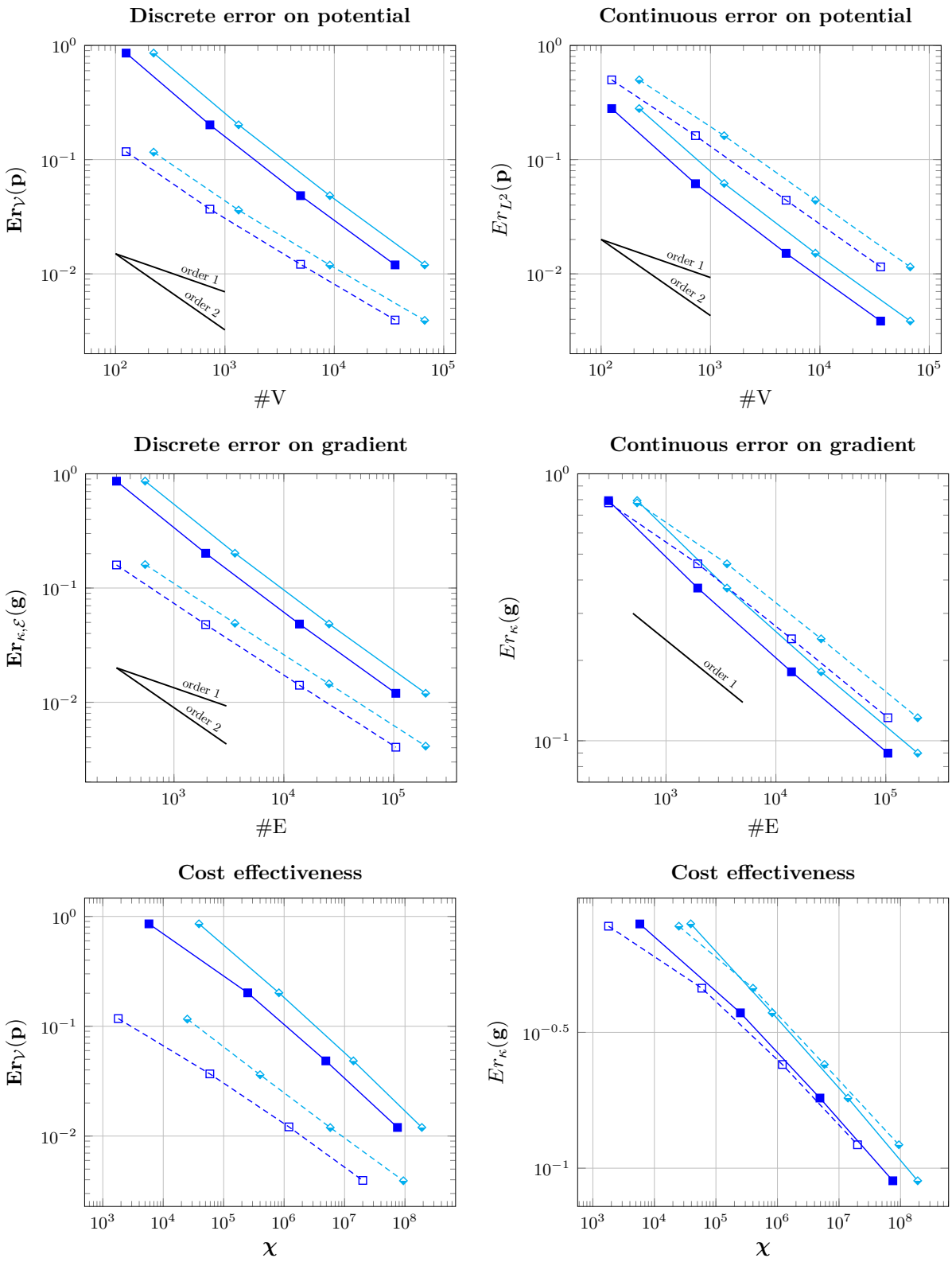

Figure 8.11 – Comparison between `Vb-DGA` (labels A) and `Vb-SUSHI` (labels B) schemes of the error on the potential (top line), of the error on the gradient (middle line), and of the cost-effectiveness (bottom line).

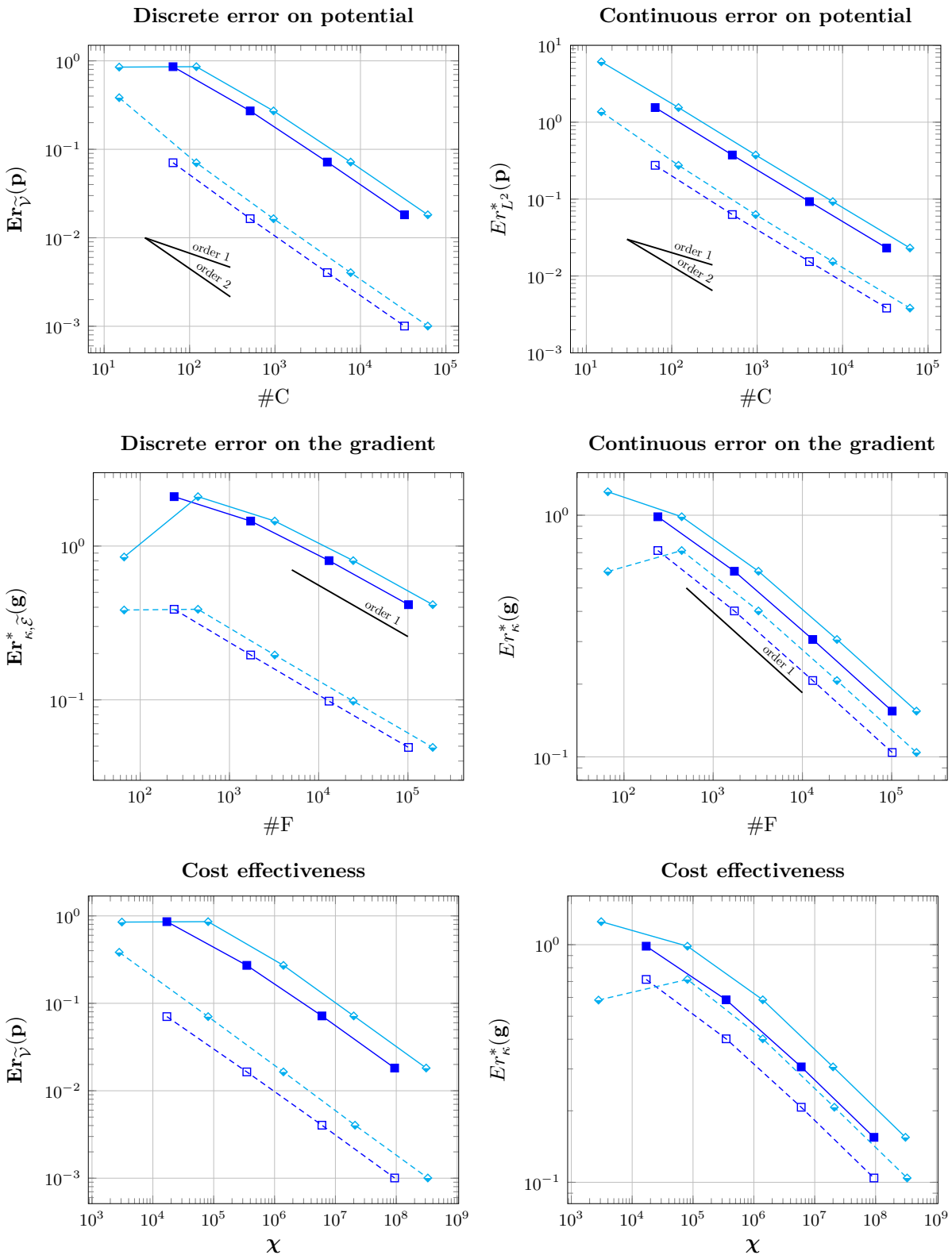

Figure 8.12 – Comparison between `HCb-DGA` (labels A) and `HCb-SUSHI` (labels B) schemes of the error on potential (top line), of the error on gradient (middle line), and of the cost-effectiveness (bottom line).

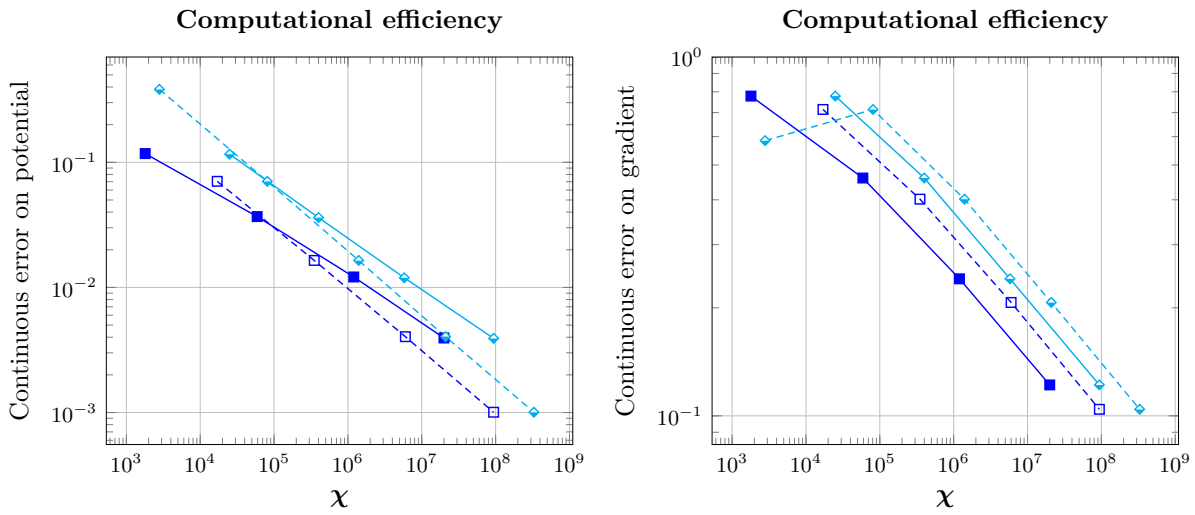

Figure 8.13 – Comparison of the cost-effectiveness between `Vb-SUSHI` (labels A) and `HCb-SUSHI` (labels B) schemes for the error on potential in continuous norm (left) and the error on gradient (right) in continuous energy norm.

Chapter 9

Stokes equations

Contents

This chapter is devoted to the analysis of CDO schemes for the Stokes equations presented in Section 4.2. As mentioned in Section 4.2, our starting point are the Stokes equations in the two-field and three-field curl formulations. Since the pressure is seen as a potential, its DoFs are located either at primal or at dual mesh vertices. The former case uses the two-field curl formulation and leads to vertex-based pressure schemes. These CDO schemes are analyzed in Section 9.1 The latter case uses the three-field curl formulation and leads to cell-based pressure schemes (since primal cells are in one-to-one correspondence with dual mesh vertices). These CDO schemes are analyzed in Section 9.2. The vertex-based pressure schemes are, to our knowledge, the first of this class on polyhedral meshes. The cell-based pressure schemes share common features with the recent MSE schemes of Kreeft & Gerritsma (2013); however, the present schemes can be deployed on polyhedral meshes. The two families of CDO schemes involve two discrete Hodge operators, one linking the velocity (seen as a circulation) to the mass flux and the other linking the vorticity to the viscous stress. One key feature of the present schemes is that they ensure local mass and momentum conservation on polyhedral meshes, while being only first order. The discrete stability hinges on novel discrete Poincaré inequalities derived in Section 7.4. Moreover, using commutators related to the consistency error (cf. Section 6.2.2), we derive *a priori* error estimates and establish first-order error estimates for smooth solutions. In addition, we show how the present CDO framework can deal with the practically important issue of discretizing the external load. Namely, we present two strategies for discretizing the external load so as to deliver tight error estimates when the external load is expected to have a large curl-free or divergence-free part (see Linke (2014) for a related work). Finally, we conclude this chapter with numerical results in Section 9.3.

In order to avoid technicalities related to harmonic forms, we often assume in what follows that Ω is simply connected and its boundary $\partial\Omega$ is connected. Whenever used, we refer to this assumption as $(\mathbf{A}_{\boldsymbol{\Omega}})$.

9.1 Vertex-based pressure schemes

9.1.1 Discrete systems

For the sake of completeness, we recall the key points of the definition of vertex-based pressure schemes (cf. Section 4.2 for more details). In vertex-based pressure schemes, the two unknowns are the pressure potential $p^* := \rho^{-1}p$ and the velocity $\underline{u}$. The starting formulation is the two-field curl formulation (4.12) defined as follows:

$$\begin{cases} \underline{\mathrm{curl}}(\mu\,\underline{\mathrm{curl}}(\underline{u})) + \rho\,\underline{\mathrm{grad}}(p^*) = \rho\underline{f}^*, & \text{in } \Omega, \\ \mathrm{div}(\rho\underline{u}) = 0, & \text{in } \Omega, \end{cases} \tag{9.1}$$

where we have introduced the external load density $\underline{f}^* := \rho^{-1}\underline{f}$. We recall that the density ρ and the viscosity μ are actually constant, and that these quantities are written explicitly in the equations to identify where a discrete Hodge operator is to be used. In what follows, we also consider the vorticity $\underline{\omega} := \underline{\mathrm{curl}}(\underline{u})$. In this section, we focus on homogeneous and natural BCs which are

$$\rho\underline{u}\cdot\underline{\nu}_{\partial\Omega} = \underline{\phi}_\nu^{\mathrm{bc}}, \quad \mu\underline{\omega}\times\underline{\nu}_{\partial\Omega} = \underline{\omega}_\tau^{\mathrm{bc}}, \qquad \text{on } \partial\Omega, \tag{9.2}$$

with data $\underline{\phi}_\nu^{\mathrm{bc}}$ and $\underline{\omega}_\tau^{\mathrm{bc}}$. The discrete system is: Find $(\mathbf{p}^*,\mathbf{u})\in\mathcal{V}_{\perp\mathbf{1}}\times\mathcal{E}$ such that

$$\begin{cases} \widetilde{\mathsf{CURL}}\cdot\mathsf{H}_\mu^{\mathcal{F}\tilde{\mathcal{E}}}\cdot\mathsf{CURL}(\mathbf{u}) + \mathsf{H}_\rho^{\mathcal{E}\tilde{\mathcal{F}}}\cdot\mathsf{GRAD}(\mathbf{p}^*) = \mathsf{S}^{\mathsf{vb}}(\rho,\underline{f}^*), \\ -\widetilde{\mathsf{DIV}}\cdot\mathsf{H}_\rho^{\mathcal{E}\tilde{\mathcal{F}}}(\mathbf{u}) = 0_{\widetilde{\mathcal{C}}}. \end{cases} \tag{9.3}$$

The space of DoFs for the pressure potential is set such that

$$\mathcal{V}_{\perp\mathbf{1}} := \{\boldsymbol{\theta}\in\mathcal{V};\ [\![\boldsymbol{\theta},\mathsf{H}_1^{\mathcal{V}\tilde{\mathcal{C}}}(\mathbf{1})]\!]_{\mathcal{V}\tilde{\mathcal{C}}} = 0\}, \tag{9.4}$$

where $\mathsf{H}_1^{\mathcal{V}\tilde{\mathcal{C}}}$ is a diagonal discrete Hodge operator with entries equal to $|\tilde{\mathrm{c}}(\mathrm{v})|$ for all $\mathrm{v}\in\mathrm{V}$ and $\mathbf{1}\in\mathcal{V}$ has all its entries equal to 1.

Remark 9.1 (Translational invariance)**.** *The translational invariance of the pressure potential* $[\![\mathbf{p}^*,\mathsf{H}_1^{\mathcal{V}\tilde{\mathcal{C}}}(\mathbf{1})]\!]_{\mathcal{V}\tilde{\mathcal{C}}} = 0$ *is equivalent to* $\sum_{\mathrm{v}\in\mathrm{V}}|\tilde{\mathrm{c}}(\mathrm{v})|\mathbf{p}_\mathrm{v}^* = 0$ *or also* $\int_\Omega \mathtt{L}_\mathcal{V}^0(\mathbf{p}^*) = 0$ *where* $\mathtt{L}_\mathcal{V}^0$ *is the local potential reconstruction operator introduced in Section 7.2.3. This last identity is the discrete counterpart of the zero mean-value condition on the pressure.*

The discrete variational formulation of system (9.3) is: Find $(\mathbf{p}^*,\mathbf{u})\in\mathcal{V}_{\perp\mathbf{1}}\times\mathcal{E}$ such that

$$\begin{cases} [\![\mathsf{CURL}(\mathbf{u}),\mathsf{H}_\mu^{\mathcal{F}\tilde{\mathcal{E}}}\cdot\mathsf{CURL}(\mathbf{w})]\!]_{\mathcal{F}\tilde{\mathcal{E}}} + [\![\mathsf{GRAD}(\mathbf{p}^*),\mathsf{H}_\rho^{\mathcal{E}\tilde{\mathcal{F}}}(\mathbf{w})]\!]_{\mathcal{E}\tilde{\mathcal{F}}} = [\![\mathbf{w},\mathsf{S}^{\mathsf{vb}}(\rho,\underline{f}^*)]\!]_{\mathcal{E}\tilde{\mathcal{F}}} & \forall\mathbf{w}\in\mathcal{E}, \\ [\![\mathsf{GRAD}(\mathbf{q}),\mathsf{H}_\rho^{\mathcal{E}\tilde{\mathcal{F}}}(\mathbf{u})]\!]_{\mathcal{E}\tilde{\mathcal{F}}} = 0 & \forall\mathbf{q}\in\mathcal{V}_{\perp\mathbf{1}}, \end{cases} \tag{9.5}$$

where we have used the adjunction property between $-\mathsf{GRAD}$ and $\widetilde{\mathsf{DIV}}$, and between CURL and $\widetilde{\mathsf{CURL}}$ (cf. Proposition 3.16). In addition, we introduce the following operators:

$$\begin{aligned} &\mathsf{A}^{\mathsf{vb}}:\mathcal{E}\to\widetilde{\mathcal{F}}, && \mathsf{B}:\mathcal{E}\to\widetilde{\mathcal{C}}, && \mathsf{B}^{\mathrm{T}}:\mathcal{V}\to\widetilde{\mathcal{F}}, \\ &\mathsf{A}^{\mathsf{vb}} := \widetilde{\mathsf{CURL}}\cdot\mathsf{H}_\mu^{\mathcal{F}\tilde{\mathcal{E}}}\cdot\mathsf{CURL}, && \mathsf{B} := -\widetilde{\mathsf{DIV}}\cdot\mathsf{H}_\rho^{\mathcal{E}\tilde{\mathcal{F}}}, && \mathsf{B}^{\mathrm{T}} := \mathsf{H}_\rho^{\mathcal{E}\tilde{\mathcal{F}}}\cdot\mathsf{GRAD}. \end{aligned} \tag{9.6}$$

The operators B and B^{T} are adjoint, and A^{vb} is selfadjoint owing to the symmetry of the two discrete Hodge operators and the discrete adjunction of $-\mathsf{GRAD}$ and $\widetilde{\mathsf{DIV}}$ and that of CURL and $\widetilde{\mathsf{CURL}}$. Using (9.6), vertex-based pressure schemes can be recast as follows: Find $(\mathbf{p}^*,\mathbf{u})\in\mathcal{V}_{\perp\mathbf{1}}\times\mathcal{E}$ such that

$$\begin{bmatrix} \mathsf{A}^{\mathsf{vb}} & \mathsf{B}^{\mathrm{T}} \\ \mathsf{B} & 0 \end{bmatrix}\begin{bmatrix} \mathbf{u} \\ \mathbf{p}^* \end{bmatrix} = \begin{bmatrix} \mathsf{S}^{\mathsf{vb}}(\rho,\underline{f}^*) \\ 0_{\widetilde{\mathcal{C}}} \end{bmatrix}. \tag{9.7}$$

The right-hand side $\mathsf{S}^{\mathsf{vb}}(\rho,\underline{f}^*)\in\widetilde{\mathcal{F}}$ discretizes the external load $\rho\underline{f}^*$. Two expressions are considered in the analysis, respectively termed discrete primal load and discrete dual load. They are defined for each edge $\mathrm{e}\in\mathrm{E}$ as follows:

$$\mathsf{S}^{\mathsf{vb}}_{\mathsf{p}}(\rho,\underline{f}^*)|_{\tilde{\mathrm{f}}(\mathrm{e})}:=(\mathsf{H}_\rho^{\mathcal{E}\widetilde{\mathcal{F}}}\cdot\mathsf{R}_{\mathcal{E}}(\underline{f}^*))|_{\tilde{\mathrm{f}}(\mathrm{e})},\tag{9.8a}$$

$$\mathsf{S}^{\mathsf{vb}}_{\mathsf{d}}(\rho,\underline{f}^*)|_{\tilde{\mathrm{f}}(\mathrm{e})}:=\mathsf{R}_{\widetilde{\mathcal{F}}}(\rho\underline{f}^*)|_{\tilde{\mathrm{f}}(\mathrm{e})}.\tag{9.8b}$$

A sufficient condition for the discrete primal and dual load to be well-defined is $\underline{f}^*\in S_{\mathcal{E}}(\Omega)$ and $\rho\underline{f}^*\in S_{\widetilde{\mathcal{F}}}(\Omega)$ respectively. A possible choice is that $\underline{f}^*\in H^s(\Omega)^3$ with $s>\frac12$ and $\underline{\mathrm{curl}}(\underline{f}^*)\in[L^4(\Omega)]^3$ in the primal case (cf. Definition 3.5) and $\rho\underline{f}^*\in H^s(\Omega)^3$ with $s>\frac12$ in the dual case (cf. Remark 3.6).

Discrete Hodge operators. The two discrete Hodge operators, $\mathsf{H}_\rho^{\mathcal{E}\widetilde{\mathcal{F}}}$ and $\mathsf{H}_\mu^{\mathcal{F}\widetilde{\mathcal{E}}}$, satisfy the three local properties (**H0**), (**H1**), and (**H2**). Specifically, the local discrete Hodge operator $\mathsf{H}_\rho^{\mathcal{E}_\mathrm{c}\widetilde{\mathcal{F}}_\mathrm{c}}$ satisfies for all $\mathrm{c}\in\mathrm{C}$:

(**H0**) [Symmetry] $\mathsf{H}_\rho^{\mathcal{E}\widetilde{\mathcal{F}}}$ is symmetric.

(**H1**) [Local stability] There exists $\eta_\rho>0$ such that, for all $\mathrm{c}\in\mathrm{C}$,

$$\eta_\rho\|\mathbf{u}\|_{2,\mathcal{E}_\mathrm{c}}^2\le\|\mathbf{u}\|_{\rho,\mathrm{c}}^2\le\eta_\rho^{-1}\|\mathbf{u}\|_{2,\mathcal{E}_\mathrm{c}}^2,\qquad\forall\mathbf{u}\in\mathcal{E}_\mathrm{c}.\tag{9.9}$$

(**H2**) [Local $\mathbb{P}_0$-consistency] The local commuting operator

$$\lfloor\rho,\,{}_{\mathrm{c}}\tilde{\mathcal{F}}_\mathrm{c}\rceil(\bullet):=\mathsf{H}_\rho^{\mathcal{E}_\mathrm{c}\widetilde{\mathcal{F}}_\mathrm{c}}\cdot\mathsf{R}_{\mathcal{E}_\mathrm{c}}(\bullet)-\mathsf{R}_{\widetilde{\mathcal{F}}_\mathrm{c}}(\rho\,\bullet)\tag{9.10}$$

satisfies $\lfloor\rho,\,{}_{\mathrm{c}}\tilde{\mathcal{F}}_\mathrm{c}\rceil(\underline{K})=0$ for any vector field $\underline{K}$ which is constant in $\mathrm{c}\in\mathrm{C}$.

Similarly, the discrete Hodge operator $\mathsf{H}_\mu^{\mathcal{F}_\mathrm{c}\widetilde{\mathcal{E}}_\mathrm{c}}$ satisfies for all $\mathrm{c}\in\mathrm{C}$:

(**H0**) [Symmetry] $\mathsf{H}_\mu^{\mathcal{F}_\mathrm{c}\widetilde{\mathcal{E}}_\mathrm{c}}$ is symmetric.

(**H1**) [Local stability] There exists $\eta_\mu>0$ such that, for all $\mathrm{c}\in\mathrm{C}$,

$$\eta_\mu\|\boldsymbol{\omega}\|_{2,\mathcal{F}_\mathrm{c}}^2\le\|\boldsymbol{\omega}\|_{\mu,\mathrm{c}}^2\le\eta_\mu^{-1}\|\boldsymbol{\omega}\|_{2,\mathcal{F}_\mathrm{c}}^2,\qquad\forall\boldsymbol{\omega}\in\mathcal{F}_\mathrm{c}.\tag{9.11}$$

(**H2**) [Local $\mathbb{P}_0$-consistency] The local commuting operator

$$\lfloor\mu,\,{}_{\mathcal{F}_\mathrm{c}}\tilde{\mathcal{E}}_\mathrm{c}\rceil(\bullet):=\mathsf{H}_\mu^{\mathcal{F}_\mathrm{c}\widetilde{\mathcal{E}}_\mathrm{c}}\cdot\mathsf{R}_{\mathcal{F}_\mathrm{c}}(\bullet)-\mathsf{R}_{\widetilde{\mathcal{E}}_\mathrm{c}}(\mu\,\bullet)\tag{9.12}$$

satisfies $\lfloor\mu,\,{}_{\mathcal{F}_\mathrm{c}}\tilde{\mathcal{E}}_\mathrm{c}\rceil(\underline{K})=0$ for any vector field $\underline{K}$ which is constant in $\mathrm{c}\in\mathrm{C}$.

Similarly to the generic definitions of Section 6.1, we define the following discrete norms induced by the two discrete Hodge operators $\mathsf{H}_\rho^{\mathcal{E}\widetilde{\mathcal{F}}}$ and $\mathsf{H}_\mu^{\mathcal{F}\widetilde{\mathcal{E}}}$:

$$\|\mathbf{u}\|_\rho^2:=[\![\mathbf{u},\mathsf{H}_\rho^{\mathcal{E}\widetilde{\mathcal{F}}}(\mathbf{u})]\!]_{\mathcal{E}\widetilde{\mathcal{F}}},\qquad\|\boldsymbol{\phi}\|_{\rho^{-1}}^2:=[\![(\mathsf{H}_\rho^{\mathcal{E}\widetilde{\mathcal{F}}})^{-1}(\boldsymbol{\phi}),\boldsymbol{\phi}]\!]_{\mathcal{E}\widetilde{\mathcal{F}}},\tag{9.13a}$$

$$\|\boldsymbol{\omega}\|_\mu^2:=[\![\boldsymbol{\omega},\mathsf{H}_\mu^{\mathcal{F}\widetilde{\mathcal{E}}}(\boldsymbol{\omega})]\!]_{\mathcal{F}\widetilde{\mathcal{E}}},\qquad\|\boldsymbol{\omega}^*\|_{\mu^{-1}}^2:=[\![(\mathsf{H}_\mu^{\mathcal{F}\widetilde{\mathcal{E}}})^{-1}(\boldsymbol{\omega}^*),\boldsymbol{\omega}^*]\!]_{\mathcal{F}\widetilde{\mathcal{E}}},\tag{9.13b}$$

for all $\mathbf{u}\in\mathcal{E}$, $\boldsymbol{\phi}\in\widetilde{\mathcal{F}}$, $\boldsymbol{\omega}\in\mathcal{F}$, and $\boldsymbol{\omega}^*\in\widetilde{\mathcal{E}}$. Owing to the Cauchy–Schwarz inequality (6.14), we infer that

$$[\![\mathbf{u},\boldsymbol{\phi}]\!]_{\mathcal{E}\widetilde{\mathcal{F}}}\le\|\mathbf{u}\|_\rho\,\|\boldsymbol{\phi}\|_{\rho^{-1}},\qquad[\![\boldsymbol{\omega},\boldsymbol{\omega}^*]\!]_{\mathcal{F}\widetilde{\mathcal{E}}}\le\|\boldsymbol{\omega}\|_\mu\,\|\boldsymbol{\omega}^*\|_{\mu^{-1}}.\tag{9.14}$$

Owing to (3.20), we infer from (**H1**) the corresponding global stability for $\mathsf{H}_\rho^{\mathcal{E}\widetilde{\mathcal{F}}}$: There exists η_ρ such that

$$\forall\mathbf{u}\in\mathcal{E},\qquad\eta_\rho\|\mathbf{u}\|_{2,\mathcal{E}}^2\le\|\mathbf{u}\|_\rho^2\le\eta_\rho^{-1}\|\mathbf{u}\|_{2,\mathcal{E}}^2,\tag{9.15}$$

and, that for $\mathsf{H}_\mu^{\mathcal{F}\widetilde{\mathcal{E}}}$: There exists η_μ such that

$$\forall\boldsymbol{\omega}\in\mathcal{F},\qquad\eta_\mu\|\boldsymbol{\omega}\|_{2,\mathcal{F}}^2\le\|\boldsymbol{\omega}\|_\mu^2\le\eta_\mu^{-1}\|\boldsymbol{\omega}\|_{2,\mathcal{F}}^2.\tag{9.16}$$

9.1.2 Stability and well-posedness

Lemma 9.2 (Coercivity)**.** *Assume* **(MR)** *and* $(\mathbf{A_\Omega})$*. Then, there exists* $\eta_{\mathsf{A}} > 0$ *(independent of the mesh size) such that, for all* $\mathbf{u} \in \operatorname{Ker}\mathsf{B}$*, the following inequality holds:*

$$[\![\mathbf{u}, \mathsf{A}^{\mathsf{vb}}(\mathbf{u})]\!]_{\mathcal{E}\widetilde{\mathcal{F}}} \geq \eta_{\mathsf{A}} \|\mathbf{u}\|_\rho^2. \tag{9.17}$$

Proof. Let us verify that $\mathbf{u} \in \operatorname{Ker}\mathsf{B}$ implies that $[\![\mathbf{u}, \mathsf{H}_\rho^{\mathcal{E}\widetilde{\mathcal{F}}}(\mathbf{v})]\!]_{\mathcal{E}\widetilde{\mathcal{F}}} = 0$ for all $\mathbf{v} \in \operatorname{Ker}\mathsf{CURL}$. Owing to $(\mathbf{A_\Omega})$ and Proposition 3.12, there is $\boldsymbol{\theta} \in \mathcal{V}$ such that $\mathbf{v} = \mathsf{GRAD}(\boldsymbol{\theta})$. As a result,

$$[\![\mathbf{u}, \mathsf{H}_\rho^{\mathcal{E}\widetilde{\mathcal{F}}}(\mathbf{v})]\!]_{\mathcal{E}\widetilde{\mathcal{F}}} = [\![\mathbf{u}, \mathsf{B}^{\mathrm{T}}(\boldsymbol{\theta})]\!]_{\mathcal{E}\widetilde{\mathcal{F}}} = [\![\boldsymbol{\theta}, \mathsf{B}(\mathbf{u})]\!]_{\mathcal{V}\widetilde{\mathcal{C}}} = 0.$$

Applying Lemma 7.47 and the stability property (6.21), we infer that

$$\eta_\rho \|\mathbf{u}\|_\rho^2 \leq \|\mathbf{u}\|_{2,\mathcal{E}}^2 \leq (C_{\mathrm{P}}^{(1)})^2 \|\mathsf{CURL}(\mathbf{u})\|_{2,\mathcal{F}}^2 \leq (C_{\mathrm{P}}^{(1)})^2 \eta_\mu^{-1} \|\mathsf{CURL}(\mathbf{u})\|_\mu^2,$$

whence we infer (9.17) with $\eta_{\mathsf{A}} = \eta_\rho \eta_\mu (C_{\mathrm{P}}^{(1)})^{-2}$ since $\|\mathsf{CURL}(\mathbf{u})\|_\mu^2 = [\![\mathbf{u}, \mathsf{A}^{\mathsf{vb}}(\mathbf{u})]\!]_{\mathcal{E}\widetilde{\mathcal{F}}}$. □

Lemma 9.3 (Discrete inf-sup condition)**.** *Assume* **(MR)***. Then, there exists* $\beta_{\mathsf{B}} > 0$ *(independent of the mesh size) such that*

$$\inf_{\boldsymbol{\theta} \in \mathcal{V}_{\perp \mathbf{1}}} \sup_{\mathbf{u} \in \mathcal{E}} \frac{[\![\boldsymbol{\theta}, \mathsf{B}(\mathbf{u})]\!]_{\mathcal{V}\widetilde{\mathcal{C}}}}{\|\boldsymbol{\theta}\|_{2,\mathcal{V}} \|\mathbf{u}\|_\rho} \geq \beta_{\mathsf{B}}. \tag{9.18}$$

Proof. For all $\boldsymbol{\theta} \in \mathcal{V}_{\perp \mathbf{1}}$, set $\mathbf{u} := \mathsf{GRAD}(\boldsymbol{\theta})$. Then, $[\![\boldsymbol{\theta}, \mathsf{B}(\mathbf{u})]\!]_{\mathcal{V}\widetilde{\mathcal{C}}} = [\![\mathbf{u}, \mathsf{B}^{\mathrm{T}}(\boldsymbol{\theta})]\!]_{\mathcal{E}\widetilde{\mathcal{F}}} = \|\mathbf{u}\|_\rho^2$ and owing to Lemma 7.45 and (9.16), we infer that $\|\boldsymbol{\theta}\|_{2,\mathcal{V}} \leq C_{\mathrm{P}}^{(0)} \eta_\rho^{-1/2} \|\mathbf{u}\|_\rho$. This yields the inf-sup condition with $\beta_{\mathsf{B}} = \eta_\rho^{1/2} (C_{\mathrm{P}}^{(0)})^{-1}$. □

A classical consequence of Lemmata 9.2 and 9.3 is the following (Brezzi & Fortin, 1991):

Corollary 9.4 (Well-posedness)**.** *Assume* **(MR)** *and* $(\mathbf{A_\Omega})$*. Then, the discrete system* (9.3) *is well-posed.*

9.1.3 Error analysis

Error analysis for discrete dual load. In what follows, we consider a discrete dual load $\mathsf{S}_{\mathsf{d}}^{\mathsf{vb}}(\rho, \underline{f}^*)$ set according to (9.8b). For simplicity, we assume that there is no quadrature error when evaluating the discrete load. We assume that $\underline{f}^* \in [H^s(\Omega)]^3$ with $s > \frac{1}{2}$ so that $\underline{f}^* \in S_{\widetilde{\mathcal{F}}}(\Omega)$ and $\mathsf{S}_{\mathsf{d}}^{\mathsf{vb}}(\rho, \underline{f}^*)$ is well-defined. Moreover, we consider the following global commuting operators:

$$\begin{aligned} \lfloor \rho,\, \varepsilon\widetilde{\mathcal{F}} \rceil(\bullet) &:= \mathsf{H}_\rho^{\mathcal{E}\widetilde{\mathcal{F}}} \cdot \mathsf{R}_{\mathcal{E}}(\bullet) - \mathsf{R}_{\widetilde{\mathcal{F}}}(\rho\, \bullet), \\ \lfloor \mu,\, \mathcal{F}\widetilde{\mathcal{E}} \rceil(\bullet) &:= \mathsf{H}_\mu^{\mathcal{F}\widetilde{\mathcal{E}}} \cdot \mathsf{R}_{\mathcal{F}}(\bullet) - \mathsf{R}_{\widetilde{\mathcal{E}}}(\mu\, \bullet). \end{aligned} \tag{9.19}$$

To ensure that $\lfloor \rho,\, \varepsilon\widetilde{\mathcal{F}} \rceil(\bullet)$ is well-defined when applied to $\underline{u}$ and $\underline{\mathrm{grad}}(p^*)$ (recall that $(\underline{u}, p^*)$ is the solution of the two-field curl formulation (9.1)), we assume that $\underline{u}, \underline{\mathrm{grad}}(p^*) \in S_{\mathcal{E}}(\Omega) \cap S_{\widetilde{\mathcal{F}}}(\Omega)$. To ensure that $\lfloor \mu,\, \mathcal{F}\widetilde{\mathcal{E}} \rceil(\bullet)$ is well-defined when applied to $\underline{\omega}$, we assume that $\underline{\omega} \in S_{\mathcal{F}}(\Omega) \cap S_{\widetilde{\mathcal{E}}}(\Omega)$.

Let $\mathbf{u}$, $\mathbf{p}^*$ solve the discrete system (9.3) and recall that $\boldsymbol{\omega} = \mathsf{CURL}(\mathbf{u})$. Then, we define the following discrete differences:

$$\boldsymbol{\delta}\mathbf{p}^* := \mathsf{R}_{\mathcal{V}}(p^*) - \mathbf{p}^*, \quad \boldsymbol{\delta}\mathbf{u} := \mathsf{R}_{\mathcal{E}}(\underline{u}) - \mathbf{u}, \quad \boldsymbol{\delta}\boldsymbol{\omega} := \mathsf{R}_{\mathcal{F}}(\underline{\omega}) - \boldsymbol{\omega}. \tag{9.20}$$

Theorem 9.5 (Error bounds with discrete dual load)**.** *Assume* **(MR)** *and* $(\mathbf{A_\Omega})$*. Let* $\underline{u}$*,* p^* *solve of the two-field curl formulation* (9.1) *with homogeneous natural BCs. Let* $\mathbf{u}$*,* $\mathbf{p}^*$ *solve the discrete system* (9.3) *with the discrete dual load* $\mathsf{S}_{\mathsf{d}}^{\mathsf{vb}}(\rho, \underline{f}^*)$*. Assume that* $\underline{f}^* \in [H^s(\Omega)]^3$ *with*

$s > \frac{1}{2}$. Assume that $\underline{u}$ and $\underline{\mathrm{grad}}(p^*) \in S_{\mathcal{E}}(\Omega) \cap S_{\widetilde{\mathcal{F}}}(\Omega)$, and $\underline{\omega} \in S_{\mathcal{F}}(\Omega) \cap S_{\widetilde{\mathcal{E}}}(\Omega)$. Then, the following error bounds hold:

$$\|\mathsf{GRAD}(\boldsymbol{\delta}\mathbf{p}^*)\|_\rho \le \|\lfloor \rho,\, {}_{\mathcal{E}}\widetilde{\mathcal{F}}\rceil(\underline{\mathrm{grad}}(p^*))\|_{\rho^{-1}}, \tag{9.21a}$$

$$\|\boldsymbol{\delta\omega}\|_\mu \lesssim \|\lfloor \rho,\, {}_{\mathcal{E}}\widetilde{\mathcal{F}}\rceil(\underline{\mathrm{grad}}(p^*))\|_{\rho^{-1}} + \|\lfloor \mu,\, {}_{\mathcal{F}}\widetilde{\mathcal{E}}\rceil(\underline{\omega})\|_{\mu^{-1}}, \tag{9.21b}$$

$$\|\boldsymbol{\delta u}\|_\rho \lesssim \|\lfloor \rho,\, {}_{\mathcal{E}}\widetilde{\mathcal{F}}\rceil(\underline{\mathrm{grad}}(p^*))\|_{\rho^{-1}} + \|\lfloor \mu,\, {}_{\mathcal{F}}\widetilde{\mathcal{E}}\rceil(\underline{\omega})\|_{\mu^{-1}} + \|\lfloor \rho,\, {}_{\mathcal{E}}\widetilde{\mathcal{F}}\rceil(\underline{u})\|_{\rho^{-1}}. \tag{9.21c}$$

Moreover, if $\underline{u}, \underline{\omega}, \underline{\mathrm{grad}}(p^*) \in [H^1(\mathrm{C})]^3$ and $\underline{f}^* \in [L^4(\Omega)]^3$, the following error estimates hold:

$$\|\mathsf{GRAD}(\boldsymbol{\delta}\mathbf{p}^*)\|_\rho \lesssim h\, \|\underline{\mathrm{grad}}(p^*)\|_{[H^1(\mathrm{C})]^3}, \tag{9.22a}$$

$$\|\boldsymbol{\delta\omega}\|_\mu \lesssim h \left(\|\underline{\mathrm{grad}}(p^*)\|_{[H^1(\mathrm{C})]^3} + \|\underline{\omega}\|_{[H^1(\mathrm{C})]^3} + \|\underline{f}^*\|_{[L^4(\Omega)]^3} \right), \tag{9.22b}$$

$$\|\boldsymbol{\delta u}\|_\rho \lesssim h \left(\|\underline{\mathrm{grad}}(p^*)\|_{[H^1(\mathrm{C})]^3} + \|\underline{\omega}\|_{[H^1(\mathrm{C})]^3} + \|\underline{f}^*\|_{[L^4(\Omega)]^3} + \|\underline{u}\|_{[H^1(\mathrm{C})]^3} \right). \tag{9.22c}$$

Proof. (1) We first derive the error equations. Applying $\mathsf{R}_{\widetilde{\mathcal{F}}}$ to the momentum and $\mathsf{R}_{\widetilde{\mathcal{C}}}$ to the mass balance equation in (9.1) yields

$$\begin{aligned} \widetilde{\mathsf{CURL}}(\mathsf{R}_{\widetilde{\mathcal{E}}}(\mu\underline{\omega})) + \mathsf{R}_{\widetilde{\mathcal{F}}}(\rho\, \underline{\mathrm{grad}}(p^*)) &= \mathsf{S}_{\mathsf{d}}^{\mathsf{vb}}(\rho, \underline{f}^*), \\ \widetilde{\mathsf{DIV}}(\mathsf{R}_{\widetilde{\mathcal{F}}}(\rho\underline{u})) &= 0_{\widetilde{\mathcal{C}}}, \end{aligned}$$

owing to the commuting property (Proposition 3.18) on the interior dual mesh entities and the homogeneous BCs (4.15) on the dual mesh entities touching the boundary $\partial\Omega$. Subtracting from the corresponding equation in (9.3) and introducing the global commuting operators leads to

$$\widetilde{\mathsf{CURL}} \cdot \mathsf{H}_\mu^{\mathcal{F}\widetilde{\mathcal{E}}}(\boldsymbol{\delta\omega}) + \mathsf{H}_\rho^{\mathcal{E}\widetilde{\mathcal{F}}} \cdot \mathsf{GRAD}(\boldsymbol{\delta}\mathbf{p}^*) = \widetilde{\mathsf{CURL}}(\lfloor \mu,\, {}_{\mathcal{F}}\widetilde{\mathcal{E}}\rceil(\underline{\omega})) + \lfloor \rho,\, {}_{\mathcal{E}}\widetilde{\mathcal{F}}\rceil(\underline{\mathrm{grad}}(p^*)), \tag{9.23a}$$

$$\widetilde{\mathsf{DIV}} \cdot \mathsf{H}_\rho^{\mathcal{E}\widetilde{\mathcal{F}}}(\boldsymbol{\delta u}) = \widetilde{\mathsf{DIV}}(\lfloor \rho,\, {}_{\mathcal{E}}\widetilde{\mathcal{F}}\rceil(\underline{u})), \tag{9.23b}$$

since $\mathsf{R}_{\mathcal{E}}(\underline{\mathrm{grad}}(p^*)) = \mathsf{GRAD}(\mathsf{R}_{\mathcal{V}}(p^*))$.

(2) *Bound on the pressure gradient.* We take the duality product of (9.23a) with $\mathsf{GRAD}(\boldsymbol{\delta}\mathbf{p}^*)$. Since $[\![\mathsf{GRAD}(\boldsymbol{\delta}\mathbf{p}^*), \widetilde{\mathsf{CURL}}(\mathbf{b})]\!]_{\mathcal{E}\widetilde{\mathcal{F}}} = [\![\mathsf{CURL}(\mathsf{GRAD}(\boldsymbol{\delta}\mathbf{p}^*)), \mathbf{b}]\!]_{\mathcal{F}\widetilde{\mathcal{E}}} = 0$ for all $\mathbf{b} \in \widetilde{\mathcal{E}}$, we infer that $\|\mathsf{GRAD}(\boldsymbol{\delta}\mathbf{p}^*)\|_\rho^2 = [\![\mathsf{GRAD}(\boldsymbol{\delta}\mathbf{p}^*), \lfloor \rho,\, {}_{\mathcal{E}}\widetilde{\mathcal{F}}\rceil(\underline{\mathrm{grad}}(p^*))]\!]_{\mathcal{E}\widetilde{\mathcal{F}}}$, whence (9.21a) follows from the Cauchy–Schwarz inequality (9.14).

(3) *Bound on the vorticity.* We use the discrete Hodge decomposition

$$\mathcal{E} = \mathrm{Im}\,\mathsf{GRAD} \overset{\perp\mathsf{H}}{\oplus} (\mathrm{Ker}\,\mathsf{CURL})^{\perp\mathsf{H}}, \tag{9.24}$$

where $(\mathrm{Ker}\,\mathsf{CURL})^{\perp\mathsf{H}} := \{\mathbf{u} \in \mathcal{E};\ [\![\mathbf{u}, \mathsf{H}_\rho^{\mathcal{E}\widetilde{\mathcal{F}}}(\mathbf{v})]\!]_{\mathcal{E}\widetilde{\mathcal{F}}} = 0,\, \forall \mathbf{v} \in \mathrm{Ker}\,\mathsf{CURL}\}$, which results from the decomposition $\mathcal{E} = \mathrm{Im}\,\mathsf{GRAD} \overset{\perp\mathsf{H}}{\oplus} (\mathrm{Im}\,\mathsf{GRAD})^{\perp\mathsf{H}}$ and $\mathrm{Im}\,\mathsf{GRAD} = \mathrm{Ker}\,\mathsf{CURL}$ owing to $(\mathbf{A_\Omega})$ and Proposition 3.12. Using (9.24), we set $\boldsymbol{\delta u} = \mathsf{GRAD}(\boldsymbol{\delta\theta}) + \boldsymbol{\delta u}_\perp$ with $\boldsymbol{\delta\theta} \in \mathcal{V}$ and $\boldsymbol{\delta u}_\perp \in (\mathrm{Ker}\,\mathsf{CURL})^{\perp\mathsf{H}}$. Observe that $\mathsf{CURL}(\boldsymbol{\delta u}_\perp) = \mathsf{CURL}(\boldsymbol{\delta u}) = \boldsymbol{\delta\omega}$ and that $\|\boldsymbol{\delta u}_\perp\|_\rho \lesssim \|\boldsymbol{\delta\omega}\|_\mu$ owing to Lemma 7.47 and the global stability (9.15) of $\mathsf{H}_\rho^{\mathcal{E}\widetilde{\mathcal{F}}}$ and (9.16) of $\mathsf{H}_\mu^{\mathcal{F}\widetilde{\mathcal{E}}}$. We take the duality product of (9.23a) with $\boldsymbol{\delta u}_\perp$. Since $[\![\boldsymbol{\delta u}_\perp, \mathsf{H}_\rho^{\mathcal{E}\widetilde{\mathcal{F}}} \cdot \mathsf{GRAD}(\boldsymbol{\delta}\mathbf{p}^*)]\!]_{\mathcal{E}\widetilde{\mathcal{F}}} = 0$, we infer that

$$\|\boldsymbol{\delta\omega}\|_\mu^2 = [\![\boldsymbol{\delta\omega}, \lfloor \mu,\, {}_{\mathcal{F}}\widetilde{\mathcal{E}}\rceil(\underline{\omega})]\!]_{\mathcal{F}\widetilde{\mathcal{E}}} + [\![\boldsymbol{\delta u}_\perp, \lfloor \rho,\, {}_{\mathcal{E}}\widetilde{\mathcal{F}}\rceil(\underline{\mathrm{grad}}(p^*))]\!]_{\mathcal{E}\widetilde{\mathcal{F}}}. \tag{9.25}$$

The estimate (9.21b) results from Cauchy–Schwarz inequalities (9.14) and $\|\boldsymbol{\delta u}_\perp\|_\rho \lesssim \|\boldsymbol{\delta\omega}\|_\mu$.

(4) *Bound on the velocity.* Since $\|\boldsymbol{\delta u}\|_\rho^2 = \|\boldsymbol{\delta u}_\perp\|_\rho^2 + \|\mathsf{GRAD}(\boldsymbol{\delta\theta})\|_\rho^2$ and $\|\boldsymbol{\delta u}_\perp\|_\rho \lesssim \|\boldsymbol{\delta\omega}\|_\mu$, it remains to estimate $\|\mathsf{GRAD}(\boldsymbol{\delta\theta})\|_\rho$. We take the duality product of (9.23b) with $\boldsymbol{\delta\theta}$. Since $[\![\boldsymbol{\delta u}_\perp, \mathsf{H}_\rho^{\varepsilon\tilde{\mathcal{F}}} \cdot \mathsf{GRAD}(\boldsymbol{\delta\theta})]\!]_{\mathcal{E}\tilde{\mathcal{F}}} = 0$, we infer that

$$\|\mathsf{GRAD}(\boldsymbol{\delta\theta})\|_\rho^2 = [\![\mathsf{GRAD}(\boldsymbol{\delta\theta}), \mathsf{H}_\rho^{\mathcal{E}\tilde{\mathcal{F}}}(\boldsymbol{\delta u})]\!]_{\mathcal{E}\tilde{\mathcal{F}}} = [\![\mathsf{GRAD}(\boldsymbol{\delta\theta}), \lfloor\rho, \varepsilon\tilde{\mathcal{F}}\rceil(\underline{u})]\!]_{\mathcal{E}\tilde{\mathcal{F}}},$$

and the Cauchy–Schwarz inequality (9.14) yields $\|\mathsf{GRAD}(\boldsymbol{\delta\theta})\|_\rho \le \|\lfloor\rho, \varepsilon\tilde{\mathcal{F}}\rceil(\underline{u})\|_{\rho^{-1}}$.

(5) Finally, the error bounds for smooth solutions result from Lemmata 6.14 and 6.16. Observe that $\underline{\mathrm{curl}}(\underline{\omega}) \in [L^4(\Omega)]^3$ since $\underline{\mathrm{curl}}(\mu\underline{\omega}) = \rho\underline{f}^* - \rho\,\underline{\mathrm{grad}}(p^*)$ (ρ and μ are constant, $\underline{f}^* \in [L^4(\Omega)]^3$, and $\underline{\mathrm{grad}}(p^*) \in [H^1(\mathrm{C})]^3$), and that $\underline{\mathrm{curl}}(\underline{u}) \in [L^4(\Omega)]^3$ since $\underline{\omega} = \underline{\mathrm{curl}}(\underline{u}) \in [H^1(\mathrm{C})]^3$. □

Error analysis for discrete primal load. In what follows, we consider the discrete primal load $\mathsf{S}_\mathsf{p}^\mathsf{vb}(\rho, \underline{f}^*)$ set according to (9.8a). A first consequence is that the regularity requirement on $\underline{f}^*$ has to be enforced so that $\underline{f}^* \in S_\mathcal{E}(\Omega)$ and $\mathsf{S}_\mathsf{p}^\mathsf{vb}(\rho, \underline{f}^*)$ is well-defined. Thus, we assume that $\underline{f}^* \in [H^s(\Omega)]^3$ with $s > \frac{1}{2}$ and $\underline{\mathrm{curl}}(\underline{f}^*) \in [L^4(\Omega)]^3$ (cf. Remark 3.6). The regularity requirements of $\underline{u}$ and $\underline{\omega}$ are identical to that of the case of a discrete dual load. A second consequence is that the global commuting operator $\lfloor\rho, \varepsilon\tilde{\mathcal{F}}\rceil(\underline{\mathrm{grad}}(p^*))$ is replaced by $\lfloor\rho, \varepsilon\tilde{\mathcal{F}}\rceil(\underline{\mathrm{curl}}(\underline{\omega}^*))$, where we recall that $\underline{\omega}^* = \mu\underline{\omega}$.

Theorem 9.6 (Error bounds with discrete primal load)**.** *Assume* **(MR)** *and* $(\mathbf{A}_\mathbf{\Omega})$*. Let* $\underline{u}$*,* p^* *solve of the two-field curl formulation* (9.1) *with homogeneous natural BCs. Let* $\mathbf{u}$*,* $\mathbf{p}^*$ *solve the discrete system* (9.3) *with the discrete primal load* $\mathsf{S}_\mathsf{p}^\mathsf{vb}(\rho, \underline{f}^*)$*. Assume that* $\underline{f}^* \in [H^s(\Omega)]^3$ *with* $s > \frac{1}{2}$ *and* $\underline{\mathrm{curl}}(\underline{f}^*) \in [L^4(\Omega)]^3$*. Assume that* $\underline{u}$ *and* $\underline{\mathrm{curl}}(\underline{\omega}^*) \in S_\mathcal{E}(\Omega) \cap S_{\tilde{\mathcal{F}}}(\Omega)$*, and* $\underline{\omega} \in S_\mathcal{F}(\Omega) \cap S_{\tilde{\mathcal{E}}}(\Omega)$*. Then, the following error bounds hold:*

$$\|\mathsf{GRAD}(\boldsymbol{\delta p}^*)\|_\rho \le \|\lfloor\rho, \varepsilon\tilde{\mathcal{F}}\rceil(\underline{\mathrm{curl}}(\underline{\omega}^*))\|_{\rho^{-1}}, \tag{9.26a}$$

$$\|\boldsymbol{\delta\omega}\|_\mu \lesssim \|\lfloor\rho, \varepsilon\tilde{\mathcal{F}}\rceil(\underline{\mathrm{curl}}(\underline{\omega}^*))\|_{\rho^{-1}} + \|\lfloor\mu, \mathcal{F}\tilde{\mathcal{E}}\rceil(\underline{\omega})\|_{\mu^{-1}}, \tag{9.26b}$$

$$\|\boldsymbol{\delta u}\|_\rho \lesssim \|\lfloor\rho, \varepsilon\tilde{\mathcal{F}}\rceil(\underline{\mathrm{curl}}(\underline{\omega}^*))\|_{\rho^{-1}} + \|\lfloor\mu, \mathcal{F}\tilde{\mathcal{E}}\rceil(\underline{\omega})\|_{\mu^{-1}} + \|\lfloor\rho, \varepsilon\tilde{\mathcal{F}}\rceil(\underline{u})\|_{\rho^{-1}}. \tag{9.26c}$$

Moreover, if $\underline{u}$*,* $\underline{\omega}$*,* $\underline{\mathrm{curl}}(\underline{\omega}^*) \in [H^1(\mathrm{C})]^3$*, the following error estimates hold:*

$$\|\mathsf{GRAD}(\boldsymbol{\delta p}^*)\|_\rho \lesssim h\left(\|\underline{\mathrm{curl}}(\underline{\omega}^*)\|_{[H^1(\mathrm{C})]^3} + \|\underline{\mathrm{curl}}(\underline{f}^*)\|_{[L^4(\Omega)]^3}\right), \tag{9.27a}$$

$$\|\boldsymbol{\delta\omega}\|_\mu \lesssim h\left(\|\underline{\mathrm{curl}}(\underline{\omega}^*)\|_{[H^1(\mathrm{C})]^3} + \|\underline{\mathrm{curl}}(\underline{f}^*)\|_{[L^4(\Omega)]^3} + \|\underline{\omega}\|_{[H^1(\mathrm{C})]^3}\right), \tag{9.27b}$$

$$\|\boldsymbol{\delta u}\|_\rho \lesssim h\left(\|\underline{\mathrm{curl}}(\underline{\omega}^*)\|_{[H^1(\mathrm{C})]^3} + \|\underline{\mathrm{curl}}(\underline{f}^*)\|_{[L^4(\Omega)]^3} + \|\underline{\omega}\|_{[H^1(\mathrm{C})]^3} + \|\underline{u}\|_{[H^1(\mathrm{C})]^3}\right). \tag{9.27c}$$

Proof. Since $\mathsf{S}_\mathsf{p}^\mathsf{vb}(\rho, \underline{f}^*) = \mathsf{S}_\mathsf{d}^\mathsf{vb}(\rho, \underline{f}^*) + \lfloor\rho, \varepsilon\tilde{\mathcal{F}}\rceil(\underline{f}^*)$, the main difference with the proof of Theorem 9.5 is that the error equation (9.23a) is to be replaced by

$$\widetilde{\mathsf{CURL}} \cdot \mathsf{H}_\mu^{\mathcal{F}\tilde{\mathcal{E}}} \cdot \mathsf{CURL}(\boldsymbol{\delta u}) + \mathsf{H}_\rho^{\mathcal{E}\tilde{\mathcal{F}}} \cdot \mathsf{GRAD}(\boldsymbol{\delta p}^*) = \widetilde{\mathsf{CURL}}(\lfloor\mu, \mathcal{F}\tilde{\mathcal{E}}\rceil(\underline{\omega})) - \lfloor\rho, \varepsilon\tilde{\mathcal{F}}\rceil(\underline{\mathrm{curl}}(\underline{\omega}^*)).$$

The rest of the proof follows the same lines and is skipped for brevity. □

Remark 9.7 (Comparison with Theorem 9.5)**.** *When the divergence-free part of the external load (i.e.,* $\underline{\mathrm{curl}}(\underline{\omega}^*)$*) is expected to dominate over the curl-free part (i.e.,* $\underline{\mathrm{grad}}(p^*)$*), using a discrete dual load is more appropriate since the error bounds do not depend on* $\underline{\mathrm{curl}}(\underline{\omega}^*)$*. Alternatively, when the curl-free part is expected to dominate over the divergence-free part, using a discrete primal load is more appropriate since the error bounds do not depend on* $\underline{\mathrm{grad}}(p^*)$*.*

9.2 Cell-based pressure schemes

9.2.1 Discrete systems

For the sake of completeness, we recall the key points of the definition of cell-based pressure schemes (cf. Section 4.2.3 for more details). Cell-based pressure schemes rely on the three-field curl formulation (4.13) defined as follows:

$$\begin{cases} -\mu^{-1}\underline{\omega}^* + \underline{\mathrm{curl}}(\rho^{-1}\underline{\phi}) = \underline{0}, & \text{in } \Omega, \\ \rho^{-1}\,\underline{\mathrm{curl}}(\underline{\omega}^*) + \underline{\mathrm{grad}}(p^*) = \underline{f}^*, & \text{in } \Omega, \\ \mathrm{div}(\underline{\phi}) = 0, & \text{in } \Omega, \end{cases} \tag{9.28}$$

where the mass flux $\underline{\phi} = \rho\underline{u}$ and the auxiliary field $\underline{\omega}^* = \mu\underline{\omega}$ (to which we loosely refer as viscous stress circulation) have been introduced. We recall that $p^* = \rho^{-1}p$ and $\underline{f}^* := \rho^{-1}\underline{f}$. In what follows, we focus on homogeneous and natural BCs which are

$$\underline{u} \times \underline{\nu}_{\partial\Omega} = \underline{u}_\tau^{\mathrm{bc}}, \quad p^* = p^{\mathrm{bc}}, \qquad \text{on } \partial\Omega, \tag{9.29}$$

with data $\underline{u}_\tau^{\mathrm{bc}}$ and p^{bc}. The discrete system is: Find $(\mathbf{p}^*, \boldsymbol{\phi}, \boldsymbol{\omega}^*) \in \widetilde{\mathcal{V}} \times \mathcal{F} \times \mathcal{E}$ such that

$$\begin{cases} -\,\mathsf{H}_{\mu^{-1}}^{\mathcal{E}\widetilde{\mathcal{F}}}(\boldsymbol{\omega}^*) + \widetilde{\mathsf{CURL}} \cdot \mathsf{H}_{\rho^{-1}}^{\mathcal{F}\widetilde{\mathcal{E}}}(\boldsymbol{\phi}) = 0_{\widetilde{\mathcal{F}}}, \\ \mathsf{H}_{\rho^{-1}}^{\mathcal{F}\widetilde{\mathcal{E}}} \cdot \mathsf{CURL}(\boldsymbol{\omega}^*) + \widetilde{\mathsf{GRAD}}(\mathbf{p}^*) = \mathsf{S}^{\mathsf{cb}}(\rho, \underline{f}^*), \\ -\,\mathsf{DIV}(\boldsymbol{\phi}) = 0_{\mathcal{C}}. \end{cases} \tag{9.30}$$

The discrete variational formulation of (9.30) is: Find $(\mathbf{p}^*, \boldsymbol{\phi}, \boldsymbol{\omega}^*) \in \widetilde{\mathcal{V}} \times \mathcal{F} \times \mathcal{E}$ such that

$$\begin{cases} -\,[\![\mathbf{w}, \mathsf{H}_{\mu^{-1}}^{\mathcal{E}\widetilde{\mathcal{F}}}(\boldsymbol{\omega}^*)]\!]_{\mathcal{E}\widetilde{\mathcal{F}}} + [\![\mathsf{CURL}(\mathbf{w}), \mathsf{H}_{\rho^{-1}}^{\mathcal{F}\widetilde{\mathcal{E}}}(\boldsymbol{\phi})]\!]_{\mathcal{F}\widetilde{\mathcal{E}}} = 0, & \forall \mathbf{w} \in \mathcal{E}, \\ [\![\mathsf{CURL}(\boldsymbol{\omega}^*), \mathsf{H}_{\rho^{-1}}^{\mathcal{F}\widetilde{\mathcal{E}}}(\boldsymbol{\psi})]\!]_{\mathcal{F}\widetilde{\mathcal{E}}} - [\![\mathsf{DIV}(\boldsymbol{\psi}), \mathbf{p}^*]\!]_{\mathcal{C}\widetilde{\mathcal{V}}} = [\![\boldsymbol{\psi}, \mathsf{S}^{\mathsf{cb}}(\rho, \underline{f}^*)]\!]_{\mathcal{F}\widetilde{\mathcal{E}}}, & \forall \boldsymbol{\psi} \in \mathcal{F}, \\ -\,[\![\mathsf{DIV}(\boldsymbol{\phi}), \mathbf{q}]\!]_{\mathcal{C}\widetilde{\mathcal{V}}} = 0, & \forall \mathbf{q} \in \widetilde{\mathcal{V}}. \end{cases} \tag{9.31}$$

We introduce the following operators:

$$\begin{array}{lllll} \mathsf{A}^{\mathsf{cb}} : \mathcal{E} \to \widetilde{\mathcal{F}}, & \mathsf{C} : \mathcal{E} \to \widetilde{\mathcal{E}}, & \mathsf{C}^{\mathrm{T}} : \mathcal{F} \to \widetilde{\mathcal{F}}, & \mathsf{D} : \mathcal{F} \to \mathcal{C}, & \mathsf{D}^{\mathrm{T}} : \widetilde{\mathcal{V}} \to \widetilde{\mathcal{E}}, \\ \mathsf{A}^{\mathsf{cb}} := -\mathsf{H}_{\mu^{-1}}^{\mathcal{E}\widetilde{\mathcal{F}}}, & \mathsf{C} := \mathsf{H}_{\rho^{-1}}^{\mathcal{F}\widetilde{\mathcal{E}}} \cdot \mathsf{CURL}, & \mathsf{C}^{\mathrm{T}} := \widetilde{\mathsf{CURL}} \cdot \mathsf{H}_{\rho^{-1}}^{\mathcal{F}\widetilde{\mathcal{E}}}, & \mathsf{D} := -\mathsf{DIV}, & \mathsf{D}^{\mathrm{T}} := \widetilde{\mathsf{GRAD}}. \end{array} \tag{9.32}$$

The operators C (resp. D) and C^{T} (resp. D^{T}) are adjoint owing to the discrete adjunction property (cf. Proposition (3.16)) and to the symmetry of $\mathsf{H}_{\rho^{-1}}^{\mathcal{F}\widetilde{\mathcal{E}}}$; moreover, A^{cb} is selfadjoint and negative definite. Using (9.32), cell-based pressure schemes can be recast as follows: Find $(\mathbf{p}^*, \boldsymbol{\phi}, \boldsymbol{\omega}^*) \in \widetilde{\mathcal{V}} \times \mathcal{F} \times \mathcal{E}$ such that

$$\begin{bmatrix} \mathsf{A}^{\mathsf{cb}} & \mathsf{C}^{\mathrm{T}} & 0 \\ \mathsf{C} & 0 & \mathsf{D}^{\mathrm{T}} \\ 0 & \mathsf{D} & 0 \end{bmatrix} \begin{bmatrix} \boldsymbol{\omega}^* \\ \boldsymbol{\phi} \\ \mathbf{p}^* \end{bmatrix} = \begin{bmatrix} 0_{\widetilde{\mathcal{F}}} \\ \mathsf{S}^{\mathsf{cb}}(\rho, \underline{f}^*) \\ 0_{\mathcal{C}} \end{bmatrix}. \tag{9.33}$$

The right-hand side $\mathsf{S}^{\mathsf{cb}}(\rho, \underline{f}^*) \in \widetilde{\mathcal{E}}$ discretizes the external load $\underline{f}^*$. Two expressions are considered in the analysis, respectively termed discrete primal load and discrete dual load, and defined for each face $\mathrm{f} \in \mathrm{F}$ as follows:

$$\mathsf{S}_{\mathsf{p}}^{\mathsf{cb}}(\rho, \underline{f}^*)|_{\tilde{\mathrm{e}}(\mathrm{f})} := \left(\mathsf{H}_{\rho^{-1}}^{\mathcal{F}\widetilde{\mathcal{E}}} \cdot \mathsf{R}_{\mathcal{F}}(\rho\underline{f}^*)\right)|_{\tilde{\mathrm{e}}(\mathrm{f})}, \tag{9.34a}$$

$$\mathsf{S}_{\mathsf{d}}^{\mathsf{cb}}(\rho, \underline{f}^*)|_{\tilde{\mathrm{e}}(\mathrm{f})} := \mathsf{R}_{\widetilde{\mathcal{E}}}(\underline{f}^*)|_{\tilde{\mathrm{e}}(\mathrm{f})}. \tag{9.34b}$$

A sufficient condition for the discrete primal (resp. dual) load to be well-defined is to require that $\rho\underline{f}^* \in H^s(\Omega)^3$ with $s > \frac{1}{2}$ (resp. $\underline{f}^* \in H^s(\Omega)^3$ with $s > \frac{1}{2}$ and $\underline{\mathrm{curl}}(\underline{f}^*) \in [L^4(\Omega)]^3$).

Discrete Hodge operators. The two discrete Hodge operators $\mathsf{H}_{\mu^{-1}}^{\mathcal{E}\widetilde{\mathcal{F}}}$ and $\mathsf{H}_{\rho^{-1}}^{\mathcal{F}\widetilde{\mathcal{E}}}$ satisfy the three local properties (**H0**), (**H1**), and (**H2**). Specifically, the local discrete Hodge operator $\mathsf{H}_{\mu^{-1}}^{\mathcal{E}_c\widetilde{\mathcal{F}}_c}$ satisfies for all $c \in C$:

(**H0**) [Symmetry] $\mathsf{H}_{\mu^{-1}}^{\mathcal{E}_c\widetilde{\mathcal{F}}_c}$ is symmetric.

(**H1**) [Local stability] There exists $\eta_{\mu^{-1}} > 0$ such that, for all $c \in C$,

$$\eta_{\mu^{-1}} \|\boldsymbol{\omega}^*\|_{2,\mathcal{E}_c}^2 \le \|\boldsymbol{\omega}^*\|_{\rho^{-1},c}^2 \le \eta_{\mu^{-1}}^{-1} \|\boldsymbol{\omega}^*\|_{2,\mathcal{E}_c}^2, \qquad \forall \boldsymbol{\omega}^* \in \mathcal{E}_c. \tag{9.35}$$

(**H2**) [Local $\mathbb{P}_0$-consistency] The local commuting operator

$$\lfloor \mu^{-1}, \varepsilon_c\tilde{\mathcal{F}}_c \rceil(\bullet) := \mathsf{H}_{\mu^{-1}}^{\mathcal{E}_c\widetilde{\mathcal{F}}_c} \cdot \mathsf{R}_{\mathcal{E}_c}(\bullet) - \mathsf{R}_{\widetilde{\mathcal{F}}_c}(\mu^{-1}\bullet) \tag{9.36}$$

satisfies $\lfloor \mu^{-1}, \varepsilon_c\tilde{\mathcal{F}}_c \rceil(\underline{K}) = 0$ for any vector field $\underline{K}$ which is constant in $c \in C$.

Specifically, the local discrete Hodge operator $\mathsf{H}_{\rho^{-1}}^{\mathcal{F}_c\widetilde{\mathcal{E}}_c}$ satisfies for all $c \in C$:

(**H0**) [Symmetry] $\mathsf{H}_{\rho^{-1}}^{\mathcal{F}_c\widetilde{\mathcal{E}}_c}$ is symmetric.

(**H1**) [Local stability] There exists $\eta_{\rho^{-1}} > 0$ such that, for all $c \in C$,

$$\eta_{\rho^{-1}} \|\boldsymbol{\phi}\|_{2,\mathcal{F}_c}^2 \le \|\boldsymbol{\phi}\|_{\rho^{-1},c}^2 \le \eta_{\rho^{-1}}^{-1} \|\boldsymbol{\phi}\|_{2,\mathcal{F}_c}^2, \qquad \forall \boldsymbol{\phi} \in \mathcal{F}_c. \tag{9.37}$$

(**H2**) [Local $\mathbb{P}_0$-consistency] The local commuting operator

$$\lfloor \rho^{-1}, \mathcal{F}_c\tilde{\varepsilon}_c \rceil(\bullet) := \mathsf{H}_{\rho^{-1}}^{\mathcal{F}_c\widetilde{\mathcal{E}}_c} \cdot \mathsf{R}_{\mathcal{F}_c}(\bullet) - \mathsf{R}_{\widetilde{\mathcal{E}}_c}(\mu\bullet) \tag{9.38}$$

satisfies $\lfloor \mu, \mathcal{F}_c\tilde{\varepsilon}_c \rceil(\underline{K}) = 0$ for any vector field $\underline{K}$ which is constant in $c \in C$.

Similarly to the generic definitions of Section 6.1, we define the following discrete norms induced by the two discrete Hodge operators $\mathsf{H}_{\mu^{-1}}^{\mathcal{E}\widetilde{\mathcal{F}}}$ and $\mathsf{H}_{\rho^{-1}}^{\mathcal{F}\widetilde{\mathcal{E}}}$:

$$\|\boldsymbol{\phi}\|_{\rho^{-1}}^2 := [\![\boldsymbol{\phi}, \mathsf{H}_{\rho^{-1}}^{\mathcal{F}\widetilde{\mathcal{E}}}(\boldsymbol{\phi})]\!]_{\mathcal{F}\widetilde{\mathcal{E}}}, \qquad \|\mathbf{u}\|_{\rho}^2 := [\![(\mathsf{H}_{\rho^{-1}}^{\mathcal{F}\widetilde{\mathcal{E}}})^{-1}(\mathbf{u}), \mathbf{u}]\!]_{\mathcal{F}\widetilde{\mathcal{E}}}, \tag{9.39a}$$

$$\|\boldsymbol{\omega}^*\|_{\mu^{-1}}^2 := [\![\boldsymbol{\omega}^*, \mathsf{H}_{\mu^{-1}}^{\mathcal{E}\widetilde{\mathcal{F}}}(\boldsymbol{\omega}^*)]\!]_{\mathcal{E}\widetilde{\mathcal{F}}}, \qquad \|\boldsymbol{\omega}\|_{\mu}^2 := [\![(\mathsf{H}_{\mu^{-1}}^{\mathcal{E}\widetilde{\mathcal{F}}})^{-1}(\boldsymbol{\omega}), \boldsymbol{\omega}]\!]_{\mathcal{E}\widetilde{\mathcal{F}}}, \tag{9.39b}$$

for all $\boldsymbol{\phi} \in \mathcal{F}$, $\mathbf{u} \in \widetilde{\mathcal{E}}$, $\boldsymbol{\omega}^* \in \mathcal{E}$, and $\boldsymbol{\omega} \in \widetilde{\mathcal{F}}$. Note that these norms differ from those defined in (9.13) for vertex-based pressure schemes. Owing to the Cauchy–Schwarz inequality (6.14), we infer that

$$[\![\boldsymbol{\phi}, \mathbf{u}]\!]_{\mathcal{F}\widetilde{\mathcal{E}}} \le \|\boldsymbol{\phi}\|_{\rho^{-1}} \|\mathbf{u}\|_{\rho}, \qquad [\![\boldsymbol{\omega}^*, \boldsymbol{\omega}]\!]_{\mathcal{E}\widetilde{\mathcal{F}}} \le \|\boldsymbol{\omega}^*\|_{\mu^{-1}} \|\boldsymbol{\omega}\|_{\mu}. \tag{9.40}$$

Owing to (3.20), we infer from (**H1**) the corresponding global stability related to $\mathsf{H}_{\mu^{-1}}^{\mathcal{E}\widetilde{\mathcal{F}}}$: There exists $\eta_{\mu^{-1}}$ such that

$$\forall \boldsymbol{\omega}^* \in \mathcal{E}, \qquad \eta_{\mu^{-1}} \|\boldsymbol{\omega}^*\|_{2,\mathcal{E}}^2 \le \|\boldsymbol{\omega}^*\|_{\mu^{-1}}^2 \le \eta_{\mu^{-1}}^{-1} \|\boldsymbol{\omega}^*\|_{2,\mathcal{E}}^2, \tag{9.41}$$

and, that related to $\mathsf{H}_{\rho^{-1}}^{\mathcal{F}\widetilde{\mathcal{E}}}$: There exists $\eta_{\rho^{-1}}$ such that

$$\forall \boldsymbol{\phi} \in \mathcal{F}, \qquad \eta_{\rho^{-1}} \|\boldsymbol{\phi}\|_{2,\mathcal{F}}^2 \le \|\boldsymbol{\phi}\|_{\rho^{-1}}^2 \le \eta_{\rho^{-1}}^{-1} \|\boldsymbol{\phi}\|_{2,\mathcal{F}}^2. \tag{9.42}$$

9.2.2 Stability and well-posedness

Lemma 9.8 (Discrete inf-sup conditions)**.** *Assume* **(MR)** *and* $(\mathbf{A_\Omega})$*. Then, there exist* $\beta_{\mathsf{C}} > 0$ *and* $\beta_{\mathsf{D}} > 0$ *(independent of the mesh size) such that*

$$\inf_{\mathbf{p}\in\widetilde{\mathcal{V}}} \sup_{\mathbf{v}\in\mathcal{F}} \frac{[\![\mathsf{D}(\mathbf{v}), \mathbf{p}]\!]_{\mathcal{C}\widetilde{\mathcal{V}}}}{\|\mathbf{p}\|_{2,\widetilde{\mathcal{V}}} \|\mathbf{v}\|_{\rho^{-1}}} \ge \beta_{\mathsf{D}}, \qquad \inf_{\phi\in\operatorname{Ker}\mathsf{D}} \sup_{\psi\in\mathcal{E}} \frac{[\![\boldsymbol{\phi}, \mathsf{C}(\boldsymbol{\psi})]\!]_{\mathcal{F}\widetilde{\mathcal{E}}}}{\|\boldsymbol{\phi}\|_{\rho^{-1}} \|\boldsymbol{\psi}\|_{\mu^{-1}}} \ge \beta_{\mathsf{C}}.$$

Proof. To prove the inf-sup condition on D, let $\mathbf{p} \in \widetilde{\mathcal{V}}$ and set $\mathbf{v} := (\mathsf{H}_{\rho^{-1}}^{\mathcal{F}\widetilde{\mathcal{E}}})^{-1}(\widetilde{\mathsf{GRAD}}(\mathbf{p}))$. Then, $\mathbf{v} \in \mathcal{F}$ and $[\![\mathsf{D}(\mathbf{v}), \mathbf{p}]\!]_{\mathcal{C}\widetilde{\mathcal{V}}} = \|\mathbf{v}\|_{\rho^{-1}}^2 = \|\widetilde{\mathsf{GRAD}}(\mathbf{p})\|_{\rho}^2$. Moreover, owing to **(MR)** and (**H1**), we infer that $\|\widetilde{\mathsf{GRAD}}(\mathbf{p})\|_{2,\widetilde{\mathcal{E}}} \lesssim \|\mathbf{v}\|_{\rho^{-1}}$; hence, using the discrete Poincaré inequality (6.35) yields $\|\mathbf{p}\|_{2,\widetilde{\mathcal{V}}} \lesssim \|\mathbf{v}\|_{\rho^{-1}}$.

To prove the inf-sup condition on C, let $\boldsymbol{\phi} \in \operatorname{Ker}\mathsf{D}$. Owing to the exact sequence property (Proposition 3.12) and $(\mathbf{A_\Omega})$, there is $\boldsymbol{\psi} \in \mathcal{E}$ s.t. $\boldsymbol{\phi} = \mathsf{CURL}(\boldsymbol{\psi})$; moreover, we can take $\boldsymbol{\psi} \in (\operatorname{Ker}\mathsf{CURL})^{\perp\mathsf{H}}$, the orthogonality being with respect to $\mathsf{H}_{\mu^{-1}}^{\mathcal{E}\widetilde{\mathcal{F}}}$. Then, $\|\boldsymbol{\phi}\|_{\rho^{-1}}^2 = [\![\boldsymbol{\phi}, \mathsf{C}(\boldsymbol{\psi})]\!]_{\mathcal{F}\widetilde{\mathcal{E}}}$ and $\|\boldsymbol{\psi}\|_{2,\mathcal{E}} \lesssim \|\boldsymbol{\phi}\|_{2,\mathcal{F}}$ owing to the discrete Poincaré inequality on CURL (cf. Lemma 7.47). The norm equivalences on $\mathcal{E}$ (9.41) and $\mathcal{F}$ (9.42) conclude the proof. □

Corollary 9.9 (Well-posedness)**.** *Assume* **(MR)** *and* $(\mathbf{A_\Omega})$*. Then, the discrete system* (9.30) *is well-posed.*

Proof. This a classical consequence of Lemma 9.8 and the fact that A^{cb} is selfadjoint and negative definite (cf. (Dubois, 2002, Theorem 1)). □

9.2.3 Error analysis

Error analysis for discrete dual load. In what follows, we consider a discrete dual load $\mathsf{S}_{\mathsf{d}}^{\mathsf{cb}}(\rho, \underline{f}^*)$ set according to (9.34b). For simplicity, we assume that there is no quadrature error when evaluating the external load. Remarks on the regularity requirements are similar to those of vertex-based pressure schemes in the case of a discrete primal load. We consider the following global commuting operators:

$$\begin{aligned} \lfloor \mu^{-1}, \varepsilon\widetilde{\mathcal{F}} \rceil(\bullet) &:= \mathsf{H}_{\mu^{-1}}^{\varepsilon\widetilde{\mathcal{F}}} \cdot \mathsf{R}_{\mathcal{E}}(\bullet) - \mathsf{R}_{\widetilde{\mathcal{F}}}(\mu^{-1}\bullet), \\ \lfloor \rho^{-1}, \mathcal{F}\widetilde{\varepsilon} \rceil(\bullet) &:= \mathsf{H}_{\rho^{-1}}^{\mathcal{F}\widetilde{\mathcal{E}}} \cdot \mathsf{R}_{\mathcal{F}}(\bullet) - \mathsf{R}_{\widetilde{\mathcal{E}}}(\rho^{-1}\bullet). \end{aligned} \tag{9.43}$$

Let $(p^*, \underline{\phi}, \underline{\omega}^*)$ solve the three-field curl formulation (9.28). To ensure that $\lfloor \rho^{-1}, \mathcal{F}\widetilde{\varepsilon} \rceil(\bullet)$ is well-defined when applied to $\underline{\phi}$ and $\underline{\mathrm{curl}}(\underline{\omega}^*)$, we assume that $\underline{\phi}$ and $\underline{\mathrm{curl}}(\underline{\omega}^*) \in S_{\mathcal{F}}(\Omega) \cap S_{\widetilde{\mathcal{E}}}(\Omega)$. To ensure that $\lfloor \mu^{-1}, \varepsilon\widetilde{\mathcal{F}} \rceil(\bullet)$ is well-defined when applied to $\underline{\omega}^*$, we assume that $\underline{\omega}^* \in S_{\mathcal{E}}(\Omega) \cap S_{\widetilde{\mathcal{F}}}(\Omega)$.

Let $(\mathbf{p}^*, \boldsymbol{\phi}, \boldsymbol{\omega}^*)$ solve the discrete system (9.30). Then, we define the following discrete differences:

$$\boldsymbol{\delta}\mathbf{p}^* := \mathsf{R}_{\widetilde{\mathcal{V}}}(p^*) - \mathbf{p}^*, \quad \boldsymbol{\delta}\boldsymbol{\phi} := \mathsf{R}_{\mathcal{F}}(\underline{\phi}) - \boldsymbol{\phi}, \quad \boldsymbol{\delta}\boldsymbol{\omega}^* := \mathsf{R}_{\mathcal{E}}(\underline{\omega}^*) - \boldsymbol{\omega}^*. \tag{9.44}$$

Theorem 9.10 (Error bounds with discrete dual load)**.** *Assume* **(MR)** *and* $(\mathbf{A_\Omega})$*. Let* $(p^*, \underline{\phi}, \underline{\omega}^*)$ *solve the three-field curl formulation* (9.28) *with homogeneous natural BCs. Let* $(\mathbf{p}^*, \boldsymbol{\phi}, \boldsymbol{\omega}^*)$ *solve the discrete system* (9.30) *with the discrete dual load* $\mathsf{S}_{\mathsf{d}}^{\mathsf{cb}}(\rho, \underline{f}^*)$*. Assume that* $\underline{f}^* \in H^s(\Omega)^3$ *with* $s > \frac{1}{2}$ *and* $\underline{\mathrm{curl}}(\underline{f}^*) \in [L^4(\Omega)]^3$*. Assume that* $\underline{\phi}$ *and* $\underline{\mathrm{curl}}(\underline{\omega}^*) \in S_{\mathcal{F}}(\Omega) \cap S_{\widetilde{\mathcal{E}}}(\Omega)$*. Assume that* $\underline{\omega}^* \in S_{\mathcal{E}}(\Omega) \cap S_{\widetilde{\mathcal{F}}}(\Omega)$*. Then, the following error bounds hold:*

$$\|\widetilde{\mathsf{GRAD}}(\boldsymbol{\delta}\mathbf{p}^*)\|_{\rho} \le \|\lfloor \rho^{-1}, \mathcal{F}\widetilde{\varepsilon} \rceil(\underline{\mathrm{curl}}\,\underline{\omega}^*)\|_{\rho}, \tag{9.45a}$$

$$\|\boldsymbol{\delta}\boldsymbol{\omega}^*\|_{\mu^{-1}} \lesssim \|\lfloor \rho^{-1}, \mathcal{F}\widetilde{\varepsilon} \rceil(\underline{\mathrm{curl}}\,\underline{\omega}^*)\|_{\rho} + \|\lfloor \mu^{-1}, \varepsilon\widetilde{\mathcal{F}} \rceil(\underline{\omega}^*)\|_{\mu}, \tag{9.45b}$$

$$\|\boldsymbol{\delta}\boldsymbol{\phi}\|_{\rho^{-1}} \lesssim \|\lfloor \rho^{-1}, \mathcal{F}\widetilde{\varepsilon} \rceil(\underline{\mathrm{curl}}\,\underline{\omega}^*)\|_{\rho} + \|\lfloor \mu^{-1}, \varepsilon\widetilde{\mathcal{F}} \rceil(\underline{\omega}^*)\|_{\mu} + \|\lfloor \rho^{-1}, \mathcal{F}\widetilde{\varepsilon} \rceil(\underline{\phi})\|_{\rho}. \tag{9.45c}$$

Moreover, if $\underline{\phi}$*,* $\underline{\omega}^*$*,* $\underline{\mathrm{curl}}(\underline{\omega}^*) \in [H^1(\mathrm{C})]^3$*, the following error estimates hold:*

$$\|\widetilde{\mathsf{GRAD}}(\boldsymbol{\delta}\mathbf{p}^*)\|_{\rho} \lesssim h\left(\|\underline{\mathrm{curl}}(\underline{\omega}^*)\|_{[H^1(\mathrm{C})]^3} + \|\underline{\mathrm{curl}}(\underline{f}^*)\|_{[L^4(\Omega)]^3}\right), \tag{9.46a}$$

$$\|\boldsymbol{\delta}\boldsymbol{\omega}^*\|_{\mu^{-1}} \lesssim h\left(\|\underline{\mathrm{curl}}(\underline{\omega}^*)\|_{[H^1(\mathrm{C})]^3} + \|\underline{\mathrm{curl}}(\underline{f}^*)\|_{[L^4(\Omega)]^3} + \|\underline{\omega}^*\|_{[H^1(\mathrm{C})]^3}\right), \tag{9.46b}$$

$$\|\boldsymbol{\delta}\boldsymbol{\phi}\|_{\rho^{-1}} \lesssim h\left(\|\underline{\mathrm{curl}}(\underline{\omega}^*)\|_{[H^1(\mathrm{C})]^3} + \|\underline{\mathrm{curl}}(\underline{f}^*)\|_{[L^4(\Omega)]^3} + \|\underline{\omega}^*\|_{[H^1(\mathrm{C})]^3} + \|\underline{\phi}\|_{[H^1(\mathrm{C})]^3}\right). \tag{9.46c}$$

Proof. (1) We first derive the error equations. Applying $\mathsf{R}_{\widetilde{\mathcal{F}}}$ to the vorticity definition, $\mathsf{R}_{\widetilde{\mathcal{E}}}$ to the momentum balance, and $\mathsf{R}_{\mathcal{C}}$ to the mass balance in (9.28) yields

$$\begin{aligned}
&-\mathsf{R}_{\widetilde{\mathcal{F}}}(\mu^{-1}\underline{\omega}^*) + \widetilde{\mathsf{CURL}}(\mathsf{R}_{\widetilde{\mathcal{E}}}(\rho^{-1}\underline{\phi})) &&= 0_{\widetilde{\mathcal{F}}},\\
&\mathsf{R}_{\widetilde{\mathcal{E}}}(\rho^{-1}\,\underline{\mathrm{curl}}(\underline{\omega}^*)) + \widetilde{\mathsf{GRAD}}(\mathsf{R}_{\widetilde{\mathcal{V}}}(p^*)) &&= \mathsf{S}_{\mathsf{d}}^{\mathsf{cb}}(\rho,\underline{f}^*),\\
&\mathsf{DIV}(\mathsf{R}_{\mathcal{F}}(\underline{\phi})) &&= 0_{\mathcal{C}},
\end{aligned}$$

owing to the commuting property (Proposition 3.18) on the interior dual mesh entities and the homogeneous BCs (4.25) on the dual mesh entities touching the boundary $\partial\Omega$. Subtracting from the corresponding equation in (9.30) and introducing the global commuting operators (9.43) leads to

$$-\mathsf{H}_{\mu^{-1}}^{\mathcal{E}\widetilde{\mathcal{F}}}(\boldsymbol{\delta\omega}^*) + \widetilde{\mathsf{CURL}}\cdot\mathsf{H}_{\rho^{-1}}^{\mathcal{F}\widetilde{\mathcal{E}}}(\boldsymbol{\delta\phi}) = -\lfloor\mu^{-1},\,\varepsilon\widetilde{\mathcal{F}}\rceil(\underline{\omega}^*) + \widetilde{\mathsf{CURL}}\cdot\lfloor\rho^{-1},\,\mathcal{F}\widetilde{\varepsilon}\rceil(\underline{\phi}), \tag{9.47a}$$

$$\mathsf{H}_{\rho^{-1}}^{\mathcal{F}\widetilde{\mathcal{E}}}\cdot\mathsf{CURL}(\boldsymbol{\delta\omega}^*) + \widetilde{\mathsf{GRAD}}(\boldsymbol{\delta p}^*) = \lfloor\rho^{-1},\,\mathcal{F}\widetilde{\varepsilon}\rceil(\underline{\mathrm{curl}}\,\underline{\omega}^*), \tag{9.47b}$$

$$\mathsf{DIV}(\boldsymbol{\delta\phi}) = 0_{\mathcal{C}}. \tag{9.47c}$$

(2) *Bound on the pressure gradient.* We take the duality product of (9.47b) with $(\mathsf{H}_{\rho^{-1}}^{\mathcal{F}\widetilde{\mathcal{E}}})^{-1}\cdot\widetilde{\mathsf{GRAD}}(\boldsymbol{\delta p}^*)$. Proceeding as in Step (2) of the proof of Theorem 9.5 yields (9.45a).

(3) *Bound on the viscous stress circulation.* We use the discrete Hodge decomposition (9.24) based on the discrete Hodge operator $\mathsf{H}_{\mu^{-1}}^{\mathcal{E}\widetilde{\mathcal{F}}}$. We set $\boldsymbol{\delta\omega}^* = \mathsf{GRAD}(\boldsymbol{\delta\theta}) + \boldsymbol{\delta\omega}_\perp^*$ with $\boldsymbol{\delta\theta}\in\mathcal{V}$ and $\boldsymbol{\delta\omega}_\perp^*\in(\operatorname{Ker}\mathsf{CURL})^{\perp_{\mathsf{H}}}$. We take the duality product of (9.47a) with $\mathsf{GRAD}(\boldsymbol{\delta\theta})$. Observing that $[\![\mathsf{GRAD}(\boldsymbol{\delta\theta}),\widetilde{\mathsf{CURL}}(\mathbf{b})]\!]_{\mathcal{E}\widetilde{\mathcal{F}}} = 0$ for all $\mathbf{b}\in\widetilde{\mathcal{E}}$ and $[\![\mathsf{GRAD}(\boldsymbol{\delta\theta}),\mathsf{H}_{\mu^{-1}}^{\mathcal{E}\widetilde{\mathcal{F}}}(\boldsymbol{\delta\omega}^*)]\!]_{\mathcal{E}\widetilde{\mathcal{F}}} = |\!|\!|\mathsf{GRAD}(\boldsymbol{\theta})|\!|\!|_{\mu^{-1}}^2$, we infer that $|\!|\!|\mathsf{GRAD}(\boldsymbol{\theta})|\!|\!|_{\mu^{-1}}\lesssim|\!|\!|\lfloor\mu^{-1},\,\varepsilon\widetilde{\mathcal{F}}\rceil(\underline{\omega}^*)|\!|\!|_{\mu}$. Then, we take the duality product of (9.47b) with $\mathsf{CURL}(\boldsymbol{\delta\omega}^*)$. This yields $|\!|\!|\mathsf{CURL}(\boldsymbol{\delta\omega}^*)|\!|\!|_{\rho^{-1}}\le|\!|\!|\lfloor\rho^{-1},\,\mathcal{F}\widetilde{\varepsilon}\rceil(\underline{\mathrm{curl}}\,\underline{\omega}^*)|\!|\!|_{\rho}$. Since $\mathsf{CURL}(\boldsymbol{\delta\omega}^*) = \mathsf{CURL}(\boldsymbol{\delta\omega}_\perp^*)$ and $\boldsymbol{\delta\omega}_\perp^*\in(\operatorname{Ker}\mathsf{CURL})^{\perp_{\mathsf{H}}}$, we infer from the discrete Poincaré inequality on CURL (cf. Lemma 7.47) that

$$|\!|\!|\boldsymbol{\delta\omega}_\perp^*|\!|\!|_{\mu^{-1}}\lesssim|\!|\!|\lfloor\rho^{-1},\,\mathcal{F}\widetilde{\varepsilon}\rceil(\underline{\mathrm{curl}}\,\underline{\omega}^*)|\!|\!|_{\rho}.$$

Finally, since $|\!|\!|\boldsymbol{\delta\omega}^*|\!|\!|_{\mu^{-1}}^2 = |\!|\!|\mathsf{GRAD}(\boldsymbol{\theta})|\!|\!|_{\mu^{-1}}^2 + |\!|\!|\boldsymbol{\delta\omega}_\perp^*|\!|\!|_{\mu^{-1}}^2$, we infer (9.45b).

(4) *Bound on the mass flux.* Owing to (9.47c), $(\mathbf{A}_{\boldsymbol{\Omega}})$, and Proposition 3.12, there is $\boldsymbol{\delta\psi}\in\mathcal{E}$ s.t. $\boldsymbol{\delta\phi} = \mathsf{CURL}(\boldsymbol{\delta\psi})$, and we can take $\boldsymbol{\delta\psi}\in(\operatorname{Ker}\mathsf{CURL})^{\perp_{\mathsf{H}}}$. We take the duality product of (9.47a) with $\boldsymbol{\delta\psi}$. For the two terms on the left-hand side, we obtain $[\![\boldsymbol{\delta\psi},\mathsf{H}_{\mu^{-1}}^{\mathcal{E}\widetilde{\mathcal{F}}}(\boldsymbol{\delta\omega}^*)]\!]_{\mathcal{E}\widetilde{\mathcal{F}}}\le|\!|\!|\boldsymbol{\delta\psi}|\!|\!|_{\mu^{-1}}|\!|\!|\boldsymbol{\delta\omega}^*|\!|\!|_{\mu^{-1}}$ and $[\![\boldsymbol{\delta\psi},\widetilde{\mathsf{CURL}}\cdot\mathsf{H}_{\rho^{-1}}^{\mathcal{F}\widetilde{\mathcal{E}}}(\boldsymbol{\delta\phi})]\!]_{\mathcal{E}\widetilde{\mathcal{F}}} = |\!|\!|\mathsf{CURL}(\boldsymbol{\delta\psi})|\!|\!|_{\rho^{-1}}^2$. Using Lemma 7.47, the Cauchy–Schwarz inequalities (9.40), and the previous error bounds lead to (9.45c).

(5) Finally, the error bounds for smooth solutions result from Lemmata 6.14 and 6.16. □

Error analysis for discrete primal load. In what follows, we consider a discrete primal load $\mathsf{S}_{\mathsf{p}}^{\mathsf{cb}}(\rho,\underline{f}^*)$ set according to (9.34a). Remarks on the regularity requirements are similar to those of vertex-based pressure schemes in the case of a discrete dual load (*i.e.* less regularity is required compared to the previous case).

Theorem 9.11 (Error bounds with discrete primal load)**.** *Assume* **(MR)** *and* $(\mathbf{A}_{\boldsymbol{\Omega}})$*. Let* $(p^*,\underline{\phi},\underline{\omega}^*)$ *solve the three-field curl formulation* (9.28) *with homogeneous natural BCs. Let* $(\mathbf{p}^*,\boldsymbol{\phi},\boldsymbol{\omega}^*)$ *solve the discrete system* (9.30) *with the discrete primal load* $\mathsf{S}_{\mathsf{p}}^{\mathsf{cb}}(\rho,\underline{f}^*)$*. Assume that* $\underline{f}^*\in H^s(\Omega)^3$ *with* $s>\frac12$*. Assume that* $\underline{\phi}$ *and* $\rho\,\underline{\mathrm{grad}}(p^*)\in S_{\mathcal{F}}(\Omega)\cap S_{\widetilde{\mathcal{E}}}(\Omega)$*. Assume that*

$\underline{\omega}^* \in S_{\mathcal{E}}(\Omega) \cap S_{\widetilde{\mathcal{F}}}(\Omega)$. *Then, the following error bounds hold:*

$$\|\widetilde{\mathsf{GRAD}}(\boldsymbol{\delta p}^*)\|_\rho \le \|\lfloor\rho^{-1},\, {}_{\mathcal{F}}\tilde{\varepsilon}\rceil(\rho\,\underline{\mathrm{grad}}(p^*))\|_\rho, \tag{9.48a}$$

$$\|\boldsymbol{\delta\omega}^*\|_{\mu^{-1}} \lesssim \|\lfloor\rho^{-1},\, {}_{\mathcal{F}}\tilde{\varepsilon}\rceil(\rho\,\underline{\mathrm{grad}}(p^*))\|_\rho + \|\lfloor\mu^{-1},\, {}_{\varepsilon}\tilde{\mathcal{F}}\rceil(\underline{\omega}^*)\|_\mu, \tag{9.48b}$$

$$\|\boldsymbol{\delta\phi}\|_{\rho^{-1}} \lesssim \|\lfloor\rho^{-1},\, {}_{\mathcal{F}}\tilde{\varepsilon}\rceil(\rho\,\underline{\mathrm{grad}}(p^*))\|_\rho + \|\lfloor\mu^{-1},\, {}_{\varepsilon}\tilde{\mathcal{F}}\rceil(\underline{\omega}^*)\|_\mu + \|\lfloor\rho^{-1},\, {}_{\mathcal{F}}\tilde{\varepsilon}\rceil(\underline{\phi})\|_\rho. \tag{9.48c}$$

Moreover, if $\underline{\phi}$, $\underline{\mathrm{grad}}(p^*)$, $\underline{\omega}^* \in [H^1(\mathrm{C})]^3$ *and* $\underline{f}^* \in [L^4(\Omega)]^3$, *the following error estimates hold:*

$$\|\widetilde{\mathsf{GRAD}}(\boldsymbol{\delta p}^*)\|_\rho \lesssim h\,\|\rho\,\underline{\mathrm{grad}}(p^*)\|_{[H^1(\mathrm{C})]^3}, \tag{9.49a}$$

$$\|\boldsymbol{\delta\omega}^*\|_{\mu^{-1}} \lesssim h\left(\|\rho\,\underline{\mathrm{grad}}(p^*)\|_{[H^1(\mathrm{C})]^3} + \|\underline{\omega}^*\|_{[H^1(\mathrm{C})]^3} + \|\underline{f}^*\|_{[L^4(\Omega)]^3}\right), \tag{9.49b}$$

$$\|\boldsymbol{\delta\phi}\|_{\rho^{-1}} \lesssim h\left(\|\rho\,\underline{\mathrm{grad}}(p^*)\|_{[H^1(\mathrm{C})]^3} + \|\underline{\omega}^*\|_{[H^1(\mathrm{C})]^3} + \|\underline{f}^*\|_{[L^4(\Omega)]^3} + \|\underline{\phi}\|_{[H^1(\mathrm{C})]^3}\right). \tag{9.49c}$$

Proof. Since $\mathsf{S}_{\mathsf{p}}^{\mathsf{cb}}(\rho, \underline{f}^*) = \mathsf{S}_{\mathsf{d}}^{\mathsf{cb}}(\rho, \underline{f}^*) + \lfloor\rho^{-1},\, {}_{\mathcal{F}}\tilde{\varepsilon}\rceil(\rho\underline{f}^*)$, the main difference with the proof of Theorem 9.10 is that the error equation (9.47b) is to be replaced by

$$\mathsf{H}_{\rho^{-1}}^{\mathcal{F}\tilde{\mathcal{E}}} \cdot \mathsf{CURL}(\boldsymbol{\delta\omega}^*) + \widetilde{\mathsf{GRAD}}(\boldsymbol{\delta p}^*) = \lfloor\rho^{-1},\, {}_{\mathcal{F}}\tilde{\varepsilon}\rceil(\rho\,\underline{\mathrm{grad}}(p^*)).$$

The rest of the proof follows the same lines and is skipped for brevity. □

Remark 9.12 (Comparison with Theorem 9.10)**.** *When the divergence-free part of the external load (i.e.,* $\underline{\mathrm{curl}}(\underline{\omega}^*)$*) is expected to dominate over the curl-free part (i.e.,* $\underline{\mathrm{grad}}(p^*)$*), using a discrete primal load is more appropriate since the error bounds do not depend on* $\underline{\mathrm{curl}}(\underline{\omega}^*)$*. Alternatively, when the curl-free part is expected to dominate over the divergence-free part, using a discrete dual load is more appropriate since the error bounds do not depend on* $\underline{\mathrm{grad}}(p^*)$*.*

9.3 Numerical results

In this section, we focus on the vertex-based pressure scheme (9.3). Numerical results for the cell-based pressure scheme (9.30) are left for future works.

9.3.1 Linear algebra aspects

The strategy for solving the linear system (9.3) takes advantage of the CDO framework, which allows us to solve only two SPD systems, since it is possible to operate an exact splitting between pressure and velocity. Applying $\widetilde{\mathsf{DIV}}$ to the momentum equation yields the following SPD system for the pressure:

$$\underbrace{\widetilde{\mathsf{DIV}} \cdot \mathsf{H}_{\rho}^{\varepsilon\tilde{\mathcal{F}}} \cdot \mathsf{GRAD}}_{\mathsf{A}_{\Delta}^{\mathsf{vb}}}(\mathbf{p}^*) = \widetilde{\mathsf{DIV}} \cdot \mathsf{S}^{\mathsf{vb}}(\rho, \underline{f}^*), \tag{9.50}$$

of size #V which is independent of $\mathbf{u}$. Then, the velocity $\mathbf{u}$ is solved by an augmented Lagrangian (AL) approach yielding the following SPD system of size #E, where the right-hand side takes into account the pressure computed in (9.50):

$$\underbrace{(\mathsf{A}^{\mathsf{vb}} + r\mathsf{B}^{\mathrm{T}} \cdot \mathsf{B})}_{\mathsf{A}_{\mathrm{AL}}^{\mathsf{vb}}}(\mathbf{u}) = \mathsf{S}^{\mathsf{vb}}(\rho, \underline{f}^*) - \mathsf{B}^{\mathrm{T}}(\mathbf{p}^*). \tag{9.51}$$

Applying $\widetilde{\mathsf{DIV}}$ to this system readily shows that the discrete velocity exactly satisfies both momentum and mass balance in (9.3). Numerical experiments suggest that a convenient value of the Lagrange multiplier r is the reciprocal of $\max_{\mathrm{e}\in\mathrm{E}}|\mathfrak{p}_{\mathrm{e}}|$ with $\mathfrak{p}_{\mathrm{e}} := \cup_{\mathrm{c}\in\mathrm{C}_{\mathrm{e}}}\mathfrak{p}_{\mathrm{e,c}}$ (cf. Section 5.2.2). Since the two systems (9.50) and (9.51) are SPD, we apply a CG algorithm preconditioned with a SSOR technique to invert the linear systems (as for elliptic problems). More sophisticated techniques like algebraic multigrid can be employed to improve the efficiency of the iterative solver.

9.3.2 Vortex test case

We first consider an adaptation of the Taylor–Green vortex test case on the unit cube $\Omega = [0,1]^3$. Mass density and viscosity are set to 1. We consider the system (9.1) with the following exact pressure and exact velocity fields:

$$\begin{aligned} p(x,y,z) &= \sin(2\pi x)\sin(2\pi y)\sin(2\pi z), \\ \underline{u}(x,y,z) &= \begin{bmatrix} \frac{1}{2}\sin(2\pi x)\cos(2\pi y)\cos(2\pi z) \\ \frac{1}{2}\cos(2\pi x)\sin(2\pi y)\cos(2\pi z) \\ -\cos(2\pi x)\cos(2\pi y)\sin(2\pi z) \end{bmatrix}. \end{aligned} \tag{9.52}$$

The external load $\underline{f}^*$ and the non-homogeneous BCs are determined from (9.52) in order to satisfy (9.1).

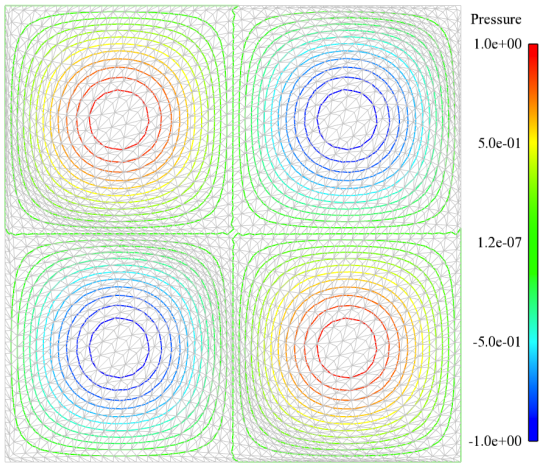

Figure 9.1 – Pressure isolines at $z = 0.75$ obtained on a `PrT` mesh corresponding to the exact solution (9.52).

We investigate numerically the vertex-based pressure scheme (9.3) on the five mesh sequences: `Hex`, `PrT`, `PrG`, `CB`, and `Ker`, previously introduced in Section 8.4. Illustrations of these meshes and quantitative information on the features of the mesh sequences are provided in Appendix A. The two discrete Hodge operators $\mathsf{H}_\rho^{\mathcal{E}\tilde{\mathcal{F}}}$ and $\mathsf{H}_\mu^{\mathcal{F}\tilde{\mathcal{E}}}$ of the discrete system (9.3) are built using local reconstruction operators which are piecewise constant (cf. Section 7.3.1). Specifically, we consider two strategies. When the two discrete Hodge operators are built using the DGA reconstruction operators, we refer to the scheme as `DGA` and, when the SUSHI-like reconstruction operators are used, we refer to the scheme as `SUSHI`.

In what follows, we consider either natural BCs defined in (9.1) or essential BCs corresponding to (9.29) in the case of vertex-based pressure schemes. The essential BCs are strongly enforced, *i.e.* we remove DoFs associated to the pressure and attached to primal vertices $\mathrm{v} \in \mathrm{V}^{\mathrm{B}}$ as well as DoFs associated to the velocity and attached to primal edges $\mathrm{e} \in \mathrm{E}^{\mathrm{B}}$. In addition, we consider either a discrete primal or dual load. So, four combinations are studied for each scheme: natural BCs with a discrete primal load, denoted by `NPL`, essential BCs with a discrete primal load `EPL`, natural BCs with a discrete dual load `NDL`, and essential BCs with a discrete dual load `EDL`.

Convergence rates. To study the convergence rates of CDO schemes for the vortex test case, we define similar quantities as for the elliptic problems. Recalling the definitions of Section 8.4.1 where the discrete errors are generically defined as follows:

$$\mathbf{Er}_{\mathcal{X}}(\mathbf{a}) := \frac{\|\mathsf{R}_{\mathcal{X}}(a) - \mathbf{a}\|_{2,\mathcal{X}}}{\|\mathsf{R}_{\mathcal{X}}(a)\|_{2,\mathcal{X}}}, \qquad \mathbf{Er}_{\alpha,\mathcal{X}}(\mathbf{a}) := \frac{\|\mathsf{R}_{\mathcal{X}}(a) - \mathbf{a}\|_{\alpha,\mathcal{X}}}{\|\mathsf{R}_{\mathcal{X}}(a)\|_{\alpha,\mathcal{X}}}, \tag{9.53}$$

where $\mathbf{a} \in \mathcal{X}$ is a generic discrete solution and a a generic exact solution. We consider the following discrete errors for the pressure $\mathbf{Er}_{\mathcal{V}}(\mathbf{p}^*)$, its gradient $\mathbf{Er}_{\rho,\mathcal{E}}(\mathbf{g})$, the velocity $\mathbf{Er}_{\rho,\mathcal{E}}(\mathbf{u})$, and the vorticity $\mathbf{Er}_{\mu,\mathcal{F}}(\boldsymbol{\omega})$. We recall the definition of the convergence rate

$$\mathrm{R} := -3\frac{\log\left(\frac{Q_i}{Q_{i-1}}\right)}{\log\left(\frac{\#\mathrm{X}_i}{\#\mathrm{X}_{i-1}}\right)}, \tag{9.54}$$

where Q_i and Q_{i-1} are the computed errors on the i^{th} and $(i-1)^{\text{th}}$ meshes of the sequence, and $\#\mathrm{X}_i$ and $\#\mathrm{X}_{i-1}$ are the numbers of DoFs related to theses errors and associated to the i^{th} and $(i-1)^{\text{th}}$ meshes of the sequence.

Synthesis

Convergence rates of the discrete errors observed on the finest meshes of each mesh sequence are reported in Table 9.1 for the pressure and its gradient, and in Table 9.2 for the velocity and the vorticity.

Error	Scheme	Case	Hex	PrT	PrG	CB	Ker
$\mathbf{Er}_{\mathcal{V}}(\mathbf{p}^*)$	NDL	DGA	2.3	2.0	2.1	2.2	1.2
		SUSHI	2.0	2.1	1.9	2.1	0.9
	NPL	DGA	4.2	1.8	1.7	1.8	1.5
		SUSHI	4.2	1.7	1.6	1.7	1.1
	EDL	DGA	2.1	2.1	2.1	2.0	1.3
		SUSHI	2.1	2.0	2.0	2.0	0.9
	EPL	DGA	4.2	2.0	2.1	1.9	1.3
		SUSHI	4.2	2.0	1.9	2.1	0.9
$\mathbf{Er}_{\rho,\mathcal{E}}(\mathbf{g})$	NDL	DGA	2.1	2.0	1.9	1.1	1.5
		SUSHI	1.9	1.9	1.8	1.1	1.0
	NPL	DGA	4.1	2.0	1.8	1.0	1.4
		SUSHI	4.1	1.9	1.8	1.3	1.0
	EDL	DGA	2.1	2.0	2.0	1.1	1.5
		SUSHI	2.1	2.0	1.9	1.0	1.0
	EPL	DGA	4.1	2.0	1.9	0.9	1.4
		SUSHI	4.1	1.9	1.9	1.0	0.9

Table 9.1 – Convergence rates of the discrete errors on the pressure and its gradient between the two finest meshes of each sequence for the four cases (NDL, NPL, EDL, and EPL) and the two schemes (DGA and SUSHI).

The results on the pressure gradient, vorticity, and velocity are in agreement with the theoretical results derived in Section 9.1., Similar convergence rates are observed with the four tested cases between DGA and SUSHI reconstruction operators for the Hex, PrT, and PrG mesh sequences. Concerning the CB mesh sequence, SUSHI reconstruction operators obtain a better convergence rates of the discrete errors for the velocity and the vorticity. Concerning the Ker mesh sequence, DGA reconstruction operators shows a better convergence rates of the discrete errors for all the computed variables. In the case of the Hex, PrT, and PrG mesh sequences, some super-convergent behavior is observed for the pressure gradient, the velocity, and the vorticity. The pressure error appears to converge at second-order for most of the cases considered herein. The exception is the Ker sequence, as for elliptic equations (cf. Section 8.4.3). This is a consequence of the variation of the values of the mesh regularity parameters during the successive

Error	Scheme	Case	Hex	PrT	PrG	CB	Ker
$\mathbf{Er}_{\rho,\mathcal{E}}(\mathbf{u})$	NDL	DGA	2.1	2.0	1.8	1.1	1.3
		SUSHI	2.1	1.9	1.8	1.4	1.0
	NPL	DGA	2.0	2.0	1.8	1.1	1.4
		SUSHI	2.1	2.0	1.8	1.4	1.2
	EDL	DGA	2.1	2.0	2.0	1.0	1.3
		SUSHI	2.1	2.0	1.9	1.3	1.1
	EPL	DGA	2.0	2.0	2.0	1.0	1.4
		SUSHI	2.1	2.0	1.9	1.3	1.1
$\mathbf{Er}_{\mu,\mathcal{F}}(\boldsymbol{\omega})$	NDL	DGA	2.0	1.9	1.7	1.0	1.3
		SUSHI	2.0	1.9	1.6	0.9	1.0
	NPL	DGA	2.0	1.9	1.7	1.0	1.4
		SUSHI	2.0	1.9	1.6	1.0	1.1
	EDL	DGA	2.0	2.0	1.9	0.9	1.3
		SUSHI	2.0	2.0	1.8	0.9	1.0
	EPL	DGA	2.0	2.0	1.9	1.0	1.4
		SUSHI	2.0	1.9	1.8	1.0	1.1

Table 9.2 – Convergence rates of the discrete errors on the velocity and the vorticity between the two finest meshes of each sequence for the four cases (NDL, NPL, EDL, and EPL) and the two schemes (DGA and SUSHI).

mesh refinements (in particular, the criteria related to the orthogonality; cf. Appendix A). A noticeable difference appears in the case of the Hex sequence with a discrete primal load (cases NPL and EPL). Namely, the pressure and its gradient are captured up to the accuracy of the quadrature rule used to compute the discrete primal load. Specifically, we consider the Gauss quadrature on edges with two points which is of order 3.

Computational effectiveness. To study the computational effectiveness of CDO schemes, we introduce $\mathrm{NNZ}(\mathsf{A}^{\mathsf{vb}}_{\Delta})$ and $\mathrm{NNZ}(\mathsf{A}^{\mathsf{vb}}_{\mathrm{AL}})$ which are the number of non-zeros of the system matrices to solve for the pressure (cf. (9.50)) and for the velocity (cf. (9.51)) respectively. $\mathrm{n}_{\mathrm{Ite}}(\mathsf{A}^{\mathsf{vb}}_{\Delta})$ and $\mathrm{n}_{\mathrm{Ite}}(\mathsf{A}^{\mathsf{vb}}_{\mathrm{AL}})$ are the corresponding number of iterations required to achieve the convergence. The convergence criterion set a tolerance of $\epsilon = 10^{-12}$ on the norm of the residual. Following the same rationale as in the elliptic case, we define the computational cost as follows:

$$\boldsymbol{\chi} := \mathrm{n}_{\mathrm{Ite}}(\mathsf{A}^{\mathsf{vb}}_{\Delta}) \times \mathrm{NNZ}(\mathsf{A}^{\mathsf{vb}}_{\Delta}) + \mathrm{n}_{\mathrm{Ite}}(\mathsf{A}^{\mathsf{vb}}_{\mathrm{AL}}) \times \mathrm{NNZ}(\mathsf{A}^{\mathsf{vb}}_{\mathrm{AL}}). \tag{9.55}$$

Since conclusion are similar in the case of natural or essential BCs. We restrict our comparison of the computational effectiveness between DGA and SUSHI reconstruction operators to natural BCs in the case of a discrete dual load in Figure 9.2 and in the case of a discrete primal load in Figure 9.3. No general conclusion can be drawn. Namely, for the Hex mesh sequence, the vertex-based pressure scheme using the SUSHI reconstruction operators turns out to be more cost-effective than that using the DGA reconstruction operators (cf. Remark 7.34). For the other mesh sequences, the vertex-based pressure scheme using the DGA reconstruction operators turns out to have a similar or better cost-effectiveness than that using the SUSHI reconstruction operators (at the exception of the CB mesh sequence for the discrete pressure error in the case of a discrete primal load).

We assign a label to each mesh sequence as depicted in Table 9.3. In what follows, we focus on the results obtained with natural BCs since the conclusions are similar with essential BCs (cf. Appendix B.2 for more details on essential BCs).

Sequence	Hex	PrT	PrG	CB	Ker
Thumbnail	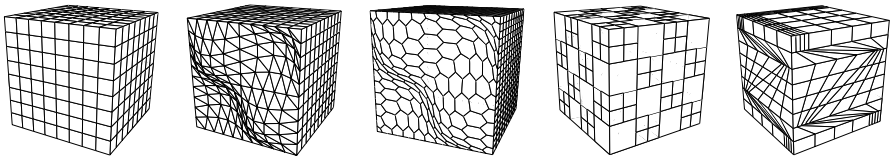				
Labels A					
Labels B					

Table 9.3 – Labels associated to each mesh sequence.

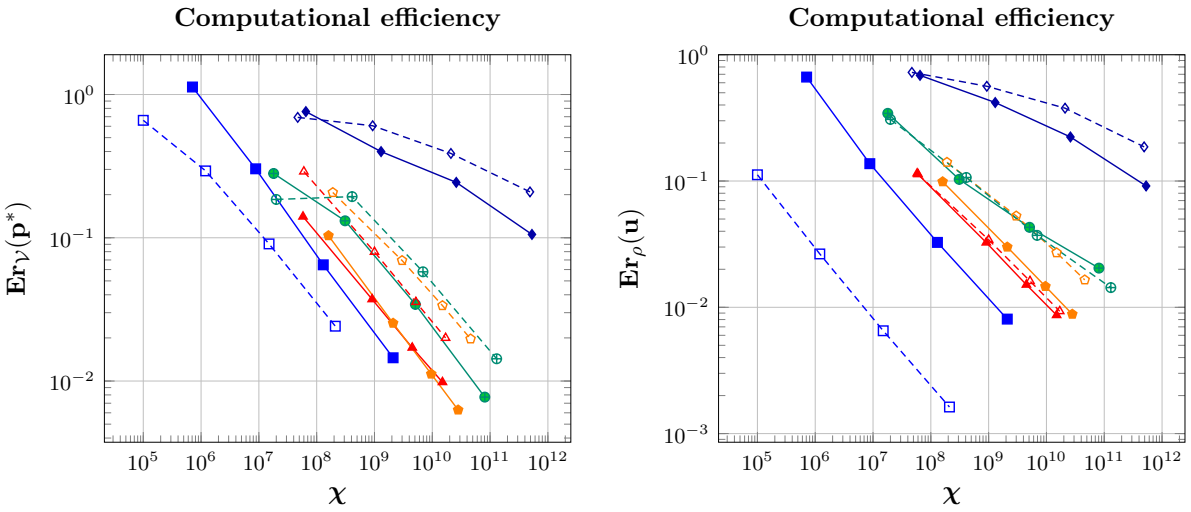

Figure 9.2 – Comparison of the cost-effectiveness between DGA (labels A) and SUSHI (labels B) reconstruction operators for the discrete error on the pressure (left) and the discrete error on the velocity (right) in the case NDL.

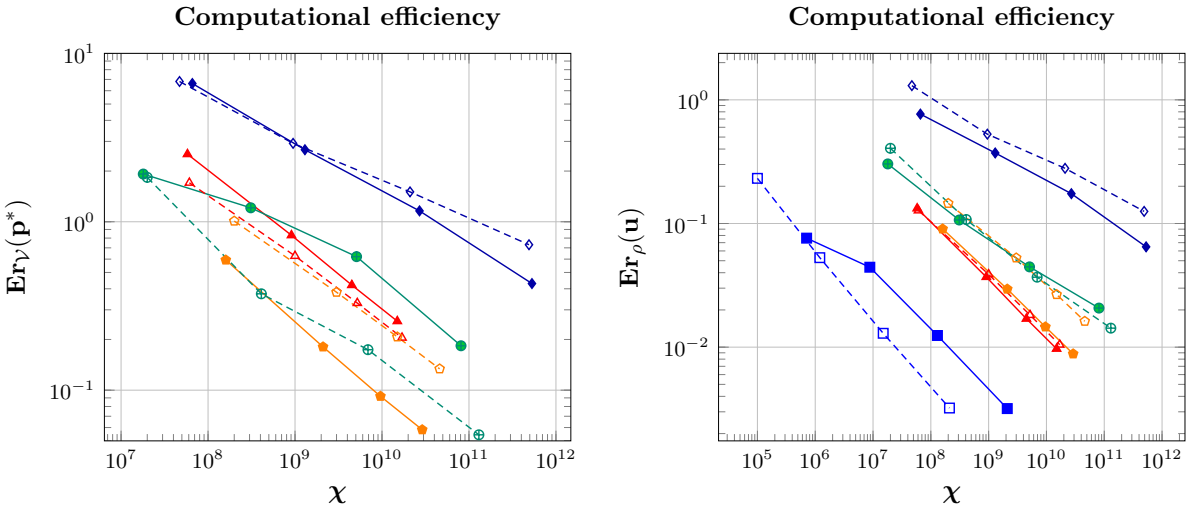

Figure 9.3 – Comparison of the cost-effectiveness between DGA (labels A) and SUSHI (labels B) reconstruction operators for the discrete error on the pressure (left) and the discrete error on the velocity (right) in the case NPL.

Results with DGA reconstruction operators

We now detail the results obtained with a vertex-based scheme using the DGA reconstruction operators. We compare the two strategies of discretization of the external load with natural BCs, *i.e.* the cases NDL and NPL. In Figure 9.4, we plot the discrete errors on the pressure, its gradient, the velocity and the vorticity. Except for the Hex mesh sequence, using a discrete dual load yields more accurate results on the pressure than using a discrete primal load. Concerning the accuracy on the velocity, nearly the same level of accuracy is obtained using the two strategies (except for the Hex mesh sequence). Similar results are plotted in Figure 9.5 for the vertex-based pressure scheme using the SUSHI reconstruction operators. The same conclusions hold. Results concerning the cases EDL and EPL are collected in Appendix B.2.

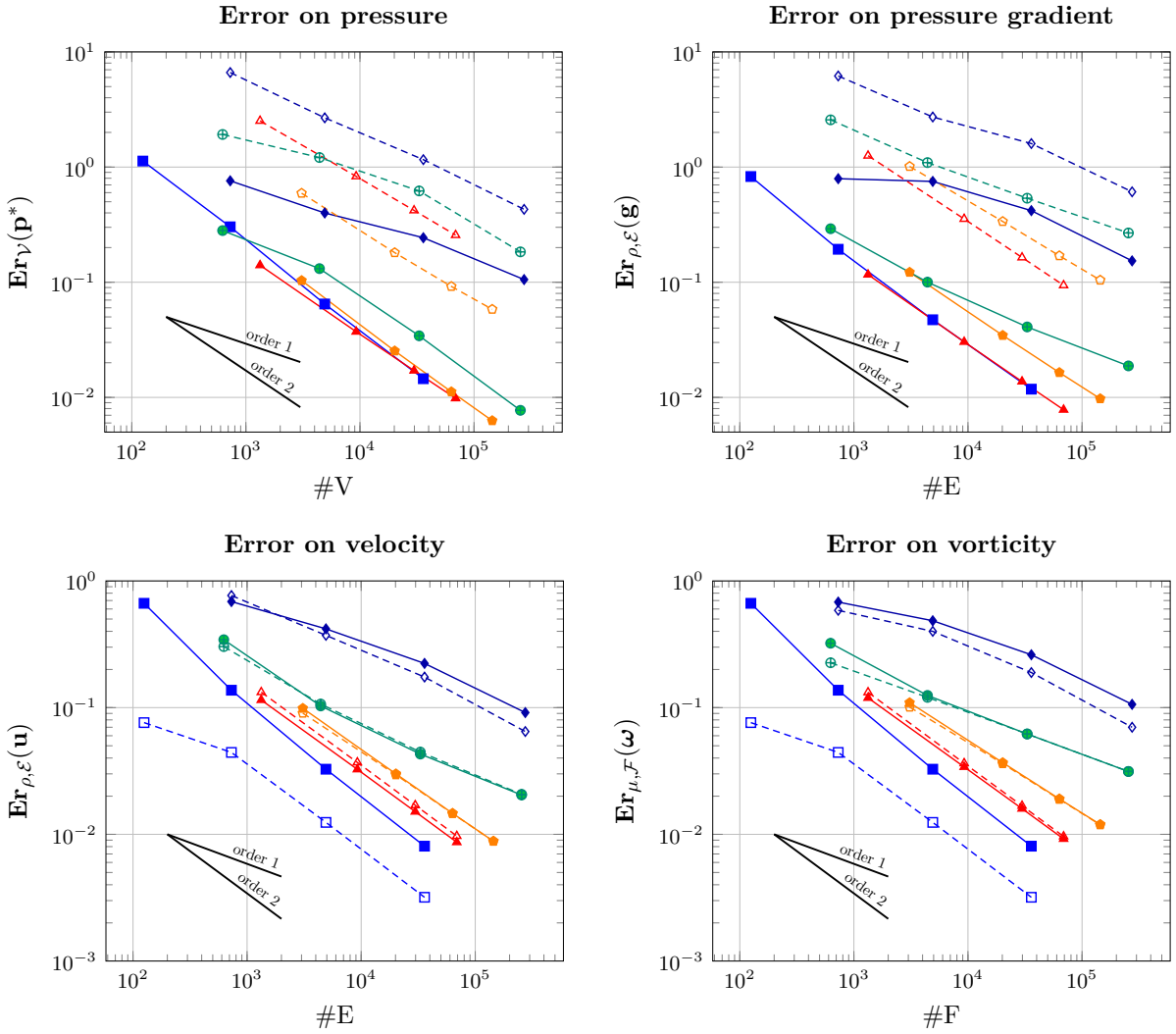

Figure 9.4 – Discrete error on the pressure (upper left), on the pressure gradient (upper right), on the velocity (lower left), and on the vorticity (lower right) for the vertex-based pressure scheme using the DGA reconstruction operators. Natural BCs are considered: NDL with labels A and NPL with labels B.

Results with SUSHI reconstruction operators

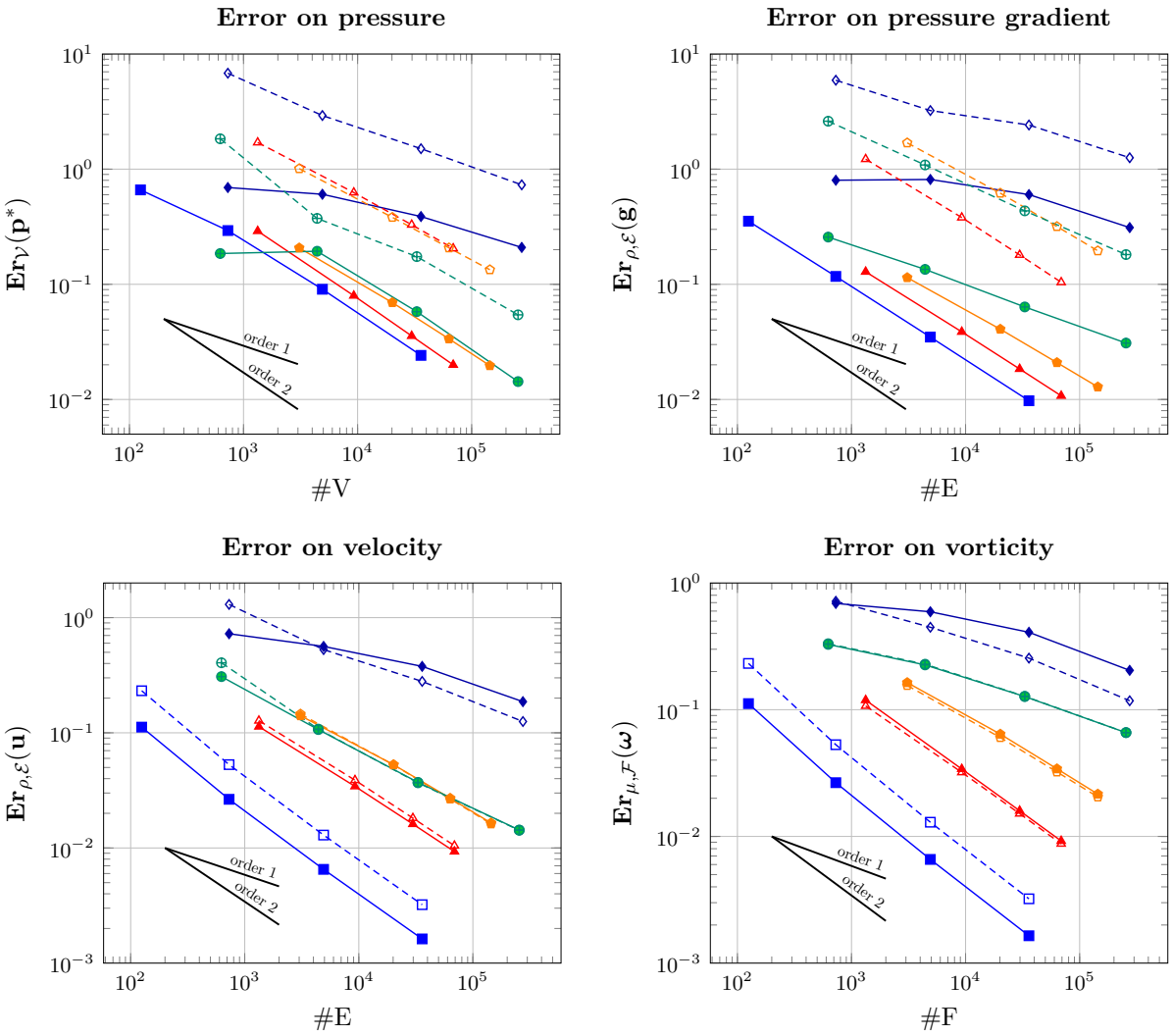

Figure 9.5 – Discrete error on the pressure (upper left), on the pressure gradient (upper right), on the velocity (lower left), and on the vorticity (lower right) for the vertex-based pressure scheme using the SUSHI reconstruction operators. Natural BCs are considered: NDL with labels A and NPL with labels B.

9.3.3 External load

Finally, we illustrate the practical advantage of the primal and dual load discretizations. We consider the vector potential $\underline{\Psi} = \underline{\mathrm{curl}}(\underline{u})$ and the scalar potential $\Theta = p$ with $\underline{u}$ and p defined in (9.52) with natural BCs, and we take for the external load

$$\rho \underline{f}^* := \chi_{\underline{u}}\, \underline{\mathrm{curl}}(\underline{\Psi}) + \chi_p\, \underline{\mathrm{grad}}(\Theta), \tag{9.56}$$

with real numbers $\chi_{\underline{u}}$ and χ_p, so that $\rho \underline{f}^*$ has a large curl-free part when $\chi_p \gg 1$ and a large divergence-free part when $\chi_{\underline{u}} \gg 1$. We observe from Figure 9.6, left, that the discrete pressure error is not affected by the large divergence-free part of the load when choosing a dual discretization. Similarly, we observe from Figure 9.6, right, that the discrete velocity error is not affected by the large curl-free part of the load when choosing a primal discretization. These numerical results are in agreement with the theoretical results derived in Theorems 9.5 and 9.6. We stress that the Hodge–Helmholtz decomposition of the external load is not used explicitly in the scheme. Similar results are obtained with the other mesh sequences.

Remark 9.13 (Quadrature effect)**.** *When the magnitude of $\chi_{\underline{u}}$ or χ_p is large, a particular care*

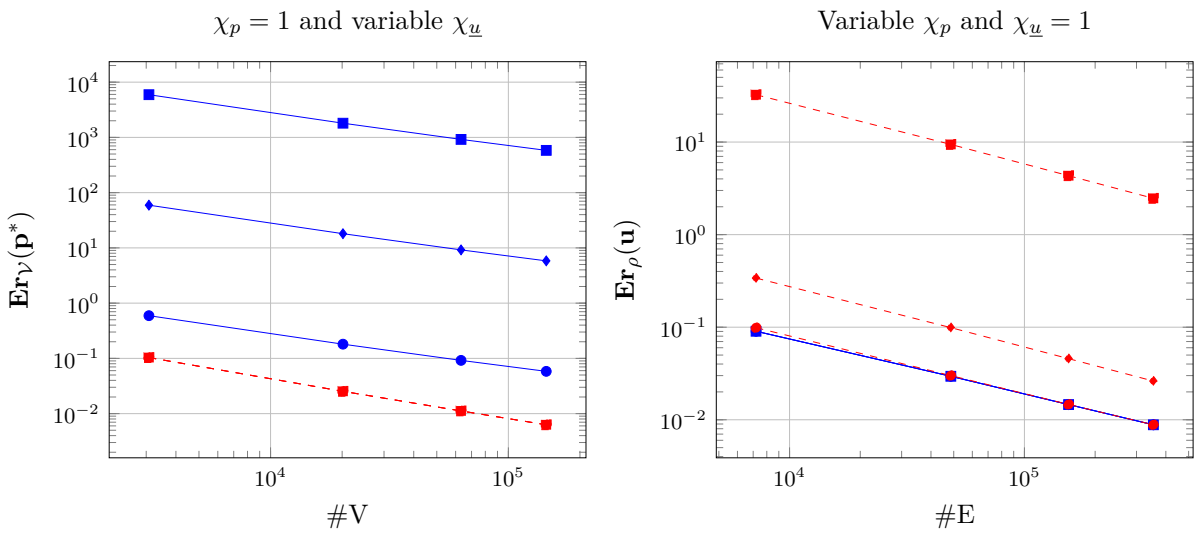

Figure 9.6 – Effect of a primal (blue solid lines) and dual (red dashed lines) discretization of the external load on the sequence of PrG meshes when one considers a large divergence-free part (left) or a large curl-free part (right). Left: Error on the pressure for $\chi_{\underline{u}} \in \{1 \text{ (circle)}, 10^2 \text{ (diamond)}, 10^4 \text{ (square)}\}$ and $\chi_p = 1$; Right: Error on the velocity for $\chi_{\underline{u}} = 1$ and $\chi_p \in \{1 \text{ (circle)}, 10^2 \text{ (diamond)}, 10^4 \text{ (square)}\}$.

has to be taken to the computation of the external load. Namely, quadrature rules of order 5 have to be used so as to recover the theoretical results for the `PrG`*,* `CB`*, and* `Ker` *mesh sequences.*

Conclusions & Perspectives

L'approche CDO (Compatible Discrete Operator) développée dans le cadre de cette thèse constitue une nouvelle approche de discrétisation des problèmes elliptiques et de Stokes sur maillages polyédriques. La première partie de cette thèse rassemble les principes constitutifs des schémas CDO. La définition des degrés de liberté, celle des opérateurs différentiels discrets sur le maillage primal et le maillage dual, ainsi que les opérateurs de Hodge discrets reliant les degrés de liberté en dualité ont été successivement explicités. La considération conjointe d'un maillage primal et d'un maillage dual a permis de regrouper sur la même base théorique deux familles de schémas CDO se différenciant par le positionnement des degrés de liberté associés au potentiel. Un positionnement aux sommets du maillage primal correspond aux schémas *vertex-based* et un positionnement aux sommets du maillage dual (*i.e.* au centre des cellules du maillage primal) aux schémas *cell-based*. Deux familles de schémas CDO ont ainsi été proposées pour discrétiser les équations elliptiques et de Stokes.

La seconde partie de ce mémoire pose les bases théoriques de l'analyse des schémas CDO sur maillages polyédriques. Deux niveaux d'analyse ont été proposés. Le premier niveau adopte une vision algébrique. Les propriétés qu'un opérateur de Hodge doit satisfaire sont la clé de voûte de l'analyse des schémas CDO. Les trois propriétés identifiées sont : la symétrie, la stabilité et la $\mathbb{P}_0$-consistance. Le second niveau d'analyse repose sur l'utilisation d'opérateurs de reconstruction. Les propriétés relatives à ces opérateurs ont été identifiées en cohérence avec l'analyse algébrique. Plusieurs exemples d'opérateurs de reconstruction ont été proposés et analysés. L'utilisation d'opérateurs de reconstruction permet de définir génériquement l'opérateur de Hodge discret d'une part et d'étendre les résultats théoriques d'autre part. Pour chaque niveau d'analyse, des inégalités de Poincaré discrètes sur les opérateurs différentiels discrets ont été également établies.

La dernière partie de ce mémoire rassemble l'analyse et les tests numériques relatifs aux schémas CDO proposés pour les équations elliptiques et de Stokes. Concernant les équations elliptiques, la stabilité et des estimations d'erreur en norme d'énergie à l'ordre 1 du gradient et du flux ont été démontrées ainsi qu'une estimation d'erreur en norme L^2 à l'ordre 2 du potentiel. Des liens avec les schémas mimétiques (MFD) et les récentes évolutions des schémas Volumes Finis (VF) ont également été établis. Concernant les équations de Stokes, la stabilité et des estimations d'erreur à l'ordre 1 du gradient de pression, de la vitesse et de la vorticité ont été démontrées. Par ailleurs, un traitement robuste des termes source ayant une forte composante solénoïdale ou irrotationnelle a été proposé. Ces schémas ont été implémentés dans un prototype basé sur *Code_Saturne* et ont été validés et comparés sur des cas tests à l'aide de plusieurs séries de maillages. Au regard des résultats obtenus en termes de robustesse, d'efficacité et de précision, l'approche CDO s'avère être une méthode de choix parmi les schémas de discrétisation d'ordre 1 sur maillages polyédriques.

Plusieurs développements complémentaires et extensions du champ d'application des schémas CDO ont été identifiés. A court terme, les travaux de recherche développés dans cette thèse seront capitalisés via l'intégration des schémas CDO dans *Code_Saturne*, en traitant d'abord les schémas discrétisant les équations elliptiques, puis ceux discrétisant les équations de Stokes. Cette intégration donnera lieu à la parallélisation des schémas CDO. Des développements supplémentaires, notamment relatifs à l'algèbre linéaire, seront à effectuer pour adapter les tech-

niques actuelles aux exigences du calcul "Hautes Performances". Le cas échéant, les conclusions portant sur l'efficacité des différents schémas CDO pourront être ré-évaluées.

Concernant les problèmes elliptiques, les développements supplémentaires identifiés regroupent l'étude du principe du maximum et l'analyse d'erreur *a posteriori*. L'adaptation des travaux de Lipnikov *et al.* (2011) dans le cadre des schémas MFD, ou ceux de Droniou & Le Potier (2011) dans le cadre des schémas VF, constitueront un point de départ pour l'étude du principe du maximum. L'analyse d'erreur *a posteriori* pourra s'appuyer sur les travaux de Ern & Vohralík (2013) en tirant profit des opérateurs de reconstruction du flux disponibles dans les schémas CDO. Les estimations d'erreur *a posteriori* ont vocation à être couplées à des techniques de raffinement/dé-raffinement automatique de maillage. La capacité des schémas CDO à traiter les polyèdres prendra à cette occasion toute son importance puisque des polyèdres apparaissent naturellement dans les zones d'agglomération de mailles ou à l'interface des zones raffinées.

Concernant le problème de Stokes, le traitement des formes harmoniques (liées à la formulation rotationnelle) et l'ajout de nouvelles conditions aux limites sont deux axes de développements identifiés. Le calcul efficace des formes harmoniques pourra s'appuyer sur les travaux récents de Dlotko & Specogna (2013). L'ajout de nouvelles conditions aux limites pourra être effectué à l'aide de techniques de pénalisation *à la Nitsche*.

Enfin, à moyen terme, l'objectif est le développement de schémas CDO pour la discrétisation des équations de Navier-Stokes. La première étape consistera à prendre en compte les termes de convection pour un champ scalaire, puis pour un champ vectoriel, afin de traiter ensuite le terme convectif des équations de Navier-Stokes. Ces travaux font actuellement l'objet d'une thèse au sein d'EDF R&D. Le développement des schémas CDO basés sur une formulation tensorielle du terme visqueux est une autre évolution envisageable. Les choix de discrétisation effectués dans les travaux de Droniou & Eymard (2009) avec les schémas MFV, ceux de Beirão da Veiga *et al.* (2010) avec les schémas MFD ou ceux de Krell & Manzini (2012) avec les schémas DDFV, pourront être une source d'inspiration. L'adaptation des modèles de turbulence de type "Simulation des Grandes Échelles" sera un autre axe de développement afin d'être en mesure de répondre aux enjeux industriels d'EDF R&D. Les travaux de Verstappen & Veldman (2003) ou ceux de la thèse de Dardalhon (2012) pourront servir de point de départ, en lien avec l'expertise des équipes d'EDF R&D dans ce domaine.

Part IV

Appendix

Appendix A

Properties of the mesh sequences

In this appendix, we collect the main features of the mesh sequences used to assess CDO schemes. We recall that these mesh sequences are taken from the FVCA benchmark:

— `Hex`: Cartesian meshes,
— `HLR`: Cartesian meshes with a locally refined subdomain (polyhedral meshes),
— `PrT`: prismatic meshes,
— `PrG`: prismatic meshes with polygonal basis (polyhedral meshes),
— `CB`: checkerboard meshes (polyhedral meshes),
— `Ker`: Kershaw meshes corresponding to hexahedral meshes with a strong non-orthogonality.

A.1 Definition of mesh quality criteria

Taking inspiration of (6.7) and (6.8), we define for each mesh the following quantities:

$$\eta_{\perp}^{\mathrm{E}} := \min_{\mathrm{c}\in\mathrm{C}} \left(\min_{\mathrm{e}\in\mathrm{E_c}} \underline{\tau}_{\mathrm{e}} \cdot \underline{\nu}_{\tilde{\mathrm{f}}_{\mathrm{c}}(\mathrm{e})} \right), \qquad 0 < \eta_{\perp}^{\mathrm{E}} \leq 1, \tag{A.1a}$$

$$\eta_{\mathrm{vol}}^{\mathrm{E}} := \min_{\mathrm{c}\in\mathrm{C}} d \left(\frac{\sum_{\mathrm{e}\in\mathrm{E_c}} |\mathrm{e}||\tilde{\mathrm{f}}_{\mathrm{c}}(\mathrm{e})|}{|\mathrm{c}|} \right) \qquad 0 < \eta_{\mathrm{vol}}^{\mathrm{E}} \leq 1, \tag{A.1b}$$

$$\eta_{\perp}^{\mathrm{F}} := \min_{\mathrm{c}\in\mathrm{C}} \left(\min_{\mathrm{f}\in\mathrm{F_c}} \underline{\tau}_{\tilde{\mathrm{e}}_{\mathrm{c}}(\mathrm{f})} \cdot \underline{\nu}_{\mathrm{f}} \right), \qquad 0 < \eta_{\perp}^{\mathrm{F}} \leq 1, \tag{A.1c}$$

$$\eta_{\mathrm{vol}}^{\mathrm{F}} := \min_{\mathrm{c}\in\mathrm{C}} d \left(\frac{\sum_{\mathrm{f}\in\mathrm{F_c}} |\mathrm{f}||\tilde{\mathrm{e}}_{\mathrm{c}}(\mathrm{f})|}{|\mathrm{c}|} \right), \qquad 0 < \eta_{\mathrm{vol}}^{\mathrm{F}} \leq 1. \tag{A.1d}$$

These four quantities allow us to evaluate the mesh quality. Namely, $\eta_{\perp}^{\mathrm{E}}$ and $\eta_{\perp}^{\mathrm{F}}$ measure the non-orthogonality of a mesh. For an orthogonal mesh, $\eta_{\perp}^{\mathrm{E}} = \eta_{\perp}^{\mathrm{F}} = 1$. The bigger the non-orthogonality is, the lower $\eta_{\perp}^{\mathrm{E}}$ and $\eta_{\perp}^{\mathrm{F}}$ are. $\eta_{\mathrm{vol}}^{\mathrm{E}}$ and $\eta_{\mathrm{vol}}^{\mathrm{F}}$ measure the non-uniformity of a mesh. A good quality mesh is near from 1. In addition to these criteria, we define the aspect ratio of the barycentric subdivision as follows:

$$\mathfrak{ar} := \sqrt{d} \min_{\mathfrak{c}\in\mathfrak{C}} \left(\frac{\min_{\mathfrak{e}\in\mathfrak{E}_{\mathfrak{c}}} |\mathfrak{e}|}{\max_{\mathfrak{e}\in\mathfrak{E}_{\mathfrak{c}}} |\mathfrak{e}|} \right), \qquad 0 < \mathfrak{ar} \leq 1, \tag{A.2}$$

where $\mathfrak{C}$ is the set of all tetrahedra constituting the simplicial submesh produced by the barycentric subdivision and $\mathfrak{e}$ is an edge of the simplicial submesh (cf. Chapter 5). For a uniform Cartesian mesh, $\mathfrak{ar} = 1$. A poor-quality mesh has an aspect ratio $\mathfrak{ar}$ near from 0. Moreover, for the sake of completeness, we collect the max number of entities in each cell ($\max_{\mathrm{c}\in\mathrm{C}} \#\mathrm{V_c}$, $\max_{\mathrm{c}\in\mathrm{C}} \#\mathrm{E_c}$, and $\max_{\mathrm{c}\in\mathrm{C}} \#\mathrm{F_c}$) as these quantities appear in the stability constants. We recall that the number of subsimplices of the barycentric subdivision of a cell $\mathrm{c} \in \mathrm{C}$ is equal to $4\#\mathrm{E_c}$.

A.2 Mesh sequences

The `Hex` mesh sequence is detailed in Figure A.1, the `HLR` mesh sequence in Figure A.2, the `PrT` mesh sequence in Figure A.3, the `PrG` mesh sequence in Figure A.4, the `CB` mesh sequence in Figure A.5, and the `Ker` mesh sequence in Figure A.6. As depicted in these figures, all the mesh sequences have constant mesh regularity criteria excepted for the `Ker` mesh sequence. Thus, the `Ker` mesh sequence is not really suited to study the convergence of a scheme. However, we keep this mesh sequence to evaluate the robustness of CDO schemes. As detailed in Table A.1, the mesh regularity criteria of the `Ker` mesh sequence are the worst among the tested mesh sequences.

Mesh sequence	`Hex`	`HLR`	`PrT`	`PrG`	`CB`	`Ker`
$\eta_{\perp}^{\mathrm{E}}$	1.0e+00	8.9e-01	3.1e-01	1.8e-01	8.9e-01	4.2e-02
$\eta_{\mathrm{vol}}^{\mathrm{F}}$	1.0e+00	9.6e-01	5.3e-01	5.2e-01	8.2e-01	1.1e-01
$\mathfrak{ar}$	1.0e+00	5.0e-01	1.5e-01	1.5e-01	5.0e-01	2.1e-02

Table A.1 – Selected mesh quality criteria for the finest mesh of each sequence.

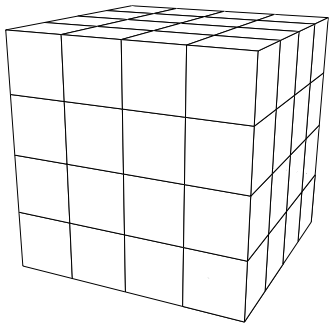

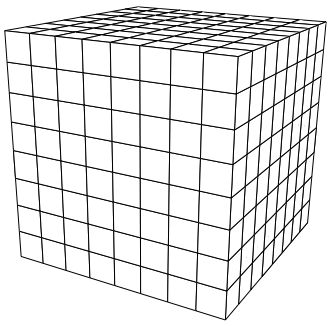

Mesh	#V	#E	#F	#C
`H4`	125	300	240	64
`H8`	729	1944	1728	512
`H16`	4913	13872	13056	4096
`H32`	35937	104544	101376	32768

Mesh	$\eta_{\perp}^{\mathrm{E}}$	$\eta_{\perp}^{\mathrm{F}}$	$\eta_{\mathrm{vol}}^{\mathrm{E}}$	$\eta_{\mathrm{vol}}^{\mathrm{F}}$
`H4`	1.0e+00	1.0e+00	1.0e+00	1.0e+00
`H8`	1.0e+00	1.0e+00	1.0e+00	1.0e+00
`H16`	1.0e+00	1.0e+00	1.0e+00	1.0e+00
`H32`	1.0e+00	1.0e+00	1.0e+00	1.0e+00

Mesh	$\mathfrak{ar}$	$\max_{c\in C} \#V_c$	$\max_{c\in C} \#E_c$	$\max_{c\in C} \#F_c$
`H4`	1.0e+00	8	12	6
`H8`	1.0e+00	8	12	6
`H16`	1.0e+00	8	12	6
`H32`	1.0e+00	8	12	6

Figure A.1 – Left: Successive refinement of the `Hex` mesh sequence. Right: Tables collecting the cardinality of primal sets, mesh quality criteria, and the regularity of the barycentric subdivision for the meshes of the `Hex` mesh sequence.

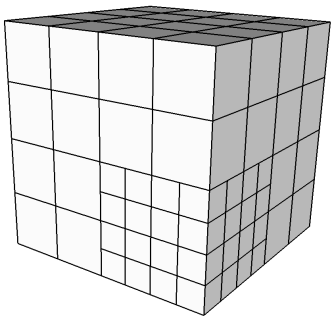

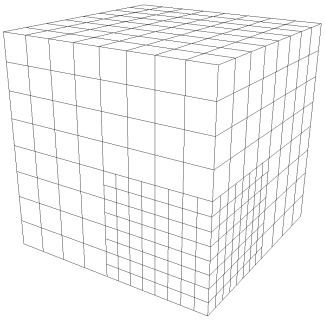

Mesh	#V	#E	#F	#C
HLR2	46	96	66	15
HLR4	223	546	444	120
HLR8	1333	3588	3216	960
HLR16	9097	25800	24384	7680
HLR32	66961	195216	189696	61440

Mesh	$\eta_{\perp}^{\mathrm{E}}$	$\eta_{\perp}^{\mathrm{F}}$	$\eta_{\mathrm{vol}}^{\mathrm{E}}$	$\eta_{\mathrm{vol}}^{\mathrm{F}}$
HLR2	8.9e-01	8.2e-01	9.6e-01	9.6e-01
HLR4	8.9e-01	8.2e-01	9.6e-01	9.6e-01
HLR8	8.9e-01	8.2e-01	9.6e-01	9.6e-01
HLR16	8.9e-01	8.2e-01	9.6e-01	9.6e-01
HLR32	8.9e-01	8.2e-01	9.6e-01	9.6e-01

Mesh	$\mathfrak{ar}$	$\max_{c\in C} \#V_c$	$\max_{c\in C} \#E_c$	$\max_{c\in C} \#F_c$
HLR2	5.0e-01	13	20	9
HLR4	5.0e-01	13	20	9
HLR8	5.0e-01	13	20	9
HLR16	5.0e-01	13	20	9
HLR32	5.0e-01	13	20	9

Figure A.2 – Left: Successive refinement of the HLR mesh sequence. Right: Tables collecting the cardinality of primal sets, mesh quality criteria, and the regularity of the barycentric subdivision for the meshes of the HLR mesh sequence.

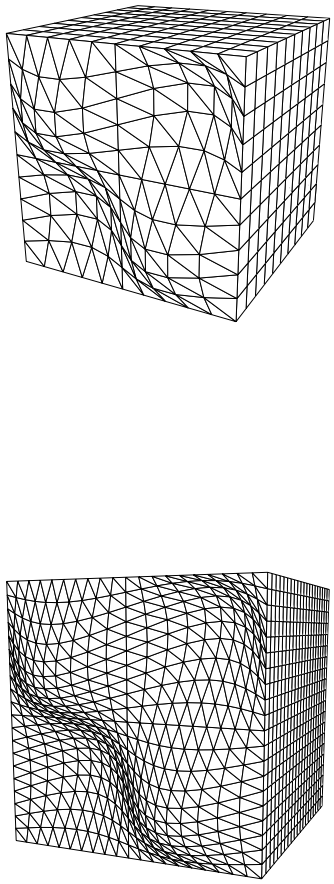

Mesh	#V	#E	#F	#C
PrT10	1331	4730	5400	2000
PrT20	9261	34860	41600	16000
PrT30	29791	114390	138600	54000
PrT40	68921	267320	326400	128000

Mesh	$\eta_{\perp}^{\mathrm{E}}$	$\eta_{\perp}^{\mathrm{F}}$	$\eta_{\mathrm{vol}}^{\mathrm{E}}$	$\eta_{\mathrm{vol}}^{\mathrm{F}}$
PrT10	2.5e-01	2.5e-01	4.5e-01	4.5e-01
PrT20	3.1e-01	3.1e-01	5.2e-01	5.2e-01
PrT30	3.1e-01	3.1e-01	5.2e-01	5.2e-01
PrT40	3.1e-01	3.1e-01	5.3e-01	5.3e-01

Mesh	$\mathfrak{at}$	$\max_{c\in C} \#V_c$	$\max_{c\in C} \#E_c$	$\max_{c\in C} \#F_c$
PrT10	1.0e-01	6	9	5
PrT20	1.3e-01	6	9	5
PrT30	1.4e-01	6	9	5
PrT40	1.5e-01	6	9	5

Figure A.3 – Left: Successive refinement of the PrT mesh sequence. Right: Tables collecting the cardinality of primal sets, mesh quality criteria, and the regularity of the barycentric subdivision for the meshes of the PrT mesh sequence.

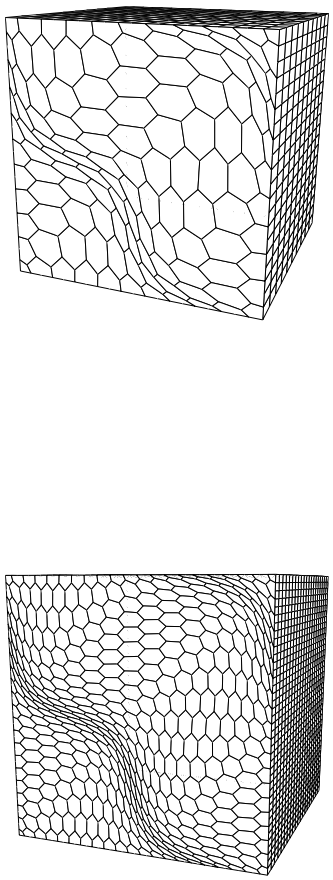

Mesh	#V	#E	#F	#C
PrG10	3080	7200	5331	1210
PrG20	20160	48600	37261	8820
PrG30	63240	154200	119791	28830
PrG40	144320	354000	276921	67240

Mesh	$\eta_{\perp}^{\mathrm{E}}$	$\eta_{\perp}^{\mathrm{F}}$	$\eta_{\mathrm{vol}}^{\mathrm{E}}$	$\eta_{\mathrm{vol}}^{\mathrm{F}}$
PrG10	2.1e-01	2.1e-01	5.9e-01	5.9e-01
PrG20	1.9e-01	1.9e-01	5.3e-01	5.3e-01
PrG30	1.8e-01	1.8e-01	5.2e-01	5.2e-01
PrG40	1.8e-01	1.8e-01	5.2e-01	5.2e-01

Mesh	$\mathfrak{ar}$	$\max_{c\in C} \#\mathrm{V_c}$	$\max_{c\in C} \#\mathrm{E_c}$	$\max_{c\in C} \#\mathrm{F_c}$
PrG10	1.8e-01	12	18	8
PrG20	1.5e-01	12	18	8
PrG30	1.5e-01	12	18	8
PrG40	1.5e-01	12	18	8

Figure A.4 – Left: Successive refinement of the PrG mesh sequence. Right: Tables collecting the cardinality of primal sets, mesh quality criteria, and the regularity of the barycentric subdivision for the meshes of the PrG mesh sequence.

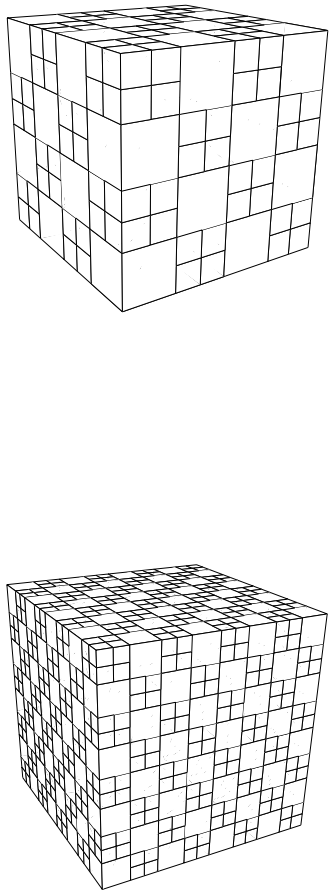

Mesh	#V	#E	#F	#C
CB2	97	216	156	36
CB4	625	1536	1200	288
CB8	4417	11520	9408	2304
CB16	33025	89088	74496	18432
CB32	254977	700416	592896	147456

Mesh	$\eta_{\perp}^{\mathrm{E}}$	$\eta_{\perp}^{\mathrm{F}}$	$\eta_{\mathrm{vol}}^{\mathrm{E}}$	$\eta_{\mathrm{vol}}^{\mathrm{F}}$
CB2	8.9e-01	8.2e-01	9.2e-01	9.0e-01
CB4	8.9e-01	8.2e-01	9.1e-01	8.2e-01
CB8	8.9e-01	8.2e-01	9.1e-01	8.2e-01
CB16	8.9e-01	8.2e-01	9.1e-01	8.2e-01
CB32	8.9e-01	8.2e-01	9.1e-01	8.2e-01

Mesh	$\mathfrak{ar}$	$\max_{c\in C} \#V_c$	$\max_{c\in C} \#E_c$	$\max_{c\in C} \#F_c$
CB2	5.0e-01	20	33	15
CB4	5.0e-01	26	48	24
CB8	5.0e-01	26	48	24
CB16	5.0e-01	26	48	24
CB32	5.0e-01	26	48	24

Figure A.5 – Left: Successive refinement of the CB mesh sequence. Right: Tables collecting the cardinality of primal sets, mesh quality criteria, and the regularity of the barycentric subdivision for the meshes of the CB mesh sequence.

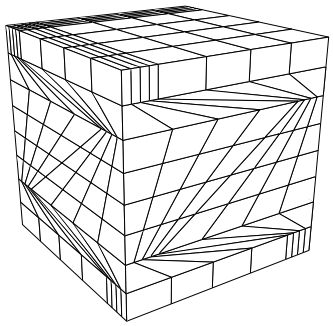

Mesh	#V	#E	#F	#C
K8	729	1944	1728	512
K16	4913	13872	13056	4096
K32	35937	104544	101376	32768
K64	274625	811200	798720	262144

Mesh	$\eta_{\perp}^{\mathrm{E}}$	$\eta_{\perp}^{\mathrm{F}}$	$\eta_{\mathrm{vol}}^{\mathrm{E}}$	$\eta_{\mathrm{vol}}^{\mathrm{F}}$
K8	6.1e-02	1.0e-01	1.4e-01	1.2e-01
K16	4.6e-02	7.3e-02	1.3e-01	1.2e-01
K32	3.9e-02	6.8e-02	1.2e-01	1.1e-01
K64	4.2e-02	7.8e-02	1.3e-01	1.1e-01

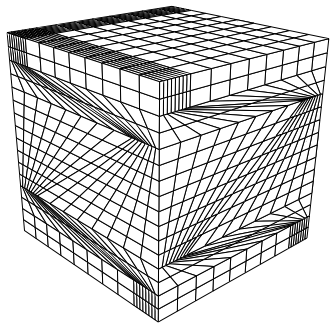

Mesh	$\mathfrak{ar}$	$\max_{c\in C} \#\mathrm{V_c}$	$\max_{c\in C} \#\mathrm{E_c}$	$\max_{c\in C} \#\mathrm{F_c}$
K8	5.0e-02	8	12	6
K16	4.3e-02	8	12	6
K32	3.6e-02	8	12	6
K64	2.1e-02	8	12	6

Figure A.6 – Left: Successive refinement of the Ker mesh sequence. Right: Tables collecting the cardinality of primal sets, mesh quality criteria and the regularity of the barycentric subdivision for the meshes of the Ker mesh sequence.

Appendix B

Additional numerical results

B.1 Elliptic problem

In this section, we collect results on mixed cell-based schemes related to the FVCA problem introduced in Section 8.4.3. Results plotted in Figures B.1, B.2, and B.3 show that mixed cell-based schemes built using the `DGA` reconstruction are more accurate and that their cost-effectiveness is better than cell-based schemes built using the `SUSHI`-like reconstruction. Labels used in the following figures are that of Table 8.7.

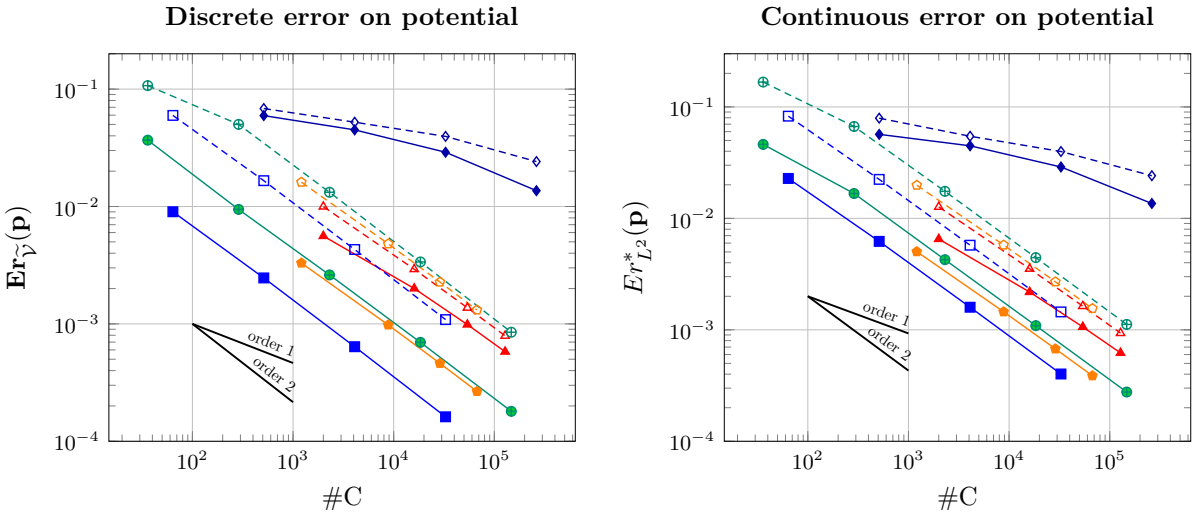

Figure B.1 – Discrete (left) and continuous (right) error on the potential for mixed cell-based schemes: `Cb-DGA` with labels A and `Cb-SUSHI` with labels B.

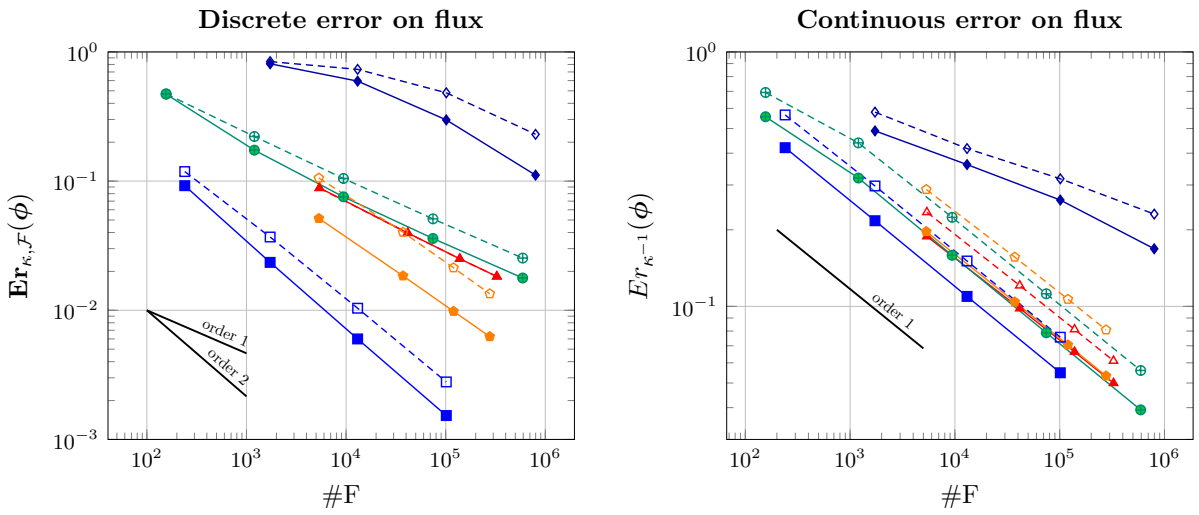

Figure B.2 – Discrete (left) and continuous (right) error on the flux for mixed cell-based scheme: `Cb-DGA` with labels A and `Cb-SUSHI` with labels B.

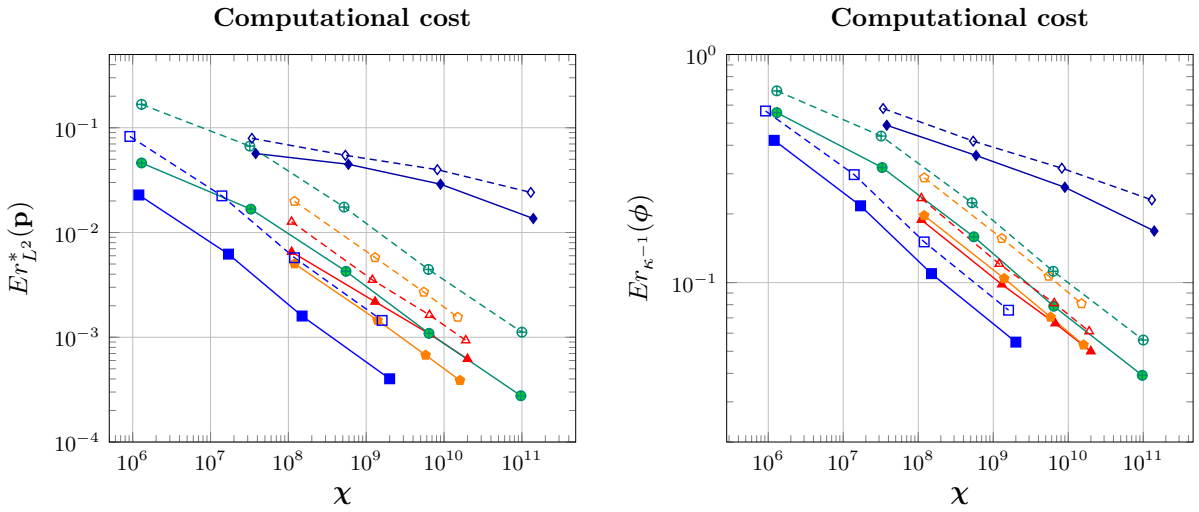

Figure B.3 – Comparison of the cost-effectiveness between `Cb-DGA` (labels A) and `Cb-SUSHI` (labels B) schemes for the continuous error on the potential (left) and the error on the flux in continuous energy norm (right).

B.2 Stokes problem

In this section, we detail the results obtained on the vortex test case (cf. Section 9.3.2) with essential BCs for vertex-based pressure schemes built using either the DGA reconstruction operators or the SUSHI-like reconstruction operators. For each tested scheme, we consider the primal and dual discretization of the external load. Labels are that of Table 9.3. Conclusions drawn from Figures B.4 (resp. B.5) are similar to those with natural BCs. The main observation is that essential BCs lead to more accurate results than natural BCs.

B.2.1 Vertex-based pressure scheme with DGA reconstruction operators

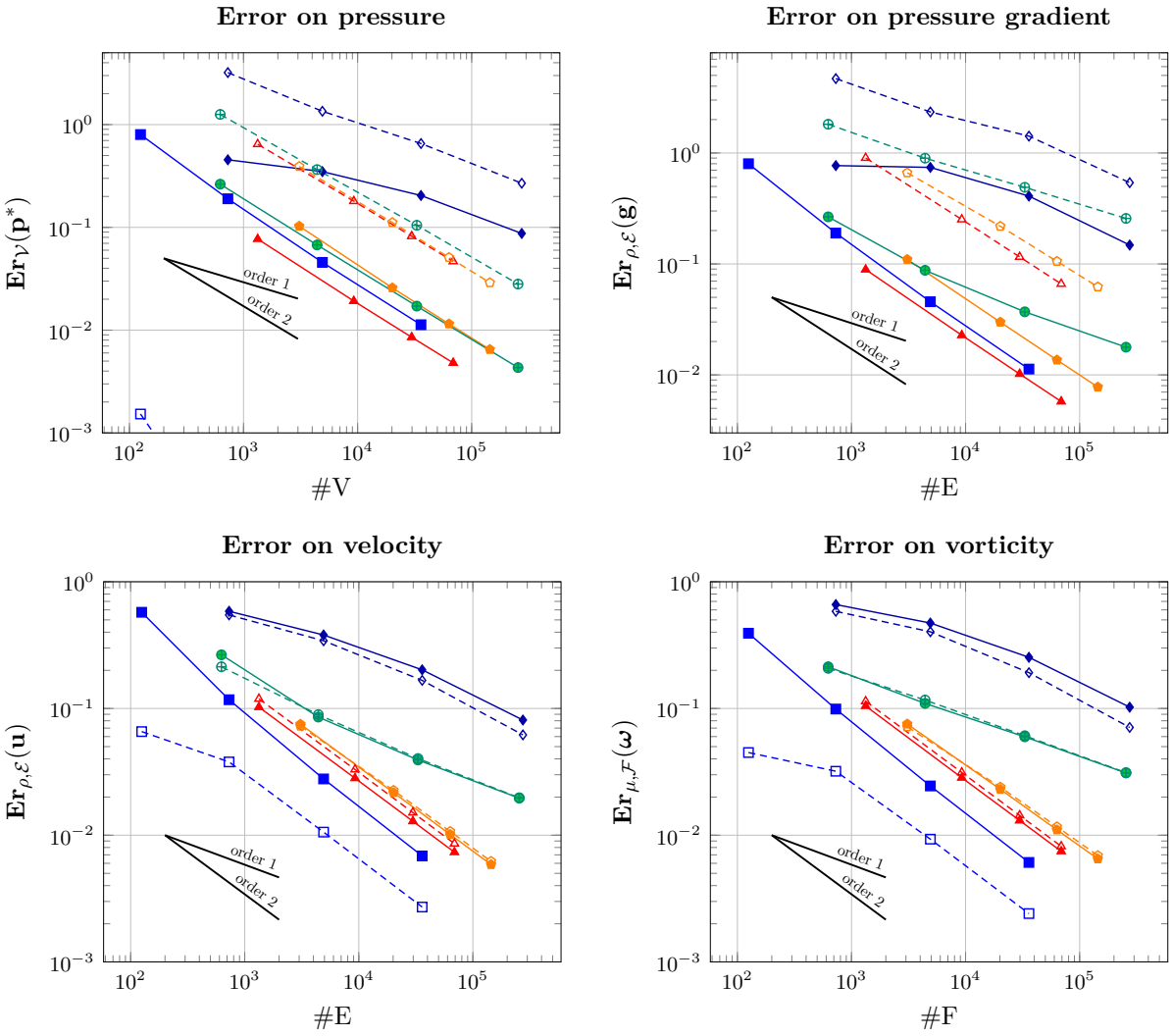

Figure B.4 – Discrete error on the pressure (upper left), on the pressure gradient (upper right), on the velocity (lower left), and on the vorticity (lower right) for the vertex-based pressure scheme using the DGA reconstruction operators. Essential BCs are considered: EDL with labels A and EPL with labels B.

B.2.2 Vertex-based pressure scheme with SUSHI reconstruction operators

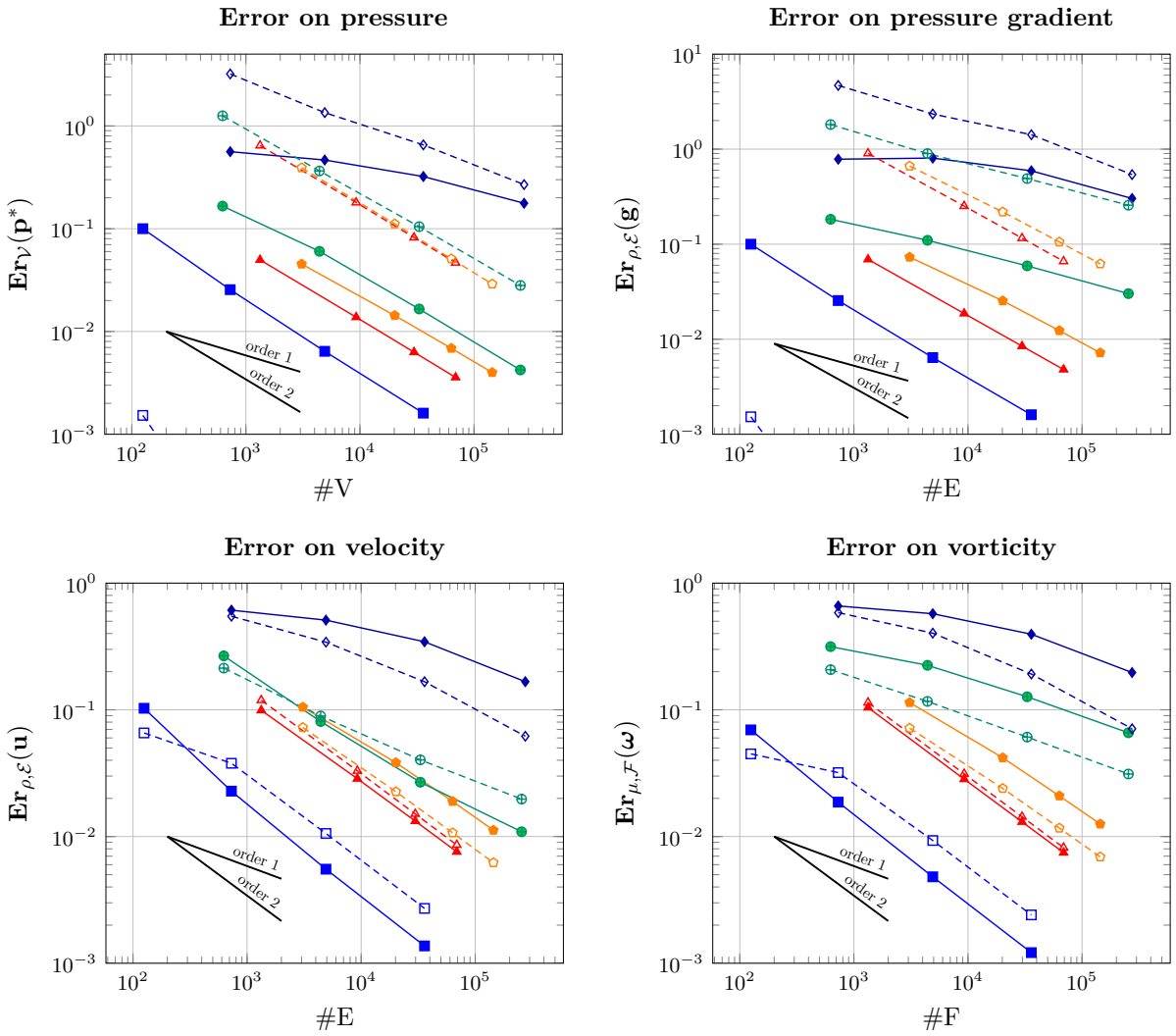

Figure B.5 – Discrete error on the pressure (upper left), on the pressure gradient (upper right), on the velocity (lower left), and on the vorticity (lower right) for the vertex-based pressure scheme using the SUSHI-like reconstruction operators. Essential BCs are considered: EDL with labels A and EPL with labels B.

List of symbols

Abbreviations

ALU	Augmented Lagrangian Uzawa
BC(s)	Boundary Condition(s)
CDO	Compatible Discrete Operator
CG	Conjugate gradient
DDFV	Discrete Duality Finite Volume
DEC	Discrete Exterior Calculus
DGA	Discrete Geometric Approach
DoF(s)	Degree(s) of freedom
FD	Finite Differences
FE	Finite Elements
FEEC	Finite Element Exterior Calculus
FES	Finite Element System
FIT	Finite Integration Technique
FV	Finite Volumes
HFV	Hybrid Finite Volume
HHO	Hybrid High Order
HMM	Hybrid Mixed Mimetic
MFD	Mimetic Finite Difference
MFV	Mixed Finite Volume
MHO	Mixed High Order
MPFA	Multi-Point Flux Approximation
MSE	Mimetic Spectral Element
PDEs	Partial Differential Equations
SPD	Symmetric Definite Positive
SSOR	Symmetric Successive OverRelaxation
TPFA	Two-Point Flux Approximation
VEM	Virtual Element Method

Operators

$\mathtt{A}_{\mathcal{X}}$	approximation operator for the DoFs space denoted by $\mathcal{X}$
$\mathtt{C}_{\mathcal{X}}$	consistent part of a reconstruction operator from $\mathcal{X}$
$\mathsf{H}_{\alpha}^{x\tilde{y}}$	discrete Hodge operator from $\mathcal{X}$ to $\widetilde{\mathcal{Y}}$ related to the material property α
$\mathsf{T}_{\mathrm{X,c}}$	projection operator from global to local DoFs spaces which are isomorphic to $\mathbb{R}^{\#\mathrm{X}}$ (global) and $\mathbb{R}^{\#\mathrm{X_c}}$ (local)
$\mathtt{L}_{\mathcal{X}}$	lifting or reconstruction operator from $\mathcal{X}$
$\mathsf{R}_{\mathcal{X}}$	reduction operator or de Rham's map on $\mathcal{X}$ DoF space
$\mathtt{S}_{\mathcal{X}}$	stabilization part of a reconstruction operator from $\mathcal{X}$
$\mathsf{GRAD}/\widetilde{\mathsf{GRAD}}$	discrete gradient operator on primal/dual mesh
$\mathsf{CURL}/\widetilde{\mathsf{CURL}}$	discrete curl operator on primal/dual mesh
$\mathsf{DIV}/\widetilde{\mathsf{DIV}}$	discrete divergence operator on primal/dual mesh

Sets and spaces

$\mathrm{v}/\tilde{\mathrm{v}}$	primal/dual vertex
$\mathrm{e}/\tilde{\mathrm{e}}$	primal/dual edge
$\mathrm{f}/\tilde{\mathrm{f}}$	primal/dual face
$\mathrm{c}/\tilde{\mathrm{c}}$	primal/dual cell
$\mathrm{x}/\tilde{\mathrm{y}}$	generic primal/dual entities. $\mathrm{x} \in \{\mathrm{v},\mathrm{e},\mathrm{f},\mathrm{c}\}$ and $\tilde{\mathrm{y}} \in \{\tilde{\mathrm{v}},\tilde{\mathrm{e}},\tilde{\mathrm{f}},\tilde{\mathrm{c}}\}$
$\mathrm{V}/\widetilde{\mathrm{V}}$	set of primal/dual vertices
$\mathrm{E}/\widetilde{\mathrm{E}}$	set of primal/dual edges
$\mathrm{F}/\widetilde{\mathrm{F}}$	set of primal/dual faces
$\mathrm{C}/\widetilde{\mathrm{C}}$	set of primal/dual cells
$\mathrm{X}/\widetilde{\mathrm{Y}}$	generic set of primal/dual entities. $\mathrm{X} \in \{\mathrm{V},\mathrm{E},\mathrm{F},\mathrm{C}\}$ and $\widetilde{\mathrm{Y}} \in \{\widetilde{\mathrm{V}},\widetilde{\mathrm{E}},\widetilde{\mathrm{F}},\widetilde{\mathrm{C}}\}$
$\mathcal{V}/\widetilde{\mathcal{V}}$	space of DoF related to primal/dual vertices
$\mathcal{E}/\widetilde{\mathcal{E}}$	space of DoF related to primal/dual edges
$\mathcal{F}/\widetilde{\mathcal{F}}$	space of DoF related to primal/dual faces
$\mathcal{C}/\widetilde{\mathcal{C}}$	space of DoF related to primal/dual cells
$\mathcal{X}/\widetilde{\mathcal{Y}}$	generic space of DoF related to primal/dual entities. $\mathcal{X} \in \{\mathcal{V},\mathcal{E},\mathcal{F},\mathcal{C}\}$ and $\widetilde{\mathcal{Y}} \in \{\widetilde{\mathcal{V}},\widetilde{\mathcal{E}},\widetilde{\mathcal{F}},\widetilde{\mathcal{C}}\}$
$\mathbb{P}_k(\mathrm{X})$	vector space of piecewise polynomials in $\underline{x} := (x_0,\ldots,x_d)$ of degree at most k; the decomposition of Ω on which the space is broken is related to entity space X
$H^s(\Omega)$	(Hilbert) space of functions whose derivatives up to order s are in $L^2(\Omega)$, *i.e.* $W^{s,2}(\Omega)$

$L^p(\Omega)$	(Lebesgue) space of functions whose p-th power is Lebesgue integrable on Ω
$W^{s,p}(\Omega)$	(Sobolev) space of functions whose derivatives up to order s are in $L^p(\Omega)$

Parameters and coefficients

d	space dimension
α	generic material property
κ	conductivity
μ	viscosity
ρ	mass density

Bibliography

Abboud, H., Chami, F. E. & Sayah, T. (2012) A priori and a posteriori estimates for three-dimensional Stokes equations with nonstandard boundary conditions. *Numer. Methods Partial Differential Equations*, **28**, 1178–1193.

Abraham, R., Marsden, J. & Ratiu, T. (1988) *Manifolds, tensor analysis, and applications*, vol. 75. Springer.

Amrouche, C., Bernardi, C., Dauge, M. & Girault, V. (1998) Vector potentials in three-dimensional non-smooth domains. *Math. Meth. Appl. Sci.*, **21**, 823–864.

Andreianov, B., Bendahmane, M., Hubert, F. & Krell, S. (2012) On 3D DDFV discretization of gradient and divergence operators. I. meshing, operators and discrete duality. *IMA Journal of Numerical Analysis*, **32**, 1574–1603.

Andreianov, B., Bendahmane, M. & Hubert, F. (2013) On3D DDFV discretization of gradient and divergence operators. II. Discrete functional analysis tools and applications to degenerate parabolic problems. *CMAM Comput. Meth. Appli. Math.*, **13**, 369–410.

Archambeau, F., Mechitoua, N. & Sakiz, M. (2004) Code_saturne: A Finite Volume code for the computation of turbulent incompressible flows - industrial applications. *IJFV*, **1**.

Arnold, D. N., Falk, R. S. & Winther, R. (2006) Finite Element Exterior Calculus, homological techniques, and applications. *Acta Numerica*, **15**, 1–155.

Arnold, D. N., Falk, R. S. & Winther, R. (2010) Finite Element Exterior Calculus: from Hodge Theory to Numerical Stability. *Bull. Amer. Math. Soc.*, **47**, 281–354. DOI: 10.1090/S0273-0979-10-01278-4.

Arnold, D. N. & Brezzi, F. (1985) Mixed and Nonconforming Finite Element methods: Implementation, postprocessing and error estimates. *M2AN Math. Model. Numer. Anal.*, **19**, 7–32.

Auchmann, B. & Kurz, S. (2006) A geometrical defined discrete Hodge operator on simplicial cells. *IEEE Transactions on Magnetics*, **42**, 643.

Back, A. & Sonnendrücker, E. (2013) Spline Discrete Differential Forms and New Finite Difference Discrete Hodge Operator. Unpublished.

Beirão da Veiga, L., Gyrya, V., Lipnikov, K. & Manzini, G. (2009) Mimetic Finite Difference Method for the Stokes Problem on Polygonal Meshes. *Journal of Computational Physics*, **228**, 7215–7232.

Beirão da Veiga, L., Lipnikov, K. & Manzini, G. (2010) Error analysis for mimetic discretization of the steady Stokes problem on polyhedral meshes. *SIAM J. Numer. Anal*, **48**, 1419–1443.

Beirão da Veiga, L., Lipnikov, K. & Manzini, G. (2011) Arbitrary-order nodal mimetic discretizations of elliptic problems on polygonal meshes. *SIAM Journal on Numerical Analysis*, **49**, 1737–1760.

Beirão da Veiga, L., Lipnikov, K. & Manzini, G. (2014) *The Mimetic Finite Difference method for Elliptic Problems*. Modeling, Simulation & Applications, vol. 11. Springer.

Beirão da Veiga, L., Brezzi, F., Cangiani, A., Manzini, G., Marini, L. D. & Russo, A. (2013) Basic principles of Virtual Element Methods. *Math. Models Methods Appl. Sci.*, **23**, 199–214.

Beirão da Veiga, L. & Lipnikov, K. (2010) A mimetic discretization of the Stokes problem with selected edge bubbles. *SIAM J. Sci. Comput.*, **32**, 875–893.

Bernardi, C. & Chorfi, N. (2006) Spectral discretization of the vorticity, velocity, and pressure formulation of the Stokes problem. *SIAM J. Numer. Anal*, **44**, 826–850.

Bessemoulin-Chatard, M., Chainais-Hillairet, C. & Filbet, F. (2014) On discrete functional inequalities for some Finite Volume schemes. HAL-00672591.

Bochev, P. & Hyman, J. M. (2005) Principles of mimetic discretizations of differential operators. *Compatible Spatial Discretization* (D. Arnold, P. Bochev, R. Lehoucq, R. A. Nicolaides & M. Shashkov eds). The IMA Volumes in mathematics and its applications, vol. 142. Springer, pp. 89–120.

Bossavit, A. (1988) Whitney forms: a class of Finite Elements for three-dimensional ccomputation in electromagnetism. *IEE Proceedings A*, **135**, 493–500.

Bossavit, A. (1998) On the geometry of electromagnetism. *J. Japan Soc. Appl. Electromagn. & Mech.*, **6**, 17–28 (no 1), 114–23 (no 2), 233–40 (no 3), 318–26 (no 4).

Bossavit, A. (1999-2000) Computational electromagnetism and geometry. *J. Japan Soc. Appl. Electromagn. & Mech.*, **7-8**, 150–9 (no 1), 294–301 (no 2), 401–8 (no 3), 102–9 (no 4), 203–9 (no 5), 372–7 (no 6).

Bossavit, A. (2001) Generalized Finite Differences in computational electromagnetics. *Progress In Electromagnetics Research*, **32**, 45–64.

Bossavit, A. (2002) Generating Whitney forms of polynomial degree one and higher. *IEEE Transactions on Magnetics*, **38**, 341–344.

Bramble, J. H. & Lee, P. (1994) On Variational Formulations for the Stokes Equations with Non-Standard Boundary Conditions. *M2AN Math. Model. Numer. Anal.*, **28**, 903–919.

Branin, F. (1966) The Algebraic-Topological Basis for Network Analogies and the Vector Calculus. In Symposium on generalized networks (12–14 April 1966).

Brezzi, F., Lipnikov, K. & Shashkov, M. (2005) Convergence of the Mimetic Finite Difference method for diffusion problems on polyhedral meshes. *SIAM J. Numer. Anal*, **43**, 1872–1896.

Brezzi, F., Buffa, A. & Lipnikov, K. (2009) Mimetic Finite Difference for elliptic problem. *Mathematical Modelling and Numerical Analysis*, **43**, 277–295.

Brezzi, F., Buffa, A. & Manzini, G. (2014) Mimetic scalar products of discrete differential forms. *J. Comput. Phys.*, **257**, 1228–1259.

Brezzi, F. & Fortin, M. (1991) *Mixed and Hydbrid Finite Element Methods*. Springer series in computational mathematics. Springer-Verlag.

Buffa, A., Rivas, J., Sangalli, G. & Vásquez, R. (2011) Isogeometric Discrete Differential Forms in Three Dimensions. *SIAM J. Numer. Anal*, **49**, 818–844.

Buffa, A. & Christiansen, S. (2007) A dual finite element complex on the barycentric refinement. *Mathematics of Computation*, **76**, 1743–1769.

Chénier, E., Eymard, R., Gallouët, T. & Herbin, R. (2014) An extension of the MAC scheme to locally refined meshes : convergence analysis for full tensor time-dependent navier–stokes equations. *Calcolo*. HAL-00751556.

Christiansen, S. H. (2008) A construction of spaces of compatible differential forms on cellular complexes. *Math. Models Methods Appl. Sci.*, **18**, 739–757.

Christiansen, S. H., Munthe-Kaas, H. Z. & Owren, B. (2011) Topics in structure-preserving discretization. *Acta Numer.*, **20**, 1–119.

Christiansen, S. & Rapetti, F. (2014) On high order Finite Element spaces of differential forms. Arxiv:1306.4835.

Ciarlet, P. (1978) *The Finite Element Method for Elliptic Problems*. North-Holland.

Clemens, M. & Weiland, T. (2001) Discrete Electromagnetism with the Finite Integration Technique. *Progress In Electromagnetics Research*, **32**, 65–87.

Codecasa, L., Specogna, R. & Trevisan, F. (2010) A new set of basis functions for the Discrete Geometric Approach. *Journal of Computational Physics*, **229**, 7401–7410.

Codecasa, L. & Trevisan, F. (2007) Constitutive equations for discrete electromagnetic problems over polyhedral grids. *Journal of Computational Physics*, **225**, 1894–1918.

Codecasa, L. & Trevisan, F. (2010a) Convergence of electromagnetic problems modelled by Discrete Geometric Approach. *CMES*, **58**, pp. 15–44.

Codecasa, L. & Trevisan, F. (2010b) Error bounds for Discrete Geometric Approach. *CMES Comput. Model. Eng. Sci.*, **59**, 155–179.

Dardalhon, F. (2012) Schémas numériques pour la simulation des grandes échelles. *Ph.D. thesis*, Université d'Aix-Marseille.

Delcourte, S. & Omnes, P. (2014) A Discrete Duality Finite Volume discretization of the vorticity-velocity-pressure formulation of the 2D Stokes problem on almost arbitrary two-dimensional grids. *Numer. Methods Partial Differential Eq.* 10.1002/num.21890.

Desbrun, M., Hirani, A. N., Leok, M. & Marsden, J. E. (2005) Discrete Exterior Calculus. http://arxiv.org/abs/math/0508341.

Desbrun, M., Kanso, E. & Tong, Y. (2006) Discrete Differential Forms for Computational Modeling. Discrete Differential Forms for Computational Modeling, pp. 287–324.

Di Pietro, D. A. (2012) Cell centered Galerkin methods for diffusive problems. *M2AN Math. Model. Numer. Anal.*, **46**, 111–144.

Di Pietro, D. A., Ern, A. & Lemaire, S. (2014) An arbitrary-order and compact-stencil discretization of diffusion on general meshes based on local reconstruction operators. *Computational Methods in Applied Mathematics*, **14**, 461–472.

Di Pietro, D. A. & Ern, A. (2012) *Mathematical Aspects of Discontinuous Galerkin Methods*. SMAI Mathématiques et Applications, vol. 69. Springer.

Di Pietro, D. A. & Ern, A. (2013) A Family of Arbitrary-order Mixed Methods for Heterogeneous Anisotropic Diffusion on General Meshes. http://hal.archives-ouvertes.fr/hal-00918482.

Di Pietro, D. A. & Ern, A. (2015) Hybrid High-Order methods for variable-diffusion problems on general meshes. *C. R. Math. Acad. Sci. Paris*, **353**, 31–34.

Di Pietro, D. A. & Lemaire, S. (2015) An extension of the Crouzeix-Raviart space to general meshes with application to quasi-incompressible linear elasticity and Stokes flow. *Math. Comp.*, **84**, 1–31.

Dlotko, P. & Specogna, R. (2013) A novel technique for cohomology computations in engineering practice. *Comput. Methods Appl. Mech. Engrg.*, **253**, 530–542.

Dodziuk, J. (1976) Finite-difference approach to the Hodge theory of harmonic forms. *Amer. J. Math.*, **98**, 79–104.

Droniou, J., Eymard, R., Gallouët, T. & Herbin, R. (2010) A Unified Approach to Mimetic Finite Difference, Hybrid Finite Volume and Mixed Finite Volume Methods. *Mathematical Models and Methods in Applied Sciences*, **20**, 265–295.

Droniou, J., Eymard, R., Gallouët, T. & Herbin, R. (2013) Gradient Schemes: a generic framework for the discretisation of linear, nonlinear and nonlocal elliptic and parabolic equations. *Mathematical Models and Methods in Applied Sciences*, **23**, 2395–2432.

Droniou, J. (2014) Finite Volume schemes for diffusion equations: Introduction to and review of modern methods. *MMathematical Models and Methods in Applied Sciences (M3AS)*, **24**, 1575–1619.

Droniou, J. & Eymard, R. (2006) A mixed finite volume scheme for anisotropic diffusion problems on any grid. *Numer. Math.*, **105**, 35–71.

Droniou, J. & Eymard, R. (2009) Study of the mixed finite volume method for Stokes and Navier-Stokes equations. *Num. Meth. for Part*, **25**, 137–171.

Droniou, J. & Le Potier, C. (2011) Construction and convergence study of schemes preserving the elliptic local maximum principle. *SIAM J. Numer. Anal.*, **49**, 459–490.

Dubois, F. (1992) Une formulation tourbillon-vitesse-presion pour le problème de Stokes. *Comptes Rendus de l'Académie des Sciences*, **314**, 277–280.

Dubois, F. (2002) Vorticity-velocity-pressure formulation for the Stokes problem. *Mathematical Methods in the Applied Sciences*, **25**, 1091–1119.

Ern, A. & Guermond, J.-L. (2004) *Theory and Pratice of Finite Elements*. Applied Mathematical Sciences, vol. 159. Springer.

Ern, A. & Vohralík, M. (2013) Adaptative inexact Newton methods with a posteriori stopping criteria for nonlinear diffusion PDEs. *SIAM J. Sci. Comput.*, **35**, 1761–1791.

Euler, T. (2007) Consistent discretization of maxwell's equations on polyhedral grids. *Ph.D. thesis*, Technischen Universität Darmstadt.

Eymard, R., Gallouët, T. & Herbin, R. (2000) Finite Volume methods. *Handbook of numerical analysis, Vol. VII*. Handb. Numer. Anal., VII. Amsterdam: North-Holland, pp. 713–1020.

Eymard, R., Gallouët, T. & Herbin, R. (2010) Discretization of heterogeneous and anisotropic diffusion problems on general nonconforming meshes SUSHI: a scheme using stabilization and hybrid interfaces. *IMA Journal of Numerical Analysis*, **30**, 1009–1043.

Eymard, R., Henry, G., Herbin, R., Hubert, F., Klöfkorn, R. & Manzini, G. (2011) 3D benchmark on discretization schemes for anisotropic diffusion problems on general grids. *Finite Volumes for Complex Applications VI - Problems & Perspectives*, vol. 2. Springer, pp. 95–130.

Eymard, R., Guichard, C. & Herbin, R. (2012) Small stencil 3D schemes for diffusive flows in porious media. *ESAIM: Mathematical Modelling and Numerical Analysis*, **46**, 265–290.

Eymard, R., Fuhrmann, J. & Linke, A. (2014) On MAC schemes on triangular Delaunay meshes, their convergence and applications to coupled flow problem. *Numer. Methods Partial Differential Eq.*, **30**, 1397–1424.

Falk, R. & Neilan, M. (2013) Stokes Complexes and the Construction of Stable Finite Elements with Pointwise Mass Conservation. *SIAM J. Numer. Anal*, **51**, 1308–1326.

Floater, M., Kós, G. & Reimers, M. (2005) Mean value coordinates in 3d. *Computer Aided Geometric Design*, **22**, 623–631.

Fortin, M. & Glowinski, M. (1983) *Augmented Lagrangian Methods: Applications to the numerical solution of boundary-value problems*. Elsevier.

Fournier, Y., Bonelle, J., Moulinec, C., Shang, Z., Sunderland, A. G. & Uribe, J. C. (2011) Optimizing Code_Saturne computations on Petascale systems. *Computers & Fluids*, **45**, 103–108.

Frankel, T. (1997) *The Geometry of Physics: an Introduction*, first edition edn. Cambridge University Press.

Gerritsma, M. (2011) Edge functions for spectral element methods. *Spectral and High Order Methods for Partial Differential Equations* (J. S. Hesthaven, E. M. Rønquist, T. J. Barth, M. Griebel, D. E. Keyes, R. M. Nieminen, D. Roose & T. Schlick eds). Lecture Notes in Computational Science and Engineering, vol. 76. Springer Berlin Heidelberg, pp. 199–207.

Gerritsma, M. (2012) An introduction to a compatible spectral discretization method. *Mechanics of Advanced Materials and Structures*, **19**, 48–67.

Gillette, A., Rand, A. & Bajaj, C. (2012) Error estimates for generalized barycentric interpolation. *Adv. Comput. Math.*, **37**, 417–439.

Gillette, A. & Bajaj, C. (2011) Dual formulations of mixed finite element methods with applications. *Computer-Aided Design*, **43**, 1213 – 1221.

Harlow, F. & Welch, J. (1965) Numerical calculations of time dependent viscous incompressible flow of fluid with a free surface. *Physics of Fluids*, **8**, 2182–2189.

Hatcher, A. (2002) *Algebraic Topology*. Cambridge University Press.

He, B. (2006) Compatible Discretizations for Maxwell Equations. *Ph.D. thesis*, The Ohio State University.

He, B. & Teixeira, F. (2006) Geometric finite element discretization of maxwell equations in primal and dual spaces. *Phys. Lett. A*, **346**, 1–14.

Hermeline, F. (2000) A Finite Volume method for the approximation of diffusion operators on distorted meshes. *J. Comput. Phys.*, **160**, 481–490.

Hiemstra, R., Toshniwal, D., Huijsman, R. & Gerritsma, M. (2013) High Order Geometric Methods with Exact Conservation Properties. *J. Comput. Phys.*, **257**, 1444–1471.

Hiptmair, R. (1999) Canonical construction of Finite Elements. *Math. Comp.*, **68**, 1325–1346.

Hiptmair, R. (2001a) Discrete Hodge operators: An algebraic perspective. *Progress In Electromagnetics Research*, **32**, 247–269.

Hiptmair, R. (2001b) High Order Whitney Forms. *Progress In Electromagnetics Research (PIER)*, **32**, 271–299.

Hormann, K. & Sukumar, N. (2008) Maximum entropy coordinates for arbitrary polytopes. *Proceedings of the Symposium on Geometry Processing*. Eurographics Association, pp. 1513–1520.

Hu, X. & Nicolaides, R. A. (1992) Covolume techniques for anisotropic media. *Numer. Math.*, **61**, 215–234.

Hyman, J. M. & Shashkov, M. (1997) Natural discretizations for the divergence, gradient, and curl on logically rectangular grids. *Computers & Mathematics with Applications*, **33**, 81–104.

Kreeft, J., Palha, A. & Gerritsma, M. (2011) Mimetic framework on curvilinear quadrilaterals of arbitrary order. arXiv:1111.4304v1.

Kreeft, J. & Gerritsma, M. (2013) Mixed mimetic spectral element method for Stokes flow: A pointwise divergence-free solution. *Journal of Computational Physics*, **240**, 284–309.

Krell, S. & Manzini, G. (2012) The Discrete Duality Finite Volume method for Stokes equations on three-dimensional polyhedral meshes. *SIAM Journal on Numerical Analysis*, **50**, 808–837.

Kron, G. (1945) Numerical solution of ordinary and partial differential equations by means of equivalent circuits. *Journal of Applied Physics*, **16**, 172–186.

Kron, G. (1953) A Set of Principles to Interconnect the Solutions of Physical Systems. *J. Appl. Phys.*, **24**, 965.

Linke, A. (2014) On the role of the Helmholtz decomposition in mixed methods for incompressible flows and a new variational crime. *Comput. Methods Appl. Mech. Engrg.*, **268**, 782–800.

Lipnikov, K., Manzini, G. & Svyatskiy, D. (2011) Analysis of the monotonicity conditions in the mimetic finite difference method for elliptic problems. *Journal of Computational Physics*, **230**, 2620–2642.

Lipnikov, K., Manzini, G. & Shashkov, M. (2014) Mimetic finite difference method. *Journal of Computational Physics*, **257**, 1163–1227.

Lipnikov, K. & Manzini, G. (2014) A high-order mimetic method on unstructured polyhedral meshes for the diffusion equation. *J. Comput. Phys.*, **272**, 360–385.

Mattiussi, C. (1997) An Analysis of Finite Volume, Finite Element, and Finite Difference Methods Using Some Concepts from Algebraic Topology. *J. Comput. Phys.*, **133**, 289–309.

Mullen, P., Memari, P., de Goes, F. & Desbrun, M. (2011) HOT: Hodge Optimized Triangulations. *ACM Transactions on Graphics*, **30**.

Munkres, J. (1984) *Elements of Algebraic Topology*. Addison-Wesley.

Nédélec, J. C. (1982) Élements Finis Mixtes Incompressibles pour l'Équation de Stokes dans $\mathbb{R}^3$. *Numer. Math.*, **39**, 97–112.

Nicolaides, R. A. & Trapp, K. A. (2006) Covolume discretization of differential forms. *Compatible Spatial Discretizations* (D. Arnold, P. Bochev, R. Lehoucq, R. Nicolaides & M. Shashkov eds). The IMA Volumes in Mathematics and its Applications, vol. 142. Springer.

Perot, J. B., Vidovic, D. & Wesseling, P. (2006) *Compatible Spatial Discretizations*, vol. 142. Springer, chapter Mimetic reconstruction of vectors, pp. 173–188.

Perot, J. B. & Nallapati, R. (2003) A moving unstructured staggered mesh method for the simulation of incompressible free-surface flows. *Journal of Computational Physics*, **184**, 192–214.

Perot, J. B. & Subramanian, V. (2007) Discrete Calculus Methods for Diffusion. *J. Comput. Phys.*, **224**, 59–81.

Rapetti, F. (2007) High order edge elements on simplicial meshes. *Mathematical Modelling and Numerical Analysis (M2AN)*, **41**, 1001–1020.

Raviart, P.-A. & Thomas, J. (1977) Primal hybrid Finite Element methods for 2nd order elliptic equations. *Math. Comp.*, **31**, 391–413.

Rufat, D., Mason, G., Mullen, P. & Desbrun, M. (2014) The chain collocation method: A spectrally accurate calculus of forms. *J. Comput. Phys.*, **257**, 1352–1372.

Shashkov, M. & Steinberg, S. (1995) Support Operator Finite Difference algorithms for general elliptic problems. *Journal of Computational Physics*, **118**, 131–151.

Tarhasaari, T., Kettunen, L. & Bossavit, A. (1999) Some realizations of a discrete Hodge operator: A reinterpretation of finite element techniques. *IEEE Transactions on magnetics*, **35**, 1494–1497.

Teixeira, F. (2013) Differential Forms in Lattice Field Theories: An Overview. *ISRN Mathematical Physics*, **2013**, 16p.

Tikhonov, A. & Samarskii, A. (1962) Homogeneous Difference Schemes. *USSR Comput. Math. and Math. Phys.*, **1**, 5–67.

Tonti, E. (1975a) *On the formal structure of physical theories*. monograph of the Italian National Research Council.

Tonti, E. (1975b) The reason for analogies between physical theories. *Applied Mathematical Modelling*, **1**, 37–50.

Tonti, E. (2001) A direct discrete formulation of field laws: The Cell Method. *CMES*, **1**.

Trapp, K. A. (2008) Inner products in covolume and mimetic methods. *ESAIM: Mathematical Modelling and Numerical Analysis*, **42**, 941–959.

Trevisan, F. & Kettunen, L. (2006) Geometric interpretation of finite-dimensional eddy-current formulations. *Internat. J. Numer. Methods Engrg.*, **67**, 1888–1908.

Verstappen, R. & Veldman, A. (2003) Symmetry-preserving discretization of turbulent flow. *J. Comput. Phys.*, **187**, 343–368.

Vohralík, M. & Wohlmuth, B. (2013) Mixed finite element methods: implementation with one unknown per element, local flux expressions, positivity, polygonal meshes, and relations to other methods. *Math. Models Methods Appl. Sci.*, **5**, 803–838.

Wachspress, E. (1975) *A rational Finite Element basis*. Mathematics in Science and Engineering, vol. 114. Academic Press.

Warren, J., Schaefer, S., Hirani, A. & Desbrun, M. (2007) Barycentric coordinates for convex sets. *Advances in Computational Mathematics*, **27**, 319–338.

Whitney, H. (1957) *Geometric integration theory*. Princeton, N. J.: Princeton University Press, pp. xv+387.

Yee, K. (1966) Numerical solution of initial boundary value problems involving maxwell's equations in isotropic media. *IEEE Transaction*, **AP-14**, 302–307.

Résumé

Cette thèse présente une nouvelle classe de schémas de discrétisation spatiale sur maillages polyédriques, nommée *Compatible Discrete Operator* (CDO) et en étudie l'application aux équations elliptiques et de Stokes. La préservation au niveau discret des caractéristiques essentielles du système continu sert de fil conducteur à la construction des opérateurs. Les opérateurs de de Rham définissent les degrés de liberté en accord avec la nature physique des champs à discrétiser. Les équations sont décomposées de manière à différencier les relations topologiques (lois de conservation) des relations constitutives (lois de fermeture). Les relations topologiques sont associées à des opérateurs différentiels discrets et les relations constitutives à des opérateurs de Hodge discrets. Une particularité de l'approche CDO est l'utilisation explicite d'un second maillage, dit dual, pour bâtir l'opérateur de Hodge discret. Deux familles de schémas CDO sont ainsi considérées : les schémas vertex-based lorsque le potentiel est discrétisé aux sommets du maillage (primal), et les schémas cell-based lorsque le potentiel est discrétisé aux sommets du maillage dual (les sommets duaux étant en bijection avec les cellules primales). Les schémas CDO associés à ces deux familles sont présentés et leur convergence est analysée. Une première analyse s'appuie sur une définition algébrique de l'opérateur de Hodge discret et permet d'identifier trois propriétés clés : symétrie, stabilité et $\mathbb{P}_0$-consistance. Une seconde analyse s'appuie sur une définition de l'opérateur de Hodge discret à l'aide d'opérateurs de reconstruction pour lesquels sont identifiées les propriétés à satisfaire. Par ailleurs, les schémas CDO fournissent une vision unifiée d'une large gamme de schémas de la littérature (éléments finis, volumes finis, schémas mimétiques...). Enfin, la validité et l'efficacité de l'approche CDO sont illustrées sur divers cas tests et plusieurs maillages polyédriques.

Mot-clés. *discrétisation compatible, discrétisation mimétique, elliptique, Stokes, opérateur de Hodge discret, maillage polyédrique.*

Abstract

This thesis presents a new class of spatial discretization schemes on polyhedral meshes, called *Compatible Discrete Operator* (CDO) schemes and their application to elliptic and Stokes equations In CDO schemes, preserving the structural properties of the continuous equations is the leading principle to design the discrete operators. De Rham maps define the degrees of freedom according to the physical nature of fields to discretize. CDO schemes operate a clear separation between topological relations (balance equations) and constitutive relations (closure laws). Topological relations are related to discrete differential operators, and constitutive relations to discrete Hodge operators. A feature of CDO schemes is the explicit use of a second mesh, called dual mesh, to build the discrete Hodge operator. Two families of CDO schemes are considered: vertex-based schemes where the potential is located at (primal) mesh vertices, and cell-based schemes where the potential is located at dual mesh vertices (dual vertices being in one-to-one correspondence with primal cells). The CDO schemes related to these two families are presented and their convergence is analyzed. A first analysis hinges on an algebraic definition of the discrete Hodge operator and allows one to identify three key properties: symmetry, stability, and $\mathbb{P}_0$-consistency. A second analysis hinges on a definition of the discrete Hodge operator using reconstruction operators, and the requirements on these reconstruction operators are identified. In addition, CDO schemes provide a unified vision on a broad class of schemes proposed in the literature (finite element, finite element, mimetic schemes...). Finally, the reliability and the efficiency of CDO schemes are assessed on various test cases and several polyhedral meshes.

Keywords. *compatible discretization, mimetic discretization, elliptic, Stokes, discrete Hodge operator, polyhedral mesh*

École des Ponts
ParisTech